A Novel Route to Tailoring the Performance of Liquid Thermoplastic Acrylic Resins for Composite Applications

Ogwa Winifred Obande

Doctor of Philosophy Thesis

University of Edinburgh

2020

Declaration

I declare that this thesis was composed by myself and that the work contained herein is my own, except where explicitly stated otherwise in the text. This work has not been submitted for any other degree or professional qualification except as specified. Any publications are my own work, except where indicated throughout the thesis.

(*Ogwa Winifred Obande*)

Acknowledgements

I owe a debt of gratitude to my supervisor, Dr Dipa Roy for her expert guidance, mentorship, and continued support over the past years of discovery. Her unwavering passion and enthusiasm for polymer and composite engineering kept me driven and engaged throughout my graduate research experience. The warmest of thanks to my second supervisor, Prof Conchúr Ó Brádaigh for his continuous advice, guidance and expert insight. His passion for research excellence has been remarkable and inspirational.

With thanks, I acknowledge the School of Engineering at the University of Edinburgh for the PhD studentship. I would like to thank Arkema GRL, France and SABIC for the provision of material samples and technical support towards this body of work. I gratefully acknowledge the support of the Henry Royce Institute for funding through the Royce PhD Equipment Access Scheme, which enabled access to Confocal Raman facilities at the Culham Centre for Fusion Energy (Royce@CCFE); EPSRC Grant Number EP/R00661X/1.

I am grateful to the members of the Composites Research Group at the University of Edinburgh for the many engaging discussions and advice over the years. I would especially like to thank Dr Eddie McCarthy for his insightful comments and discussions; Dr Francisca Martinez-Hergueta for invaluable impact characterisation and non-destructive evaluation (NDE) insights; Mr Eddie Monteith for the technical support he provided over the years; Mr Mark Jones and Ms Kate Ó'Rourke Masters students, whose research constituted valuable insights that shaped this work.

I acknowledge the support of the School of Engineering (University of Limerick, Ireland) for access to impact test facilities; Dr Hamed Yazdani Nezhad and Dr Pavan Sri Addepalli of Cranfield University for impact testing and NDE; Dr Jenni Garden and Ms Weronika Gruzska of the School of Chemical at the University of Edinburgh for applied chemistry analyses and expertise; and Mr Christian Wurzer of the UK Biochar Research Centre, the University of Edinburgh for support with thermogravimetric analyses.

Finally, I wish to thank Prof John Summerscales and Dr Francisca Martinez-Hergueta, my esteemed viva examiners: for insightful feedback and critique, which were invaluable to the production of this final, improved version of my thesis.

I dedicate this thesis firstly, to God Almighty, who gives me strength and wisdom to do all things.

To my family, Mum (Mrs Enayi T. Obande), Dad (Dr Ogbe D. Obande), Emmanuel, Jake, Jamie, Ochanya, Bosco, Ogbe, Joe & Blessing,
I am incredibly grateful and blessed to have had you all on my team. You were my loudest cheerleaders through this journey.
We did it!

omnia possum in eo qui me confortat

Abstract

As strict government directives continue to incentivise research activities aimed at addressing environmental issues such as the sustainability of fuel resources, reduction of greenhouse gas emissions, and waste management, more and more sectors are adopting ideological shifts towards greener practices. This has positioned continuous fibre-reinforced thermoplastic (CF-RTP) composites as ideal candidate materials in many sectors where their thermosetting (TS) counterparts once dominated. Such a shift is particularly important for the transport sector, which has turned towards *lightweighting* for improved fuel economy and the minimisation of greenhouse gas emissions. While the attractive characteristics of traditional thermoplastic (TP) resins have long been known, their high-melt viscosities rendered them impractical for many sectors due to the requirement for high temperatures and pressures for the production of CF-RTPs. Consequently, TS matrices, have historically been preferred for composite applications at the expense of matrix toughness, recyclability, thermoformability and weldability, which are intrinsic properties of TPs.

Liquid thermoplastic (LTP) resins are attractive, emerging solutions for the shortfalls of traditional thermoplastics (cost-prohibitive processing methodologies) and thermosets (poor end-of-life resource recovery and brittle failure behaviour). Their use facilitates the low-cost fabrication of CF-RTP composites via liquid composite moulding methodologies. CF-RTP composites possess unique attributes that position them as ideal candidate materials for the production of lightweight vehicles with more favourable end-of-life resource recovery than their TS counterparts.

The recent development of room-temperature-processible, LTP resins for the composites markets has garnered considerable research interest. Elium® resins are LTP acrylics, which have become highly desirable, due to favourably low viscosities under ambient processing conditions without specialised or heated tooling. They have been shown to be thermoformable, recyclable, weldable; and are suitable for the production of large-scale components for the renewable energy sector. Their adoption into other sectors (e.g.: transport and marine) can be beneficial from a post-processibility perspective. Acrylics are, however, commodity TPs resins. They are known to be susceptible to solvent attack and strain-rate-dependent embrittlement and have relatively poor thermal stability.

This PhD project aims to explore viable tailoring concepts for liquid reactive acrylic resins, which may be applied without deleterious effects on the glass transition temperature and processibility. The reactivity of the acrylic resin can be exploited to dissolve a telechelic poly(phenylene ether) (PPE) resin for in-situ polymerisation of tailored blends. PPE is a linear, amorphous engineering TP with exceptional thermal stability, and solvent and moisture resistance. It has demonstrable hybridisation efficiency, evidenced by its successful application in blended composite matrices. Thus, a low-molecular, vinyl-functionalised, oligomeric PPE resin was selected based on its ability to reactively participate in the free-radical polymerisation reaction, which can facilitate chemical interactions with the acrylic resin's chemistry. Complementary analytical techniques have been employed on unreinforced blends with compositional variation as part of a parametric down-selection study to determine the optimum PPE content. In addition to identifying the optimum composition, these analyses revealed the formation of multi-species blends, comprising a cross-linked acrylic/PPE network, with interpenetrating constituents (a grafted acrylic/PPE reacted product and a linear acrylic homopolymer).

The viability of this innovative hybridisation approach for room-temperature resin infusion of CF-RTP composites and their subsequent post-processing (by thermoforming) was assessed. A glass-fibre reinforced PPE-modified acrylic laminate was produced and rigorously characterised against an unmodified acrylic-matrix composite to study the hybridisation efficiency. Benchmarking revealed exceptional solvent resistance and thermal stability in the PPE-modified acrylic-matrix composites, confirming the effective contributions of the PPE modifier and this hybridisation methodology. Despite containing a lightly cross-linked network, it was found that the prepared blends retained the desirable thermoformability of the acrylic matrix, confirming that performance tailoring was not performed at the expense of post-processibility.

Lay Summary

The recent acceleration in the market growth of thermoplastic composites is due to the strict targets set by global government directives. These targets are focused on addressing issues surrounding the sustainability of fuel resources, greenhouse gas emissions and waste management. Fibre-reinforced composites as lightweight materials, already fulfil the weight-reduction requirements for improved fuel economy and reduction of greenhouse gas emissions in the transport and aviation sectors. However, the low-cost processibility of thermoset (TS) resins means they have dominated the composites industry as preferred matrices. On the other hand, thermoplastic (TP) polymers offer excellent reprocessibility and toughness but are more challenging and expensive to combine with fibres, due to their high-melt viscosities. Acrylic liquid thermoplastic (LTP) resins have attracted considerable research attention because they effectively bridge the gap between the low-cost processibility of TS resins and the post-processibility of TPs. These reactive, room-temperature-processible resins have already been demonstrated as recyclable, thermoformable/reshapable and weldable. They have been successfully used to produce large-scale demonstrators for the renewable sector without specialised heated tools. Some drawbacks that need to be addressed with acrylic LTPs include their vulnerability to solvent attack, brittle response under certain loading conditions and poor thermal stability.

This PhD project aims to develop, apply, and evaluate an innovative resin system based on a tailored acrylic LTP resin for composite applications. Given the reactivity of the acrylic LTP resins, a higher performance resin (poly(phenylene ether), PPE) has been selected to co-react with the acrylic system to produce tailored blends with enhanced performance. The specific grade of PPE resin used has good chemical compatibility with the acrylic resin. Ultimately, the goal of this project was to enhance the performance of the acrylic resin for composite applications without compromising the resin's desirable room-temperature-processibility and the reprocessibility of the end-product. Both unreinforced and glass fibre-reinforced acrylic/PPE blends were successfully produced using room-temperature moulding methodologies. It was found that co-reacting the liquid acrylic and PPE resins effectively produced complex blends comprising chemically favourable interactions, which enhanced solvent resistance and thermal stability while maintaining a good degree of reshapabilty.

Table of Contents

Declaration i

Acknowledgements ii

Abstract iv

Lay Summary vi

List of Figures xii

List of Tables xxvi

PART I: INTRODUCTION & RESEARCH MOTIVATION 1

Chapter 1 Introduction 2

1.1 Thesis outline 4

Chapter references 6

Chapter 2 Literature review 13

2.1 Polymerisation reactions, thermal and rheological behaviour of liquid reactive acrylic resins 13

2.1.1 Influence of initiator content on polymerisation reactions 14

2.1.2 Influence of temperature 17

2.1.3 Polymerisation exotherm 18

2.2 Fabrication of continuous fibre-reinforced acrylic-matrix composites 19

2.3 Mechanical Properties of acrylic-matrix composites 22

2.3.1 Glass fibre-reinforced acrylic-matrix composites 22

2.3.2 Carbon fibre-reinforced acrylic-matrix composites 25

2.3.3 Flax fibre-reinforced acrylic-matrix composites 35

2.4 Dynamic mechanical (thermomechanical) properties 38

2.5 Effects of fibre sizing on the properties of acrylic-matrix composites 40

2.6 Toughening of acrylic-matrix composites 42

2.7 Hybrid thermoplastic composites using *in situ* polymerised acrylics 48

2.8 Advantages of thermoplastic acrylic-matrix composites 51

2.8.1 Reshaping by thermoforming acrylic-matrix composites 51

2.8.2 Joining of acrylic-matrix composites 51

2.8.3 Recycling and recovery of constituents 52
2.9 Summary of comparative works 53
Chapter references 56
Chapter 3 PhD research motivation 67
3.1 Gaps in existing knowledge 67
3.2 Research opportunities 67
3.3 Thesis aim and objectives 69
3.3.1 Material selection and benchmarking of acrylic-matrix composite performance against an epoxy-matrix composite 69
3.3.2 Development and characterisation of reactive hybrid matrices 70
3.3.3 Fabrication and characterisation of the hybrid-matrix system 70
Chapter references 71
PART II: BENCHMARKING THE PERFORMANCE OF A GLASS FIBRE-REINFORCED THERMOPLASTIC ACRYLIC-MATRIX COMPOSITE 73
Chapter 4 Preliminary studies & material selection 74
4.1 Materials & fabrication method 75
4.2 Characterisation of viscoelastic and drop-weight impact performance 77
4.3 Results and discussion 79
4.3.1 Viscoelastic performance 79
4.3.2 Drop-weight impact damage resistance 81
4.4 Conclusions 84
4.5 Implications for subsequent studies 84
Chapter References 85
Chapter 5 Comparative performance of vacuum-infused thermoplastic acrylic- and thermoset epoxy-matrix composites 87
5.1 Materials and methods 87
5.1.1 Materials and laminate specifications 87
5.1.2 Matched-mould vacuum infusion moulding of laminates 88
5.1.3 Evaluation of laminate quality 89
5.1.4 Mechanical and thermomechanical testing 89

5.2 Results and discussions 94
5.2.1 Transverse tensile properties 94
5.2.2 Longitudinal flexural performance 95
5.2.3 Transverse flexural performance 98
5.2.4 Short beam shear properties 100
5.2.5 Interlaminar fracture toughness test results 103
5.2.6 Dynamic mechanical analyses 107
5.2.7 Drop-weight impact response 108
5.3 Chapter conclusions 120
5.4 Chapter references 127
PART III: DEVELOPMENT OF ACRYLIC/POLY(PHENYLENE ETHER) (PPE) HYBRID MATRIX & CHARACTERISATION OF GLASS FIBRE-REINFORCED ACRYLIC/PPE COMPOSITE 130
Chaper 6 Development, preparation and evaluation of unreinforced acrylic/PPE hybrid polymers 131
6.1 Considerations for thermoplastic-thermoplastic hybrid matrix development 131
6.1.1 Polyphenylene ether (PPE) 131
6.2 Possibilities for thermoplastic-thermoplastic hybrid matrices 134
6.3 Materials and methods 135
6.3.1 Materials 135
6.3.2 Preparation of modified resins 136
6.3.3 Mould casting process 137
6.3.4 Nuclear magnetic resonance (NMR) spectroscopy 138
6.3.5 Solvent resistance in acetone 139
6.3.6 Dynamic mechanical analysis 139
6.3.7 Thermogravimetric analysis 140
6.3.8 Morphological assessments on fractured unreinforced polymers 140
6.4 Results and discussions 142
6.4.1 Results of solution-state polymer analyses 142
6.4.2 Solvent resistance results 146
6.4.3 Dynamic mechanical analysis 150

6.4.4 Results of thermogravimetric analysis 153
6.4.5 Effects of modification on the flexural behaviour 159
6.4.6 Effects of PPE-modification on morphology 160
6.5 Complementary discussions 166
6.6 Chapter conclusion 170
Chapter references 172
Chapter 7 Fabrication and evaluation of glass fibre-reinforced acrylic-PPE composites 182
7.1 Materials and methods 182
7.1.1 Liquid resin infusion moulding of glass fibre-reinforced acrylic-PPE composites 182
7.1.2 Solvent resistance in acetone 184
7.1.3 Thermal and thermomechanical characterisation 184
7.1.4 Mechanical characterisation and microscopic inspection 185
7.1.5 Drop-weight impact characterisation 188
7.2 Results and discussions 188
7.2.1 Solvent resistance in acetone 188
7.2.2 Dynamic mechanical analysis 191
7.2.3 Thermogravimetric analysis 196
7.2.4 Transverse tensile properties 199
7.2.5 Longitudinal flexural performance 202
7.2.6 Transverse flexural performance 204
7.2.7 Short beam shear properties 207
7.2.8 Characterisation of interlaminar fracture toughness 209
7.2.9 Drop-weight impact response 218
7.3 Complementary summary of observations 232
7.4 Chapter conclusions 233
Chapter references 235
PART IV: INSIGHTS, THESIS CONTRIBUTIONS & CONCLUSIONS 242
Chapter 8 Thesis contributions to the current state of knowledge 243
8.1 Comparative study of thermoplastic (acrylic) and thermoset (epoxy) composites 243

8.2 Development of a novel hybridisation route for composite applications using in-situ polymerisable thermoplastic matrices 243
8.3 Insights into chemical interactions in acrylic-PPE hybrid matrices and composites 244
8.4 The development of potential repair and joining methodologies for thermoplastic acrylic-matrix composites 245
8.5 Considerations for the use of acrylic resins 246
8.6 Recommendations for further research 246
Chapter references 250
Chapter 9 Thesis conclusions 251
PART V: AUXILIARY CHAPTERS 254
Appendix A 255
Nomenclature and Acronyms 255
A.1 Acronyms and Material Designations 255
A.2 Variables and Parameters 261
Latin Letters, Variables and Symbols 261
Greek Letters and Symbols 265
Appendix B Insights from complementary research and collaborations 267
B.1 New possibilities with liquid acrylic resins and their hybrids 267
B.1.1 Thermoplastic fibre-metal laminates 267
B.1.2 Waste management and infusion repair 268
B.1.3 Impact damage repair 271
B.1.4 Selective modification strategies 273
References 275
Appendix C Supplementary Information 278
C.1 Supplementary Information for Chapter 6 278
C.2 Supplementary Information for Chapter 7 280
References 292
Appendix D: Peer-Reviewed Publications of the Author 293
D.1 Published Journal Articles 293
D.2 Research collaborations and involvements 294

List of Figures

Figure	Caption	Page
Figure 2-1	Dynamic-mechanical analysis results showing the effect of initiator contents of (a) 0.8 %, (b) 1.2 %, and (c) 1.6 % on tangent delta (tanδ) as a function of temperature (T) (Copyright permission from Wiley. Adapted from Figure 7 in [26]).	14
Figure 2-2	Results of the thermogravimetric analyses on samples polymerised with initiator contents of 0.8 wt. %, 1.2 wt. % and 1.6 wt. %. Valleys corresponding to the first and second mass loss events are marked as 1 and 2, respectively (Copyright permission from Wiley. Adapted from Fig. 8 in [8]).	15
Figure 2-3	Degree of conversion as a function of temperature for Elium® 150 samples polymerised with 0.8 wt. %, 1.2 wt. % and 1.6 wt. % of initiator (Copyright permission from Wiley [26]).	16
Figure 2-4	An (a) optimised three-step thermal cycle for Elium® 150 resin and (b) DSC validation results for the cycle as developed by de Andrade Raponi et al. [13] (Copyright permission from Elsevier [13]).	18
Figure 2-5	Conventional liquid resin infusion process set-up.	20
Figure 2-6	Impact-face damage states on glass fibre-reinforced polyester, epoxy and acrylic composites subjected to impact events of 10 J, 20 J and 30 J (Copyright permission from Elsevier. Adapted from Fig. 8 in [46]).	25
Figure 2-7	Scanning electron micrographs showing flexural failure modes of thin-ply carbon fibre-reinforced (a) & (c) epoxy and (b) & (d) acrylic composites (Copyright permission from Elsevier [48]).	27
Figure 2-8	Flexural failure modes of thin-ply carbon fibre-reinforced acrylic composites: (a), (c) & (e) without annealing; and (b), (d) & (f) with annealing (Copyright permission from Elsevier [48]).	28
Figure 2-9	Impact side and reverse side damage following impact events at 25, 42 and 52 J (Copyright permission from Elsevier. Reproduced from Figs. 12, 14 & 16 in [21]).	29

Figure 2-10	Micrographs showing damage sustained by carbon fibre-reinforced (a), (b) & (c) acrylic and (d), (e) & (f) epoxy composites following drop-weight impacts at 25, 42 and 52 J, respectively (Copyright permission from Elsevier. Reproduced from Figs. 13, 14 & 15 [21]).	29
Figure 2-11	(a) Representative load-displacement curves showing mode-I crack propagation behaviour, (b) representative R-curves, and (c) mode-I fracture toughness values of carbon fibre-reinforced acrylic and epoxy composites (Copyright permission from Elsevier. Reproduced from Figs. 3-5 in [32]).	31
Figure 2-12	Load-displacement curves for carbon fibre-reinforced (a) Elium® 150, (b) epoxy; and (c) mode-II interlaminar fracture toughness determined from same (Copyright permission from Elsevier. Reproduced from Figs. 6-8 in [35]).	33
Figure 2-13	SEM micrographs of mode-II fracture surfaces of CF/acrylic and CF/epoxy (Copyright permission from Elsevier. Reproduced from Figs. 11 & 12 in [35]).	34
Figure 2-14	SEM micrographs of exposed fibre surfaces following mode-II fracture toughness testing on CF/acrylic and CF/epoxy composites (Copyright permission from Elsevier. Reproduced from Figs. 11 & 12 in [35]).	35
Figure 2-15	Low- and high-magnification SEM micrographs of double cantilever fracture surfaces of UHMWPE-acrylic samples containing (a & b) untreated fibres, (c & d) PDA-treated fibres, and (e & f) PDA+MWCNT-treated fibres (Copyright permission from Elsevier. Adapted from Fig. 7 in [59]).	41
Figure 2-16	Structure of self-assembling acrylic block copolymer (Copyright permission from Elsevier. Reproduced from Fig. 1a in [19]).	43
Figure 2-17	Demonstration of thermoformability (a) flattening a curved section and (b) producing a curved prototype from glass-reinforced acrylic laminates (Copyright permission from Elsevier. Reproduced from Fig. 9 & 10 in [5]).	51
Figure 2-18	Welding configuration used by Bhudolia et al. [43] (Copyright permission from Elsevier. Fig. 1 in [43]).	52
Figure 2-19	Recovery of fibres and polymer matrix from in situ polymerised glass/acrylic laminate by dissolution as	53

demonstrated by Cousins et al. [5] (Copyright permission from Elsevier. Reproduced from Fig. 5 in [5]).

Figure 3-1 Diagrammatic representations of thermoplastics (amorphous, semi-crystalline) and cross-linked thermosets. 68

Figure 4-1 (a) A schematic diagram and (b) photograph of the resin infusion set-up used for laminate fabrication. 76

Figure 4-2 Drop-weight impact test experimental set-up. 78

Figure 4-3 Experimental set-up for damage area image acquisition. 79

Figure 4-4 Single-frequency DMA thermograms showing damping behaviour (*tan delta*) as a function of temperature. 79

Figure 4-5 Multi-frequency DMA thermograms showing the evolution of *tan delta* (damping parameter) with frequency at 25°C. 80

Figure 4-6 Impact and back face images (cropped) showing the damage states of GF/E180 and GF/IN-2 coupons following impact events at 15 J, respectively. The scale bar (50 mm) applies to all images. 81

Figure 4-7 Impact and back face images (cropped) showing the damage states of GF/E180 and GF/IN-2 coupons following impact events at 30 J, respectively. The scale bar (50 mm) applies to all images. 82

Figure 4-8 Representative damage states for (a) GF/E180 at 15 J, (b) GF/IN-2 at 15 J, (c) GF/E180 at 30 J, and (d) GF/IN-2 at 30 J. ROI: region of interest. 83

Figure 5-1 Adjustable-cavity vacuum infusion mould supplied by Composite Integration used for the fabrication of test laminates. 88

Figure 5-2 Schematic showing FAI coupon extraction from impact-damaged coupons. 93

Figure 5-3 Transverse stress-strain behaviour of all GF/acrylic and GF/epoxy samples. 95

Figure 5-4 Representative failure modes in both materials following transverse tensile testing with loading direction schematically represented. 95

Figure 5-5	Stress-strain curves of (a) GF/acrylic, (b) GF/epoxy and (c) representative curves showing characteristic behaviour of both materials in response to longitudinal flexural loading.	96
Figure 5-6	Images showing representative modes of (a) compressive failure, (b) tensile failure, on upper and lower surfaces, respectively; and (c) regions of compressive and tensile failure on GF/acrylic sample edges of longitudinal flexure specimens. Note: (d), (e) and (f) are the same features on GF/epoxy samples, respectively.	98
Figure 5-7	Stress-strain curves of (a) GF/acrylic and (b) GF/epoxy and (c) representative curves showing characteristic behaviour of both materials in response to transverse flexural loading.	99
Figure 5-8	Images of representative failures (tensile side) on three samples of (a) GF/acrylic and (b) GF/epoxy following transverse flexural testing.	100
Figure 5-9	Load-displacement curves obtained from short beam shear tests for all (a) GF/acrylic and (b) GF/epoxy samples and (c) a comparison of two representative curves from both materials.	101
Figure 5-10	SEM micrographs showing representative GF/acrylic short beam shear failure modes at magnifications of 25× in (a), 50× in (b), and 200× in (c) and (d).	102
Figure 5-11	SEM micrographs showing representative GF/epoxy short beam shear failure modes at magnifications of 25× in (a), 50× in (b), and 200× in (c) and (d).	102
Figure 5-12	Representative (a) load-displacement curves and (b) resistance curves (R-curves) obtained from DCB testing of GF/acrylic and GF/epoxy, and (c) is a chart comparing their average $G_{IC\text{-}Init.}$ and $G_{IC\text{-}Prop.}$ values.	104
Figure 5-13	Images of representative delamination behaviour observed during DCB testing of (a)-(b) GF/acrylic and (c)-(d) GF/epoxy at equivalent test times. The relative extents of fibre bridging are evident.	105
Figure 5-14	SEM micrographs of mode-I fracture surfaces of GF/acrylic (a-b) and GF/epoxy (c-d).	107
Figure 5-15	Thermomechanical results showing the effect of temperature on storage modulus and tan delta in DMA testing. Testing carried out in the longitudinal direction.	107

Figure 5-16	Representative force-displacement curves for GF/epoxy and GF/acrylic samples subjected to (a) 30 J and (b) 50 J.	109
Figure 5-17	Representative energy-time curves for GF/epoxy and GF/acrylic samples subjected to (a) 30 J and (b) 50 J.	110
Figure 5-18	(a) & (b) Back-lit images of impact-damaged samples, and representative (c) & (d) macroscopic images of samples of GF/epoxy and GF/acrylic following impact events at 30 J, respectively.	111
Figure 5-19	(a) & (b) Back-lit images of impact-damaged samples, and representative (c) & (d) macroscopic images of samples of GF/epoxy and GF/acrylic following impact events at 50 J, respectively.	112
Figure 5-20	Damaged area fractions as functions of impact energy.	113
Figure 5-21	Energy profile diagram of GF/acrylic and GF/epoxy composite materials for drop-weight impacts at 30 J and 50 J.	115
Figure 5-22	Flexure-after-impact (FAI) stress-strain curves of (a) pristine, (b) 30 J and (c) 50 J impact-damaged coupons of GF/epoxy and GF/acrylic samples.	117
Figure 5-23	(a) Flexural strength and (b) flexural modulus results of flexure-after-impact tests conducted on pristine, 30 J and 50 J impact-damaged coupons of GF/epoxy and GF/acrylic samples.	118
Figure 5-24	Post-impact property reduction as functions of matrix type and impact energy. *Percentage reductions are with respect to properties obtained from pristine samples.	119
Figure 6-1	Representative chemical structure of PPE.	134
Figure 6-2	Representative chemical structure of vinyl-functionalised PPE as published by the manufacturer [33]. Note, Y was used by the manufacturer to denote proprietary information pertinent to the grade of PPE employed in this study.	135
Figure 6-3	Schematics of the resin blend preparation procedure and the observed characteristics of each blend after mixing and leaving undisturbed for 24 h.	137

Figure 6-4	The cast polymer samples were placed over the word "TEST" to assess the influence of PPE content on transparency and colour of PPE-modified blends.	138
Figure 6-5	Schematic depicting the experimental set-up employed for obtaining fractured (unreinforced) specimens for microscopic investigations.	141
Figure 6-6	Schematics showing the region of interest for SEM microscopy.	141
Figure 6-7	Overlaid ^{1}H NMR spectra of the acrylic/PPE blends and the starting materials in the presence and absence of BPO in $CDCl_3$. The key ^{1}H NMR signals from the acrylic monomer (*, red), PPE oligomer (*, blue) and acrylic polymer (#, green) are highlighted.	143
Figure 6-8	Basic structures of block and random copolymers and cross-linked polymers.	144
Figure 6-9	DOSY NMR spectrum of A95/P5 and A90/P10 blends in $CDCl_3$.	146
Figure 6-10	Mass losses after the exposure of unreinforced polymer samples to acetone for 60 minutes (blue) and 72 hours (red) showing the influence of PPE modifier content on solvent resistance. Note: A lesser mass loss corresponds to superior solvent resistance.	147
Figure 6-11	Time-lapse images of unmodified acrylic (A100/P0) and PPE-modified acrylic blends with compositional variations (A97/P3 – A85/P15) subjected to prolonged (72 h) exposure in acetone — nominal sample dimensions (mm): 8 × 8.	149
Figure 6-12	Representative DMA thermograms showing the effects of PPE content on damping behaviour (tan delta) and T_g. Note: the PPE used has a Tg of 160°C [33].	150
Figure 6-13	T_g values and tan delta peak heights from DMA experiments on polymer matrix samples. Results are based on averaged duplicates. Note: the PPE used has a Tg of 160°C [33].	151
Figure 6-14	Diagrammatic representation showing the determination of half peak width and peak factor from DMA thermograms.	152

Figure 6-15	Half tan delta peak widths and peak factors determined from DMA experiments on polymer matrix samples. Results are based on averaged duplicates.	152
Figure 6-16	Graphical illustration of the characteristic parameters for TGA curves.	153
Figure 6-17	Representative thermograms from TGA on unmodified acrylic polymer (A100/P0) and PPE-modified acrylic blends A97/P3, A95/P5, A90/P10 and A85/P15. Zones 1-3 are characteristic degradation zones and are presented as inset graphs for improved visibility.	154
Figure 6-18	Representative DTG thermograms for unmodified acrylic polymer (A100/P0), PPE oligomer (A0/P100) and their blends: A97/P3, A95/P5, A90/P10 and A85/P15. Zone 1 is an inset graph for improved visibility of unique degradation behaviour exhibited by all blends.	156
Figure 6-19	Graphical illustration of key DTG parameters.	157
Figure 6-20	Flexural load-displacement curves from flexural testing of neat acrylic A100/P0, and PPE-modified acrylic blends (A97/P3, A95/P5, A90/P10 and A85/P15).	160
Figure 6-21	Confocal Raman micrographs showing compositional maps for the PPE-modified acrylic blends as obtained from flexural fracture surfaces. The correlation map depicts acrylic- and PPE-rich phases in cyan and yellow; matrix cracks are visible as irregular deep blue vein-like features, respectively.	161
Figure 6-22	SEM micrographs of flexural fracture surfaces of acrylic and PPE-modified acrylic polymer samples. Note: (a)-(e) are low-magnification micrographs and (f)-(j) are high-magnification micrographs of A100/P0, A97/P3, A95/P5, A90/P10 and A85/P1, respectively.	162
Figure 6-23	SEM micrographs showing the main fracture mechanisms on fractured (flexural) acrylic and PPE-modified acrylic matrix samples.	164
Figure 6-24	Chemical structures of the reactants (acrylic monomer, PPE oligomer and dibenzoyl peroxide radical) and the proposed cross-linked acrylic/PPE structure formed.	166
Figure 6-25	Results of reshapabilty trials conducted on the acrylic/PPE blends, A100/P0 as the thermoplastic control, and a cast epoxy sample as a thermoset control. All samples are 40-mm	167

dia. discs except for A97/P3, which measures 25 mm × 8 mm × 4 mm due to material constraints.

Figure 6-26 (a) The proposed polymer architecture within the PPE-modified acrylic blends, showing a lightly cross-linked acrylic/PPE network, a branched or grafted acrylic/PPE species, and a highly entangled, linear acrylic polymer species; (b) a simplified form of same. 169

Figure 7-1 Diagrammatic representation of the experimental set-up for composite fabrication. The upper and lower mould halves of the adjustable-cavity vacuum infusion mould are shown in blue. 183

Figure 7-2 Mass losses after the exposure of glass fibre-reinforced polymer samples to acetone for 60 minutes (blue) and 72 hours (red) showing the influence of PPE modifier content on solvent resistance. Note: A lesser mass loss corresponds to superior solvent resistance. 188

Figure 7-3 Time-lapse images of glass fibre-reinforced acrylic (GF/A100/P0) and glass fibre-reinforced acrylic/PPE (GF/A95/P5) composites subjected to prolonged (72 h) exposure in acetone. Nominal sample dimensions (mm): 8 × 8. 190

Figure 7-4 DMA thermograms for glass fibre-reinforced (a) acrylic (GF/A100/P0) and (b) PPE-modified acrylic (GF/A95/P5) composites showing damping response (tan delta), and (c) representative thermograms with averaged results for each material. 192

Figure 7-5 An idealised representation of the T_{gN} values used in the analysis for the GF/A95/P5 sample, where T_{g1} and T_{g2} are the glass transition temperatures (Kelvin) for the acrylic homopolymer and PPE-rich phases of the hybrid matrix, respectively. 193

Figure 7-6 TGA and DTG plots of glass fibre-reinforced acrylic (GF/A100/P0) and PPE-modified acrylic (GF/A95/P5) composites. 197

Figure 7-7 Representative curves and results for GF/A100/P0 (red) and GF/A95/P5 (blue) following loading in transverse tension. Stress-strain curves for all samples are provided in Appendix C.2.1.1 (Figure C-2 & Figure C-3). 199

Figure 7-8	Representative macroscopic and back-lit images of failed transverse tensile test specimens of GF/A100/P0 ((a) & (c)) and GF/A95/P5 ((b) & (d)).	200
Figure 7-9	Representative curves and results for GF/A100/P0 (red) and GF/A95/P5 (blue) following loading in longitudinal flexure. Stress-strain curves for all samples are provided in Appendix C.2.1.1 (Figure C-10 & Figure C-11).	202
Figure 7-10	Macroscopic images of failure behaviour on the compressive and transverse sides of representative samples of GF/A100/P0 and GF/A95/P5. Side views of representative samples are also presented to show differences in deformation behaviour. All images feature 10 mm scale bar.	203
Figure 7-11	Representative curves and results for GF/A100/P0 (red) and GF/A95/P5 (blue) following loading in transverse flexure. Stress-strain curves for all samples are provided in Appendix C.2.1.1 (Figure C-12 & Figure C-13)	205
Figure 7-12	Macroscopic images of representative transverse flexural failure on sides subjected to tensile stress states of (a) GF/A100/P0 and (b) GF/A95/P5 samples.	206
Figure 7-13	Stress-displacement curves for (a) GF/A100/P0 and (b) GF/A95/P5 following loading in short beam shear. Note: τ_{max} is the corresponding shear strength and $\tau_{1.5\,mm}$ is the stress at 1.5 mm displacement for all samples, respectively.	208
Figure 7-14	Representative macroscopic failure resulting from short beam shear loading of GF/A100/P0 and GF/A95/P5.	209
Figure 7-15	(a) Representative load-displacement curves and (b) R-curves for GF/A100/P0 (red) and GF/A95/P5 (blue) following double cantilever beam testing.	210
Figure 7-16	(a) In-situ test images obtained during double cantilever beam testing to show the crack-opening behaviour of GF/A100/P0 and GF/A95/P5. Nominal thicknesses for GF/A100/P0 and GF/A95/P5 are 3.8 mm and 3.3 mm, respectively.	212
Figure 7-17	SEM micrographs showing mode-I fracture surfaces of (a), (b) & (c) GF/A100/P0 and (d)-(f) GF/A95/P5. The large broken arrows show the direction of crack propagation. In (f), arrows highlight paths of microcrack formation.	213
Figure 7-18	SEM micrographs showing fracture mechanisms in the GF/A95/P5 sample. Different stages of craze formation can	214

	be seen in (a), and ruptured craze fibrils and microcrack formation can be seen in (b). The large broken arrows show the direction of crack propagation.	
Figure 7-19	(a) SEM micrographs of GF/A95/P5 DCB fracture surface showing domains (Feature 1) and (b) shows evidence of shear banding (Feature 2) mechanism.	216
Figure 7-20	SEM micrograph showing GF/A95/P5 fracture surface; Features 1, 2, 3 and 4 are domains, craze-like microcracking, drawn matrix ribbons bounding parabolas and plastic flow of the matrix, respectively.	217
Figure 7-21	Representative force-displacement (a) &(c), and energy-time (b) & (d) curves for GF/A100/P0 and GF/A95/P5, following impacts at 30 J and 50 J, respectively.	219
Figure 7-22	High-contrast, back-lit images showing the damage states following 30-J impact events on GF/A100/P0 and GF/A95/P5 coupons.	221
Figure 7-23	High-contrast, back-lit images showing the damage states following 50-J impact events on GF/A100/P0 and GF/A95/P5 coupons.	222
Figure 7-24	(a) Damaged area fraction and (b) damage index as functions of impact energy for GF/A100/P0 and GF/A95/P5.	223
Figure 7-25	Energy profile diagram for GF/A100/P0 and GF/A95/P5 for drop-weight impacts performed at 30 J and 50 J.	225
Figure 7-26	Flexural stress-strain curves for pristine (undamaged), bidirectional GF/A100/P0 and GF/A95/P5 samples.	226
Figure 7-27	Flexural stress-strain curves for 30-J impact-damaged bidirectional GF/A100/P0 and GF/A95/P5 samples.	227
Figure 7-28	Flexural stress-strain curves for 50-J impact-damaged bidirectional GF/A100/P0 and GF/A95/P5 samples.	228
Figure 7-29	Post-impact flexural strength as a function of impact damage states for GF/A100/P0 and GF/A95/P5.	229
Figure 7-30	Post-impact flexural modulus as a function of impact damage states for GF/A100/P0 and GF/A95/P5.	230
Figure 7-31	Residual post-impact properties as functions of matrix type and impact energy. *Percentage reductions are FAI strengths	231

and moduli normalised with respect to corresponding nominal values.

Figure 9-1 Illustrative summary of the preliminary miscibility trials conducted to assess the phase stability of the acrylic/PPE resin blends for room-temperature resin infusion processing. Further details are available in Chapter 6. 252

Figure 9-2 A summary of the key findings of this chapter. Axis Min and Max values are provided in parenthesis for scaling purposes. †: No T_{end}^2 value for A100/P0; the T_{end}^1 value was used for graphing purposes only. Note: Solvent resistance is the inverse of mass fraction lost during exposure to acetone; subscripts, 60 min and 72 h for solvent resistance imply the results for 60 min and 72 h exposure, respectively. 253

Figure 9-3 The proposed polymer architecture within the PPE-modified acrylic blends, showing a lightly cross-linked acrylic/PPE network, a branched or grafted acrylic/PPE species, and a highly entangled, linear acrylic polymer species. A detailed description of all considerations and theories that informed the identification of this structure can be found in Chapter 6 (Section 6.5). 254

Figure 9-4 Results of thermoformability trials conducted on the acrylic/PPE blends, A100/P0 as the thermoplastic control, and epoxy as a thermoset control. All samples are 40-mm dia. discs except for A97/P3, which measures 25 mm × 8 mm × 4 mm due to material availability constraints. Previously presented in Section 6.5 and prepared as detailed in Appendix C.1.1.2 (Figure C-2). 255

Figure 9-5 Summary of the chemical and thermal analyses results for glass fibre-reinforced acrylic (GF/A100/P0) and PPE-modified acrylic (GF/A95/P5) composites as presented in Chapter 7. All symbols are used as listed in the Nomenclature section (Appendix A). 257

Figure 9-6 Summary of the mechanical and thermomechanical properties for glass fibre-reinforced acrylic (GF/A100/P0) and PPE-modified acrylic (GF/A95/P5) composites as presented in Chapter 7. All symbols are used as listed in the Nomenclature section (Appendix A). 258

Figure 9-7 Summary of the drop-weight impact performance of glass fibre-reinforced acrylic (GF/A100/P0) and PPE-modified acrylic (GF/A95/P5) composites as presented in Chapter 7. 271

All symbols are used as listed in the Nomenclature section (Appendix A).

Figure 9-8 Summary of the impact tolerance (the post-impact flexural properties) of glass fibre-reinforced acrylic (GF/A100/P0) and PPE-modified acrylic (GF/A95/P5) composites as presented in Chapter 7. All symbols are used as listed in the Nomenclature section (Appendix A). 272

Figure B-1 (a) VARTM set-up and (b) perforation design of the Al alloy sheet utilised for TP-FML fabrication [1]. 268

Figure B-2 (a) Low- and (b) high-magnification SEM micrographs showing the interface between the fibre-reinforced acrylic and the aluminium substrates of the TP-FML [1]. 268

Figure B-3 Two-stage production sequence for the fabrication of the "repaired" laminate. Adapted from a Masters project report by O'Rourke [14]. 270

Figure B-4 High-contrast back-lit images of impact-damaged coupons before and after hot-press repair (Temperature: 200°C; Pressure: 29.5 bar; Duration: 3 minutes). 271

Figure B-5 Post-impact flexural (a) strength, (b) modulus as functions of damage and repair conditions. 272

Figure B-6 Scanning electron micrographs of mode-I interlaminar fracture surfaces of acrylic-PPE hybrid matrix composites prepared using loose powder and preforming approaches. Note: these micrographs are a compilation of those reported by Jones [15]. 274

Figure C-1 Activation energies for degradation reactions for acrylic and PPE-modified acrylic polymers; results show the influence of PPE content on thermal stability. These energies were assessed using the data in Section 6.4.4. 278

Figure C-2 Methodology for ascertaining the reshapability of unreinforced neat and PPE-modified acrylic samples. 40-mm dia. disc samples were used for an epoxy reference, A100/P0, A95/P5, A90/P10 and A85/P15 samples. Due to material availability, a different geometry was used for the A95/P5 sample, which measured (25 × 8 × 4) mm. The associated results are presented and discussed in Section 6.5 (Figure 6-25). 279

Figure C-3	Transverse tensile stress-strain responses for all GF/A100/P0 samples. A representative chart was presented for this material in Section 7.2.4 (Figure 7-7).	280
Figure C-4	Transverse tensile stress-strain responses for all GF/A95/P5 samples. A representative chart was presented for this material in Section 7.2.4 (Figure 7-7).	281
Figure C-5	Longitudinal flexural stress-strain responses for all GF/100/P0 samples. A representative chart was presented for this material in Section 7.2.5 (Figure 7-9).	282
Figure C-6	Longitudinal flexural stress-strain curves for quasi-unidirectional, glass fibre-reinforced GF/A100/P0. A representative chart was presented for this material in Section 7.2.5 (Figure 7-9).	283
Figure C-7	Transverse flexural stress-strain curves for quasi-unidirectional, glass fibre-reinforced GF/A100/P0. A representative chart was presented for this material in Section 7.2.6 (Figure 7-11).	284
Figure C-8	Transverse flexural stress-strain curves for quasi-unidirectional, glass fibre-reinforced GF/A95/P5. A representative chart was presented for this material in Section 7.2.6 (Figure 7-11).	285
Figure C-9	Illustrative representation of the hot-press moulding attempted for the production of neat unreinforced PPE for characterisation. Results were unfavourable for testing as shown in Figure C-3.	286
Figure C-10	Fragments of neat, unreinforced PPE obtained from the attempted hot-press moulding of plaques for testing as detailed in Figure C-2. The plaque exhibited poor handleability and was not suited for the extraction of samples for testing.	287
Figure C-11	(a)A graphical representation of the microdroplet test method attempted for characterising the fibre-matrix interface, (b) the targeted geometry, and (c) the obtained samples were not suitable for testing.	288
Figure C-12	SEM micrographs of GF/A100/P0 ((a) & (c), and GF/A95/P5 (b) & (d) fracture surfaces. Greater matrix coverage on fibres on GF/A95/P5 is indicative of enhanced interfacial adhesion.	290

Figure C-13 Evidence of pronounced matrix ductility on the DCB fracture surface of a GF/A95/P5 sample. 291

List of Tables

Table	Caption	Page
Table 1-1	An overview of published works by chapter.	5
Table 2-1	Summary of critical findings on the influence of initiator content on the polymerisation behaviour of liquid acrylic resins. Data sourced from [26].	17
Table 2-2	Summary of reported processing techniques of acrylic matrix composites and resulting fibre (V_f) and void (V_v) volume fractions, by resin grade and fibre type.	21
Table 2-3	Summary of tensile properties reported for flax fibre-reinforced acrylic composites.	36
Table 2-4	Summary of some thermomechanical properties reported in published works for acrylic-based matrices and composites.	39
Table 2-5	Overview of works on the effects of toughening on the impact performance of acrylic-matrix composites.	44
Table 2-6	A summary of the effects of Nanostrength®-toughening on glass transition temperatures of unreinforced acrylic polymers.	48
Table 2-7	Overview of some published works on acrylic-matrix hybrid composites.	50
Table 2-8	Summary of published literature on the comparative performance of acrylic composites against comparable epoxy composites.	55
Table 4-1	DMA test information.	77
Table 4-2	Drop-weight impact test parameters.	78
Table 5-1	Summary mechanical and thermomechanical properties reported as specified in matrix technical datasheets and relevant publications.	87
Table 5-2	Summary mechanical and thermomechanical properties reported as specified in matrix technical datasheets and relevant publications.	89

Table 5-3	Details of test parameters and specimen dimensions.	91
Table 5-4	Details of impact test parameters.	91
Table 5-5	Tensile, flexural and shear properties.	94
Table 5-6	Summary of thermomechanical results.	108
Table 5-7	Summary of comparative impact properties of GF/epoxy and GF/acrylic samples.	114
Table 5-8	Chapter overview of evaluated properties (Mechanical properties). *Percentage difference expressed with respect to GF/epoxy values; where + and – symbols represent higher and lower GF/acroylic values, respectively.	124
Table 5-9	Chapter overview of mode-I interlaminar fracture toughness properties. *Percentage difference expressed with respect to GF/epoxy values; where + and – symbols represent higher and lower GF/acrylic values, respectively.	125
Table 5-10	Chapter overview of evaluated properties (Drop-weight impact properties). *Percentage difference expressed with respect to GF/epoxy values; where + and – symbols represent higher and lower GF/acrylic values, respectively.	125
Table 5-11	Chapter overview of evaluated properties (Damage tolerance; flexure-after-impact) -cont. *Percentage difference expressed with respect to GF/epoxy values; where + and – symbols represent higher and lower GF/acrylic values, respectively.	125
Table 5-12	Chapter overview of evaluated properties (Thermomechanical properties). *Percentage difference expressed with respect to GF/epoxy values; where + and – symbols represent higher and lower GF/acrylic values, respectively.	126
Table 6-1	Summary of research contributions on the development of PPE- and PPO-based blended material systems.	132
Table 6-2	Overview of neat acrylic and blend compositions, where A and P indicate acrylic and PPE constituents, respectively.	136
Table 6-3	Summary of analyses performed by material type and composition.	140

Table 6-4	Summary of thermogravimetric results for polymeric showing the effects of PPE-modification on thermal stability. Values are averaged from duplicates.	155
Table 6-5	Summary of derivative thermogravimetric results for polymeric showing the effects of PPE-modification on thermal stability. Values are averaged from duplicates.	159
Table 7-1	Summary of materials used for composite fabrication.	182
Table 7-2	Summary of comparative laminate properties.	184
Table 7-3	Test specification for the mechanical characterisation of samples from quasi-unidirectional laminates.	187
Table 7-4	Summary of values used in the estimation of the constituents (acrylic and PPE) within the reacted product to yield a T_{g2} value of 120°C (373 K).	194
Table 7-5	Summary of thermogravimetric results of composite samples showing the effects of PPE-modification on thermal stability.	198
Table B-1	Summary of the results reported for infusion repair by O'Rourke [14].	270
Table B-2	Summary of PPE-modified acrylic laminates investigated by Jones [15].	273

PART I: INTRODUCTION & RESEARCH MOTIVATION

Chapter 1 Introduction

Fibre-reinforced polymer (FRP) composites are particularly attractive for their exceptional specific strength and stiffness properties; and are known to be highly durable. Thus, they are ideal candidate materials across many sectors, particularly for weight-critical applications. The use of thermoplastic (TP) polymer matrices offers benefits in fracture toughness, damage tolerance, recyclability, welding and thermoformability compared to their thermosetting (TS) counterparts [1–3]. However, their high melt viscosities necessitate processing at high temperatures and pressures to achieve desired polymer flow and consolidation of saturated plies [4,5]. Consequently, processing methodologies for the production of TP polymer matrix composites are considered cost-prohibitive for many sectors.

The demand for TP-FRP has increased significantly in light of global changes in government legislation, which set targets for mass reduction in road vehicles and the minimisation of landfill-bound waste streams. Thus, to meet this demand, research activities in recent years have focused on the development of novel material systems and alternative methodologies that facilitate cost- and energy-efficient production of continuous fibre-reinforced thermoplastic composites.

TP precursors such as cyclic butylene terephthalate (CBT) [6–10], caprolactam [11,12] and laurolactam [13,14] have attracted significant attention for the reactive processing of TP-matrix composites. The low viscosities of these reactive monomers and oligomers are ideal for low-pressure infiltration into dry fibre preforms, and subsequently, in-situ polymerising into polybutylene terephthalate (PBT), polyamide-6 (PA-6) and polyamide-12 (PA-12), respectively. While being innovative alternatives to conventional TP matrices, these materials require mould heating to achieve temperatures above 150°C (PA-6 and PA-12) and 180°C (PBT). As a result, specialised tooling and energy costs become prohibitively expensive for the fabrication of large-scale structures, particularly for applications in the wind energy sector, where blade lengths continue to increase to meet growing global energy demand [15–17].

More recently, a family of TP acrylic monomer resins, which are suited to liquid resin infusion (LRI) processing of composites at room temperature has become the subject of extensive research. Such research efforts have focused on rigorous benchmarking of their

mechanical and thermomechanical performance against epoxy systems spanning commodity and intermediate-performance epoxies [18–30].

In general, composites based on these acrylic resin systems exhibit comparable performance with non-aerospace-grade epoxy-matrix composites in terms of general mechanical properties. However, acrylic-based composites have been reported to possess inferior longitudinal tensile and compressive strengths [22], transverse flexural performance [26] and impact damage resistance [19]. Concerning their thermomechanical performance, lower glass transition temperatures have been reported for these resins [26]; this may also be indicative of lower thermal stability compared to epoxy-based composites [31].

Moreover, acrylics as commodity amorphous TP polymers are highly susceptible to solvent attack [32], which makes them unsuitable for certain applications and environments. Improving solvent resistance can be highly beneficial for acrylic-matrix composites to increase their acceptance in a broader range of applications. This is particularly of importance for automotive applications, for which solvent and chemical resistance are desirable in matrices to overcome the effects of prolonged in-service exposure to chemicals (gasoline, motor oil, antifreeze, paint, cleaning solvents and road salts) [33].

Several works have focused on acrylic-matrix modification to realise enhanced-performance composites [30,34–36], further highlighting the need to design and develop hybrids based on these resins for tailored performance.

Current modification practices for liquid acrylic resins involve the incorporation of self-assembling acrylic-based block copolymers based on nanophasic morphology. A routinely used block copolymer modifier is Nanostrength™; based on Arkema's proprietary alkoxyamine technology, it comprises polymethylmethacrylate-b-polybutylacrylate-b-polymethylmethacrylate. Its use is reported to enhance impact properties, rigidity and the overall transparency of the matrix [37].

Interestingly, with the exception of works on melt-mixed TP blends [38–45], the modification of TP matrices for composite applications has not been the subject of extensive research in the same way that TS-matrix modification has. This may be because

high-melt viscosities of traditional TP polymer matrices often limit the extent to which modifiers can be incorporated.

Due to their low viscosities, liquid TP resins for composite applications are thus ideal candidate materials for the same modification methodologies utilised for liquid TS resin systems. TS resin systems, such as epoxies are often tailored with the addition of other polymeric phases, which may be elastomeric or thermoplastic [46–54]. The use of TP modifiers can be highly beneficial because their use does not have deleterious effects on glass transition temperature in the resulting blend in the way that elastomeric modifiers do [38] and they can enhance the fracture toughness property of the brittle TS matrix.

Another motivation behind the addition of higher performance engineering TPs into liquid thermosetting resins is the need to circumvent challenges associated with their processibility [55,56]. This approach involves the use of these liquid resins as reactive solvents within which higher molecular weight TPs can be dissolved for subsequent processing by liquid composite moulding methodologies. Thus, this is an attractive way to produce composite structures with tailored-performance hybrid matrices.

Poly(phenylene oxide) (PPO), also known as poly(phenylene ether) (PPE) is a relatively low-cost engineering thermoplastic that has become one of the most important engineering polymers today. Arguably the main limiting factor to the broader applicability of PPE as a standalone composite matrix is its poor processibility [57–60].

1.1 Thesis outline

This thesis has been structured around peer-reviewed publications (as detailed in Table 1-1). Each publication relates to a specific objective of this research and collectively provides an in-depth understanding of the development, characteristics and wider-reaching impact of reactive hybridisation of a liquid thermoplastic matrix and a higher performance thermoplastic oligomer for composite applications.

Details of these publications are summarised in Table 1-1 along with the current impact factors for the respective journals to which they were submitted. Appendix D in Part V of this thesis may be consulted for further information on these articles and other relevant research activities and involvements that pertain to this body of work.

Table 1-1. An overview of published works by chapter.

Chapter	*Publication Title* *[Authors]*	*Journal* *[Impact Factor]*	*Status*
2	**Obande, W., Ó Brádaigh, C., Ray, D., 2021. Continuous fibre-reinforced thermoplastic acrylic-matrix composites prepared by liquid resin infusion–A review** [Obande, W.; Ó Brádaigh, C. M.; Ray, D.]	Composites Part B: Engineering [7.635]	Published
4	**Viscoelastic and Drop-Weight Impact Properties of an Acrylic-Matrix Composite and a Conventional Thermoset Composite – A Comparative Study** [Obande, W.; Ray, D.; Ó Brádaigh, C. M.]	Materials Letters [3.204]	Published
5	**Mechanical and Thermomechanical Characterisation of Vacuum-Infused Thermoplastic- and Thermoset-Based Composites** [Obande, W.; Mamalis, D.; Ray, D.; Yang, L.; Ó Brádaigh, C. M.]	Materials & Design [6.289]	Published
6	**Enhancing the solvent resistance and thermomechanical properties of thermoplastic acrylic polymers and composites via reactive hybridisation** [Obande, W.; Gruszka, W.; Garden, J.; Wurzer, C.; Ó Brádaigh, C. M.; Ray, D.]	Materials & Design [6.289]	Published
7	**Thermoplastic hybrid-matrix composites prepared by a room-temperature vacuum infusion and in-situ polymerisation process** [Obande, W.; Ó Brádaigh, C. M.; Ray, D.]	Composites Communications [4.915]	Published

In the interest of providing a comprehensive overview of the body of work presented in this thesis, chapters are presented sequentially, in line with the evolution of the objectives rather than a chronological order of the publications on which they are based.

The main chapters of this thesis are broadly divided into the following four parts:

PART I. Introduction and motivation: **Chapters 1-3**

PART II. Benchmarking the performance of glass fibre-reinforced acrylic-matrix composite: **Chapters 4 & 5**

PART III. Development of acrylic/PPE hybrid matrix and characterisation of glass fibre-reinforced acrylic/PPE composite: **Chapters 6 & 7**

PART IV. Research contributions, thesis conclusions & outlook: **Chapters 8 & 9**

Chapter references

[1] Hinkley JA, Johnston NJ, O'Brien TK. Interlaminar fracture toughness of thermoplastic composites. Adv Thermoplast Matrix Compos Mater 1989:251–63. https://doi.org/10.1520/stp24606s.

[2] Nash N. Inclusion of a thermoplastic phase to improve impact and post-impact performances of carbon fibre reinforced thermosetting composites — A review. Mater Des 2015;85:582–97. https://doi.org/10.1016/J.MATDES.2015.07.001.

[3] Kim K-Y, Ye L, Phoa K-M. Interlaminar fracture toughness of CF/PEI and GF/PEI composites at elevated temperatures. Appl Compos Mater 2004;11:173–90.

[4] Howes JC, Loos AC, Hinkley JA. The Effect of Processing on Autohesive Strength Development in Thermoplastic Resins and Composites. Adv Thermoplast Matrix Compos Mater 2008:17–33. https://doi.org/10.1520/stp24593s.

[5] Akca E, Gursel A. A Review on the Matrix Toughness of Thermoplastic Materials. Period Eng Nat Sci 2015;3:1–8. https://doi.org/10.21533/pen.v3i2.52.

[6] Coll SM, Murtagh AM, Ó Brádaigh CM. Resin film infusion of cyclic pBT composites: a fundamental study. Proc. SAMPE Eur. 25th Int. Jubil. Conf., Paris: 2004.

[7] Parton H, Verpoest I. In situ polymerization of thermoplastic composites based on cyclic oligomers. Polym Compos 2005;26:60–5.

[8] Yan C, Liu L, Zhu Y, Xu H, Liu D. Properties of polymerized cyclic butylene terephthalate and its composites via ring-opening polymerization. J Thermoplast Compos Mater 2018;31:181–201. https://doi.org/10.1177/0892705717697774.

[9] Abt T, Sánchez-Soto M. A review of the recent advances in cyclic butylene terephthalate technology and its composites. Crit Rev Solid State Mater Sci 2017;42:173–217. https://doi.org/10.1080/10408436.2016.1160820.

[10] Balogh G. Development of cyclic butylene terephthalate matrix composites. Budapest University of Technology and Economics [Doctoral Thesis], 2012.

[11] Van Rijswijk K, Teuwen JJE, Bersee HEN, Beukers A. Textile fiber-reinforced anionic polyamide-6 composites. Part I: The vacuum infusion process. Compos Part A Appl Sci Manuf 2008;40:1–10. https://doi.org/10.1016/j.compositesa.2008.03.018.

[12] Pillay S, Vaidya UK, Janowski GM. Effects of moisture and UV exposure on liquid molded carbon fabric reinforced nylon 6 composite laminates. Compos Sci Technol 2009;69:839–46. https://doi.org/10.1016/j.compscitech.2008.03.021.

[13] Ó Máirtín P, McDonnell P, Connor M, Eder R, Ó Brádaigh CM. Process investigation of a liquid PA-12/carbon fibre moulding system. Compos Part A 2001;32:915–23.

[14] Zingraff L, Michaud V, Bourban PE, Månson JAE. Resin transfer moulding of anionically polymerised polyamide 12. Compos Part A Appl Sci Manuf 2005;36:1675–86. https://doi.org/10.1016/j.compositesa.2005.03.023.

[15] Ó Brádaigh CM, Doyle A, Doyle D, Feerick PJ. Electrically-heated ceramic composite tooling for out-of-autoclave manufacturing of large composite structures. Int SAMPE Tech Conf 2011.

[16] Doyle A, Feerick P, Mallon P, Ó Brádaigh C, Doyle D. A heated mould for moulding polymeric composites, a method for making such mould and its use 2012.

[17] Gardiner G. Thermoplastic wind blades: To be or Not? CompositesWorld 2012:30–5.

[18] Chilali A, Zouari W, Assarar M, Kebir H, Ayad R. Analysis of the mechanical behaviour of flax and glass fabrics-reinforced thermoplastic and thermoset resins. J Reinf Plast Compos 2016;35:1217–32. https://doi.org/10.1177/0731684416645203.

[19] Obande W, Ray D, Ó Brádaigh CM. Viscoelastic and drop-weight impact properties of an acrylic-matrix composite and a conventional thermoset composite – A comparative study. Mater Lett 2019;238.

https://doi.org/10.1016/j.matlet.2018.11.137.

[20] Aronica A, Fossati D. Mechanical Properties of Carbon Fiber Composite Materials. Politecnico di Milano [Master's Thesis], 2014.

[21] Aronica A, Fossati D. Effects of resin and processing on mechanical properties of carbon fibre composites. Politecnico di Milano [Master's Thesis], 2015.

[22] Baley C, Lan M, Bourmaud A, Le Duigou A. Compressive and tensile behaviour of unidirectional composites reinforced by natural fibres: Influence of fibres (flax and jute), matrix and fibre volume fraction. Mater Today Commun 2018;16:300–6. https://doi.org/10.1016/j.mtcomm.2018.07.003.

[23] Chilali A, Assarar M, Zouari W, Kebir H, Ayad R. Effect of geometric dimensions and fibre orientation on 3D moisture diffusion in flax fibre reinforced thermoplastic and thermosetting composites. Compos Part A Appl Sci Manuf 2017;95:75–86. https://doi.org/10.1016/j.compositesa.2016.12.020.

[24] Bhudolia SKK, Perrotey P, Joshi SCC. Optimizing polymer infusion process for thin ply textile composites with novel matrix system. Materials (Basel) 2017;10. https://doi.org/10.3390/ma10030293.

[25] Lorriot T, El Yagoubi J, Fourel J, Tison F. Non-conventional glass fiber NCF composites with thermoset and thermoplastic matrices. 20th Int. Conf. Compos. Mater., Copenhagen: 2015.

[26] Obande W, Mamalis D, Ray D, Yang L, Ó Brádaigh CM. Mechanical and thermomechanical characterisation of vacuum-infused thermoplastic- and thermoset-based composites. Mater Des 2019;175. https://doi.org/10.1016/j.matdes.2019.107828.

[27] Murray RE, Penumadu D, Cousins D, Beach R, Snowberg D, Berry D, et al. Manufacturing and flexural characterization of infusion-reacted thermoplastic wind turbine blade subcomponents. Appl Compos Mater 2019;27:945–61. https://doi.org/10.1007/s10443-019-9760-2.

[28] Davies P, Arhant M. Fatigue behaviour of acrylic matrix composites: influence of

seawater. Appl Compos Mater 2019;26:507–18. https://doi.org/10.1007/s10443-018-9713-1.

[29] Bhudolia SK, Perrotey P, Joshi SC. Mode I fracture toughness and fractographic investigation of carbon fibre composites with liquid Methylmethacrylate thermoplastic matrix. Compos Part B Eng 2018;134:246–53. https://doi.org/10.1016/j.compositesb.2017.09.057.

[30] Kinvi-Dossou G, Matadi Boumbimba R, Bonfoh N, Garzon-Hernandez S, Garcia-Gonzalez D, Gerard P, et al. Innovative acrylic thermoplastic composites versus conventional composites: Improving the impact performances. Compos Struct 2019;217:1–13. https://doi.org/10.1016/j.compstruct.2019.02.090.

[31] Carlos Quagliano Amado J. Thermal Resistance Properties of Polyurethanes and Its Composites. Thermosoftening Plast., IntechOpen; 2020. https://doi.org/10.5772/intechopen.87039.

[32] Woishnis WA, Ebnesajjad S, editors. Acrylic Polymers and Copolymers. Chem. Resist. Thermoplast., 2012, p. 1–106. https://doi.org/10.1016/b978-1-4557-7896-6.00001-7.

[33] Mallick PK. Thermoplastics and thermoplastic-matrix composites for lightweight automotive structures. Mater. Des. Manuf. Light. Veh., Elsevier Ltd.; 2010, p. 174–207. https://doi.org/10.1533/9781845697822.1.174.

[34] Bhudolia SK, Joshi SC. Low-velocity impact response of carbon fibre composites with novel liquid Methylmethacrylate thermoplastic matrix. Compos Struct 2018;203:696–708. https://doi.org/10.1016/j.compstruct.2018.07.066.

[35] Matadi Boumbimba R, Coulibaly M, Khabouchi A, Kinvi-Dossou G, Bonfoh N, Gerard P. Glass fibres reinforced acrylic thermoplastic resin-based tri-block copolymers composites: Low velocity impact response at various temperatures. Compos Struct 2017;160:939–51. https://doi.org/10.1016/j.compstruct.2016.10.127.

[36] Pini T. Fracture behaviour of thermoplastic acrylic resins and their relevant

unidirectional carbon fibre composites: rate and temperature effects. Politecnico Milano 1863 [Doctoral Thesis], 2017.

[37] Arkema. Nanostrength®: self-assembling block copolymers - Arkema n.d.

[38] Khanh T, Nguyen L, Sébastien †, Livi S, Soares BG, Benes H, et al. Toughening of Epoxy/Ionic Liquid Networks with Thermoplastics Based on Poly(2,6-dimethyl-1,4-phenylene ether) (PPE) 2016. https://doi.org/10.1021/acssuschemeng.6b02479.

[39] Ajitha AR, Thomas S. Introduction: Polymer blends, thermodynamics, miscibility, phase separation, and compatibilization. Elsevier Inc.; 2019. https://doi.org/10.1016/B978-0-12-816006-0.00001-3.

[40] Kar GP, Biswas S, Bose S. Tailoring the interface of an immiscible polymer blend by a mutually miscible homopolymer grafted onto graphene oxide: Outstanding mechanical properties. Phys Chem Chem Phys 2015;17:1811–21. https://doi.org/10.1039/c4cp04481a.

[41] Robeson LM. Fundamentals of polymer blends. Polym. blends a Compr. Rev., 2007.

[42] Varsavas SD, Kaynak C. Effects of glass fiber reinforcement and thermoplastic elastomer blending on the mechanical performance of polylactide. Compos Commun 2018;8:24–30. https://doi.org/10.1016/j.coco.2018.03.003.

[43] Pecorini TJ, Hertzberg RW. The fracture behavior of rubber-toughened, short-fiber composites of nylon 6,6. Polym Compos 1994;15:174–83. https://doi.org/10.1002/pc.750150303.

[44] Parker DS, Yee AF. Factors Influencing the Mode I Interlaminar Fracture Toughness of a Rubber Toughened Thermoplastic Matrix Composite. J Thermoplast Compos Mater 1989;2:2–18. https://doi.org/10.1177/089270578900200101.

[45] Tjong SC, Xu SA, Mai YW. Impact fracture toughness of short glass fiber-reinforced polyamide 6,6 hybrid composites containing elastomer particles using

essential work of fracture concept. Mater Sci Eng A 2003;347:338–45. https://doi.org/10.1016/S0921-5093(02)00609-3.

[46] Lee SE, Jeong E, Lee MY, Lee MK, Lee YS. Improvement of the mechanical and thermal properties of polyethersulfone-modified epoxy composites. J Ind Eng Chem 2016;33:73–9. https://doi.org/10.1016/j.jiec.2015.09.022.

[47] Mimura K, Ito H, Fujioka H. Improvement of thermal and mechanical properties by control of morphologies in PES-modified epoxy resins. Polymer (Guildf) 2000;41:4451–9. https://doi.org/10.1016/S0032-3861(99)00700-4.

[48] Zhao P, Liang X, Chen J, Ran Q, Gu Y. Poly(ether imide)-modified benzoxazine blends: Influences of phase separation and hydrogen bonding interactions on the curing reaction. J Appl Polym Sci 2013;128:2865–74. https://doi.org/10.1002/app.38459.

[49] Biolley N, Pascal T, Sillion B. Polyimide-modified epoxy system: time-temperature-transformation diagrams, mechanical and thermal properties. Polymer (Guildf) 1994;35:558–64. https://doi.org/10.1016/0032-3861(94)90511-8.

[50] Hamerton I, McNamara LT, Howlin BJ, Smith PA, Cross P, Ward S. Toughening mechanisms in aromatic polybenzoxazines using thermoplastic oligomers and telechelics. Macromolecules 2014;47:1946–58. https://doi.org/10.1021/ma5002436.

[51] Orhan T, Ates S, Hacaloglu J, Yagci Y. Thermal degradation characteristics of polysulfones with benzoxazine end groups. J Anal Appl Pyrolysis 2012;94:146–52. https://doi.org/10.1016/j.jaap.2011.12.001.

[52] Del Saz-Orozco B, Ray D, Kervennic A, McGrail PT, Stanley WF. Toughening of carbon fibre/polybenzoxazine composites by incorporating polyethersulfone into the interlaminar region. Mater Des 2016;93:297–303. https://doi.org/10.1016/j.matdes.2015.12.138.

[53] Di Pasquale G, Motta O, Recca A, Carter JT, McGrail PT, Acierno D. New high-

performance thermoplastic toughened epoxy thermosets. Polymer (Guildf) 1997;38:4345–8. https://doi.org/10.1016/S0032-3861(96)01031-2.

[54] Hamerton I, McNamara LT, Howlin BJ, Smith PA, Cross P, Ward S. Developing toughened aromatic polybenzoxazines using thermoplastic oligomers and telechelics, part 1: Preparation and characterization of the functionalized oligomers. J Appl Polym Sci 2014;131. https://doi.org/10.1002/app.40875.

[55] Ronak B. Fracture mechanics of nanostructured polymer blends with janus particles. University of Bayreuth [Doctoral Thesis], 2018.

[56] Nelissen LNIH. A novel route to blends of polystyrene and poly(2,6-dimethyl-1,4-phenylene ether)□: synthesis, properties and applications 1991. https://doi.org/10.6100/IR352941.

[57] Venderbosch RW, Meijer HEH, Lemstra PJ. Processing of intractable polymers using reactive solvents: 1. Poly(2,6-dimethyl-1,4-phenylene ether)/epoxy resin. Polymer (Guildf) 1994;35:4349–57. https://doi.org/10.1016/0032-3861(94)90092-2.

[58] Venderbosch RW, Meijer HEH, Lemstra PJ. Processing of intractable polymers using reactive solvents: 2. Poly(2,6-dimethyl-1,4-phenylene ether) as a matrix material for high performance composites. Polymer (Guildf) 1995;36:1167–78. https://doi.org/10.1016/0032-3861(95)93918-C.

[59] Cong H, Yu B, Yuan H, Tian C, Yang S. Preparation and characterization of nanocomposites with polyphenylene oxide. In: Mittal V, editor. Manuf. nanocomposites with Eng. Plast., Woodhead Publishing; 2015.

[60] Li Y, Xie T, Yang G. Effects of polyphenylene oxide content on morphology, thermal, and mechanical properties of polyphenylene oxide/polyamide 6 blends. J Appl Polym Sci 2006;99:2076–81. https://doi.org/10.1002/app.22687.

Chapter 2 Literature review

Recent research activities on reactive TP resins have led to the development of Elium®, a family of liquid TP acrylic resins, which are *in situ* polymerisable at room temperature. With viscosities as low as 100 mPa.s, these acrylic resins are considered more cost-effective than the first-generation reactive resins described in Chapter 1. Moreover, their suitability for the production of large-scale components by resin infusion [1–4]; and their thermoformability and recyclability [5] have recently been demonstrated.

The following sections present a comprehensive review of the advancements to date in the use of reactive acrylic resins as attractive solutions to the challenges associated with traditional thermosetting and thermoplastic matrices for composite applications. Published works on the mechanical and thermomechanical performance of *in situ* polymerisable acrylic matrices and their composites are reviewed and discussed herein. A broad summary of comparative analyses performed to date alongside comparable thermosetting composites is also presented.

2.1 Polymerisation reactions, thermal and rheological behaviour of liquid reactive acrylic resins

Acrylics polymerise by free radical polymerisation and undergo three characteristic reactions. (i) Initiation is typically brought about by radical peroxides (initiators), which comprise unpaired electrons that can combine with monomers via covalent bonding to create reactive radical sites on the monomers. (ii) This is followed by chain propagation reaction, with unreacted monomer molecules successively being 'captured' and newly unpaired electrons becoming available at growing chain ends. (iii) Termination can subsequently occur by recombination, usually in the presence of another radical, or a termination agent to bring growth to an end. Process parameters such as initiator concentration, temperature and pressure, have been reported to significantly influence the rates of radical polymerisation reactions and also the resultant molecular weight and molecular weight distribution [6,7]. Understanding the effects of these parameters on the resulting acrylic polymer system is an essential step in fostering an established knowledge base on optimum processing conditions. Presented herein, is a brief overview of published works on the polymerisation behaviour of acrylics as a function of processing conditions.

2.1.1 Influence of initiator content on polymerisation reactions

Using the Elium® 150 grade of liquid acrylic resin and a commercial organic peroxide, it was shown that initiator content influences the reaction stages of free radical polymerisation [8]. Both high (1.6 %) and low (0.8 %) initiator contents promote slower initiation and termination reaction rates than an intermediate concentration (1.2 %). Combined with observations of higher onset temperatures (75°C) for the high and low concentrations, and lower temperature (58°C) for the intermediate concentration, the authors concluded that these observations were associated with the availability of the radical species provided by the initiator. It was suggested that for the lower radical concentration (0.8 %), fewer acrylic monomer molecules were initiated and thus, the growth of a few long chains culminated in the observed behaviour. In contrast, higher concentration (1.6 %) promoted concurrent growth of several short chains. It can thus, be deduced that in all cases, these effects are combinatory effects of the competitive chain growth and ultimate termination reactions. Interestingly, the lowest initiator content was found to cause an instantaneous, exponential increase in viscosity up to the terminal cycle temperature (rheological study). Increasing the initiator content was reported to reduce the viscosity at all polymerisation reaction stages.

A positive correlation exists between the initiator content and glass transition temperature (Figure 2-1), with equivalent values reported for 1.2 % and 1.6 % concentrations [8].

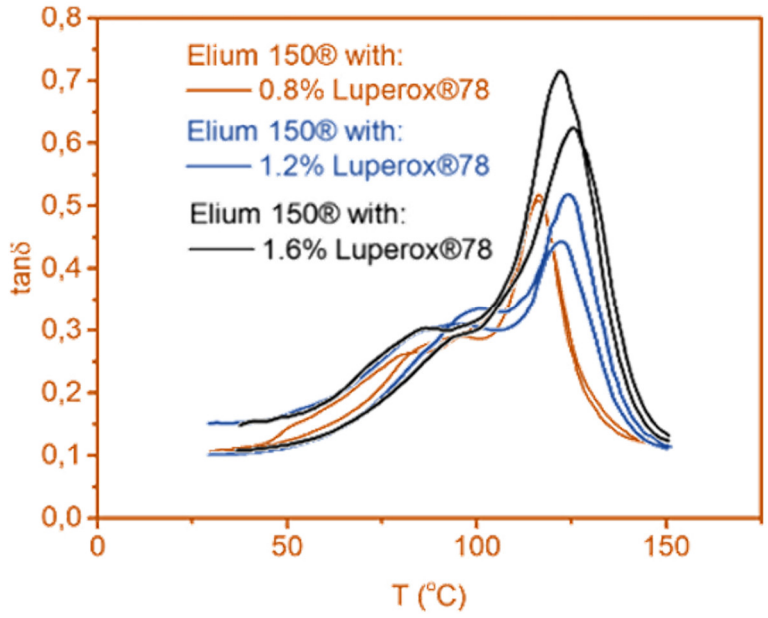


Figure 2-1. Dynamic-mechanical analysis results showing the effect of initiator contents of (a) 0.8 %, (b) 1.2 %, and (c) 1.6 % on tangent delta (tanδ) as a function of temperature (T) (Copyright permission from Wiley. Adapted from Figure 7 in [26]).

While no effects were observed on tan delta peak amplitudes between the samples containing 0.8 % and 1.2 % of initiator content, a pronounced increase was observed for the sample polymerised with 1.6 wt. % of the initiator.

The same authors reported no major effects of initiator content on the thermal degradation behaviour on polymerised samples. All samples were shown to undergo two mass loss stages, evidenced by the two valleys in the derivative thermogravimetric (DTG) curves (Figure 2-2).

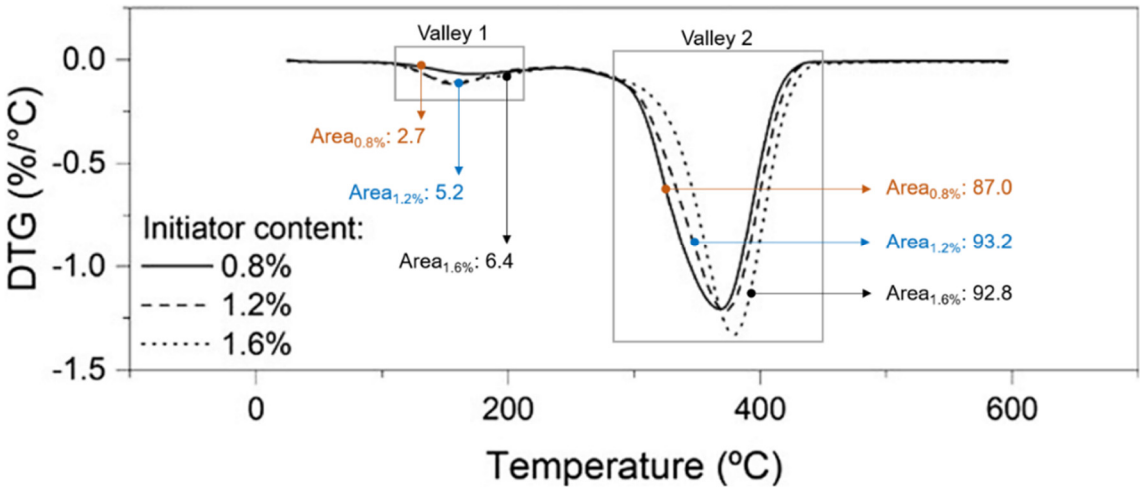


Figure 2-2. . Results of the thermogravimetric analyses on samples polymerised with initiator contents of 0.8 wt. %, 1.2 wt. % and 1.6 wt. %. Valleys corresponding to the first and second mass loss events are marked as 1 and 2, respectively (Copyright permission from Wiley. Adapted from Fig. 8 in [8]).

For samples polymerised using initiator contents of 0.8 %, 1.2 % and 1.6 %, respectively, the valleys are as follows. (i) *Valley 1*: occurred at 113°C, 115°C and 108°C, and was said to be related to the depolymerisation of head-to-head linkages (from recombination termination reactions) and residual monomers. (ii) *Valley 2*: occurred at 298°C, 302°C and 326°C. This valley was said to be associated with random scission. Evidently, an increase in initiator content promoted the formation of more head-to-head linkages. Interestingly, a third characteristic decomposition valley, which is typically observed for acrylic-based polymers due to the decomposition of unsaturated chain ends at temperatures of around 230°C was said to be absent due to copolymerisation with oxygen during the polymerisation process. This work highlights the importance of further exploration of the thermal stability and flammability of reactive acrylic polymers and their composites. Acrylics are known to depolymerise at elevated temperatures, releasing flammable monomers, which has in-service fire hazard implications [9]. Already, it has been shown using non-woven intumescent mats

[10] and a phosphorus-carbon-based flame retardant [11] that the flame retardance and smoke suppression properties of acrylic-matrix composites can be significantly enhanced.

On the influence of initiator content on the degree of conversion, the samples containing 0.8 wt. % and 1.6 wt. % of initiator appeared to exhibit slower initiation and propagation rates as shown in Figure 2-3 [8].

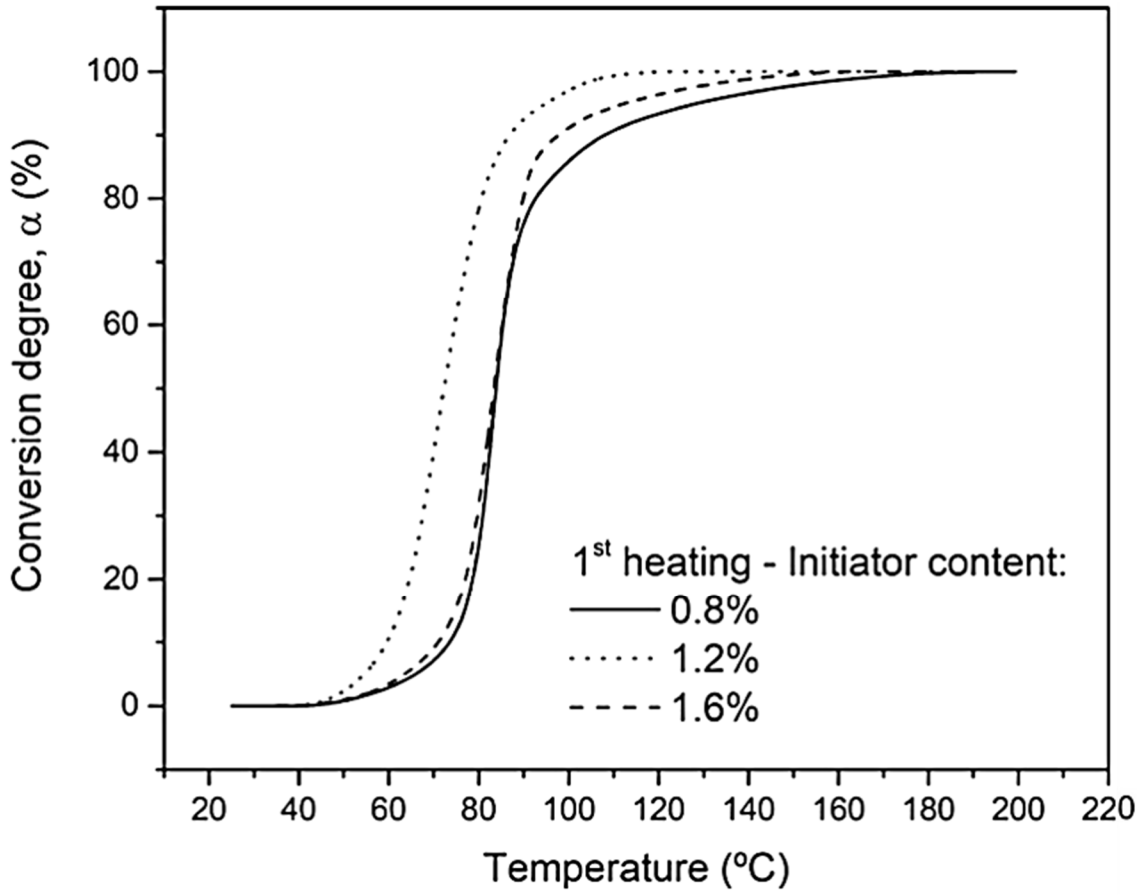


Figure 2-3. Degree of conversion as a function of temperature for Elium® 150 samples polymerised with 0.8 wt. %, 1.2 wt. % and 1.6 wt. % of initiator (Copyright permission from Wiley [26]).

The work by de Andrade Raponi et al. [8] provides an understanding of the influence of initiator content for Elium® 150 resin; key findings are summarised in Table 2-1. While this is an essential study in advancing knowledge on the behaviour of Elium® 150, it is worth noting that compositional differences exist between the grades of this novel family of acrylic resins. As such, research attention must be invested in fostering an understanding of the effects of initiator content on the properties of other grades of Elium®.

Table 2-1. Summary of critical findings on the influence of initiator content on the polymerisation behaviour of liquid acrylic resins. Data sourced from [26].

	Polymerisation				*Rheology*	*Glass transition*	*Decomposition*	
Initiator content (wt. %)	$T_{100\,\%}$ *(°C)*	T_{onset} *(°C)*	T_{max} *(°C)*	$-\Delta H$ *(J/g)*	T_{gel} *(°C)*	T_g *(°C)*	T_{onset} *Peak 1 (°C)*	T_{onset} *Peak 2 (°C)*
0.8	199.3	75.9	82.6	129.4	87.0	116.2	113	298
1.2	122.4	57.9	70.4	150.7	84.4	123.4	115	302
1.6	163.9	74.0	81.8	210.7	87.5	123.3	108	326

2.1.2 Influence of temperature

The polymerisation of first-generation acrylate monomers has been shown to be influenced by temperature due to its effects on the polymerisation time, the formation of voids, and the risk of exothermic runaways [12]. de Andrade Raponi et al. [13] showed that temperature significantly influences the termination step of polymerisation reactions for unreinforced Elium® 150 containing 1.2 % of a commercial organic peroxide, and invariably, its degree of conversion. A key contribution of this work was the proposal of a three-stage thermal processing cycle (Figure 2-4 (a)), comprising sequential isothermal segments at 25°C (25 min), 80°C (30 min) and 110°C (120 min), with heating rates of 4°C/min. The first segment was employed to promote a slow reaction rate to limit the formation of thermally-induced voids. No exothermic peaks were revealed by DSC analysis of the polymerised sample (Figure 2-4(b)), which implies that no further polymerisation was detected. As with the work by de Andrade Raponi et al. [8] an obvious limitation is that this study focused solely on process optimisation for this specific grade of acrylic resin, and the proposed process parameters may not be directly applicable to other grades given the compositional variations that may exist in this family of acrylic resins. Thus, further studies of this nature covering several grades may prove beneficial. Interestingly, the manufacturers remarked on the suitability of this resin grade for room-temperature polymerisation; however, suggest a post-polymerisation heating step at 80°C for 4 h for enhanced mechanical performance [14].

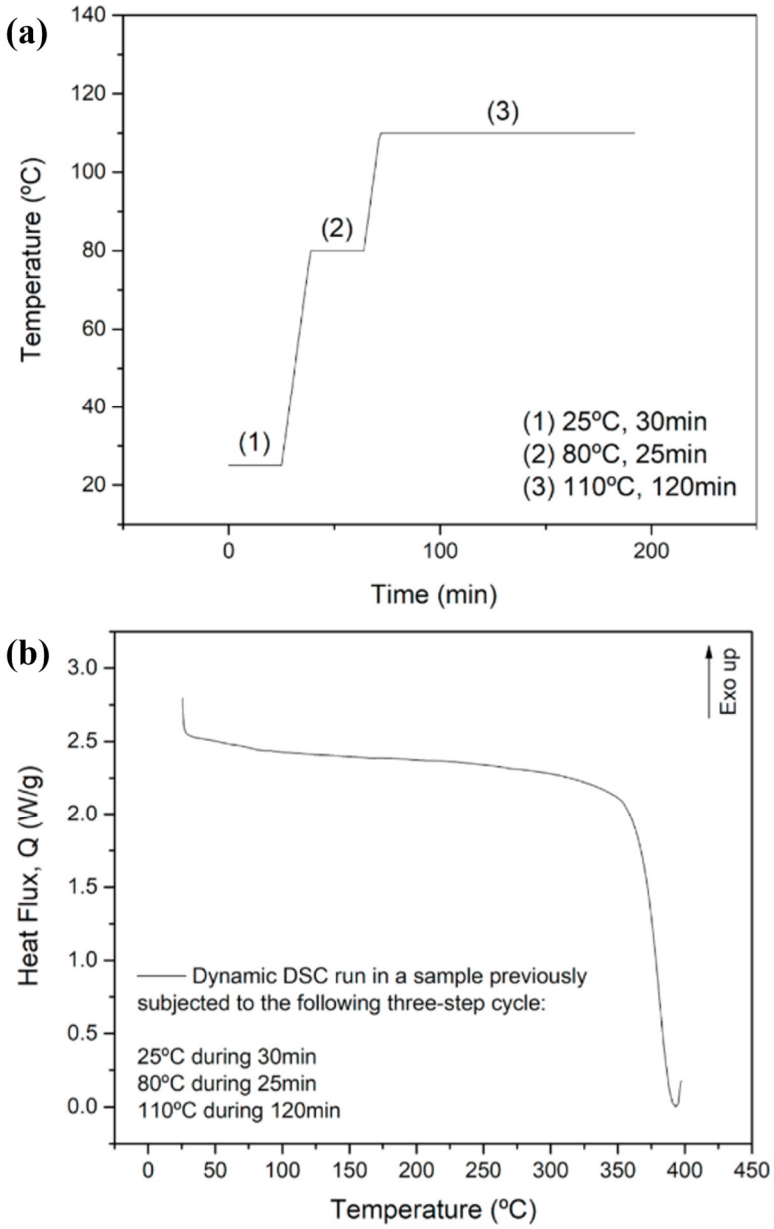


Figure 2-4. An (a) optimised three-step thermal cycle for Elium® 150 resin and (b) DSC validation results for the cycle as developed by de Andrade Raponi et al. [13] (Copyright permission from Elsevier [13]).

2.1.3 Polymerisation exotherm

Murray et al. [15] reported the need for a proprietary exothermic-control agent for the production of thick sections of glass fibre-reinforced acrylic laminates. In a similar study [1], the need for such measures in the production of thick components (>12 mm) was highlighted. These findings are supported by Charlier et al. [16] who reported constant heat flow and reaction rate up to 40 % conversion, followed by an instantaneous increase in reaction rate up to 100 % conversion. This rate change was believed to be attributed to an

auto-acceleration phenomenon (the gel effect), known to induce a high degree of exothermicity in bulk free radical polymerisation. Peak exotherm temperatures of 45°C [17] and 77-90°C [5] have been reported for thin and thick sections, respectively. An increase in laminate thickness from 3.8 mm to 11.3 mm has been shown to result in a corresponding increase in peak exotherm temperature of 21.5°C [18].

2.2 Fabrication of continuous fibre-reinforced acrylic-matrix composites

Most published works on the properties of *in situ* polymerised acrylic-matrix composites have employed a vacuum-assisted resin transfer moulding (VARTM) technique [19–24]; however, resin transfer moulding (RTM) [21,25–27] and wet lay-up and press moulding [28] have also been used.

Depending on the variant of liquid resin infusion method used (such as those in Hindersmann's overview [29]), an array of auxiliary materials are used to aid liquid resin infusion and the subsequent release or demoulding process. In most cases, the set-up shown in Figure 2-5 is employed, where a flexible membrane or bag is used in conjunction with a rigid tool base. Traditional liquid resin infusions are typically preceded by a resin degassing process for the removal of dissolved gases and micro-bubbles within liquid resins such as epoxy [30]. However, the short pot life and infusion window (~40 min) of these acrylic resin systems makes degassing impractical. Where it has been attempted on E−280, no significant benefits were reported [20]. With the exception of the work done by Cousins et al. [5], no authors reported a resin degassing step for acrylic-based laminates. Across most of the reviewed works, a conventional liquid resin infusion configuration with a flexible membrane was employed. Additionally, vacuum RTM (VRTM) or RTM Light was also reported using an innovative adjustable-thickness tool with two rigid mould halves [24,31] where vacuum is used for both clamping and resin flow [29].

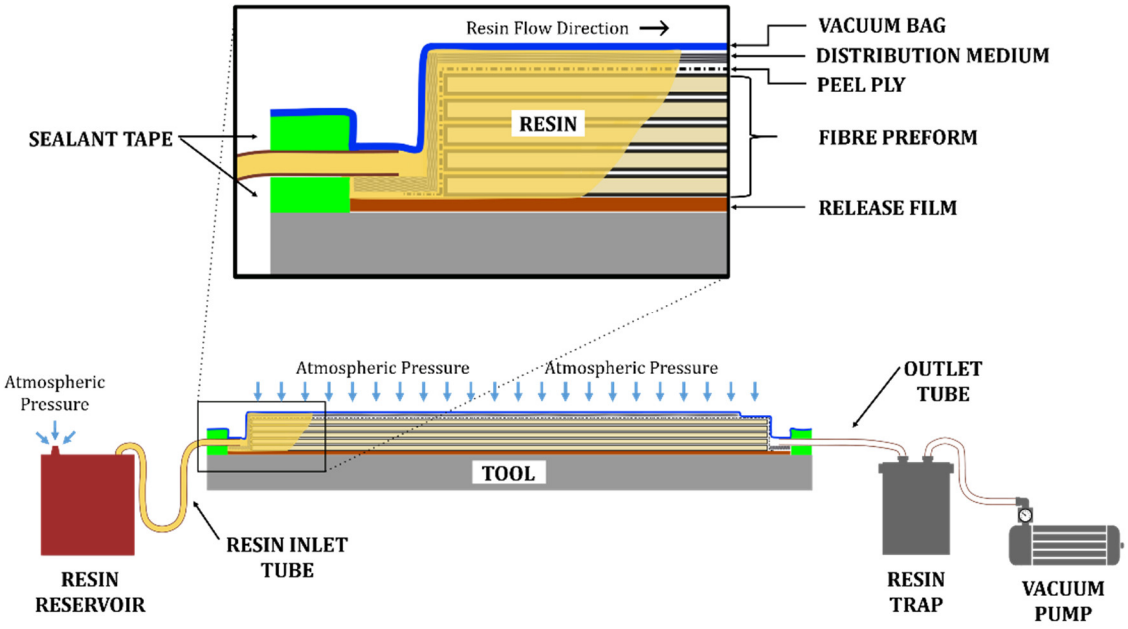


Figure 2-5. Conventional liquid resin infusion process set-up.

A two-stage technique for the fabrication of flax fibre-reinforced acrylic was reported by Baley et al. [28]. (i) The initial manual impregnation stage produced fully wetted-out preforms, which were subsequently (ii) hot-press moulded for enhanced void elimination and consolidation. While this resin grade (Elium® 150) does not require heating during the polymerisation process [14], the use of heat during and after the polymerisation step was reported by the authors as recommendations from the manufacturer. Heating was also reported by Boufaida et al. [27] for RTM fabrication of acrylic-based laminates; this was said to be needed for thermal activation of the polymerisation process due to the incompatibility of the fibre sizing employed with the intrinsic activation agent in the initiator. While the precise grade of acrylic resin used by Boufaida et al. [27] was not specified, the suitability of the RTM process for producing acrylic-matrix laminates has also been demonstrated by Bhudolia et al. [21] using Elium® 280 with carbon fibre reinforcements (with a thermoplastic-compatible sizing agent). Table 2-2 presents an overview of some of the typical fabrication processes for acrylic matrix composites and the laminate quality achieved by resin grade and fibre type.

Table 2-2. Summary of reported processing techniques of acrylic matrix composites and resulting fibre (V_f) and void (V_v) volume fractions, by resin grade and fibre type.

Reinforcement	*Elium®*	*Process*	V_f *(%)*	V_v (%)	*Reference*
Carbon	280	i. Liquid resin infusion ii. RTM	i. 48 – 60 ii. 57	i. 0.1 – 1 ii. N/S	i. [20,22,32,33] ii. [21]
Carbon	150	i. Hand layup & vacuum moulding† ii. Liquid resin infusion	i. N/S ii. N/S	i. N/S ii. N/S	i. [34] ii. [35]
Carbon	N/S	Liquid resin infusion	60	N/S	[36]
Glass	180, 188 O	Liquid resin infusion	47-49.5	0.4	[24,37]
Glass	150	Liquid resin infusion	N/S	N/S	[38]
Glass	N/S	Liquid resin infusion	i. 54.2 ii. 46.5 iii. 52.4	i. N/S ii. 7 iii. 1.3	i. [15] ii. [23] iii. [39]
Flax	RT 150	i. Hand layup & press moulding ii. Liquid resin infusion	i. 48 ii. 35 – 40	i. N/S ii. 2.5 – 7.5	i. [28] ii. [40]
Flax	N/S	Liquid resin infusion	37.1	5	[39]

†: thermally post-processed, **N/S:** Not specified

2.3 Mechanical Properties of acrylic-matrix composites

2.3.1 Glass fibre-reinforced acrylic-matrix composites

2.3.1.1 Tensile properties

Lorriot et al. [23] reported comparable longitudinal tensile strengths (~860 MPa) and moduli (40 GPa) in glass fibre-reinforced acrylic and epoxy laminates, reporting marginally higher (5 %) failure strain in the acrylic-based composite. Similar comparability was reported by Chilali et al. [39]. However, due to much lower fibre volume fraction (37 %), the reported tensile strength (380 MPa) and modulus (23 GPa) are considerably lower than those determined by other authors who achieved fibre volume fractions above 46 %. Cousins [41] identified a marked superiority in the tensile strength and modulus of an acrylic composite over its epoxy counterpart, reporting strengths of 916 MPa and 723 MPa, respectively. Even higher longitudinal tensile strength (1241 MPa) and modulus (52.7 GPa) were reported by Zoller et al. [42], possibly owing to higher fibre weight fractions (81 %) attained, the use of a different grade of acrylic resin (Elium® 595 E) or the effects of the pultrusion process on fibre alignment. Obande et al. [24] characterised the transverse tensile properties of acrylic- and epoxy-based glass FRPs and reported a superiority in strength for the acrylic system; strengths of 73 MPa and 54 MPa were reported, respectively. Equivalent transverse tensile moduli were reported for both materials at 13 GPa.

2.3.1.2 Compressive properties

The compressive performance of glass fibre-reinforced acrylics has not been extensively studied. Cousins [41] comparatively assessed glass fibre-reinforced acrylic and epoxy composites and reported equivalent strengths (~600 MPa) and moduli (~34 GPa) for both materials. Substantially higher average compressive strength (1044 MPa) and modulus (~52 GPa) values were reported for pultruded glass fibre-reinforced acrylic composite material based on Elium® C595 E [42]. While no details of fibre volume or mass fractions were provided for the materials reported by Cousins [41], the high fibre mass fraction of 81 % was reported by Zoller et al. [42] possibly explains the high compressive strength and modulus. Besides, the use of the pultrusion process may confer a high degree of fibre alignment, which is known to influence the longitudinal compressive performance of composites [43]. To the best of our knowledge, no other works focus on assessing the compressive performance of glass fibre-reinforced acrylic composites. The lack of published literature on this area highlights the need for more benchmarking studies on the compressive

properties of glass-reinforced acrylic composites alongside more traditional thermoset matrix-based composites.

2.3.1.3 Flexural properties

Cousins [41] measured higher flexural strengths in the acrylic-based composite (1006 MPa) than the epoxy-based reference material (809 MPa); the authors reported moduli of values of ~37.5 GPa and ~35 GPa, respectively. No fibre volume fractions were reported for these materials. As with the tensile and compressive properties in Sections 2.3.1.1 and 2.3.1.2, Zoller et al. [42] showed that it was possible to achieve high-flexural-performance glass fibre-reinforced acrylics based on Elium® C595 E by pultrusion. The average longitudinal flexural strength and modulus for this material were 1291 MPa and 44.7 GPa, respectively. Davies and Arhant [44] reported flexural strengths of 703 MPa and 606 MPa, and moduli of 40.1 GPa and 38.2 GPa for glass fibre-reinforced acrylic and epoxy composites with fibre volume fractions of 52 and 53 %, respectively. These trends were also observed by Obande et al. [24], who reported strengths of 879 MPa and 869 MPa, and moduli of 40 GPa and 38 GPa for glass fibre-reinforced acrylic and epoxy composites with fibre volume fractions of 49.5 %, respectively. In the same study, the authors observed the opposite trend for transverse flexural performance, reporting strengths of 91 MPa and 94 MPa, and moduli of 11 GPa and 12 GPa for the acrylic- and epoxy-based materials, respectively. Interestingly, despite possessing consistently higher longitudinal characteristics, composites produced from other grades of the acrylic resin and produced using other techniques, the material studied by Zoller et al. [42] exhibited lower transverse flexural strength (68.9 MPa) and modulus (11.5 GPa) than that reported by Obande et al. [24].

2.3.1.4 Shear properties

In-plane shear properties of a glass fibre-reinforced acrylic matrix and an epoxy-based counterpart were studied by Lorriot et al. [23]. The authors reported higher shear modulus (~31 %) in the epoxy-matrix composite and comparable shear strengths in both materials. Chilali et al. [39] reported comparable performance during in-plane shear strengths, with both acrylic- and epoxy-matrix composites yielding strengths of ~68 MPa and moduli or ~6 GPa. Cousins [41] found that an acrylic-based FRP possessed 8 % lower short beam shear strength than its epoxy-based counterpart, reporting strengths of ~50 MPa and 54 MPa, respectively. Obande et al. [24] also studied the short beam shear behaviour of glass fibre-reinforced acrylic and epoxy composites and reported comparable shear strengths in both

materials, with the acrylic-based composite being marginally higher at 58 MPa (+2 %) than its epoxy counterpart. Dissimilar damage evolution was described by the authors, who found that epoxy-matrix samples exhibited a more pronounced onset of failure beyond load peaks, dropping by up to 30 % from the peak load. In contrast, a smoother and more gradual drop in load was observed with acrylic samples. For unidirectional glass fibre-reinforced acrylics, Davies and Arhant [44] reported 21 % higher short beam shear strengths than a comparable epoxy-based composite. Despite the authors exploiting specialised acrylic-compatible sizing on their reinforcements, an average short beam shear strength of 46 GPa was reported for the acrylic-based samples. The grade of acrylic resin used in this work (Elium® 180) and that used by Obande et al. [24], Elium® 188 belong to the same class of Elium® resins [45] and as such, should exhibit similar performance for the same type of reinforcement. Moreover, short beam shear behaviour should ideally be enhanced in work by Davies and Arhant [44], particularly given the benefits that specialised sizing formulation potentially confer and the fact that marginally higher fibre volume fraction (52 %) was reported for this work. In contrast, Obande et al. [24] achieved a volume fraction of 49.5 %. These observations highlight the need for comparative benchmarking studies on sizing technology for these acrylic matrices.

2.3.1.5 Impact properties

Kinvi-Dossou et al. [46] conducted a study in which acrylic-matrix composites containing woven reinforcements were deemed more damage resistant than their polyester- and epoxy-based counterparts. As shown in Figure 2-6, the damaged envelope grows considerably for the polyester- and epoxy-matrix composites, with evidence of gross delamination being observable. Only minimal damage states are presented for the acrylic composite samples at these energy levels. The authors believe that the superior impact strength is attributed to improved interfacial adhesion between the glass fibres and the acrylic matrix, but provide no strong evidence to support this claim. In addition, the impact performance of the acrylic laminate was also reported to be enhanced by shear banding within the matrix, which contributes to the dissipation of bulk strain energy and gives way to shear localisation. A further remark by the authors suggests that this acrylic is considerably more ductile than the epoxy and polyester matrix, which are described as brittle. It is worth noting that acrylics have been shown to possess low failure strain and strain-dependent embrittlement [24,37,47] as brittle amorphous thermoplastic materials.

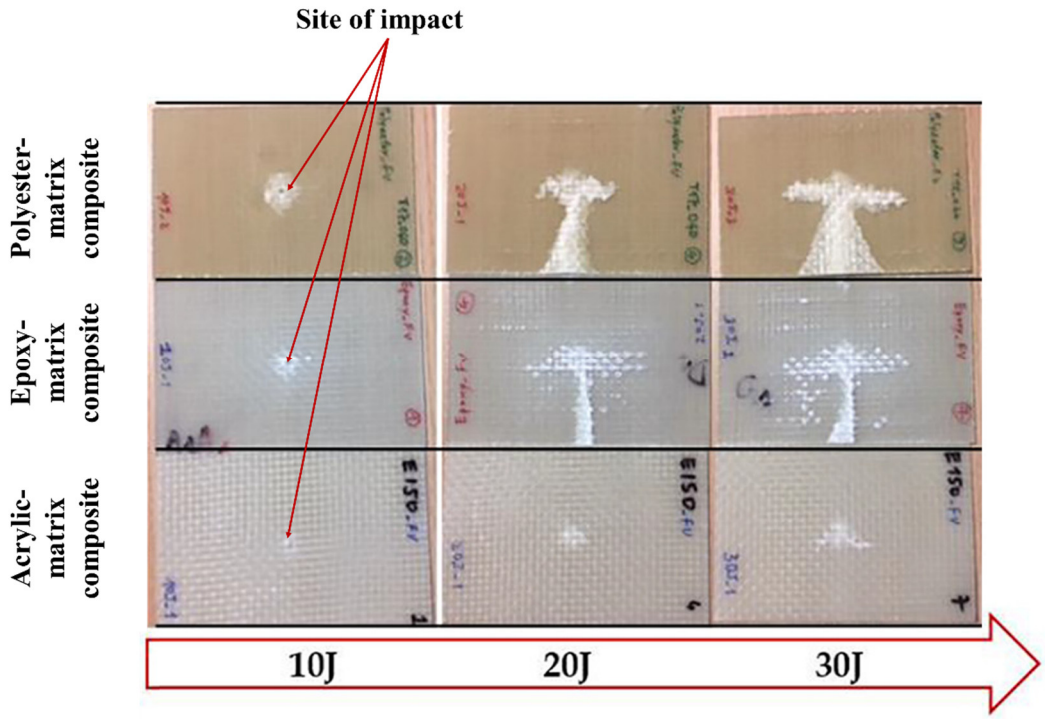


Figure 2-6. Impact-face damage states on glass fibre-reinforced polyester, epoxy and acrylic composites subjected to impact events of 10 J, 20 J and 30 J (Copyright permission from Elsevier. Adapted from Fig. 8 in [46]).

Cadieu et al. [38] assessed the effects of rate on the out-of-plane loading response of glass fibre-reinforced Elium® 150 using quasi-static indentation and drop-weight impact; it was concluded that higher loading rates result in lower penetration depth and higher stiffness, which result in higher elastic energy and conversely, lower dissipated energy. At low impact energies and low indentation, no rate effects were reported for the area of the damaged zone. At higher energy levels, however, a more substantial reduction is observed in the damaged area at the shorter timescale. Damage mechanisms were not reported to be affected by the loading rate; the authors observed delamination, matrix cracking and fibre-related failure at all loading rates.

2.3.2 Carbon fibre-reinforced acrylic-matrix composites

2.3.2.1 Tensile properties

The tensile properties of cross-ply acrylic and epoxy FRPs were studied by Bhudolia et al. [22]. While localised brittle fractures were observed in the epoxy-based material, fibre splitting and fracture, and delamination were reported as the predominant modes in the acrylic-based FRP. Ultimately, the epoxy material had superior strength (1216.9 MPa) and modulus (66.7 GPa) than its thermoplastic counterpart, which had values of 1004.3 MPa and

53.1 GPa, respectively. A major limitation of this study is that dissimilar reinforcement systems were used, making it challenging to draw definitive conclusions. Interestingly, Davies and Arhant [44] reported lower tensile strength (831 MPa) and higher modulus (71.9 GPa) for thick-ply carbon fibre-reinforced acrylic composite.

2.3.2.2 Flexural properties

The flexural properties of an acrylic-based material were comparatively evaluated alongside a baseline epoxy system. In this work, Bhudolia et al. [22] reported 33.3 % and 9.5 % higher strength and modulus values, respectively in the epoxy FRP, which failed on both the tensile and compressive sides. However, only compressive failure was observed in the acrylic composite, which had average strength and modulus values of 671.1 MPa and 52.1 GPa, respectively. These findings were, however, affected by the ply configuration in each laminate. Conventional thick-ply non-crimp fabric (NCF) was used in the fabrication of the acrylic laminate, whereas, its epoxy-based counterpart contained thin-ply NCF reinforcement.

For thick-ply laminates with similar stacking sequences, Davies and Arhant [44] reported lower mean flexural strength (589.5 MPa) and higher modulus (102.7 GPa). Bhudolia et al. [48] also presented findings on the flexural behaviour of thin-ply carbon fibre-reinforced acrylic and epoxy composites. Using quasi-isotropic laminates with fibre volume fractions of 58.3 % and 60 %, respectively, the authors reported flexural strengths of 813.2 MPa and 835.3 MPa for the acrylic- and epoxy-based materials, respectively. Their moduli were found to be comparable at ~51 GPa. Differences in failure behaviour were highlighted; Figure 2-7 shows the failure characteristics reported by the authors. A greater extent of visible matrix deformation on the side in compression was reported for the acrylic-based composite; delamination was observed in its epoxy counterpart.

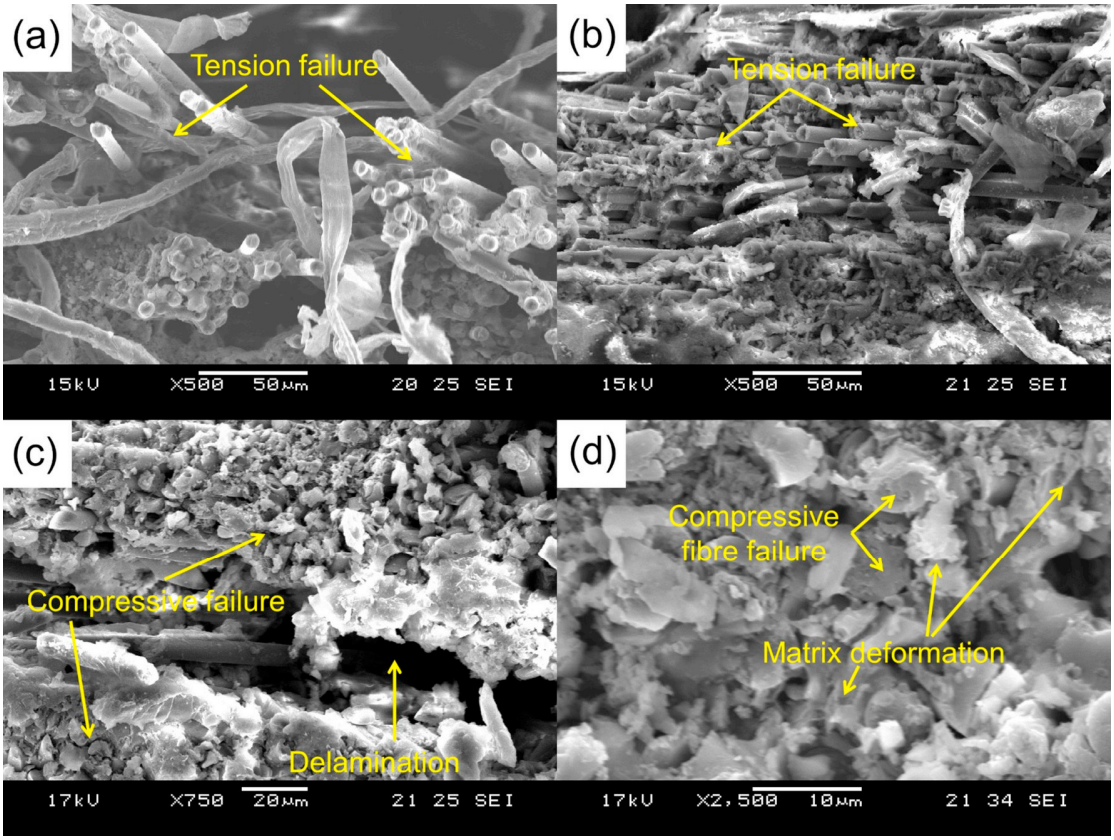


Figure 2-7. Scanning electron micrographs showing flexural failure modes of thin-ply carbon fibre-reinforced (a) & (c) epoxy and (b) & (d) acrylic composites (Copyright permission from Elsevier [48]).

This work also represents the first implementation of annealing for this family of acrylic resins. Although similar to the post-processing cycles recommended by the manufacturers for some grades of Elium® resin, it was performed in a hot press (80°C for 2 h) as opposed to a free-standing heating cycle. This annealing process was said to facilitate targeted microstructural reorganisation, a more complete polymerisation reaction, enhanced matrix ductility and interfacial adhesion as shown in Figure 2-8. The grade of Elium® under consideration in this work was not disclosed, which indirectly limits the transferability of the findings presented by the authors. It is unclear if the insufficient polymerisation reported in this work was associated with sizing effects as previously suggested by Boufaida et al. [27].

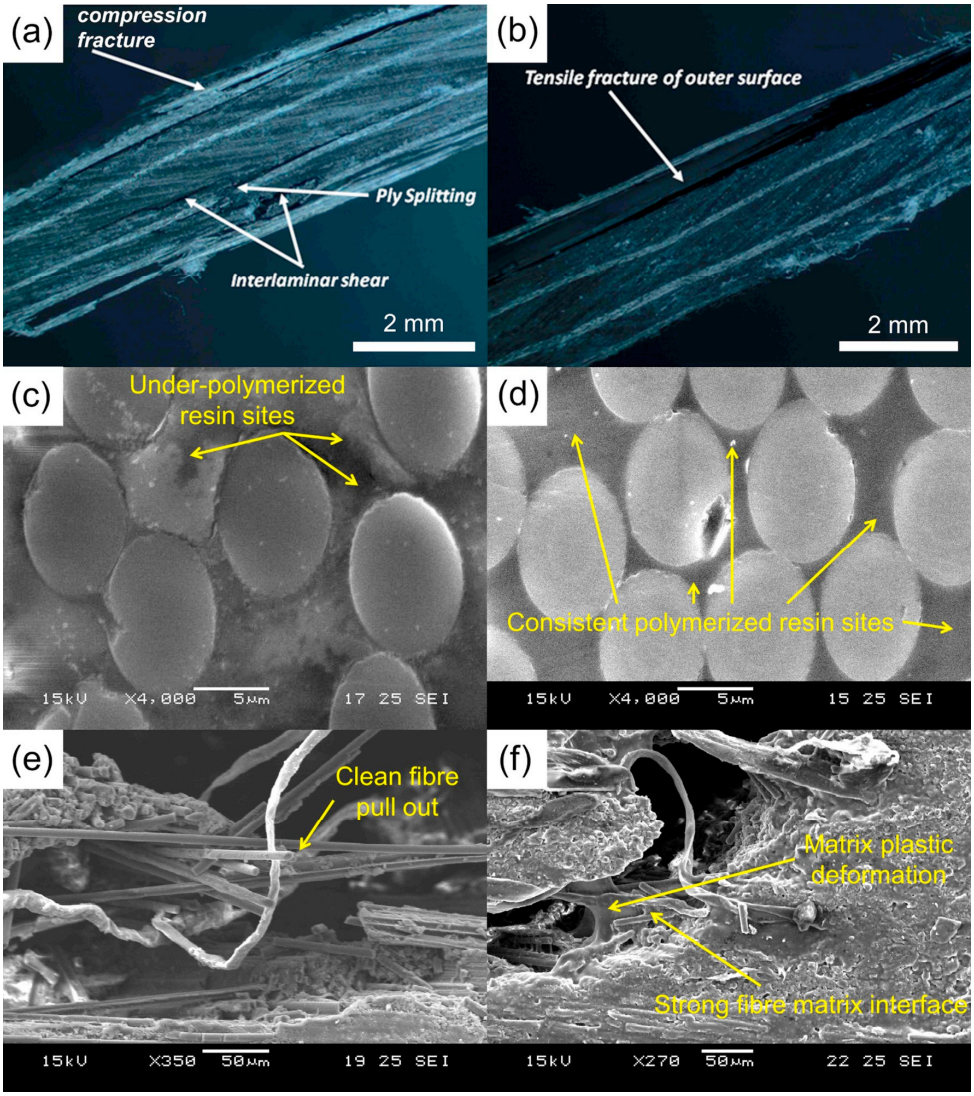


Figure 2-8. Flexural failure modes of thin-ply carbon fibre-reinforced acrylic composites: (a), (c) & (e) without annealing; and (b), (d) & (f) with annealing (Copyright permission from Elsevier [48]).

2.3.2.3 Impact properties

Carbon fibre-reinforced acrylic composites have been shown to possess superior structural integrity during impact compared to equivalent epoxy-based composites. The acrylic-matrix composite was reported to be capable of undergoing more elastic deflection before the maximum impact load was reached [21]. The authors also reported strain sensitivity in this material, with increasing energy levels giving rise to greater elastic-plastic deformations relative to the epoxy-matrix composite. This had direct consequences on the resulting damage states of both materials (Figure 2-9 and Figure 2-10); a larger extent of delamination and catastrophic failure characteristics were observed in the carbon fibre-reinforced epoxy samples for 42-J and 52-J impacts.

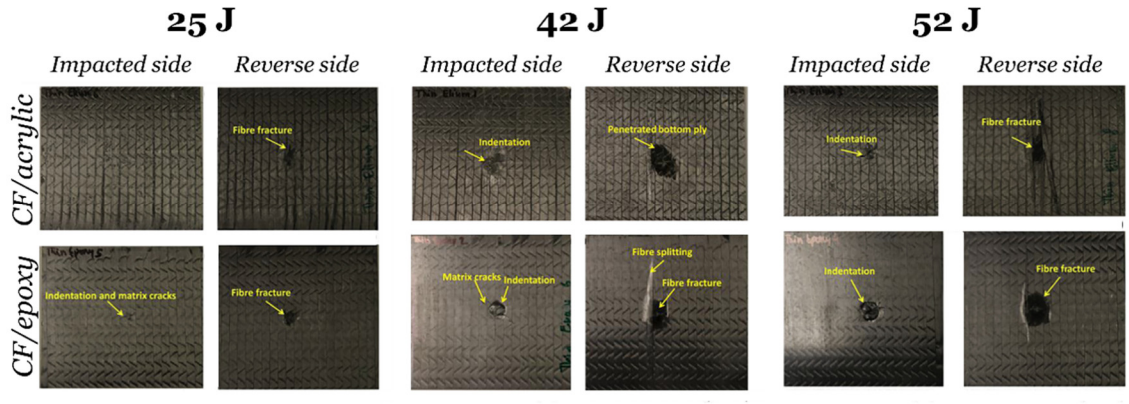


Figure 2-9. Impact side and reverse side damage following impact events at 25, 42 and 52 J (Copyright permission from Elsevier. Reproduced from Figs. 12, 14 & 16 in [21]).

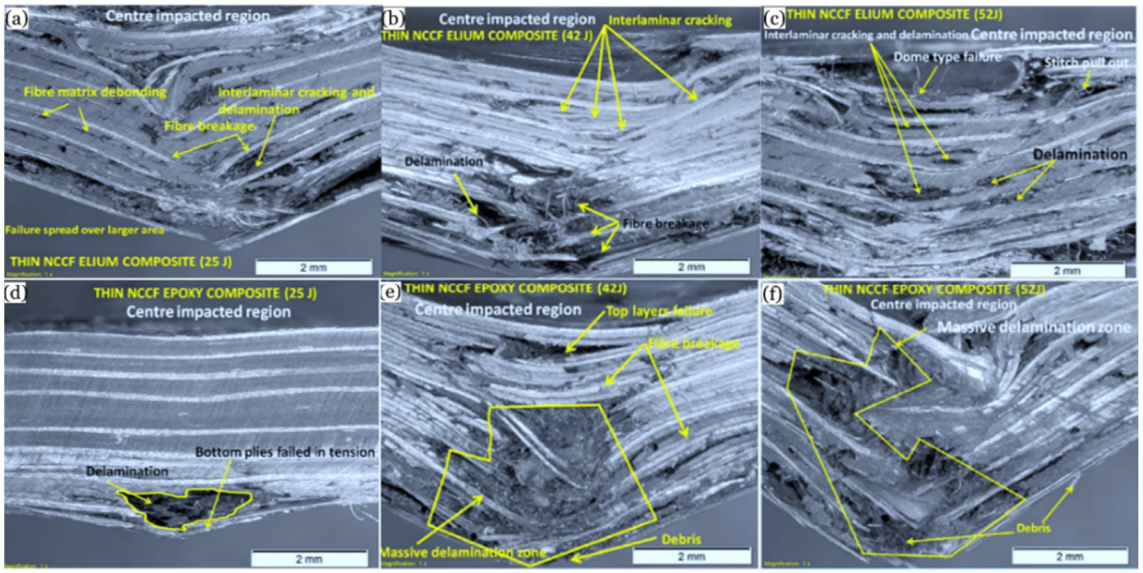


Figure 2-10. Micrographs showing damage sustained by carbon fibre-reinforced (a), (b) & (c) acrylic and (d), (e) & (f) epoxy composites following drop-weight impacts at 25, 42 and 52 J, respectively (Copyright permission from Elsevier. Reproduced from Figs. 13, 14 & 15 [21]).

Interestingly, impacts at a lower energy level (25 J) appeared to produce more severe and extensive damage states in the acrylic-based material such as fibre fractures and interlaminar cracking (Figure 2-10a); delamination and tensile failure of backface plies can be seen for the epoxy-matrix composite (Figure 2-10d). The authors also suggested that plastic zone development at the tips of interlaminar cracks contributed positively towards enhancing the ductility of the acrylic-matrix composite. It was also proposed that shear crack propagation was favoured by superior interfacial strength in the carbon fibre-reinforced acrylic material. In a similar study, the use of thin-ply carbon fibre reinforcement has also been shown by

Bhudolia et al. [49] to produce more impact damage-resistant acrylic-matrix composites than the use of standard thick-ply reinforcement. Thin-ply carbon fibre-reinforced acrylic composites were reported to exhibit more favourable elastic-plastic deformation, leading to smaller delamination zones than in the thick-ply variant.

2.3.2.4 Mode-I interlaminar fracture toughness

Bhudolia et al. [32] compared the mode-I interlaminar fracture toughness (G_{IC}) and fracture behaviour of quasi-isotropic thin-ply carbon-reinforced acrylic and epoxy laminates. The acrylic FRP possessed superior mode-I fracture toughness due to crack arresting mechanisms such as crack deflection behind the crack tip, crack branching and multi-plane propagation of cracks. Upon further microstructural inspection of the fracture surfaces, evidence of fibre bridging, strong interfacial strength, ductile drawing and crazing, fibre splitting and pull-out were also reported. The surface of the epoxy-based FRP exhibited clean fibre failure and pull-out, brittle propagation of matrix cracks and scarp formation.

Interestingly, textured micro-flow was also reported, indicating some degree of micro-scale ductility. As shown in Figure 2-11(a), a linear response was observed in the pre-peak regions of all samples. Evidence of early failure was observed in the acrylic samples before peak load (Point 1); however, major failure only initiated beyond the load peak. Higher peak loads were reported for the acrylic-based samples than their epoxy counterpart, indicating superior resistance to crack initiation.

Furthermore, higher load peaks were observed in the acrylic-matrix composites than their epoxy-based counterpart. The displacements between the first (1, 1' & 1") and second (2, 2' & 2") load drops were categorically different for each material; as can be seen in Figure 2-11(a), this displacement is highest in the thin-ply CF/acrylic material and lowest in its thin-ply epoxy-based counterpart. The authors suggest that this is indicative of superior bond strength and adhesion in the CF/acrylic materials. Resin-rich volumes and microvoids within the thick-ply variant of acrylic composite (relative to the thin-ply variant) were cited as sources of variation between thick- and thin-ply configurations.

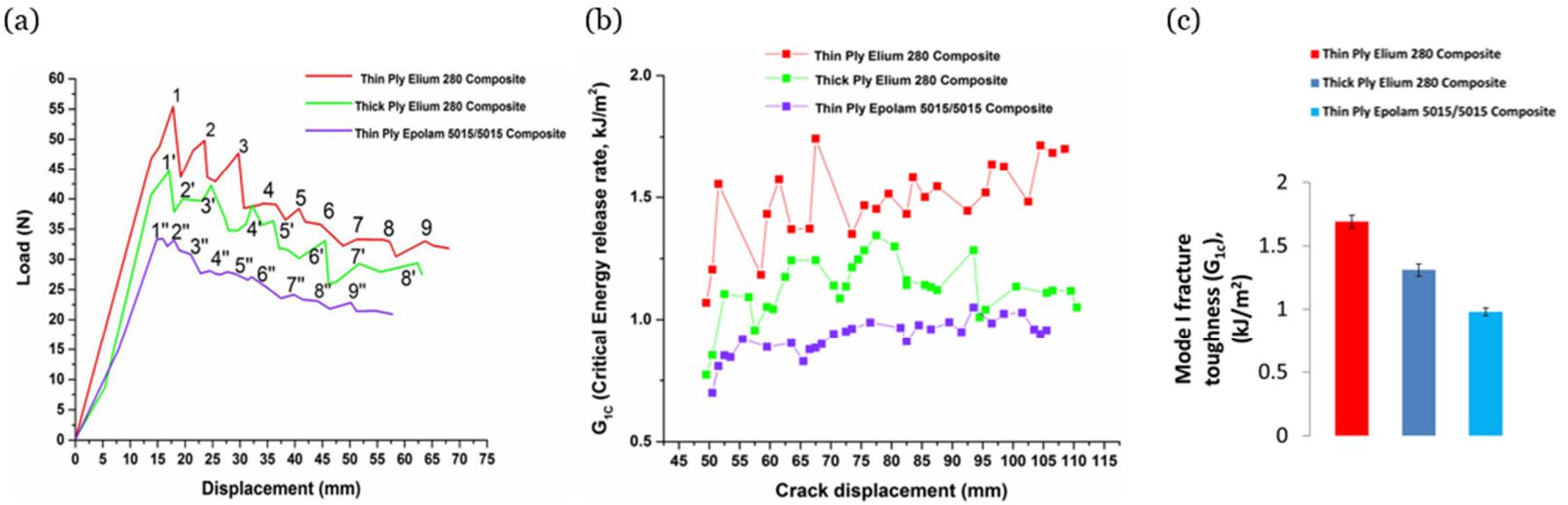


Figure 2-11. (a) Representative load-displacement curves showing mode-I crack propagation behaviour, (b) representative R-curves, and (c) mode-I fracture toughness values of carbon fibre-reinforced acrylic and epoxy composites (Copyright permission from Elsevier. Reproduced from Figs. 3-5 in [32]).

The authors also reported higher initiation and fracture toughness energy values in both thin- and thick-ply acrylic-based samples (Figure 2-11(b)), which also had a higher G_{IC} value than the epoxy-based material (Figure 2-11(c)). Ply thickness is believed to influence the vulnerability of a laminate to delamination and thus, should significantly affect fracture toughness behaviour [50]. Bhudolia et al. [32] found that a reduction in ply thickness increased interlaminar fracture resistance. It is worth noting, however, that the thick-ply acrylic-based composite possessed intermediate fracture toughness and crack growth resistance in comparison to the thin-ply epoxy-based composite material. Overall, it can be seen that matrix type had a more significant effect on G_{IC} than ply thickness. Bhudolia et al. [22] also drew similar conclusions from the characterisation of two cross-ply carbon laminates (acrylic- and epoxy-based). It was found that the thick-ply acrylic-based material possessed double the fracture toughness of the epoxy-based reference. Thermoset- and thermoplastic-compatible sizing systems were employed for the thin- and thick-ply reinforcements, respectively.

Additionally, while more severe fibre bridging was reported in the thin-ply epoxy material, the authors found that fibre pull-out and rupture were the dominant mechanisms within the thick-ply acrylic composite. Although the authors contribute vital information on material characteristics and failure behaviour, an obvious incomparability of the two materials under investigation exists due to each system comprising a different matrix, ply thickness and sizing system. Thus, the findings of the study cannot be considered conclusive due to the interplay of the matrix, sizing and ply thickness effects, which coexist within the materials under investigation.

Despite offering benefits in delaying matrix crack and delamination, the use of thin-ply reinforcements in composites has been thought to give rise to brittle failure behaviour and compromised damage tolerance [51,52]. In light of the conclusions drawn by Bhudolia et al. [32], it becomes evident that both thick-ply and thin-ply acrylic-matrix composites exhibit desirable resistance to crack initiation and propagation.

2.3.2.5 Mode-II interlaminar fracture toughness

Evaluating the mode-II fracture toughness of acrylic- and epoxy- based laminates reinforced with plain-woven carbon fabric, Barbosa et al. [35] found that woven carbon fibre-reinforced acrylic exhibited superior Mode-II propagation toughness (+40 %) than its epoxy-matrix

counterpart, which had a mode-II fracture toughness of 201 J/m^2. The load-displacement responses for both materials are presented in Figure 2-12 (a) and Figure 2-12 (b). The authors state that the higher peak load in the epoxy-matrix composite is indicative of superiority in *suppressing* the occurrence of delamination; i.e., a higher energy requirement for initiation. It was also suggested that the magnitude of the load drop corresponds to the material's ability to arrest delamination.

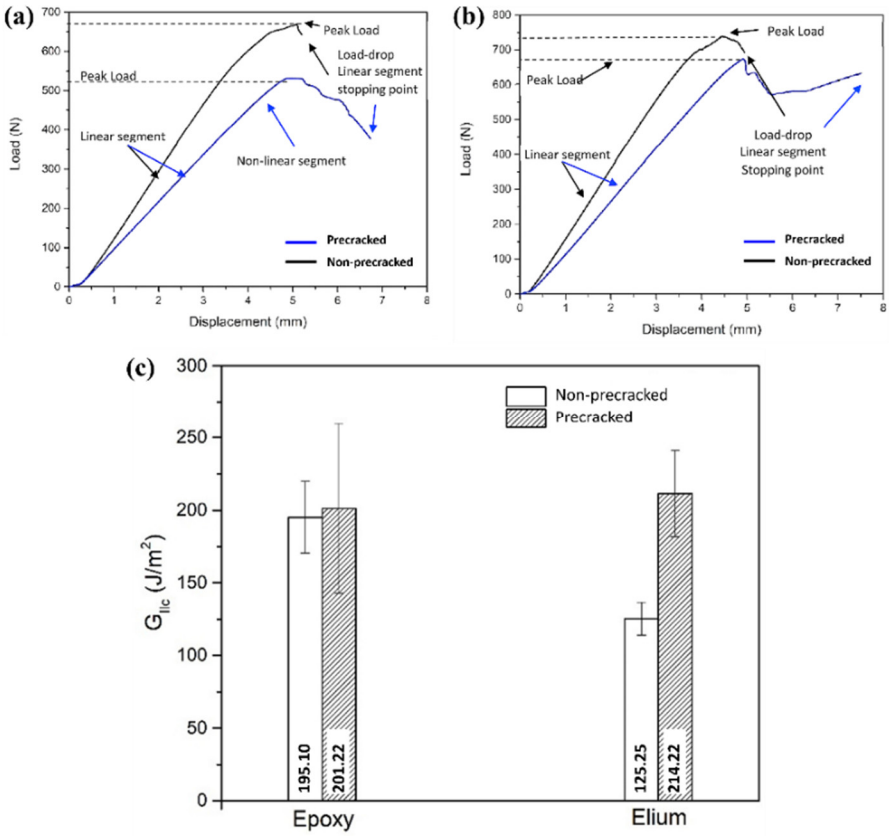


Figure 2-12. Load-displacement curves for carbon fibre-reinforced (a) Elium® 150, (b) epoxy; and (c) mode-II interlaminar fracture toughness determined from same (Copyright permission from Elsevier. Reproduced from Figs. 6-8 in [35]).

As shown in Figure 2-12 (c), the acrylic-matrix composite exhibited sensitivity to the test configuration (i.e., precracked vs non-precracked). The authors reported a variation of 41 % in the G_{IIC} values between precracked and non-precracked acrylic-based samples, compared to only a 3 % variation in epoxy-based samples. This corresponded to a 36 % lower average non-precracked G_{IIC} value and a 6 % higher average precracked G_{IIC} than its epoxy-based counterpart. Differences in interfacial adhesion are suggested as potential sources of these variations in the acrylic-matrix composite; however, no attempts are made to support this

claim. The authors believe that in addition to crack propagation, some of the energy absorbed is linked with plastic deformation within matrix-rich zones. This plastic deformation is thought to alter the fracture surface considerably and may mask important fractographic characteristics.

SEM fractographic inspection (Figure 2-13) revealed characteristic mode-II fracture behaviour on the surfaces of both materials, namely, shear cusps. Cusps are shear-induced fracture features that develop at the interface due to interlaminar shear stresses, which may cause matrix cleavage. They develop in the matrix-rich regions between fibres, following the direction of failure propagation.

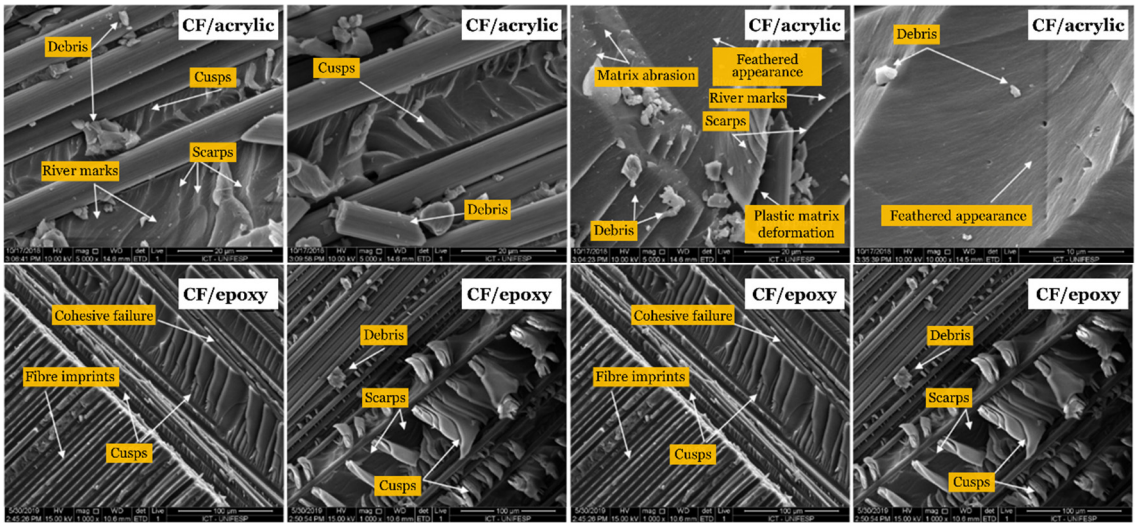


Figure 2-13. SEM micrographs of mode-II fracture surfaces of CF/acrylic and CF/epoxy (Copyright permission from Elsevier. Reproduced from Figs. 11 & 12 in [35]).

The authors consider the scale and distribution of cusps observed as the distinguishing attributes of both materials. Moreover, distinctive features observed solely on the surface of the CF/acrylic material were river marks, plastic matrix deformation, matrix abrasion, and localised feathered appearance of the matrix surface. The authors gave valuable insights into these features, suggesting that matrix abrasions were indicative of high loading rates and relative motion of fibre and matrix surfaces. In contrast, plastic deformation of the matrix was attributed to the viscoelastic behaviour of the acrylic matrix causing extension of fracture planes. Interestingly, cohesive failure and fibre imprints were unique to the CF/epoxy material. However, it is worth noting that the mismatched magnifications of the micrographs presented by the authors limit the extent of comparability of the observed fractographic features in terms of size and distribution of shear cusps.

It was also suggested that the superior crack resistance exhibited by this thermoplastic-matrix composite stems from two mechanisms – plastic matrix deformation and interfacial debonding; which the authors remarked are beneficial in composites subjected to mode-II loading.

Micrographs of the fibre surfaces shown in Figure 2-14 reveal comparable fibre coverage following fracture, indicating that the use of multi-compatible sizing technology may not adversely affect the performance of the acrylic-based system. The authors did, however, suggest that even further enhancements may be realised in the crack resistance of the acrylic-based composites by using specially sized fabrics compatible with acrylic resin systems.

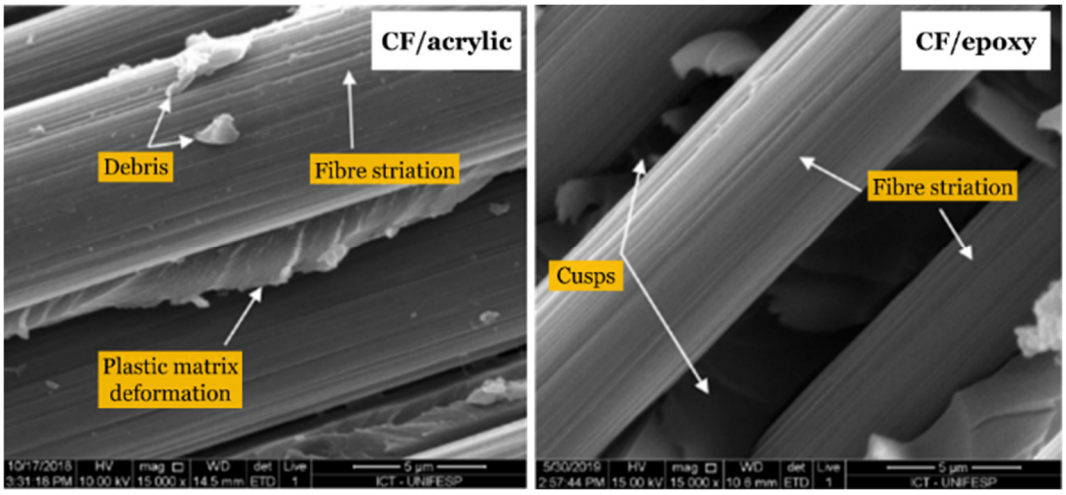


Figure 2-14. SEM micrographs of exposed fibre surfaces following mode-II fracture toughness testing on CF/acrylic and CF/epoxy composites (Copyright permission from Elsevier. Reproduced from Figs. 11 & 12 in [35]).

2.3.3 Flax fibre-reinforced acrylic-matrix composites

2.3.3.1 Tensile properties

Baley et al. [28] conducted a parametric study to assess the longitudinal tensile behaviour of flax fibre-reinforced acrylic composites alongside polyamide-, polypropylene-, and epoxy-based counterparts. For this review, the measurements reported by the authors have been normalised to equivalent fibre volume fractions of 50 %. Although matrix type yielded marginal effects on the tensile moduli across all samples, the most significant influence was observed in strengths. The acrylic-matrix composite was found to be superior in tensile strength to the flax fibre-reinforced polypropylene (23 %) and maleic anhydride-grafted polypropylene (7 %). However, its tensile strength was 58 % lower than the epoxy-based laminate and comparable to the polyamide-based material. Chilali et al. [39] also studied the

static tensile behaviour of woven flax fibre-reinforced epoxy and acrylic laminates alongside their unreinforced forms. The authors observed ductile and quasi-linear behaviour in the unreinforced acrylic and epoxy matrices, with failure strains of 2.3 % and 1.1 %, respectively. For reinforced composites, three distinct stress-strain characteristic regions were identified. (i) Both the acrylic- and epoxy-based materials were reported to exhibit an initial linear elastic region; (ii) a region of slight non-linearity followed, with a loss of stiffness being reported; and (iii) lastly, stress increased linearly up to ultimate failure, with both materials failing abruptly thereafter. This variation was been reported by Haggui et al. [53,54], who describe the same trend in stress-strain response for unidirectional flax fibre-reinforced acrylics. All authors attribute the second stage (non-linear) with the creation and evolution of damage. However, the authors present different explanations for the third and final stage. Haggui et al. [53,54] suggest that this quasi-linear behaviour is associated with multiplication or intensification of damage, leading up to ultimate failure, whereas, Chilali et al. [39] proposed contributions from microfibrillar reorientation associated with flax fibres. As shown in Table 2-3, tensile properties reported by Chilali et al. [39] appear to be significantly lower than those reported by other authors. However, this may be due to the differences in reinforcement architecture used.

Table 2-3. Summary of tensile properties reported for flax fibre-reinforced acrylic composites.

	Type	V_f	V_f*	*σ (MPa)*	*σ** (MPa)*	*E (GPa)*	*E** (GPa)*
Baley et al. [28]	UD	48	50	243.8	**254.0**	27.6	**28.8**
Chilali et al. [39]	UD	37.1	50	130	**175.2**	13.53	**18.2**
Haggui et al. [53,54]	UD	38	50	210	**276.3**	23	**30.3**
Monti et al. [40]	2/2 Twill	~37.5	50	225	**300**	23.3	**31.1**

Data normalisation has been performed to a target V_f (marked *) of 50 % for this review.
Reported data and normalised data (marked **) have been presented.
UD: Unidirectional.

Interestingly, this work highlights that the incorporation of fibres positively contributed (~+20 %) to the failure strain of the epoxy. However, in the acrylic material, a reduction in failure strain (~-22 %) was reported.

2.3.3.2 Compressive properties

Baley et al. [28] presented findings of a study on the comparative compressive performance of unidirectional flax fibre-reinforced acrylic and epoxy composites. The authors reported 7%, 27% and 5% lower compressive strength in the acrylic-based material than its epoxy

(115 MPa), polyamide (134 MPa), and polypropylene/maleic anhydride-grafted polypropylene (110 MPa) counterparts, respectively. However, it had 28% higher compressive strength than flax fibre-reinforced polypropylene (75 MPa). In terms of tensile strength, it was superior to the flax fibre-reinforced polypropylene (193 MPa; +23%) and maleic anhydride-grafted polypropylene (234 MPa; +7%). However, its tensile strength was 58% lower than the epoxy-based laminate (408 MPa) and comparable to the polyamide-based material (258 MPa). These results clearly show a more considerable influence of the matrix used on compressive strength than on tensile strength, a property known to be fibre-dominated. The authors attribute the poor compressive performance of the acrylic to weak interfacial strength between the flax fibres and acrylic matrix. These results clearly show a considerable influence of the matrix used on compressive strength, which itself is known to be matrix-dominated.

2.3.3.3 Flexural properties

Haggui et al. [53] evaluated the flexural behaviour of bidirectional flax fibre-reinforced acrylic laminates using three-point bend tests. A three-stage stress-strain behaviour was described, with an initial linear region preceding a nonlinear and terminal quasi-linear one. The authors also reported transverse microcracking as the incipient damage mechanism, occurring during the nonlinear phase of testing. Haggui et al. [53]. studied the cyclic flexural performance of flax fibre-reinforced acrylics and identified a two-stage degradation of stiffness. The authors concluded that a critical number of cycles (c. 104) exists, below which the rate of degradation is relatively slow. This was believed to be related to damage initiation and microcracking phenomena, which precede the rapid accumulation of transverse cracking and subsequent delamination growth up to 9 × 105 cycles.

2.3.3.4 Shear properties

Chilali et al. [39] assessed the shear performance of flax fibre-reinforced acrylic and epoxy laminates by in-plane shear testing and reported a superiority (~10 %) in shear modulus for the epoxy-based material. Both flax fibre-reinforced acrylic and epoxy materials were reported to exhibit equivalent ultimate shear strengths at approximately 23 GPa; however, normalising the reported data as described in Section 2.3.3.1 revealed an even greater difference in the measured values. The epoxy-based laminate possessed higher (+16 %) shear strength than the acrylic material.

2.4 Dynamic mechanical (thermomechanical) properties

Several works have studied the thermomechanical behaviour of thermoplastic acrylic matrices and their glass fibre-reinforced composites. Acrylic-based composites have been reported to exhibit comparable (and in some cases, superior) performance to their thermosetting counterparts, such as epoxy-matrix composites with *Tg* values in the range of 67°C - 127°C being reported [8,24,33,36,37,42,55,56]. Table 2-4 presents a summary of some of the key reported thermomechanical properties of acrylic matrix composites in published literature.

Table 2-4. Summary of some thermomechanical properties reported in published works for acrylic-based matrices and composites.

Materials	*Methods*	*Results*	*References*
Matrix: Elium® 180, 188 Reinforcement: UD Glass NCF Sizing: Multi-compatible	Manufacturing: Liquid resin infusion Characterisation: Dynamic mechanical analysis	i. T_g: 115 °C *Tan delta* peak: 0.53	[37]
		ii. T_g: 106 °C *Tan delta* peak: 0.76	[24]
Matrix: Elium® --- Reinforcement: - Sizing: -	Manufacturing: - Characterisation: Dynamic mechanical analysis	i. *Tg*: 125 °C *Tan delta* peak: -	[36]
		ii. *Tg*: 127°C *Tan delta* peak: -	[56]
Matrix: Elium® 150† Reinforcement: - Sizing: - †Various initiator contents: 0.8-1.6 wt. %	Manufacturing: Silicone mould casting Characterisation: Dynamic mechanical analysis	T_g: 116° C, 123° C, 123 °C *Tan delta* peak: ~0.5, ~0.45, ~0.65 *0.8 wt. %, 1.2 wt. % and 1.6 wt. %, respectively*	[8]
Matrix: Elium® C595 E Reinforcement: - Sizing: -	Manufacturing: - Characterisation: Dynamic mechanical analysis	T_g: 109 °C *Tan delta* peak: -	
Matrix: Elium® C595 E Reinforcement: UD Glass Sizing: contains a vinyl group	Manufacturing: Pultrusion Characterisation: Dynamic mechanical analysis	*As produced* T_g: 119 °C *Tan delta* peak: -	[42]
		Processed at 190°C; 10 min T_g: 122 °C *Tan delta* peak: -	
Matrix: Elium® 150 Reinforcement: - Sizing: -	Manufacturing: - Characterisation: Dynamic mechanical analysis	T_g: 110 - 120°C *Tan delta* peak: 1.3 (matrix only)	
Reinforcement: Carbon fabric* (thin- and thick-ply) Sizing: - *quasi-isotropic lay-up	Manufacturing: Liquid resin infusion Characterisation: Dynamic mechanical analysis	*Tan delta* peak: 0.59 (thin-ply) *Tan delta* peak: 0.51 (thick-ply	[33]

2.5 Effects of fibre sizing on the properties of acrylic-matrix composites

Given the infancy of this class of resins, its chemistry is not as well-known as traditional thermosets, which are associated with well-established supply chains and dedicated sizing technologies. Until recently, much of the published literature on acrylic-matrix composites comprised fibre reinforcements with multi-compatible sizing. With advancing research, there are now specially sized reinforcement systems available for acrylic matrix composites. However, being based on novel technology, these systems require comprehensive characterisation. Several authors have investigated the effects of such acrylic-sized reinforcements against their multi-compatible counterparts. The following section summarises the findings to date.

Boufaida et al. [27] studied the influence of sizing on the properties of glass fibre-reinforced acrylic composites using fibres sized with multi-compatible (MC) and acrylic-compatible (AC) formulations. Fibre-matrix interfacial strength was assessed in the materials using monotonic and fatigue in-plane shear testing. Although no notable influences were reported on modulus and strength, the authors reported a lower threshold for the development of progressive damage in MC-sized samples in response to monotonic loading. An enhancement of only 4 % in strength was reported for the use of AC sizing. On the influence of sizing on fatigue damage development, both MC- and AC-sized acrylic composites were characterised with respect to a reference laminate with no sizing (NS). It was found that the use of MC-sized fabrics results in enhanced fatigue performance (~7 % compared to the NS reference). However, a more significant difference was reported for the AC-sized material, corresponding to a 22 % improvement with respect to the NS reference. Although this study evaluated macromechanical performance, their findings were in agreement with those of Beguinel et al. [57], who studied the effects of fibre sizing on the interfacial shear strength (IFSS) of glass fibres with acrylic-compatible and polypropylene-compatible sizings, and carbon fibres with acrylic-compatible- and epoxy-sizings. Microbond test samples were prepared using a reactive acrylic matrix on single tensioned fibres. Improved IFSS values were reported for glass- and carbon-reinforced acrylic samples comprising fibres with acrylic-compatible sizing (compared to those employing multi-compatible sizing formulations). Moreover,

Davies et al. [58] suggest that the use of appropriate sizings may affect the durability of glass fibre-reinforced acrylic composites.

Shanmugam et al. [59] demonstrated fibre surface functionalisation of ultra-high molecular weight polyethylene (UHMWPE) as a viable means of improving mode-I interlaminar fracture toughness. The authors studied the effect of treating fibres with two polydopamine (PDA)-based coatings for composite applications. As evident in Figure 2-15, the effects of these treatments on fracture behaviour were significant.

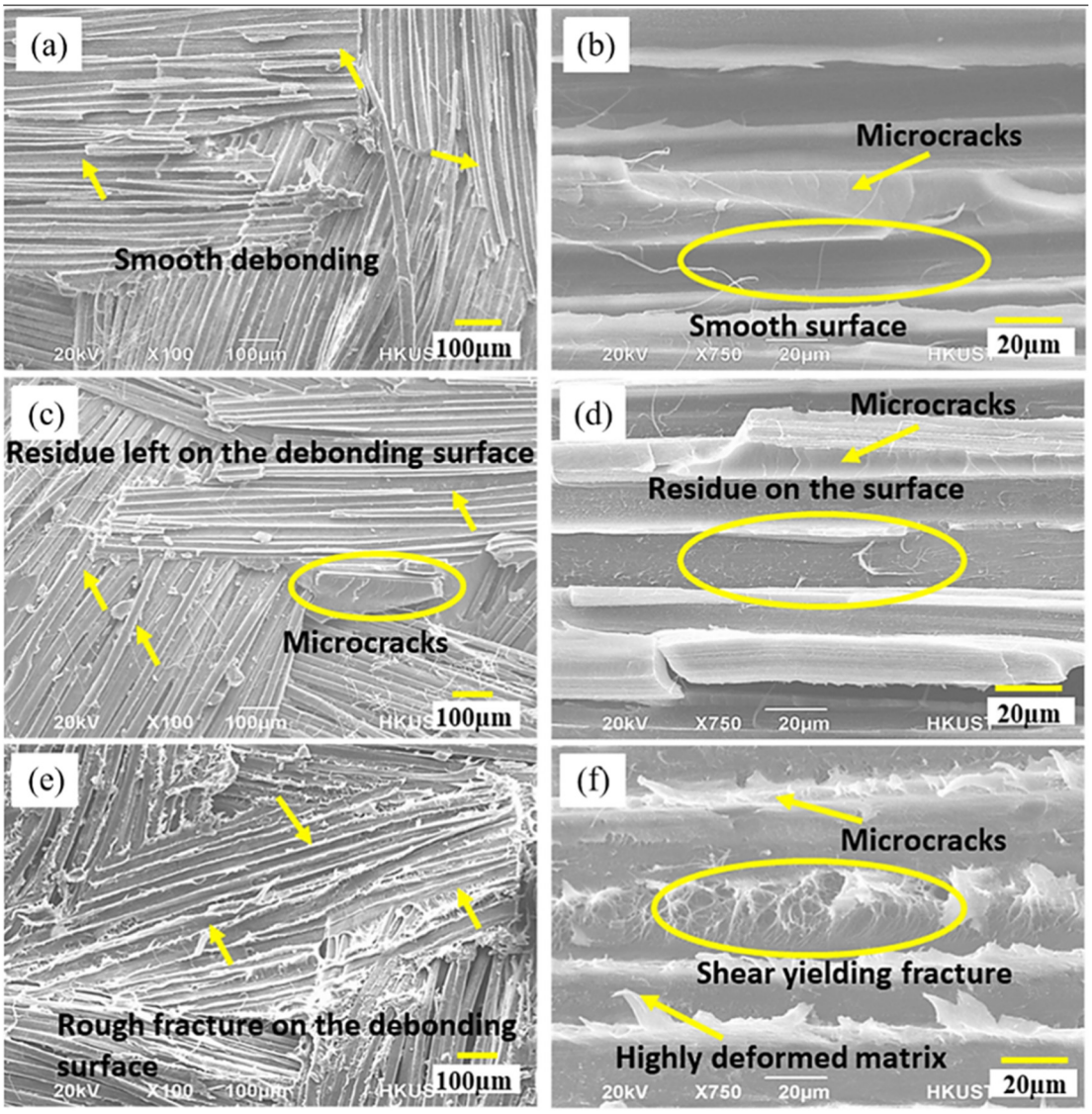


Figure 2-15. Low- and high-magnification SEM micrographs of double cantilever fracture surfaces of UHMWPE-acrylic samples containing (a & b) untreated fibres, (c & d) PDA-treated fibres, and (e & f) PDA+MWCNT-treated fibres (Copyright permission from Elsevier. Adapted from Fig. 7 in [59]).

Comparing the fracture behaviour of the FRP (Figure 2-15a and Figure 2-15b) with untreated fibre to that containing PDA-treated fibres (Figure 2-15c and Figure 2-15d), the authors reported smooth fibre surfaces with the use of untreated fibres and the presence of residue on treated fibre. Thus, it was evident that fibre functionalisation with PDA alone resulted in enhanced interfacial adhesion with the Elium® 188 matrix used, corresponding to a 19.6 % improvement in average fracture toughness. Furthermore, the enhancements achieved with the sample shown in Figure 2-15e and Figure 2-15f were realised with the incorporation of 0.03 wt. % of multi-walled carbon nanotubes (MWCNT) into the PDA coating. For this sample, an improvement of 42.5 % in fracture toughness was reported relative to the untreated reference.

These works highlight the requirement of specialised sizing technologies for these acrylic resins; however, several authors [15,24,25,37,60] have shown that the use of MC-sized reinforcement does not result in any adverse effects on the quality and performance of the composites. Interestingly, these authors report the use of Elium® 180 or 188 resins with MC-sized glass fibre reinforcement. These studies may highlight the suitability of the Elium® 18* family of resins for use with existing glass fibre sizing technologies. Besides, in a study by Charlier et al. [60], the IFSS of an unspecified Elium® resin with MC-sized and AC-sized glass fibres were micromechanically assessed by fragmentation and microdroplet testing. No significant improvements in IFSS were reported with the use of specialised sizings for acrylic matrices on glass fibres. These findings constitute important knowledge, given that the use of appropriate glass fibre sizing technology is a prerequisite for effective interfacial stress transfer, desirable fibre strength and the ultimate resistance to aggressive physical, chemical and environmental degradation agents [61].

2.6 Toughening of acrylic-matrix composites

Matrix toughness is known to contribute significantly to the performance of a laminate, particularly its interlaminar fracture behaviour [56], which affects damage tolerance [36]. Thermoplastic matrices are naturally superior in toughness than their thermosetting counterparts, and as such, typically exhibit higher mode-I interlaminar fracture toughness and other matrix-dominated characteristics. However, in these works [21,22,32], acrylic-based composites were only marginally higher in mode-I interlaminar fracture toughness than their epoxy-based counterparts – highlighting a requirement for the development of appropriate toughening strategies. To date, the intrinsic toughness of traditional high-

performance thermoplastic matrix obviates the requirement for toughening; as such, the effects of a strategically developed approach for acrylic-based composites need to be understood.

The influence of toughening on unreinforced and reinforced acrylic matrices have been investigated in several works [19,36,46,56,62,63]. All studies focused on benchmarking a toughened acrylic matrix – Elium Impact® alongside an untoughened grade. This modified grade reportedly contains 10 wt. % of a self-assembling acrylic block copolymer additive, Nanostrength®. However, the base grade of Elium® within the so-called Elium Impact® is not specified in any of the cited works. Nanostrength® is based on Arkema's proprietary alcoxyamine technology, comprising polymethylmethacrylate-b-polybutylacrylate-b-polymethylmethacrylate (shown in Figure 2-16).



Figure 2-16. Structure of self-assembling acrylic block copolymer (Copyright permission from Elsevier. Reproduced from Fig. 1a in [19]).

In addition to Nanostrength®, acrylonitrile butadiene styrene (ABS) has also been applied as a toughening agent [46]. Like Nanostrength®, ABS is a block copolymer but contains a uniformly dispersed phase of rubber within a styrene-acrylonitrile matrix. The effects of the incorporation of these toughening agents on the performance of acrylic-matrix composites will be discussed herein. Table 2-5 presents an overview of published works in this area.

The use of Nanostrength® within a glass fibre-reinforced acrylic hybrid laminate has been shown to reduce the energy absorbed for damage development compared to the equivalent untoughened laminate [19]. Similarly, Kinvi-Dossou et al. [46] reported enhanced impact strength in Nanostrength®-toughened acrylic, both in unreinforced and glass fibre-reinforced forms as detailed in Table 2-5.

Table 2-5. Overview of works on the effects of toughening on the impact performance of acrylic-matrix composites.

Materials and Methods	*Summary of results*	*Comments*	*Ref.*
• Elium® 150 • Nanostrength® • Glass fibre (woven) *Fabrication process* • Resin infusion *Test specifications* • Nanostrength® content → 5, 10 & 15 wt. % • Drop-weight impact →30, 40 & 50 J • Test temperature → -80, 20 & 80°C	• Enhanced impact damage resistance (20°C and 80°C impacts only). Nanostrength® addition was said to increase the matrix ductility and limit damage extension at these temperatures. • 10 wt. % Nanostrength® content exhibited superior performance in most cases. Changes in absorbed energy based on comparisons of the laminate prepared with 10 wt. % of Nanostrength® with the unmodified reference laminate: ▪ *-80°C impacts* → -4 % (30 J); -35 % (40 J); -13 % (50 J) ▪ *20°C impacts* → -31 % (30 J); -5 % (40 J); +7 % (50 J) ▪ *80°C impacts* → -6 % (30 J); -17 % (40 J); -10 % (50 J) • Proposed toughening mechanisms: crack-bridging, micelle cavitation, shear banding and crack tip shielding.	The authors explore a breadth of variables, which are insightful for the composites community in terms of the impact behaviour of toughened acrylic-matrix composites. However, the discussion of findings provided was mainly qualitative and hypothesis-driven. Such work would benefit from a more systematic discussion of the individual variables under investigation. Moreover, no quantitative damage zone assessments were performed.	[19]
• Elium® 150 • ABS (10 wt. %) • Nanostrength® (10 wt. %) • Glass fibre	• Marginal to moderate enhancement impact resistance achieved with Nanostrength® and ABS toughening of acrylic polymer and composite. Changes in absorbed energy in toughened laminates (compared with the unmodified laminate): ▪ *ABS-toughened acrylic* →-19 % (40 J); -0 % (50 J); -7 % (60 J) ▪ *Nanostrength®-toughened acrylic* →-16 % (40 J); +8 % (50 J); -2 % (60 J)	The authors logically provide the findings and discussions, based on comparisons of unreinforced polymers and reinforced composites, toughened and untoughened composites, and the effects of energy levels under investigation. However, no quantitative damage zone assessments were performed.	[46]

Table 2-5. Overview of works on the effects of toughening on the impact performance of acrylic-matrix composites. (contd.)

Materials and Methods (contd.)	*Summary of results (contd.)*	*Comments (contd.)*	*Ref.*
Fabrication process • Resin infusion *Test specifications* • Drop-weight impact & Charpy impact	• Improvements in impact strength were also reported with respect to unmodified acrylic polymer and composites (Charpy impact): ▪ *ABS-toughened acrylic* →+238 % (unreinforced polymer); +29 % (composite) ▪ *Nanostrength®-toughened acrylic* →+43 % (unreinforced polymer); +8.3 % (composite) • Proposed toughening mechanisms for Nanostrength® and ABS: crack-bridging, void coalescence, micelle cavitation, shear banding and crack tip shielding.		[46]

However, ABS-toughening proved more effective at enhancing polymer and composite impact strengths than Nanostrength®-toughening. In the same work, the authors also studied the drop-weight impact performance of the same materials; however, impacts under 40 J did not appear to be influenced by toughening. Both tougheners contain rubber nanophases, which are said to become grafted to the matrix during the *in situ* polymerisation process, rendering it more ductile. This enhanced ductility is reported to facilitate plastic deformation within the matrix in response to low-velocity impacts. In the case of Nanostrength®, it is believed to play a vital role in crack bridging and suppressing the coalescence of voids and microcracks. The authors also suggest that the self-assembling ability of Nanostrength® is essential to the micelle-cavitation mechanism, which not only toughens the matrix but induces shear banding and resists the initiation of delamination. These conclusions are in agreement with those drawn by Boumbimba et al. [19]. They are further supported by the works of Pini et al. [36,63,64], who extensively studied the fracture behaviour of untoughened and toughened acrylic-matrix systems and identified the dominant roles played by crazing, cavitation and shearing in Nanostrength®-toughened acrylic matrices. Pini et al. [36] suggested a transition from crazing to cavitation and shearing depending on temperature and strain-rate conditions, and reported differences in the respective dependences of mode-I fracture toughness on crack propagation rates for the toughened and untoughened acrylic-matrix composites. The fracture toughness of the toughened-matrix composite exhibited inverse proportionality to strain-rate; as the crack propagation rate increased, the authors reported a decreasing trend in fracture toughness. Interestingly, no rate effects were reported for the unmodified-matrix composite. These observations are further explained in work by Pini [47], which showed that higher displacement rates (and lower temperatures) promote multiple crazing in the Nanostrength®-toughened acrylic matrix. Conversely, cavitation and shear yielding are the dominant mechanisms at lower displacement rates (and higher temperatures). The rubber particles within the toughened acrylic matrix are said to both initiate and control the crazing behaviour. While a few larger crazes were reported for unmodified acrylic matrix, toughening was said to give rise to the formation of a large number of smaller crazes. The relative increase in the volume saturated by these smaller crazes is believed to contribute to favourable energy absorption within the toughened-matrix. Cavitation in the vicinity of rubber particles was said to promote matrix plasticity as opposed to being a primary energy absorption mechanism. Another role of cavitation

in the toughened-matrix is to induce shear yielding, which like crazing, constitutes a major energy absorption.

Pini [47] also reported positive effects of toughening on interfacial adhesion. Unmodified acrylic-matrix composites exhibited inferior interfacial strength to the toughened composites, which showed evidence of cohesive fracture of the fibre-matrix interface. However, fibre bridging was more prevalent in the unmodified composite during testing. Finally, the author reported more effective toughness transfer from unreinforced matrix to reinforced composite in the case of the unmodified matrix for which full transfer was reported due to the absence of interactions between the fibres and the process zone in the matrix-rich layer. This was not the case for the toughened materials, where only a partial transfer was reported. The author attributes this with contributions from fibre-process zone interactions. A smaller process zone (as in the untoughened matrix) was thought to be constrained by adjacent fibres. As the size of the process zone increases (with the incorporation of a toughening phase), its development is thought to be more affected by the presence of the fibres. Furthermore, the crack tip opening distance and thickness of the interlaminar resin-rich layer were shown to be influenced by the presence of a toughening phase within the matrix. Pini cites rheological differences in the toughened and untoughened material as the source of these observed differences.

In general, rubber toughening of polymeric materials is known to compromise their mechanical [65,66] and thermomechanical performance by decreasing T_g [67]. Owing to their non-reactive backbone, block copolymers like Nanostrength® are said to be unique in that their use reportedly yields no reduction in T_g [68]. To date, mechanical and thermomechanical characterisation of Nanostrength®-toughened acrylic matrices and their composites remain mostly unexplored. However, the work of Pini [47] provides valuable insights into fracture behaviour. The author reported a deleterious effect of Nanostrength®-toughening on matrix stiffness due to the presence of the rubber phase. The authors reported enhancements in tensile failure strains at a constant displacement rate of 1 mm/min over a range of test temperatures (0-60°C). Unmodified acrylic matrix (grade unspecified) exhibited brittle failure characteristics with strains of ~0.025-0.2, whereas the incorporation of 10 wt. % of Nanostrength into the same matrix system produced more ductile failure with strains of ~0.2-0.9. Table 2-6 presents a summary of key published works on the thermomechanical performance of Nanostrength®-

toughened acrylic (Elium Impact®). Due to the paucity of works on the thermomechanical properties of toughened acrylic-matrix composites, only findings on toughened unreinforced acrylic polymer have been presented in Table 2-6.

Table 2-6. A summary of the effects of Nanostrength®-toughening on glass transition temperatures of unreinforced acrylic polymers.

Matrix	*Glass transition temperature (°C)*	*Reference*
Elium®	125	Pini et al. [36]
	127	Pini et al. [56]
Elium Impact®	-25, 125	Pini et al. [36]
	-25, 130	Pini et al. [56]

2.7 Hybrid thermoplastic composites using *in situ* polymerised acrylics

Matrix- and fibre-based hybridisation have been shown as viable means of providing essential performance enhancements while concurrently targeting the reduction of mass and overall costs [69,70]. Recent advancements in liquid acrylic-matrix hybrid composites are discussed herein.

Kazemi et al. [71] reported improvements of up to 150 % in the compressive strength of woven carbon fibre/ultra-high molecular weight polyethylene (UHMWPE) fibre-reinforced acrylic composite systems with respect to UHMWPE fibre-reinforced acrylic reference laminates. Unsurprisingly, this corresponded to 27 % lower strengths in the hybrids relative to the carbon fibre-reinforced acrylic reference laminate due to the superiority of carbon fibres in performance. While studies of this type play vital roles in improving our understanding of carbon and UHMWPE as reinforcements in acrylic-matrix hybrid composites, the authors fail to provide comprehensive conclusions of their findings. No remark was made on the implication of such hybrids. Nonetheless, this study does demonstrate the potential for realising cost-effective (compared to carbon-only FRPs), stronger and stiffer (compared to UHMWPE-only FRPs) thermoplastic-matrix hybrid systems by a conventional room-temperature vacuum infusion. In another study [72], similar hybrids were shown to enhance impact performance, evidenced by a lesser (47 %) reduction in structural integrity and an 18 % reduction in absorbed energy.

Fibre-metal laminates (FML) are a class of hybrids comprising thin metal sheets interleafing FRPs layers. They were developed to exploit the weight-saving benefits of composites in a relatively cost-effective manner with possible enhancements in flame retardance, damage tolerance, fatigue and impact properties [73,74]. Some of the earliest works in this area focused on the use of thermosetting matrices (e.g.: glass-reinforced epoxy-based FMLs). This was due to the historic challenges associated with melt processing methodologies for thermoplastic alternatives. The rise in the popularity of liquid reactive thermoplastic resins has opened doors of opportunity for this class of hybrids as it facilitates resin infusion processing of thermoplastic FMLs. Although the mode-I interlaminar fracture toughness reported by Mamalis et al. [75] was lower than the reference acrylic-based laminate, the authors remarked that the value reported for the FML was ~237 % higher than values reported in literature for a thermoset FML.

An overview of works in this area demonstrating the suitability of liquid thermoplastic acrylic resins is presented in Table 2-7.

Table 2-7. Overview of some published works on acrylic-matrix hybrid composites.

Materials	*Fabrication Methodology*	*Summary of results*	*Ref.*

• Elium® 188
• BPO
• UHMWPE (woven; 12 plies)
• Ti6Al4V titanium (1.5-mm thick)
• PDA
• CNT (multi-walled)
	• Alloy surface activation → anodisation, alkali etching and annealing of the alloy sheet.
	• Fibre surface functionalisation → PDA or PDA & CNT fibre coating.
	  • Laminate 1 → Untreated
	  • Laminate 2 → Only alloy surface activation
	  • Laminate 3 → Alloy surface activation + PDA fibre treatment;
	  • Laminate 4 → Alloy surface activation + PDA & CNT fibre treatment.
		• Mode-I fracture toughness improvements were reported relative to the untreated reference laminate (Laminate 1). The most significant improvements in crack growth resistance were exhibited by Laminate 4.
		  • Laminate 2 → +528 %;
		  • Laminate 3 → +636 %;
		  • Laminate 4 → +916 %.
			[76]

• Elium® 180
• BPO
• Glass fabric (UD; 6 plies)
• 6082-T6 aluminium (0.71-mm thick)
• CN104 epoxy acrylate coating
	• Alloy surface activation → chemical etching (alkali, acid, acid-alkali and alkali-acid) or anodisation or atmospheric plasma.
	• Alkali-etched aluminium was used in FMLs to promote mechanical interlocking in addition to enhanced chemical adhesion using the CN104 coating.
	  • Laminate 1 → Acrylic-matrix FRP
	  • Laminate 2 → TP-FML
		• Performance of Laminate 2 (relative to the conventional reference laminate (Laminate 1):
		  • Flexural strength → +10 %;
		  • Flexural modulus → +23 %;
		  • Interlaminar shear strength → +41 %;
		  • Mode-I fracture toughness → -78 %.
			[75]

***FML:** fibre-metal laminate; **BPO:** dibenzoyl peroxide initiator; **UHMWPE:** ultra-high molecular weight polyethylene; **PDA:** polydopamine; **CNT:** carbon nanotubes; **UD:** unidirectional; **FRP:** fibre-reinforced polymer; **TP-:** thermoplastic-*

2.8 Advantages of thermoplastic acrylic-matrix composites

2.8.1 Reshaping by thermoforming acrylic-matrix composites

Cousins et al. [5,41] successfully demonstrated the thermoformability of continuous fibre-reinforced acrylic composites. An acrylic-matrix prototype spar cap section was flattened (120°C, 5.4 kPa, 8 h; radio-frequency press) as shown in Figure 2-17a, and a prototype single-curvature component (Figure 2-17b) was also produced as part of this study. Such works are essential to the cross-sectoral appeal; particularly for the automotive industry where *in situ* polymerised blanks could be readily thermoformed, facilitating mass-production of complex geometries. However, further investigation would be essential to understand the effects of thermal reprocessing on matrix, fibre and interfacial properties.

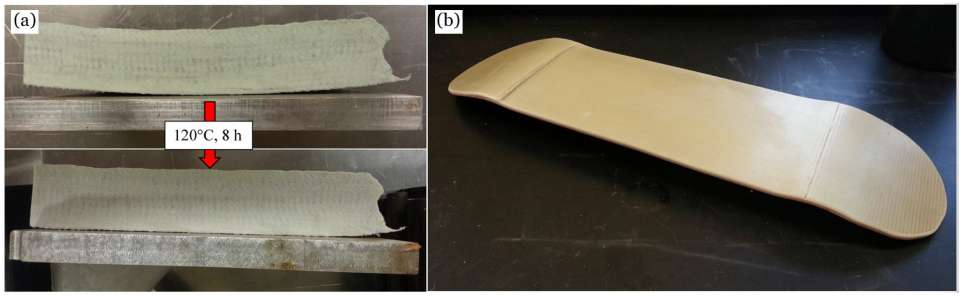


Figure 2-17. Demonstration of thermoformability (a) flattening a curved section and (b) producing a curved prototype from glass-reinforced acrylic laminates (Copyright permission from Elsevier. Reproduced from Fig. 9 & 10 in [5]).

2.8.2 Joining of acrylic-matrix composites

Welding is an attractive alternative to mechanical fasteners and adhesive joining. The former adds undesired weight and may cause drilling-induced delamination and bearing failure, and the bondline achieved with the latter is sensitive to harsh chemical environments, which can compromise static and dynamic structural performance [25]. Some recent works have demonstrated the weldability of glass fibre-reinforced acrylic composites [25,26,77]. Fusion welding of glass fibre-reinforced acrylic substrates to form lap-shear coupons was readily realised above 110°C (T_g of Elium® 188) using several element types (fine stainless steel mesh, woven carbon and unidirectional carbon fabrics) [25]. Bhudolia et al. [26] comparatively assessed ultrasonically welded and adhesively bonded carbon fibre-reinforced acrylic joints based on Elium® 150. The authors reported the use of an integrated semi-hemispherical energy director design for some of the welded joints and Arkema's methacrylate-based adhesive system (Bostik SAF 30 5) for the adhesively bonded reference coupons. The joint configurations used for welded samples

are schematically represented in Figure 2-18 with the volume of neat resin used in forming the energy director within the joints also presented.

Configuration		Resin Volume (mm^3)
ELC_IED		150.7
ELC_FED (0.5mm ELF)		312.5

Figure 2-18. Welding configuration used by Bhudolia et al. [43] (Copyright permission from Elsevier. Fig. 1 in [43]).

Energy directors have also been shown by Bhudolia et al. [26,77] to cut down on joining time compared to adhesive bonding by 99.8 %. Additionally, Bhudolia et al. [26] reported 23 % higher static lap shear strengths and 12 % higher fatigue strengths in welded joints compared to their adhesively bonded counterparts. The authors observed fibre impingement and shear cusps as the primary failure mechanisms, concluding that these promoted strong interfacial adhesion. Murray et al. [25] reported up to 100 % higher static lap shear strengths in resistance- and induction-welded coupons relative to adhesively bonded variants. It was also suggested that even greater potential enhancements of joint performance may be realised using fibre-reinforced heating elements with improved sizing technology and infusion quality.

2.8.3 Recycling and recovery of constituents

Cousins et al. [5] demonstrated the viability of acrylic-matrix composites for recycling by conventional recovery methodologies employed today such as pyrolysis, mechanical grinding and dissolution. The authors compared the recoverable constituents as well as the energy and cost requirements for all techniques, concluding that dissolution was the most favourable approach based on full-scale fibre and polymer recovery as shown in Figure 2-19. Compared to virgin fibres, recovered fibres were reported to exhibit no loss in tensile strength, with a 12 % reduction in stiffness. This loss in stiffness was attributed to operator-induced fibre misalignments during the dissolution recovery process. Additionally, pyrolysis was reported to result in the loss of fibre length scale and sizing; whereas dissolution facilitated not only their retention but also the recovery of the acrylic polymer. Pyrolysis was deemed less viable for the acrylic-matrix composite, as this required 78 % more decomposition energy than the requirement for the epoxy-based

reference. By mass, grinding and dissolution consumed the lowest and highest energies, respectively. The works of the authors essentially address the paucity in published works identified by Baley et al. [28] on the recyclability of these novel acrylic-matrix composites.

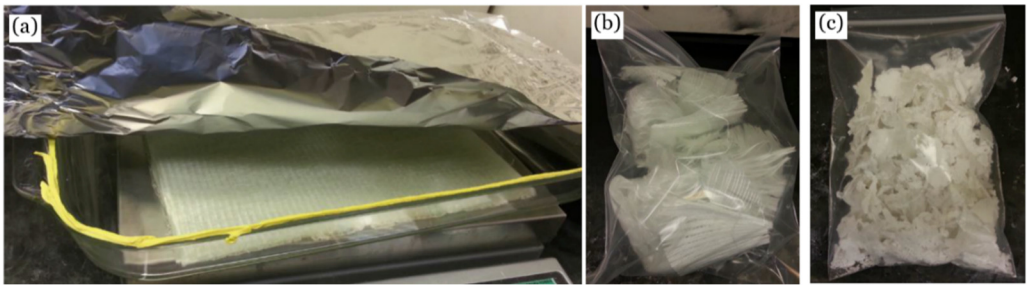


Figure 2-19: Recovery of fibres and polymer matrix from *in situ* polymerised glass/acrylic laminate by dissolution as demonstrated by Cousins et al. [5] (Copyright permission from Elsevier. Reproduced from Fig. 5 in [5]).

Although the findings reported by Cousins et al. [5] suggest no loss of sizing using the dissolution approach, surface analyses could substantiate this conclusion and contribute to increased confidence in these materials as potential future-proof solutions in terms of overall end-of-life value. Dissolution in acetone has also been demonstrated as a potential route to material recovery [78].

These works go a long way towards answering important research questions, which have profound ecological implications. Full or partial recovery of resources from end-of-life components manufactured from acrylic-matrix composites can mean better end-of-life waste management. In terms of tonnage, retired thermoset-matrix composite blades account for a large percentage of landfill-bound waste; corresponding to nearly 10 tonnes per megawatt. It is said that current practices in the marine sector mean that all end-of-life composite waste is typically disposed of in landfill due to contamination with oils, paints and core materials [79]. Given the energy-intensive production methods involved in the fabrication of such components, the use of thermoplastic-based composites has not only been identified as a viable solution to minimising environmental impact but has far-reaching economic implications [5].

2.9 Summary of comparative works

Several authors have published works on the comparative performance of acrylic composites alongside thermoset composites. An overview of existing literature by characterisation and reinforcement type is presented in Table 2-8.

These works have effectively established the knowledge base on the these materials' mechanical characteristics, with extensive efforts in characterising tensile, compressive, shear, impact, and fracture toughness [19,20,46,56,62,80–82,21,28,32,36,37,39,40,44]. Much applied research has been conducted towards understanding their fatigue [44,53,54], moisture diffusivity and marine ageing [83–87], interfacial adhesion [27,57], damage evolution and fracture behaviour [39,47,64,86,88,89], and even the effects of processing on properties [20,90]. Moreover, the thermomechanical properties of this acrylic family and their composites have also been studied by some researchers [33,34,37,64].

Chilali et al. [39] reported comparable tensile and shear performance in both acrylic-based and epoxy-based composites. They also observed superior damage resistance in flax-acrylic composites with respect to a comparable flax-epoxy material, no differences in the extent of damage and residual performance were reported between their glass-reinforced counterparts. Their findings on the tensile performance of the glass-reinforced composites are in agreement with published work by Lorriot et al. [23]; however, Baley et al. [28] reported significantly lower (-40 %) tensile strength in glass-reinforced acrylic than glass-reinforced epoxy. Kinvi-Dossou et al. [46] reported superior impact performance in glass-acrylic composites than their thermoset counterparts; however, Obande et al. [37] found that despite exhibiting more energy dissipative behaviour, glass-acrylic composites were less impact damage resistant than their epoxy counterparts.

With the exception of work published by Cousins [41], the general mechanical properties (tensile, compressive, flexural and shear) of acrylic and comparable epoxy composites have not been evaluated comprehensively. As shown in Table 2-8, no one study comparatively evaluates general mechanical properties, fracture toughness, damage behaviour and thermomechanical characteristics using a complementary approach. Despite attracting considerable research interest is not as well understood as traditional matrix systems such as epoxies. There exists a need for rigorous benchmarking towards the development of a robust performance database of acrylic matrices in composites.

Table 2-8. Summary of published literature on the comparative performance of acrylic composites against comparable epoxy composites.

Properties characterised										
Tensile	Compressive	Flexural	Shear	Fracture toughness	Impact	Fatigue	Moisture diffusivity & ageing	Damage and fracture behaviour	Damage & viscoelasticity	
FF, GF			FF, GF					FF, GF		Chilali et al. [39]
					GF				GF	Obande et al. [37]
GF, CF		GF, CF				GF, CF	GF, CF			Davies and Arhant [44]
				CF						Bhudolia et al. [32]
					GF					Kinvi-Dossou et al. [46]
					CF					Bhudolia and Joshi [21]
			CF							Bhudolia et al. [20]
			CF		CF					Aronica and Fossati [80]
FF, JF	FF, JF									Baley et al. [28]
							FF, GF			Freund et al. [85]
							GF, CF			Davies et al. [84]
							CF			Davies [83]
							FF			Chilali et al. [87]
							FF	FF		Chilali et al. [86]
								CF	CF	Bhudolia et al. [33]
GF			GF							Lorriot et al. [23]
GF	GF	GF	GF							Cousins [41]
GF, CF		GF, CF	GF, CF				GF, CF			Davies et al. [58]
		GF								Murray et al. [15]
FF, GF, CF and JF indicate the usage of flax, glass, carbon and jute reinforcements in the cited work(s).										

Chapter references

[1] Murray RE, Snowberg D, Berry D, Beach R, Rooney S, Swan D, et al. Manufacturing a 9-meter thermoplastic composite wind turbine blade. 32nd Tech Conf Am Soc Compos 2017 2017;1:29–43. https://doi.org/10.12783/asc2017/15166.

[2] Arkema. Elium resin: a disruptive innovation in the world of composites. Innov Webzine 2019.

[3] Arkema. Growing in Asia and North America. 2016.

[4] Murray RE, Beach R, Barnes D, Snowberg D, Berry D, Rooney S, et al. Structural validation of a thermoplastic composite wind turbine blade with comparison to a thermoset composite blade. Renew Energy 2021;164:1100–7. https://doi.org/10.1016/j.renene.2020.10.040.

[5] Cousins DS, Suzuki Y, Murray RE, Samaniuk JR, Stebner AP. Recycling glass fiber thermoplastic composites from wind turbine blades. J Clean Prod 2019;209:1252–63. https://doi.org/10.1016/j.jclepro.2018.10.286.

[6] Ehrenstein GW. Polymeric materials. Munich: Carl Hanser Verlag; 2001.

[7] McCrum NG, Buckley CP, Bucknall CB. Principles of polymer engineering. 2nd ed. Oxford University Press; 1997.

[8] de Andrade Raponi O, Barbosa LCM, de Souza BR, Ancelotti Junior AC. Study of the influence of initiator content in the polymerization reaction of a thermoplastic liquid resin for advanced composite manufacturing. Adv Polym Technol 2018;37:3579–87. https://doi.org/10.1002/adv.22142.

[9] Qin Y, Summerscales J, Graham-Jones J, Meng M, Pemberton R. Monomer selection for in situ polymerization infusion manufacture of natural-fiber reinforced thermoplastic-matrix marine composites. Polymers (Basel) 2020;12:1–25. https://doi.org/10.3390/polym12122928.

[10] Khalili P, Blinzler B, Kádár R, Blomqvist P, Sandinge A, Bisschop R, et al. Ramie fabric Elium®composites with flame retardant coating: Flammability, smoke,

viscoelastic and mechanical properties. Compos Part A Appl Sci Manuf 2020;137:105986. https://doi.org/10.1016/j.compositesa.2020.105986.

[11] Khalili P, Blinzler B, Kádár R, Bisschop R, Försth M, Blomqvist P. Flammability, smoke, mechanical behaviours and morphology of flame retarded natural fibre/Elium®composite. Materials (Basel) 2019;12. https://doi.org/10.3390/ma12172648.

[12] van Rijswijk K, Bersee HEN. Reactive processing of textile fiber-reinforced thermoplastic composites - An overview. Compos Part A Appl Sci Manuf 2007;38:666–81. https://doi.org/10.1016/j.compositesa.2006.05.007.

[13] de Andrade Raponi O, de Souza BR, Barbosa LCM, Ancelotti Junior AC. Thermal, rheological, and dielectric analyses of the polymerization reaction of a liquid thermoplastic resin for infusion manufacturing of composite materials. Polym Test 2018;71:32–7. https://doi.org/10.1016/j.polymertesting.2018.08.024.

[14] Arkema. ELIUM®150 technical datasheet – Liquid thermoplastic resin for glass-reinforced composite 2017.

[15] Murray RE, Penumadu D, Cousins D, Beach R, Snowberg D, Berry D, et al. Manufacturing and flexural characterization of infusion-reacted thermoplastic wind turbine blade subcomponents. Appl Compos Mater 2019;27:945–61. https://doi.org/10.1007/s10443-019-9760-2.

[16] Charlier Q, Fontanier J-CC, Lortie F, Pascault J-PP, Gerard J-FF. Rheokinetic study of acrylic reactive mixtures dedicated to fast processing of fiber-reinforced thermoplastic composites. J Appl Polym Sci 2019;136:1–9. https://doi.org/10.1002/app.47391.

[17] Pantelelis N, Bistekos E, Emmerich R, Gerard P, Zoller A, Gallardo RR. Compression RTM of reactive thermoplastic composites using microwaves and cure monitoring. Procedia CIRP 2019;85:249–54. https://doi.org/10.1016/j.procir.2019.10.005.

[18] Han N, Baran I, Zanjani JSM, Yuksel O, An LL, Akkerman R. Experimental and

computational analysis of the polymerization overheating in thick glass/Elium®acrylic thermoplastic resin composites. Compos Part B Eng 2020. https://doi.org/10.1016/j.compositesb.2020.108430.

[19] Matadi Boumbimba R, Coulibaly M, Khabouchi A, Kinvi-Dossou G, Bonfoh N, Gerard P. Glass fibres reinforced acrylic thermoplastic resin-based tri-block copolymers composites: Low velocity impact response at various temperatures. Compos Struct 2017;160:939–51. https://doi.org/10.1016/j.compstruct.2016.10.127.

[20] Bhudolia SKK, Perrotey P, Joshi SCC. Optimizing polymer infusion process for thin ply textile composites with novel matrix system. Materials (Basel) 2017;10. https://doi.org/10.3390/ma10030293.

[21] Bhudolia SK, Joshi SC. Low-velocity impact response of carbon fibre composites with novel liquid Methylmethacrylate thermoplastic matrix. Compos Struct 2018;203:696–708. https://doi.org/10.1016/j.compstruct.2018.07.066.

[22] Bhudolia SK, Perrotey P, Joshi SC. Experimental investigation on suitability of carbon fibre thin plies for racquets. Proc Inst Mech Eng Part P J Sport Eng Technol 2016;230:64–72. https://doi.org/10.1177/1754337115598489.

[23] Lorriot T, El Yagoubi J, Fourel J, Tison F. Non-conventional glass fiber NCF composites with thermoset and thermoplastic matrices. 20th Int. Conf. Compos. Mater., Copenhagen: 2015.

[24] Obande W, Mamalis D, Ray D, Yang L, Ó Brádaigh CM. Mechanical and thermomechanical characterisation of vacuum-infused thermoplastic- and thermoset-based composites. Mater Des 2019;175. https://doi.org/10.1016/j.matdes.2019.107828.

[25] Murray RE, Roadman J, Beach R. Fusion joining of thermoplastic composite wind turbine blades: Lap-shear bond characterization. Renew Energy 2019;140:501–12. https://doi.org/10.1016/j.renene.2019.03.085.

[26] Bhudolia SK, Gohel G, Kah Fai L, Barsotti RJ. Fatigue response of ultrasonically

welded carbon/Elium® thermoplastic composites. Mater Lett 2020;264:127362. https://doi.org/10.1016/j.matlet.2020.127362.

[27] Boufaida Z, Farge L, André S, Meshaka Y. Influence of the fiber/matrix strength on the mechanical properties of a glass fiber/thermoplastic-matrix plain weave fabric composite. Compos Part A Appl Sci Manuf 2015;75:28–38. https://doi.org/10.1016/j.compositesa.2015.04.012.

[28] Baley C, Lan M, Bourmaud A, Le Duigou A. Compressive and tensile behaviour of unidirectional composites reinforced by natural fibres: Influence of fibres (flax and jute), matrix and fibre volume fraction. Mater Today Commun 2018;16:300–6. https://doi.org/10.1016/j.mtcomm.2018.07.003.

[29] Hindersmann A. Confusion about infusion: An overview of infusion processes. Compos Part A Appl Sci Manuf 2019. https://doi.org/10.1016/j.compositesa.2019.105583.

[30] Afendi M, Banks WM, Kirkwood D. Bubble free resin for infusion process. Compos Part A Appl Sci Manuf 2005;36:739–46. https://doi.org/10.1016/j.compositesa.2004.10.030.

[31] Obande W, Ó Brádaigh CM, Ray D. Thermoplastic hybrid-matrix composite prepared by a room-temperature vacuum infusion and in-situ polymerisation process. Compos Commun 2020. https://doi.org/10.1016/j.coco.2020.100439.

[32] Bhudolia SK, Perrotey P, Joshi SC. Mode I fracture toughness and fractographic investigation of carbon fibre composites with liquid Methylmethacrylate thermoplastic matrix. Compos Part B Eng 2018;134:246–53. https://doi.org/10.1016/j.compositesb.2017.09.057.

[33] Bhudolia SK, Perrotey P, Joshi SC. Enhanced vibration damping and dynamic mechanical characteristics of composites with novel pseudo-thermoset matrix system. Compos Struct 2017;179:502–13. https://doi.org/10.1016/j.compstruct.2017.07.093.

[34] Fredi G, Dorigato A, Pegoretti A. Novel reactive thermoplastic resin as a matrix

for laminates containing phase change microcapsules. Polym Compos 2019. https://doi.org/10.1002/pc.25233.

[35] Barbosa LCM, Bortoluzzi DB, Ancelotti AC. Analysis of fracture toughness in mode II and fractographic study of composites based on Elium®150 thermoplastic matrix. Compos Part B Eng 2019;175:107082. https://doi.org/10.1016/j.compositesb.2019.107082.

[36] Pini T, Briatico-Vangosa F, Frassine R, Rink M. Time dependent fracture behaviour of a carbon fibre composite based on a (rubber toughened) acrylic polymer. Procedia Struct Integr 2016;2:253–60. https://doi.org/10.1016/j.prostr.2016.06.033.

[37] Obande W, Ray D, Ó Brádaigh CM. Viscoelastic and drop-weight impact properties of an acrylic-matrix composite and a conventional thermoset composite – A comparative study. Mater Lett 2019;238. https://doi.org/10.1016/j.matlet.2018.11.137.

[38] Cadieu L, Kopp JB, Jumel J, Bega J, Froustey C. Strain rate effect on the mechanical properties of a glass fibre reinforced acrylic matrix laminate. An experimental approach. Compos Struct 2019;223:110952. https://doi.org/10.1016/j.compstruct.2019.110952.

[39] Chilali A, Zouari W, Assarar M, Kebir H, Ayad R. Analysis of the mechanical behaviour of flax and glass fabrics-reinforced thermoplastic and thermoset resins. J Reinf Plast Compos 2016;35:1217–32. https://doi.org/10.1177/0731684416645203.

[40] Monti A, El Mahi A, Jendli Z, Guillaumat L. Mechanical behaviour and damage mechanisms analysis of a flax-fibre reinforced composite by acoustic emission. Compos Part A Appl Sci Manuf 2016;90:100–10. https://doi.org/10.1016/j.compositesa.2016.07.002.

[41] Cousins DS. Advanced thermoplastic composites for wind turbine blade manufacturing. Colorado School of Mines [Doctoral Thesis], 2018.

[42] Zoller A, Escalé P, Gérard P. Pultrusion of bendable continuous fibers reinforced composites with reactive acrylic thermoplastic Elium®resin. Front Mater 2019;6:1–9. https://doi.org/10.3389/fmats.2019.00290.

[43] Lee J, Soutis C. A study on the compressive strength of thick carbon fibre-epoxy laminates. Compos Sci Technol 2007;67:2015–26. https://doi.org/10.1016/j.compscitech.2006.12.001.

[44] Davies P, Arhant M. Fatigue behaviour of acrylic matrix composites: influence of seawater. Appl Compos Mater 2019;26:507–18. https://doi.org/10.1007/s10443-018-9713-1.

[45] Arkema. Liquid thermoplastic resin for tougher composites 2017. https://www.arkema-americas.com/export/shared/.content/media/downloads/products-documentations/incubator/brochure-elium-2017.pdf.

[46] Kinvi-Dossou G, Matadi Boumbimba R, Bonfoh N, Garzon-Hernandez S, Garcia-Gonzalez D, Gerard P, et al. Innovative acrylic thermoplastic composites versus conventional composites: Improving the impact performances. Compos Struct 2019;217:1–13. https://doi.org/10.1016/j.compstruct.2019.02.090.

[47] Pini T. Fracture behaviour of thermoplastic acrylic resins and their relevant unidirectional carbon fibre composites: rate and temperature effects. Politecnico Milano 1863 [Doctoral Thesis], 2017.

[48] Bhudolia SK, Joshi SC, Bert A, Di YB, Makam R, Gohel G. Flexural characteristics of novel carbon methylmethacrylate composites. Compos Commun 2019;13:129–33. https://doi.org/10.1016/j.coco.2019.04.007.

[49] Bhudolia SK, Joshi SC, Bert A, Gohel GR, Raama M. Energy Characteristics and Failure Mechanisms for Textile Spread Tow Thin Ply Thermoplastic Composites under Low-velocity Impact. Fibers Polym 2019;20:1716–25. https://doi.org/10.1007/s12221-019-9295-z.

[50] Jalalvand M, Czél G, Wisnom MR. Parametric study of failure mechanisms and

optimal configurations of pseudo-ductile thin-ply UD hybrid composites. Compos Part A Appl Sci Manuf 2015;74:123–31. https://doi.org/10.1016/j.compositesa.2015.04.001.

[51] Cugnoni J, Amacher R, Kohler S, Brunner J, Kramer E, Dransfeld C, et al. Towards aerospace grade thin-ply composites: Effect of ply thickness, fibre, matrix and interlayer toughening on strength and damage tolerance. Compos Sci Technol 2018;168:467–77. https://doi.org/10.1016/j.compscitech.2018.08.037.

[52] Frossard G. Fracture of thin-ply composites effects of ply thickness. École Polytechnique Fédérale de Lausanne [Doctoral Thesis], 2017.

[53] Haggui M, El Mahi A, Jendli Z, Akrout A, Haddar M. Damage analysis of flax fibre/elium composite under static and fatigue testing. In: Haddar M, Chaari F, Benamara A, Chouchane M, Karra C, Aifaoui N, editors. Des. Model. Mech. Syst., Cham: Springer International Publishing; 2018, p. 681–91.

[54] Haggui M, El Mahi A, Jendli Z, Akrout A, Haddar M. Static and fatigue characterization of flax fiber reinforced thermoplastic composites by acoustic emission. Appl Acoust 2019;147:100–10. https://doi.org/10.1016/j.apacoust.2018.03.011.

[55] Barbosa LCM, Gomes G, Junior ACA. Prediction of temperature-frequency-dependent mechanical properties of composites based on thermoplastic liquid resin reinforced with carbon fibers using artificial neural networks. Int J Adv Manuf Technol 2019. https://doi.org/10.1007/s00170-019-04486-4.

[56] Pini T, Caimmi F, Briatico-Vangosa F, Frassine R, Rink M. Fracture initiation and propagation in unidirectional CF composites based on thermoplastic acrylic resins. Eng Fract Mech 2017;184:51–8. https://doi.org/10.1016/j.engfracmech.2017.08.023.

[57] Johanna B, Jean-François G, Frédéric L, Pierre G, Jérôme M. New continuous fiber reinforced thermoplastic composites: An analysis of interfacial adhesion from the micro scale to the macro scale. ICCM Int Conf Compos Mater 2015;2015-July:19–24.

[58] Davies P, Le Gac PYY, Le Gall M. Influence of sea water aging on the mechanical behaviour of acrylic matrix composites. Appl Compos Mater 2017;24:97–111. https://doi.org/10.1007/s10443-016-9516-1.

[59] Shanmugam L, Kazemi ME, Rao Z, Lu D, Wang X, Wang B, et al. Enhanced Mode I fracture toughness of UHMWPE fabric/thermoplastic laminates with combined surface treatments of polydopamine and functionalized carbon nanotubes. Compos Part B Eng 2019;178:107450. https://doi.org/10.1016/j.compositesb.2019.107450.

[60] Charlier Q, Lortie F, Gerard P, Gerard JF. Interfacial adhesion between glass fibers and acrylic-based matrices as studied by micromechanical testing. ICCM Int Conf Compos Mater 2015;2015-July:19–24.

[61] Thomason JL. Glass fibre sizing: A review. Compos Part A Appl Sci Manuf 2019;127. https://doi.org/10.1016/j.compositesa.2019.105619.

[62] Pini T, Briatico-Vangosa F, Frassine R, Rink M. Matrix toughness transfer and fibre bridging laws in acrylic resin based CF composites. Eng Fract Mech 2018;203:115–25. https://doi.org/10.1016/j.engfracmech.2018.03.026.

[63] Pini T, Castellani L, Briatico-Vangosa F, Frassine R, Rink M. Damage mechanisms in a toughened acrylic resin: Effect of temperature and thermal history. Polym Eng Sci 2019;59:566–72. https://doi.org/10.1002/pen.24971.

[64] Pini T, Briatico-Vangosa F, Frassine R, Rink M. Fracture toughness of acrylic resins: Viscoelastic effects and deformation mechanisms. Polym Eng Sci 2018;58:369–76. https://doi.org/10.1002/pen.24583.

[65] Keskin R, Adanur S. Improving toughness of polypropylene with thermoplastic elastomers in injection molding. Polym - Plast Technol Eng 2011;50:20–8. https://doi.org/10.1080/03602559.2010.512344.

[66] Tamas-Benyei P, Bitay E, Kishi H, Matsuda S, Czigany T. Toughening of epoxy resin: The effect of water jet milling on worn tire rubber particles. Polymers (Basel) 2019;11. https://doi.org/10.3390/polym11030529.

[67] Utaloff K, Kothmann MH, Ciesielski M, Döring M, Neumeyer T, Altstädt V, et al. Improvement of fracture toughness and glass transition temperature of DGEBA-based epoxy systems using toughening and crosslinking modifiers. Polym Eng Sci 2019;59:86–95. https://doi.org/10.1002/pen.24870.

[68] Barsotti R, Fine T, Inoubli R, Gerard P, Schmidt S, Macy N, et al. Nanostrength® Block Copolymers for Epoxy Toughening. Meet. Thermoset Resin Formul. Assoc., Chicago, Illinois: 2008.

[69] Safri SNA, Sultan MTH, Jawaid M, Jayakrishna K. Impact behaviour of hybrid composites for structural applications: A review. Compos Part B Eng 2018;133:112–21. https://doi.org/10.1016/j.compositesb.2017.09.008.

[70] Bunea M, Cîrciumaru A, Buciumeanu M, Bîrsan IG, Silva FS. Low velocity impact response of fabric reinforced hybrid composites with stratified filled epoxy matrix. Compos Sci Technol 2018;169:242–8. https://doi.org/10.1016/j.compscitech.2018.11.024.

[71] Kazemi ME, Shanmugam L, Lu D, Wang X, Wang B, Yang J. Mechanical properties and failure modes of hybrid fiber reinforced polymer composites with a novel liquid thermoplastic resin, Elium®. Compos Part A Appl Sci Manuf 2019;125:105523. https://doi.org/10.1016/j.compositesa.2019.105523.

[72] Kazemi ME, Shanmugam L, Dadashi A, Shakouri M, Lu D, Du Z, et al. Investigating the roles of fiber, resin, and stacking sequence on the low-velocity impact response of novel hybrid thermoplastic composites. Compos Part B Eng 2021;207:108554. https://doi.org/10.1016/j.compositesb.2020.108554.

[73] Vlot A, Gunnik JW, editors. Fibre metal laminates: an introduction. Springer Science & Business Media; 2011. https://doi.org/DOI 10.1007/978-94-010-0995-9.

[74] Vogelesang LB, Vlot A. Development of fibre metal laminates for advanced aerospace structures. J Mater Process Technol 2000;103:1–5. https://doi.org/10.1016/S0924-0136(00)00411-8.

[75] Mamalis D, Obande W, Koutsos V, Blackford JR, Ó Brádaigh CM, Ray D. Novel thermoplastic fibre-metal laminates manufactured by vacuum resin infusion: The effect of surface treatments on interfacial bonding. Mater Des 2019;162. https://doi.org/10.1016/j.matdes.2018.11.048.

[76] Shanmugam L, Kazemi ME, Rao Z, Yang L, Yang J. On the metal thermoplastic composite interface of Ti alloy/UHMWPE-Elium® laminates. Compos Part B Eng 2020;181:107578. https://doi.org/10.1016/j.compositesb.2019.107578.

[77] Bhudolia SK, Gohel G, Fai LK, Barsotti RJ. Investigation on ultrasonic welding attributes of novel carbon/Elium®composites. Materials (Basel) 2020;13:10–5. https://doi.org/10.3390/ma13051117.

[78] Gebhardt M, Chakraborty S, Manolakis I, Meiners D. Closed-loop room temperature recycling of Elium CFRPs and its influence on the 2nd generation composite properties. J Sci Alliance Plast Technol 2020;16:179–210.

[79] Summerscales J, Singh MM, Wittamore K. Disposal of composite boats and other marine composites. Elsevier Ltd.; 2016. https://doi.org/10.1016/B978-1-78242-250-1.00008-9.

[80] Aronica A, Fossati D. Effects of resin and processing on mechanical properties of carbon fibre composites. Politecnico di Milano [Master's Thesis], 2015.

[81] Aronica A, Fossati D. Mechanical Properties of Carbon Fiber Composite Materials. Politecnico di Milano [Master's Thesis], 2014.

[82] Shah SZH, Megat-Yusoff PSM, Karuppanan S, Choudhry RS, Ahmad F, Sajid Z, et al. Performance comparison of resin-infused thermoplastic and thermoset 3D fabric composites under impact loading. Int J Mech Sci 2021. https://doi.org/10.1016/j.ijmecsci.2020.105984.

[83] Davies P. Environmental degradation of composites for marine structures: new materials and new applications. Philos Trans R Soc A Math Phys Eng Sci 2016;374:1–14. https://doi.org/10.1098/rsta.2015.0272.

[84] Davies P, Le Gac P-Y, Le Gall M, Arhant M. Marine ageing behaviour of new

environmentally friendly composites. In: Davies P, Rajapakse YDS, editors. Durab. Compos. a Mar. Environ. 2, Cham: Springer International Publishing; 2018, p. 225–37. https://doi.org/10.1007/978-3-319-65145-3_12.

[85] Freund L, Bouchart V, Perrin H, Chevrier P. Hydrothermal aging of natural fibers composite: determination of diffusivity parameters. ECCM 2016 - Proceeding 17th Eur. Conf. Compos. Mater., 2016.

[86] Chilali A, Zouari W, Assarar M, Kebir H, Ayad R. Effect of water ageing on the load-unload cyclic behaviour of flax fibre-reinforced thermoplastic and thermosetting composites. Compos Struct 2018;183:309–19. https://doi.org/10.1016/j.compstruct.2017.03.077.

[87] Chilali A, Assarar M, Zouari W, Kebir H, Ayad R. Effect of geometric dimensions and fibre orientation on 3D moisture diffusion in flax fibre reinforced thermoplastic and thermosetting composites. Compos Part A Appl Sci Manuf 2017;95:75–86. https://doi.org/10.1016/j.compositesa.2016.12.020.

[88] Haggui M, Jendli Z, Akrout A, El Mahi A. Damage identification in flax fibre composite with thermoplastic matrix under quasi-static loading. Int Conf Adv Mater Mech Manuf 2016:1–4.

[89] Haggui M, El Mahi A, Jendli Z, Akrout A. Damage characterization of flax fibre composite using linear and nonlinear vibration resonant techniques. 26th Annu Int Conf Compos Eng 2018.

[90] Lin Q, Ferriol M, Cochez M, Vahabi H, Vagner C. Continuous fiber-reinforced thermoplastic composites: influence of processing on fire retardant properties. Fire Mater 2017;41:646–53. https://doi.org/10.1002/fam.2406.

Chapter 3 PhD research motivation

Based on the review of existing literature presented in Chapter 2, some gaps in existing knowledge are worthy of immediate attention. Closing these gaps in the current database of the performance of acrylic-matrix composites will serve to improve the understanding of these innovative liquid acrylic resin for composite applications and will inform decision-making on new and unexplored areas for their application. In addition to these gaps, research opportunities have been identified to explore routes by which the envelope of applicability of these novel resin-based composites may be expanded.

The gaps and open research areas presented in this chapter are those which have motivated this body of work and from which the aims and objectives are derived.

3.1 Gaps in existing knowledge

Given the recent introduction of liquid acrylic monomeric resins, the database of their performance as composite matrices is considerably less mature than that of traditional epoxy matrix systems. Not much is known about the mode-I fracture toughness properties of non-carbon fibre-reinforced acrylic composites (e.g.: those containing glass fibre reinforcements), as such, this warrants further attention.

Moreover, despite demonstrable suitability for the fabrication of large-scale components such as those required for the wind [1–3] and marine sectors [4,5], the performance of the flagship grades for these sectors (Elium® 180 & 188O) remain relatively unexplored. Much attention has been given to understanding the behaviour of Elium® 150 and its fibre-reinforced composites [6–9]. Thus, there exists a clear gap in knowledge, which must be addressed.

3.2 Research opportunities

Based on the published works reviewed in Chapter 2, these liquid acrylic resins often exhibit comparable or marginally superior mechanical and thermomechanical performance to non-aerospace epoxy-based composites.

In addition to the research opportunities gleaned from the review in Chapter 2, other considerations are presented below.

Acrylics are commodity amorphous thermoplastics, a class of materials, which are known to be susceptible to solvent-related degradation [10,11]. This has wide-reaching implications and has meant that amorphous thermoplastics had been relegated to non-structural composite applications in favour of thermosets and their partially crystalline thermoplastic counterparts. Apart from their vulnerability in aggressive environments, other factors must be considered. As shown in Figure 3-1, crystalline regions, which cause a step-change in density upon reordering within partially crystalline polymers are markedly absent in amorphous thermoplastics. Thus, they are superior in dimensional stability, with minimal volumetric change expected during solidification. This offers great benefits for the composites industry as thermal processing of such a matrix is not likely to result in severe accumulation of internal stresses.

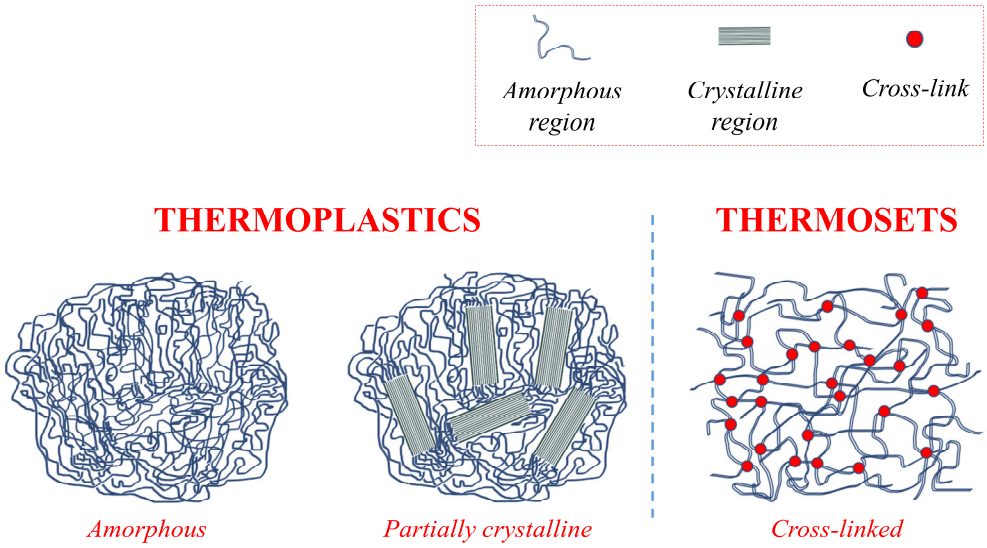


Figure 3-1. Diagrammatic representations of thermoplastics (amorphous, partially crystalline) and cross-linked thermosets.

While the cost-competitiveness, low-viscosity and room-temperature processibility, and reprocessibility of liquid acrylic resins make them excellent candidates for addressing current environmental challenges associated with the use of thermosetting matrices for composite applications, more work needs to be done to extend their applicability. It is worth noting that there are drawbacks associated with the absence of rigid structures such as crystalline domains (in partially crystalline thermoplastics) and cross-links (in thermosets) within their molecular structure. For engineering and high-performance amorphous thermoplastics, such as poly(ether imide) (PEI), these drawbacks may be

masked. Without a doubt, moving down to commodity amorphous polymers invariably results in a drop in strength, stiffness, thermomechanical performance and thermal stability [12]. Inspired by previous studies on the tailoring of liquid acrylic-matrix composites properties [9,13–15] by exploiting its low viscosity and in-situ polymerisation capabilities, the reactive nature of these novel resins may hold the key to addressing these drawbacks. Their low viscosity and reactivity offer benefits for bulk matrix modification prior to infiltration into reinforcement fabrics and in-situ polymerisation.

3.3 Thesis aim and objectives

Motivated by the open research opportunities discussed in Section 3.2, this PhD research aims to investigate routes by which thermoplastic-thermoplastic hybrid-matrix composites based on liquid acrylic resin technology may be prepared by room-temperature vacuum infusion and in-situ polymerisation processes.

Ultimately, this research aims to answer the question: *"Can an in-situ polymerisable hybrid matrix be developed by a reactive hybridisation route for composite applications based on liquid acrylic resin technology?"* Thus, this body of work is focused on the development of a simple, yet effective strategy for tailoring the performance of liquid thermoplastic acrylic resins for broader applicability within the field of composite materials.

In view of this overarching aim and the need to address the gaps in the performance database of composites based on these novel resin systems (discussed in Section 3.1), the objectives of this thesis are hereby methodically defined.

3.3.1 Material selection and benchmarking of acrylic-matrix composite performance against an epoxy-matrix composite

Before delving into the development of hybrids, it is pivotal to conduct a preliminary screening study for material selection. Acrylic-matrix composites have been previously studied using liquid composite moulding processes, with vacuum infusion and resin transfer moulding being suitable for a broad range of Elium® grades. This part of the study explores the use of a standard vacuum infusion process to obtain laminates for preliminary screening assessments of mechanical and thermomechanical performance.

Besides, to close the aforementioned gaps in knowledge for these resins as composite matrices, an integral part of this objective is to comparatively characterise the acrylic-

matrix composite with respect to a more traditional thermoset epoxy-matrix counterpart. A combination of thermomechanical and mechanical analytical techniques have been used to get a comprehensive overview of material behaviour over a range of conditions. Knowledge gained from this phase of work provides a baseline for subsequent tailoring of the selected acrylic matrix.

3.3.2 Development and characterisation of reactive hybrid matrices

To fulfil the aim of this project, it was essential to consider all factors contributing to the favourable qualities of the base acrylic resin. Thus, these were incorporated as integral parts of the material selection criteria. The desired hybridisation route and the use of additional constituents/co-reactants must satisfy the following conditions:

- **Maintain the cost-effectiveness** of the base acrylic resin;
- Induce no deleterious effects on the **processibility and reprocessibility** of the thermoplastic acrylic constituent.
- Utilise **functional groups for enhanced reactivity** between all constituents;
- Confer **performance enhancements** with no reduction in the glass transition temperature of original properties.

Following the selection of the additional co-reactant for hybridisation of the base acrylic monomeric resin, the effects of compositional variations are characterised with respect to the neat acrylic material using a combination of analytical techniques including confocal Raman microscopy, nuclear magnetic resonance spectroscopy and dynamic mechanical analysis performed on unreinforced polymer samples.

3.3.3 Fabrication and characterisation of the hybrid-matrix system

Based on the findings of the experiments conducted as part of the objectives defined in Section 3.3.2, the best performing composition of constituents for the hybrid matrix is selected. The objective broadly defined in this section involves the validation of the optimal composition by evaluating the reinforced form of the hybrid matrix. This composition is thereafter employed for the fabrication of glass fibre-reinforced hybrid-matrix laminates to gain an in-depth understanding of the effects of hybridisation. Using a combination of the techniques applied to fulfil the objectives described in Sections 3.3.1 and 3.3.2, the quality and properties of the hybrid-matrix composites are comprehensively

evaluated in comparison with the benchmarked acrylic composite material described in Section 3.3.1.

Finally, physical insights into the behaviour of the hybrid-matrix composite and new opportunities for its application are also presented in detail.

Chapter references

[1] Murray RE, Snowberg D, Berry D, Beach R, Rooney S, Swan D, et al. Manufacturing a 9-meter thermoplastic composite wind turbine blade. 32nd Tech Conf Am Soc Compos 2017 2017;1:29–43. https://doi.org/10.12783/asc2017/15166.

[2] Cousins DS, Suzuki Y, Murray RE, Samaniuk JR, Stebner AP. Recycling glass fiber thermoplastic composites from wind turbine blades. J Clean Prod 2019;209:1252–63. https://doi.org/10.1016/j.jclepro.2018.10.286.

[3] Murray RE, Beach R, Barnes D, Snowberg D, Berry D, Rooney S, et al. Structural validation of a thermoplastic composite wind turbine blade with comparison to a thermoset composite blade. Renew Energy 2021;164:1100–7. https://doi.org/10.1016/j.renene.2020.10.040.

[4] Davies P, Arhant M. Fatigue behaviour of acrylic matrix composites: influence of seawater. Appl Compos Mater 2019;26:507–18. https://doi.org/10.1007/s10443-018-9713-1.

[5] Davies P, Le Gac PYY, Le Gall M. Influence of sea water aging on the mechanical behaviour of acrylic matrix composites. Appl Compos Mater 2017;24:97–111. https://doi.org/10.1007/s10443-016-9516-1.

[6] Aronica A, Fossati D. Effects of resin and processing on mechanical properties of carbon fibre composites. Politecnico di Milano [Master's Thesis], 2015.

[7] de Andrade Raponi O, Barbosa LCM, de Souza BR, Ancelotti Junior AC. Study of the influence of initiator content in the polymerization reaction of a thermoplastic liquid resin for advanced composite manufacturing. Adv Polym Technol 2018;37:3579–87. https://doi.org/10.1002/adv.22142.

[8] Bhudolia SK, Perrotey P, Joshi SC. Experimental investigation on suitability of carbon fibre thin plies for racquets. Proc Inst Mech Eng Part P J Sport Eng Technol 2016;230:64–72. https://doi.org/10.1177/1754337115598489.

[9] Matadi Boumbimba R, Coulibaly M, Khabouchi A, Kinvi-Dossou G, Bonfoh N, Gerard P. Glass fibres reinforced acrylic thermoplastic resin-based tri-block copolymers composites: Low velocity impact response at various temperatures. Compos Struct 2017;160:939–51. https://doi.org/10.1016/j.compstruct.2016.10.127.

[10] Cogswell FN. Thermoplastic aromatic polymer composites. 1992. https://doi.org/10.1533/9781845699253.

[11] Meyer GW, Pak SJ, Lee YJ, McGrath JE. New high-performance thermosetting polymer matrix material systems. Polymer (Guildf) 1995. https://doi.org/10.1016/0032-3861(95)95311-N.

[12] An in-depth guide to choosing the right thermoplastic for your component | Knowledge Centre | Essentra Components UK n.d.

[13] Pini T, Castellani L, Briatico-Vangosa F, Frassine R, Rink M. Damage mechanisms in a toughened acrylic resin: Effect of temperature and thermal history. Polym Eng Sci 2019;59:566–72. https://doi.org/10.1002/pen.24971.

[14] Pini T, Caimmi F, Briatico-Vangosa F, Frassine R, Rink M. Fracture initiation and propagation in unidirectional CF composites based on thermoplastic acrylic resins. Eng Fract Mech 2017;184:51–8. https://doi.org/10.1016/j.engfracmech.2017.08.023.

[15] Pini T, Briatico-Vangosa F, Frassine R, Rink M. Matrix toughness transfer and fibre bridging laws in acrylic resin based CF composites. Eng Fract Mech 2018;203:115–25. https://doi.org/10.1016/j.engfracmech.2018.03.026.

PART II: BENCHMARKING THE PERFORMANCE OF A GLASS FIBRE-REINFORCED THERMOPLASTIC ACRYLIC-MATRIX COMPOSITE

Chapter 4 Preliminary studies & material selection

Inspired by the gaps identified and discussed in Chapters 2 and 3, respectively, this Chapter presents a preliminary study conducted to aid in decision-making for the material selection and manufacturing processes.

Acrylics are known to exhibit strain-rate-dependent embrittlement [1]; thus, two characterisation techniques were selected to gain insights into the damage resistance and viscoelastic properties of the material systems. Glass transition temperature (T_g) is a good indicator of a material's performance (thermal and mechanical)[2] as moving from high-performance polymers to their commodity counterparts invariably means a reduction in T_g. Thus, T_g determination is an essential step towards assessing the comparability of the prospective resin systems.

Based on the paucity of literature on Elium® 180 & 188 O resins before the author's own work, these resins needed to be explored to contribute to the knowledge base for the use of liquid acrylic resin systems for marine and wind energy applications. With guidance from technical experts at Arkema GRL, France, it was discovered that Elium® 180 and Elium® 188 O were virtually identical in formulation and thus, may be used interchangeably. Both formulations require a powder-based dibenzoyl peroxide initiator; however, the -188 O grade contains a fragrance additive, whereas the -180 grade is fragrance-free. Due to the immediate availability of material samples, Elium® 180 was selected for this preliminary study.

Three primary criteria were considered for this preliminary material selection phase in selecting the appropriate epoxy resin for benchmarking: (i) *room-temperature processibility*, (ii) *cost*, and (iii) *availability*. As part of the objectives of this study was to comparatively assess the performance of the acrylic resin against that of a non-aerospace grade epoxy resin, a commercially available epoxy resin system was sourced based on availability from Easy Composites Ltd., UK. The two-part resin system – IN-2 Infusion Epoxy was selected based on comparability of processing temperature and curing time. Ultimately, the work described in this chapter focuses on assessing the epoxy resin for its suitability based on the final selection criterion, performance.

In selecting the reinforcement for this phase of the research project, unidirectional glass fibre reinforcement with multicompatible sizing was desired to enhance the direct

comparability between the material systems. However, extensive sourcing activities proved unfruitful within the timescale of this study and a quasi-unidirectional non-crimp fabric was selected. At the time of this study, it was not possible to source any reinforcements with multicompatible-sized fibre, as such, an epoxy-sized variant was employed. A standard vacuum infusion technique offered the best compromise between time, cost and quality for this stage of the research project.

In the interest of clarity, the laminates discussed in this chapter have been assigned a unique identification context based on the precise grade names of the resins used to distinguish them from those studied in subsequent chapters of this thesis, where new and more appropriate contexts are defined. Thus, where "GF/E180" and "GF/IN-2" are used in Chapter 4, they refer to glass-fibre reinforced laminates comprising Elium® 180 acrylic resin and IN-2 Infusion epoxy resin systems, respectively.

4.1 Materials & fabrication method

A room-temperature infusible thermoplastic acrylic resin, Elium® 180 (Arkema GRL, France) was selected for preliminary characterisation studies in comparison to a cold-cure epoxy resin, IN-2 Infusion Epoxy (Easy Composites Ltd., UK). In addition to its ease of processibility, the epoxy resin system was selected due to availability and cost considerations. 4 mm-thick laminates comprising eight plies of stitched non-crimp E-glass fabric (Saertex GmbH & Co. KG, Germany) were produced for each resin system. The fabric used comprised 0°-direction fibres (520 g/m2), 90°-direction fibres (54 g/m2) and 110 Tex polyester stitching (17 g/m2) for a total areal weight of 591 g/m2. A stacking sequence of $[45/0/-45/90]_s$ or more simply, [45/0/-45/90/90/-45/0/45] was used. While the precise formulation of sizing employed by the manufactures was not disclosed, the fabric was sized for epoxy-compatibility as a multicompatible alternative was not available at the time of the study.

With the exception of initiators/hardeners and post-curing requirements, each test laminate was identically produced using a standard room temperature vacuum infusion process as shown in Figure 4-1.

Eight square plies of dry fabric measuring 500 mm in length were cut and assembled to make a preform for each infusion. Each preform was placed over a rigid tool base (with the relevant auxiliary infusion aids) and subsequently sealed under a flexible vacuum bag

for evacuation and infusion. Leak testing was performed to assess vacuum integrity for each run, with a target of <5 mbar/min over 10 minutes.

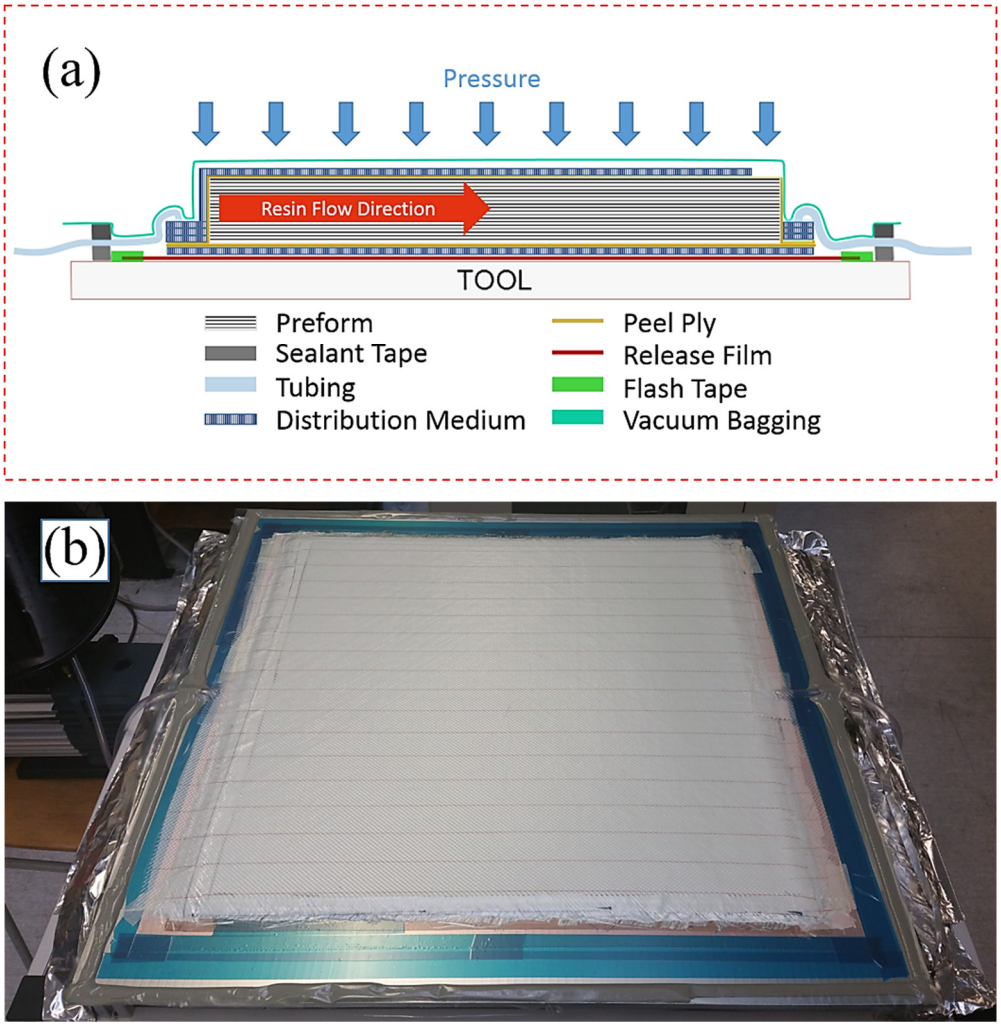


Figure 4-1. (a) A schematic diagram and (b) photograph of the resin infusion set-up used for laminate fabrication.

After resin infusion, the acrylic-matrix laminate was left in-situ for 24 hours at room temperature to polymerise; thereafter, the laminate was demoulded for coupon extraction with no post-cure requirements prescribed by the resin manufacturer. For the epoxy-matrix laminate, the same duration was required for room temperature cure. However, following the resin manufacturer's recommendations, the laminate was subjected to a free-standing post-cure by heating from 40°C to 70°C in a convection oven in increments of 10°C with isothermal heating segments of 2 hours maintained at each temperature.

The polymerisation of the acrylic resin was achieved using a dibenzoyl peroxide initiator, BP-50-FT (100:3 by weight of resin). The slow AT30 hardener supplied by Easy Composites, Ltd. UK) was used to initiate cure in the epoxy resin (100:30 by weight of resin).

An estimated fibre volume fraction of 47 % was attained for both laminates as shown below in Equation 4-1 [3]:

$$V_f = \frac{n.AW_f}{\rho_f.t} \times 100$$

Equation 4-1

Where V_f is the fibre volume fraction (%), n is the number of plies, AW_f is the fibre areal weight (g/m^2), ρ_f (g/m^3) and t is the thickness (m).

4.2 Characterisation of viscoelastic and drop-weight impact performance

Single-frequency (SF) and multi-frequency (MF) dynamical mechanical analyses (DMA) were performed as detailed in Table 4-1 to study the viscoelastic behaviours of both materials. All samples were loaded in a 3-point bend configuration on a Triton 2000 series analyser.

Table 4-1. DMA test information.

Test Parameters	
Standard	BS ISO 6721 – 11
Specimen dimensions (mm)	35 × 5
Heating rate (°C/min)	3
Amplitude (μm)	10
Temperature range (°C)	**SF:** Ambient – 170; **MF:** Ambient – 45
Frequency (Hz)	**SF:** 1; **MF:** 0.01 – 100
Span (mm)	30

The drop-weight impact characteristics of both material systems were also comparatively assessed using the experimental set-up shown in Figure 4-2.

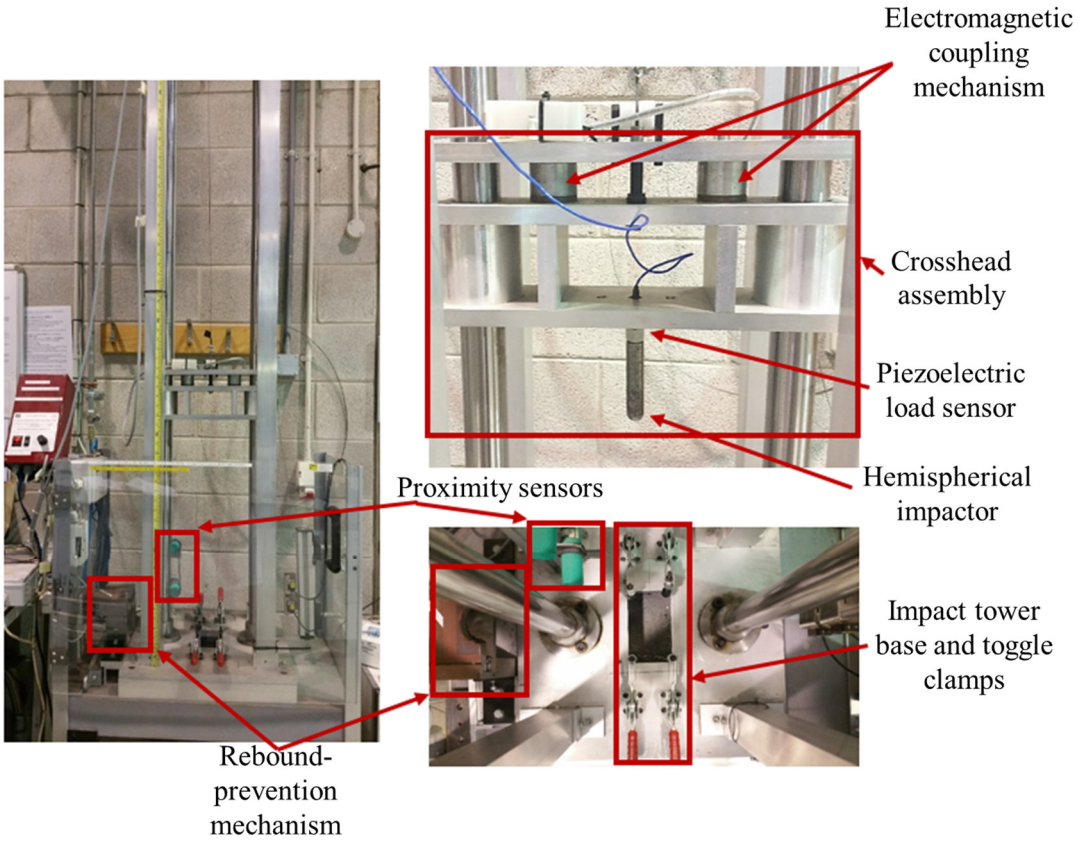


Figure 4-2. Drop-weight impact test experimental set-up.

Six specimens were tested at each energy level per material. The test parameters used are defined in Table 4-2.

Table 4-2. Drop-weight impact test parameters.

Test Parameters	
Standard	ASTM D7136
Specimen dimensions (mm)	150 × 100
Impactor mass (kg)	4.2
Drop height (m)	**15 J**: 0.55; **30 J**: 1.05
Impact velocity (ms^{-1})	**15 J**: 2.25; **30 J**: 3.11

High-contrast imaging of the impact-damaged coupons facilitated computation of damaged areas as a measure of damage resistance as shown in Figure 4-3. Damage areas were measured using digital image processing software (Image J, National Institutes of Health).

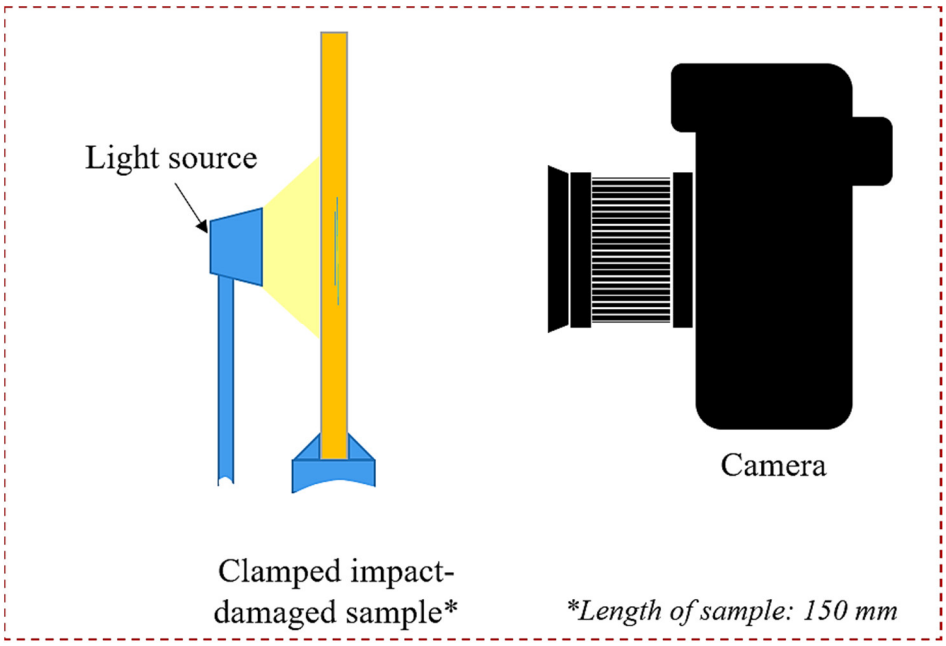


Figure 4-3. Experimental set-up for damage area image acquisition.

4.3 Results and discussion

4.3.1 Viscoelastic performance

Glass transition (T_g) temperatures were determined as temperatures corresponding to the *tan delta* (damping) peak as shown in Figure 4-4.

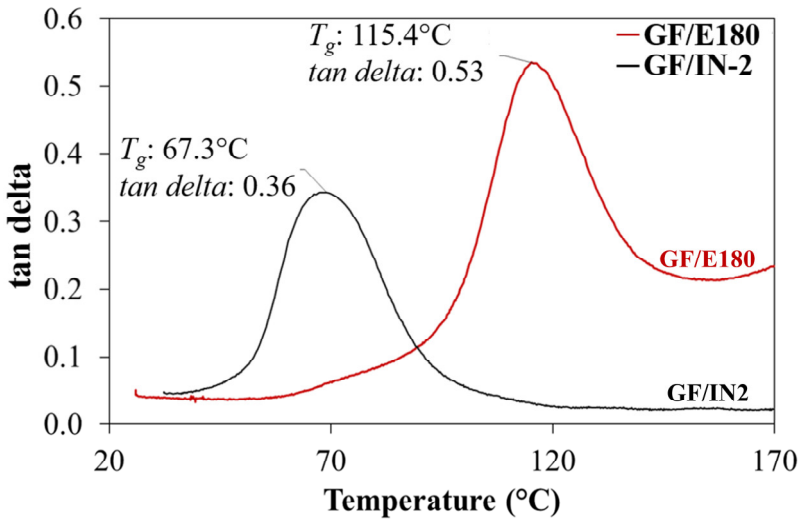


Figure 4-4. Single-frequency DMA thermograms showing damping behaviour (*tan delta*) as a function of temperature.

The T_g values recorded were 67°C and 115°C for GF/IN-2 and GF/E180, respectively. This mismatch in T_g highlights the incomparability of these materials for comprehensive

characterisation of properties. More importantly, it also suggests differences in the windows of applicability of these matrix systems, which has direct consequences on the conclusiveness of any prospective findings from a more in-depth comparative performance study.

Interestingly, a higher and broader *tan delta* peak was observed in GF/E180, which demonstrate a greater dissipative (damping) capacity than that of GF/IN-2. These attributes also suggest differences in the polymer chain mobility, which may originate from intrinsic structures of each matrix type or the respective fibre-matrix interfacial strengths within both composite material systems [4–8]. To rule out the likelihood of sizing-incompatibility playing a role, an alternative reinforcement system with acrylic-compatible or multicompatible sizing technology must be sourced for the remainder of this body of work.

Results of the multi-frequency DMA tests performed are shown in Figure 4-5. Given their dissimilar T_g values, multi-frequency scan results were analysed at a reference temperature of 25°C to facilitate direct comparisons between the materials' viscoelastic behaviours.

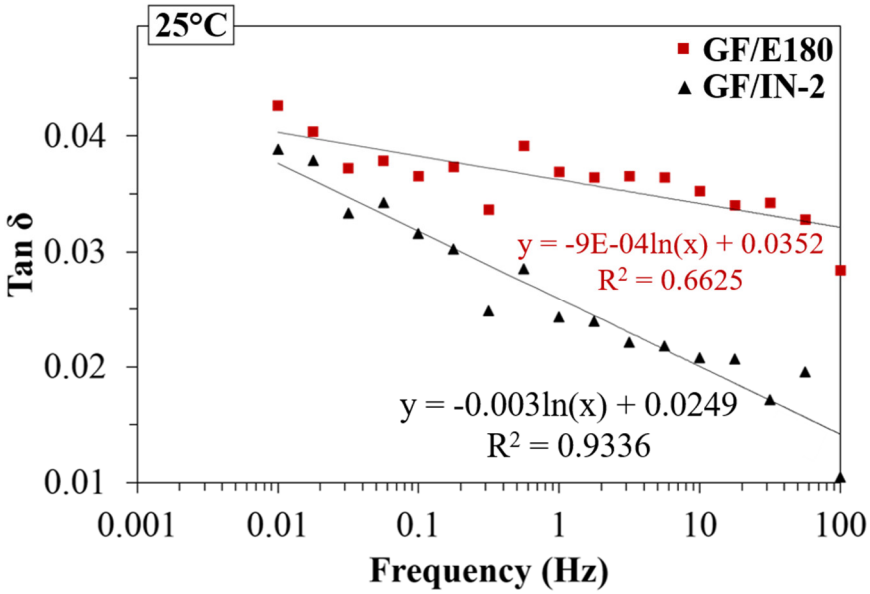


Figure 4-5. Multi-frequency DMA thermograms showing the evolution of *tan delta* (damping parameter) with frequency at 25°C.

GF/E180 not only exhibited higher (8.7 %) damping behaviour but had a higher damping retention capacity than GF/IN-2 at higher frequencies, evidenced by up to 66 % of a loss in damping/dissipative capacity (GF/IN-2) from 0.01 Hz to 100 Hz, compared to 26 %

(GF/E180) and the slopes of the respective trend lines shown in Figure 4-5. A higher frequency is analogous to a higher strain-rate regime of testing; thus, it is apparent that the epoxy-based composite exhibits greater strain-rate sensitivity than the acrylic-matrix composite.

As an amorphous thermoplastic matrix, the chains within the acrylic matrix are likely able to dissipate the applied energy and subsequently expend it through short-range motion. The rigid nature of the cross-linked chains within the GF/IN-2 reduces the extent to which it can dissipate energy at 25°C. For both materials, there is a time-dependent response because, at higher frequencies, the molecules undergo limited dissipation. Both SF and MF scans showed higher energy dissipation in the case of GF/E180.

4.3.2 Drop-weight impact damage resistance

Using the technique described in Section 4.2 and illustrated in Figure 4-3, the images collated in Figure 4-6.

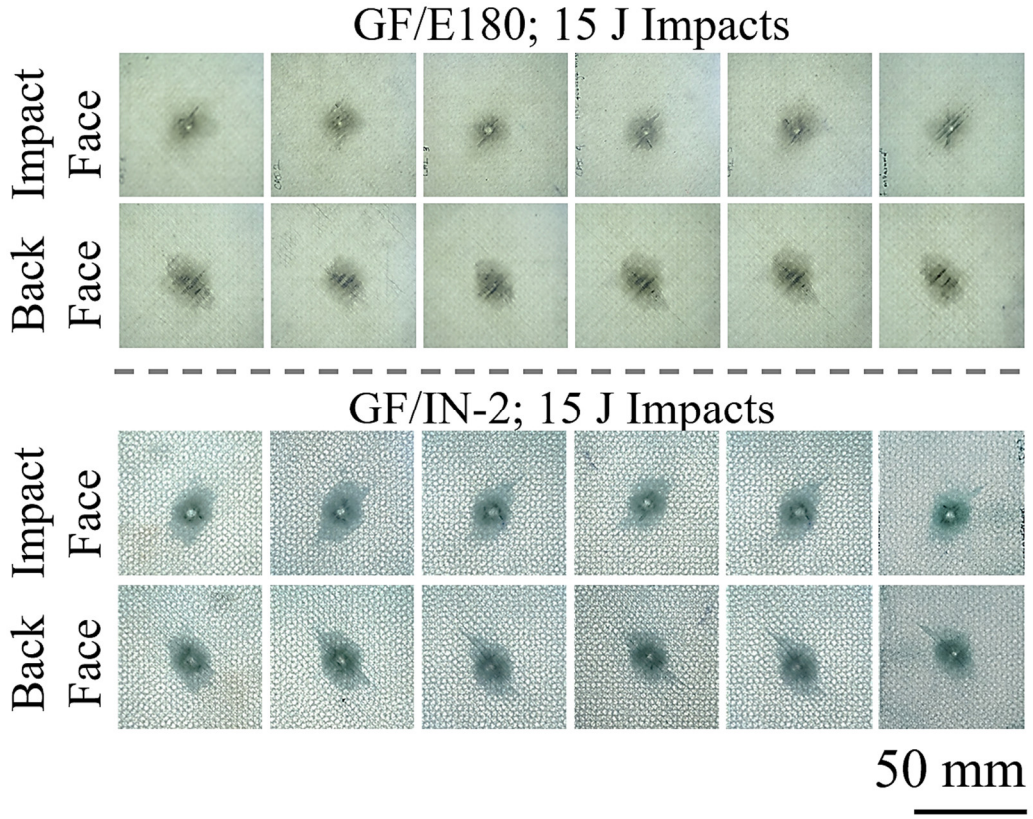


Figure 4-6. Impact and back face images (cropped) showing the damage states of GF/E180 and GF/IN-2 coupons following impact events at 15 J, respectively. The scale bar (50 mm) applies to all images.

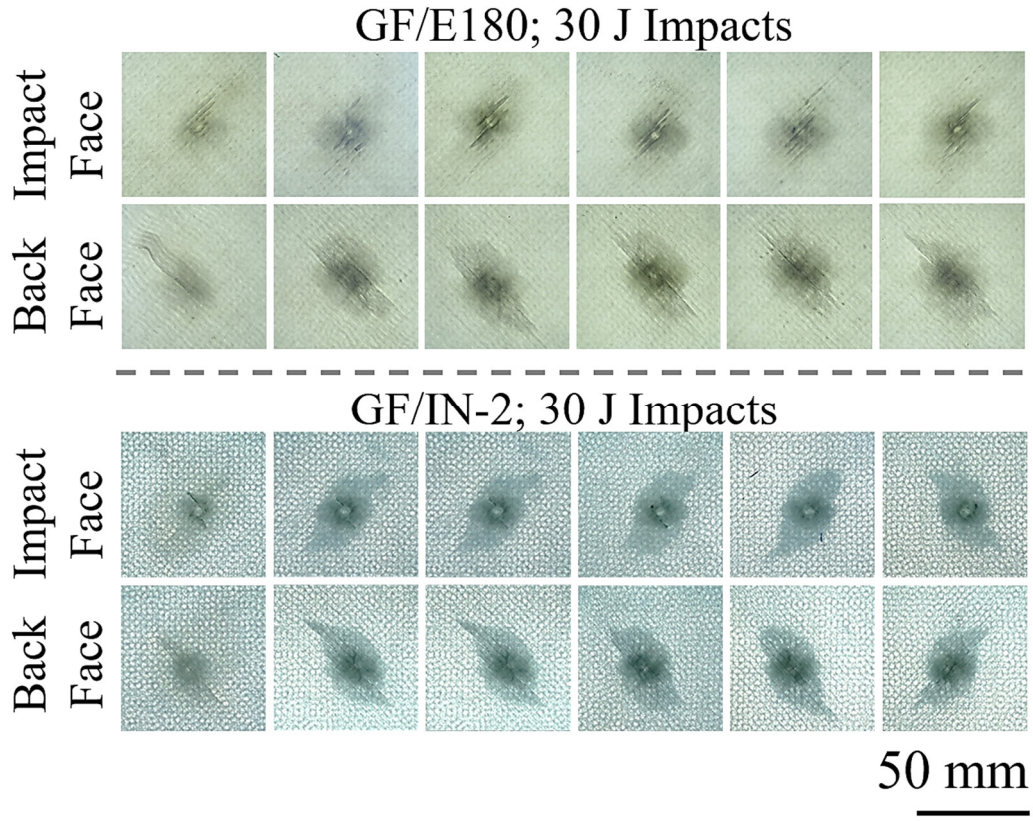


Figure 4-7. Impact and back face images (cropped) showing the damage states of GF/E180 and GF/IN-2 coupons following impact events at 30 J, respectively. The scale bar (50 mm) applies to all images.

Damage areas were assessed as shown in Figure 4-8 with representative images also presented. The damage areas for GF/E180 and GF/IN-2 were measured as 4.4 ± 0.9 % and 3.9 ± 0.3 % for coupons subjected to 15 J impacts, and 7.4 ± 0.5 % and 6.6 ± 0.5 % for 30 J impacts, respectively. Thus, GF/IN-2 was marginally more damage resistant.

The impact performance of FRPs involves a combination of several complex and interrelated processes, which include energy dissipation (elastic deflection and rebound) and absorption (creation of fracture surfaces); the extent of the latter controls the resultant damage processes. From a stress perspective, the inherent anisotropy of laminated FRPs gives rise to two states of stress — namely bending and interlaminar shear [9]. Their interplay results in matrix cracking and interfacial debonding, which ultimately lead to delamination and fibre fracture. As such, matrix toughness, ductility and interfacial strength play significant roles in impact performance.

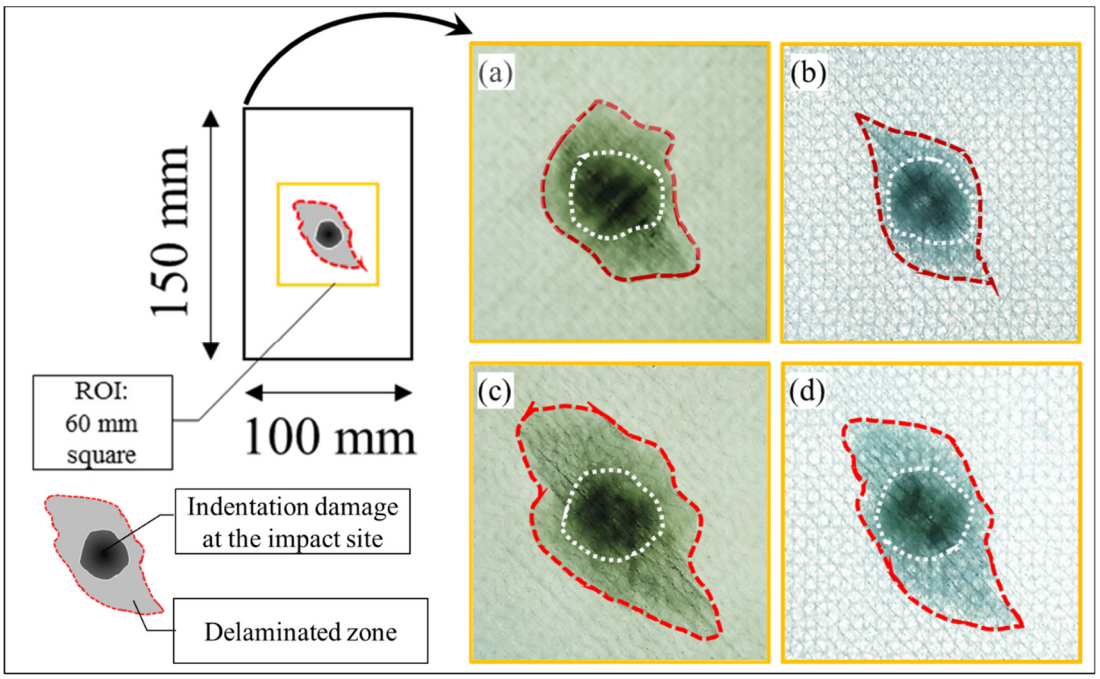


Figure 4-8. Representative damage states for (a) GF/E180 at 15 J, (b) GF/IN-2 at 15 J, (c) GF/E180 at 30 J, and (d) GF/IN-2 at 30 J. ROI: region of interest.

The observations from the viscoelastic study were not reflected in the impact testing. To understand the lack of correlation between the viscoelastic and impact responses of GF/E180 and GF/IN-2, some possible influencing factors are proposed.

Brittle amorphous thermoplastics (BATPs) such as acrylics exhibit microscopic ductility and undergo ductile-to-brittle transition at high strain rates due to strain localisation [1,10]. This microscopic ductility in matrices such as the acrylic under investigation typically does not translate into macroscopic failure behaviour because of their post-yield behaviour. This poor translatability is thought to be due to the formation of crazes normal to the applied stress direction as a result of macroscopic strain softening and limited strain hardening, the latter of which gives rise to low failure strain [1,10]. While crazes are known to be precursors to macroscopic cracks, they typically feature fibrillary bridging, which allows for microscopic plastic drawing. This drawing constitutes the bulk of fracture toughness in BATPs [11]. Additionally, the presence of fibres in BATPs inhibits plastic zone development [12], which induces a triaxial stress state in the matrix and limits the dissipation of energy [13]. Despite being brittle and amorphous, epoxies do not commonly exhibit this post-yield deformation behaviour because their cross-links increase their strain hardening moduli [12,14]. Thus, introducing physical cross-links or a

high degree of entanglement may be an effective way of translating the microductility of acrylics to their macroscopic fracture behaviour.

Even with superior dissipative characteristics, GF/E180 contains an acrylic matrix, which is prone to strain-dependent embrittlement [1] and has low failure strain [10]. Furthermore, a high damping peak does not necessarily predict high impact strength, because the nature of chain deformation occurring within the polymer – i.e., main or side chain ultimately determines how much of a correlation exists between both behaviours [15].

4.4 Conclusions

A comparative study was conducted to evaluate the viscoelastic and impact behaviours of GF/E180 and GF/IN-2. GF/E180 was found to have a higher (~9 %) damping factor and superior (66 %) retention of this property at the highest test frequency of 100 Hz. Improved damping characteristics typically predict impact damage resistance, however, when subjected to 15 and 30 J impact events, GF/E180 was less damage resistant. The observations of this study are in agreement with those of Heijboer [15] on viscoelastic and impact responses of unreinforced acrylic polymer. These findings are important for benchmarking these acrylic resins as a new class of resins for composite applications. Plausible factors associated with the lack of correlation between the viscoelastic behaviour and drop-weight impact responses of the materials under investigation were proposed based on established knowledge from published works, which constitute interesting observations that warrant further investigations to substantiate.

4.5 Implications for subsequent studies

From the findings presented in Section 4.3.1 and conclusions drawn in Section 4.4, it is apparent that the execution of the objectives of the remainder of this work requires the following:

- **An epoxy resin with a more closely matched glass transition temperature.** Although some insights have been gained from the study of these materials, the dissimilar glass transition temperatures would limit their direct comparability.
- **A unidirectional (or quasi-unidirectional) glass fibre reinforcement system with acrylic- or multicompatible sizing.** This is essential to ensure that the epoxy reference material is not preferentially paired with epoxy-sized

reinforcement, which would play a role in interfacial adhesion between the fibre and matrix within unfavourably paired constituents of the acrylic-based composite. The selection of multicompatible-sized reinforcement having reactivity with vinyl groups would be ideal.

- **A vacuum infusion process would be suitable for subsequent laminate fabrication.** However, given the number of laminates the full body of work would require, minimisation of process-related waste is desirable. A simple, yet effective vacuum infusion-based process with minimal usage of consumables and auxiliary materials is preferred. This would ensure that in trying to study a resin system ideally low-moderate ecological impact, the process design maintains the same ecological philosophy.
- The introduction of physical cross-links, high entanglement and chain rigidity into the acrylic matrix may be an effective way to tune macroscopic fracture behaviour.

Chapter References

[1] Wu H, Ma G, Xia Y. Experimental study of tensile properties of PMMA at intermediate strain rate. Mater Lett 2004;58:3681–5. https://doi.org/10.1016/j.matlet.2004.07.022.

[2] Park SA, Jeon H, Kim H, Shin SH, Choy S, Hwang DS, et al. Sustainable and recyclable super engineering thermoplastic from biorenewable monomer. Nat Commun 2019;10:1–11. https://doi.org/10.1038/s41467-019-10582-6.

[3] Summerscales J. MATS347 Composites Design and Manufacture n.d. https://ecm-academics.plymouth.ac.uk/jsummerscales/MATS347/MATS347A1 basics.htm (accessed May 27, 2021).

[4] Kim MW, Song YS, Youn JR. Effects of interfacial adhesion and crystallization on the thermoresistance of poly(lactic acid)/mica composites. Compos Part A Appl Sci Manuf 2010;41:1817–22. https://doi.org/10.1016/j.compositesa.2010.08.016.

[5] Hameed N, Sreekumar PA, Francis B, Yang W, Thomas S. Morphology, dynamic mechanical and thermal studies on poly(styrene-co-acrylonitrile) modified epoxy resin/glass fibre composites. Compos Part A Appl Sci Manuf 2007;38:2422–32. https://doi.org/10.1016/j.compositesa.2007.08.009.

[6] Afaghi-Khatibi A, Mai YW. Characterisation of fibre/matrix interfacial degradation under cyclic fatigue loading using dynamic mechanical analysis. Compos Part A Appl Sci Manuf 2002;33:1585–92. https://doi.org/10.1016/S1359-835X(02)00117-3.

[7] Jang BZ. Advanced Polymer Composites: Principles and Applications (Pdl Handbook Series). n.d.

[8] Ko YS, Forsman WC, Dziemianowicz TS. Carbon fiber-reinforced composites: Effect of fiber surface on polymer properties. Polym Eng Sci 1982;22:805–14. https://doi.org/10.1002/pen.760221304.

[9] Abrate S. Impact Engineering of Composite Structures. vol. 526. Vienna: Springer Vienna; 2011. https://doi.org/10.1007/978-3-7091-0523-8.

[10] van Casteren IA. Control of microstructures to induce ductility in brittle amorphous polymers. Technische Universiteit Einhoven, 2003. https://doi.org/10.6100/IR566897.

[11] Tervoort TA, Govaert LE. Craze-initiation kinetics in polystyrene. J Polym Sci Part B Polym Phys 2004. https://doi.org/10.1002/polb.20093.

[12] Bradley WL. Relationship of Matrix Toughness to Interlaminar Fracture Toughness. In: Friedrich K, editor. Appl. Fract. Mech. to Compos. Mater., Elsevier Science Publishers B.V.; 1989, p. 159–87. https://doi.org/10.1016/B978-0-444-87286-9.50009-7.

[13] De Kok JMM. Deformation, yield and fracture of unidirectional composites in transverse loading. 1. Influence of fibre volume fraction and test-temperature. Technische Universiteit Eindhoven, 1995. https://doi.org/10.6100/IR436701.

[14] Wendlandt M, Tervoort TA, Suter UW. Strain-hardening modulus of cross-linked glassy poly(methyl methacrylate). J Polym Sci Part B Polym Phys 2010. https://doi.org/10.1002/polb.21979.

[15] Heijboer J. Dynamic mechanical properties and impact strength. J Polym Sci Part C Polym 1968. https://doi.org/10.106/0013-7944(72)90066-5.

Chapter 5 Comparative performance of vacuum-infused thermoplastic acrylic- and thermoset epoxy-matrix composites

5.1 Materials and methods

5.1.1 Materials and laminate specifications

The materials under investigation in this study were glass fibre-reinforced acrylic (GF/acrylic) and epoxy (GF/epoxy) laminates, comprising eight plies of non-crimp E-glass fabric (TEST2594-125-50; Ahlstrom-Munksjö). Fibres in 0°- and 90°-directions and PES stitching account for 600, 36 and 10 g/m^2, respectively of the total areal weight of 646 g/m^2. For the GF/acrylic laminate, Elium® 188 O resin (Arkema) was used with BP-50-FT organic peroxide initiator (United Initiators). A two-part epoxy resin system SR 1710/SD 7820 (Sicomin Epoxy Systems), was used for the GF/epoxy laminate. The comparability of glass transition temperature (T_g) of unreinforced matrices was the main selection criterion for the reference epoxy system. It is worth noting that the mixed resin viscosities (as specified by the manufacturers) were dissimilar for both resins. Elium® 188 O had a viscosity of 100 mPa.s at 25°C, whereas the value specified for the epoxy was 450 mPa.s at 30°C. Table 5-1 shows the properties of both resin systems. With the exception of T_g for Elium® 188 O, all values have been sourced from relevant datasheets. Reinforcement with multi-compatible sizing was sourced for this investigation due to the limited availability of specially sized fabrics for acrylics at the time.

Table 5-1. Summary mechanical and thermomechanical properties reported as specified in matrix technical datasheets and relevant publications.

Property	Elium® 188 O [1]	SR1710/SD 7820 [2]
Tensile strength (MPa)	66	78
Tensile modulus (GPa)	3.2	2.8
Elongation at break (%)	2.8	6.2
Flexural strength (MPa)	111	117
Flexural modulus (GPa)	2.9	2.8
Glass transition temperature (°C)	120†	127

†: *value for Elium® 280 sourced from published literature* [3]

5.1.2 Matched-mould vacuum infusion moulding of laminates

Laminates were manufactured using an adjustable-cavity vacuum infusion mould supplied by Composite Integration Figure 5-1. For each processing cycle, square fabric plies measuring 485 mm in length were cut and dried in a convection oven (60°C overnight). For all test laminates, eight plies were carefully assembled into the cavity with a pre-set height of 4 mm; the entire mould surface had been pre-treated with Zyvax® Watershield, a chemical release agent. Following the vacuum-assisted clamping and evacuation of the mould cavity, a 2-minute leak test was performed for a target maximum leak rate of 5 mbar/min. All infusions were performed at room temperature, followed by 24 h at room temperature. The GF/epoxy laminate was subjected to a two-part, freestanding post-cure (8 h at 60°C and 4 h at 100°C). The GF/acrylic laminate did not require post-processing; however, the recommended time of 8 h was extended to 24 h to ensure full polymerisation. The use of the low-viscosity acrylic resin resulted in significantly shorter infusion times (5.5 minutes) than the use of its epoxy counterpart (26.7 minutes).

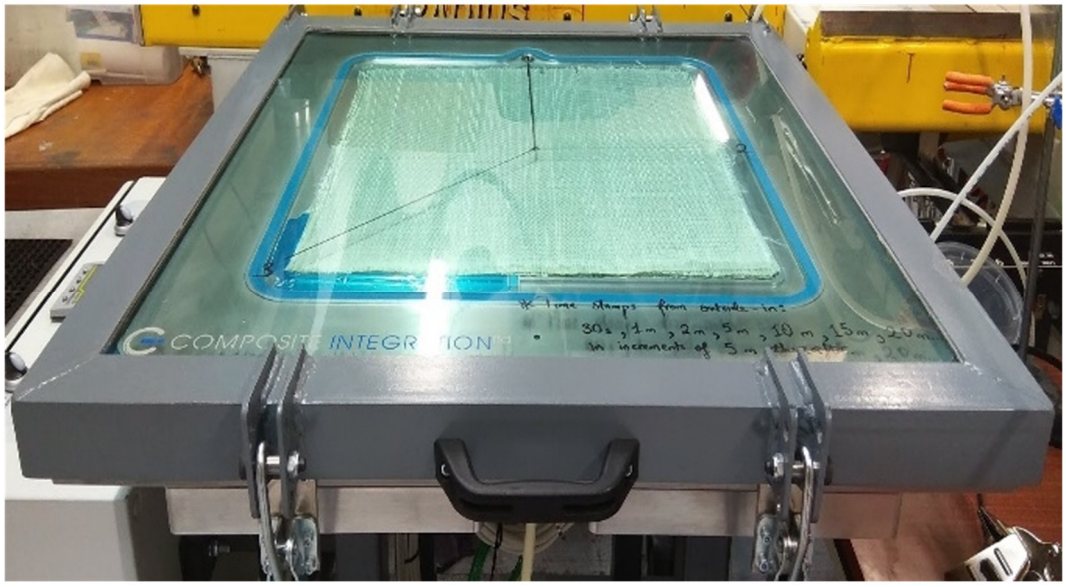


Figure 5-1 Adjustable-cavity vacuum infusion mould supplied by Composite Integration used for the fabrication of test laminates.

A water-lubricated diamond-coated saw blade was used to cut specimens from the fabricated laminates following relevant test standards. Drying was performed in a convection oven at 50°C for 72 h to ensure samples were free of moisture from the cutting process prior to testing. With the exception of transverse tensile and flexural test specimens, longitudinal specimens were utilised for all other test methods.

Table 5-2. Summary mechanical and thermomechanical properties reported as specified in matrix technical datasheets and relevant publications.

	Quasi-unidirectional laminate	Bidirectional laminate
Lay-up	$[0]_8$	$[0/90/90/0]_2$
Average laminate thickness (mm)	*GF/acrylic:* 3.8 ± 0.02	*GF/acrylic:* 3.8 ± 0.09
	GF/epoxy: 3.9 ± 0.03	*GF/epoxy:* 3.9 ± 0.04
Used in Section(s)	5.1.4.1 – 5.1.4.6	5.1.4.7
	5.2.1 – 5.2.6	5.2.7

5.1.3 Evaluation of laminate quality

Fibre volume and void fractions were determined by the matrix burn-off technique (ASTM D3171) to assess the quality of the laminates produced. Fibre volume fractions were the same (49.5 %) in both cases; however, the void contents were 0.4 % and 1.3 % in GF/acrylic and GF/epoxy, respectively. The lower void content in the case of GF/acrylic can be attributed to the low infusion viscosity of the acrylic resin and agrees with observations by Chilali et al. [4].

5.1.4 Mechanical and thermomechanical testing

5.1.4.1 Tensile testing

Transverse tensile testing was conducted in accordance with ASTM D3039. Six samples measuring 250 mm × 25 mm were loaded at 2 mm/min until failure on an MTS Criterion (Model 45) test frame with a 300-kN load cell (*Model/Serial No.: LPS.305/578061; Calibration Certificate No.: E269020119113333*). To prevent slippage between the grip face and specimen ends during testing, 240 grit emery cloths were used at sample ends; hydraulic gripping jaws were used (grip pressure: 60 bar). Using video extensometry (Imetrum UVX & Manta G-146B/G-146C), strains were computed from recorded real-time deformations; all samples were speckled with matt black paint before testing.

5.1.4.2 Flexural testing

The longitudinal and transverse flexural properties (strengths and moduli) of GF/acrylic and GF/epoxy were determined by three-point loading in accordance with ASTM D7264 using a sample span-to-thickness ratio of 32:1, corresponding to sample lengths of 154 mm and a crosshead speed of 1 mm/min. Loading nose and supports were hardened steel pins of 6-mm diameter. Six samples were tested for each material under transverse loading

conditions, whereas five samples were loaded longitudinally from each laminate. Testing was performed on an Instron (3369) test frame fitted with a 10 kN load cell (Instron 2530-10 kN; *Serial No.: 142956; Calibration Certificate No.: E321102820105802*) while Mid-span deflections were tracked and recorded using the video extensometer described in Section 5.1.4.1. Sample edges were speckled with a fine-tip permanent marker to facilitate video extensometry.

5.1.4.3 Short beam shear testing

To evaluate the short beam shear performance of GF/acrylic and GF/epoxy, six coupons measuring 8 mm × 24 mm were loaded to failure by short beam shear testing (in accordance with ASTM D2344). The test frame detailed in Section 5.1.4.1 was used. Testing was performed at a crosshead speed of 1 mm/min. A span-to-thickness ratio of 4:1 was used to ensure samples were subjected to a shear stress state. Cylindrical loading nose and supports were used with diameters of 6 mm and 3 mm, respectively.

5.1.4.4 Mode-I fracture toughness testing

Double cantilever beam (DCB) testing was performed in accordance with ASTM D5528 for the determination of mode-I interlaminar fracture toughness. Testing was performed on the Instron test frame detailed in Section 5.1.4.1. Self-releasing films (13-μm thick perfluoroalkoxy alkane) were implanted at the mid-plane of each laminate during fabrication to create a 63-mm long initiation site for delamination. Samples were carefully cut from the test laminate to maintain the length of the original initiation site and dimensions (175 mm × 25 mm). Steel loading blocks (25 mm × 25 mm × 16 mm) were bonded to the *pre-cracked* sample ends for load introduction and high-contrast speckles were applied as described in Section 5.1.4.1 to sample edges to facilitate automatic tracking of delamination length using a video extensometer (refer to Section 5.1.4.1 for specifications). For each test, loading was performed at a rate of 1 mm/min for a minimum delamination length of 50 mm. Load, opening (crosshead) displacement and delamination length were recorded.

5.1.4.5 Scanning electron microscopy

Scanning electron microscopy was used as a means of qualitatively assessing failure behaviour following short beam shear (SBS) and DCB testing. Samples were prepared with a 40-nm sputter coating of gold to enhance surface conductivity and imaged at 5 kV

on a JEOL JSM series instrument. SBS sample edges were coated; whereas on DCB samples, the coating was applied to exposed interlaminar fracture surfaces (created during testing).

5.1.4.6 Dynamic mechanical analyses

Dynamical mechanical analysis (DMA) was performed in accordance with BS ISO 6721-11 to assess the thermomechanical properties of both materials. The test and specimen specifications are detailed in Table 5-3. Storage and loss moduli, and tan delta were recorded as functions of temperature throughout testing.

Table 5-3. Details of test parameters and specimen dimensions.

Analyser	Q800-V21.1 TA instruments (0800-0786)
Mode	Three-point bending (longitudinal)
Nominal specimen dimensions	60 mm × 10 mm × 4 mm (50-mm span)
Temperature profile	Ambient – 180°C (3°C/min)
Displacement amplitude	50 μm
Frequency	1 Hz

5.1.4.7 Drop-weight impact response

The damage resistance of bidirectional laminate samples of GF/acrylic and GF/epoxy materials were comparatively evaluated using the drop-weight impact following ASTM D7136. Samples measuring 150 $mm_{[0°]}$ × 100 $mm_{[90°]}$ were subjected to impact events at 30 J and 50 J using a drop-weight impact tower instrumented with a load cell and laser sensors for the acquisition of load, displacement and velocity data. The samples were clamped onto a rigid base with an opening per the test standard using toggle clamps with rubber tips. Additionally, a high-speed camera (recording at 4000 frames per second) was used to validate the height to attain the energy levels and to obtain the corresponding impact velocities. The summary of impact test parameters is presented in Table 5-4.

Table 5-4. Details of impact test parameters.

	30 J	50 J
Tower	Rosand Type 5	
Drop heights (m)	1.34	2.33
Velocity (m/s)	5.1	6.6
Mass (kg)	2.28	2.28

Post-impact damage evaluations were conducted using the methodology described in Section 4.2 and depicted in Figure 4-3. The damage areas were obtained as fractions of the total coupon face area as measures of impact damage resistance. Note that for each impact energy level, the target energies were not attained due to losses (frictional, sound, etc.); thus, the incident energies for the respective levels were used for computations instead of the target energies.

Finally, damage index [5,6] and damage degree [7] were computed for each material at both energy levels. Damage index is the ratio of absorbed energy to elastic energy and facilitates a comparison of the post-impact structural integrity in that a higher damage index is indicative of a higher extent of damage. Similarly, the damage degree is the ratio of absorbed energy to incident energy, and also describes the extent of structural damage, where values less than 1 denote rebounding impacts and values greater than 1 imply perforation.

5.1.4.8 Impact damage tolerance (flexure-after-impact)

Given the life-limiting nature of damage resulting from drop-weight impact events, one of the most important parameters to consider in the evaluation of impact performance is damage tolerance. Damage tolerance refers to the structural integrity of a structure after it has sustained damage; as such, it is essential to assessing the post-impact structural efficiency of composites.

Flexure-after-impact (FAI) testing was conducted to assess the damage tolerance of the impacted coupons obtained from the method described in Section 5.1.4.7. Such an approach has been demonstrated to be a suitable alternative to compression-after-impact and is favourable due to the requirement for smaller specimens [8–10]. FAI samples measuring 150 $mm_{[0°]}$ × 45 $mm_{[90°]}$ were carefully sectioned from each GF/acrylic and GF/epoxy impact-damaged coupon as depicted in Figure 5-2. After the cutting process, oven-drying was performed as described in Section 5.1.2 to eliminate surface and entrapped moisture within each sample from lubricant used during the process.

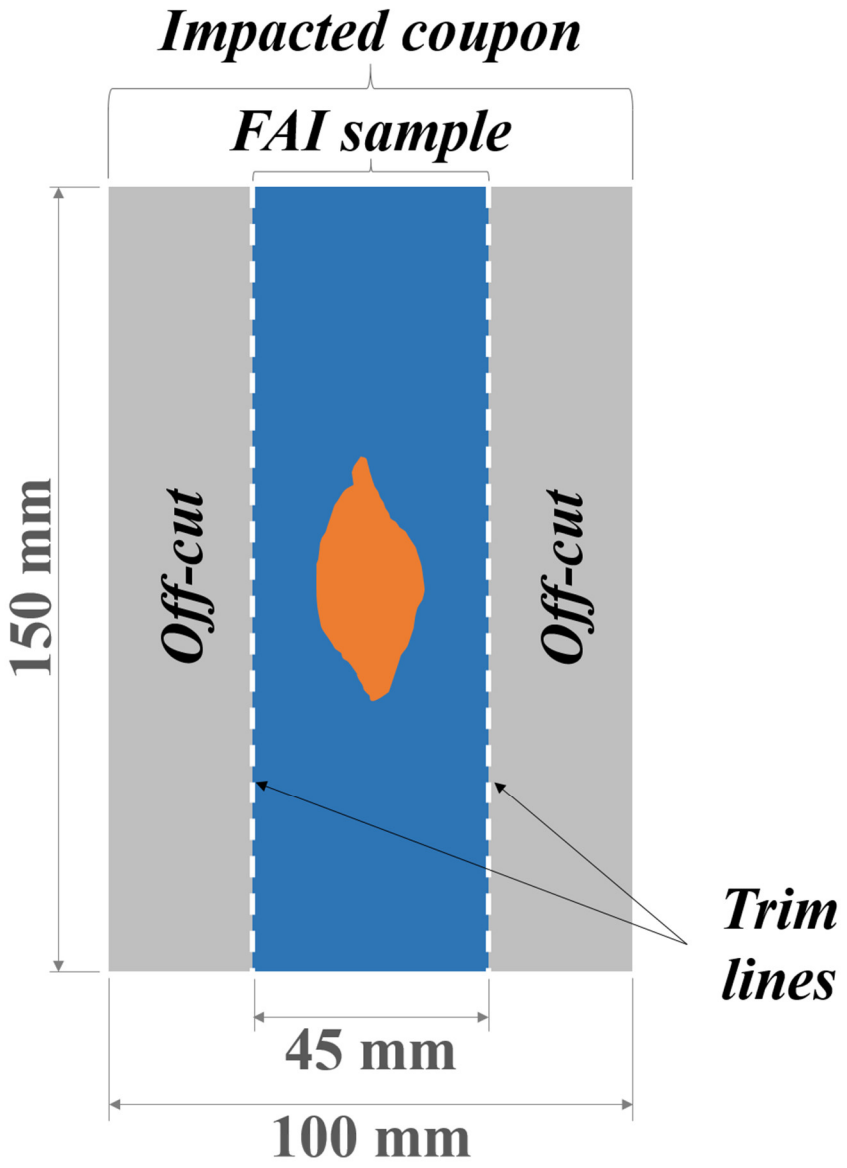


Figure 5-2. Schematic showing FAI coupon extraction from impact-damaged coupons.

All sectioned samples and off-cuts were dried as described in Section 5.1.2 to remove possible traces of moisture from the cutting process. Flexural testing was performed over a support span of 120 mm at a rate of 2 mm/min using the test frame, fixture and configuration described in 5.1.4.2. Sample edges were speckled and imaged as described in Sections 5.1.4.1 and 5.1.4.2 for real-time acquisition of mid-span deflection.

To experimentally determine the undamaged flexural strengths and moduli of both bidirectional fibre-reinforced composites, the off-cuts from the impacted coupons were also speckled and tested in an identical manner using the same span and crosshead speed.

While the use of pristine samples with identical geometry to those described for FAI testing was desirable, this was not possible due to material constraints. The "undamaged" samples were the 25-mm wide off-cuts of the trimming operation shown in Figure 5-2. From a geometry and condition perspective, these samples are not ideal. However, the results obtained from these tests provide vital estimates of the required properties for comparison with residual properties from FAI tests.

5.2 Results and discussions

A summary of the tensile, flexural and short beam shear properties reported and discussed in Sections 5.2.1 to 5.2.4 is presented in Table 5-5.

Table 5-5. Tensile, flexural and shear properties.

		GF/acrylic	GF/epoxy
Tensile Properties (Transverse)	Strength (MPa)	73 ± 3.9	54 ± 4.1
	Modulus (GPa)	13 ± 0.6	13 ± 0.5
	Failure Strain (%)	1.2 ± 0.3	2.1 ± 0.2
Flexural Properties (Longitudinal)	Strength (MPa)	879 ± 49	869 ± 42
	Modulus (GPa)	40 ± 1.7	38 ± 2.3
	Failure Strain (%)	3.3 ± 0.4	3.4 ± 0.6
Flexural Properties (Transverse)	Strength (MPa)	91 ± 5.4	94 ± 7.2
	Modulus (GPa)	11 ± 0.2	12 ± 0.4
	Failure Strain (%)	1.7 ± 0.3	2.0 ± 0.2
Short Beam Shear Properties	Strength (MPa)	58 ± 1.7	57 ± 1.0

5.2.1 Transverse tensile properties

Representative stress-strain responses for GF/acrylic and GF/epoxy are presented in Figure 5-3 and are given in Table 5-5. GF/acrylic exhibited significantly higher average transverse tensile strengths at 73 MPa, compared to 54 MPa for the GF/epoxy specimens. For both materials, strain is observed to increase linearly with increasing applied stress. GF/acrylic samples showed evidence of plastic deformation at strains above 0.4 % and continue to yield gradually until the point of ultimate specimen fracture. In contrast, lower transverse tensile strengths were observed for the GF/epoxy samples, with higher strains observed at failure. GF/epoxy had higher failure strains (2.1 ± 0.2 %) than GF/acrylic (1.2 ± 0.3 %).

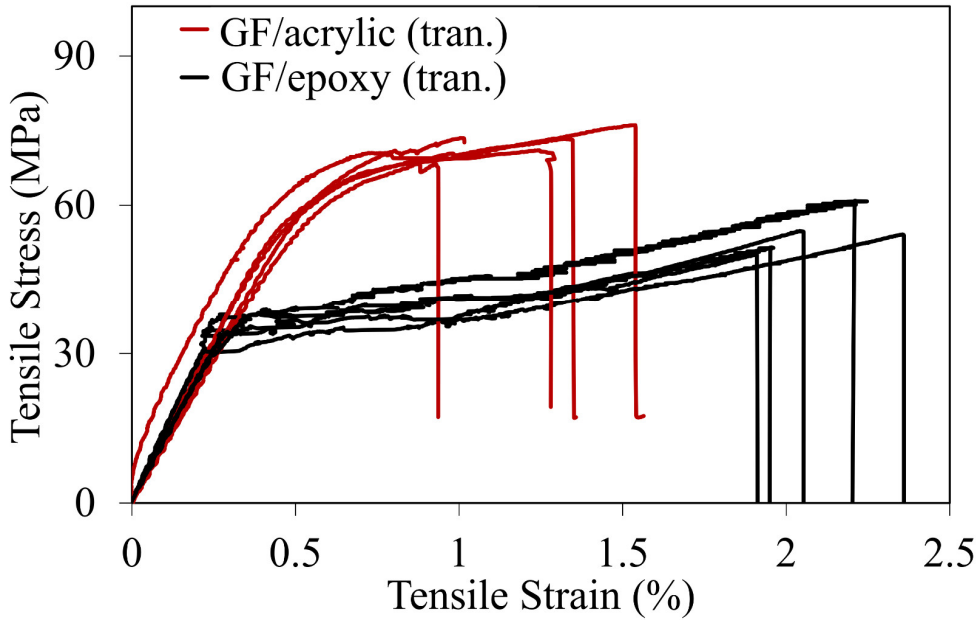


Figure 5-3. Transverse stress-strain behaviour of all GF/acrylic and GF/epoxy samples.

As shown in Figure 5-4, a series of horizontal cracks were observed in all GF/epoxy specimens. In the case of GF/acrylic, only a few cracks were seen to appear before the main failure event. Evidence of fibre-splitting along the loading direction, originating from the sparsely distributed 90°-fibres were only observed in GF/acrylic samples.

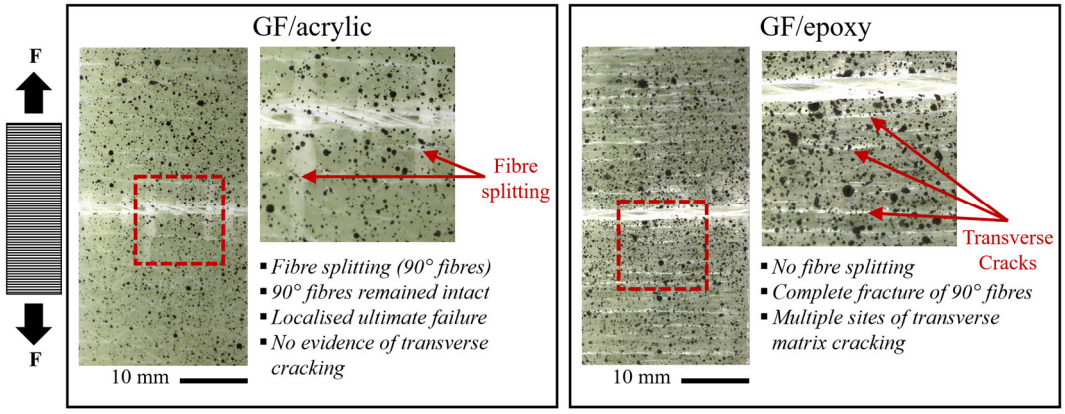


Figure 5-4. Representative failure modes in both materials following transverse tensile testing with loading direction schematically represented.

5.2.2 Longitudinal flexural performance

Figure 5-5 shows representative stress-strain behaviour of the materials under investigation following longitudinal flexural loading to failure.

As previously presented in Table 5-5, GF/acrylic exhibited marginally higher strength (average of 880 MPa) and modulus (average of 40 GPa) compared to averages of 870

MPa and 38 GPa for GF/epoxy, respectively. In addition, up to failure, its stress-strain response was similar to that of GF/epoxy.

From Figure 5-5, a monotonic linear increase in stress exists in both materials up to the limit of proportionality; thereafter, evidence of plastic deformation is seen until the onset of severe compressive failure (Point 1). However, they exhibit dissimilar damage evolution beyond this point. In both materials, ultimate tensile fibre fracture (Point 2) is observed as a discrete and sudden loss in stiffness; however, in GF/acrylic samples, this was preceded by an extended period where marginal stress reductions were observed with increasing strain. This behaviour is indicative of progressive matrix cracking [11]. In the case of the GF/epoxy samples, more sudden load drops and stepped reduction in stress are observed until ultimate failure. The strain window between onset and ultimate failure events, i.e., between Points 1 and 2 was broader (~26 %) in GF/acrylic samples.

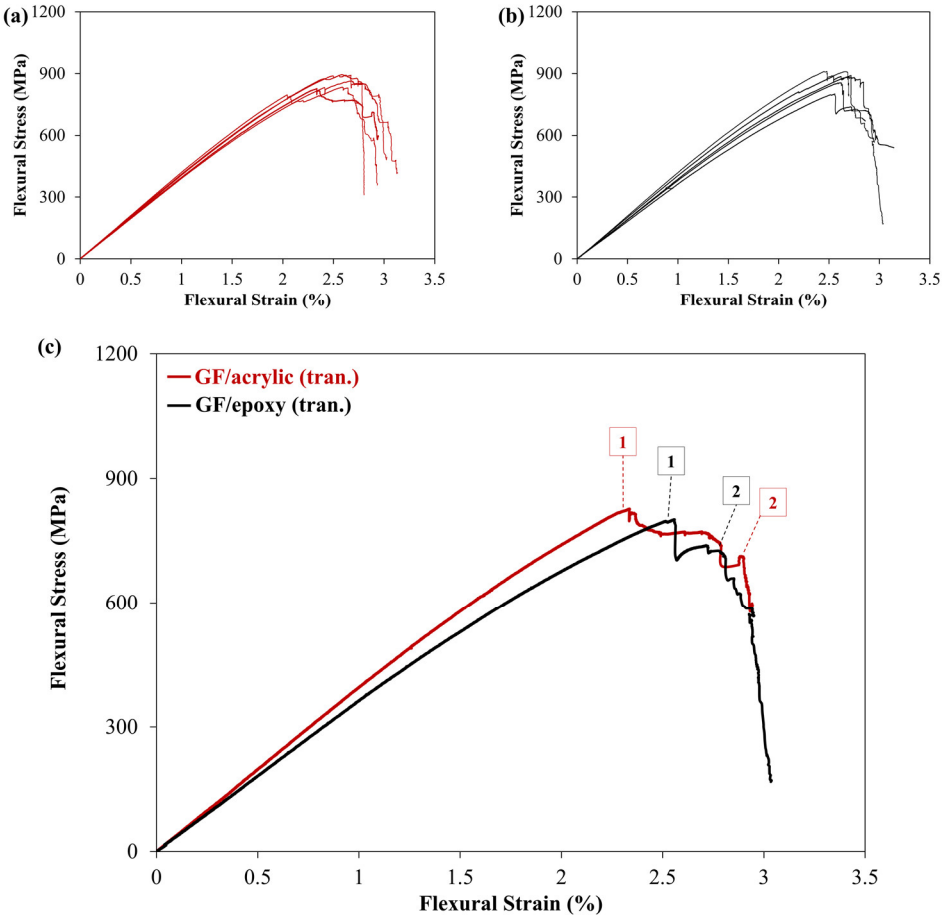


Figure 5-5 Stress-strain curves of (a) GF/acrylic, (b) GF/epoxy and (c) representative curves showing characteristic behaviour of both materials in response to longitudinal flexural loading.

Damage initiation in both materials occurred on the side in compression, with evidence of compressive fibre fractures being observed before tensile fibre fracture. In the case of GF/epoxy samples, tensile matrix damage events coincided with compressive fibre fracture. However, it is worth noting that as these observations were based on edge detection of damage modes, other undetected failure events may have occurred before those reported.

Post-mortem inspections of ultimate compressive, tensile and through-thickness (edge) failure modes were conducted on all samples. Representative images obtained during these inspections are presented in Figure 5-6 Focusing on the damage on the compressive sides (Figure 5-6a & Figure 5-6d) of test samples from both materials, distinct failure types are observed; GF/acrylic samples showed evidence of micro-buckling under the loading nose and severe delamination in tows on outer edges. On the other hand, matrix crushing was more prominent in GF/epoxy, without edge effect as observed with GF/acrylic. A lesser extent of surface buckling was evident. Distinct, ultimate tensile failure modes were also observed in both materials. While all samples showed characteristics of tow separation and delamination, GF/acrylic tows remained mostly intact (Figure 5-6b), whereas GF/epoxy tows suffered more intra-tow matrix cracks and debonding, leading to a shinier appearance (Figure 5-6e). Damage in GF/acrylic was spread over a longer length, while more localised damage occurred in GF/epoxy. Comparing the distribution of damage mechanisms through the thickness as shown in Figure 5-6c and Figure 5-6f, a similar extent of fibre-related damage processes (such as kinking and fracture) were observed in both materials. Although distinct regions of compressive and tensile failure were observed in all samples, GF/acrylic samples showed more *hourglass-shaped* distribution of these regions, with upper and lower regions joining. In contrast, GF/epoxy samples had two discrete upper and lower bounds in the distribution of failure.

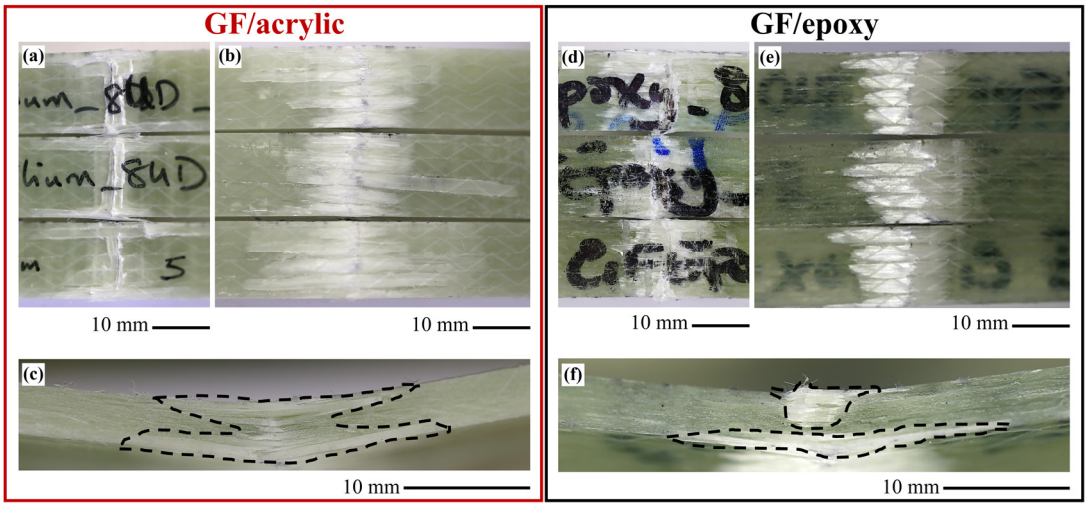


Figure 5-6. Images showing representative modes of (a) compressive failure, (b) tensile failure, on upper and lower surfaces, respectively; and (c) regions of compressive and tensile failure on GF/acrylic sample edges of longitudinal flexure specimens. Note: (d), (e) and (f) are the same features on GF/epoxy samples, respectively.

5.2.3 Transverse flexural performance

Representative stress-strain responses to transverse flexural loading are shown in Figure 5-7 and strengths and moduli were presented in Table 5-5. Despite its superiority in transverse tensile performance as discussed in Section 5.2.1, the GF/acrylic material exhibited marginally lower transverse strength (91 MPa) and modulus (11 GPa). The GF/epoxy material had a strength of 94 MPa and a modulus of 12 GPa. This difference in trends between transverse tensile and flexural properties is believed to the associated with the fact that transverse flexural properties are considerably less sensitive to defect density in the gauge length than transverse tensile properties. Transverse tensile properties are highly susceptible to the distribution of flaws, given the larger volume in the gauge section compared with the transverse flexural test geometry. Consequently, the transverse flexural testing results may more accurately evaluate matrix and interfacial strengths [12,13]

As shown in Figure 5-7, both materials exhibit a short linear elastic region, however, in the case of GF/acrylic; this region is followed by some non-linearity until failure, indicating a higher degree of plastic deformation before failure. Conversely, GF/epoxy samples showed evidence of earlier onset of damage after the initial linear region. In all epoxy-based samples, this region was followed by oscillations in stress-strain response (indicating progressive accumulation of minor damage events) until the occurrence of

ultimate failure. Unlike the longitudinal stress-strain responses where a broader region of linearity was observed (indicating fibre-dominated flexural behaviour), a high extent of non-linearity exists in the transverse stress-strain curves due to the matrix-dominated nature of the failure observed.

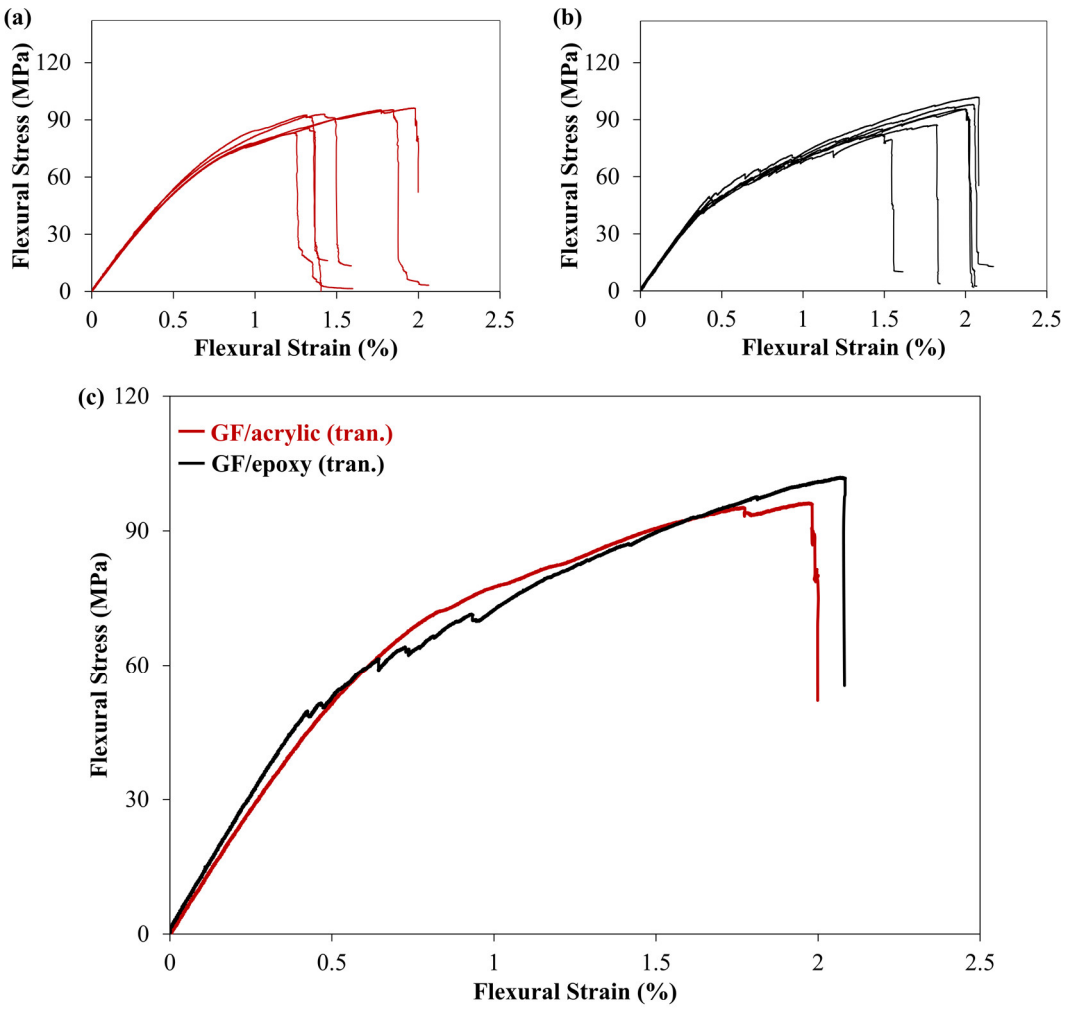


Figure 5-7. Stress-strain curves of (a) GF/acrylic and (b) GF/epoxy and (c) representative curves showing characteristic behaviour of both materials in response to transverse flexural loading.

As shown in Figure 5-8, multiple transverse cracks were observed on GF/Epoxy samples, explaining the oscillations observed in stress-strain behaviour (Figure 5-7) leading to ultimate failure.

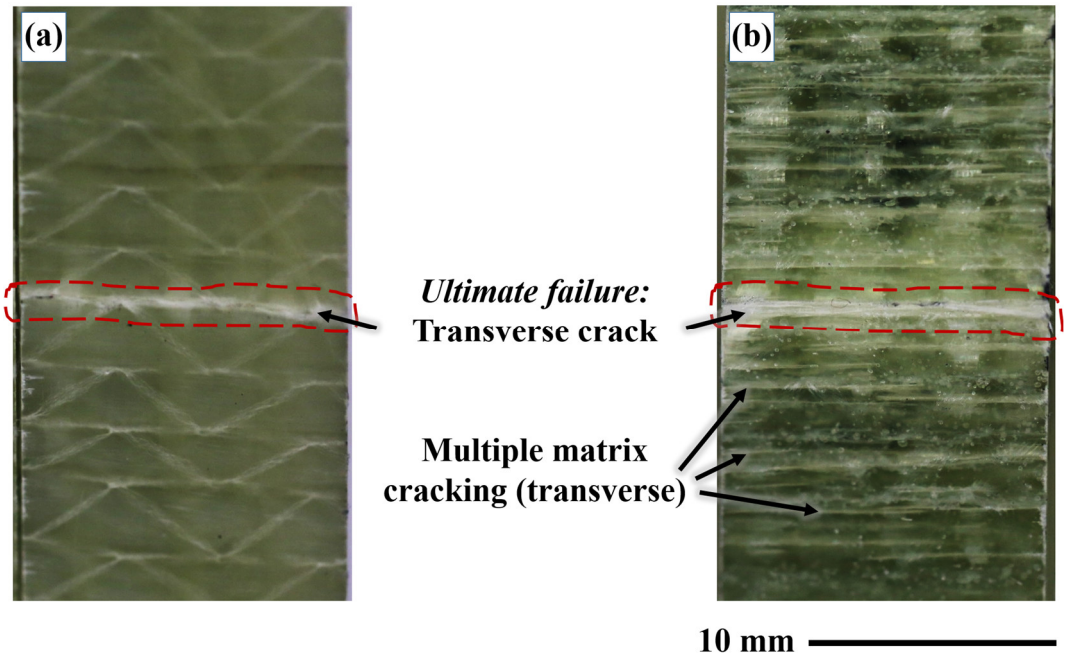


Figure 5-8. Images of representative failures (tensile side) on three samples of (a) GF/acrylic and (b) GF/epoxy following transverse flexural testing.

5.2.4 Short beam shear properties

In this section, the results of short beam shear testing for the determination of short beam shear strengths are presented in Table 5-5 and discussed. GF/acrylic had comparable shear strength (58 MPa) with GF/epoxy (57 MPa). Figure 5-9 shows all load-displacement curves for both materials.

Load-displacement curves reveal similar pre-peak behaviour in both materials. A linear region is observed for all samples and is followed by some nonlinear deformation before peak load. Beyond this point, GF/acrylic samples did not exhibit abrupt load drops; their curves revealed evidence of severe inelastic deformation with localised stable crack propagation. In contrast, a more noticeable onset of failure is observed in GF/epoxy samples as load drops of about 20-30 % from respective load peaks. Larger areas are bounded by the GF/acrylic curves than those observed under GF/epoxy curves, indicating higher energy absorption. It can thus be assumed that more fracture energy was available within GF/acrylic samples.

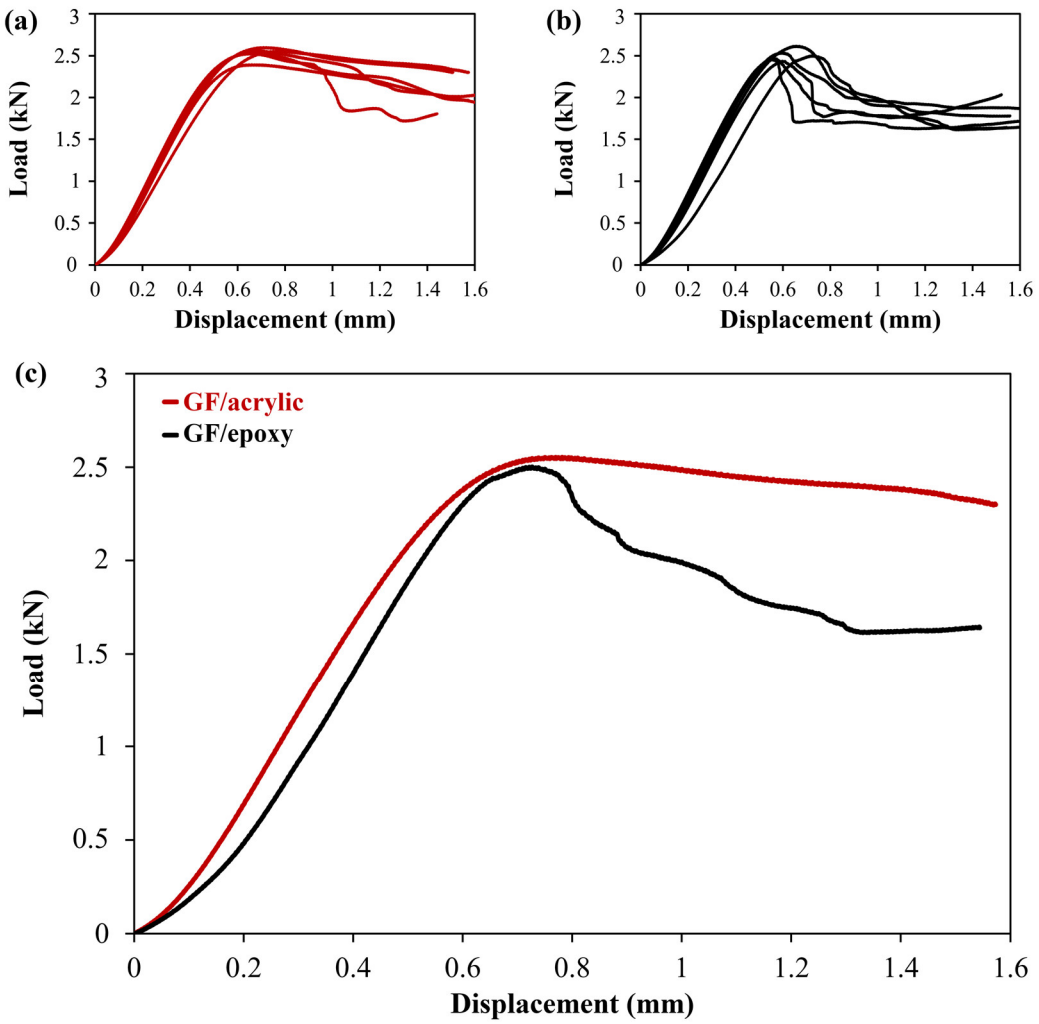


Figure 5-9. Load-displacement curves obtained from short beam shear tests for all (a) GF/acrylic and (b) GF/epoxy samples and (c) a comparison of two representative curves from both materials.

Post-mortem SEM inspections on edges of failed specimens were conducted to substantiate observed load-displacement behaviour. As shown in Figure 5-10, evidence of interlaminar shear and plastic deformation are visible in GF/acrylic, with ductile fracture characteristics observed.

The damage characteristics of GF/epoxy shown in Figure 5-11 are consistent with interlaminar shear failure; brittle shear cusps [14] were present, with no plasticity being observed. Both materials had multiple cracks uniformly dispersed throughout the thickness. All cracks observed in the GF/epoxy sample were near 90° fibres, which were dispersed throughout each ply. In contrast, cracks in GF/acrylic did not occur around these fibres. The observation of more delamination in GF/acrylic than GF/epoxy is in

agreement with the assumptions made from the load-displacement curves in terms of fracture energy absorption.

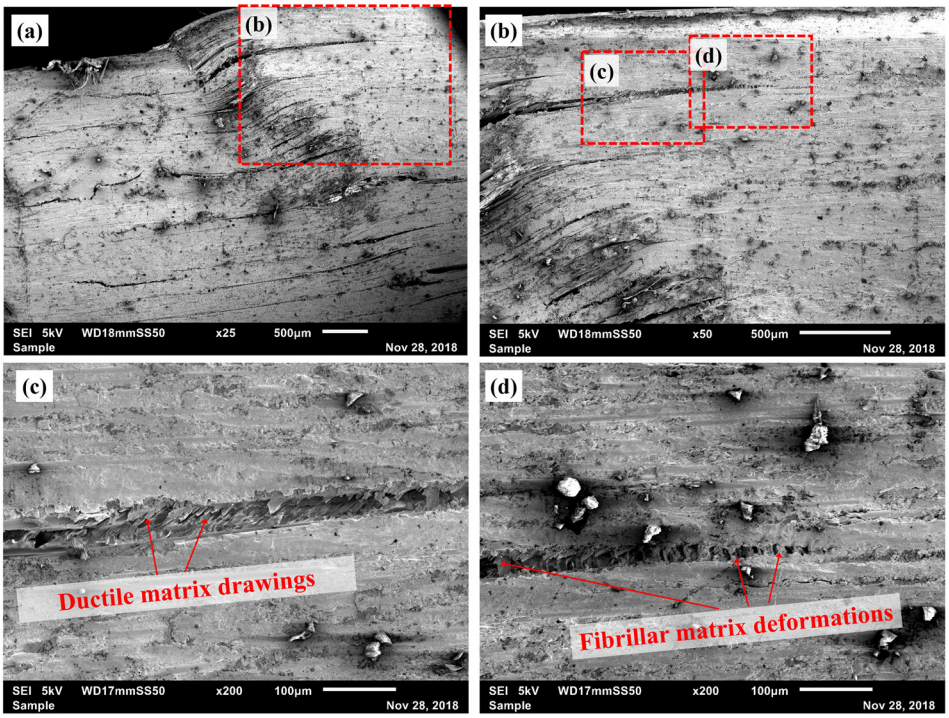


Figure 5-10. SEM micrographs showing representative GF/acrylic short beam shear failure modes at magnifications of 25× in (a), 50× in (b), and 200× in (c) and (d).

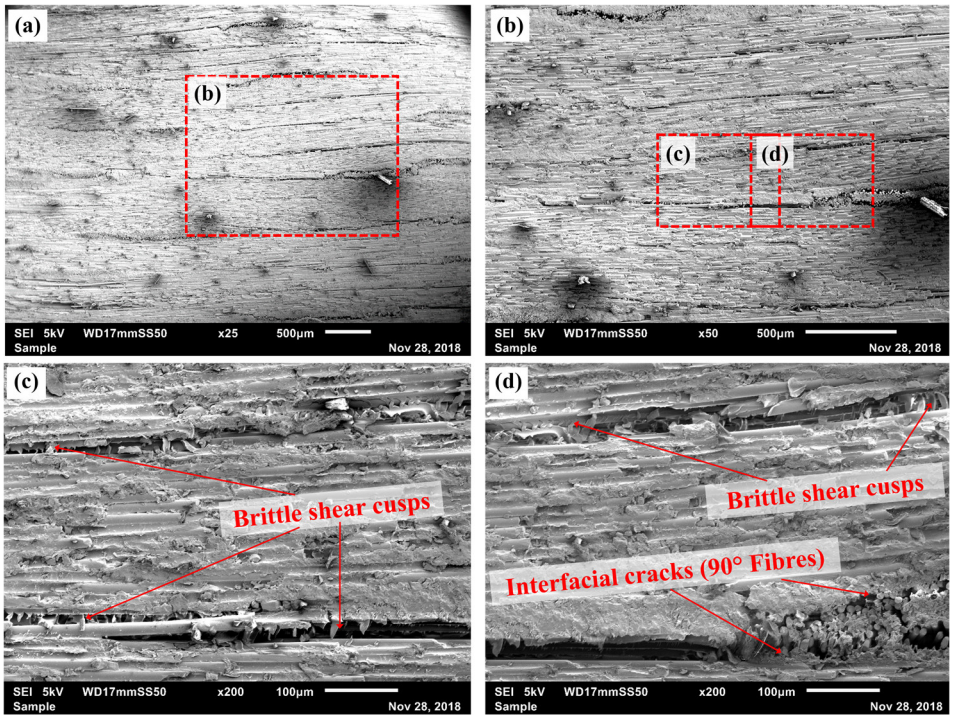


Figure 5-11. SEM micrographs showing representative GF/epoxy short beam shear failure modes at magnifications of 25× in (a), 50× in (b), and 200× in (c) and (d).

5.2.5 Interlaminar fracture toughness test results

It has been shown in preceding sections that GF/acrylic significantly outperforms GF/epoxy in terms of transverse tensile strength while exhibiting similar interlaminar short beam shear and flexural properties (in both longitudinal and transverse directions). This section discusses the observations from double cantilever beam fracture testing. The mode-I fracture toughness values reported here are average strain energies released during initiation ($G_{IC\text{-}Init.}$) and propagation ($G_{IC\text{-}Prop.}$), calculated using the modified beam theory method as per the test standard, with the onset of non-linearity being used to evaluate the former.

GF/acrylic exhibited superior mode-I fracture toughness, with a mean $G_{IC\text{-}Prop.}$ of 1814 J/m^2 compared to the value of 1574 J/m^2 for GF/epoxy, with 19 % higher initiation fracture toughness than GF/epoxy. Representative load-displacement curves, R-curves and comparisons of mean initiation and propagation toughness values are presented in Figure 5-12.

All samples exhibited an initial non-linearity during the *take-up* portion of load introduction and simultaneous opening of the specimen before crack initiation. Following this, a monotonic increase in load was observed before delamination initiation. A minor pre-peak load-drop is evident in both materials. Upon initiation, the load-displacement curves of both materials revealed minor oscillations and load-drops, which are consistent with stick-slip delamination behaviour and are indicative of unstable propagation [15,16].

From Figure 5-13, a greater extent of fibre bridging (at the crack tip) is observed in GF/acrylic (Figure 5-13a) than in GF/epoxy (Figure 5-13b). Moreover, crack bridging occurred throughout testing due to the presence of 90° tows in the fabric used.

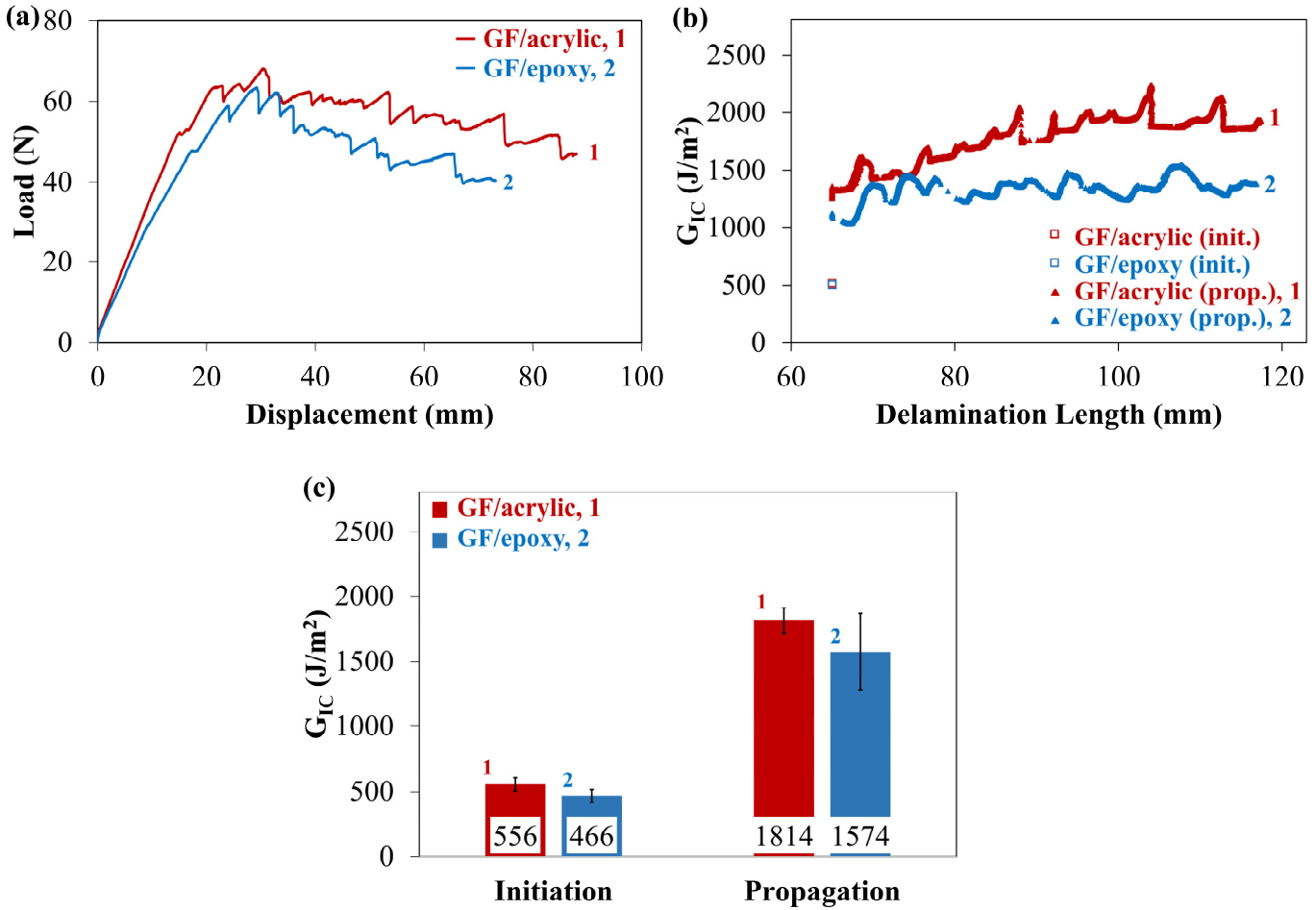


Figure 5-12. Representative (a) load-displacement curves and (b) resistance curves (R-curves) obtained from DCB testing of GF/acrylic and GF/epoxy, and (c) is a chart comparing their average $G_{IC\text{-}Init.}$ and $G_{IC\text{-}Prop.}$ values.

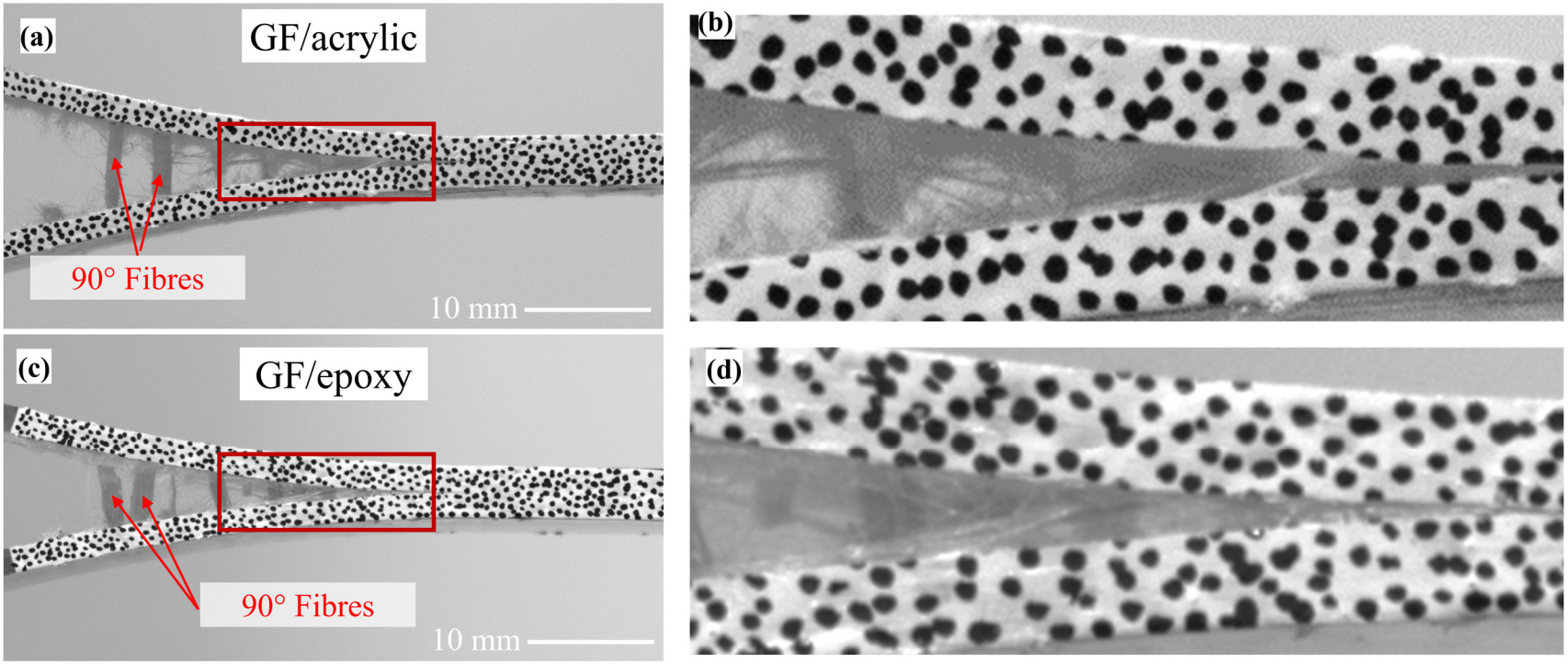


Figure 5-13 Images of representative delamination behaviour observed during DCB testing of (a)-(b) GF/acrylic and (c)-(d) GF/epoxy at equivalent test times. The relative extents of fibre bridging are evident.

This was evident in both materials and occurred throughout testing; as such, the load-displacement curves (Figure 5-12a) and the R-curves (Figure 5-12b) are not representative of purely unidirectional specimens. It is highly likely that some of the load drops and the evolution of mode-I fracture resistance with increasing crack length correspond to secondary energy-dissipation processes such as tow rupture and debonding events [16]. However, as the same reinforcement was used in both materials, the associated effects on the comparability of these materials are considered negligible. As is evident in Figure 5-12b, the delamination resistance of GF/acrylic increases with increasing crack growth, whereas that of GF/epoxy remains relatively constant. The increase in delamination resistance in the GF/acrylic material may be attributed to inelastic matrix deformation and the aforementioned higher extent of fibre bridging. The latter may be due to superiority in adhesion at the fibre-matrix interface; however, micrographic inspections of each material's faying surfaces were conducted to gain further insights.

Complementary scanning electron micrographic inspections of fracture surfaces (Figure 5-14); however, distinct failure modes are visible in both materials. The presence of ductile matrix deformation on the GF/acrylic fracture surface indicated ductile matrix fracture, providing evidence for the increase in resistance observed on the R-curve for GF/acrylic samples. Besides, only cusps, mirror zones and hackle zones were observed in GF/epoxy, which are characteristics of brittle matrix fracture. These micrographic observations are consistent with those from short beam test specimens in the context of ductile and brittle matrix fracture characteristics. Moreover, an exceptional level of fibre-matrix adhesion was observed in GF/acrylic (Figure 5-14a) compared with its epoxy counterpart (Figure 5-14b), providing evidence to support the previously proposed mechanisms for increased resistance with increasing crack length observed for this material. This observation also explains the superiority in transverse tensile strength in the GF/acrylic material and confirms that the use of fabric with multi-compatible sizing resulted in a desirable strong interfacial adhesion. In addition, matrix fractures observed in GF/acrylic were distinctly duller in appearance and seemed to have a rougher texture, further confirming ductile behaviour at a microscopic scale. All epoxy matrix fractures had brittle characteristics (i.e., exhibited sheen and smoothness).

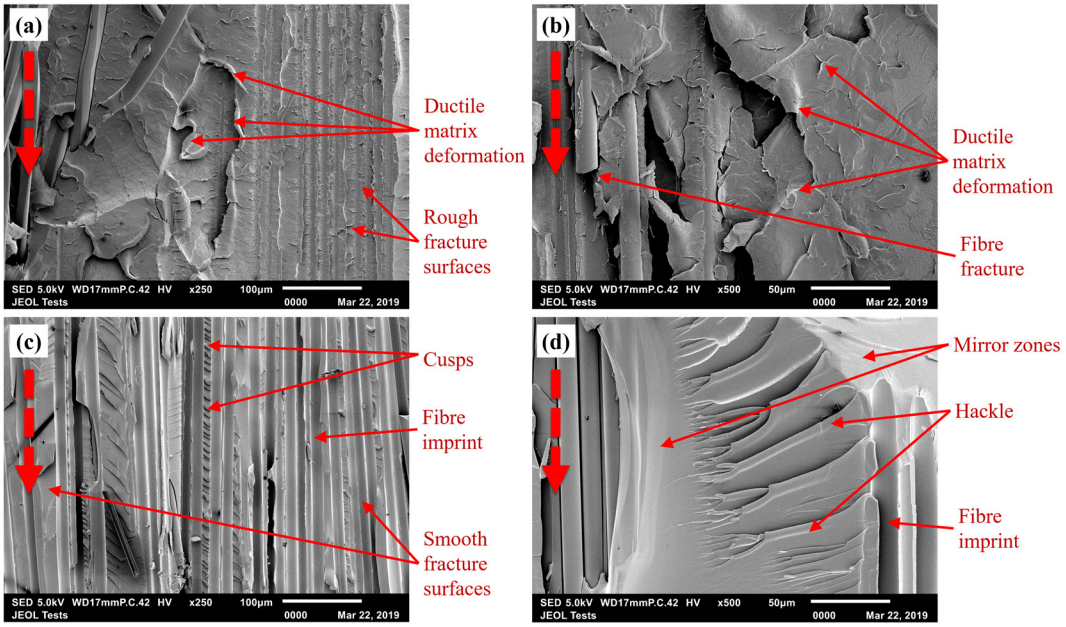


Figure 5-14. SEM micrographs of mode-I fracture surfaces of GF/acrylic (a-b) and GF/epoxy (c-d).

5.2.6 Dynamic mechanical analyses

The viscoelastic responses of both materials with temperature are shown in Figure 5-15 The section that follows discusses differences in tan delta and storage modulus for both materials in the context of damping behaviour associated with each matrix type.

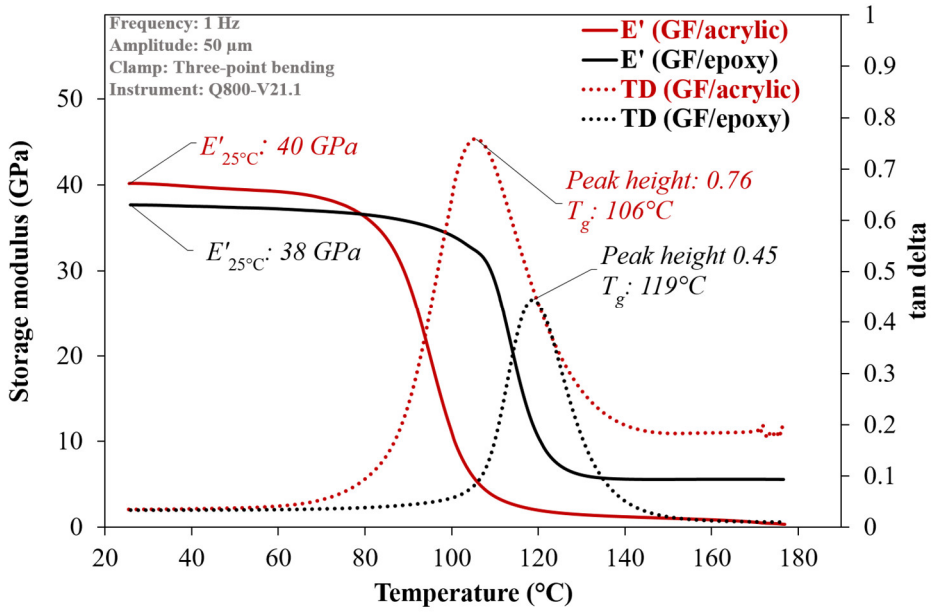


Figure 5-15. Thermomechanical results showing the effect of temperature on storage modulus and tan delta in DMA testing. Testing carried out in the longitudinal direction.

The thermomechanical properties of GF/acrylic and GF/epoxy obtained from the DMA experiments are presented in Table 5-6.

Table 5-6. Summary of thermomechanical results.

	T_g, tan delta (°C)	Height of tan delta peak	Storage modulus at onset (GPa)
GF/acrylic	106	0.76	40
GF/epoxy	119	0.45	38

GF/acrylic was found to exhibit superior damping behaviour, as evidenced by the higher tan delta peak and the larger area under this peak, compared to GF/epoxy. The term "damping" here is used to indicate the energy dissipative efficiency of the materials [17,18]. The area bounded under the tan delta curve is proportional to the degree of molecular mobility, which in turn correlates to damping properties [19,20]. Thus, having higher peak intensity and larger area under its tan delta curve, GF/acrylic exhibits better damping behaviour. Being a thermoplastic amorphous polymer, i.e., possessing no crosslinks, the polymer chains in GF/acrylic can undergo instantaneous short-range deformation to dissipate the applied stresses. Conversely, the cross-linked 3D-network structure of the matrix in GF/epoxy inhibits deformations of the same magnitude as observed in GF/acrylic. The effects of cross-links on the height of tan delta peaks have been previously studied by Bandzierz et al. [21]. These results indicate that GF/acrylic would tend towards highly inelastic response, whereas elastic response dominates in GF/epoxy.

5.2.7 Drop-weight impact response

5.2.7.1 Damage resistance

Figure 5-16 shows representative curves obtained from samples of each bidirectional laminate following impacts at 30 J and 50 J. All GF/acrylic and GF/epoxy samples exhibited comparable force-deflection behaviour with slight variations in the maximum contact forces and deflections between the materials within the respective energy levels. During an impact event, the impact striker's kinetic energy is converted to elastic energy within the target (or coupon), with some portion of energy also absorbed in the creation of damage. As a result of this conversion, contact force increases rapidly until the striker arrests at a maximum force value. Depending on the proportion of elastically stored

energy available, the impact striker may rebound or perforate the coupon if most of the energy is absorbed in the creation of damage. The shape of the force-displacement curve, i.e., opened or closed loops are indicative of the post-contact travel behaviour of the striker relative to the coupon. An opened loop signifies perforation of the coupon by the striker, whereas, a closed loop provides evidence for striker rebound [22]. This can be seen for each material (and at both energy levels), where the contact force increases with deflection up to a peak value and then progressively decreases back to zero as the impactor rebounds. Thus, all impact events yielded non-perforative damage mechanisms.

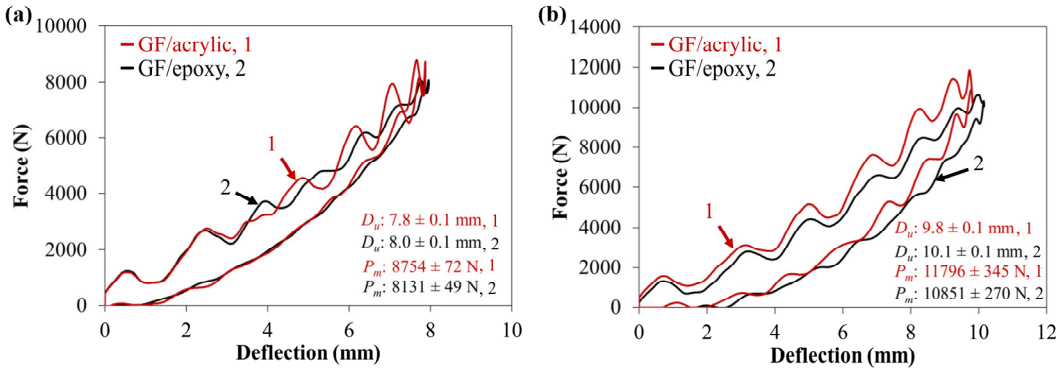


Figure 5-16. Representative force-displacement curves for GF/epoxy and GF/acrylic samples subjected to (a) 30 J and (b) 50 J.

The wave-like signature observed on the force-deflection curves presented in Figure 5-16a and Figure 5-16b of all samples were likely induced by frictional effects [6]. These undulations prohibited the precise determination of stiffness and dynamic modulus as slopes of the pre-peak portion of these curves [22]. However, it is evident that for both 30 J and 50 J impact events, the GF/acrylic material exhibits relatively higher stiffness and dynamic modulus.

Furthermore, results such as those shown in Figure 5-16 revealed that impacts at 30 J and 50 J were associated with higher (7.7 % and 8.7 %) peak contact forces in the GF/acrylic material, and lower (2.5 % and 3 %) maximum deflections than in the GF/epoxy reference material, respectively. Higher impact loads in the GF/acrylic coupons provide evidence of superior pre-damage load-bearing capacity than in its thermoset-based counterpart. The lower ultimate deflection suggests inferior ductility in the acrylic-matrix composite relative to the epoxy-based material. However, overall, there exists minor comparability in the ultimate deflections for both composite materials, as only marginal differences exist between them. The curves for both materials (at both energy levels)

showed no evidence of major damage development, which typically results in a significant load-drop and change in deflection between the peak load and ultimate deflection of the coupons [22]. Rather, relatively smooth post-peak transitions occur between these points during testing.

It is apparent that from the corresponding energy-time curves for both materials at 30 J (Figure 5-17a) and 50 J (Figure 5-17b) that absorbed energies (and consequently, elastic energies) are comparable between both material systems. This comparability holds for both energy levels. Thus, it would appear within both composite systems, a similar extent of energy is absorbed (for damage development) and dissipated (elastically).

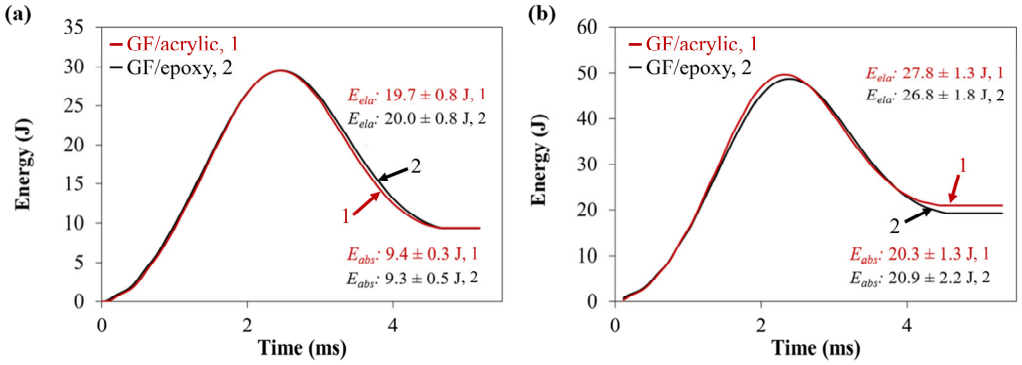


Figure 5-17. Representative energy-time curves for GF/epoxy and GF/acrylic samples subjected to (a) 30 J and (b) 50 J.

The backlit images of all coupons subjected to 30 J impacts are shown in Figure 5-18a and Figure 5-18b. These images revealed a near-rhomboidal damage shape for all coupons. The representative macroscopic images of impact face and back face damage states for each material after 30 J impacts are presented in Figure 5-18c and Figure 5-18d, respectively. From these images, striker indentation and longitudinal matrix cracking are evident as common damage mechanisms on the impact face. However, GF/epoxy samples exhibited an additional mechanism in form of extensive fibre tow splitting (Figure 5-18c). This may be associated with the differences in matrix ductility as observed in Section 5.2.5. However, evidence from force-displacement curves in terms of the lower ultimate deflection of the GF/acrylic coupons suggests it exhibits relatively lower matrix ductility. Thus, it is plausible that the acrylic matrix only possesses superior microstructural ductility compared to the epoxy matrix, which does not effectively translate to macroscopic failure behaviour [23,24].

Furthermore, while both materials exhibited extensive delamination as the predominant mechanism observable on the back face, longitudinal matrix cracking (Figure 5-18c) was also observed for epoxy-based coupons. Such matrix cracks have been reported to be brittle matrix behaviour in previous works [25,26].

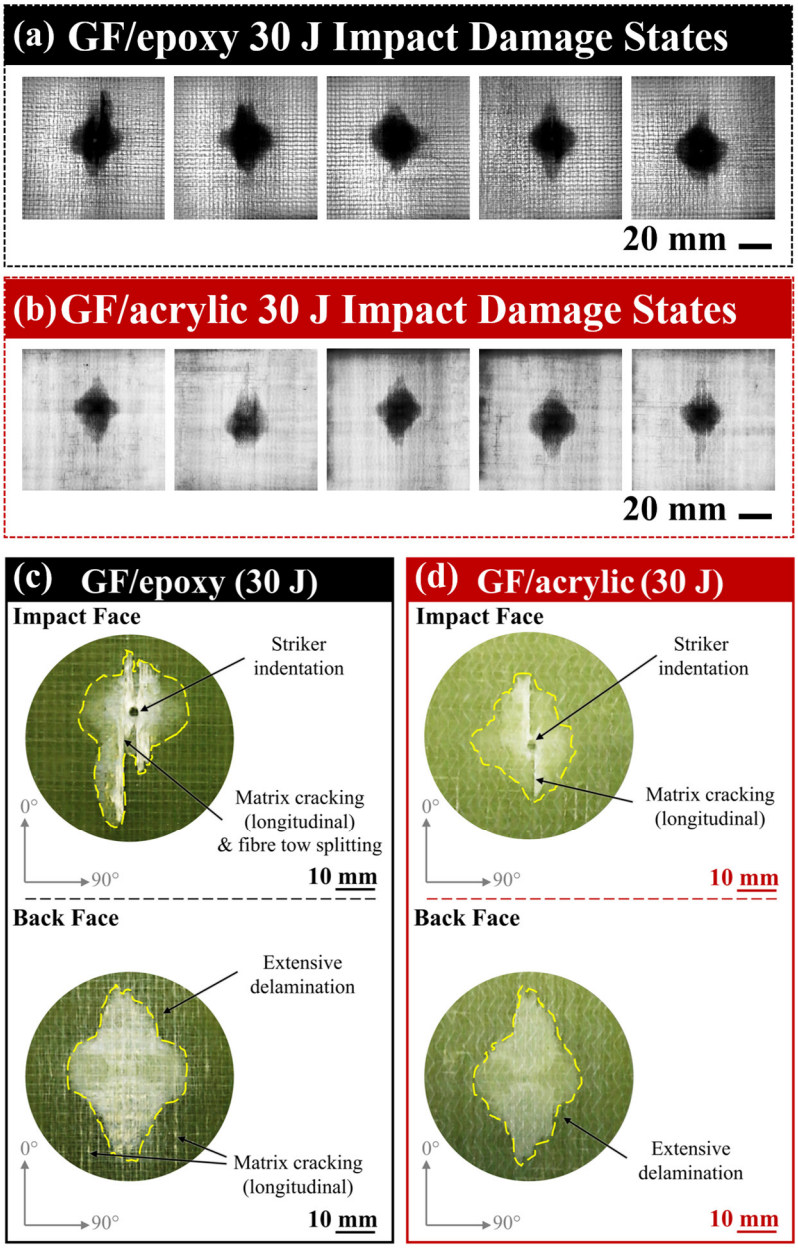


Figure 5-18. (a) & (b) Back-lit images of impact-damaged samples, and representative (c) & (d) macroscopic images of samples of GF/epoxy and GF/acrylic following impact events at 30 J, respectively.

Similar observations were also made for the 50 J impact damage states, which are presented in Figure 5-19. Beginning with Figure 5-19a and Figure 5-19b, the damage

shapes revealed by back-light imaging for the 50 J impacts was also consistent with the characteristic rhomboidal damaged areas observed for 30 J impacts.

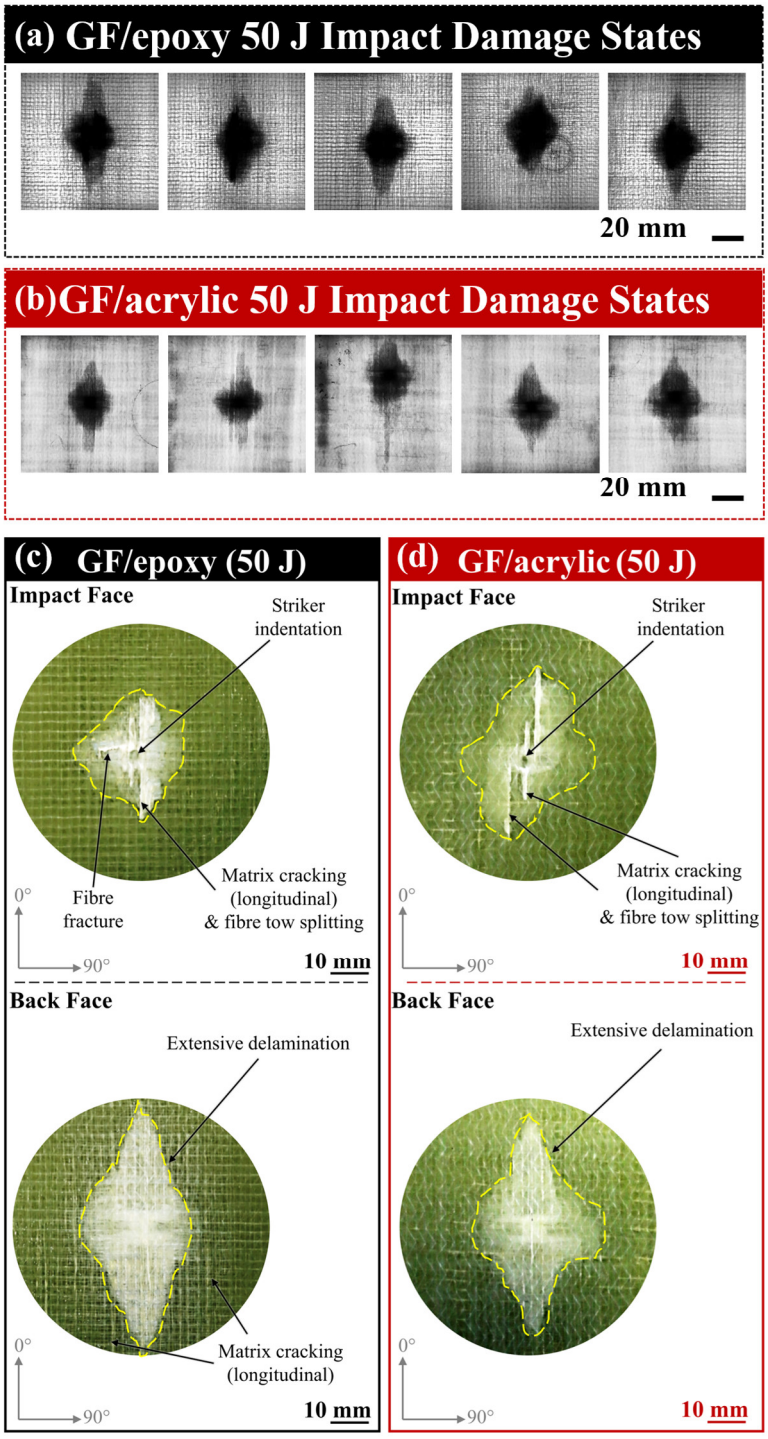


Figure 5-19. (a) & (b) Back-lit images of impact-damaged samples, and representative (c) & (d) macroscopic images of samples of GF/epoxy and GF/acrylic following impact events at 50 J, respectively.

However, macroscopic images shown in Figure 5-19 revealed that the higher impact energy facilitated the creation of more severe damage mechanisms in both materials. On

the impact face, the additional energy results in fibre fracture and tow splitting in the GF/epoxy and GF/acrylic coupons, respectively. These new damage mechanisms were observed in addition to those previously reported for the 30 J impacts on these materials.

In terms of impact damage resistance, the back-lit images of the coupons shown in Figure 5-18 and Figure 5-19 were used to compute the damaged area fractions presented in Figure 5-20 for the respective materials and impact energy levels. Damaged area fractions were computed with respect to the total coupon face area and are not representative of full damaged volumes.

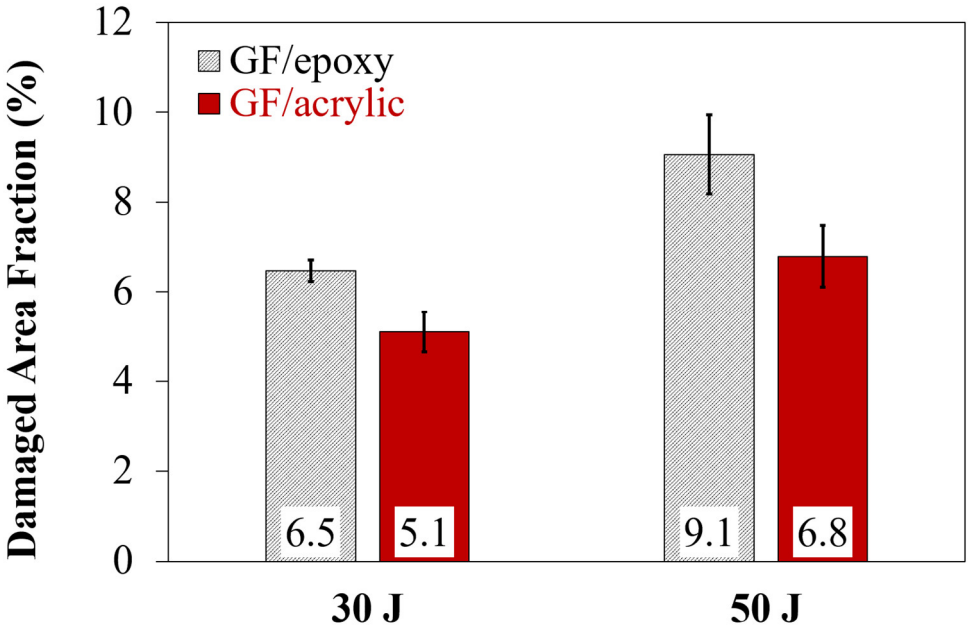


Figure 5-20. Damaged area fractions as functions of impact energy.

The GF/acrylic material presented 22 % and 25 % lower damage areas in response to 30-J and 50-J impacts, respectively. Additionally, a 20-J increase in impact energy produced a 33 % increase in damage area in the GF/acrylic material, compared to a 40 % increase in its GF/epoxy counterpart. Combined with the lower damage area at the respective energy levels, this lower change in damage area with increasing energy in the GF/acrylic composite provides strong evidence of superior impact damage resistance and lesser sensitivity to impact energy in terms of its damage resistance. This is in agreement with the findings discussed in Section 4.3.1, where the multi-frequency dynamic thermal analysis results in Figure 4-5 highlighted a greater strain-rate sensitivity in the epoxy-based composite than its acrylic-matrix composite. However, acrylics are known to be highly

susceptible to high strain rate embrittlement [27], so these results also suggest that the conditions employed in this present body of work are below the strain rate regime where the sensitivity is most prominent.

Furthermore, in light of the similar absorbed energies reported for both materials, these results suggest that other damage mechanism may be present within the GF/acrylic samples, which were not detectable by the damage assessment techniques employed in this study. While damage area determination facilitates the evaluation of in-plane damage mechanisms (with respect to the coupon face) such as delamination, other mechanisms such as matrix cracking, interfacial debonding, and fibre-related damage such as pull-out and fracture may not be readily detected in this way. Furthermore, given the bidirectional architecture of the reinforcement used, it is worth noting that both longitudinal and transverse fractures in these materials would cause the same degree of discrepancy between the measured damaged areas and energy absorption.

Corresponding damage degrees and indices were calculated for both materials at the two energy levels to explore differences in energy absorption that may provide vital insights into underlying mechanisms. These parameters and all other properties discussed in this section have been summarised for enhanced comparability in Table 5-7.

Table 5-7. Summary of comparative impact properties of GF/epoxy and GF/acrylic samples.

Evaluated properties	*30 J*		*50 J*	
	GF/epoxy	*GF/acrylic*	*GF/epoxy*	*GF/acrylic*
Peak load (N)	8131 ± 49	8754 ± 72	10851 ± 270	11796 ± 345
Ultimate deflection (mm)	8.0 ± 0.1	7.8 ± 0.1	10.1 ± 0.1	9.8 ±0.1
Incident energy (J)	29.3 ± 0.7	29.1 ± 0.8	47.7 ± 0.6	48.0 ± 0.7
Elastic energy (J)	20.0 ± 0.8	19.7 ± 0.8	26.8 ± 1.8	27.8 ± 1.3
Absorbed energy (J)	9.3 ± 0.5	9.4 ± 0.3	20.9 ± 2.2	20.3 ± 1.3
Damaged area (%)	6.5 ± 0.2	5.1 ± 0.4	9.1 ± 0.9	6.8 ± 0.7
Damage index	0.32 ± 0.02	0.32 ± 0.01	0.44 ± 0.04	0.42 ± 0.03
Damage degree	0.47 ± 0.04	0.48 ± 0.03	0.79 ± 0.14	0.73 ± 0.08

Comparisons of the damage indices for both materials revealed no discernible differences between the GF/acrylic and GF/epoxy materials at 30 J. However, an increase in impact energy to 50 J produced a ~5 % lower damage index in the GF/acrylic material with respect to its GF/epoxy counterpart. This suggests a marginally lower sensitivity of the GF/acrylic material's energy absorption (damage-related) to changes in impact energy, which is in agreement with the observations from the damaged areas and those in Section 4.3.1. Given that the damage index is a function of the absorbed and elastically dissipated energies within the system, these findings also highlight that the GF/acrylic material at 50 J favours a greater extent of elastic dissipation of energy. Similarly, at the lower impact energy (30 J), both materials exhibit comparable damage degrees. However, as with damage index, an increase in impact energy to 50 J produces a lower (~8 %) damage degree in the GF/acrylic material compared to the GF/epoxy reference material. Furthermore, due to the rebound of the striker, and thus, the absence of penetration and perforation, all damage degree values are less than 1. Nonetheless, the GF/epoxy material tends more towards one as the impact energy increases to 50 J, suggesting proximity to its penetration threshold.

The energy profile diagram in Figure 5-21 was produced by plotting the absorbed energies against impact energies for GF/acrylic and GF/epoxy materials. This diagram revealed that both materials fall considerably below the equal energy line at both energy levels.

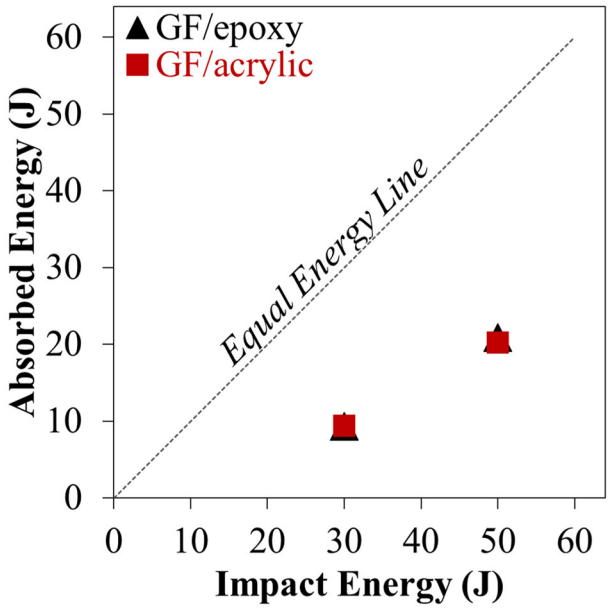


Figure 5-21. Energy profile diagram of GF/acrylic and GF/epoxy composite materials for drop-weight impacts at 30 J and 50 J.

This method facilitates a direct comparison between the impact and absorbed energies for the identification of penetration and perforation thresholds following drop-weight impact events. Penetration threshold is the critical energy value corresponding to the first point of non-rebounding deflection into the coupon body in the thickness direction. It is the point at which the absorbed energy is approximately equal to the impact energy. Perforation threshold is the point associated with full penetration of the impactor body out of the coupon body; thus, it is observed at energies over the penetration threshold [28,29]. Thus, it can be concluded that the energy levels employed in this study are well below the penetration and perforation thresholds of both materials. Further testing at higher energy levels and with more data points would be required for the extrapolation of the perforation and penetration thresholds of these materials.

The overall similarities in the magnitudes of the damage indices and degrees, and energy profiles of these materials makes it difficult to gain insights into the internal distribution of damage mechanisms as discussed in Section 5.2.7.1. However, further post-impact assessments presented in Section 5.2.7.2, may facilitate more in-depth discussions.

5.2.7.2 Impact damage tolerance (flexural-after-impact)

Flexural stress-strain curves obtained from the FAI tests performed on impact-damaged coupons as described in Section 5.1.4.8 are presented in Figure 5-22. As can be seen in Figure 5-22a, all pristine samples tested for both materials exhibit similar stress-strain behaviour, with an initial linear increase in flexural stress with strain up to ~ 1.4 % strain, followed by a slight region of inelasticity before ultimate failure. No discernible differences can be seen in stress-strain evolution for undamaged GF/acrylic and GF/epoxy samples. Interestingly, despite exhibiting repeatable elastic and inelastic zones for the respective material types, the stress-strain curves in Figure 5-22b & Figure 5-22c revealed a considerable amount of scatter in their pre-failure and ultimate failure behaviour. However, some trends are revealed that are worthy of discussion.

As with pristine samples, GF/acrylic and GF/epoxy samples subjected to 30 J events exhibited elastic evolution of stress relative to strain up to ~1.4 % as can be seen in Figure 5-22b. No evidence of damage initiation was observed at this point. In the GF/acrylic material, however, an earlier onset of damage is evident in the zone of inelasticity, with a slight load-drop, likely resulting from matrix damage development.

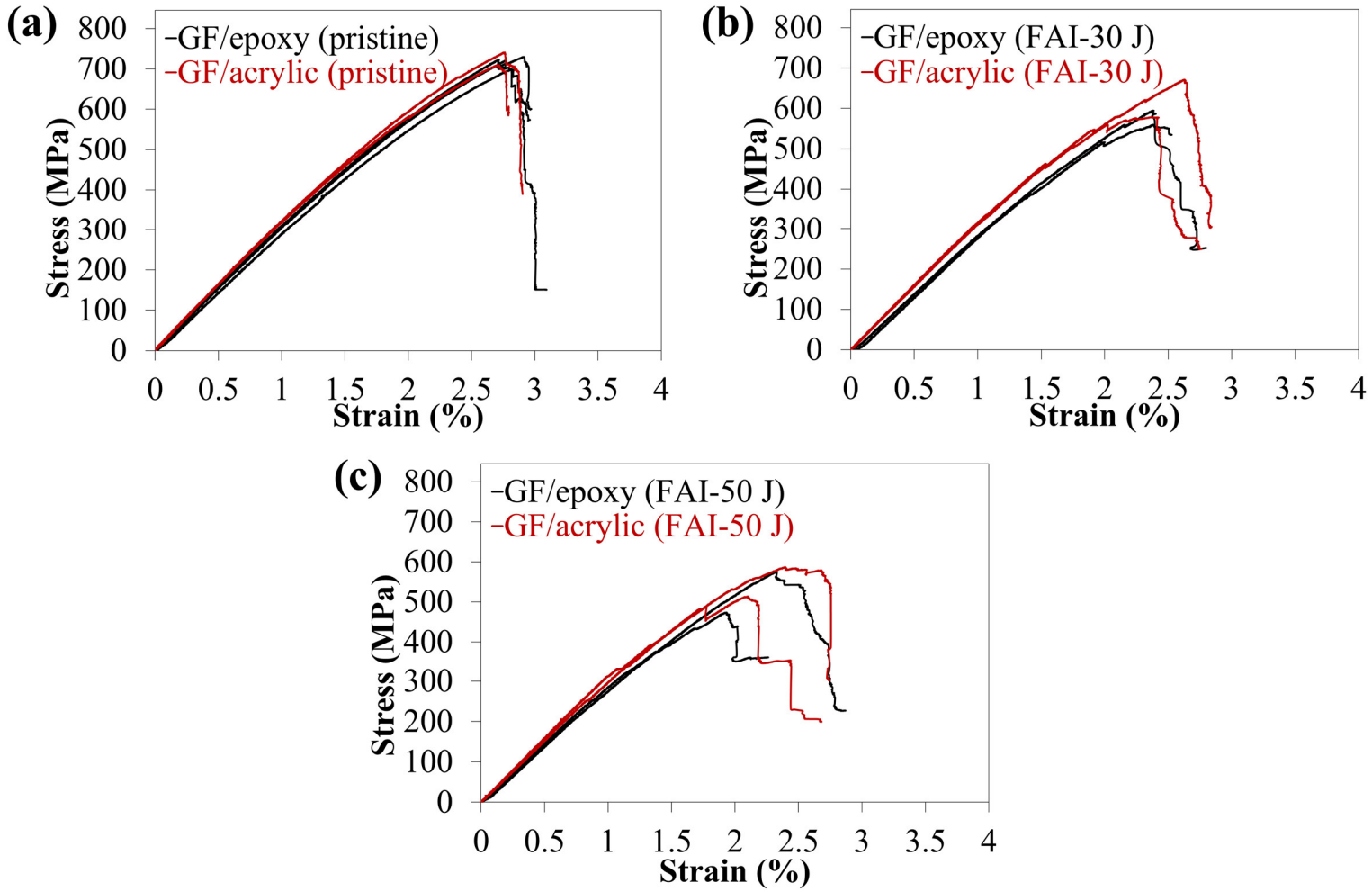


Figure 5-22. Flexure-after-impact (FAI) stress-strain curves of (a) pristine, (b) 30 J and (c) 50 J impact-damaged coupons of GF/epoxy and GF/acrylic samples.

Similar trends can be observed in Figure 5-22c, the results of FAI on 50 J impact-damaged samples; however, it is worth noting that both GF/acrylic and GF/epoxy transition from elastic to inelastic stress-strain evolution at ~1 % strain. From this transition point, the two GF/acrylic samples exhibit earlier damage onsets in form of small load-drops, which continue to occur in succession up to their respective ultimate failure stresses. A broader range of flexural failure strains was observed for 50-J FAI tests. Figure 5-23 shows the post-impact flexural strengths and moduli as functions of damage states of the tested samples (i.e., pristine, 30 J impact-damaged and 50 J impact-damaged).

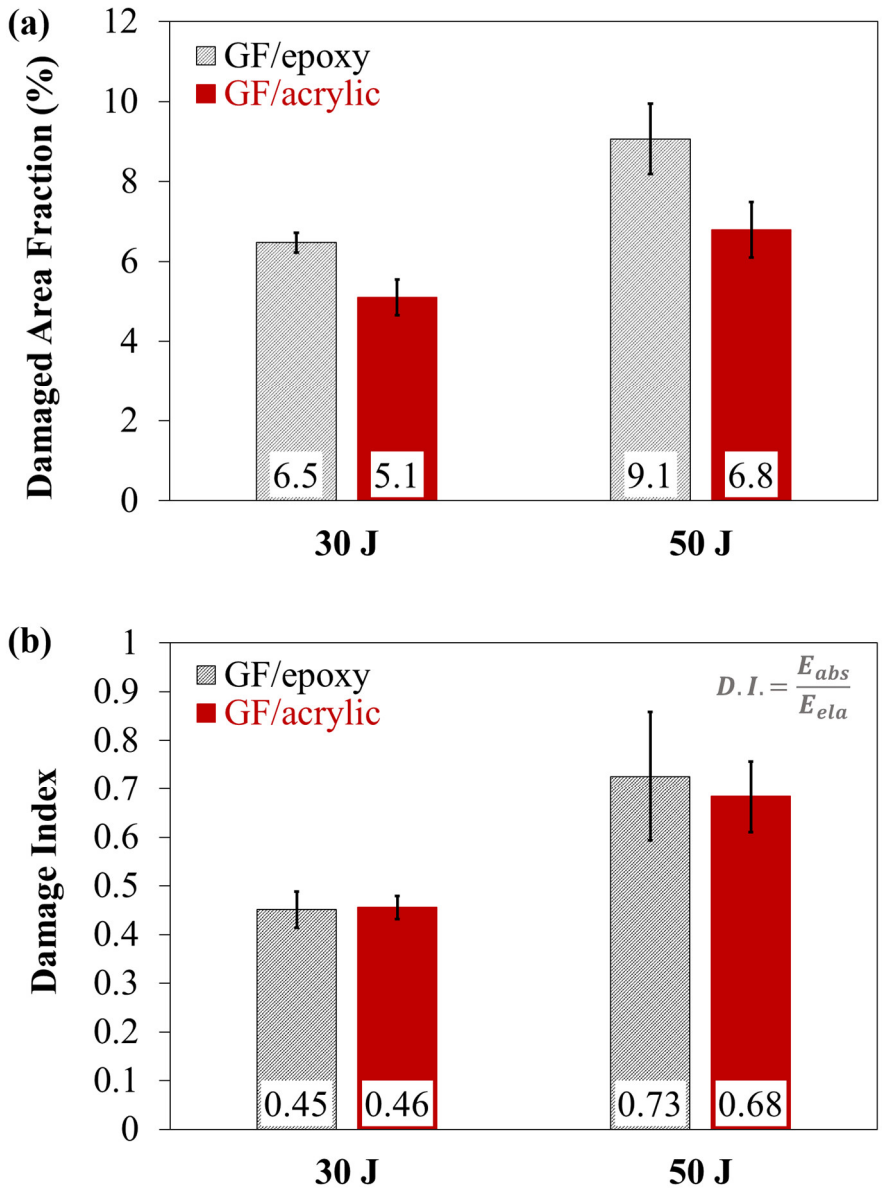
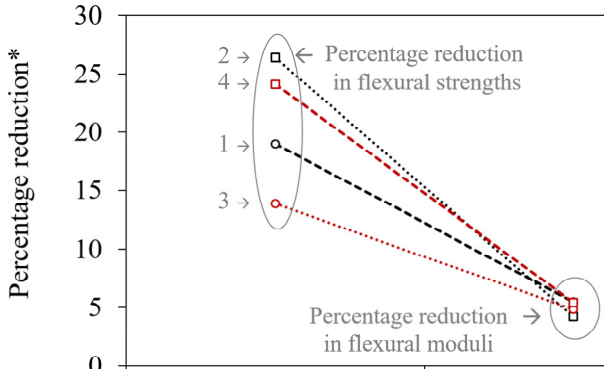


Figure 5-23. (a) Flexural strength and (b) flexural modulus results of flexure-after-impact tests conducted on pristine, 30 J and 50 J impact-damaged coupons of GF/epoxy and GF/acrylic samples.

Beginning with a comparison between the materials in each damage state, it can be seen in Figure 5-23a that GF/acrylic possessed 2 % (pristine), 8 % (30 J FAI) and 5 % (50 J FAI) higher flexural strength than GF/epoxy. A similar trend was observed for flexural modulus, for which GF/acrylic exhibited 1 % (pristine), 6 % (30 J FAI) and 5 % (50 J FAI) higher values.

A comparison of post-impact and undamaged (pristine) material performance is presented in Figure 5-24. Flexural strength reductions were more severe in the GF/epoxy material at each energy level with respect to the corresponding GF/acrylic counterparts. This was evidenced by a 19 % and 26 % reduction in strength following 30 J and 50 J impacts on GF/epoxy samples, compared to 14 % and 24 % in the GF/acrylic material, respectively. Given the comparability of the pristine (nominal) performance between these two materials, the differences in post-impact flexural properties highlight more pronounced deteriorations in the structural integrity of the GF/epoxy composite material at both impact energy levels. Moreover, they also suggest that the acrylic matrix possesses a superior ability to restrain the extension of the damage envelope from the impact-induced damage mechanisms. This may be due to the higher mode-I interlaminar fracture toughness as previously reported in Section 5.2.5, where it was found that GF/acrylic possessed higher initiation (19 %) and propagation (15 %) than GF/epoxy.



		% reduction in strength	% reduction in modulus
1 →	GF/epoxy (30 J)	19	5
2 →	GF/epoxy (50 J)	26	4
3 →	GF/acrylic (30 J)	14	5
4 →	GF/acrylic (50 J)	24	5

Figure 5-24. Post-impact property reduction as functions of matrix type and impact energy. *Percentage reductions are with respect to properties obtained from pristine samples.

The bidirectional architecture of the reinforcements used in these samples, residual strength will likely be governed by the integrity of the fibres in the longitudinal direction. The comparative performance reveals a greater reduction in strength with respect to the pristine or nominal strength in the GF/epoxy samples. This strongly suggests that more 0° fibre fractures occurred within this material than in the GF/acrylic samples, and also rules out the relative dominance of fractures of longitudinal fibres in the impact energy absorption mechanisms for GF/acrylic samples as previously discussed in Section 5.2.7.1. In addition to the role played by impact damage mechanisms on the relative reduction of post-impact flexural strength, the through-thickness distribution of damage within a given sample is also known to influence the extent of reduction of strength. Also, the post-impact flexural strength of stitched composite laminates is known to be more sensitive to fibre fractures than other impact damage mechanisms [10].

In terms of flexural modulus, all samples exhibit only a marginal reduction relative to their nominal moduli. Residual flexural modulus does not appear to be influenced by matrix type or energy level. However, residual flexural modulus is known to be considerably less sensitive to the presence of impact damage than residual flexural strength [9,30,31]. It is expected that more severe damage formation, with extensive fibre fractures, delamination and perforation may result in a more dramatic reduction in the flexural moduli of the impact-damaged GF/acrylic and GF/epoxy materials.

5.3 Chapter conclusions

This chapter comparatively assessed the mechanical and thermomechanical performance of a vacuum-infused thermoplastic acrylic composite against a traditional epoxy-based system. The processing of the thermoplastic system was associated with shorter cycle times (due to low viscosity infiltration and no requirement for post-processing). Moreover, the use of reinforcement fabric with multicompatible sizing resulted in good interfacial adhesion in GF/acrylic.

- GF/acrylic exhibited superior transverse tensile performance, with 33 % higher strength relative to the GF/epoxy material. While both materials possessed equivalent moduli, their strain development characteristics were considerably distinct. The GF/acrylic samples exhibited elastic stress-strain behaviour up to 0.4 % and thereafter, plastic deformation occurred until failure at much lower

strains than the epoxy-matrix material. The GF/epoxy material appeared to undergo progressive matrix cracking, which saturated the gauge length up to ultimate failure. Despite the absence of yielding behaviour, the GF/epoxy samples failed at significantly 43 % higher strains than GF/acrylic samples.

- The GF/acrylic material was found to possess good mode-I fracture toughness and delamination resistance, with 19 % and 15 % higher $G_{IC\text{-}Init.}$ and $G_{IC\text{-}Prop.}$ than the GF/epoxy reference, respectively. Micrographic inspections of the faying surfaces revealed microscopic ductility in GF/acrylic and brittle fracture mechanisms in GF/epoxy.
- GF/acrylic had a higher tan delta peak (+69 %) than GF/epoxy, suggesting a superiority in damping or energy dissipation capacity. This provides evidence that GF/acrylic is likely to tend towards inelastic response and undergo instantaneous, short-range deformation in response to applied stresses than its epoxy-based counterpart.
- Good comparability was observed for the following properties:
    - Longitudinal flexural strength and modulus, for which the GF/acrylic material exhibited 1 % and 5 % higher values than those obtained for the GF/epoxy material.
    - Short beam shear strengths were on average 2% higher in the GF/acrylic material than GF/epoxy. Micrographic inspections of short beam shear failure behaviour revealed fibrillary matrix deformation and inelastic drawing in the acrylic-based composite, whereas, brittle shear cusps and interfacial cracks in the vicinity of 90° fibres were observed for the GF/epoxy sample.
- Interestingly, despite exhibiting superior transverse tensile properties, the GF/acrylic material possessed inferior transverse flexural strength (-3 %) and modulus (-8 %) than the GF/epoxy material. It also failed at a considerably lower average strain (-15%). While transverse cracks were also observed for the epoxy-based materials, which were consistent with those observed during transverse tensile testing, the strain evolution of this material was more comparable with the GF/acrylic laminate. With the exception of distinctive characteristics associated with matrix cracking in the GF/epoxy material, all samples presented similar extents of inelastic behaviour up to ultimate failure.

- GF/acrylic coupons were more impact damage-resistant than their epoxy-based counterparts in response to both 30 J and 50 J drop-weight impact events. This was evidenced by the larger mean areas of the damaged zones in the GF/epoxy coupons. 30 J impacts produced damaged zones that were 6.5 % and 5.1 % of the full coupon face area in the GF/epoxy and GF/acrylic coupons, respectively. Similarly, the damage areas in coupons subjected to 50 J were 9.1 % and 6.8 %, respectively. Interestingly, both materials were comparable in terms of absorbed energy, providing strong evidence of additional non-detectible damage mechanisms within the GF/acrylic material. Moreover, the GF/acrylic coupons exhibited a lesser sensitivity to increasing impact damage in terms of their damage resistance. Increasing the impact energy from 30 J to 50 J resulted in a 33 % increase in damage area in the GF/acrylic material, compared to a 40 % increase in the GF/epoxy material. However, an assessment of the damage parameters (indices and degrees) of both materials showed a good degree of comparability, further confirming that additional impact-induced damage mechanisms were responsible for the mismatch between the respective absorbed energies and measured damaged areas.
- The materials' corresponding damage tolerances were assessed by a flexural test method performed on resized impacted coupons and compared with the undamaged samples. These tests revealed superior performance in the GF/acrylic coupons (with respect to those of GF/epoxy) across each damage state.
    - Residual strengths of 30-J impacted GF/acrylic and GF/epoxy coupons were 14 % and 19 % lower than their respective undamaged strengths, respectively. 50 J impacts resulted in 24 % and 26 % reductions in GF/acrylic and GF/epoxy coupons respectively. Overall, the greatest reductions were observed in the GF/epoxy, confirming that the acrylic matrix possesses superior resistance to damage extension under the conditions investigated.
    - Residual flexural modulus did not appear to vary with matrix type and impact energy level. All materials exhibited comparable marginal reductions in flexural modulus with respect to their respective pristine states. This provides evidence that non-fibre-related damage mechanisms were induced by both energy levels within both materials. Thus,

interfacial, matrix and delamination failures were most likely the dominant mechanisms within these materials.

- The acrylic matrix possesses a superior ability to inhibit the extension of the damage envelope from the impact-induced damage mechanisms during post-impact testing. This was evidenced by lesser reductions in the GF/acrylic material's residual flexural strengths than those of the GF/epoxy. This is plausibly attributed to its aforementioned superiority in mode-I interlaminar fracture toughness.

The findings and observations presented in this chapter will not only serve to foster an understanding of acrylic matrices in continuous fibre-reinforced composite applications but are essential baselines for the wider aim of this body of work. Routes developed for modifications will be validated using various test methods, including those presented herein. Thus, these results provide a broader context for the chapters that follow. Overviews of the evaluated properties discussed throughout this chapter have been presented from Table 5-8 to Table 5-12, with percentage changes expressed with respect to corresponding GF/epoxy values.

Table 5-8. Chapter overview of evaluated properties (Mechanical properties). *Percentage difference expressed with respect to GF/epoxy values; where + and – symbols represent higher and lower GF/acrylic values, respectively.

	GF/epoxy	***GF/acrylic***	***Percentage Difference****
Tensile Properties (Transverse)			
Strength (MPa)	54	73	+35
Modulus (GPa)	13	13	+0
Failure strain (%)	2.1	1.2	-43
Flexural Properties (Longitudinal)			
Strength (MPa)	869	879	+1
Modulus (GPa)	38	40	+5
Failure strain (%)	3.4	3.3	-3
Flexural Properties (Transverse)			
Strength (MPa)	94	91	-3
Modulus (GPa)	12	11	-8
Failure strain (%)	2.0	1.7	-15
Short Beam Shear Properties			
Strength (MPa)	57	58	+2

Table 5-9. Chapter overview of mode-I interlaminar fracture toughness properties. *Percentage difference expressed with respect to GF/epoxy values; where + and – symbols represent higher and lower GF/acrylic values, respectively.

	GF/epoxy	***GF/acrylic***	***Percentage Difference****
Mode-I Interlaminar Fracture Toughness			
Initiation (J/m^2)	466	556	+19
Propagation (J/m^2)	1574	1814	+15

Table 5-10. Chapter overview of evaluated properties (Drop-weight impact properties). *Percentage difference expressed with respect to GF/epoxy values; where + and – symbols represent higher and lower GF/acrylic values, respectively.

	30 J			***50 J***		
	GF/epoxy	***GF/acrylic***	***Percentage Difference****	***GF/epoxy***	***GF/acrylic***	***Percentage Difference****
Impact Damage Resistance						
Peak load (N)	8131	8754	+8	10851	11796	+9
Ultimate deflection (mm)	8.0	7.8	-3	10.1	9.8	-3
Elastic energy (J)	20.0	19.7	-2	26.8	27.8	+4
Absorbed energy (J)	9.3	9.4	+1	20.9	20.3	-3
Damaged area (%)	6.5	5.1	N/A	9.1	6.8	N/A

Table 5-11. Chapter overview of evaluated properties (Damage tolerance; flexure-after-impact) -cont. *Percentage difference expressed with respect to GF/epoxy values; where + and – symbols represent higher and lower GF/acrylic values, respectively.

	30 J			***50 J***		
	GF/epoxy	***GF/acrylic***	***Percentage Difference****	***GF/epoxy***	***GF/acrylic***	***Percentage Difference****
Impact Damage Tolerance						
Residual flexural strength (MPa)	577.1	624.6	+8	524.4	550.1	+5
Residual flexural modulus (GPa)	30.1	31.4	+4	30.5	31.2	+2
Loss in flexural strength (%)	19	14	N/A	26	24	N/A
Loss in flexural modulus (%)	5	5	N/A	4	5	N/A

Table 5-12. Chapter overview of evaluated properties (Thermomechanical properties). *Percentage difference expressed with respect to GF/epoxy values; where + and – symbols represent higher and lower GF/acrylic values, respectively.

	GF/epoxy	***GF/acrylic***	***Percentage Difference****
Thermomechanical properties			
Glass transition temperature (°C)	119	106	-11
Tan delta	0.45	0.76	+69

5.4 Chapter references

[1] Arkema. Liquid thermoplastic resin for tougher composites 2017. https://www.arkema-americas.com/export/shared/.content/media/downloads/products-documentations/incubator/brochure-elium-2017.pdf.

[2] Sicomin Epoxy Systems. Technical Datasheet – SR 1710 inj / SD 7820 Epoxy system for infusion and injection processes 2014. http://sicomin.com/datasheets/product-pdf1265.pdf (accessed May 27, 2021).

[3] Bhudolia SKK, Perrotey P, Joshi SCC. Optimizing polymer infusion process for thin ply textile composites with novel matrix system. Materials (Basel) 2017;10. https://doi.org/10.3390/ma10030293.

[4] Chilali A, Zouari W, Assarar M, Kebir H, Ayad R. Analysis of the mechanical behaviour of flax and glass fabrics-reinforced thermoplastic and thermoset resins. J Reinf Plast Compos 2016;35:1217–32. https://doi.org/10.1177/0731684416645203.

[5] Ali M, Joshi SC. Impact Damage Resistance of CFRP Prepreg Laminates with Dispersed CSP Particles into Ply Interfaces. Int J Damage Mech 2012;21:1106–27. https://doi.org/10.1177/1056789511429143.

[6] Bhudolia SK, Joshi SC. Low-velocity impact response of carbon fibre composites with novel liquid Methylmethacrylate thermoplastic matrix. Compos Struct 2018;203:696–708. https://doi.org/10.1016/j.compstruct.2018.07.066.

[7] Belingardi G, Vadori R. Low velocity impact tests of laminate glass-fiber-epoxy matrix composite material plates. Int J Impact Eng 2002;27:213–29. https://doi.org/10.1016/S0734-743X(01)00040-9.

[8] Hart KR, Chia PXL, Sheridan LE, Wetzel ED, Sottos NR, White SR. Comparison of Compression-After-Impact and Flexure-After-Impact protocols for 2D and 3D woven fiber-reinforced composites. Compos Part A Appl Sci Manuf 2017;101:471–9. https://doi.org/10.1016/j.compositesa.2017.07.005.

[9] Yuan B, Ye M, Hu Y, Cheng F, Hu X. Flexure and flexure-after-impact properties of carbon fibre composites interleaved with ultra-thin non-woven aramid fibre veils. Compos Part A Appl Sci Manuf 2020;131:105813. https://doi.org/10.1016/j.compositesa.2020.105813.

[10] Francesconi L, Aymerich F. Effect of stitching on the flexure after impact behavior of thin laminated composites. Proc Inst Mech Eng Part C 2017;232:1375. https://doi.org/10.1177/0954406217712745.

[11] Zhang D, Waas AM, Yen CF. Progressive damage and failure response of hybrid 3D textile composites subjected to flexural loading, part I: Experimental studies. Int J Solids Struct 2015;75–76:309–20. https://doi.org/10.1016/j.ijsolstr.2015.06.034.

[12] Hamada H, Ishibashi S, Maekawa Z. Evaluation of transverse tensile strength of unidirectional CFRP laminate. In: Hogg PJ, Schulte K, Wittich H, editors. Compos. Test. Stand. (Eccm-Cts 2), CRC Press; 1994, p. 259.

[13] Adams D. Transverse flexure testing : CompositesWorld. Compos World 2010.

[14] Hiley MJ. Fractographic study of static and fatigue failures in polymer composites Fractographic study of static and fatigue failures in polymer composites. Plast Tubber Compos 1999;28:210–27. https://doi.org/10.1179/146580199101540358.

[15] Almansour FA, Dhakal HN, Zhang ZY. Effect of water absorption on Mode I interlaminar fracture toughness of flax/basalt reinforced vinyl ester hybrid composites. Compos Struct 2017;168:813–25. https://doi.org/10.1016/j.compstruct.2017.02.081.

[16] Bensadoun F, Verpoest I, Van Vuure AW. Interlaminar fracture toughness of flax-epoxy composites. J Reinf Plast Compos 2017;36:121–36. https://doi.org/10.1177/0731684416672925.

[17] Eliades T, Zinelis S, Kim D-G, Brantley W. Structure/property relationships in orthodontic polymers. Elsevier Ltd; 2017. https://doi.org/10.1016/b978-0-08-

100383-1.00002-3.

[18] Sudheer M. Thermomechanical properties of epoxy /PTW composites. J Mech Eng Autom 2016;6:18–21. https://doi.org/10.5923/c.jmea.201601.04.

[19] Chaudhari V, Chandekar H, Saboo J, Mascarenhas A. Studies on thermo-mechanical properties of chemically treated jute-polyester composite. IOP Conf Ser Mater Sci Eng 2018;330. https://doi.org/10.1088/1757-899X/330/1/012032.

[20] Mousa A, Heinrich G, Wagenknecht U. Wood-like material from thermoplastic polymer and landfill bio-materials: DMA, TGA and solvent resistance properties. Polym from Renew Resour 2015;6:25–42. https://doi.org/10.1177/204124791500600102.

[21] Bandzierz K, Reuvekamp L, Dryzek J, Dierkes W, Blume A, Bielinski D. Influence of network structure on glass transition temperature of elastomers. Materials (Basel) 2016;9. https://doi.org/10.3390/MA9070607.

[22] Shah SZH, Megat-Yusoff PSM, Karuppanan S, Choudhry RS, Ahmad F, Sajid Z, et al. Performance comparison of resin-infused thermoplastic and thermoset 3D fabric composites under impact loading. Int J Mech Sci 2021. https://doi.org/10.1016/j.ijmecsci.2020.105984.

[23] van Casteren IA. Control of microstructures to induce ductility in brittle amorphous polymers. Technische Universiteit Einhoven, 2003. https://doi.org/10.6100/IR566897.

[24] Klompen ETJ. Mechanical properties of solid polymers: constitutive modelling of long and short term behaviour. Technische Universiteit Eindhoven, 2005. https://doi.org/10.1016/b978-0-444-82877-4.50020-2.

[25] Arumugam V, Adhithya A, Sidharth P, Santulli C. Failure modes characterization of impacted carbon fibre reinforced plastics laminates under compression loading using acoustic emission. J Compos Mater 2014;48:3457–68. https://doi.org/10.1177/0021998313509504.

[26] Vieille B, Casado VM, Bouvet C. Influence of matrix toughness and ductility on

the compression-after-impact behavior of woven-ply thermoplastic- and thermosetting-composites: A comparative study. Compos Struct 2014;110:207–18. https://doi.org/10.1016/j.compstruct.2013.12.008.

[27] Wu H, Ma G, Xia Y. Experimental study of tensile properties of PMMA at intermediate strain rate. Mater Lett 2004;58:3681–5. https://doi.org/10.1016/j.matlet.2004.07.022.

[28] Bektaş NB, Ağir I. Impact response of composite plates manufactured with stitch-bonded non-crimp glass fiber fabrics. Sci Eng Compos Mater 2014;21:111–20. https://doi.org/10.1515/secm-2012-0066.

[29] Evci C, Uyandıran İ. The effect of the impactor diameter and temperature on low velocity impact behavior of CFRP laminates. Proc. 6th Int. Adv. Appl. Phys. Mater. Sci. Congr. Exhib. AIP Conf. Proc. 1809, vol. 1809, AIP Publishing; 2017, p. 20010–4. https://doi.org/10.1063/1.4975429.

[30] Zhang ZY, Richardson MOW. Low velocity impact induced damage evaluation and its effect on the residual flexural properties of pultruded GRP composites. Compos Struct 2007;81:195–201. https://doi.org/10.1016/j.compstruct.2006.08.019.

[31] Liu Q, Guo O, Ju Y, Lin Y, Li Q. Impact responses and residual flexural properties of narrow CFRP laminates. Compos Struct 2014;111:332–9. https://doi.org/10.1016/j.compstruct.2014.01.018.

PART III: DEVELOPMENT OF ACRYLIC/POLY(PHENYLENE ETHER) (PPE) HYBRID MATRIX & CHARACTERISATION OF GLASS FIBRE-REINFORCED ACRYLIC/PPE COMPOSITE

Chaper 6 Development, preparation and evaluation of unreinforced acrylic/PPE hybrid polymers

6.1 Considerations for thermoplastic-thermoplastic hybrid matrix development

Current modification practices for liquid acrylic resins involve the incorporation of self-assembling acrylic-based block copolymers based on nanophasic morphology. Its use is reported to enhance impact properties, rigidity and the overall transparency of the matrix [1]. Research contributions in this area are extensively discussed in Section 2.6. The trademarked modifier – Nanostrength™ is based on Arkema's proprietary alkoxyamine technology, comprising polymethylmethacrylate-b-polybutylacrylate-b-polymethylmethacrylate.

While thermosetting matrices are routinely modified, with a vast body of literature on associated modification strategies and toughening mechanism, the modification of thermoplastic matrices for composite applications has not been the subject of extensive research. This may be because high-melt viscosities of traditional thermoplastic polymer matrices often limit the extent to which modifiers can be incorporated. In light of the recent surge in demand and popularity of thermoplastic matrices for composite applications, strategic incorporation of engineering and high-performance thermoplastics into a lower performance thermoplastic may offer attractive benefits towards enhancing the applicability of the latter.

6.1.1 Polyphenylene ether (PPE)

Poly(phenylene oxide) (PPO), also known as poly(phenylene ether) (PPE) is a relatively low-cost engineering thermoplastic that has become one of the most important engineering polymers today. Arguably the main limiting factor to the broader applicability of PPE as a standalone composite matrix is its poor processibility [2–5]. As can be seen from the published works summarised in Table 6-1, much of the research contributions have employed melt blending methodologies, with limited exploration of reinforced PPE-modified matrices. Thus, a clear gap exists that motivates this research.

Table 6-1. Summary of research contributions on the development of PPE- and PPO-based blended material systems.

Materials	*Composition(s)*	*Process(es)*	*Remarks*	*References*
Polyamide-6 (PA6) PPE	PA6:30 wt. % PPE: 70 wt. %	Melt blending	Unreinforced; Compatibiliser: Tetra-functional epoxy monomer	[6]
PA6 PPO	PA6: 70-100 wt. % PPO: 0-30 wt. %	Melt blending	Unreinforced; Compatibiliser: Fumaric acid; Melt-strength enhancer required: Polypropylene	[7]
Glycol-modified polyethylene terephthalate (PETG) PPE	PETG: 40-90 wt. % PPE: 10-60 wt. %	Melt blending	Unreinforced; Compatibiliser: poly(styrene-co-maleic anhydride)	[8]
PA6 PPE	PA6: 30-70 wt. % PPE: 30-70 wt. %	Melt blending	Unreinforced; Compatibilser: poly(methylene(phenylene isocyanate))	[9]
PA6 PPE	PA6: 50 wt. % PPE: 50 wt. %	Melt blending	Unreinforced; Compatibiliser: poly(styrene-co-maleic anhydride) Elastomeric-toughening was also investigated as part of this work	[10]
Polypropylene (PP) PPO	PP: 20-80 wt. % PPO: 20-80 wt. %	Tumble and melt blending	Unreinforced; Compatibiliser: poly(styrene-b-isopropene-b-styrene) and poly(styrene-ethylene-butylene-styrene)	[11]

Table 6-1 cont.

Materials	*Composition(s)*	*Process(es)*	*Remarks*	*References*
PA6 PPE	PA6: 30 wt. % PPE: 70 wt. %	Melt blending	Unreinforced; Compatibiliser: phenolic novolac epoxy	[12]
PA6 PPO	PA6: 30-70 wt. % PPO: 30-70 wt. %	Melt blending	Unreinforced; Compatibiliser: styrene-maleic anhydride	[13,14]
PA6 PPO	PA6: 50 wt. % PPO: 50 wt. %	Melt blending	Unreinforced; Compatibiliser: styrene-co-glycidyl methacrylate	[15]
PA66 PPO	PA66: 40-60 wt. % PPO: 40-60 wt. %	Melt blending	Unreinforced; Compatibiliser: styrene-maleic anhydride	[16]
PA6 PPE	PA6: 30 wt. % PPE:70 wt. %	Melt blending	Unreinforced; Compatibiliser: styrene-acrylic acid	[17]
Polystyrene (PS) PPE PA6 Chopped and long glass fibre (GF)	PS: 40 wt. % PPE: 40 wt. % PA6: 20 wt. % *GF: 30-40 wt. % (in composite)	Melt blending	Reinforced (discontinuous and random); Compatibiliser: maleic anhydride;	[18]
Syndiotactic polystyrene (sPS) PPE	sPS: 50-75 wt. % PPE: 25-50 wt. %	Coprecipitation and compression moulding	Unreinforced; No compatibiliser required Coprecipitation: bottom-up method, particularly suited to nanoparticle synthesis	[19]
ε-caprolactam (PA6 precursor) PPO	PA6 precursor: 94-100 wt. % PPO: 0-6 wt. %	In-situ polymerisation	Unreinforced; No compatibiliser required	[5,20]

6.2 Possibilities for thermoplastic-thermoplastic hybrid matrices

Due to their low viscosities, liquid thermoplastic resins are ideal candidate materials for the same modification methodologies utilised for liquid thermosetting resin systems for composite applications. Thermosetting resin systems, such as epoxies, are often tailored with the addition of other polymeric phases, which may be elastomeric or thermoplastic [21–29]. The use of thermoplastic modifiers can be highly beneficial because their use does not have deleterious effects on glass transition temperature in the resulting blend in the way that elastomeric modifiers do [30] and in addition to that, they enhance the fracture toughness property of the brittle thermosets.

Another motivation behind the addition of higher performance engineering thermoplastics into liquid thermosetting resins is the need to circumvent challenges associated with their processibility [31,32]. This approach involves the use of these liquid thermosetting resins as reactive solvents within which higher molecular weight thermoplastics can be dissolved for subsequent processing by liquid composite moulding methodologies; and thus, is an attractive way to produce composite structures with hybrid matrices with tailored performance.

The chapter presents an innovative approach of incorporating PPE into acrylic resins to modify the matrix properties for composite applications. A liquid thermoplastic acrylic resin system was modified using PPE. PPE is typically used in the form represented in Figure 6-1, with characteristic phenyl and methyl groups present. A phenyl group is an aromatic group of atoms with alternating single and double bonds, whereas a methyl group comprises a carbon atom bonded to three hydrogen atoms.

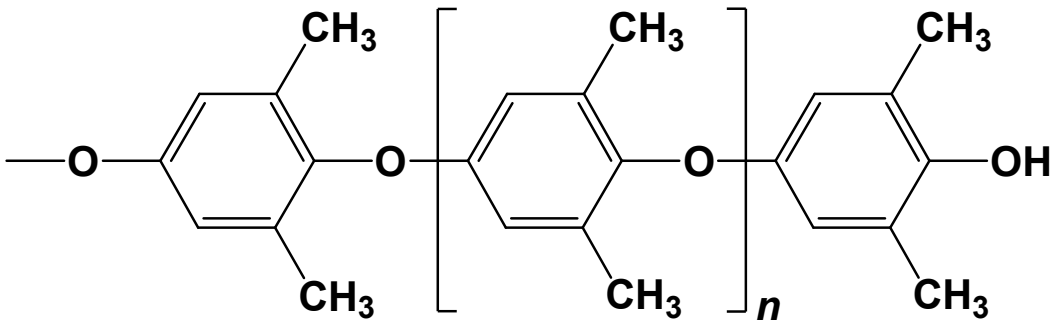


Figure 6-1. Representative chemical structure of PPE.

In this work, a grade of telechelic PPE with chain-end vinyl functionality was selected to facilitate chemical reactivity between its vinyl end groups and the growing acrylic chains via free-radical polymerisation. A telechelic molecule is one with end-group functionality. The representative structure of this grade is provided in Figure 6-2.

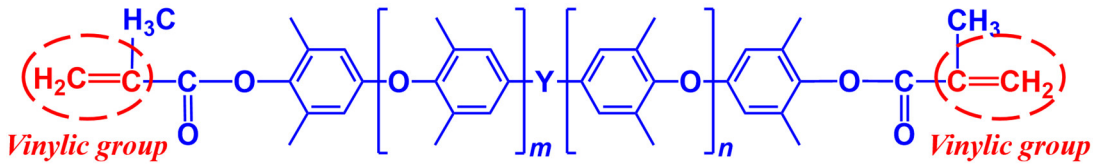


Figure 6-2. Representative chemical structure of vinyl-functionalised PPE as published by the manufacturer [33]. Note, *Y* was used by the manufacturer to denote proprietary information pertinent to the grade of PPE employed in this study.

A similar approach was previously employed by Bennett and Summers [34], and Viersen [35]. However, in this present work, a telechelic PPE oligomer is directly applied to a reactive acrylic resin as opposed to the used of styrene as a reactive solvent for PPE and inter-polymerised acrylic-modified polyisoprene as was done by Bennet and Summers. Although PPE and acrylic were copolymerised by Viersen, the intermediate blend was employed as a compatibiliser for a tertiary component. More importantly, Bennett and Summers reported improved toughness, solvent resistance and resistance to heat distortion in the blends prepared using this approach, attributing the enhanced toughness to the contributions of the elastomer (polyisoprene) constituent. The use of PPE can result in significantly improved solvent resistance, as will be shown later in this chapter.

The resulting polymer blends were characterised using various analytical techniques to assess the effects of hybridisation on their polymerisation behaviour, chemical structure, phase morphology, fracture behaviour, solvent resistance, thermomechanical performance, and thermal stability with respect to the unmodified acrylic polymer.

6.3 Materials and methods

6.3.1 Materials

A liquid thermoplastic acrylic resin (Elium® 188 O – Arkema) was reactively modified with a PPE oligomer to investigate an innovative route to modifying liquid acrylic resins for composite applications. The PPE used was NORYL™ SA9000 resin (SABIC) – a low-molecular-weight grade (M_n: 2300 Da) with vinyl functional groups.

Table 6-2 summarises the polymers produced and studied in this work. Hereafter, the polymers (reference and blends) will be referred to as A100/P0, A97/P3, A95/P5, A90/P10, A85/P15 and A0/P100.

Table 6-2. Overview of neat acrylic and blend compositions, where A and P indicate acrylic and PPE constituents, respectively.

	Elium® 188 O (by weight)	*NORYL™ SA9000 (by weight)*
A100/P0	100	0
A97/P3	97	3
A95/P5	95	5
A90/P10	90	10
A85/P15	85	15
A0/P100	0	100

6.3.2 Preparation of modified resins

PPE was dissolved into liquid acrylic resin in the compositional range of 3 to 15 % by weight of acrylic resin, as shown in Table 6-2. The liquid acrylic resin acted as a reactive solvent for the PPE oligomer.

A preliminary miscibility and solubility trial was conducted to assess the maximum PPE content dissolvable in the liquid acrylic resin. Resin blends were mixed, as shown in Figure 6-3, with hand mixing performed until the PPE powder was fully dissolved into the resin, and a homogenous mixture was obtained. The resin mixtures were covered and left undisturbed for a 24-h period. Upon visual inspection, resins containing the higher concentrations of PPE (A90/P10 and A85/P15) appeared to exhibit two distinct liquid phases after 24 h. In contrast, lower PPE contents (A97/P3 and A95/P5) did not exhibit this effect in their respective resin blends.

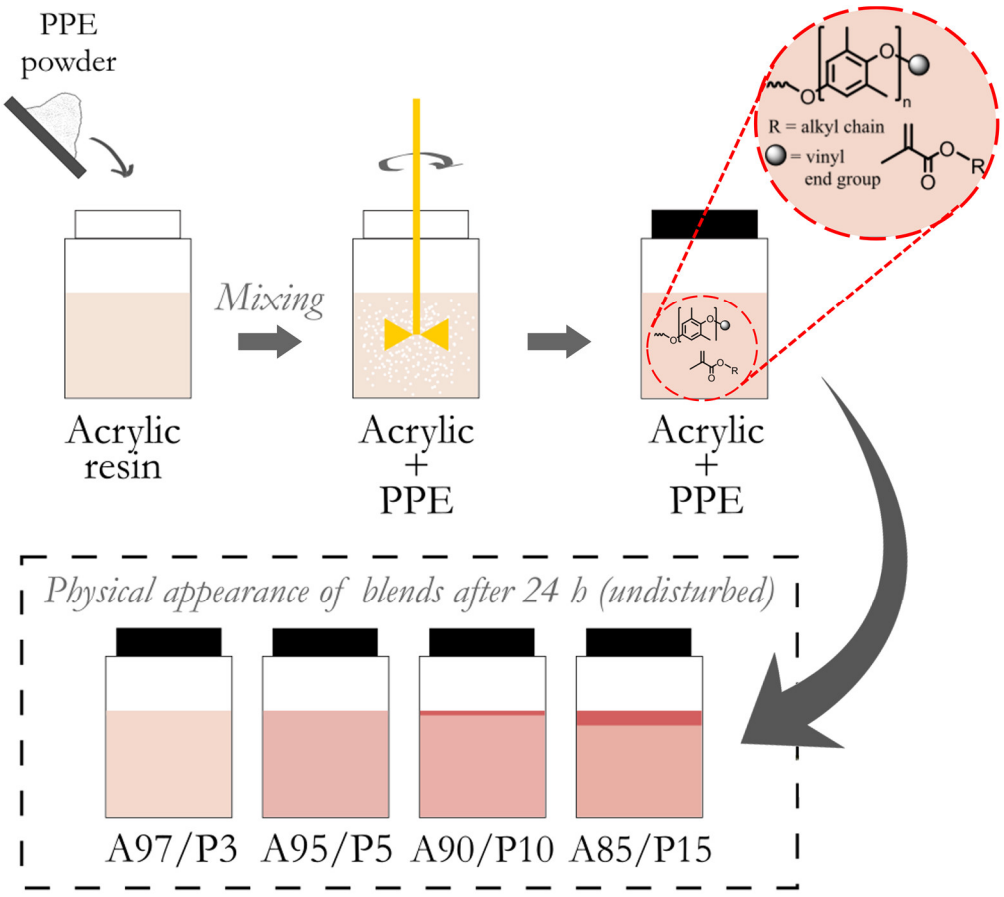


Figure 6-3. Schematics of the resin blend preparation procedure and the observed characteristics of each blend after mixing and leaving undisturbed for 24 h.

6.3.3 Mould casting process

BP50FT (United Initiators), a dibenzoyl peroxide (BPO) initiator was added to the resins 24 h after preparation at a mix ratio of 100:3 (by weight). Samples with nominal dimensions of 50 mm × 9 mm × 3 mm were polymerised at room temperature for 24 h in silicone moulds. PTFE-covered steel plates were used to cover the moulds throughout the polymerisation to prevent the evaporation and foaming of the liquid resin.

It was found that the blend composition significantly influences the transparency of the samples. As shown in Figure 6-4, the word "TEST" (Figure 6-4a) is partially visible through the sample of unmodified acrylic matrix sample (A100/P0) shown in Figure 6-4b, which has a more translucent appearance. As the content of PPE is progressively increased, the relative opacity of the samples also increased.

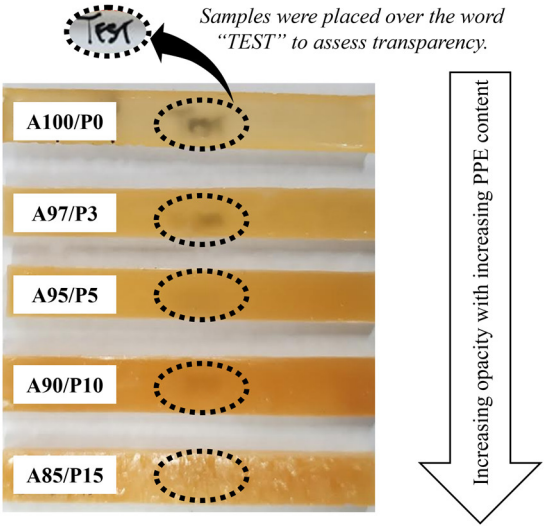


Figure 6-4. The cast polymer samples were placed over the word "TEST" to assess the influence of PPE content on the transparency and colour of PPE-modified blends.

Although every effort was made to obtain void-free samples for testing, foaming of the acrylic monomer during polymerisation limited the number of testable samples produced and the extent of evaluation methods applied (e.g.: void content determination). Such foaming has been reported by Han et al. [36] for acrylic-based resins, giving rise to bubble and porosity formation. This was thought to be associated with the resin temperature (from the exothermic polymerisation reaction) exceeding its boiling point (100°C). While void content determination was not possible during this work, the absence of macrovoids on the scanning electron micrographs confirmed that no macrovoids were forms in the obtained samples used for testing. Moreover, it was not possible at the time of this study to obtain neat PPE samples as castings for characterisation due to the poor processibility of PPE. Attempts to prepare castings using hot-press moulding as described in Appendix C.2.1.2.1 (Figure 2.14) did not yield high-quality sheets, but rather, produced highly brittle, fragile and fragmented shards as detailed in Appendix C.2.1.2.1 (Figure C-15).

Details of the obtained samples and specific sample preparation information for each type of characterisation have been provided in this Chapter's relevant methodology sections.

6.3.4 Nuclear magnetic resonance (NMR) spectroscopy

Note: This section and discussions on NMR spectroscopy were completed in collaboration with the Chemistry Department at the University of Edinburgh. The chemical structures of unmodified acrylic and PPE in the presence and absence of BPO,

as well as acrylic/PPE blends (PPE content: 5-10 wt. %), were analysed by ^{1}H and 2D NMR experiments (^{1}H-^{1}H COrrelated SpectroscopY (COSY), ^{1}H-^{13}C Heteronuclear Single Quantum Coherence (HSQC) spectroscopy and Diffusion-Ordered SpectroscopY (DOSY)). NMR spectra were recorded on a Bruker AVA500 spectrometer at 298 K (500 MHz) in $CDCl_3$ and were referenced to the residual $CDCl_3$ peaks (^{1}H: δ 7.26 ppm, ^{13}C: 77.2 ppm). Only the soluble portions of the reactive A95/P5 and A90/P10 blends were analysed by NMR spectroscopy in $CDCl_3$. The solubility of the reactive blends in $CDCl_3$ was improved by heating (50°C) and sonicating the blends in $CDCl_3$ for approximately 2 hours or leaving the samples in excess $CDCl_3$ overnight. Both blends also exhibited low solubility in other common NMR spectroscopy solvents (tetrahydrofuran (THF)-d_8, pyridine-d_5 and toluene-d_8).

6.3.5 Solvent resistance in acetone

Solvent resistance analyses were performed in acetone to study the influence of PPE-modifier content on the unreinforced acrylic matrix system. Two independent sets of experiments were conducted; polymerised samples of unmodified acrylic and acrylic/PPE blends (PPE content: 3-15 wt. %) were sectioned, weighed and placed in acetone at room temperature for 60 minutes and 72 hours. All polymer sample masses were in the range of 216 – 275 mg. For each material and test duration, a single sample was analysed per container. Samples with a 60-minute exposure time were immersed in acetone for the test duration after preparation and carefully removed, dried and weighed after completing the experiment. Data collection for the 72-h study involved routine inspections at set intervals up to 300 minutes, during which visible geometrical changes were recorded until the end of the experiment. Beyond this point, samples were inspected at the 24-h mark and 72-h mark, respectively. All coupons were removed from the solvent, dried and weighed at the end of the respective test durations.

6.3.6 Dynamic mechanical analysis

Dynamic mechanical analysis (DMA) was performed on polymer samples to study the influence of PPE-modifier content on T_g and damping behaviour using a DMA 8000 analyser (Perkin Elmer). Samples measuring 40 mm × 8 mm × 4 mm were dynamically loaded at a fixed frequency of 1 Hz using a dual cantilever bending configuration. Polymeric samples were analysed with a 10-micron amplitude. Each sample was heated from ambient temperature to 180°C at 3°C/min.

6.3.7 Thermogravimetric analysis

Thermogravimetric analysis (TGA) was performed using a Mettler Toledo TGA/DSC 1 analyser to analyse the thermal stability of polymer samples. Samples weighing 10 mg (polymer samples) were heated from 25°C to 600°C (10°C/min) under a nitrogen flow rate of 50 ml/min. In addition to comparing the evolution of mass loss and derivative thermograms (DTG), activation energies were comparatively assessed. Activation energies were determined using the method reported by Ray et al. [37].

A summary of all analytical techniques applied and the corresponding materials (by composition and type) utilised is presented in Table 6-3. With the exception of Sol.-res., M, NR, O, O+BPO and P, all identification codes and acronyms are as previously described.

Table 6-3. Summary of analyses performed by material type and composition.

	NMR	*DMA*	*TGA*	*Sol. res.*
A100/P0	✓M; P	✓P	✓P	✓P
A97/P3	✗	✓P(R)	✓P(R)	✓P(R)
A95/P5	✓P(R), P(NR)	✓P(R)	✓P(R)	✓P(R)
A90/P10	✓P(R), P(NR)	✓P(R)	✓P(R)	✓P(R)
A85/P15	✗	✓P(R)	✓P(R)	✓P(R)
A0/P100	✓O, O+BPO	✗	✓O	✗

M: Acrylic monomer (as-received) with no BPO initiator; **P:** Acrylic polymer; **P(R):** Reactive acrylic/PPE blend; **P(NR):** non-reactive blend; **O:** PPE oligomer (as-received); **O+BPO:** PPE oligomer with dibenzoyl peroxide initiator.

✓**:** Analysis performed; ✗**:** Analysis not performed.

NMR: Nuclear magnetic resonance spectroscopy; **DMA:** Dynamic mechanical analysis; **TGA:** Thermogravimetric analysis; **Sol. res.:** Solvent Resistance.

6.3.8 Morphological assessments on fractured unreinforced polymers

Single polymeric samples prepared as described in Section 6.3.3 were fractured in non-standard loading in a three-point bending configuration similar to ISO 14130, in that a narrow span (10 mm) was used. The unreinforced samples were fractured using a crosshead speed of 10 mm/min. The loading nose and supports used were 6-mm-diameter hardened steel pins as shown in Figure 6-5.

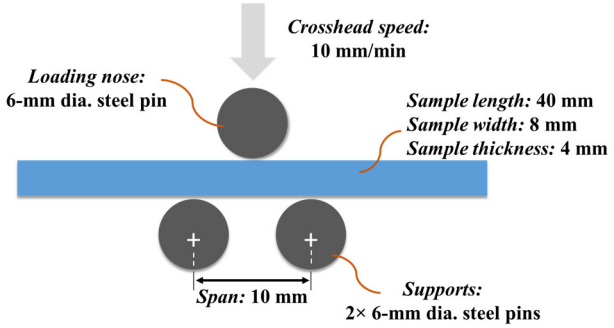


Figure 6-5. Schematic depicting the experimental set-up employed for obtaining fractured (unreinforced) specimens for microscopic investigations.

6.3.8.1 Confocal Raman microscopy

Fractured samples were non-destructively imaged using a confocal Raman microscopy technique to identify the presence of mono- or bi-phasic species within each blend. The sample was maintained at constant focus using a *TrueSurface*® tool to enhance the visualisation precision across the fracture surface (irrespective of topographical variations). An Alpha 300 AR instrument (WiTec GmbH, Germany) was used for this study.

6.3.8.2 Scanning electron microscopy (SEM)

SEM inspections were performed using secondary electron imaging to gain insights into the influence of PPE-modification on the fracture behaviour of the unreinforced polymers. Figure 6-6 shows the region of interest for SEM inspection of the fracture surface.

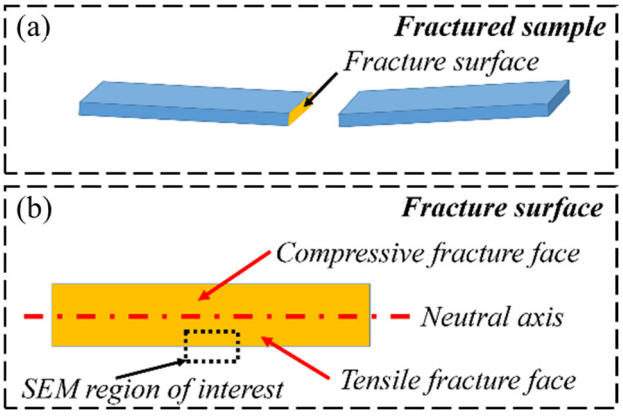


Figure 6-6. Schematics showing the region of interest for SEM microscopy.

6.4 Results and discussions

6.4.1 Results of solution-state polymer analyses

The chemical composition of acrylic/PPE blends, A95/P5 (P(R)) and A90/P10 (P(R)) was probed by NMR spectroscopy in $CDCl_3$ and compared to acrylic polymer (A100/P0 (P)) and PPE oligomer (A0/P100 (O)) (Figure 6-7). The acrylic polymer was studied alongside the as-received acrylic monomer (A100/P0 (M)) for insightful comparisons. Moreover, the as-received PPE oligomer (A0/P100 (O)) was compared with a mixture of PPE and dibenzoyl peroxide initiator (A0/P100 (O+BPO)) to ascertain the homopolymerisation potential of the PPE in the absence of the acrylic monomer.

While acrylic monomer and polymer, and PPE oligomer were all soluble in $CDCl_3$ at room temperature, the A95/P5 (P(R)) and A90/P10 (P(R)) blends required heat (50°C), sonication (approx. 2 h) and excess $CDCl_3$ to dissolve partially. These differences in solubility suggest that A95/P5 (P(R)) and A90/P10 (P(R)) formed reactive blends. To substantiate this, non-reactive blends A95/P5 (P(NR)) and A90/P10 (P(NR)) were prepared by mixing as-received acrylic monomer with as-received PPE oligomer in the aforementioned ratios (Table 6-2). These non-reactive blends displayed complete solubility in $CDCl_3$. The solubility differences between the reactive and non-reactive blends suggest that the less soluble components of A95/P5 (P(R)) and A90/P10 (P(R)) are likely to be a high-molecular-weight copolymer or a cross-linked acrylic/PPE species, or a combination of both. Interestingly, while A95/P5 (P(R)) and A90/P10 (P(R)) blends exhibited noticeable swelling upon solvation in $CDCl_3$, no swelling was observed with the A95/P5 (P(NR)) and A90/P10 (P(NR)). Swelling has previously been associated with the formation of cross-linked structures [38], with higher swelling ratios observed at lower cross-linker concentrations (<20 %) of divinylbenzene in methyl methacrylate (MMA)-divinylbenzene cross-linked copolymers. An important distinction between the cited work and this current research is that cross-linking was not the targeted hybridisation route in this work.

Comparative NMR analysis of A100/P0 (M) and A100/P0 (P) confirmed that polymerisation of the acrylic occurs under the reaction conditions employed (Figure 6-7). This was evidenced by the appearance of a new ^1H signal. In contrast, no change was evident in the ^1H NMR spectra for A0/P100 (O) and A0/P100 (O+BPO) (Figure 6-7); thus, PPE does not homopolymerise under the reaction conditions employed.

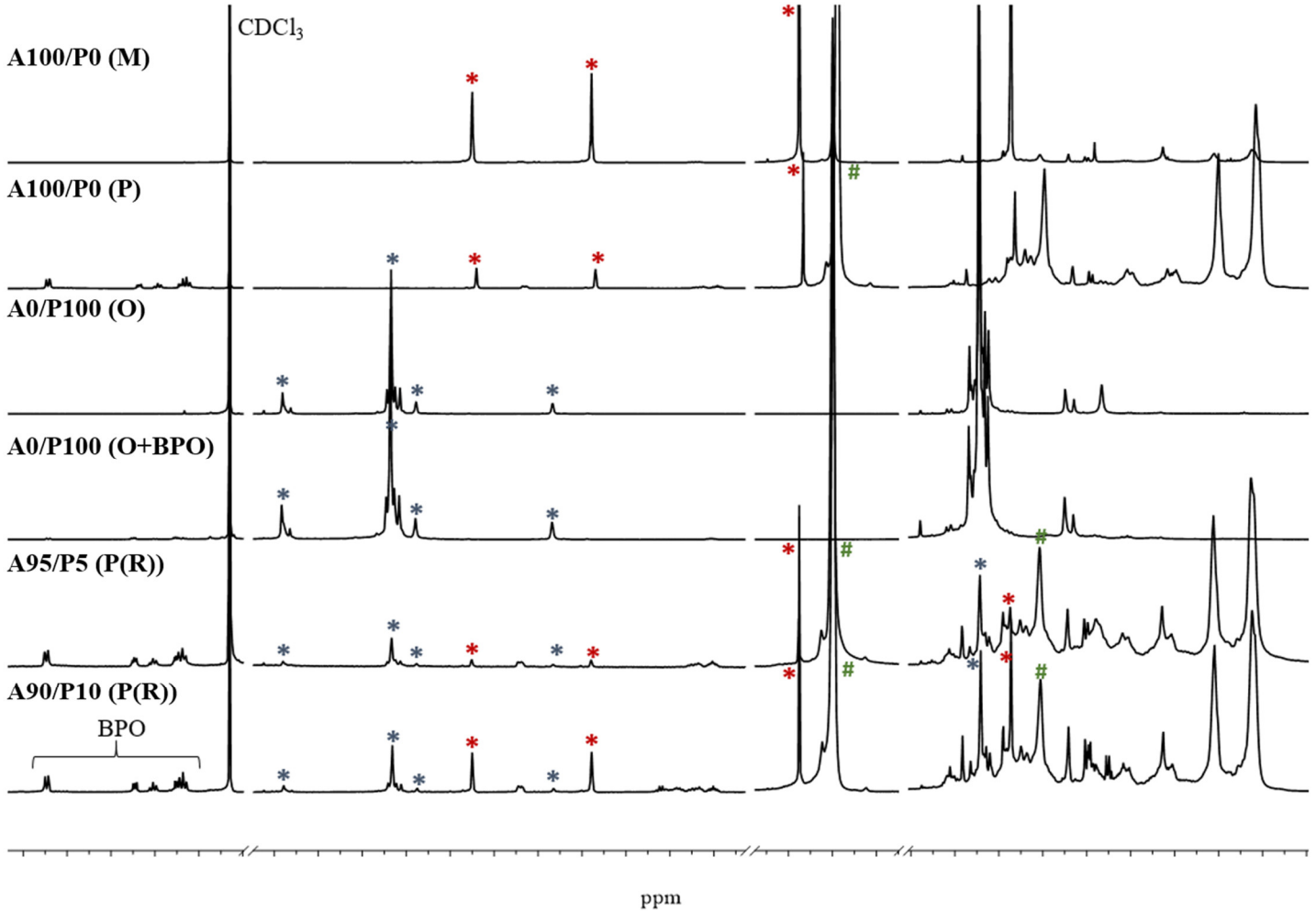


Figure 6-7. Overlaid ^{1}H NMR spectra of the acrylic/PPE blends and the starting materials in the presence and absence of BPO in $CDCl_3$. The key ^{1}H NMR signals from the acrylic monomer (*, red), PPE oligomer (*, blue) and acrylic polymer (#, green) are highlighted.

Notably, ^{1}H NMR spectra of PPE with and without BPO displayed low-intensity ^{1}H signals in the downfield region ($^{1}H^{3-5}$), which were tentatively attributed to vinylic end groups in PPE oligomer (Figure 6-7). HSQC analysis indicated that the $^{1}H^{3}$ signal correlates with a different, more downfield ^{13}C resonance than the $^{1}H^{4}$ and $^{1}H^{5}$ signals; $^{1}H^{4}$ and $^{1}H^{5}$ correlated with a single ^{13}C resonance within the expected ^{13}C NMR shift range for a disubstituted vinyl moiety. Therefore NMR analysis, suggests that $^{1}H^{3}$ protons are most likely aromatic, whereas $^{1}H^{4}$ and $^{1}H^{5}$ correspond to vinyl protons on disubstituted vinyl moieties in PPE oligomer end groups [39]. Using the M_n of the commercially available PPE oligomer (2300 Da), along with the relative integrals of the $^{1}H^{3-5}$ and aromatic PPE oligomer backbone signals, suggests that the PPE oligomer contains multiple reactive aromatic vinyl end groups per chain and may, therefore, form cross-links between acrylic polymer chains. Although these vinyl functional groups appear to be unreactive towards homopolymerisation under the conditions tested, these groups are likely involved in copolymerisation/cross-linking reactions in the presence of the acrylic.

The reactivity differences between the acrylic and PPE, combined with NMR studies, suggest that the formation of block copolymers does not occur under the conditions employed in this work. Rather, the generation of random/graft copolymers or cross-linked polymers is more likely (Figure 6-8).

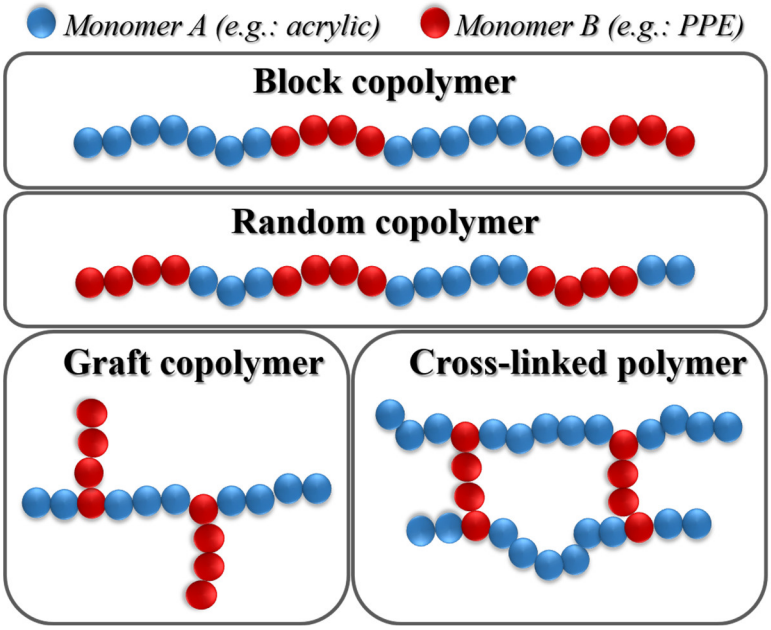


Figure 6-8. Basic structures of block and random copolymers and cross-linked polymers.

Although in-depth characterisation of the blends was limited by their low solubility in common NMR solvents, ^{1}H NMR analysis of the soluble portions of A95/P5 and A90/P10 blends indicated multi-component mixtures, which comprised acrylic polymer, unreacted PPE oligomer and acrylic monomer, as well as BPO (Figure 6-7). While the insoluble portions of the reactive blends (A95/P5 and A90/P10) could not be analysed, ^{1}H NMR analysis showed that the acrylic polymer is the major component of the soluble portions (based on the relative intensities of the acrylic polymer -OR ^{1}H NMR signal *vs.* the acrylic monomer and PPE oligomer). Although close inspection of baseline signals in the ^{1}H NMR spectra revealed several unknown species, these could be attributed to trace components present in the starting materials and impurities from sample preparation (Figure 6-7); none were associated with acrylic polymer/PPE linkages. DOSY NMR analysis supported these observations, indicating that separate PPE oligomer and acrylic polymer molecules were present in the soluble portions of the reactive A95/P5 and A90/P10 blends as these species give different diffusion coefficients as annotated in Figure 6-9.

Mechanical and cryogrinding (using liquid nitrogen) in a mortar and pestle were considered as alternative routes to attaining samples for solid-state NMR. However, the blended samples were not readily pulverised. Taken together with the ^{1}H NMR data of the soluble components, the insolubility, resistance to mechanical and cryogrinding, and swelling of the A95/P5 and A90/P10 blends suggest that these are reactive blends, rather than (non-reactive) blended aggregates of acrylic polymer and PPE oligomer. Indeed, the low solubility and swelling suggest the formation of high-molecular-weight copolymeric or cross-linked acrylic/PPE species. While the resistance to grinding and lack of solubility limited the determination of the precise chemical structure of the A95/P5 and A90/P10 blends, by both solid- and solution-state NMR spectroscopy, this low solubility offers potential benefits in terms of solvent resistance and thermal stability. Moreover, the observed resistance to pulverisation in the blends suggests enhanced mechanical properties such as toughness. This will be explored in further detail in subsequent chapters.

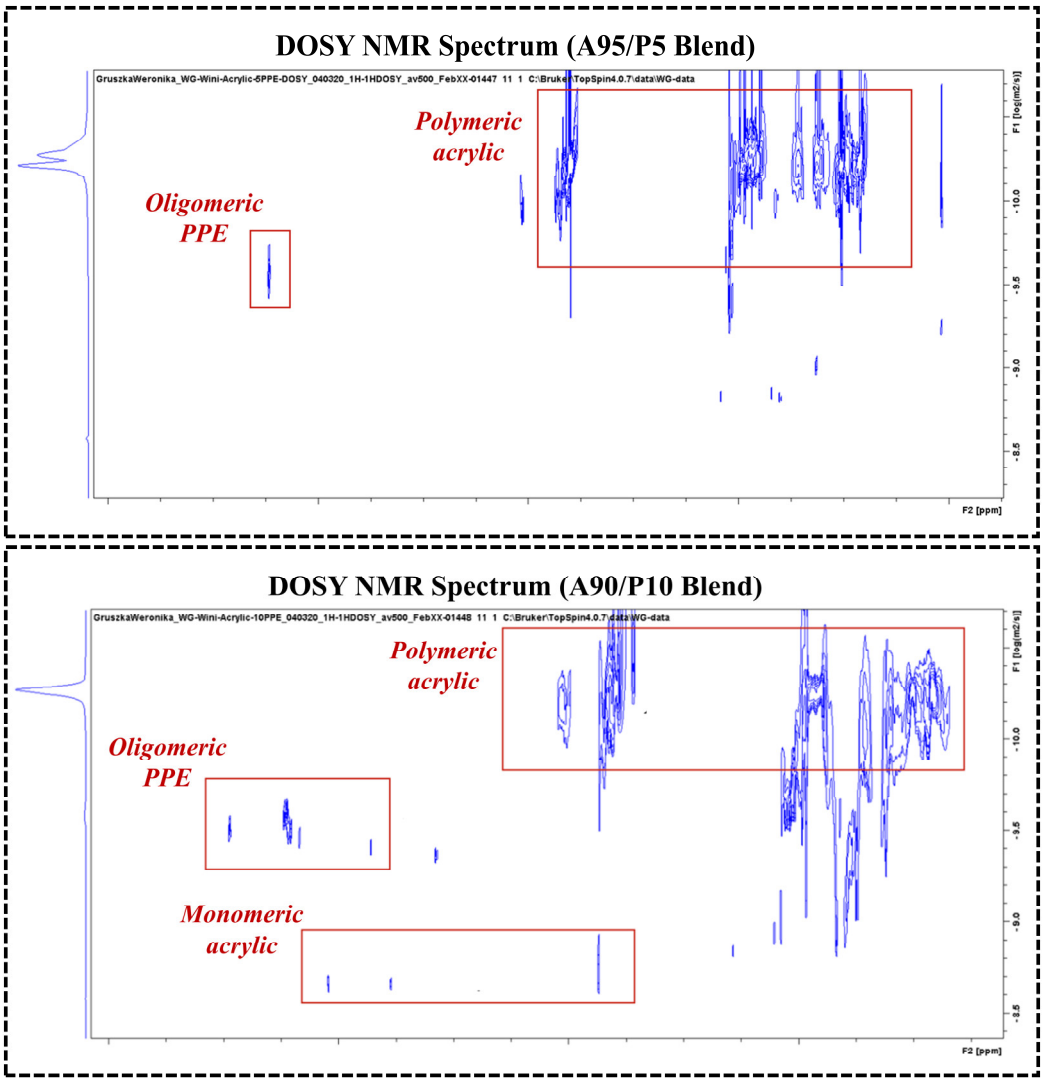


Figure 6-9. DOSY NMR spectrum of A95/P5 and A90/P10 blends in $CDCl_3$.

6.4.2 Solvent resistance results

Figure 6-10 shows the results of solvent resistance experiments on unreinforced polymers. Following exposure to acetone for 60 min at room temperature, all acrylic/PPE blend polymer samples exhibited a lesser extent of mass loss after 60 min in acetone than the unmodified acrylic (A100/P0) sample. A 37 % mass loss was observed with the A100/P0 sample, whereas the blends sustained mass losses in the range of 10-18 %, with noticeable swelling observed during the inspections conducted upon withdrawal of the samples from acetone for drying. Except for the A97/P3 sample, which lost only 12 % of its original mass, an increase in PPE content from 5 wt. % (A95/P5) to 15 wt. %

(A85/P15) results in a consistent increase in solvent resistance, evidenced by corresponding terminal mass losses of 18 % and 10 %, respectively.

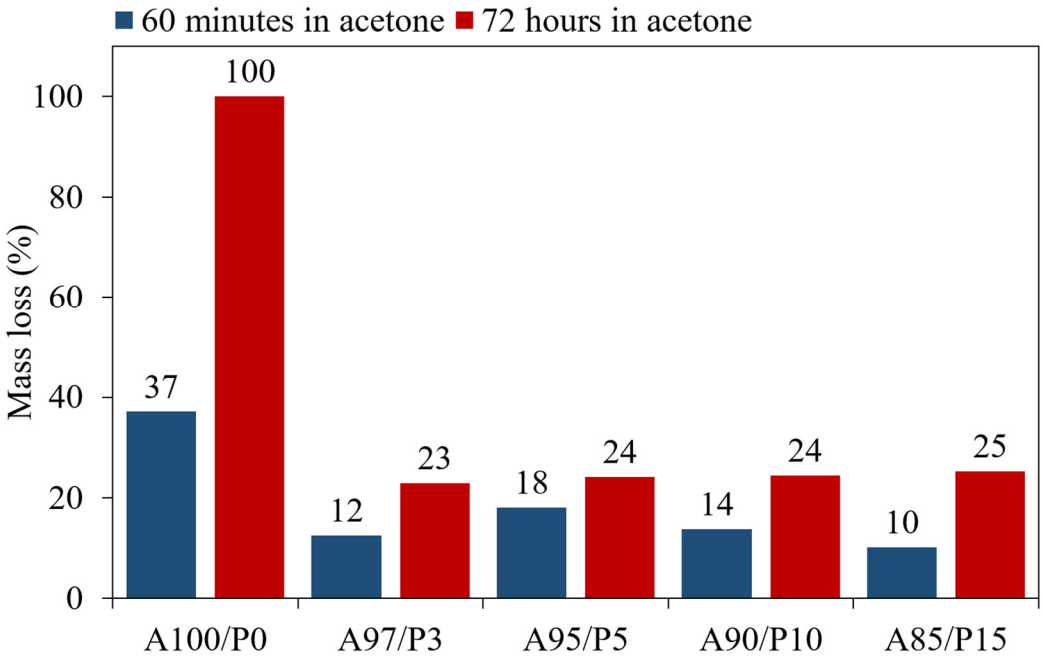


Figure 6-10. Mass losses after the exposure of unreinforced polymer samples to acetone for 60 minutes (blue) and 72 hours (red) showing the influence of PPE modifier content on solvent resistance. Note: A lesser mass loss corresponds to superior solvent resistance.

For 72-hour exposure experiments, the A100/P0 was found to completely dissolve after 300 minutes, following a progressive visible loss of volume. In contrast, all blends sustained 23-25 % of mass loss and exhibited swelling as the initial response within 30 minutes of exposure. Interestingly, increasing the PPE concentration within the blends did not appear to result in significant changes in the terminal mass in acetone after 72 hours. These observations provide strong evidence that PPE content plays a vital role in the dissolution rate and consequently, initial mass loss of acrylic/PPE blends.

The rate of dissolution of polymers is known to be influenced by polymer characteristics such as molecular weight, the chemical structure and composition of the polymer backbone, segmental stiffness and dispersity. Moreover, polymers with high molecular weights are believed to undergo substantial swelling before dissolution ensues [40]; and polymers with cross-linked structure can undergo swelling without dissolution [38]. Given that the addition of PPE into the blends adds aromatic groups within their structure, where the unmodified acrylic only contains aliphatic polymer chains, obvious differences

in the backbone structure, composition, molecular weight and segmental stiffness are likely to arise between the polymer blends.

The variations in initial dissolution behaviour observed in the 60-minute experiments with increasing PPE content are possibly associated with differences in polymer chain mobility [40,41]. At a molecular level, the variation of respective chain mobilities may be substantial enough to give rise to varying reptation times and disengagement rates. This may provide evidence of strong interchain interactions between phenyl groups within the PPE modifier. This hypothesis is supported by Darvell [42], who suggested that weak interchain forces promote a self-perpetuating ingress of solvent into polymers and swelling itself increases the free volume for solvent diffusion. Given that weak interchain forces are readily overcome by the volumetric changes that solvent attack induces.

Time-lapse images of observations from the 72-hour exposure experiments are shown in Figure 6-11. The A100/P0 sample can be seen to undergo progressive mass loss until dissolution at 300 minutes. In contrast, the PPE-modified hybrid polymers appear to exhibit whitening, with considerable swelling being observed across all samples until the full study duration was elapsed. These results provide further evidence of a significant effect of PPE incorporation on the molecular weight [40] and the possibility of cross-linked [38] acrylic/PPE species arising from the reactions of the acrylic monomer with multi-vinyl PPE oligomer. Moreover, dispersity also plays a role in the rate of dissolution and may explain the enhanced solvent resistance observed with the blend polymers [40].

Interestingly, A90/P10 and A85/P15 exhibit signs of attack on the edges with minor cracks observed. However, during 24-hour inspections, these appear to 'heal'. This implies that the volumetric change associated with the dissolution of the soluble constituent is less than or equivalent to the volumetric change resulting from the swelling of the insoluble constituent. Thus, any healing effects may be attributed to swelling after craze formation. Given that the swelling is known to be indicative of a cross-linked structure [38] and that non-cross-linked polymers typically undergo dissolution, which can locally result in microfibril or craze formation [43], these observations are highly insightful. Not only do they highlight differences between the higher (A90/P10 and A85/P15) and lower (A97/P3 and A95/P5) PPE loadings, but they provide strong evidence of the formation of both cross-linked and non-cross-linked species within the blends. It is plausible that

the lower PPE concentrations produce fewer cross-linked zones with the dominant phase being highly entangled [44–46].

It is worth noting that white sediments were observed in the solvent from 60 minutes for all hybrid polymers. These sediments remained in the solvent until the experiment was completed. The size of dispersed sediment appeared to increase with increasing PPE content. These observations may indicate the presence of a small quantity of unreacted PPE oligomer within the polymerised samples, which is in agreement with observations from NMR analysis of these materials as discussed in Section 6.4.1.

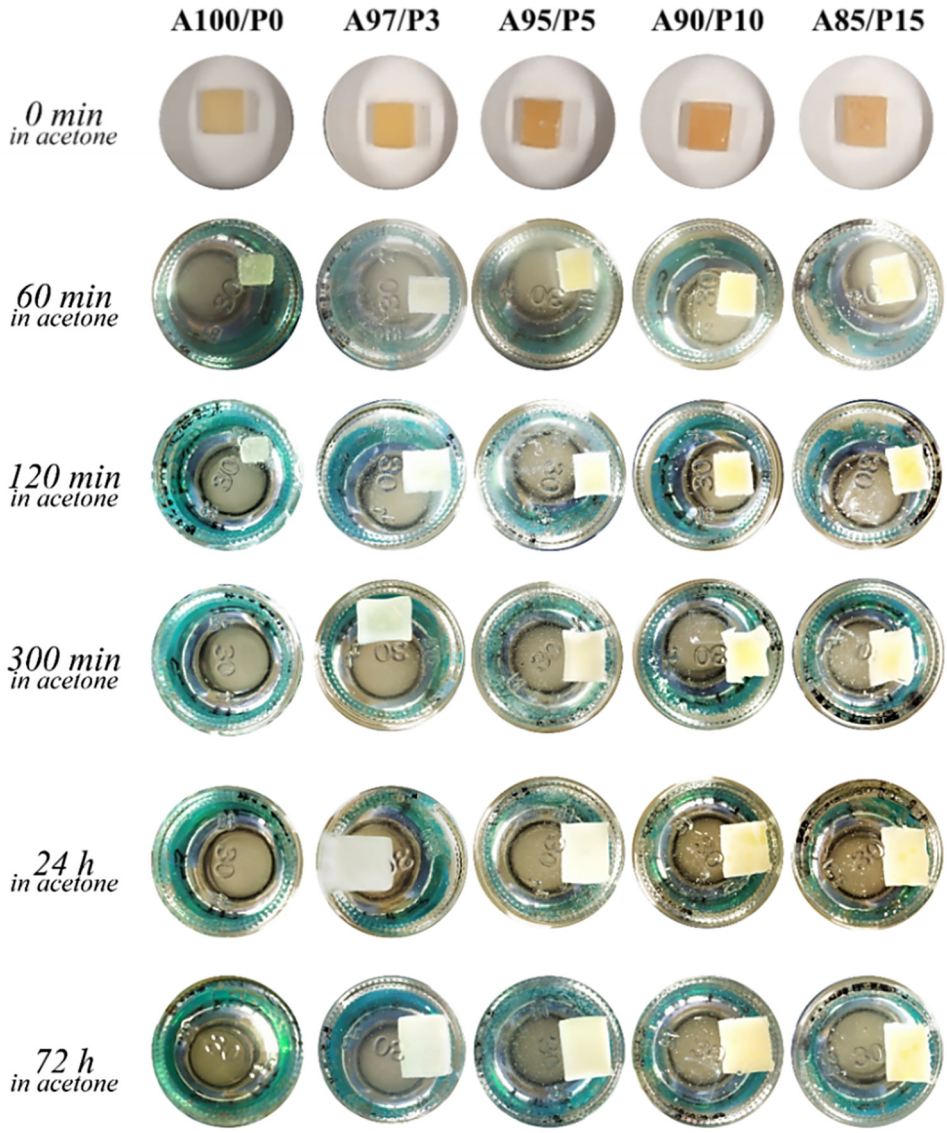


Figure 6-11. Time-lapse images of unmodified acrylic (A100/P0) and PPE-modified acrylic blends with compositional variations (A97/P3 – A85/P15) subjected to prolonged (72 h) exposure in acetone — nominal sample dimensions (mm): 8 × 8.

6.4.3 Dynamic mechanical analysis

From single-frequency DMA scans at 1 Hz, the effects of PPE-modification on the glass transition temperatures and tan delta peak heights were studied alongside the unmodified acrylic polymer matrix material. T_g values were determined as the temperature corresponding to the maximum tan delta value. The representative thermograms obtained from each material presented in Figure 6-12 reveal single tan delta peaks for all blends.

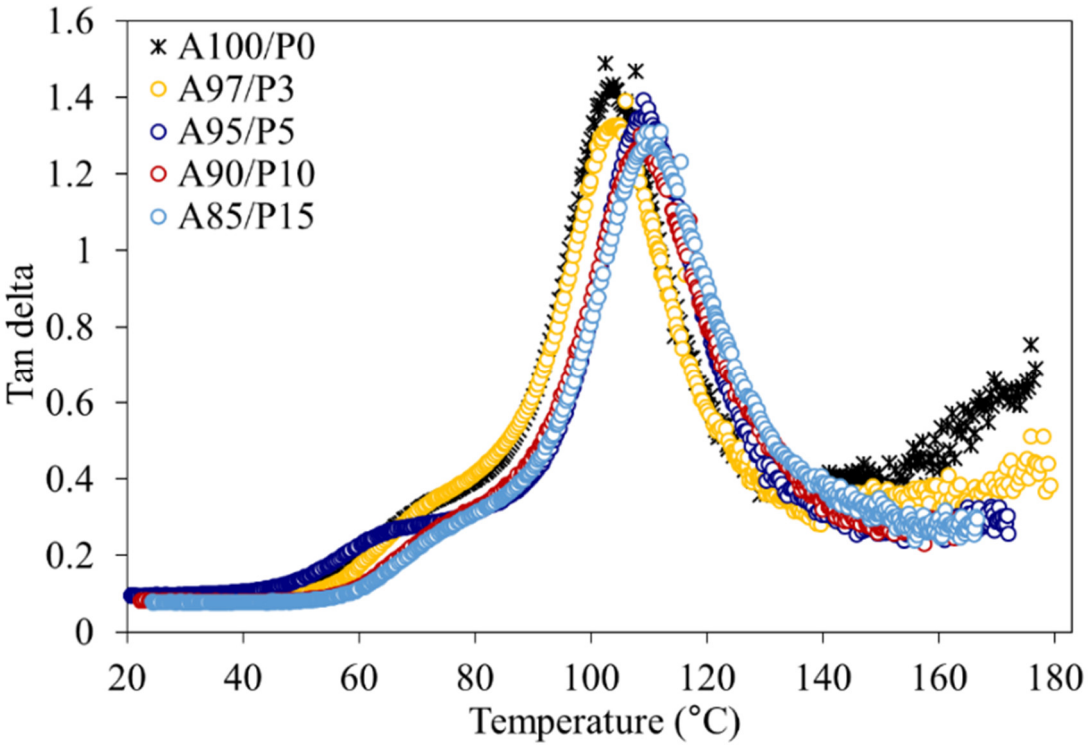


Figure 6-12. Representative DMA thermograms showing the effects of PPE content on damping behaviour (tan delta) and T_g. Note: the PPE used has a T_g of 160°C [33].

As shown in Figure 6-13, increasing the PPE content within the blends causes an overall increase in T_g by up to ~6°C. This suggests decreased chain mobility due to increased rigidity and π- π interactions due to the phenyl rings [47] of the PPE phase.

A lowering effect was also observed for the tan delta peak heights, with values decreasing by up to ~0.2 (-12 %). These trends are more pronounced up to 5 wt. % addition of PPE, as in the A95/P5 material; however, as PPE content is increased up to 15 wt. % (A85/P15), the contributions are less prominent. Given that tan delta is a ratio of loss to storage modulus, which describes the degree of viscoelastic damping within a material and the extent of polymer segmental mobility, the overall reductions in tan delta peak

height with increasing PPE content suggests a reduction in the viscoelastic response of the blends compared to the unmodified acrylic polymer matrix.

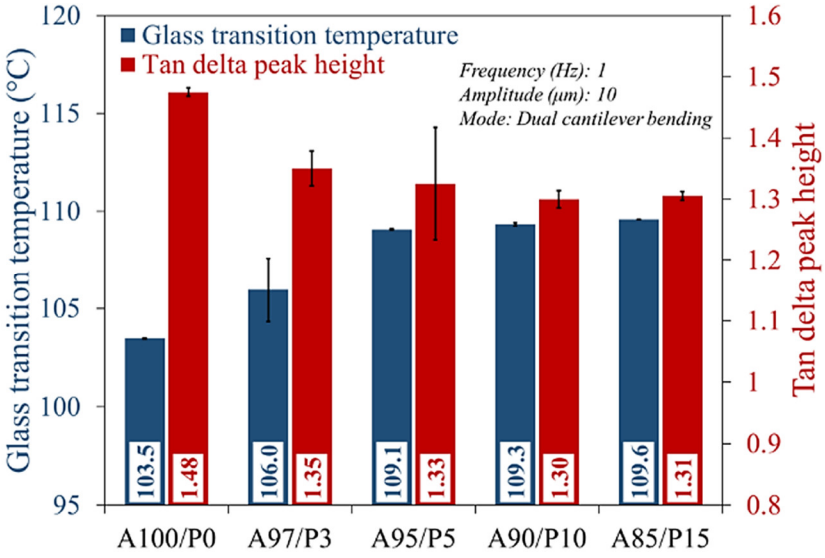


Figure 6-13. T_g values and tan delta peak heights from DMA experiments on polymer matrix samples. Results are based on averaged duplicates. Note: the PPE used has a T_g of 160°C [33].

This may be due to increased rigidity caused by the phenyl moieties in PPE or may be indicative of the existence of a cross-linked species, which would likely decrease the chain mobility [48]. Despite the absence of a cross-linking agent, the presence of the vinyl-functionalised PPE oligomer may have triggered spontaneous localised cross-linking alongside the formation of a non-cross-linked acrylic-rich constituent. Using a high-molecular-weight vinyl-pendant PPO, Huang et al. [49] proposed that a higher vinyl-pendant ratio was more likely to undergo a cross-linking reaction during polymerisation than a lower ratio. This is because an increased number of pendant vinyl groups can participate in the polymerisation process to form cross-linked structures. Interestingly, increasing glass transition temperatures were also thought to be attributed to the presence of cross-links within the vinyl-pendant PPO structure.

While this present research employed a low-molecular-weight, vinyl-end-functionalised PPE, it is plausible that increased glass transition temperatures in the blends with respect to A100/P0 was a contribution of cross-linked structures.

The effects of PPE modification on half peak width and peak factor were also assessed. Peak factor is a representation of the intrinsic heterogeneity within the polymer system [50]. It is calculated as the ratio of the corresponding half peak width and peak height for

each material, obtained as shown in Figure 6-14. Within blended polymeric systems with dissimilar T_g values, broad tan delta peaks indicate the occurrence of diffuse domains [51,52]. Both peak width [53] and peak factor are attributed to the heterogeneity of broad dispersity [50,54]; however, peak width also correlates to the distribution of relaxation times within the polymer [55].

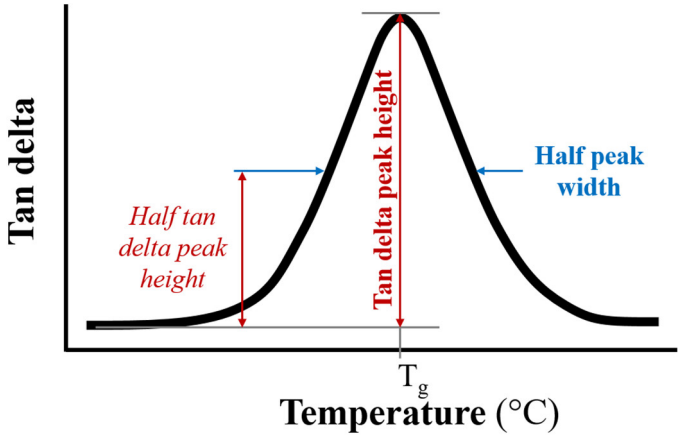


Figure 6-14. Diagrammatic representation showing the determination of half peak width and peak factor from DMA thermograms.

Using this approach, the parameters in Figure 6-15 were obtained. The addition of PPE results in an overall increase in both the half peak width and peak factor, relative to the unmodified A100/P0 polymer. An increasing trend in both half peak widths and peak factors can also be observed with increasing PPE content.

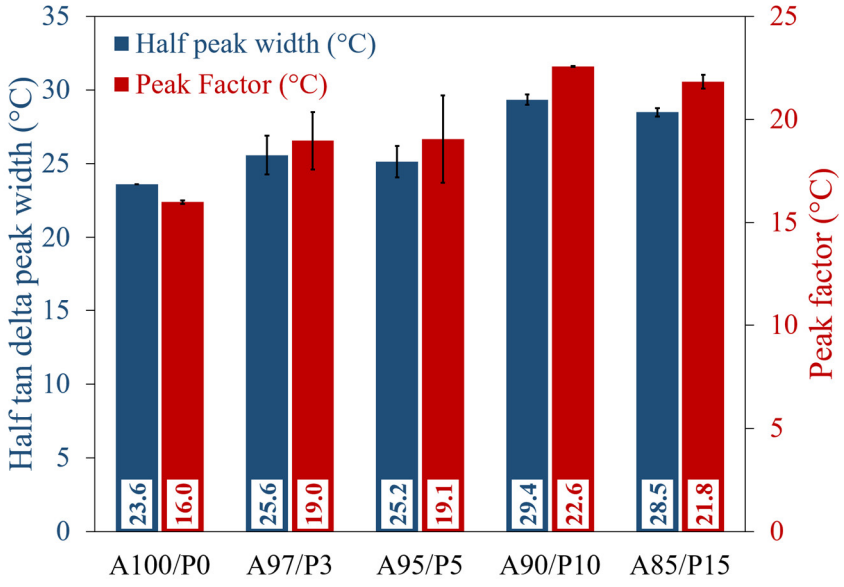


Figure 6-15. Half tan delta peak widths and peak factors determined from DMA experiments on polymer matrix samples. Results are based on averaged duplicates.

Thus, the correlation between the PPE content and both peak width and peak factor suggests the co-existence of composition-dependent acrylic-rich and PPE-rich phases within the blends.

6.4.4 Results of thermogravimetric analysis

The thermal stabilities of the acrylic and PPE-modified acrylic blends were analysed by thermogravimetric analysis (TGA). The graphical representation showing in Figure 6-16.

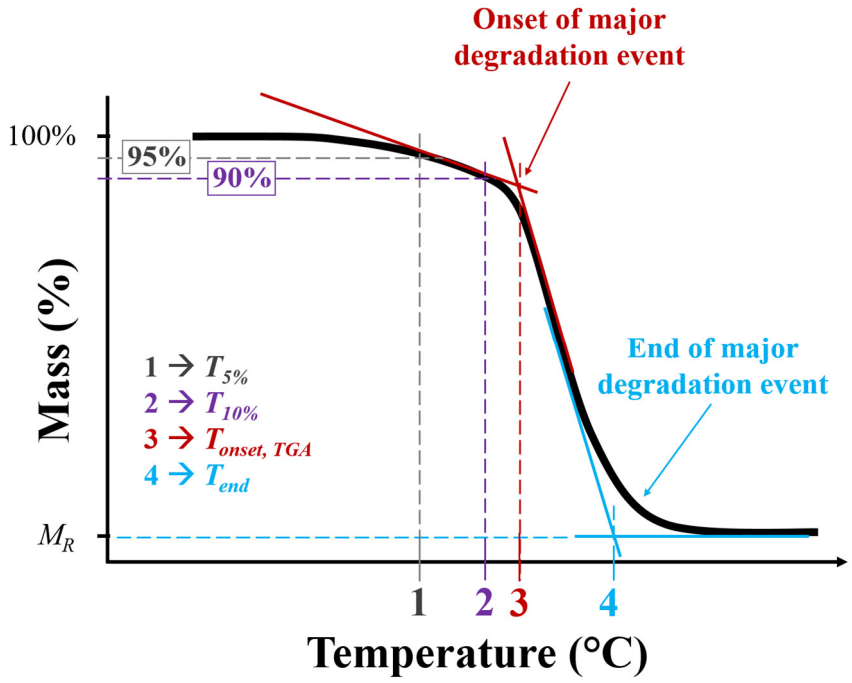


Figure 6-16. Graphical illustration of the characteristic parameters for TGA curves.

The representative thermogravimetric mass loss behaviour for all polymers are shown in Figure 6-17; two samples were analysed per material. PPE oligomer (A0/P100) appears to undergo a single-stage degradation process under the experimental conditions employed. Negligible mass loss was observed under 438°C, its onset temperature for major degradation ($T_{onset\text{-}TGA}$). This degradation behaviour is consistent with observations in published literature, which cite a major step between 430 and 500°C. This step is reported to occur as a result of thermal Fries-type chain rearrangements [56,57].

For A100/P0 samples and PPE-modified acrylic polymer samples, the slopes of their respective thermograms can be seen to change more significantly, particularly in Zone 1 (see popout plot of the inset). This is indicative of minor thermal degradation between 90°C and 110°C.

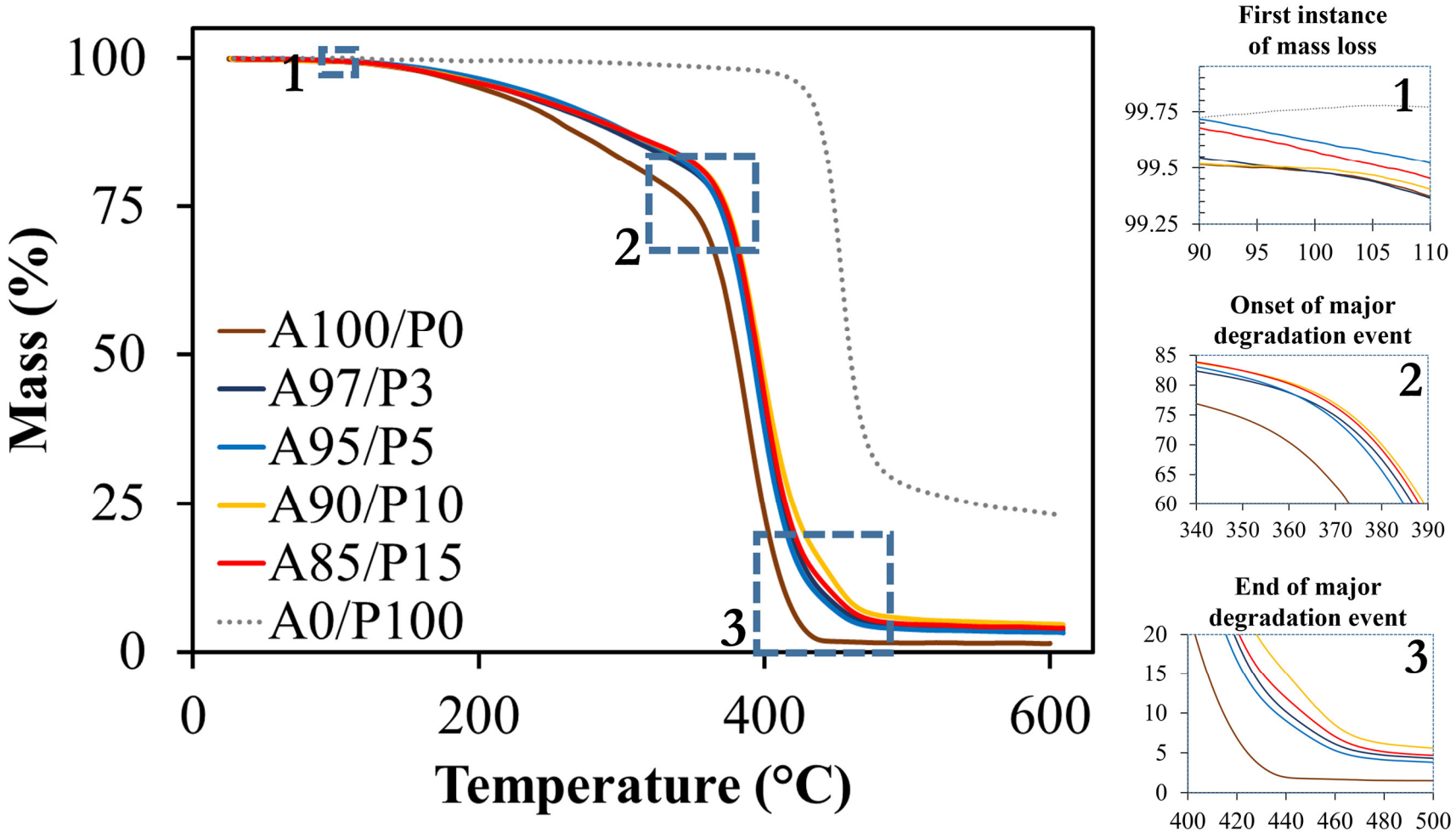


Figure 6-17. Representative thermograms from TGA on unmodified acrylic polymer (A100/P0) and PPE-modified acrylic blends A97/P3, A95/P5, A90/P10 and A85/P15. Zones 1-3 are characteristic degradation zones and are presented as inset graphs for improved visibility.

Evidently, the A100/P0 and the PPE-modified acrylic blends exhibit more sudden respective mass losses up to the $T_{onset\text{-}TGA}$. The incorporation of PPE delays the onset of major degradation, $T_{onset\text{-}TGA}$ by 7-10°C under the degradation conditions used as can be seen in Table 6-4.

Table 6-4. Summary of thermogravimetric results for polymeric showing the effects of PPE-modification on thermal stability. Values are averaged from duplicates.

	TGA curve parameters				
	$T_{onset,\ TGA}$ [a]	$T_{5\%}$ [b]	$T_{10\%}$ [c]	$T_{end,\ TGA}$ [d]	M_R [e]
	(°C)	*(°C)*	*(°C)*	*(°C)*	*%*
A100/P0	355 ± 3.2	205 ± 6	255 ± 4.6	419 ± 1.9	1 ± 0.6
A97/P3	362 ± 1.3	216 ± 6	274 ± 4.2	426 ± 0.1	4 ± 0.0
A95/P5	362 ± 2.2	225 ± 4	282 ± 2.8	423 ± 0.9	3 ± 0.4
A90/P10	365 ± 2.8	222 ± 13	286 ± 11.2	431 ± 0.2	4 ± 0.5
A85/P15	363 ± 0.1	211 ± 2	274 ± 3.9	428 ± 1.9	4 ± 0.3
A0/P100	438 ± 0.1	426 ± 1	438 ± 0.4	471 ± 0.7	23 ± 0.1

a, d $T_{onset,\ TGA}$ **&** $T_{end,\ TGA}$**:** Onset and end temperatures for the main degradation event as determined from the intersection of tangents to the inflexion at of the TGA curves (Figure 6-17), respectively.

b, c $T_{N\%}$**:** Temperatures corresponding to N% mass loss using the TGA thermograms.

e M_R**:** Residual mass at the end of the thermal cycle.

In addition to comparing the effect of PPE content on $T_{onset\text{-}TGA}$, it may be useful to compare the temperatures previously presented in Figure 6-16. $T_{5\%}$ and $T_{10\%}$ are temperatures corresponding to mass losses of 5 % and 10 %. The PPE-modified acrylic blends possessed up to 10 % and 12 % higher $T_{5\%}$ and $T_{10\%}$ values, respectively relative to the unmodified acrylic polymer. Thus, incorporating PPE oligomer into the acrylic polymer system results in improved thermal stability in terms of delaying thermal degradation events. However, at the PPE concentrations employed in this present work, no distinct trends or correlations were discernible between PPE loading and the extent of improvements attained. The representative DTG plots shown in Figure 6-18 reveal that A100/P0 undergoes a major degradation event with a valley occurring ca. 300-445°C. Evidence of a unique, minor degradation event in the A100/P0 material can be seen between 225°C-300°C.

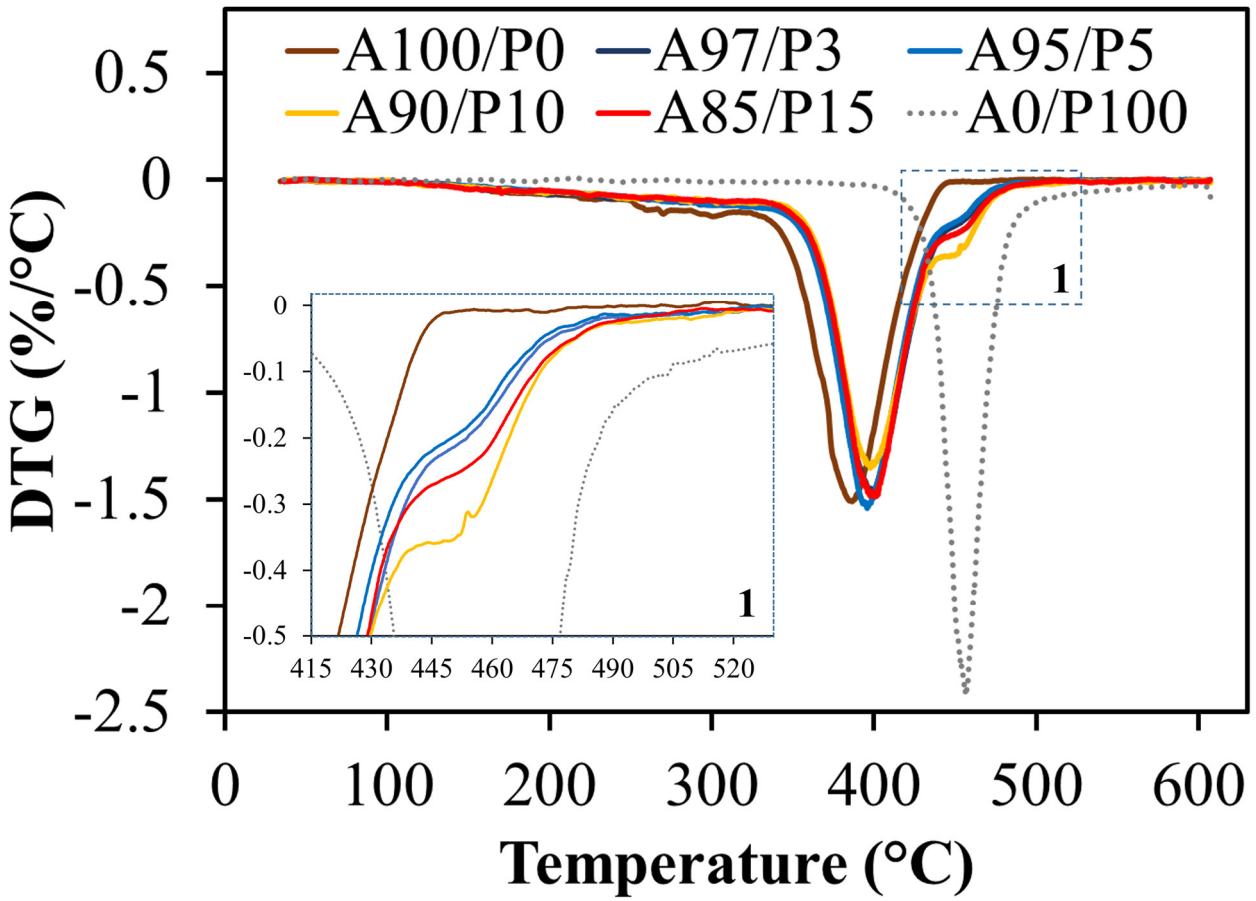


Figure 6-18. Representative DTG thermograms for unmodified acrylic polymer (A100/P0), PPE oligomer (A0/P100) and their blends: A97/P3, A95/P5, A90/P10 and A85/P15. Zone 1 is an inset graph for improved visibility of unique degradation behaviour exhibited by all blends.

Polymethylmethacrylate-based polymers are reported to undergo three-stage thermal degradation processes; with head-to-head linkage-induced scission (150-264°C), unsaturated chain-end-induced scission (264°C-335°C) and random main chain scission (335°C-425°C) [58–60]. However, in a recent study on a similar grade of acrylic resin (Elium® 150), de Andrade Raponi et al. [61] reported two distinct degradation stages. All samples studied by the authors exhibited minor DTG valleys ($T_{onset\text{-}DTG}$: 108°C-115°C) and major degradation valleys ($T_{onset\text{-}DTG}$: 298°C-326°C). A graphical representation illustrating each DTG parameter ($T_{onset\text{-}DTG}$, T_{end}^{1} and T_{end}^{2}) is provided in Figure 6-19.

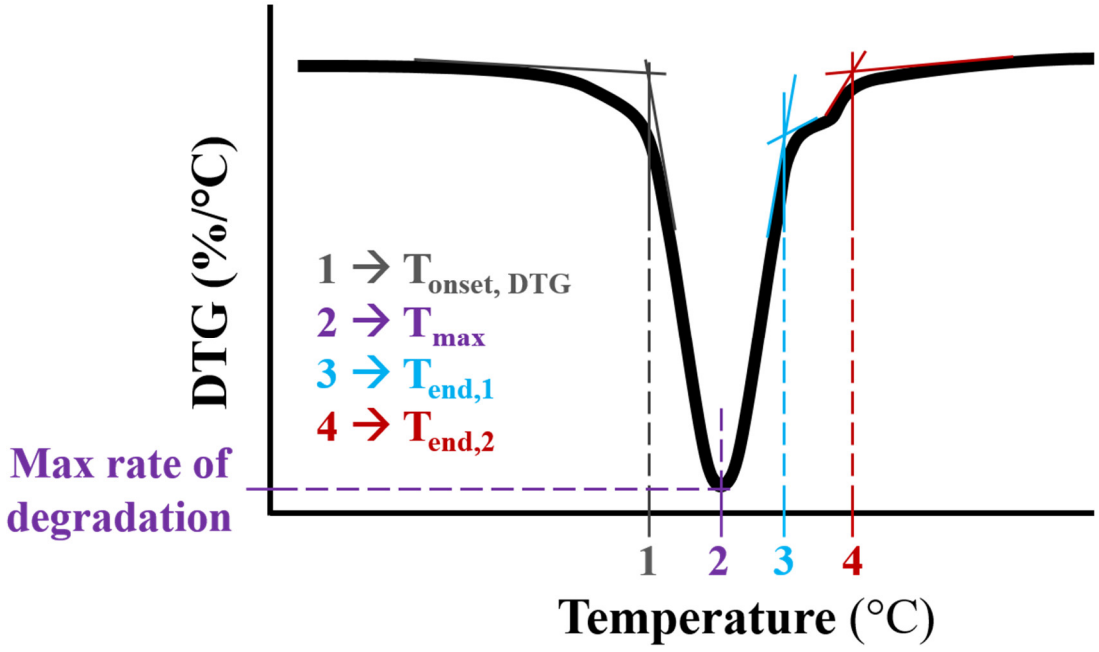


Figure 6-19. Graphical illustration of key DTG parameters.

The occurrence of the unique, minor degradation event in A100/P0 between 225°C and 300°C is thought to be attributed to the degradation of unsaturated chain ends [61]. Interestingly, no preceding major degradation events were observed. The main stage of degradation occurring between 300°C and 445°C is linked to random scission of main polymer chains [58,59]. Interestingly, while TGA thermograms showed minor mass losses between 90°C and 110°C for all acrylic-based polymers and blends, the early-onset degradation step reported by de Andrade Raponi et al. [61] as occurring between 150°C and 230°C was characteristically absent from the DTG thermograms of the materials in this present work. This step is known to be induced by the breakdown of weak head-to-

head linkages. These linkages are formed during the termination reaction (by combination) of the polymerisation process. Thus, this step's absence may indicate that alternative termination reactions must have been prevalent within the polymers under investigation [60]. The absence of this step may also suggest that shorter chain lengths dominate within each polymer material. Longer chain lengths are more susceptible to defects such as head-to-head linkages and are thus, more thermally labile [62].

Given that unsaturated chain-end-induced degradation was observed for A100/P0, the absence of such a step for the PPE-modified acrylic blends may provide vital insight into structural differences between PPE-modified and unmodified acrylic polymer. Unsaturated chain ends are formed along with saturated chain ends. This occurs due to termination by disproportionation reactions during the free-radical polymerisation process [63]. Therefore, this evidence suggests that the presence of PPE changes the ratios underpinning the termination reactions during the polymerisation process of these PPE-modified acrylic blends.

Furthermore, all PPE-modified acrylic blends exhibit elevated temperature degradation events, occurring between ~430°C and ~480°C, where a slower degradation rate is evident. This late-stage event is likely due to contributions from PPE-rich phases within the blended polymer systems and may be linked with the aforementioned Fries-type rearrangements associated with PPE chains. This distinct behaviour with the blends provides strong evidence of chemical interactions between the acrylic and PPE components of the blends, mainly because thermal degradation here is driven by main chain scission. Thus, this confirms that the presence of PPE chemically interacts with the acrylic and alters the chemical structure of the blends compared to the acrylic reference. This is further supported by the fact that the blends' end-stage degradation events coincide with the A0/P100 valley's peak temperature, as shown in Zone 1 of (Figure 6-18).

A summary of all characteristics determined from the DTG thermograms is presented in Table 6-5.

Table 6-5. Summary of derivative thermogravimetric results for polymeric showing the effects of PPE-modification on thermal stability. Values are averaged from duplicates.

	DTG curve parameters			
	$T_{onset,\ DTG}$ [a]	$T_{end,\ DTG\text{-}1}$ [b]	$T_{end,\ DTG\text{-}2}$ [c]	T_{max} [d]
	(°C)	*(°C)*	*(°C)*	*(°C)*
A100/P0	347 ± 3.8	433 ± 4.8	–	388 ± 3.7
A97/P3	363 ± 0.1	439 ± 2.3	476 ± 0.2	399 ± 0.1
A95/P5	359 ± 1.6	435 ± 0.1	474 ± 1.3	396 ± 0.1
A90/P10	360 ± 1.1	435 ± 0.0	476 ± 3.6	398 ± 0.1
A85/P15	363 ± 2.5	434 ± 0.1	479 ± 2.1	399 ± 1.3
A0/P100	429 ± 0.5	482 ± 0.1	–	457 ± 0.3

[a] $T_{onset,\ DTG}$: Onset temperatures corresponding to the pre-peak inflexion points of DTG curves as determined from the intersection of tangents.

[b, c] $T_{end,\ DTG\text{-}N}$: End temperatures corresponding to the post-peak inflexion points of DTG curves as determined from the intersection of tangents. Where N=1 & 2 are presented, two inflexion points exist.

[d] $T_{max\text{-}DTG}$: Temperatures corresponding to the maximum rate of degradation; i.e., the valleys or peaks of the DTG curves.

6.4.5 Effects of modification on the flexural behaviour

With the exception of the A85/P15 sample, PPE modification appeared to produce PPE-modified acrylic blends with enhanced flexural properties (strength and stiffness) relative to the unmodified acrylic (A100/P0) as can be seen in Figure 6-20. This may be attributed to more pronounced effects of the trace amounts of unreacted PPE as previously discussed in Section 6.3.5. Such effects would be exacerbated by the increased availability of PPE species within the system competing with oxygen radicals. Oxygen inhibition is well-documented and is known to affect free-radical polymerisation [64,65]. Thus, localised sites with trace unreacted PPE powder are likely to act as defects, which would ultimately have deleterious effects on the samples' load-bearing capacity. However, this may be circumvented if the blends are prepared in the absence of oxygen, effectively avoiding oxygen inhibition.

Although mid-span deflections were not measured during testing, all hybrid samples exhibited superior stiffness than the A100/P0 sample. The observed increase in stiffness may indicate that incorporating PPE into the acrylic matrix produces a modulus-increasing effect in the resulting matrix.

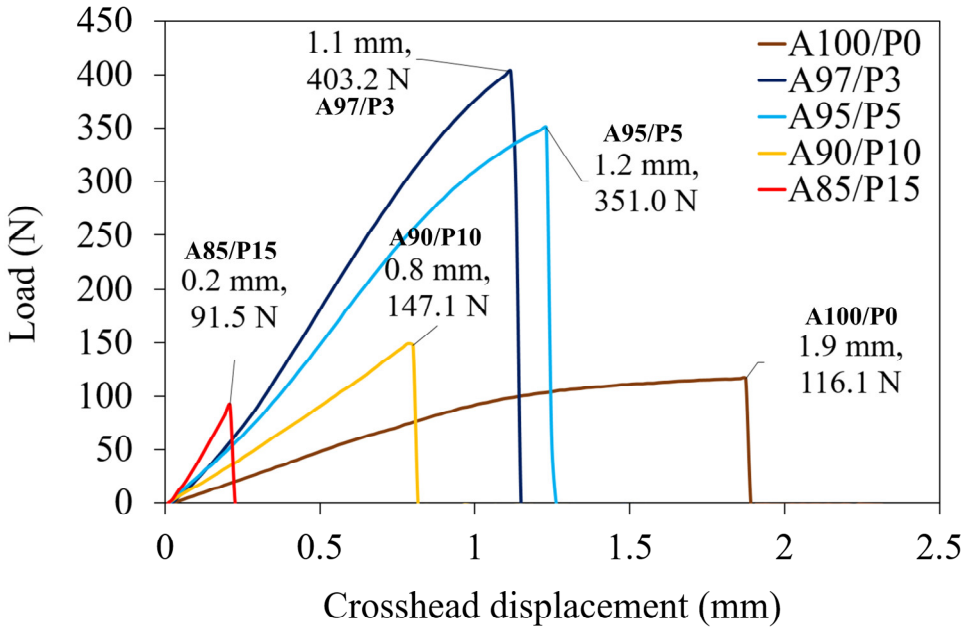


Figure 6-20. Flexural load-displacement curves from flexural testing of neat acrylic A100/P0, and PPE-modified acrylic blends (A97/P3, A95/P5, A90/P10 and A85/P15).

Due to the challenges encountered with polymerisation-induced foaming in the production of unreinforced polymer samples, these results are based on single-sample tests and are thus, not conclusive. However, these results provide interesting insights that are worthy of further investigation, particularly in terms of reinforced composite mechanical properties.

While the precise mechanism by which these enhancements cannot yet be identified, complementary microscopic assessments provide important insights on possible interacting morphological factors.

6.4.6 Effects of PPE-modification on morphology

The hypothesis proposed throughout this Chapter on the contributions of a biphasic morphology to observed behaviour is substantiated by evidence from confocal Raman microscopy, as shown in Figure 6-21.

As is evident from these compositional maps, all blends exhibit binary phase separation. PPE-rich domains appear to be dispersed within an acrylic-rich host matrix. The dispersed domains appear to vary in size, distribution and intensity within each blend. These phases appear to interact and are not mutually exclusive.

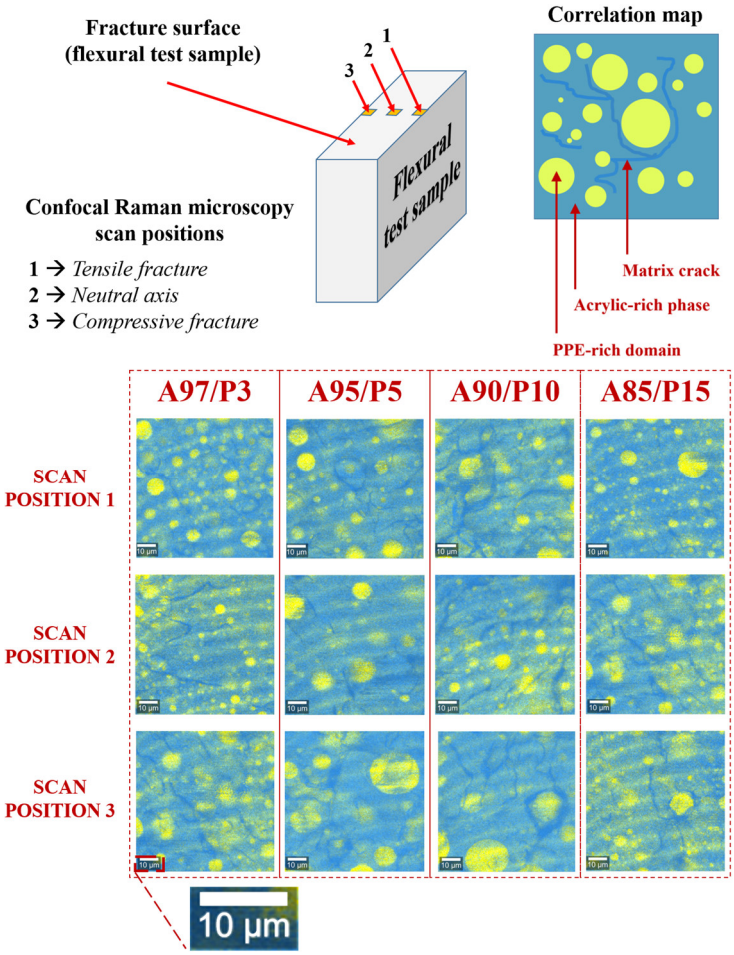


Figure 6-21. Confocal Raman micrographs showing compositional maps for the PPE-modified acrylic blends as obtained from flexural fracture surfaces. The correlation map depicts acrylic- and PPE-rich phases in cyan and yellow; matrix cracks are visible as irregular deep blue vein-like features, respectively.

Some domains exhibit a more distinct boundary, whereas other boundaries are more diffuse in appearance, suggesting multi-species mixtures. It is worth noting that the exact proportion of each component (acrylic and PPE) within the domain and host matrix is not exactly discernible using this technique. This biphasic morphology was confirmed from SEMs of the regions of interest as described in Figure 6-6. These micrographs are presented in Figure 6-23.

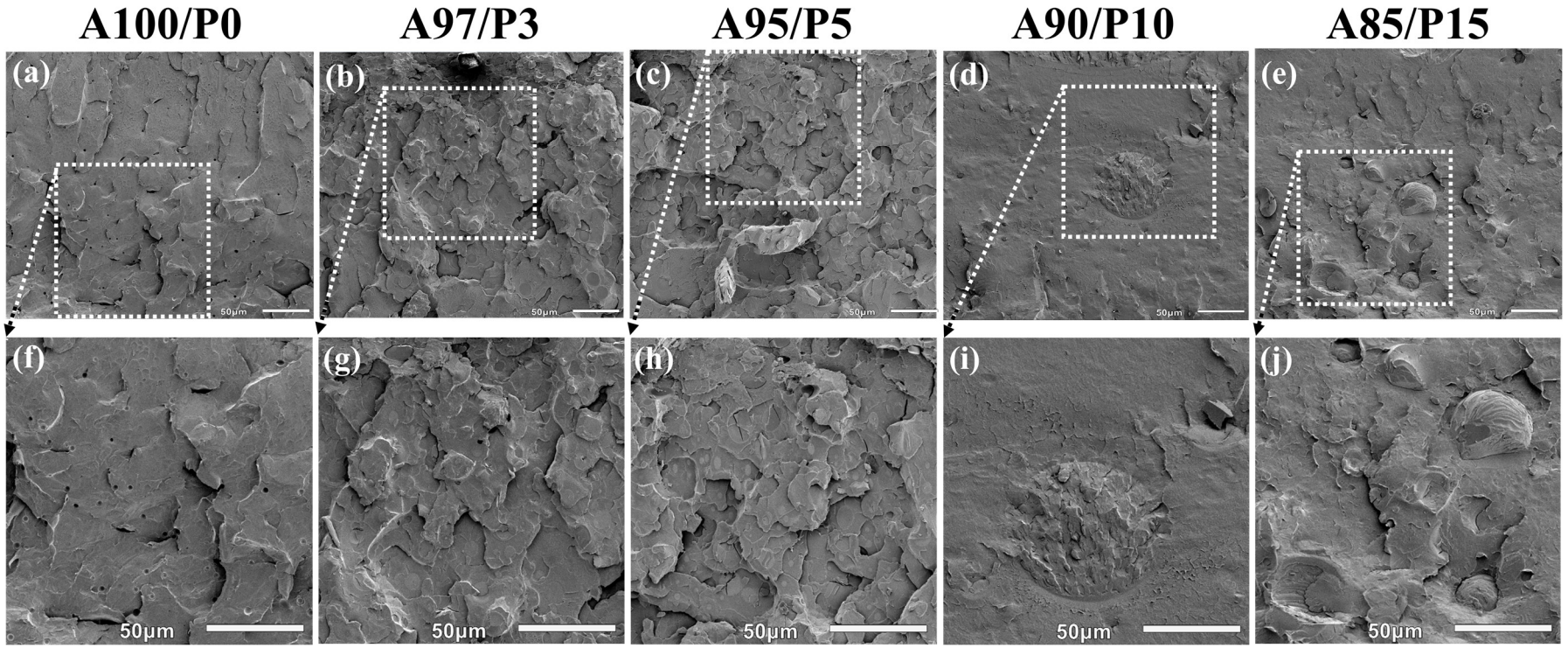


Figure 6-22. SEM micrographs of flexural fracture surfaces of acrylic and PPE-modified acrylic polymer samples. Note: (a)-(e) are low-magnification micrographs and (f)-(j) are high-magnification micrographs of A100/P0, A97/P3, A95/P5, A90/P10 and A85/P1, respectively.

From Figure 6-22, it can be seen that the fracture topography for the A100/P0 sample (Figure 6-22a and Figure 6-22f) appears relatively flat and relatively homogenous. Conversely, the micrographs for the A97/P3 (Figure 6-22b and Figure 6-22g) and A95/P5 (Figure 6-22c and Figure 6-22h) revealed considerably more multi-planar fracture features, suggesting that crack-deflection mechanisms played significant roles [66]. Higher PPE-content blends, A90/P10 (Figure 6-22d Figure 6-22i) and A85/P15 (Figure 6-22e and Figure 6-22j) exhibited highly heterogeneous fracture characteristics, with highly-textured domains surrounded by a phase with relatively flat topography.

Higher magnification micrographs (Figure 6-23) were obtained to facilitate fracture mechanisms classification for each sample. From Figure 6-23a, dimples (Feature 1, Figure 6-23a) and microvoids (Feature 2, Figure 6-23a) can be seen for the A100/P0 sample. In addition to these features, cavitated microvoids were also evident (Feature 3, Figure 6-23a). The dimples/parabolic features, believed to be associated with textured microflow, are boundaries between primary and secondary cracks forming due to coplanar interactions between competing cracks. Secondary cracks form ahead of the main crack due to the presence of inhomogeneities such as microvoids and crazes [67,68]. These microvoids occur as a result of weak interchain forces during the extension of chains [42], thus, confirming the observations in 6.4.2 where weak interchain forces were proposed as the causative factor for solvent ingress in the A100/P0 material.

Evidence of microvoid formation can also be seen in the micrographs of A97/P3 (Figure 6-23b) and A95/P5 (Figure 6-23c) samples; however, these features were only observed within the PPE-rich domains (Feature 5). Both samples appear to exhibit similar behaviour in terms of microcracks (Feature 4) and ruptures (Features 6). These two features possibly have their origins in damage imitation at the microvoids within the domains. Overall, all domains within these samples appear relatively smooth, with more texture surfaces observed for the surrounding bulk phase, possibly indicating brittle fracture of the domains for PPE loadings. At higher loadings of PPE, the domains appear considerably larger and more heterogeneously distributes. This is not only evident in Figure 6-22d and Figure 6-22e, but can be seen in the scale of the domains in Figure 6-23d and Figure 6-23e for A90/P10 and A85/P15, respectively. Interestingly, while the overall fracture surface for these samples did not show evidence of comparable

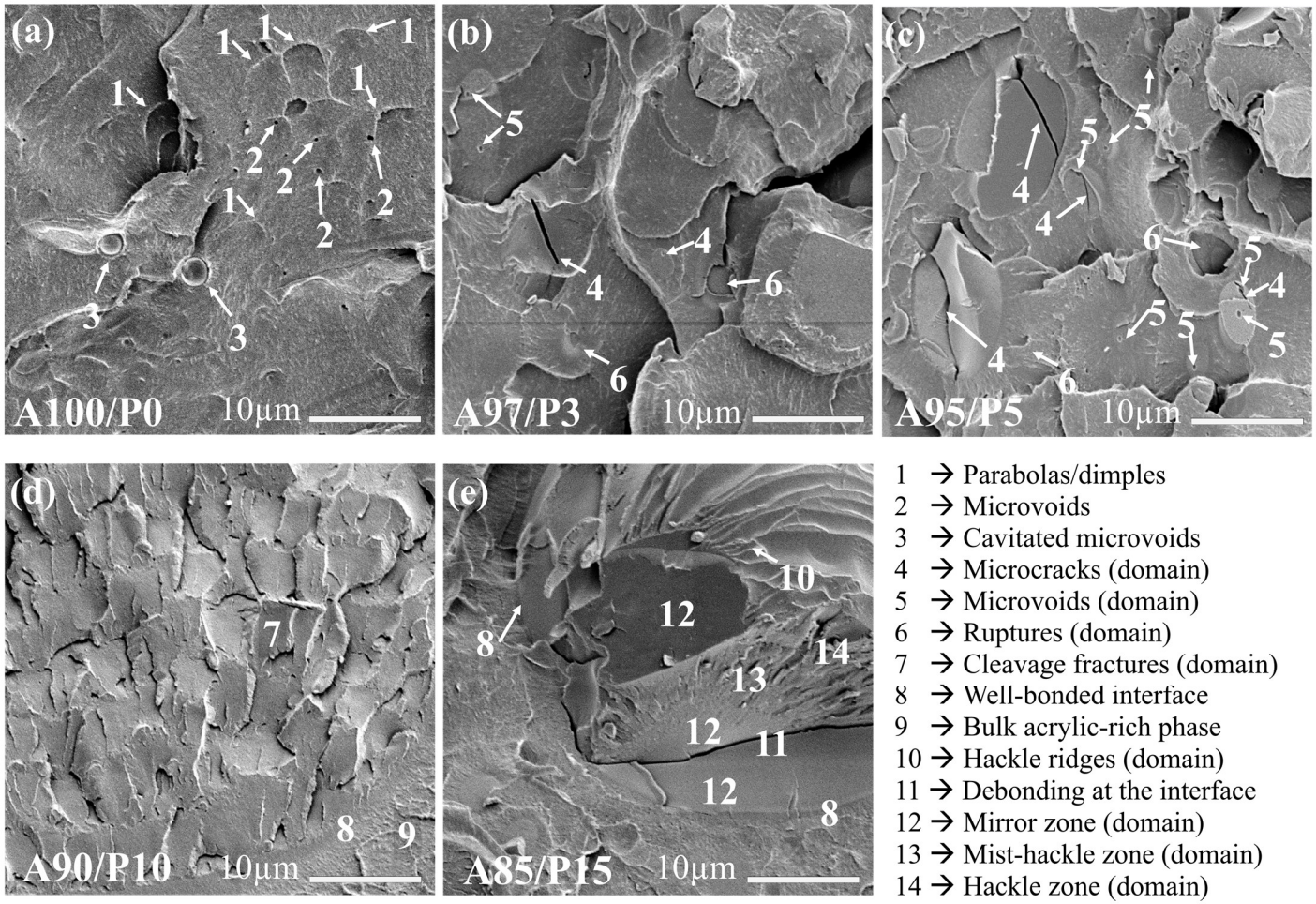


Figure 6-23. SEM micrographs showing the main fracture mechanisms on fractured (flexural) acrylic and PPE-modified acrylic matrix samples.

crack-deflection as observed for the A97/P3 and A95/P5 samples, unique domain failure characteristics were evident. For A90/P10, this was evidenced by cleavage fractures on the domain (Feature 7, Figure 6-23d). While cleavage fracture is considered a brittle fracture mechanism, it also constitutes intrinsic toughness in brittle polymers [69]. Moreover, the domain remained well-bonded (Feature 8, Figure 6-23d) to the bulk acrylic-rich phase, with a diffuse boundary. The A85/P15 sample appears to have an exposed and partially debonded domain, which remains well-bonded (Feature 8, Figure 6-23e) and also appears debonded (Feature 11, Figure 6-23e). The exposed part of the domain protrudes considerably from the surface and reveals brittle failure characteristics: hackle ridges, mirror mist-hackle and hackle zones (Features 10, 12, 13 and 14, Figure 6-23d), respectively. It is plausible that cleavage fracture resulted from completion between the main crack and nanoscale domain microcracking [70]. The dissimilarities between the lower and higher PPE loadings are thus, likely attributed to the relative differences in the contributions of graft acrylic/PPE copolymer, linear amorphous acrylic and cross-linked acrylic/PPE species as described in detail in Section 6.5.

Furthermore, as with the observations from confocal Raman microscopy, size and distribution variations are evident with increasing PPE content. Although smaller versions of these domains are apparent within the samples with lower PPE content (A97/P3 and A95/P5), they seem to be more prominent at higher PPE concentrations (A90/P10 and A85/P15), large domains are evident, varying in size from 50-140 μm. These domains appear to exhibit highly dissimilar, but characteristically brittle fracture behaviour to the surrounding matrix, further supporting the hypothesis of the formation of multi-species blends. Moreover, diffuse domains and well-bonded interfaces such as those observed for the blends in this work have been said to be indicative of low cross-linking densities [71].

While the precise composition of each domain has not been determined as part of this study, the evidence from confocal Raman and scanning electron microscopic techniques confirm the co-existence of acrylic- and PPE-rich phases within these blends. Besides, the SEM micrographs reveal that compositional variations play a significant role in the fracture behaviour of the polymer blends, highlighting that performance tailoring is indeed possible using this approach. These findings, thus, reveal that even slight variations

in the PPE content can yield a great degree of microstructural and fracture behavioural tuning.

6.5 Complementary discussions

In the preceding sections of this chapter, the contributions of the telechelicity of the PPE oligomer used in this study to cross-linking was discussed. Based on a vinyl functionality of 1.9 for the PPE formulation (specified by the manufacturer [33]), the formation of cross-linked acrylic/PPE species is highly likely within the blends based on the number of reactive sites as shown in Figure 6-24. It is worth remarking that the vinylic groups are present to promote chemical compatibility between the aliphatic acrylic and the aromatic PPE. The occurrence of cross-linking would thus constitute one of many reaction possibilities, and if appropriately controlled, could offer the potential to confer desirable properties in the resulting blend.

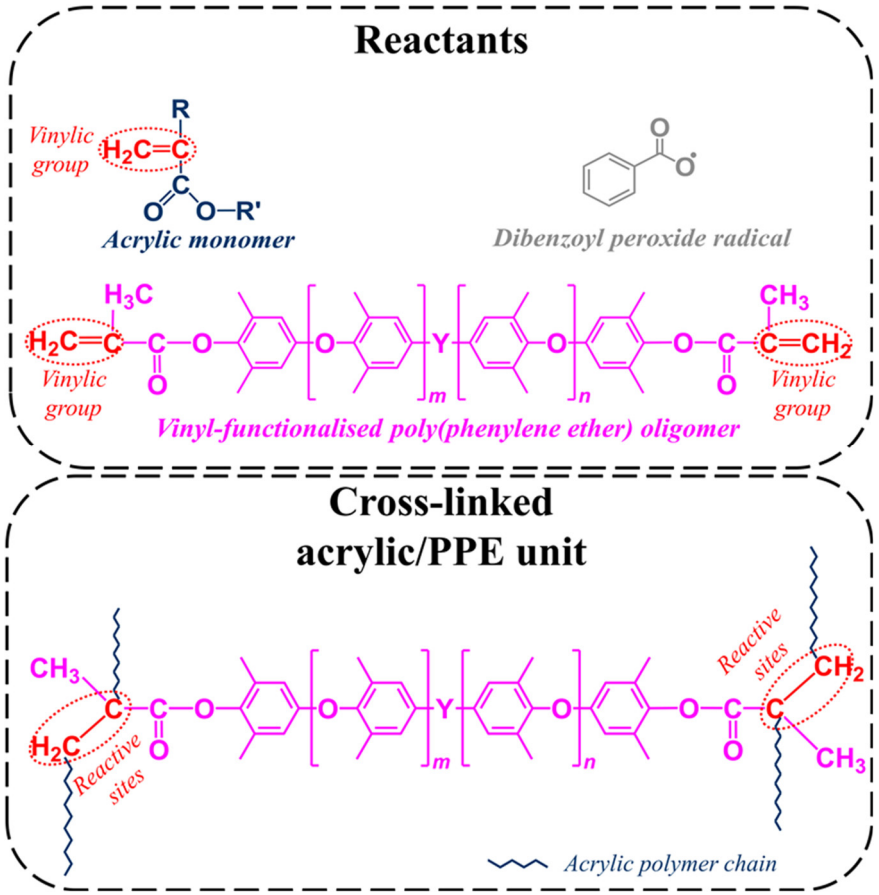


Figure 6-24. Chemical structures of the reactants (acrylic monomer, PPE oligomer and dibenzoyl peroxide radical) and the proposed cross-linked acrylic/PPE structure formed.

Moreover, as shown in Figure 6-7 and discussed in Section 6.3.4, the grade of PPE used cannot homopolymerise; meaning that no PPE-PPE interactions are expected during the polymerisation process. Rather, the telechelicity of PPE facilitates its participation in the propagation reaction with growing acrylic chains. Thus, the formation of linear and branched/grafted copolymers during the polymerisation process is not plausible.

A small-scale feasibility study was conducted as described in Appendix C.1.1.2 (Figure C-2) to explore the effects of the presence of crosslinks on the reshapability of the blends. These trials revealed that the presence of cross-links did not have deleterious effects on the post-processibility of the unreinforced PPE-modified acrylic blends.

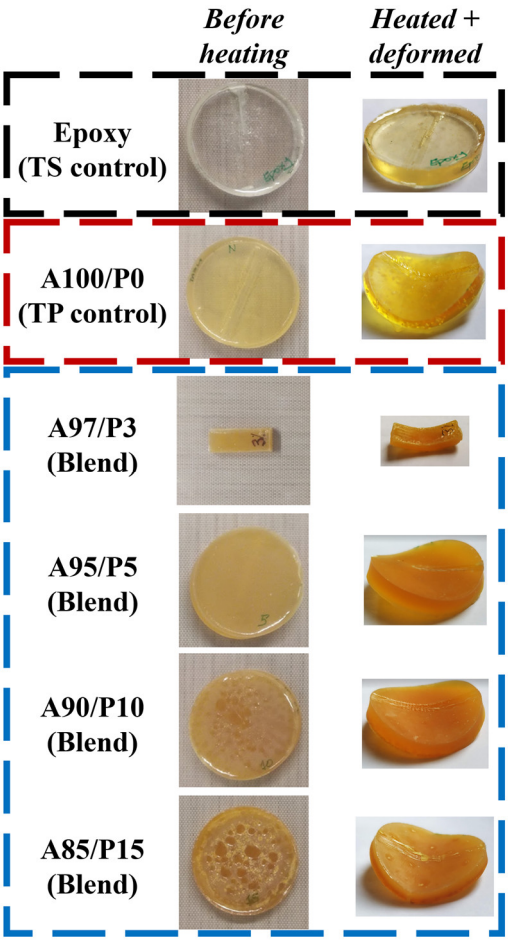


Figure 6-25. Results of reshapabilty trials conducted on the acrylic/PPE blends, A100/P0 as the thermoplastic control, and a cast epoxy sample as a thermoset control. All samples are 40-mm dia. discs except for A97/P3, which measures 25 mm × 8 mm × 4 mm due to material constraints.

Thus, it was demonstrated that the thermoplastic blends produced in this chapter exhibit the desirable characteristics of thermosets (possessing excellent solvent resistance, thermal stability, and easy infusibility at room temperature), while also retaining the post-processibility of thermoplastics. Such duality of characteristics has been previously reported for materials such as vitrimers and covalent adaptable networks (CANs), which are known to offer excellent reprocessibility despite containing cross-linked networks [72–74]. In addition to retaining the post-processibility of thermoplastics, which facilitates reshaping even after polymerisation and solidification, these attributes are highly advantageous and offer numerous potentials for composite applications.

Combined with the micrographic evidence from confocal Raman imaging and SEM imaging, thermogravimetric analysis and solvent resistance trials, the thermoformability of these blends confirms that both acrylic-rich and cross-linked acrylic/PPE. Moreover, the results of thermoforming trials suggest a good extent of chain mobility must be possible despite the presence of cross-links. Thus, these results confirm that the blends may only be slightly cross-linked or that cross-links form clusters.

The degree and density of cross-linking are expected to be highly influenced by the relative reactivities of PPE and acrylic. Variations in the extent of steric hindrance resulting from the presence of bulky phenyl groups [75,76] will likely result in volumetric congestion around each successive acrylic/PPE interaction at the reactive site. In addition, an increase in the solution viscosity is expected to result in the trapping or burying of some substituents. Consequently, some of the PPE macromolecules may only be partially saturated upon the termination of the polymerisation reaction, with perhaps trace amounts of unreacted PPE entrapped by cross-linked and branched chains. The latter may perhaps account for the observation of unreacted PPE. Branched or grafted chains may be effectively anchored and trapped within the network within such structures, and thus, their presence is not expected to compromise the solvent resistance of the blends [77].

Moreover, no specialised approach for tuning or controlling the cross-linking or grafting processes; thus, spatial variations are expected within each blend system. Finally, based on these observations and correlation to published works, the chain architecture in Figure 6-26 is proposed.

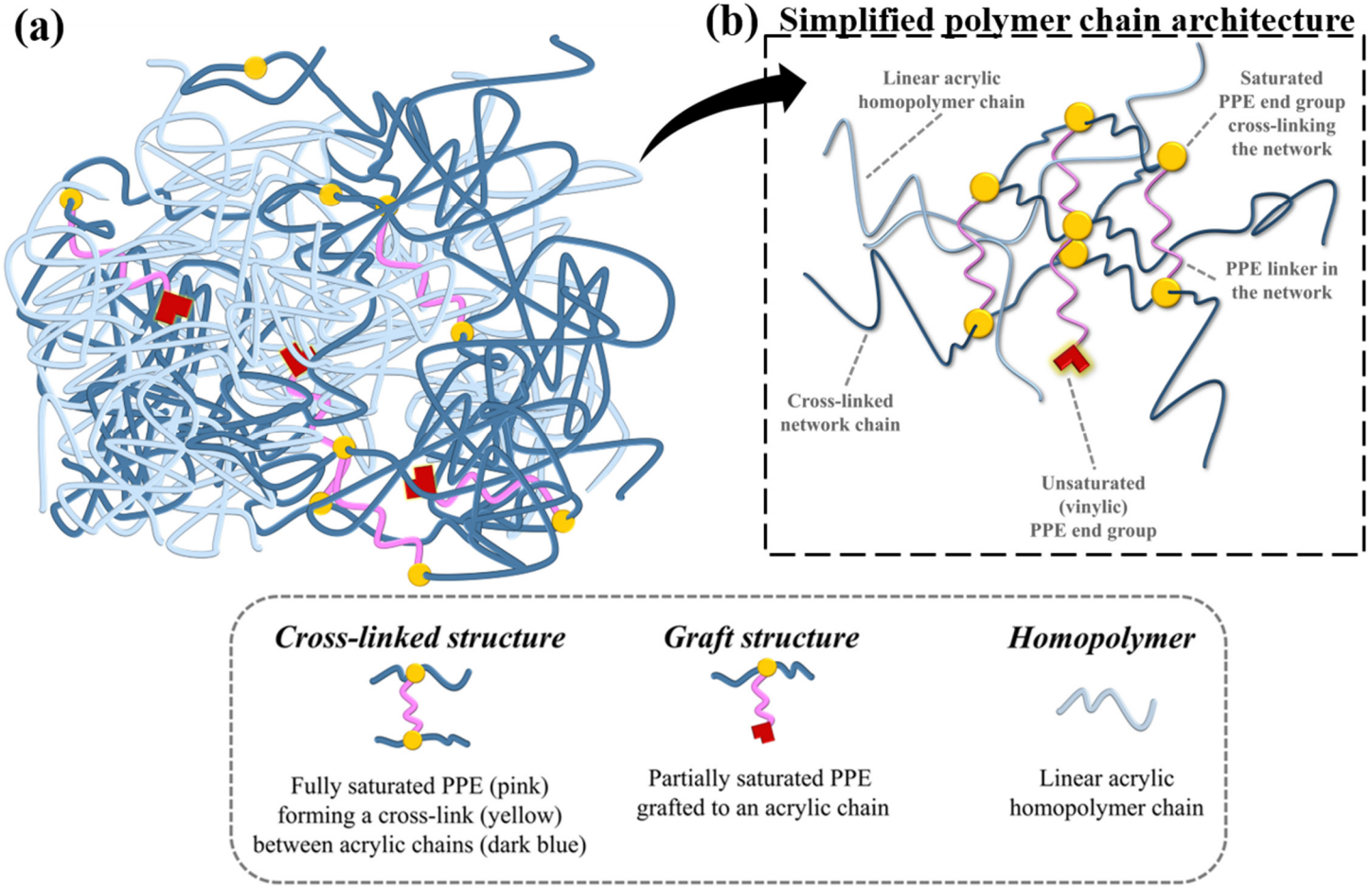


Figure 6-26. (a) The proposed polymer architecture within the PPE-modified acrylic blends, showing a lightly cross-linked acrylic/PPE network, a branched or grafted acrylic/PPE species, and a highly entangled, linear acrylic polymer species; (b) a simplified form of same.

Remarkably, such architecture has been previously reported by Röttger [78], who showed that dioxaborolane-based vitrimers exhibit excellent solvent resistance in THF, retaining up to 95% of their original mass. The same materials were reported to remain thermoformable even with cross-linked constituents. This is similar to the findings presented herein and may provide interesting insights into the behaviour of the blends considered in this present work. However, the formation of a vitrimer is highly unexpected, as vitrimers characteristically require the ester-alcohol transesterification reactions. Thus, it is not believed that the blends in this work are vitrimeric in nature.

Moreover, the process employed in this chapter may produce a material similar to interpenetrating polymer networks (IPNs), at least one of the polymers is synthesised in the presence of the other [79–84]. A distinguishing characteristic of IPNs is that one (semi-IPN) or both (full IPN) are cross-linked to form a network. Although the novel polymer blends presented in this chapter were not prepared with a traditional cross-linker, it has been shown that the telechelic PPE employed can promote cross-linking. Thus, the resulting blend architecture is likely similar to a semi-IPN with both linear acrylic and branched/grafted acrylic/PPE species interpenetrating within a lightly cross-linked acrylic/PPE network. Consequently, published work on semi-IPN may prove beneficial in providing insights into the acrylic/PPE blend behaviour as a composite matrix in Chapter 7.

6.6 Chapter conclusion

The work presented in this chapter represents the first of its kind on the development and characterisation of thermoplastic acrylic/PPE blends for the room-temperature fabrication of composites. PPE content was varied for polymer blends in a composition range of 3-15 wt. %.

The following conclusions can be derived from the work presented herein:

- Good solvent resistance (and thus, low solubility) of the acrylic/PPE polymer blends in $CDCl_3$ and other common NMR spectroscopy solvents prohibited accurate determination of the exact chemical nature of the whole acrylic/PPE blend samples.

- NMR spectroscopy of the soluble portions of the acrylic/PPE blends (in $CDCl_3$) indicated multi-component mixtures comprising individual molecules of monomeric and acrylic polymer, PPE oligomer and BPO. The good solubility of simple mixtures of independent acrylic polymer and PPE oligomer molecules in $CDCl_3$ suggests that the blends' insoluble portions contain more complex reacted acrylic/PPE species.

- Good solvent resistance of the acrylic/PPE blends was observed in acetone; although neat acrylic polymer fully dissolved after 300 minutes of exposure to acetone, all blended polymers exhibited excellent mass retention (~77-75 %).

- Increasing the PPE content within unreinforced blended polymers was found to increase T_g by up to 6°C compared to neat acrylic polymer samples. A marginal decreasing trend of tan delta peak height was observed, suggesting increased rigidity from the phenyl moieties of PPE.

- TGA results revealed that PPE modification of the acrylic matrix appears to confer enhanced thermal stability on acrylic/PPE blends as evidenced by onset retardation and residual mass. Unique secondary end-stage degradation behaviour also provides evidence of the presence of complex acrylic/PPE species.

- Based on these observations, micrographic evidence, and accepted theory published in literature, the formation of cross-linked acrylic/PPE network with interpenetrating, a grafted acrylic/PPE phase and a linear, homopolymerised acrylic species has been proposed.

The results of the miscibility trials (Section 6.3.2), solvent resistance experiment (Section 6.4.2), and activation energies (Appendix C.1.1.1) revealed that 5 wt. % was the ideal PPE content for the fabrication of fibre-reinforced hybrid-matrix composite laminates by a vacuum infusion process. The selection was made based on resin stability during the processing window for infiltration and polymerisation, enhanced solvent resistance, and thermal stability.

Chapter references

[1] Arkema. Nanostrength®: self-assembling block copolymers - Arkema n.d.

[2] Venderbosch RW, Meijer HEH, Lemstra PJ. Processing of intractable polymers using reactive solvents: 1. Poly(2,6-dimethyl-1,4-phenylene ether)/epoxy resin. Polymer (Guildf) 1994;35:4349–57. https://doi.org/10.1016/0032-3861(94)90092-2.

[3] Venderbosch RW, Meijer HEH, Lemstra PJ. Processing of intractable polymers using reactive solvents: 2. Poly(2,6-dimethyl-1,4-phenylene ether) as a matrix material for high performance composites. Polymer (Guildf) 1995;36:1167–78. https://doi.org/10.1016/0032-3861(95)93918-C.

[4] Cong H, Yu B, Yuan H, Tian C, Yang S. Preparation and characterization of nanocomposites with polyphenylene oxide. In: Mittal V, editor. Manuf. nanocomposites with Eng. Plast., Woodhead Publishing; 2015.

[5] Li Y, Xie T, Yang G. Effects of polyphenylene oxide content on morphology, thermal, and mechanical properties of polyphenylene oxide/polyamide 6 blends. J Appl Polym Sci 2006;99:2076–81. https://doi.org/10.1002/app.22687.

[6] Chiang CR, Chang FC. Polymer blends of polyamide-6 (PA6) and poly(phenylene ether) (PPE) compatibilized by a multifunctional epoxy coupler. J Polym Sci Part B Polym Phys 1998;36:1805–19. https://doi.org/10.1002/(SICI)1099-0488(199808)36:11<1805::AID-POLB2>3.0.CO;2-P.

[7] Gupta AP, Bharduwaj VR. Studies on the effect of polyamide-6 onto modified polyphenylene oxide matrix in presence of fumaric acid as a compatibilizer. Polym - Plast Technol Eng 2007. https://doi.org/10.1080/03602550701274052.

[8] Kim IG, Hong SY, Park BO, Choi HJ, Lee JH. Polyphenylene ether/glycol modified polyethylene terephthalate blends and their physical characteristics. J Macromol Sci Part B Phys 2012. https://doi.org/10.1080/00222348.2011.610207.

[9] Chiang C-R, Ju M-Y, Chang F-C. Polymer Blends of PA6 and PPE Compatibilized by Poly[methylene(phenylene isocyanate)] (PMPI) Coupler. Polym Eng Sci 1998;38:622–33.

[10] Chiou K-C, Wu S-C, Wu H-D, Chang F-C. Compatibilization and elastomer toughening of polyamide-6 (PA6)/poly(phenylene ether) (PPE) blends. J Appl Polym Sci 1999;74:23–32. https://doi.org/10.1002/(sici)1097-4628(19991003)74:1<23::aid-app3>3.0.co;2-u.

[11] Hong X, Nie G, Lin Z, Rong J. Structure and Properties of PPO/PP Blends Compatibilized by Triblock Copolymer SEBS and SEPS. Polym - Plast Technol Eng 2012. https://doi.org/10.1080/03602559.2012.671422.

[12] Chiang C-R, Tseng C-R, Chang F-C. Polymer blends of PA6 and PPE compatibilized by phenolic novolac epoxy coupler. J Polym Res 1997. https://doi.org/10.1007/s10965-006-0012-4.

[13] Chiang C-R, Chang F-C. Polymer blends of polyamide-6 (PA6) and poly(phenylene oxide) (PPO) compatibilized by styrene-maleic anhydride (SMA) copolymer. Polymer (Guildf) 1997. https://doi.org/10.1016/S0032-3861(96)00015-8.

[14] Wang S, Li B, Zhang Y. Compatibilization of poly(2,6-dimethyl-1,4-phenylene oxide)/polyamide 6 blends with styrene-maleic anhydride copolymer: Mechanical properties, morphology, crystallization, and melting behavior. J Appl Polym Sci 2010;118:3545–51. https://doi.org/10.1002/app.32730.

[15] Chiang C, Chang F. Polymer blends of polyamide□ 6 and poly(phenylene oxide) compatibilized by styrene□ co□ glycidyl methacrylate. J Appl Polym Sci 1996. https://doi.org/10.1002/(sici)1097-4628(19960926)61:13<2411::aid-app21>3.3.co;2-v.

[16] Aksit A, Geis N, Aksit M, Altstädt V. Properties of styrene-maleic anhydride copolymer compatibilized polyamide 66/Poly (Phenylene ether) blends: Effect of blend ratio and compatibilizer content. Materials (Basel) 2020.

https://doi.org/10.3390/ma13153400.

[17] Jo WH, Kim HC. Morphology, rheological and mechanical properties of poly(phenylene ether) and polyamide-6 blends with a compatibilizer. Polym Bull 1992. https://doi.org/10.1007/BF00309707.

[18] Hadimani P, Narasimha Murthy HN, Mudbidre R. Thermal and mechanical properties of glass fibre reinforced polyphenylene ether/polystyrene/nylon-6 ternary blends. Polym Polym Compos 2020. https://doi.org/10.1177/0967391120949490.

[19] Stack S, O'Donoghue O, Birkinshaw C. The thermal stability and thermal degradation of blends of syndiotactic polystyrene and polyphenylene ether. Polym Degrad Stab 2003. https://doi.org/10.1016/S0141-3910(02)00235-5.

[20] Liu A, Xie T, Yang G. Effect of Na+-MMT Platelets on Monomer Casting Polyamide 6/Polyphenylene Oxide Blends. Macromol Chem Phys 2006;207:2180–7. https://doi.org/10.1002/macp.200600358.

[21] Lee SE, Jeong E, Lee MY, Lee MK, Lee YS. Improvement of the mechanical and thermal properties of polyethersulfone-modified epoxy composites. J Ind Eng Chem 2016;33:73–9. https://doi.org/10.1016/j.jiec.2015.09.022.

[22] Mimura K, Ito H, Fujioka H. Improvement of thermal and mechanical properties by control of morphologies in PES-modified epoxy resins. Polymer (Guildf) 2000;41:4451–9. https://doi.org/10.1016/S0032-3861(99)00700-4.

[23] Zhao P, Liang X, Chen J, Ran Q, Gu Y. Poly(ether imide)-modified benzoxazine blends: Influences of phase separation and hydrogen bonding interactions on the curing reaction. J Appl Polym Sci 2013;128:2865–74. https://doi.org/10.1002/app.38459.

[24] Biolley N, Pascal T, Sillion B. Polyimide-modified epoxy system: time-temperature-transformation diagrams, mechanical and thermal properties. Polymer (Guildf) 1994;35:558–64. https://doi.org/10.1016/0032-3861(94)90511-8.

[25] Hamerton I, McNamara LT, Howlin BJ, Smith PA, Cross P, Ward S. Toughening mechanisms in aromatic polybenzoxazines using thermoplastic oligomers and telechelics. Macromolecules 2014;47:1946–58. https://doi.org/10.1021/ma5002436.

[26] Orhan T, Ates S, Hacaloglu J, Yagci Y. Thermal degradation characteristics of polysulfones with benzoxazine end groups. J Anal Appl Pyrolysis 2012;94:146–52. https://doi.org/10.1016/j.jaap.2011.12.001.

[27] Del Saz-Orozco B, Ray D, Kervennic A, McGrail PT, Stanley WF. Toughening of carbon fibre/polybenzoxazine composites by incorporating polyethersulfone into the interlaminar region. Mater Des 2016;93:297–303. https://doi.org/10.1016/j.matdes.2015.12.138.

[28] Di Pasquale G, Motta O, Recca A, Carter JT, McGrail PT, Acierno D. New high-performance thermoplastic toughened epoxy thermosets. Polymer (Guildf) 1997;38:4345–8. https://doi.org/10.1016/S0032-3861(96)01031-2.

[29] Hamerton I, McNamara LT, Howlin BJ, Smith PA, Cross P, Ward S. Developing toughened aromatic polybenzoxazines using thermoplastic oligomers and telechelics, part 1: Preparation and characterization of the functionalized oligomers. J Appl Polym Sci 2014;131. https://doi.org/10.1002/app.40875.

[30] Khanh T, Nguyen L, Sébastien †, Livi S, Soares BG, Benes H, et al. Toughening of Epoxy/Ionic Liquid Networks with Thermoplastics Based on Poly(2,6-dimethyl-1,4-phenylene ether) (PPE) 2016. https://doi.org/10.1021/acssuschemeng.6b02479.

[31] Ronak B. Fracture mechanics of nanostructured polymer blends with janus particles. University of Bayreuth [Doctoral Thesis], 2018.

[32] Nelissen LNIH. A novel route to blends of polystyrene and poly(2,6-dimethyl-1,4-phenylene ether)□ : synthesis, properties and applications 1991. https://doi.org/10.6100/IR352941.

[33] SABIC. NORYL™ SA9000 resin solubility guide 2019. https://www.sabic.com/en/products/documents/sabic-noryl-sa9000-solvent-guide/en.

[34] Bennett JG, Summers RM. Composition of a polyphenylene ether and an acrylic resin modified polyisoprene. United States Patent Office [US3794606A], 1974. https://doi.org/10.1145/178951.178972.

[35] Viersen FJ, Colantuoni P, Mamalis I. Compatibilization of poly(2,6□ dimethyl□ 1,4□ phenylene ether)/poly(vinylidene difluoride) blends. Die Angew Makromol Chemie 1993. https://doi.org/10.1002/apmc.1993.052060111.

[36] Han N, Baran I, Zanjani JSM, Yuksel O, An LL, Akkerman R. Experimental and computational analysis of the polymerization overheating in thick glass/Elium®acrylic thermoplastic resin composites. Compos Part B Eng 2020. https://doi.org/10.1016/j.compositesb.2020.108430.

[37] Ray D, Banerjee S, Mohanty AK, Misra M. Thermal and electrical behavior of vinylester resin matrix composites filled with fly ash particles. Polym Compos 2008;29:58–62. https://doi.org/10.1002/pc.20354.

[38] Uhl FM, Levchik GF, Levchik S V, Dick C, Liggat JJ, Snape CE, et al. Thermal stability of cross-linked polymers: Methyl methacrylate with divinylbenzene and styrene with dimethacrylates. Polym Degrad Stab 2001;71:317–25. https://doi.org/10.1016/S0141-3910(00)00181-6.

[39] Reich HJ. Chem 605 - Structure Determination Using Spectroscopic Methods 2020.

[40] Miller-Chou BA, Koenig JL. A review of polymer dissolution. Prog Polym Sci 2003;28:1223–70. https://doi.org/10.1016/S0079-6700(03)00045-5.

[41] Devotta I, Badiger M V, Rajamohanan PR, Ganapathy S, Mashelkar RA. Unusual retardation and enhancement in polymer dissolution: role of disengagement dynamics. Chem Eng Sci 1995;50:2557–69.

[42] Darvell BW. Materials science for dentistry. 2018.

https://doi.org/10.1016/C2015-0-05454-5.

[43] Ito MM, Gibbons AH, Qin D, Yamamoto D, Jiang H, Yamaguchi D, et al. Structural colour using organized microfibrillation in glassy polymer films. Nature 2019. https://doi.org/10.1038/s41586-019-1299-8.

[44] Fujiyabu T, Yoshikawa Y, il Chung U, Sakai T. Structure-property relationship of a model network containing solvent. Sci Technol Adv Mater 2019. https://doi.org/10.1080/14686996.2019.1618685.

[45] Hawke LGD, Ahmadi M, Goldansaz H, van Ruymbeke E. Viscoelastic properties of linear associating poly(n-butyl acrylate) chains. J Rheol (N Y N Y) 2016. https://doi.org/10.1122/1.4942231.

[46] Huang C, Huang G, Li S, Luo M, Liu H, Fu X, et al. Research on architecture and composition of natural network in natural rubber. Polymer (Guildf) 2018. https://doi.org/10.1016/j.polymer.2018.08.057.

[47] Nakano T. π-stacked polymers and molecules: Theory, synthesis, and properties. 2014. https://doi.org/10.1007/978-4-431-54129-5.

[48] Zhang M, Bareille O, Salvia M. Cure and damage monitoring of flax fiber-reinforced epoxy composite repairs for civil engineering structures using embedded piezo micro-patches. Constr Build Mater 2019. https://doi.org/10.1016/j.conbuildmat.2019.07.179.

[49] Huang CC, Yang MS, Liang M. Synthesis of new thermosetting poly(2,6-dimethyl-1, 4-phenylene oxide)s containing epoxide pendant groups. J Polym Sci Part A Polym Chem 2006. https://doi.org/10.1002/pola.21679.

[50] Romo-Uribe A. Dynamic Mechanical Thermal Analysis of Epoxy/Thermoplastic Blends 23. Handb. Epoxy Blends, 2017, p. 675–706. https://doi.org/10.1007/978-3-319-40043-3_23.

[51] Arora KS, Baah F, Canard GM, Setze DE. DMA of new acrylic- polyurethane

hybrids. Eur Coatings J 2001;2001.

[52] Gamage NJW, Hill DJT, Lukey CA, Pomery PJ. Thermal characterization of polyester-melamine coating matrices prepared under nonisothermal conditions. J Polym Sci Part A Polym Chem 2003;41:1603–21. https://doi.org/10.1002/pola.10698.

[53] Bacchi A, Yih JA, Platta J, Knight J, Pfeifer CS. Shrinkage/stress reduction and mechanical properties improvement in restorative composites formulated with thio-urethane oligomers. J Mech Behav Biomed Mater 2018;78:235–40. https://doi.org/10.1016/j.jmbbm.2017.11.011.

[54] Miyagawa H, Rich MJ, Drzal LT. Amine-cured epoxy/clay nanocomposites. I. Processing and chemical characterization. J Polym Sci Part B Polym Phys 2004. https://doi.org/10.1002/polb.20288.

[55] Kannurpatti AR, Anseth JW, Bowman CN. A study of the evolution of mechanical properties and structural heterogeneity of polymer networks formed by photopolymerizations of multifunctional (meth)acrylates. Polymer (Guildf) 1998;39:2507–13. https://doi.org/10.1016/S0032-3861(97)00585-5.

[56] Peters EN. Poly(phenylene ether) based amphiphilic block copolymers. Polymers (Basel) 2017;9. https://doi.org/10.3390/polym9090433.

[57] Wypych G. Data on Specific Polymers. Handb Mater Weather 2013:351–546. https://doi.org/10.1016/b978-1-895198-62-1.50017-2.

[58] Castellanos SG, Fernández VVA, Aguilar J, Moscoso-Sánchez FJ, Ceja I, Canché-Escamilla G, et al. Synthesis and characterization of poly(methyl methacrylate)-boehmite nanocomposites by direct microemulsion polymerization combined with the in-situ sol-gel method. Polymer (Guildf) 2019;163:134–43. https://doi.org/10.1016/j.polymer.2018.12.053.

[59] Röchow ET, Häußler L, Korwitz A, Pospiech D. Thermal decomposition of phosphonate-containing methacrylate-based copolymers. Polym Degrad Stab 2018;152:235–43. https://doi.org/10.1016/j.polymdegradstab.2018.04.036.

[60] Viratyaporn W, Lehman RL. Effect of nanoparticles on the thermal stability of PMMA nanocomposites prepared by in situ bulk polymerization. J Therm Anal Calorim 2011;103:267–73. https://doi.org/10.1007/s10973-010-1051-y.

[61] de Andrade Raponi O, Barbosa LCM, de Souza BR, Ancelotti Junior AC. Study of the influence of initiator content in the polymerization reaction of a thermoplastic liquid resin for advanced composite manufacturing. Adv Polym Technol 2018;37:3579–87. https://doi.org/10.1002/adv.22142.

[62] Percec V, Pugh C, Nuyken O, Pask SD. Macromonomers, Oligomers and Telechelic Polymers. Compr. Polym. Sci. Suppl., Elsevier; 1989, p. 281–357. https://doi.org/10.1016/b978-0-08-096701-1.00189-0.

[63] Nakamura Y, Yamago S. Termination Mechanism in the Radical Polymerization of Methyl Methacrylate and Styrene Determined by the Reaction of Structurally Well-Defined Polymer End Radicals. Macromolecules 2015;48:6450–6. https://doi.org/10.1021/acs.macromol.5b01532.

[64] Vallittu PK. Oxygen inhibition of autopolymerization of polymethylmethacrylate-glass fibre composite. J Mater Sci Mater Med 1997. https://doi.org/10.1023/A:1018578210453.

[65] Andrzejewska E. Free-radical photopolymerization of multifunctional monomers. Three-Dimensional Microfabr. Using Two-phot. Polym., 2019. https://doi.org/10.1016/B978-0-12-817827-0.00002-3.

[66] Zhang Q, Liang S, Sui G, Yang X. Influence of matrix modulus on the mechanical and interfacial properties of carbon fiber filament wound composites. RSC Adv 2015;5:25208–14. https://doi.org/10.1039/c5ra00098j.

[67] Greenhalgh ES. Delamination-dominated failures in polymer composites. In: Greenhalgh ES, editor. Fail. Anal. Fractography Polym. Compos., Woodhead Publishing; 2009, p. 164–237. https://doi.org/10.1533/9781845696818.164.

[68] Wenbo L, Tingqing Y. Computer simulation of conic-shaped patterns on fracture

surfaces of polymers. J Appl Polym Sci 2003. https://doi.org/10.1002/app.12352.

[69] Swadener JG, Liechti KM, Lozanne ALD. The intrinsic toughness and adhesion mechanisms of a glass/epoxy interface. J Mech Phys Solids 1999. https://doi.org/10.1016/S0022-5096(98)00084-2.

[70] Zorc B, Zorc M, Kosec B, Nagode A. Effect of the shape of styrene-acrylonitrile water-filter housings on the destructive pressure, crack-initiation, propagation conditions and fracture toughness of styrene-acrylonitrile. Polymers (Basel) 2020;12. https://doi.org/10.3390/polym12020280.

[71] Sawaryn C, Landfester K, Taden A. Advanced chemically induced phase separation in thermosets: Polybenzoxazines toughened with multifunctional thermoplastic main-chain benzoxazine prepolymers. Polymer (Guildf) 2011. https://doi.org/10.1016/j.polymer.2011.04.064.

[72] Han H, Xu X. Poly(methyl methacrylate)–epoxy vitrimer composites. J Appl Polym Sci 2018. https://doi.org/10.1002/app.46307.

[73] Li Q, Ma S, Lu N, Qiu J, Ye J, Liu Y, et al. Concurrent thiol–ene competitive reactions provide reprocessable, degradable and creep-resistant dynamic–permanent hybrid covalent networks. Green Chem 2020. https://doi.org/10.1039/d0gc02823a.

[74] Van Zee NJ, Nicolaÿ R. Vitrimers: Permanently crosslinked polymers with dynamic network topology. Prog Polym Sci 2020. https://doi.org/10.1016/j.progpolymsci.2020.101233.

[75] Flory PJ. Principles of polymer chemistry. 1953.

[76] Yamada B, Zetterlund PB, Sato E. Utility of propenyl groups in free radical polymerization: Effects of steric hindrance on formation and reaction behavior as versatile intermediates. Prog Polym Sci 2006;31:835–77. https://doi.org/10.1016/j.progpolymsci.2006.08.005.

[77] Plenderleith RA, Pateman CJ, Rodenburg C, Haycock JW, Claeyssens F,

Sammon C, et al. Arginine-glycine-aspartic acid functional branched semi-interpenetrating hydrogels. Soft Matter 2015. https://doi.org/10.1039/c5sm00695c.

[78] Röttger M, Domenech T, Van Der Weegen R, Breuillac A, Nicolaÿ R, Leibler L. High-performance vitrimers from commodity thermoplastics through dioxaborolane metathesis. Science 2017;356:62–5. https://doi.org/10.1126/science.aah5281.

[79] Athawale VD, Kolekar SL, Raut SS. Recent developments in polyurethanes and poly(acrylates) interpenetrating polymer networks. J Macromol Sci - Polym Rev 2003. https://doi.org/10.1081/MC-120018018.

[80] Karabanova L V, Boiteux G, Seytre G, Stevenson I, Lloyd AW, Mikhalovsky S V, et al. Phase separation in the polyurethane/ poly(2-hydroxyethyl methacrylate) semi-interpenetrating polymer networks synthesized by different ways. Polym Eng Sci 2008. https://doi.org/10.1002/pen.20965.

[81] Karabanova L V, Mikhalovsky S V, Lloyd AW, Boiteux G, Sergeeva LM, Novikova TI, et al. Gradient semi-interpenetrating polymer networks based on polyurethane and poly(vinyl pyrrolidone). J Mater Chem 2005. https://doi.org/10.1039/b410178b.

[82] Sperling LH, Mishra V. The Current Status of Interpenetrating Polymer Networks. Polym Adv Technol 1996;7:197–208. https://doi.org/10.1002/(SICI)1099-1581(199604)7:4<197::AID-PAT514>3.0.CO;2-4.

[83] Sperling LH, Hu R. Interpenetrating polymer networks. Polym. Blends Handb., 2014. https://doi.org/10.1007/978-94-007-6064-6_8.

[84] Lipatov YS, Chramova TS, Sergeeva LM, Karabanova L V. Some properties of intermediate regions in interpenetrating polymeric networks. J Polym Sci Polym Chem Ed 1977. https://doi.org/10.1002/pol.1977.170150216.

Chapter 7 Fabrication and evaluation of glass fibre-reinforced acrylic-PPE composites

7.1 Materials and methods

In light of the findings of the solubility and miscibility trials conducted in Section 6.1.2, 5 wt. % was selected as the optimum loading of PPE in the acrylic-PPE hybrid matrix for laminate fabrication. The trials revealed that beyond 5 wt. %, the resin mixtures exhibited pronounced phase instability when left undisturbed for 24 h after mixing. Thus, 5 wt. % was deemed the most suitable blend composition to study for liquid resin infusion of glass fibre-reinforced composites. The laminates studied in this chapter were produced using a quasi-unidirectional glass fabric supplied by Ahlstrom Munksjö as reinforcement. The fabric comprised 90°-fibres as ~6 % of its composition, with a total areal weight of 646 gsm. Table 7-1 provides an overview of the materials used. Hereafter, the laminates are referred to as GF/A100/P0 and GF/A95/P5 in corresponding sections of this chapter.

Table 7-1. Summary of materials used for composite fabrication.

		Elium® 188 O [a] *(by weight)*	*NORYL™ SA9000* [b] *(by weight)*	*Used in Section(s)*
Unidirectional Laminates $[0]_8$	*GF/A100/P0* [c, d]	100	0	7.1.2 - 7.1.4
	GF/A95/P5 [c, d]	95	5	7.1.2 - 7.1.4
Bidirectional Laminates $[0/90/90/0]_S$	*GF/A100/P0* [c, d]	100	0	7.1.5
	GF/A95/P5 [c, d]	95	5	7.1.5

[a] A Liquid acrylic resin [A] supplied by Arkema GRL, France.

[b] An oligomeric PPE oligomer [P] with vinyl functionality, supplied by SABIC.

[c] Fabric TEST2594 – a quasi-unidirectional (UD) glass non-crimp fabric (NCF) supplied by Ahlstrom-Munksjö. GF: glass fibre.

[d] Polymerised using a dibenzoyl peroxide initiator – BP50FT supplied by United Initiators.

7.1.1 Liquid resin infusion moulding of glass fibre-reinforced acrylic-PPE composites

Two eight-ply test laminates were prepared by a room-temperature liquid resin infusion and in-situ polymerisation process.

Following the preparation and characterisation of the resin blends described in Section 6.1.2, Blend A95/P5 was selected for the production of glass fibre-reinforced laminates. This selection was based on observations described therein and schematically illustrated in Figure 6-1 from preliminary miscibility and solubility trials. The addition of PPE up to 5 wt. % presented the most stable behaviour in terms of overall resin homogeneity. In the interest of attaining full wet-out or saturation of the glass fabric preform during infiltration using a homogenous mix, only a 5 wt. % matrix blend was studied.

The adjustable-cavity mould (Composite Integration Ltd.) described in Section 5.1.2 was used to produce the glass fibre-reinforced laminates in this Chapter. Eight unidirectional plies of glass fabric measuring 485 mm × 485 mm were cut and assembled into a preform for a target thickness of 4 mm (or target fibre volume fraction of 50 %). The preform was dried in a convection oven overnight at 60°C, and loaded into the cavity. The BP50FT initiator (3 parts) was added to the modified resin (100 parts) and mixed as described for the polymeric matrices. A room-temperature infusion was performed, and the laminate was demoulded after polymerisation at room temperature (24 h). Figure 7-1 shows a schematic representation of the experimental set-up for laminate fabrication.

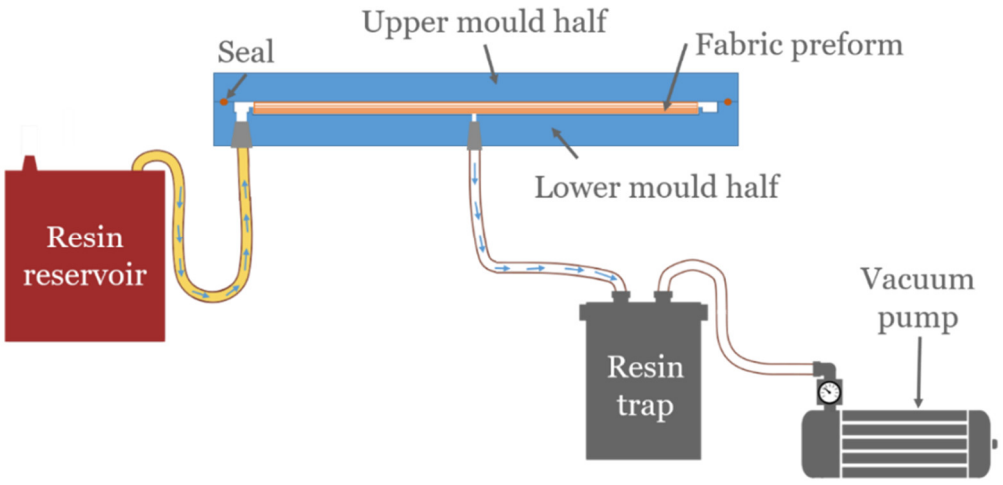


Figure 7-1. Diagrammatic representation of the experimental set-up for composite fabrication. The upper and lower mould halves of the adjustable-cavity mould are shown in blue.

Saturation times to attain full wet-out of the glass fabric during the fabrication of the GF/A100/P0 and GF/A95/P5 laminates were 5.5 minutes and 35 minutes, respectively. Further information on flow front tracking and saturation time determination are

contained in Section 5.1.2. Using the matrix burn-off technique described in Section 5.1.4, the fibre and void volume fractions evaluated for GF/A100/P0 were 49.5 % and 0.4 %, and for GF/A95/P5 were 57 % and 0.8 %, respectively. The corresponding fibre mass fractions were 68 % and 75 %, respectively. These values are summarised in Table 7-2. Although every care was taken to achieve the same fibre volume fraction by maintaining the preform configuration and the mould cavity height was measured to be the same using the same depth gauge and method, different fibre volume fractions were measured for both material systems.

Table 7-2. Summary of comparative laminate properties.

	Fibre volume fraction (%)	*Fibre mass fraction (%)*	*Void content (%)*	*Thickness (mm)*
GF/A100/P0	49.5	68	0.4	3.8
GF/A95/P5	57	75	0.8	3.3

7.1.2 Solvent resistance in acetone

Glass fibre-reinforced laminate (GF/A100/P0 and GF/A95/P5) samples with masses in the range of 410 – 490 mg were also exposed to acetone under the same conditions as their polymeric counterparts. This was done to understand the effects of fibre reinforcement and to assess the potential improvements with PPE incorporation compared to the unmodified acrylic-matrix composite discussed in Chapter 5. For each material system and test duration, two durations were considered. Samples with a 60-minute exposure time were immersed in acetone for the test duration after preparation and carefully removed, dried and weighed after completing the experiment. Data collection for the 72-hour study involved routine inspections at set intervals up to 300 minutes, during which visible geometrical changes were recorded until the end of the experiment. Beyond this point, samples were inspected at the 24-h mark and 72-h mark, respectively. All coupons were removed from the solvent, dried and weighed at the end of the respective test durations.

7.1.3 Thermal and thermomechanical characterisation

7.1.3.1 Dynamic mechanical analysis

Dynamic mechanical analysis (DMA) was performed to study the influence of PPE-modifier content on T_g and damping behaviour using a DMA 8000 analyser (Perkin Elmer). Samples measuring 40 mm × 8 mm × 4 mm were dynamically loaded at a fixed

frequency of 1 Hz using a dual cantilever bending configuration. Each sample was heated from ambient temperature to 180°C at 3°C/min.

Although the Fox empirical model [1] has limited applicability for blends with intermolecular interactions, it has been applied to gain preliminary insights into the plausible proportions of the hybrid matrix constituents. A similar approach has been previously reported in work by Karabanova et al. [2] who studied semi-interpenetrating polymer networks (semi-IPNs) based on polyurethane and poly(2-hydroxyethyl methacrylate). As previously discussed in Chapter 6, the knowledge presented in semi-IPN literature may offer interesting insights for this research. Additionally, mass data from the solvent resistance characterisation described in 7.1.2 have been used in conjunction with the Fox function to obtain better approximations of the compositions of the soluble and insoluble constituents of the blend. The results of this analysis are discussed accordingly in Section 7.2.2.

7.1.3.2 Thermogravimetric analysis

Thermogravimetric analysis (TGA) was performed using a Mettler Toledo TGA/DSC 1 analyser to assess the thermal stability of glass fibre-reinforced polymer samples. Samples weighing 5 mg were heated from 25°C to 600°C (10°C/min) under a nitrogen flow rate of 50 ml/min. In addition to comparing the evolution of mass loss and derivative thermograms (DTG), activation energies were comparatively assessed.

7.1.4 Mechanical characterisation and microscopic inspection

Mechanical characterisation of the glass fibre-reinforced acrylic-PPE laminate was conducted with respect to the performance of the unmodified acrylic-matrix composite. As summarised in Table 7-3, quasi-unidirectional samples were subjected to testing to assess tensile (ASTM D3039), flexural (ASTM D7264), short beam shear (ASTM D2344) and mode-I interlaminar fracture toughness (ASTM D5528) properties for direct comparability to findings reported in Chapter 5 (Section 5.1.4) for the glass fibre-reinforced acrylic material.

With the exception of mode-I interlaminar testing, the stipulated minimum number of samples were tested where possible for all standard test methods. While a sufficient number of samples were tested during the mode-I interlaminar characterisation of both

materials, some GF/A95/P5 samples were discarded due to undesirable test-related failures. Thus, for this material, fewer samples were tested due to material constraints,

For tensile and flexural test methods, data collected was used to assess strengths, moduli and failure strains. Only shear strengths were determined from the short beam shear tests. Crack lengths, crosshead displacement and loading histories were logged for mode-I interlaminar fracture toughness tests to assess the initiation and propagation fracture toughness. Finally, microscopic inspection on the initiation fracture behaviour was performed to gain vital complementary insights.

Table 7-3. Test specification for the mechanical characterisation of samples from quasi-unidirectional laminates.

Type of test	***Tension***	***Flexure (3-point)***		***Shear***	***ILFT*** [a]	***SEM*** [b]
Direction	*Transverse*	*Longitudinal*	*Transverse*	*Longitudinal*	*Longitudinal*	-
As described in	*Section 5.1.4.1* *ASTM D3039*	*Section 5.1.4.2* *ASTM D7264*		*Section 5.1.4.3* *ASTM D2344*	*Section 5.1.4.4* *ASTM D5528*	*Section 5.1.4.5* -
No. of samples	5† 5‡	GF/A100/P0: 6† GF/A95/P5: 8‡		GF/A100/P0: 6† GF/A95/P5: 9‡	GF/A100/P0: 5† GF/A95/P5: 3‡*	GF/A100/P0: 1† GF/A95/P5: 1‡
Nominal Dimensions (mm)	250 × 25 × 3.8† 250 × 25 × 3.3‡	154 × 13 × 3.8† 154 × 13 × 3.3‡		24 × 8 × **3.8**† 24 × 8 × **3.3**‡	60 × 9 × **3.8**† 60 × 9 × **3.3**‡	25 × 25 × **3.8**† 25 × 25 × **3.3**‡
Test speed (mm/min)	2	1		1	1	-
Other test specifications [c]	60 bar (G.P.)	32:1 (S-to-T) 6/6 (N/S)		4:1 (S-to-T) 6/3 (N/S)	a_0: 63 mm	-
Instrument(s) used	MTS Criterion 300-kN load cell [d] V.E. [f]	Instron-3369 10-kN load cell [e] V.E. [f]		Instron-3369 10-kN load cell [e] –	Instron-3369 10-kN load cell [e] V.E. [f]	JEOL JSM series SEM

[a] **ILFT:** Mode-I interlaminar fracture toughness. *: The GF/A95/P5 results were averaged over 3 samples due to material constraints. Symbols † and ‡ indicate GF/A100/P0 and GF/A95/P5 parameters, respectively. [b] **SEM:** Scanning electron microscopy on Mode-I ILFT samples. Samples extracted from the initiation zone were used imaged at 5 kV after applying a 40-nm gold coating to enhance surface conductivity. [c] **G.P.:** Grip pressure; **S-to-T:** span-to-thickness ratio; **a_0:** crack initiator length; **N/S:** loading nose & support pin diameter in mm. A perfluoroalkoxy alkane film (13-μm thick) was used as an artificial delamination initiator of length, a_0. [d] Model 45 Test frame with a 300-kN load cell (Model/Serial No.: LPS.305/578061; Calibration Certificate No.: E269020119113333). [e] 10-kN load cell (Instron 2530-10 kN; Serial No.: 142956; Calibration Certificate No.: E321102820105802). [f] **V.E.:** video extensometer (Imetrum UVX & Manta G-146B/G-146C) used for real-time tracking of tensile deformations, flexural deflections & crack lengths.

7.1.5 Drop-weight impact characterisation

7.1.5.1 Impact damage resistance

Bidirectional (cross-ply) laminates were produced from the quasi-unidirectional for impact testing with a $[0/90/90/0]_2$ lay-up. Samples measuring 150 $mm_{[0°]}$ × 100 $mm_{[90°]}$ were subjected to impact events at 30 J and 50 J, as previously described in Section 5.1.4.7. Impact damage resistance was evaluated as a function of the size of damage (area) sustained within the coupon.

7.1.5.2 Impact damage tolerance

To assess the effects of PPE modification on damage tolerance, post-impact flexural test samples were prepared and characterised as described in Section 5.1.4.8. The resized samples for the determination of pristine and residual properties nominally measured 150 $mm_{[0°]}$ × 25 $mm_{[90°]}$ and 150 $mm_{[0°]}$ × 45 $mm_{[90°]}$, respectively. Due to material constraints, a minimum of 2 samples was tested for each material, damage state (i.e., pristine or damaged) and energy level.

7.2 Results and discussions

7.2.1 Solvent resistance in acetone

Figure 7-2 shows the results of solvent resistance experiments on glass fibre-reinforced acrylic (GF/A100/P0) and acrylic/PPE (GF/A95/P5) composite samples.

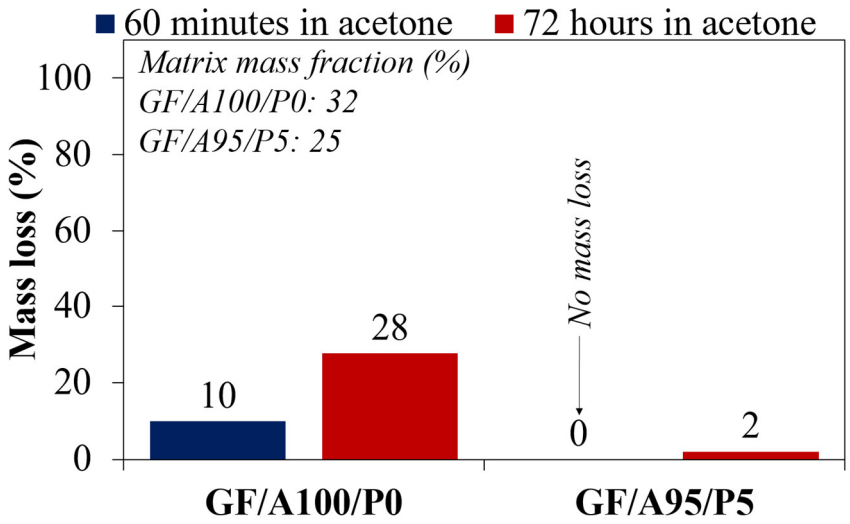


Figure 7-2. Mass losses after the exposure of glass fibre-reinforced polymer samples to acetone for 60 minutes (blue) and 72 hours (red) showing the influence of PPE modifier content on solvent resistance. Note: A lesser mass loss corresponds to superior solvent resistance.

60-minute solvent resistance experiments on the fibre-reinforced acrylic (GF/A100/P0) and acrylic/PPE (GF/A95/P5) revealed that the incorporation of PPE into the acrylic resin system contributes positively to the resistance to initial ingress and subsequent dissolution. No evidence of mass loss was measured after 60 minutes. In the unmodified acrylic composite sample (GF/A100/P0), a 10 % loss in mass was recorded.

Dissolution of glassy polymeric films and particles has been described by Devotta et al. [3] as occurring via three main stages. The diffusion of the solvent causes its ingress into the polymer matrix, which results in the creation of a distinct boundary where the unswollen glassy polymer meets the swollen rubbery gel phase. It is assumed that the boundary features a steep solvent concentration gradient – highest within the gel region, and lowest in the unswollen phase. Eventually, reptative disengagement gives rise to the relatively high molecular mobility of the polymer into the solvent. The formation of the swollen gel region is thought to be due to solvent-induced plasticisation [4].

Disengagement is typically not an instantaneous process, and its commencement is primarily driven by the reptation time as it is preceded by polymer chain mobility and reptation in succession. Amongst other factors, it is believed that the mobility of the disengaging molecule and the degree of disentanglement, considerably influence the disengagement rate, and thus, the swelling and dissolution behaviour of the polymeric molecules within the composite. In reality, the swelling-dissolution phenomenon is dynamic and highly complex, with the disengagement rate being initially negligible until the reptation time is exceeded [3,4].

Thus, these results suggest significant differences in the disengagement times for both matrices and possibly highlight other underlying interacting mechanisms as PPE is introduced. The variation of respective chain mobilities may be substantial enough to give rise to varying reptation times and disengagement rates at a molecular level. These variations can result from the presence of the cross-linked species, evidence of which was previously discussed in Chapter 6. Other sources of variation may include the presence of bulky phenyl moieties within the backbone.

Following the longer time-scale exposure (72 hours), it becomes clear that the use of the PPE-modified matrix results in even more significant improvement of the solvent resistance of the GF/A95/P5 (only 2 % of mass loss) over its unmodified acrylic

counterpart (GF/A100/P0), which lost 28 % of its original mass. With a matrix mass fraction of 32 ± 0.3 % in the composite, this recorded mass loss for the GF/A100/P0 sample is similar in magnitude to its matrix mass fraction. As such, it indicates that complete dissolution of the acrylic matrix occurred, which is in agreement with visual observations during data collection (shown in Figure 7-3).

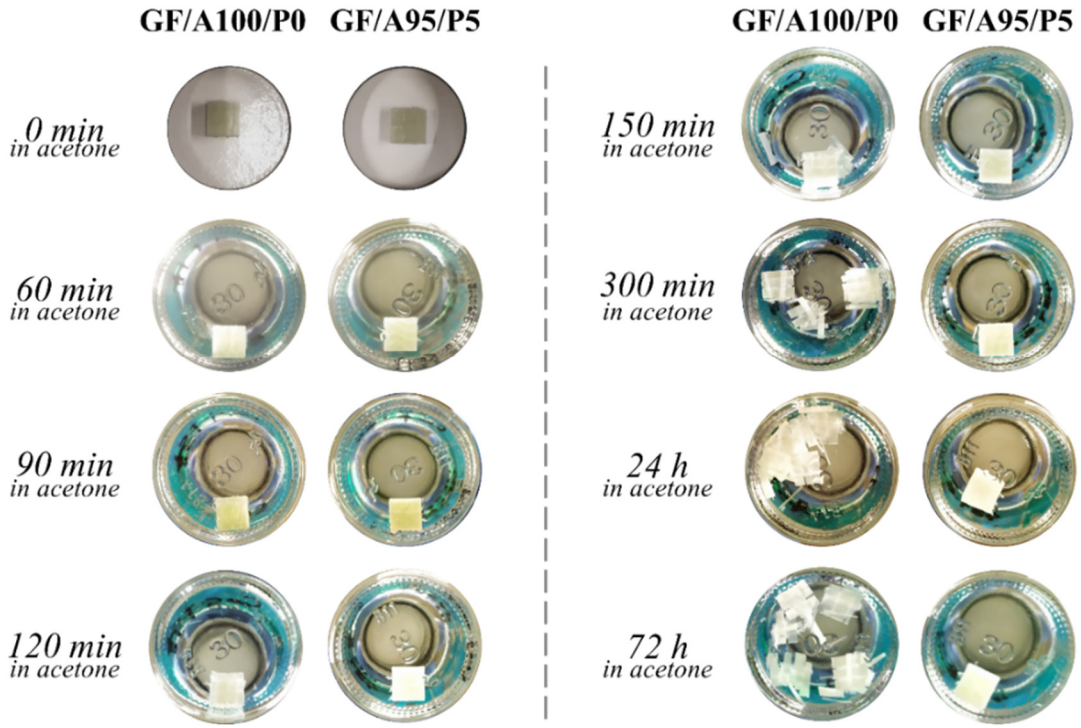


Figure 7-3. Time-lapse images of glass fibre-reinforced acrylic (GF/A100/P0) and glass fibre-reinforced acrylic/PPE (GF/A95/P5) composites subjected to prolonged (72 h) exposure in acetone. Nominal sample dimensions (mm): 8 × 8.

After 90 minutes of exposure, the integrity of the coupon appeared compromised, with layers beginning to fray along exposed edges. After 150 minutes, partial delamination of the top and bottom plies had occurred, with full delamination of the top ply following after 210 minutes. From this point onwards, the remaining plies progressively delaminated, until the ultimate dissolution of the matrix at 300 minutes. At the 300-minute interval, only fibres were visible within the solvent and upon sample recovery at completion.

In contrast, only partial whitening was observed in the GF/A95/P5 sample after 150 minutes, with some evidence of matrix dissolution (exposed fibres) along the sample

edges. Thereafter, no change was observed until the sample was recovered at 72 hours. These changes corresponded to only a 2 % mass loss, a significant performance improvement compared to a 28 % mass loss for the unmodified acrylic (GF/A100/P0) composite. It is worth noting that the matrix mass fractions for GF/A100/P0 and GF/A95/P5 are 32 % and 25 %, respectively; thus, the residual mass of the GF/A100/P0 is almost wholly constituted by glass fibres. Finally, no white sediments were observed as with unreinforced polymer samples in Figure 6-10 and discussed in Section 6.4.2, providing strong evidence that no unreacted PPE was contained within the reinforced 5 wt. % PPE-modified acrylic composite. It can be assumed that varying the conditions of the polymerisation reactions from in-air casting for the unreinforced polymer to vacuum resin infusion for the reinforced laminate played a key role. The absence of oxygen during the resin infusion process under vacuum would avoid potential oxygen-inhibition effects due to oxygen's biradical nature, given the vulnerability of acrylates to this phenomenon [5,6].

Overall, this study demonstrates significantly enhanced solvent resistance for the PPE-modified acrylic-matrix composite, which opens up opportunities for broadened applicability. High-solvent-resistant materials are desirable for numerous sectors and are expected to be particularly advantageous for the automotive sector. The low mass loss after prolonged exposure may also be correlated to good thermomechanical and mechanical property retention after exposure to harsh chemical environments. However, quantifying the extent of retentions requires further exploration.

7.2.2 Dynamic mechanical analysis

Figure 7-4 shows representative thermograms obtained from DMA experiments on glass fibre-reinforced PPE-modified acrylic (GF/A95/P5) matrix composite and an unmodified acrylic composite (GF/A100/P0). Prominent differences in damping behaviour are observed. The GF/A100/P0 material exhibited a distinct, single tan delta peak. In contrast, despite the observation of single peaks for the unreinforced A95/P5 in Section 6.4.3, the peak for GF/A95/P5 appears to broaden with mild evidence of peak splitting, indicating the presence of multi-species phases within the blend-matrix composite. The distance between tan delta peaks in blends correlates to the extent of phase separation between their constituents [7]. Thus, these observations support the hypothesis that the PPE-modified acrylic composite comprises a cross-linked network,

within which a graft acrylic/PPE copolymer and a linear acrylic homopolymer are interpenetrated. The differences between the unreinforced and reinforced A95/P5 matrix provide further evidence of the differences between the polymerisation conditions between both materials. A broader distribution of chain lengths was likely favoured during resin infusion under vacuum than those obtained by casting, results of which were discussed in Section 6.4.3. Moreover, the effects of fibres on the growth kinetics of the polymer chains is also another source of variation between the two methodologies.

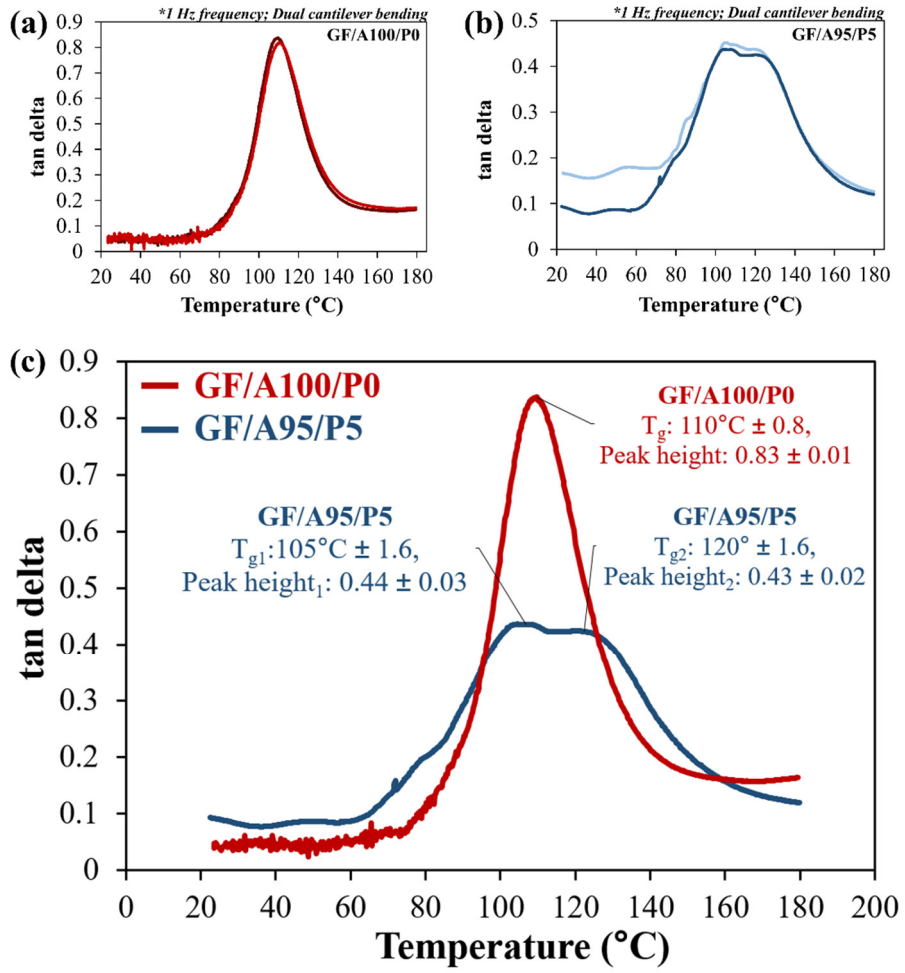


Figure 7-4. DMA results for glass fibre-reinforced (a) acrylic (GF/A100/P0) and (b) PPE-modified acrylic (GF/A95/P5) composites showing damping response (tan delta), and (c) representative thermograms with averaged results for each material. Lay-up: $[0]_8$.

The corresponding T_g values for GF/A95/P5 are 105°C and 120°C, as shown in Figure 7-4. The T_g values for neat acrylic and PPE are 104°C (rounded value from results in Figure 6-12) and 160°C [7], respectively. Thus, T_{g1} is most likely attributed to the presence

of an acrylic homopolymer species, as evidenced by NMR spectroscopy in Figure 6-4. On the other hand, T_{g2} is a unique intermediate temperature between the two blend components, and possibly provides evidence of a reacted product of the acrylic and PPE constituents coexisting with the acrylic homopolymer. Based on the observed T_g values, the hybrid matrix system was assumed to bi-phasic in nature, comprising an acrylic (or acrylic-rich phase) and a PPE-rich acrylic/PPE The Fox equation was applied using Equation 7-1 and as detailed in Section C.1.1.3 to estimate the composition of the acrylic/PPE reacted product that would give rise to a T_{g2}.

$$\frac{1}{T_{gN}} = \frac{\varphi_{2,A}}{T_{gN,A}} + \frac{\varphi_{2,B}}{T_{gN,B}} \qquad \text{Equation 7-1}$$

Where $\varphi_{2,A}$ and $\varphi_{2,B}$ are mass fractions of acrylic and PPE, respectively, the sum of which equals unity; T_{gN} is the glass transition temperature corresponding to the peaks shown in Figure 7-5; $T_{gN,A}$ and $T_{gN,B}$ are the glass transition temperatures of the acrylic and PPE constituents, respectively. Note: all T_g values were used in Kelvin.

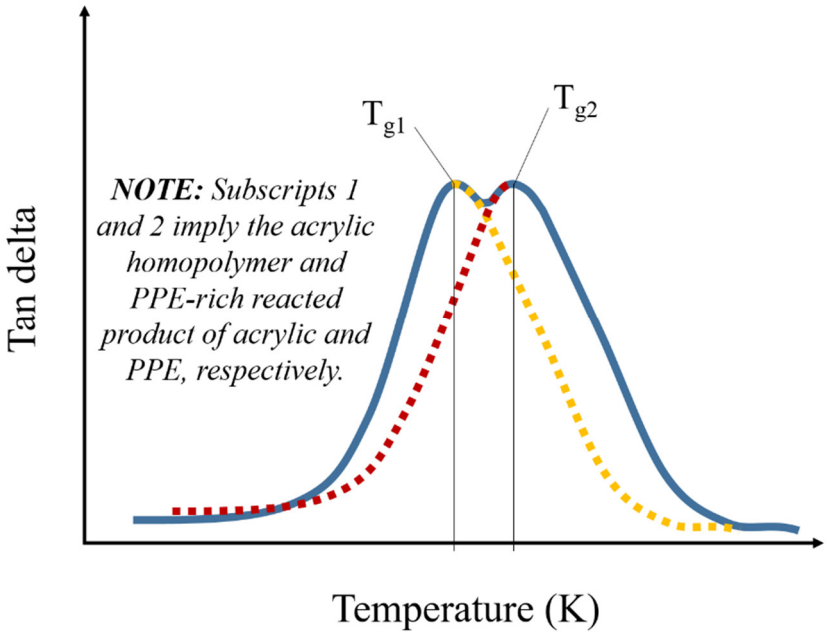


Figure 7-5. An idealised representation of the T_{gN} values used in the analysis for the GF/A95/P5 sample, where T_{g1} and T_{g2} are the glass transition temperatures (Kelvin) for the acrylic homopolymer and PPE-rich phases of the hybrid matrix, respectively.

Using the properties summarised in Table 7-4, $\varphi_{2,A}$ and $\varphi_{2,B}$ within the reacted product were estimated to be 0.69 and 0.31, respectively.

Table 7-4. Summary of values used to estimate the constituents (acrylic and PPE) within the reacted product to yield a T_{g2} value of 120°C (373 K).

Properties	*Values used*	*Source*
T_{g2}	393 K	Figure 7-4
$T_{g2,A}$	377 K	Figure 6-12
$T_{g2,B}$	433 K	[8]

Moreover, based on the observation of two T_g values, the full blended system (S_B) can be represented by a summation of the mass fractions corresponding to T_{g1} (φ_1) and T_{g2} ($\varphi_{2,A} + \varphi_{2,B}$). T_{g1} relies solely on contributions from the acrylic phase, and T_g involves contributions from both acrylic and PPE phases. Thus, assuming that all the PPE (5 wt. %) within the full blended system (S_B) is directly proportional to $\varphi_{2,B}$ according to the Fox Equation (Equation 7-1), $\varphi_{2,A}$ yields a corresponding mass fraction estimate in S_B of $\left(\frac{0.69 \times 0.05}{0.31}\right) = 0.11$. The total mass fraction of acrylic/PPE reacted product is 16 wt. %, based on combined acrylic and PPE mass fractions in S_B, i.e. 11 wt. % and 5 wt. %. Accordingly, 84 % of the total 95 wt. % of acrylic supplied for the polymerisation reaction was consumed in the formation of the homopolymer, whereas 16 % formed a reacted product with PPE.

These results provide further evidence of the formation of a complex co-reacted acrylic/PPE species. As discussed in Chapter 6, although no traditional cross-linker was employed as part of this study, the multiple vinyl functional groups of the PPE oligomer used in the hybridisation of the acrylic matrix facilitated the formation of a lightly cross-linked structure.

In light of the relative mass loss of GF/A95/P5 following prolonged exposure to acetone in Section 7.2.1, these estimated mass fractions may hold the key to understanding the hybrid-matrix structure. Solvent resistance studies revealed that mass retention of approximately 98 % of the original mass was possible as a result of PPE modification. However, in this section, it was estimated that the acrylic homopolymer constituted 84 wt. % of the full hybrid matrix system. Neat acrylic has been shown in Section 7.2.1 to be fully vulnerable to acetone attack under the same conditions. Based on the architecture proposed in Chapter 6 (Figure 6-25), the bulk of the linear, acrylic homopolymer is expected to interpenetrate a cross-linked acrylic/PPE network alongside a graft

copolymer. The cross-linked and grafted acrylic/PPE phase possible makes up approximately 16 wt. % of the full matrix. In such a structure, the network can effectively serve as a scaffold and may promote a great extent of entanglement between linear acrylic and PPE-grafted acrylic chains. Given that solvent resistance is influenced by disengagement and reptation times of polymer chains, this architecture is highly likely to favour the trapping of entanglements and thus, provide an anchor for a large extent of the acrylic homopolymer [9–11], which in itself would be vulnerable to solvent attack.

Furthermore, changes in T_g are typically indicative of changes in chain length and mobility. As discussed in Section 6.1.3, this increase in T_g with the addition of PPE indicates relative reductions in chain flexibility, available free volume and chain mobility. These observations may be due to the contributions of phenyl moieties in the PPE and cross-links to the overall rigidity. It is also apparent that the PPE-modified acrylic-matrix composite exhibited a broader peak, which provides further evidence of structural and molecular heterogeneity within the matrix.

Interestingly, the severity of the reduction in peak height in the GF/A95/P5 samples supports the hypothesis on the presence of cross-links and phenyl moieties within the PPE-modified acrylic composite enhancing the rigidity of the matrix. Cross-links are known to give rise to reduced intensities in damping peaks [12].

Moreover, the low tan delta peak values may also provide crucial information on the fibre-matrix interfacial behaviour. It is well known that composites with poor interfacial strength exhibit superior damping ability, evidenced by increased peak heights [13,14]. Thus, a diminished peak height provides strong evidence that incorporating PPE into the acrylic matrix does not appear to deteriorate interfacial adhesion between the blend matrix and the reinforcing fibres.

While attempts were made to characterise the fibre-matrix interfacial strength quantitatively, the acrylic monomer's inherent volatility prohibited sample preparation (detailed in Appendix C.2.1.2.2 (Figure C-16)). As such, a qualitative approach was sought to compare the interfacial adhesion of both materials. The empirical equation employed by Ibarra and Paños [15] and Poletto [16] was applied as defined in Equation 7-2 to obtain the interfacial adhesion parameter, A. This formula is based on established knowledge

that a stronger interface typically reduces the macromolecular mobility of the matrix neighbouring the reinforcing phase. Consequently, the $tan\ \delta_c$ value also reduces.

Moreover, the determination of the A parameter is underpinned by the assumptions that $tan\ \delta_i$, the interphase damping parameter is negligible. Thus, the adhesion parameter can be related to the damping behaviour of the composite and matrix, as well as the fibre volume fraction [15,16]. Lower $\boldsymbol{A}$ values are indicative of superior interfacial adhesion.

$$A = \left(\frac{1}{1 - V_f}\right)\left(\frac{tan\ \delta_c}{tan\ \delta_m}\right) - 1 \qquad \text{Equation 7-2}$$

The variables $tan\ \delta_c$ and $tan\ \delta_m$ represent the peak tan delta values for the composite material system and its matrix constituent, respectively; and V_f is the fibre volume fraction of the composite. Using this approach, the $\boldsymbol{A}$ parameter for the GF/A100/P0 and GF/A95/P5 materials were determined to be 0.11 and -0.24, respectively. Thus, this constitutes positive hybridisation effects in terms of fibre-matrix adhesion behaviour.

7.2.3 Thermogravimetric analysis

These trends also hold for comparisons between the GF/A100/P0 and GF/A95/P5 composites, with most parameters being marginally improved. Figure 7-6 shows the TGA and DTG curves of both the reinforced acrylic (GF/A100/P0) and PPE-modified acrylic (GF/A95/P5) composites. The oscillations observed in the DTG plots are artefacts from the instrument due to the use of relatively small sample sizes for these experiments.

Unlike the results of unreinforced polymers in Section 6.4.4, the decomposition behaviour observed in the GF/A100/P0 and GF/A95/P5 composites are similar in terms of both materials undergoing a single degradation stage. Moreover, both materials exhibit dissimilar behaviour to their respective unreinforced counterparts, indicating that both the presence of fibres and polymerisation under vacuum may affect the resulting hybrid material. As with the unreinforced polymer samples studied in Chapter 6, the presence of PPE within the blended-matrix composite results in improved thermal stability. In Zone 1 of Figure 7-6, it is evident that the GF/A95/P5 can withstand a higher temperature before mass loss initiates. From Zone 2, it is evident that the blended-matrix composite sustains lower overall mass loss under the experimental conditions utilised.

The presence of PPE within the GF/A95/P5 sample results in a reduced rate of degradation as is evident in the DTG curve where a lower valley peak is observed compared to the GF/A100/P0 composite sample. Moreover, a 16°C temperature shift is also evident.

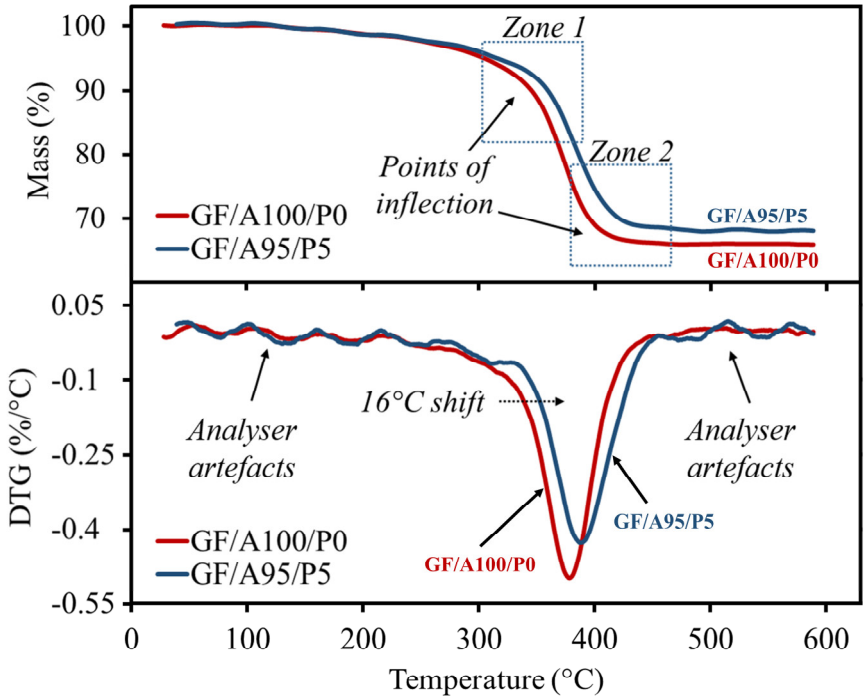


Figure 7-6. TGA and DTG plots of glass fibre-reinforced acrylic (GF/A100/P0) and PPE-modified acrylic (GF/A95/P5) composites.

Table 7-5 provides an overview of the parameters determined to estimate the composites under investigation. $T_{5\%}$ and $T_{10\%}$ are 205°C and 345°C for GF/A100/P0 and increase by 9°C and 15°Cwith the GF/A95/P5 sample, respectively.

As was the case with DMA observations, differences in GF/A100/P0 and GF/A95/P5 behaviour with their respective unreinforced counterparts presented in Chapter 6 are attributed to the differences in the processing conditions and the presence of fibres. While the casting process for unreinforced samples was performed in air, all composite laminates were prepared under vacuum. Interactions between the matrix, fibres and sizing are expected to affect the polymerisation reaction and the resulting polymers.

For enhanced comparability, all evaluated parameters discussed in Section 7.2.2 from the TGA and DTG curves of both materials are reported in Table 7-5.

Table 7-5. Summary of thermogravimetric results of composite samples showing the effects of PPE-modification on thermal stability.

	TGA curve parameters [a-e]					*DTG curve parameters* [f-h]		
	$T_{onset\text{-}TGA}$ [a]	T_{end} [b]	$T_{5\%}$ [c]	$T_{10\%}$ [d]	M_R [e]	$T_{onset\text{-}DTG}$ [f]	T_{end} [g]	T_{max} [h]
	(°C)	*(°C)*	*(°C)*	*(°C)*	*%*	*(°C)*	*(°C)*	*(°C)*
GF/A100/P0	334	409	205	345	66	334	419	378
GF/A95/P5	348	413	216	360	68	347	439	389

a, b $T_{onset\text{-}TGA}$: Onset and end temperatures for the main degradation event as determined from the intersection of tangents to the inflexion at Zones 1 and 2 of the TGA curves (Figure 7-6), respectively.

c, d $T_{N\,\%}$: Temperatures corresponding to N% of mass loss using the TGA mass loss curves.

e M_R: Residual mass at the end of the thermal cycle. Note: these are primarily fibres, given the mass fractions reported in Section 7.1.1.

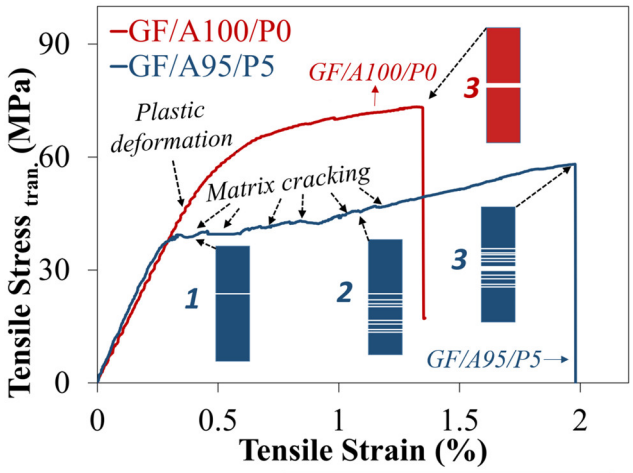
f $T_{onset\text{-}DTG}$: Onset temperatures corresponding to the pre-peak inflexion points of DTG curves as determined from the intersection of tangents.

g T_{end}: End temperatures corresponding to the post-peak inflexion points of DTG curves as determined from the intersection of tangents.

h T_{max}: Temperatures corresponding to the degradation rate; i.e., the valleys or peaks of the DTG curves.

7.2.4 Transverse tensile properties

Representative stress-strain responses and average transverse tensile strengths, moduli and failure strains of the GF/A100/P0 and GF/A95/P5 materials are presented in Figure 7-7. All other stress-strain curves are presented in Appendix C.2.1.1. Both materials exhibit similar linear behaviour initially; however, an earlier onset of damage initiation was observed with the GF/A95/P5 samples. After the linear-elastic region, a knee-point (Point 1) can be seen for all samples with mild plastic deformation. Strain-hardening behaviour occurred thereafter. This behaviour is known to occur due to the sliding, alignment/orientation and stretching of polymer chains [17]. Matrix cracking accumulates between Point 1 and Point 3 (Figure 7-7) before ultimate failure. Similar stress-strain evolution was observed for epoxy-matrix composites in Chapter 5 (Section 5.2.1). However, the epoxy-matrix composite exhibited no plasticity at the knee-point, and its stress-strain curves exhibited more pronounced evidence of matrix cracking than the GF/A95/P5 samples.



	GF/A100/P0	GF/A95/P5
Strength (MPa)	73 ± 3.9	60 ± 1.2
Modulus (GPa)	13 ± 0.6	14 ± 1.0
Failure strain (%)	1.2 ± 0.3	1.9 ± 0.1
Elastic Limit (%)	0.4 ± 0.1	0.3 ± 0.0

Figure 7-7. Representative curves and results for GF/A100/P0 (red) and GF/A95/P5 (blue) following loading in transverse tension. Stress-strain curves for all samples are provided in Appendix C.2.1.1 (Figure C-2 & Figure C-3). Lay-up: $[0]_8$.

Thus, this stress-strain evolution behaviour may constitute a cross-link-induced response to transverse tensile loading. This hypothesis is further supported by the work of

Nakajima et al. [18] who reported similar tensile behaviour in cross-linked hydrogels. The mild plasticity and reduction in damage development between Point 1 and Point 3 (Figure 7-7) relative to the GF/epoxy material and are possibly contributions of the non-cross-linked constituents within the PPE-modified acrylic composite. Visual evidence of the aforementioned cracks can be seen clearly in Figure 7-8b, which resemble the failure behaviour observed for GF/epoxy samples in Figure 5-4. In contrast, the GF/A100/P0 material undergoes plastic deformation up to failure, with no observable macroscopic transverse cracks along the sample length, as shown in Figure 7-8a.

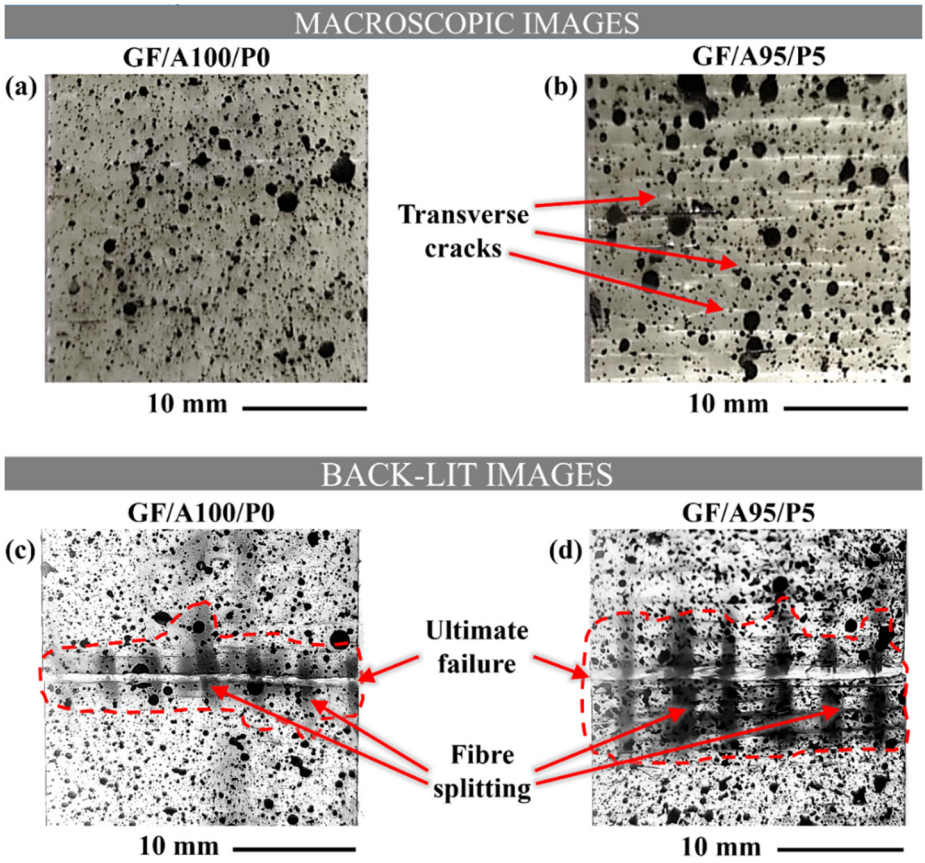


Figure 7-8. Representative macroscopic and back-lit images of failed transverse tensile test specimens of GF/A100/P0 ((a) & (c)) and GF/A95/P5 ((b) & (d)). Lay-up: $[0]_8$.

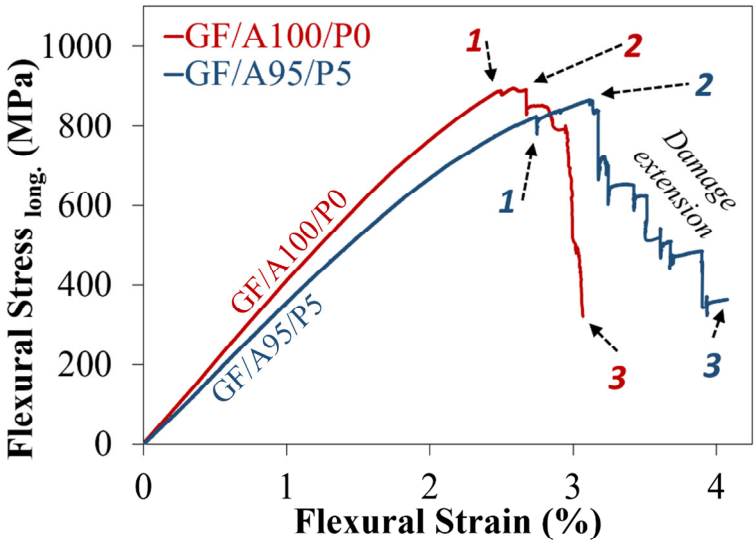
Furthermore, back-lit imaging on samples of both materials revealed similar fibre splitting damage in the longitudinal direction. As shown in Figure 7-8c and Figure 7-8d, these longitudinal fibres are the same 90°-fibres present within the quasi-unidirectional fabric, previously described in Sections 5.2.1 and 5.2.5.

Moreover, the damaged zones in GF/A95/P5 samples (Figure 7-8d) were more extensive than those observed in GF/A100/P0 (Figure 7-8c), possibly indicating more brittle fracture behaviour in the GF/A95/P5 material. The observation of both matrix cracks and plastic deformation behaviour in the GF/A95/P5 material suggests that the hybrid material exhibits both macroscopic ductile and brittle characteristics. This observation provides further evidence to support the hypothesis of a multi-species blend system, within which the reacted product of acrylic and PPE forms both cross-linked and non-cross-linked (grafted) species, coexisting with the amorphous acrylic homopolymer species as proposed in Section 6. It is plausible that the cross-linked species in the reacted product contribute to localised matrix cracking when their failure strain is exceeded — possibly explaining the pronounced damaged zone near the ultimate fracture site. Conversely, disengagement and stretching of the homopolymer acrylic and the grafted acrylic/PPE chains are likely to contribute to the enhanced ductility, evidenced by a 58 % higher failure strain in the GF/A95/P5 relative to the unmodified GF/A100/P0 reference material.

While an increase in ductility is typically at the expense of modulus or strength, matrix hybridisation results in a slight increase in modulus (+8 %), with a reduced (-18 %) transverse tensile strength (Figure 7-7). Thus, hybridisation appears to increase both transverse composite modulus and ductility. With the hypothesis of the formation of a spatially inhomogeneous polymer structure with multi-component mixtures, contributions from the cross-linked species and phenyl moieties must also be considered. Concerning cross-links, it is well known that cross-links can significantly reduce chain mobility. The greater the cross-link density of a polymer, the lower its ductility [19–23]. Thus, it can also be inferred from the increased failure strain that the hybrid matrix does not possess a high cross-link density, but intermittent and dispersed low cross-link density is more probable given the slight increase in modulus. Furthermore, phenyl moieties within PPE-derived macromolecules would be expected to have stiffening effects on the polymer backbone [24,25]. Finally, higher areas bounded under GF/A95/P5 curves suggests enhanced toughness, which may be attributed to intrinsic toughening mechanisms.

7.2.5 Longitudinal flexural performance

Results from longitudinal flexural tests are presented in Figure 7-9. Both materials exhibit a three-stage stress-strain evolution: (i) an initial linear-elastic region, followed by (ii) slight non-linearity, and (iii) onset of damage (Point 1). Post-peak strain evolution between Point 2 and 3 appears more confined in GF/A100/P0 samples than in GF/A95/P5. Progressive damage extension occurs over a broader range of strains for GF/A95/P5, which can be attributed to extended delamination, severe tow splitting processes and tow rupture.



	GF/A100/P0	GF/A95/P5
Strength (MPa)	879 ± 49	810 ± 37
Modulus (GPa)	40 ± 1.7	35 ± 0.8
Failure strain (%)	3.3 ± 0.4	3.9 ± 0.4

Figure 7-9. Representative curves and results for GF/A100/P0 (red) and GF/A95/P5 (blue) following loading in longitudinal flexure. Stress-strain curves for all samples are provided in Appendix C.2.1.1 (Figure C-10 & Figure C-11). Lay-up: $[0]_8$.

These failure modes are evident from the macroscopic image of compressive side failure for GF/A95/P5 shown in Figure 7-10. More brittle fibre fracture was observed for the GF/A95/P5 samples on the compressive side than the GF/A100/P0 samples. Both materials exhibit similar tensile side failure, which is not unexpected, as longitudinal tensile behaviour is known to be fibre-dominated. Given the fibre-dominance of this property, their normalised strengths and moduli (to 50% V_f) are also provided. Normalised

strengths were 888 MPa and 711 MPa; and normalised moduli were 40 GPa and 31 GPa for GF/A100/P0 and GF/A95/P5, respectively.

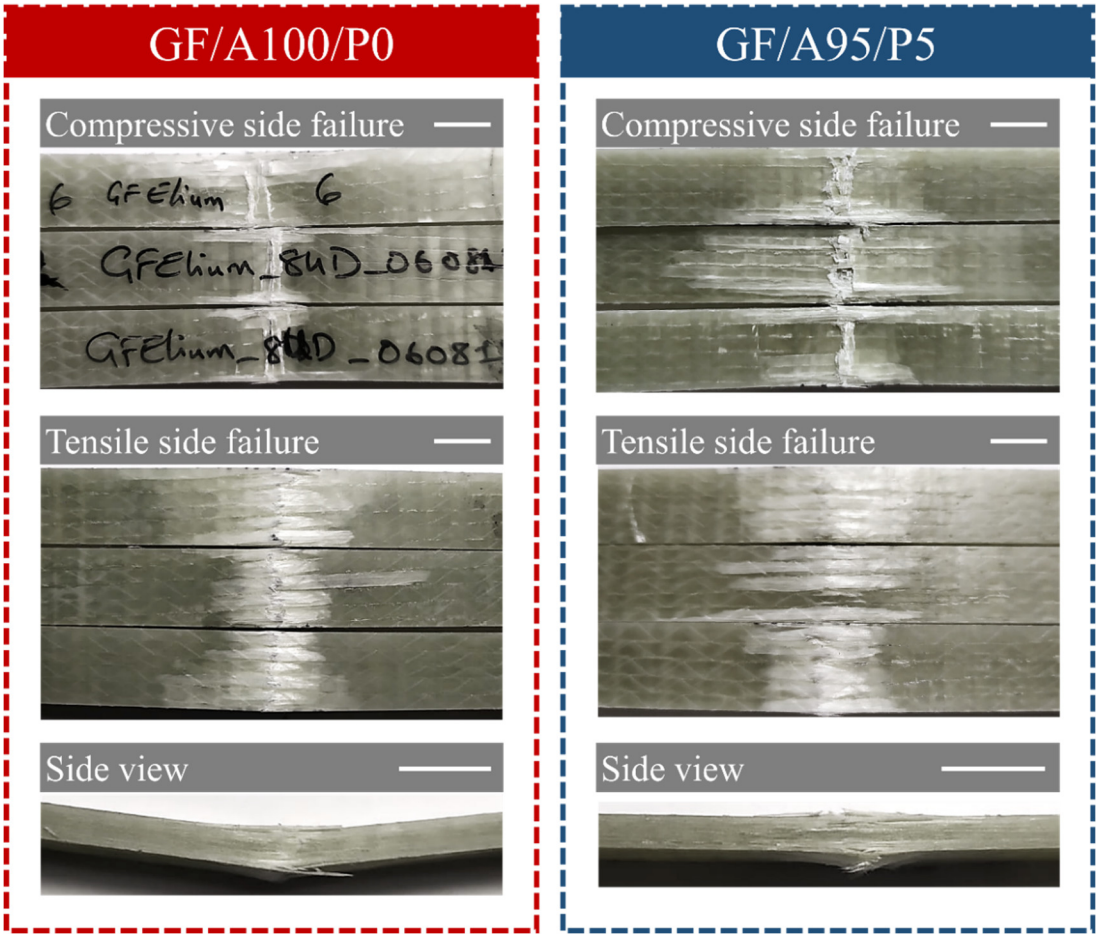


Figure 7-10. Macroscopic images of failure behaviour on the compressive and transverse sides of representative samples of GF/A100/P0 and GF/A95/P5. Side views of representative samples are also presented to show differences in deformation behaviour. All images feature a 10 mm scale bar. Lay-up: $[0]_8$.

In terms of deformation behaviour, all GF/A00/P0 samples exhibited gross order plastic deformation, evidenced by the permanent distortion of the failed sample, as shown in the side view in Figure 7-10. Interestingly, only one GF/A95/P5 exhibited similar deformation behaviour; all other samples were flat with no evidence of deformation. Together with the observation of more extensive delaminated zones, this may indicate a greater extent of brittleness in the GF/A95/P5 samples.

The incorporation of PPE into the matrix produces a laminate with lower longitudinal flexural strength (-8 %) and modulus (-18 %). The results were normalised to account for

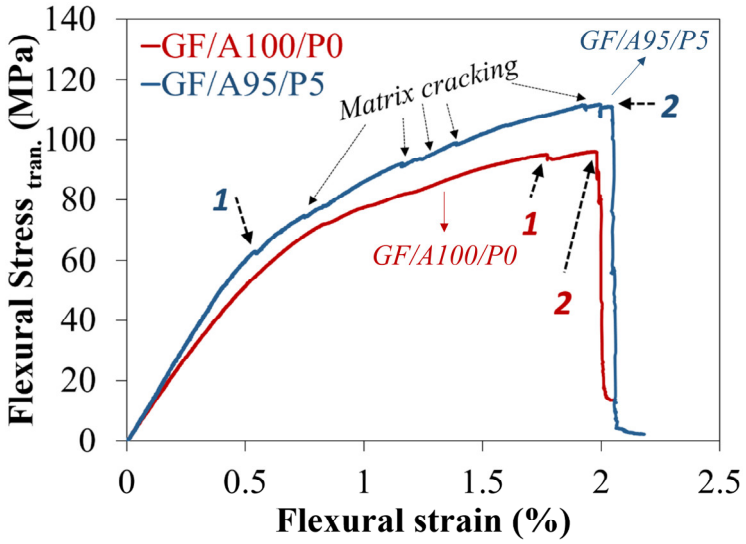
the differences in fibre volume fractions. In doing so, it was found that the GF/A95/P5 material possessed 20 % and 23 % lower mean strength and modulus than the GF/A100/P0 material. Given that higher fibre volume fractions typically results in higher strength and modulus, these reductions in strength and modulus relative to the unmodified acrylic-matrix composite are unexpected. It has been previously suggested that V_f values higher than 60 % [26] and 78 % [27] may be undesirable from a fibre-contact and stress transfer perspective. The V_f for the GF/A95/P5 is 57 % and may well explain the inferiority in strength and modulus for this material. However, further investigations are required to substantiate this.

Despite the observation of brittle characteristics, the GF/A95/P5 material also exhibits markedly higher (18 %) failure strain than the GF/A100/P0, which is consistent with transverse tensile test results discussed in Section 7.2.4. And as with transverse tensile results, a greater area appears to be bound under the curves of the GF/A95/P5 samples, suggesting enhanced toughness with respect to the unmodified GF/A100/P0 reference material. However, this toughness does not appear to contribute positively to delamination resistance under the present conditions of investigation. Higher failure strain and enhanced toughness would typically be expected to be accompanied by ductile failure characteristics and improved resistance to delamination. Thus, these results highlight a duality of attributes in the hybrid-matrix composite, and may directly result from the previously described contributions of a brittle cross-linked acrylic/PPE species, non-cross-link acrylic/PPE species and acrylic homopolymer within the matrix. Such a structure is highly desirable in the hybrid material as it suggests that more precise tuning of the blend microstructure may realise selective property enhancements.

7.2.6 Transverse flexural performance

In Figure 7-11, the results of transverse flexural tests are presented. Both materials exhibit an initial region of linearity, beyond which, plastic deformation ensues with a distinct onset of failure (Point 1) and abrupt ultimate failure at Point 2. This ultimate failure behaviour likely results from sequential transverse matrix and interfacial damage modes, which ultimately result in axial interfacial debonding (of 90° tows) and tow rupture.

All GF/A95/P5 samples undergo cumulative matrix cracking in plies under tension, evidenced between Points 1 and 2 in Figure 7-11; and supported by macroscopic failure behaviour revealed in Figure 7-12.



	GF/A100/P0	GF/A95/P5
Strength (MPa)	91 ± 5.4	105 ± 5.0
Modulus (GPa)	11 ± 0.2	13 ± 0.6
Failure strain (%)	1.7 ± 0.3	2.1 ± 0.2

Figure 7-11. Representative curves and results for GF/A100/P0 (red) and GF/A95/P5 (blue) following loading in transverse flexure. Stress-strain curves for all samples are provided in Appendix C.2.1.1 (Figure C-12 & Figure C-13). Lay-up: $[0]_8$.

The onset and accumulation of damage after the linear-elastic region was similar to the behaviour observed for samples subjected to transverse tensile loading. However, no knee-point was evident here; the GF/A95/P5 samples exhibited similar stress-strain evolution to the GF/A100/P0 samples. PPE modification resulted in improved transverse flexural strength (+15 %), modulus (+18 %) and failure strain (+24 %) relative to the unmodified reference.

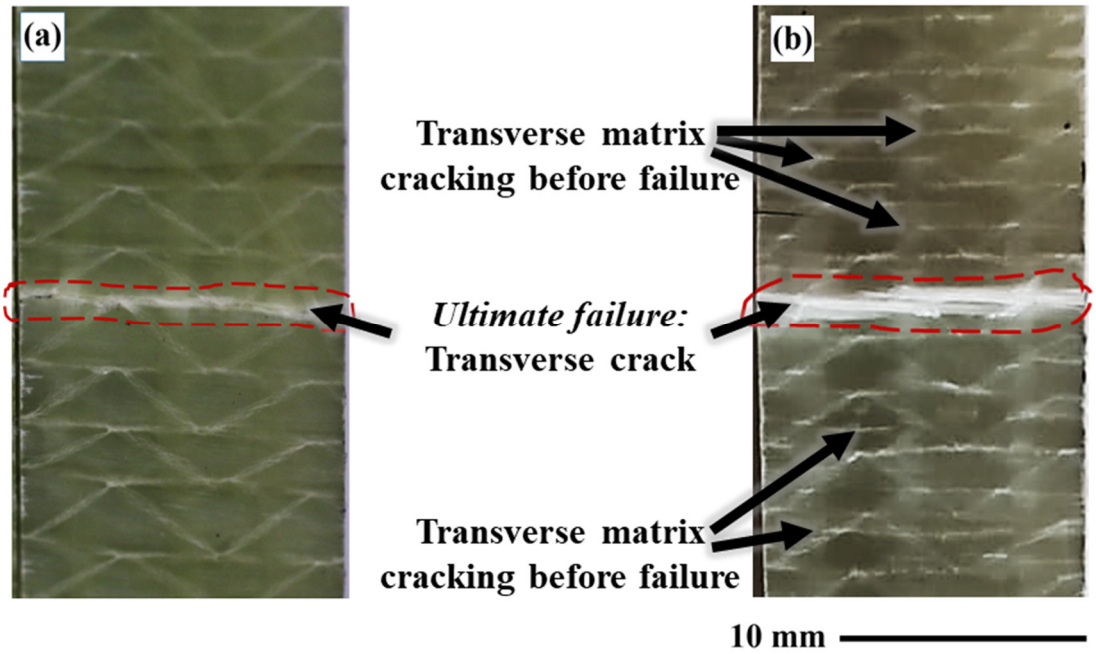


Figure 7-12. Macroscopic images of representative transverse flexural failure on sides subjected to tensile stress states of (a) GF/A100/P0 and (b) GF/A95/P5 samples. Lay-up: $[0]_8$.

Unlike the epoxy-matrix composite in Chapter 5 (Figure 5-3 and Figure 5-7), the relative trends in the transverse tensile behaviour of GF/A95/P5 did not correlate with its flexural stress-strain responses. While mild plasticity gave way to a sharper knee-point in the transverse tensile samples' strain evolution, a more gradual yield behaviour was observed for transverse flexural testing. Differences in the trends between the comparative transverse tensile and flexural performance are tentatively attributed to the sensitivity of the transverse tensile testing to defect distribution across the gauge length [28]. However, given that flexural loading induces both tensile and compressive stress states, it is unlikely that the resultant stress-strain evolution would reflect pure tensile behaviour. Of course, microcracking and microplastic deformation processes are likely to affect the contributions of compressive stresses [29]. Thus, it can be concluded that hybridisation has improved the composite transverse flexural strength, modulus, ductility and overall toughness.

Although modulus and ductility are rarely enhanced simultaneously, such behaviour has been previously reported for hybrid-matrix composites [30]. This behaviour may be attributed to the stiffening effects of the lightly cross-linked network in this present work.

The enhanced ductility would appear to be contributions from the stretching and disengagement of the interpenetrating grafted acrylic/PPE and linear acrylic polymer chains within the PPE-modified acrylic-matrix of the composite.

These results are more in line with the expected composite performance in light of the observations discussed in Section 6.1.5 where the results of flexural testing of unreinforced A95/P5 matrix revealed possibly enhanced strength and modulus relative to A100/P0 (based on peak load and apparent stiffness from their corresponding load-displacement responses). The enhanced ductility here may be positive hybridisation effects resulting from the intrinsic toughening mechanisms.

7.2.7 Short beam shear properties

Figure 7-13 shows the short beam shear test results for the GF/A100/P0 and GF/A95/P5 materials. Both materials exhibit some initial elasticity, followed by plastic deformation as the matrix begins to yield. Some fibre rotation takes place, facilitating load take-up in tension, and giving rise to a slight hardening effect on approach of ultimate shear stress (τ_{max}). For materials with relatively high interfacial shear strength, this is followed by delamination as the matrix yield strength is exceeded [31].

Both materials exhibit unique post-failure softening. The curves of GF/A95/P5 samples exhibited more abrupt losses in stiffness up to displacements of 1.5 mm. This can be seen as 9-MPa and 16-MPa reductions in stress between the stress values τ_{max} and $\tau_{1.5\ mm}$ for GF/A100/P0 and GF/A95/P5 as shown in Figure 7-13a and Figure 7-13b, respectively. Given that the interlaminar shear strength of composites is known to correlate well with their interfacial shear strength [32], both materials appear to exhibit comparable interfacial shear strengths. Therefore, the differences in the degrees of post-failure softening observed for both materials must not be associated with differences in interfacial adhesion. Post-peak softening is believed to be associated with damage accumulation within the sample [33] and thus, an inspection of damaged states may provide further insights.

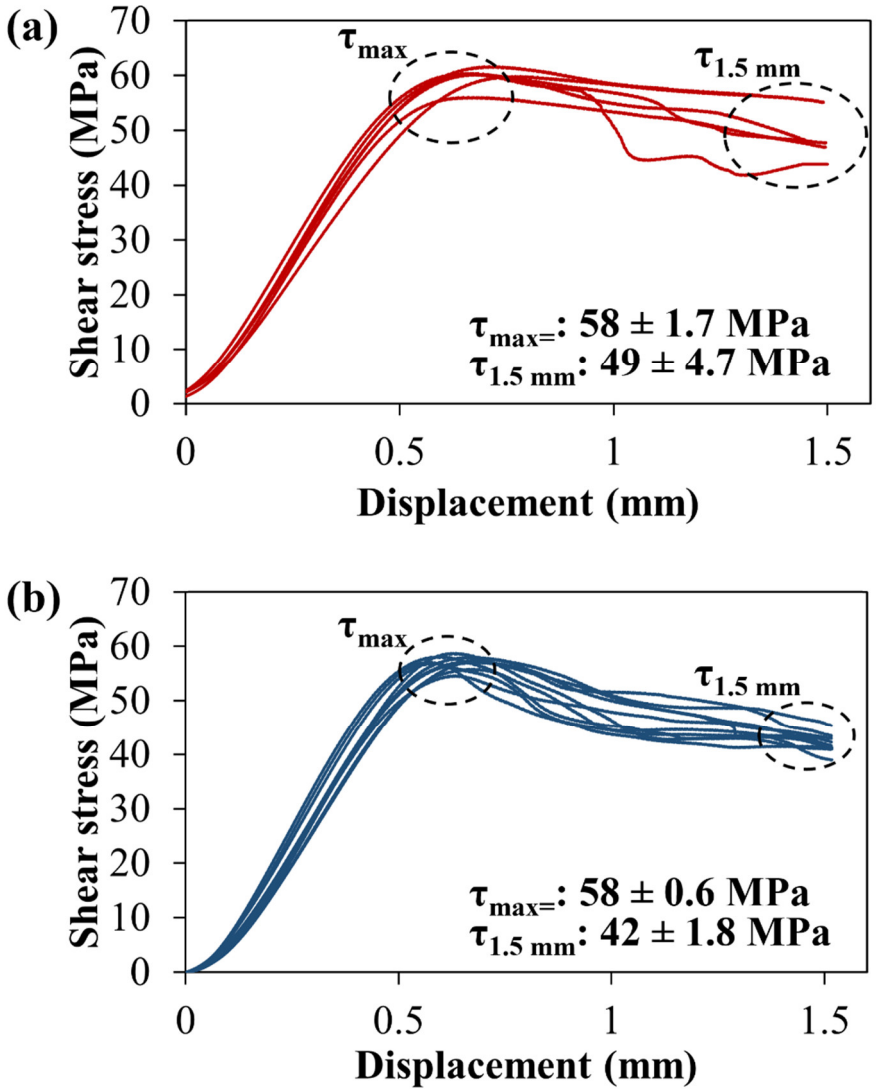


Figure 7-13. Stress-displacement curves for (a) GF/A100/P0 and (b) GF/A95/P5 following loading in short beam shear. Note: τ_{max} is the corresponding shear strength, and $\tau_{1.5\ mm}$ is the stress at 1.5 mm displacement for all samples, respectively. Lay-up: $[0]_8$.

Post-mortem sample inspections revealed markedly different damage extents and mechanisms between both materials, as is evident from the representative macroscopic images of the damage states in Figure 7-14. While the GF/A100/P0 samples exhibited predominantly inelastic deformation, with evidence of interlaminar shear failure, GF/A95/P5 underwent shear failure with the occurrence of edge-delamination.

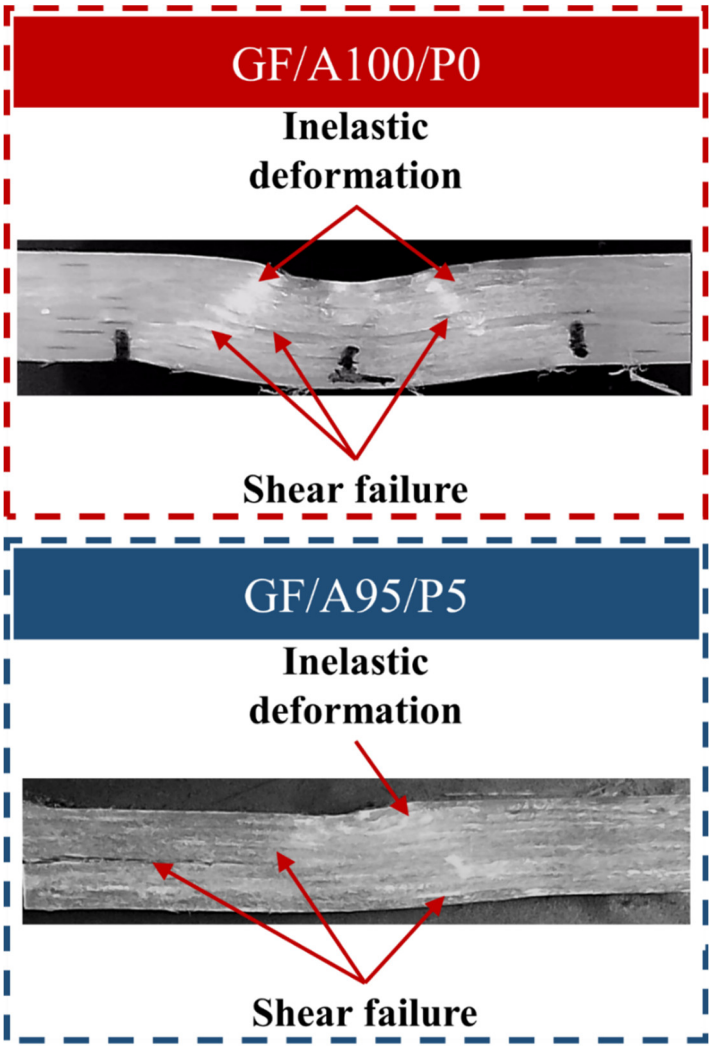


Figure 7-14. Representative macroscopic failure resulting from short beam shear loading of GF/A100/P0 and GF/A95/P5. Lay-up: $[0]_8$.

The damage accumulation and severity of delaminations were most likely the causes of the strain-softening observed in the GF/A95/P5 samples. Having established that both materials possessed comparable interfacial strengths, the prevalence of delaminations on the PPE-modified-matrix composite samples suggests lower delamination resistance, consistent with observations from Section 7.2.5 where further insights on the crack propagation behaviour of the PPE-modified acrylic composite are discussed.

7.2.8 Characterisation of interlaminar fracture toughness

DCB load-displacement curves for GF/A100/P0 and GF/A95/P5 samples are presented in Figure 7-15a and Figure 7-15b. Representative DCB load-displacement curves and obtained results are shown in Figure 7-15c; representative resistance curves (R-curves) are

shown in Figure 7-15d. As with the results presented in Section 5.2.5, $G_{IC\text{-}Init.}$ (onset of non-linearity) and $G_{IC\text{-}Prop.}$ are strain energies released during initiation and propagation, respectively using the modified beam theory approach (ASTM D5528).

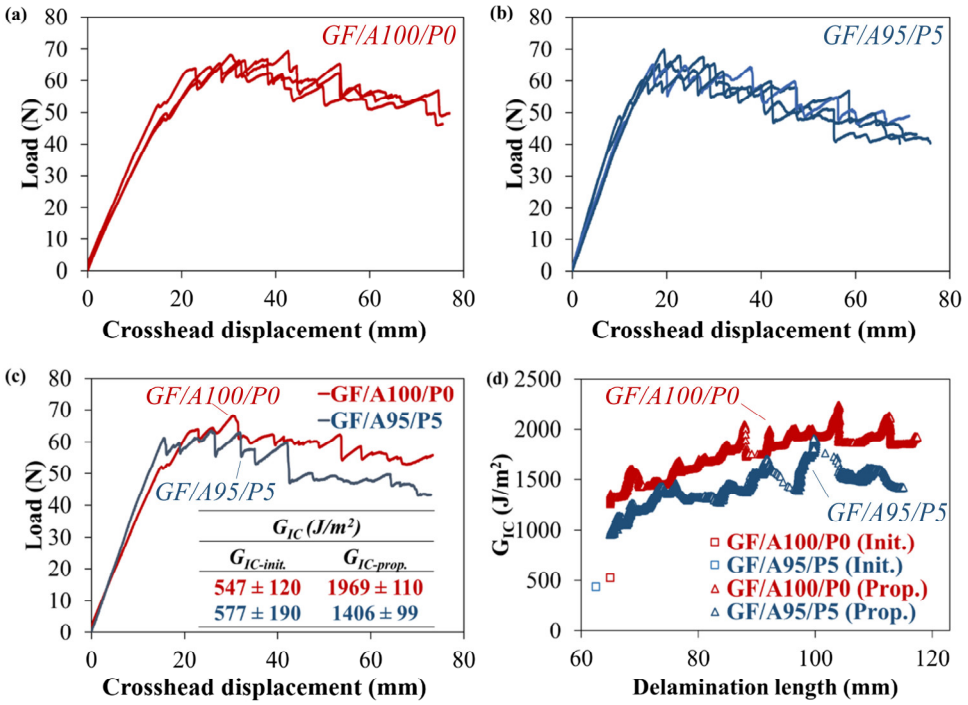


Figure 7-15. Load-displacement curves from double cantilever beam testing of (a) GF/A100/P0 and (b) GF/A95/P5, (c) representative load-displacement curves with an inset table of results, and (d) R-curves for the same materials. Lay-up: $[0]_8$.

Despite exhibiting superior longitudinal flexural stiffness, GF/A100/P0 samples had slightly lower crack opening stiffness up to initiation, which may be explained by the higher V_f in the GF/A95/P5 laminate. Both materials underwent stick-slip crack growth behaviour, which is believed to be partly due to the presence of 90°-fibres within the fabric.

As can be seen in the inset table of results (Figure 7-15c), matrix hybridisation confers a 5 % increase in initiation fracture toughness ($G_{IC\text{-}init.}$); however, propagation fracture toughness ($G_{IC\text{-}prop.}$) decreased by 29 %. The initiation fracture toughness of non-precracked composites is primarily influenced by the matrix toughness [34,35]. Moderate and lower cross-linking densities are believed to be favourable for superior crack initiation resistance due to enhanced post-yield deformation of the matrix resulting from strain

localisation [36]. Combined positive effects of intrinsic toughening and light cross-link density likely contribute to the GF/A95/P5 samples' superior initiation fracture toughness. This hypothesis is supported by the observation of relatively higher ductility in the PPE-modified acrylic composite in the preceding sections of this chapter and the hypothesis of a lightly cross-linked network.

Concerning the propagation fracture toughness, it is widely accepted that less ductile matrices exhibit better matrix toughness transfer for composite propagation fracture toughness because they favour more fibre-dominated, extrinsic toughening mechanisms. Conversely, more ductile materials are reported to exhibit more intrinsic toughening mechanisms, which are said to be evidenced in R-curve behaviour, where the absence of an increasing slope is indicative of a system with purely intrinsic mechanisms at play [37]. Interestingly, R-curves (Figure 7-15d) did not reveal discernibly distinct propagation behaviour between both materials. The slopes of the R-curves for both materials can be seen to increase with increasing crack length, indicating that the resistance to crack growth in both materials is highly dependent on the crack extension. Given the similarities in the R-curve characteristics of both materials, the aforementioned contributions of fibre-related extrinsic toughening mechanisms must be further explored. The in-situ test images shown in Figure 7-16 reveal different fibre bridging and fibre pull-out characteristics for both materials. It can be seen that the 90° tows within the GF/A100/P0 sample undergo debonding in response to the loading process and can be seen to traverse the delamination plane.

In contrast, no 90° tows were evident for the GF/A95/P5, suggesting that the enhanced interfacial adhesion in the hybrid matrix prevented debonding and likely resulted in crack growth within the matrix as opposed to the interface. Consequently, frictional dissipative phenomena such as fibre bridging and pull-out are likely to be more limited within this system. Similar observations were made by Pini [34] who reported more fibre bridging in unmodified acrylic-matrix composite due to inferior interfacial adhesion relative to its modified counterpart.

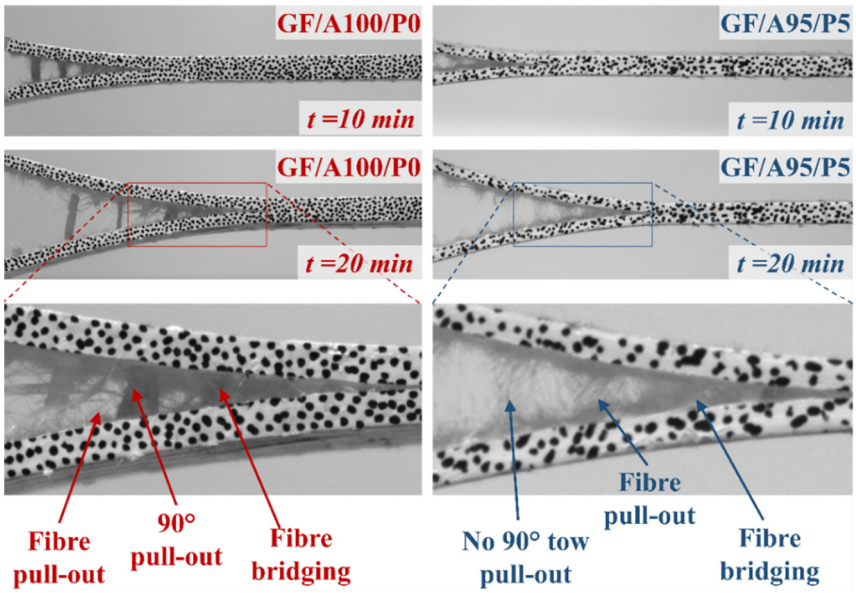


Figure 7-16. (a) In-situ test images obtained during double cantilever beam testing to show the crack-opening behaviour of GF/A100/P0 and GF/A95/P5. Laminate thicknesses for GF/A100/P0 and GF/A95/P5 are 3.8 mm and 3.3 mm, respectively. Lay-up: $[0]_8$.

7.2.8.1 Scanning electron microscopic inspection of fracture behaviour

Figure 7-17 (a)-(f) presents DCB fracture surfaces of GF/A100/P0 and GF/A95/P5 samples obtained using SEM. Both surfaces appear texturally coarse and dull, indicating comparable ductility on a microscopic scale. Although both materials also exhibit similarities in interfacial adhesion Figure C-12, more matrix coverage on the fibres within the GF/A95/P5 sample revealed enhanced interfacial adhesion due to hybridisation.

The GF/A95/P5 sample showed evidence of microcrack formation (Figure 7-17f and Figure 7-18a) and multiple crazing sites (Figure 7-18b), features that were not observed for GF/A100/P0. The microcracks appeared as long craze-like interpenetrating paths across the fracture surface; however, no coalescence was observed at their intersection points. Given that crazing is a dominant plastic deformation mechanism observed in amorphous TP matrices [38,39], these observations support the proposed factors contributing to enhanced $G_{IC\text{-}init.}$ in the GF/A95/P5 material.

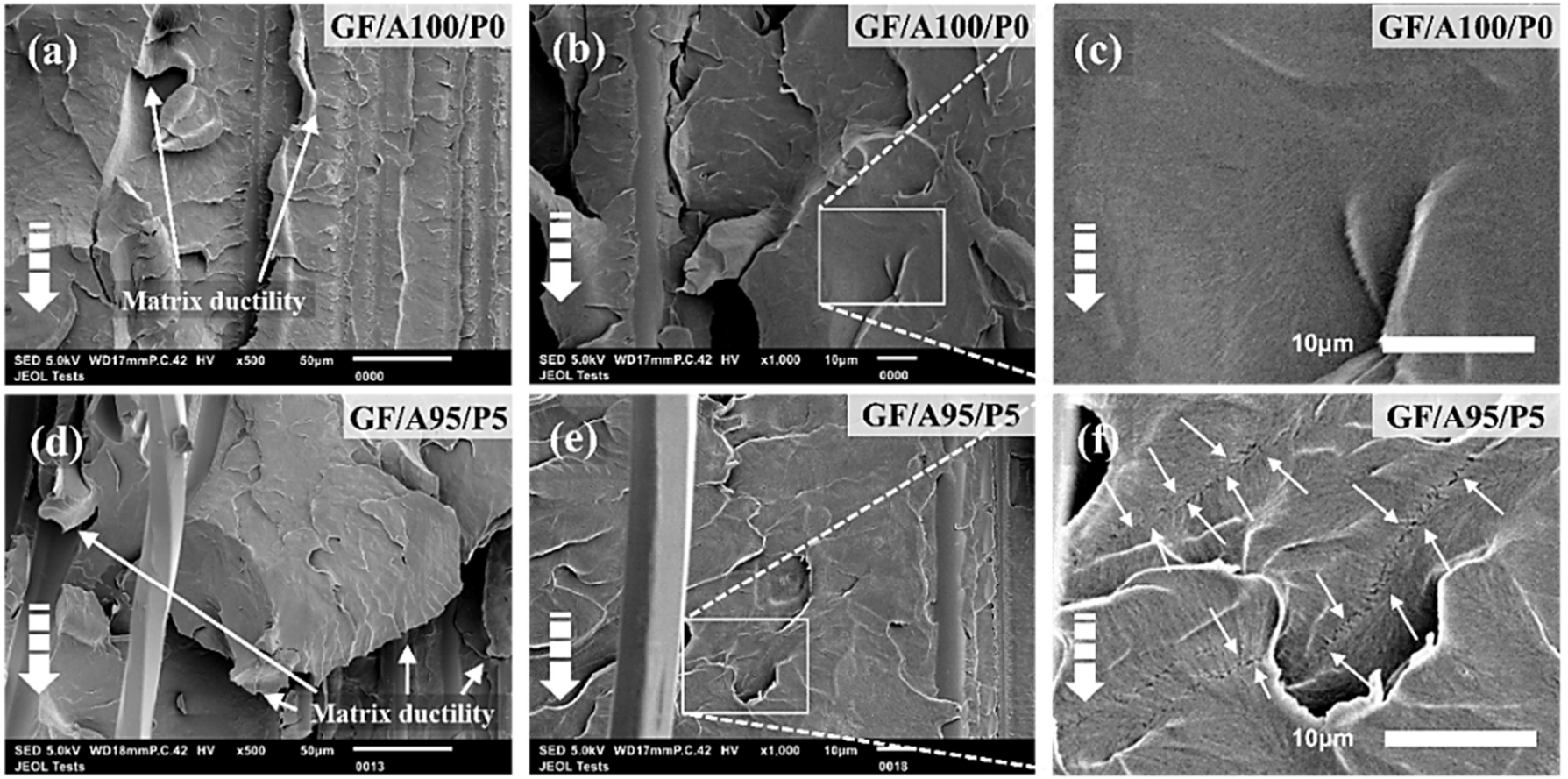


Figure 7-17. SEM micrographs showing mode-I fracture surfaces of (a), (b) & (c) GF/A100/P0 and (d)-(f) GF/A95/P5. The large broken arrows show the direction of crack propagation — arrows in (f), highlight paths of microcrack formation.

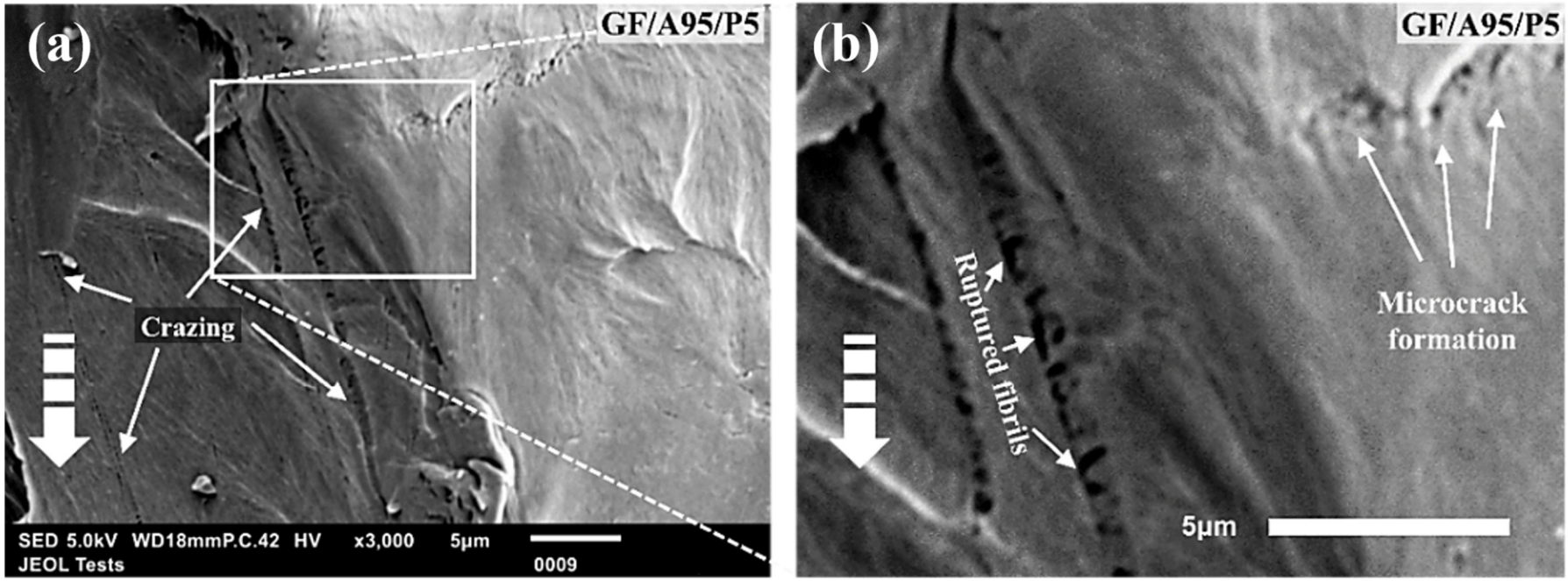


Figure 7-18. SEM micrographs showing fracture mechanisms in the GF/A95/P5 sample. Different stages of craze formation can be seen in (a), and ruptured craze fibrils and microcrack formation can be seen in (b). The large broken arrows show the direction of crack propagation.

Another factor, which may limit the extent of fibre bridging in the GF/A95/P5 material may be its plausibly higher matrix modulus due to contributions from cross-links and phenyl moieties. Zhang et al. [40] studied the effects of matrix modulus on failure modes in carbon fibre-reinforced matrices under shear stress and reported that low-modulus matrices were more likely to have interfacial failure than those with high moduli. The dominant mode reported for high-modulus matrices was matrix failure. The authors attributed this to the enhanced stress transfer efficiency of higher modulus matrices. Although glass fibres were used as reinforcements within this present work and this section is concerned with the materials' behaviour in response to mode-I interlaminar loading, the cited work can still provide valuable insights that may provide useful insight for the findings presented and discussed in this section. It has also been shown in this chapter (Section 7.2.2) that the PPE-modified acrylic matrix exhibited enhanced interfacial adhesion with the glass fibre reinforcement. Good interfacial adhesion has also been reported to limit the extent of fibre bridging, as it invariably limits shear-driven frictional sliding, a key energy absorption mechanism [41,42].

Therefore, it is likely that the lower propagation fracture toughness of the PPE-modified acrylic-matrix composite results from competitive intrinsic and extrinsic toughening mechanisms. The enhanced interfacial adhesion in the GF/A95/P5 material may have limited the extent of fibre bridging in the way of the crack tip, which invariably restricted effective crack-tip shielding. Established theory states that the total work involved in fracture comprises two characteristic regions or zones: the process zone and the plastic zone [43]. The plastic zone volume determines the plastic work within a material system and is considered an important factor in determining a material's fracture behaviour. It has been suggested in published literature [34,44] that adjacent plies can constrain the development of sufficiently large plastic zones in the matrix-rich interlaminar region of more ductile matrices. This is an important consideration for the PPE-modified acrylic-matrix composite under investigation in this work as the development of the plastic zone can be hindered by thinner interlaminar resin-rich zones [45]. Given the higher fibre volume fraction attained for the GF/A95/P5 laminate, which is a relatively thinner laminate than the GF/A100/P0 reference, it is likely that this factor led to limited development of the plastic zone. In Sections 7.2.4 and 7.2.6, it was observed that the

hybrid matrix exhibited behaviour consistent with intrinsic toughening mechanisms, which would typically be expected to translate to its macroscopic mode-I fracture behaviour. However, the poor toughness transfer (from intrinsic toughening mechanisms exhibited by the matrix to the propagation fracture toughness) is possibly attributed to the limited extent of crack-tip shielding (resulting from limited fibre bridging) and inadequate plastic zone development (thin interlaminar resin-rich layer). This is supported by the work of Pini [34]. Further insights are provided in Section 7.3, where these factors are discussed in a complementary manner with other observations provided in this chapter.

Domains are discernible across the fracture surface of the GF/A95/P5 sample (Feature 1, Figure 7-19 and Figure 7-20). Moreover, shear banding was also observed on the matrix surface (Feature 2, Figure 7-19).

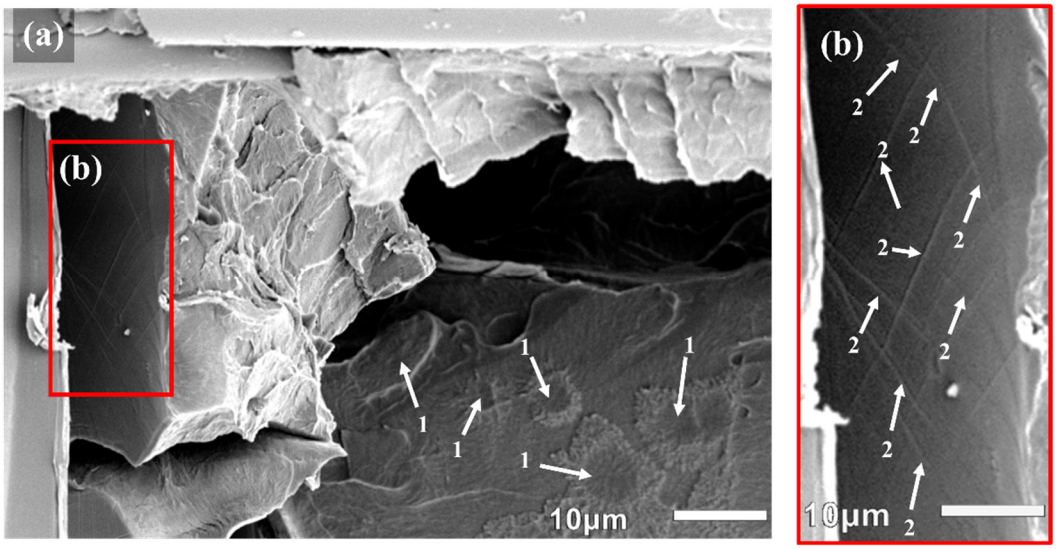


Figure 7-19. (a) SEM micrographs of GF/A95/P5 DCB fracture surface showing domains (Feature 1) and (b) shows evidence of shear banding (Feature 2) mechanism.

In addition to these features, evidence of the same craze-like microcrack formation observed in Figure 7-17f can be seen as Feature 2 in Figure 7-20. Similar parabolas to those observed on the fracture surface of the A100/P0 sample (Feature 1, Figure 6-22); however, the ones observed for GF/A95/P5 are larger and do not feature the characteristic voids associated with the A100/P0 parabolas. Instead, these parabolas comprise rigid obstacles, resembling domains (Feature 1, Figure 7-20) and are bounded

by drawn ribbons of the matrix (Feature 3, Figure 7-20). It is plausible that secondary cracks initiated at the domains, merging with the primary crack. This process appears to have occurred in succession, with arrest points between the domains. Given the ribbon-like drawing of the matrix, this process likely occurred as a slow fracture process, resulting in ductile fracture characteristics as opposed to brittle characteristics. Overall, this material exhibited pronounced ductility throughout, with highly drawn matrix deformation (Figure C-13).

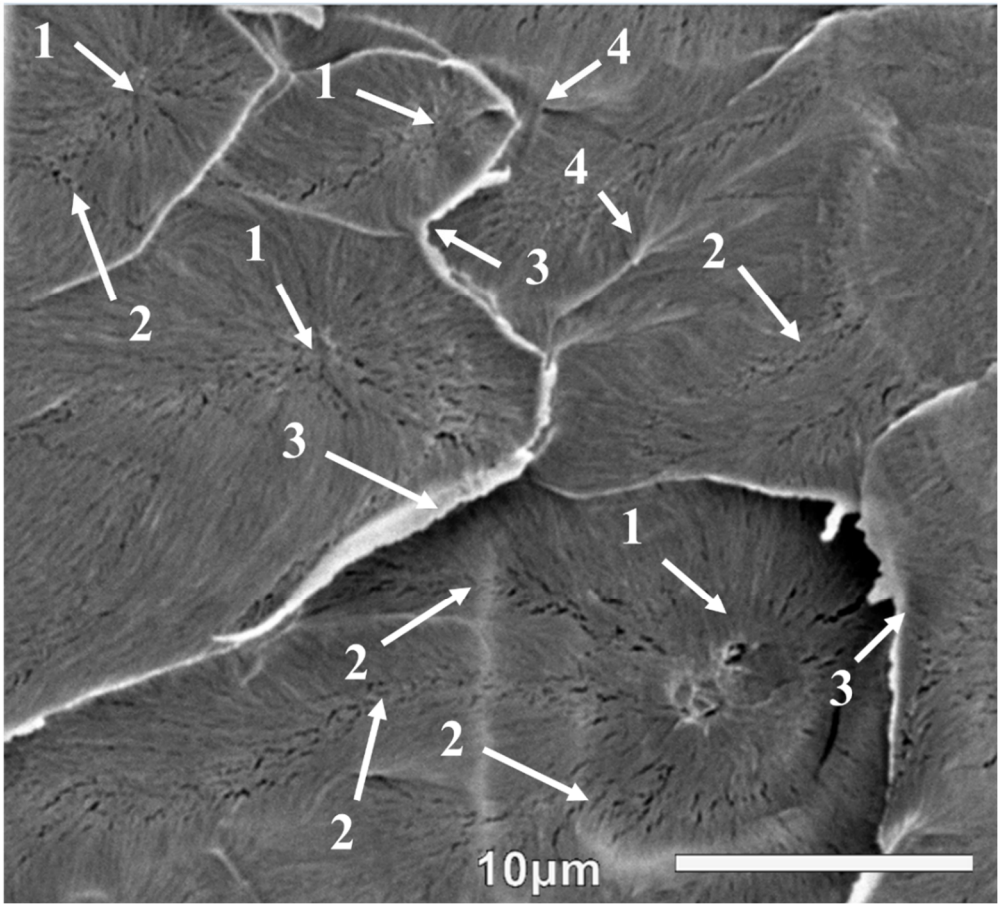


Figure 7-20. SEM micrograph showing GF/A95/P5 fracture surface; Features 1, 2, 3 and 4 are domains, craze-like microcracking, drawn matrix ribbons bounding parabolas and plastic flow of the matrix, respectively.

Given the observed fracture behaviour, it may be possible to explore further refinement of the microstructure to investigate the effects of domain size and distribution on the mode-I fracture propagation toughness. Effective control of the morphology of polymer blends is known to be beneficial for toughening [46]. Moreover, strategic tuning of the homopolymerisation of the PPE employed may be useful to control the inter-cross-link

and inter-entanglement molecular weight. Inter-entanglement molecular weight is known to influence the fracture and crazing behaviour in amorphous polymers [47].

7.2.9 Drop-weight impact response

Representative force-deflection curves and energy-time curves, together with mean values and standard deviations of ultimate deflection, peak load, and elastic and absorbed energies are presented in Figure 7-21. Due to the pronounced undulations in the force-deflection curves (Figure 7-21a and Figure 7-21b), which are likely frictional effects from the drop-weight tower [48], a precise evaluation of damage initiation cannot be performed on these results. However, given that across all samples, contact force increases nonlinearly up to the ultimate deflection value and decreases to zero during the unloading phase of the impact events, ultimate deflections and peak forces can be compared within the respective energy levels. As previously described in Chapter 5 (Section 5.2.7.1), the shape of the force-displacement curves (closed loops) are indicative of impact events with no penetration of perforation. Thus, no penetration or perforation is expected under the conditions employed for this study [49].

30-J impacts resulted in 6 % higher mean deflection in the GF/A95/P5 relative to the GF/A100/P0 material, and 50-J impacts resulted in 4 % higher mean deflection, respectively. Peak contact force was 5 % higher in the GF/A100/P0 for both impact energy levels, with respect to GF/A95/P5. This suggests a marginally higher post-damage initiation stiffness in the GF/A100/P0 coupons than those of the GF/A95/P5 material [50]. As such, this may highlight a more significant deterioration of the structural integrity of GF/A95/P5 at damage initiation. No discernible differences were observed in their sensitivities to energy level for these parameters. Increasing the impact energy to 50 J correspondingly increased the ultimate deflections by 23 % for GF/A100/P0 and 26 % for GF/A95/P5. Interestingly, the peak force increased by 35 % for both materials.

As with the materials discussed in Chapter 5 (Section 5.2.7.1), the absence of a massive load-drop and extended post-peak deformation signifies that no major damage development occurs in the materials considered in this chapter. Figure 7-21b and Figure 7-21d show a greater contribution of elastic responses to the conversion of kinetic energy for the GF/A100/P0 coupons. Elastic energies at 30 J and 50 J were 4 % and 7 % higher

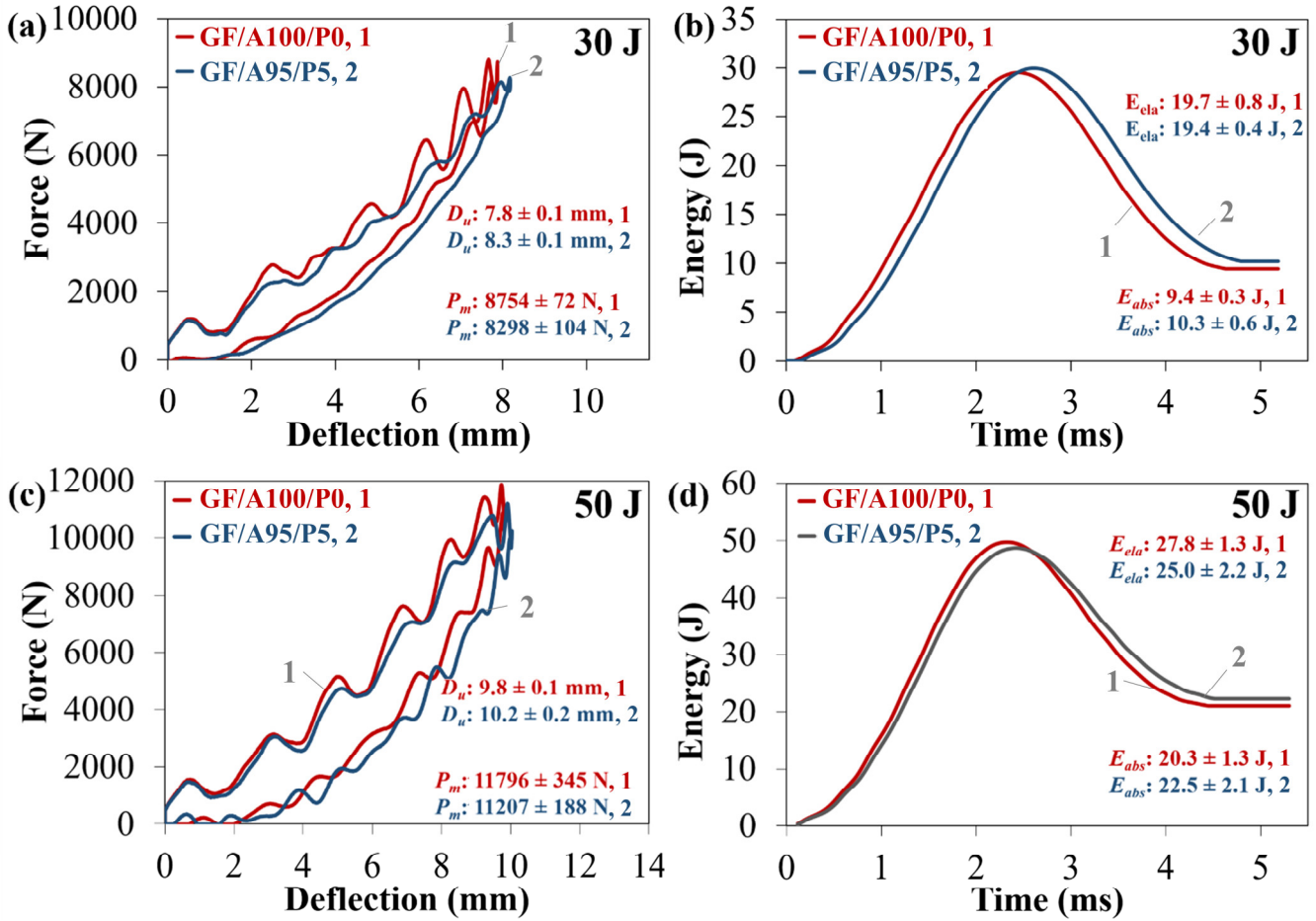


Figure 7-21. Representative force-displacement (a) &(c), and energy-time (b) & (d) curves for GF/A100/P0 and GF/A95/P5, following impacts at 30 J and 50 J, respectively. Lay-up: $[0/90/90/0]_S$.

in the GF/A100/P0 samples, with respect to the GF/A95/P5 coupons, respectively. Similarly, the GF/A95/P5 absorbed 10 % and 11 % higher energies during the 30 J and 50-J impact, respectively. Although this is possibly attributed to the intrinsic microstructural toughening mechanisms discussed in the preceding chapter, the contributions of macroscopic damage development to energy absorption within the system must not be ignored. The creation of damage and fracture surfaces in the form of mechanisms such as matrix cracking, fibre-matrix interfacial debonding, fibre failure and delamination accounts for a considerable extent of absorbed energy during drop-weight impact events; consequently, these results suggest a greater extent of damage likely occurred within the PPE-modified coupons (GF/A95/P5).

To evaluate damage states, back-lit images were obtained as previously described in Section 4.2 and as graphically represented in Figure 4-3. The imaged damage states resulting from the 30 J and 50-J impact events are presented in Figure 7-22 and Figure 7-23, respectively. These figures also include macroscopic images of the impact site (impact face and back face). As shown in Figure 7-22 and Figure 7-23, all samples present a near-rhomboidal shape of damage. Striker indentation can be seen clearly on the impact faces and extensive delamination on the back face of all samples at all energy levels. While fibre splitting was evident for the GF/A95/P5 samples at both energy levels, no fibre splitting is observed for the GF/A100/P0 samples at 30 J. However, 50-J impact events produced more severe impact face damage modes for the GF/A100/P0 samples, with extensive matrix cracking and tow splitting observed.

For more quantitative comparisons, damaged areas were evaluated as fractions of the coupon face areas. The damage area fractions shown in Figure 7-24a correlate with the observations for the absorbed energies of these materials. 30-J impacts resulted in 10 % higher damaged area fraction in the GF/A95/P5 coupons, with respect to those of the GF/A100/P0 material. For 50-J impacts, 22 % higher damaged area fractions were measured on average. Figure 7-24b shows the ratio of absorbed energy to elastic energy, the damage index term previously introduced in Section 5.2.7. A low damage index would suggest greater elastic contributions, whereas, higher values indicate absorption-dominated kinetic energy conversion.

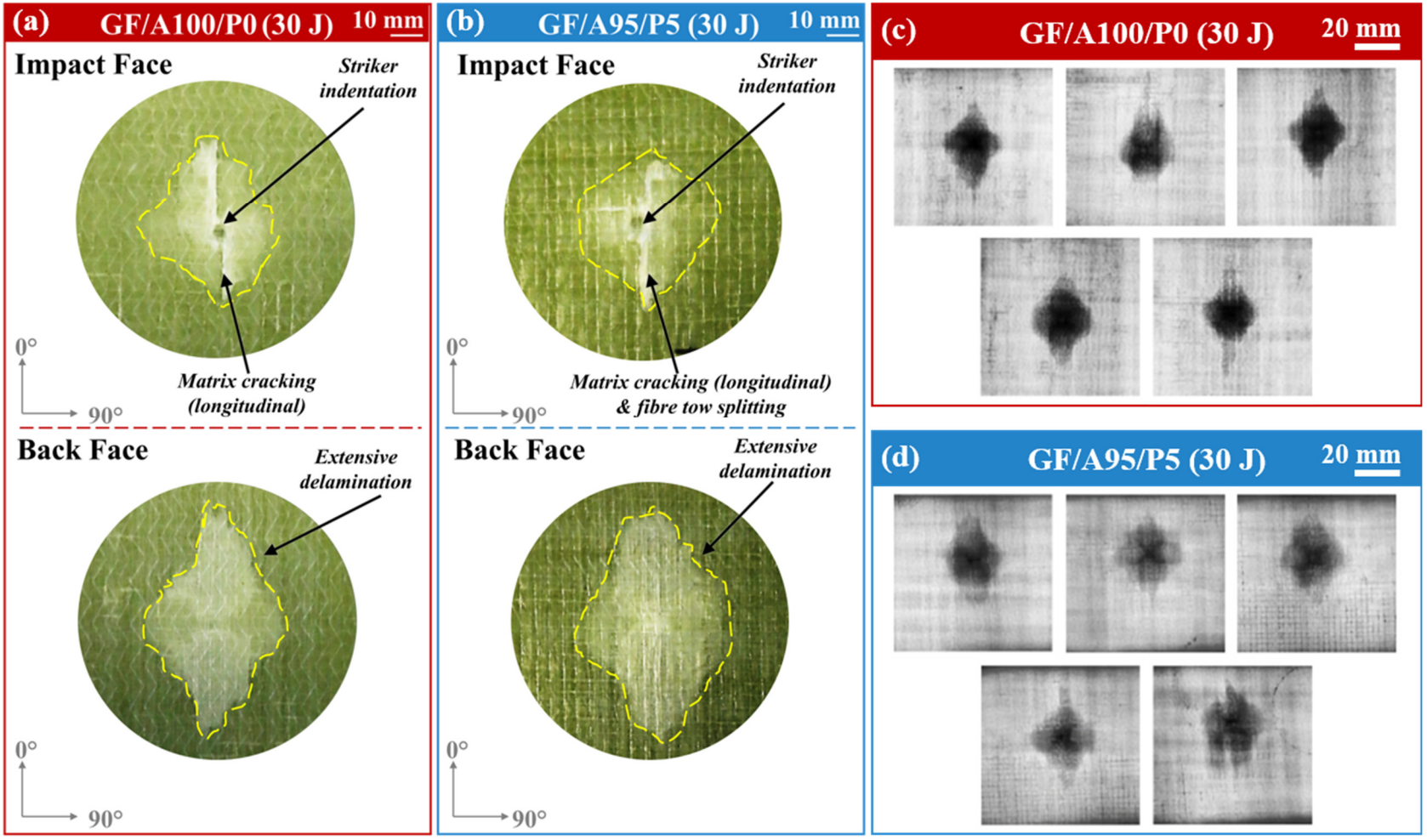


Figure 7-22. High-contrast, back-lit images showing the damage states following 30-J impact events on GF/A100/P0 and GF/A95/P5 coupons.

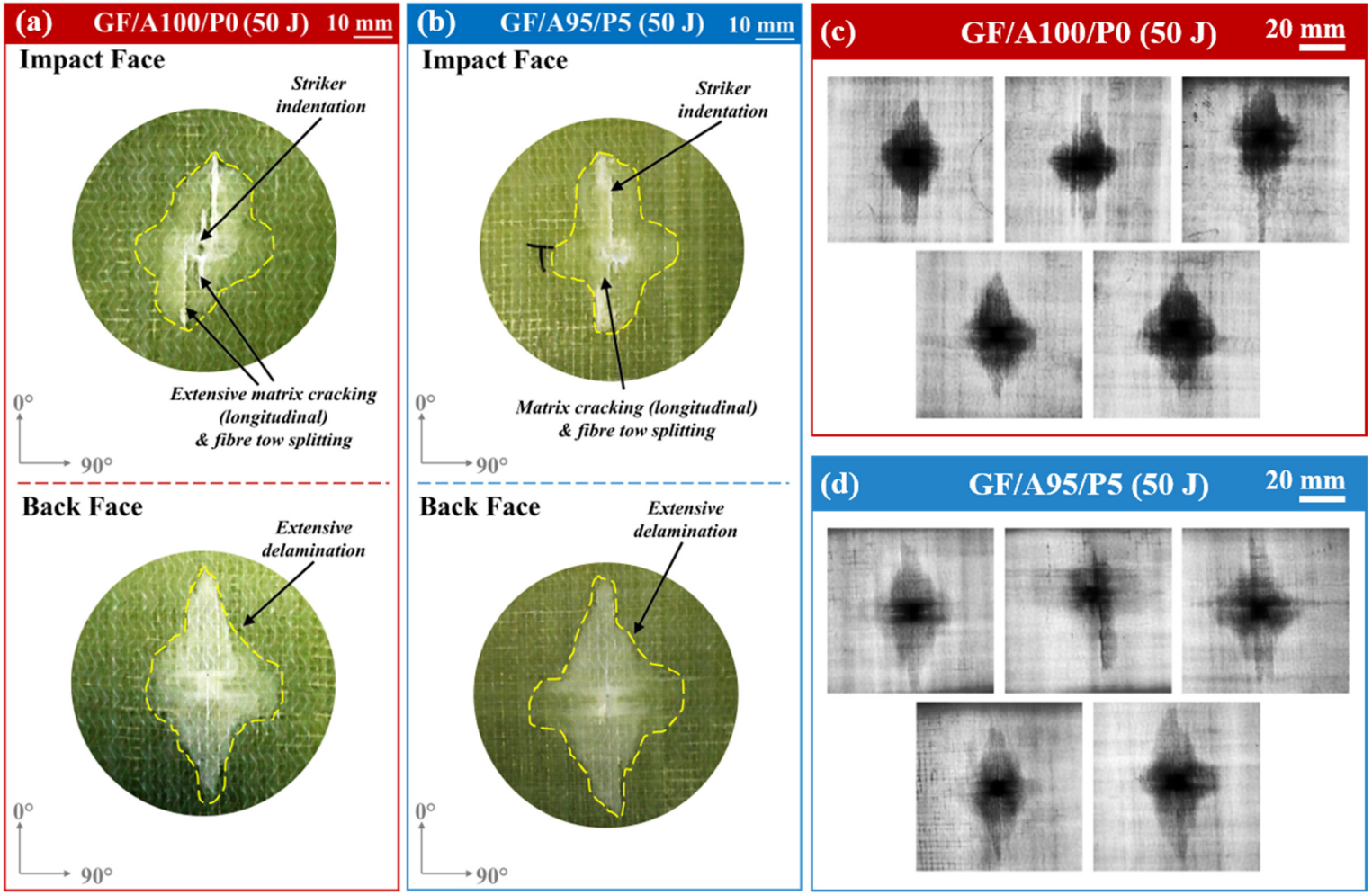


Figure 7-23. High-contrast, back-lit images showing the damage states following 50-J impact events on GF/A100/P0 and GF/A95/P5 coupons.

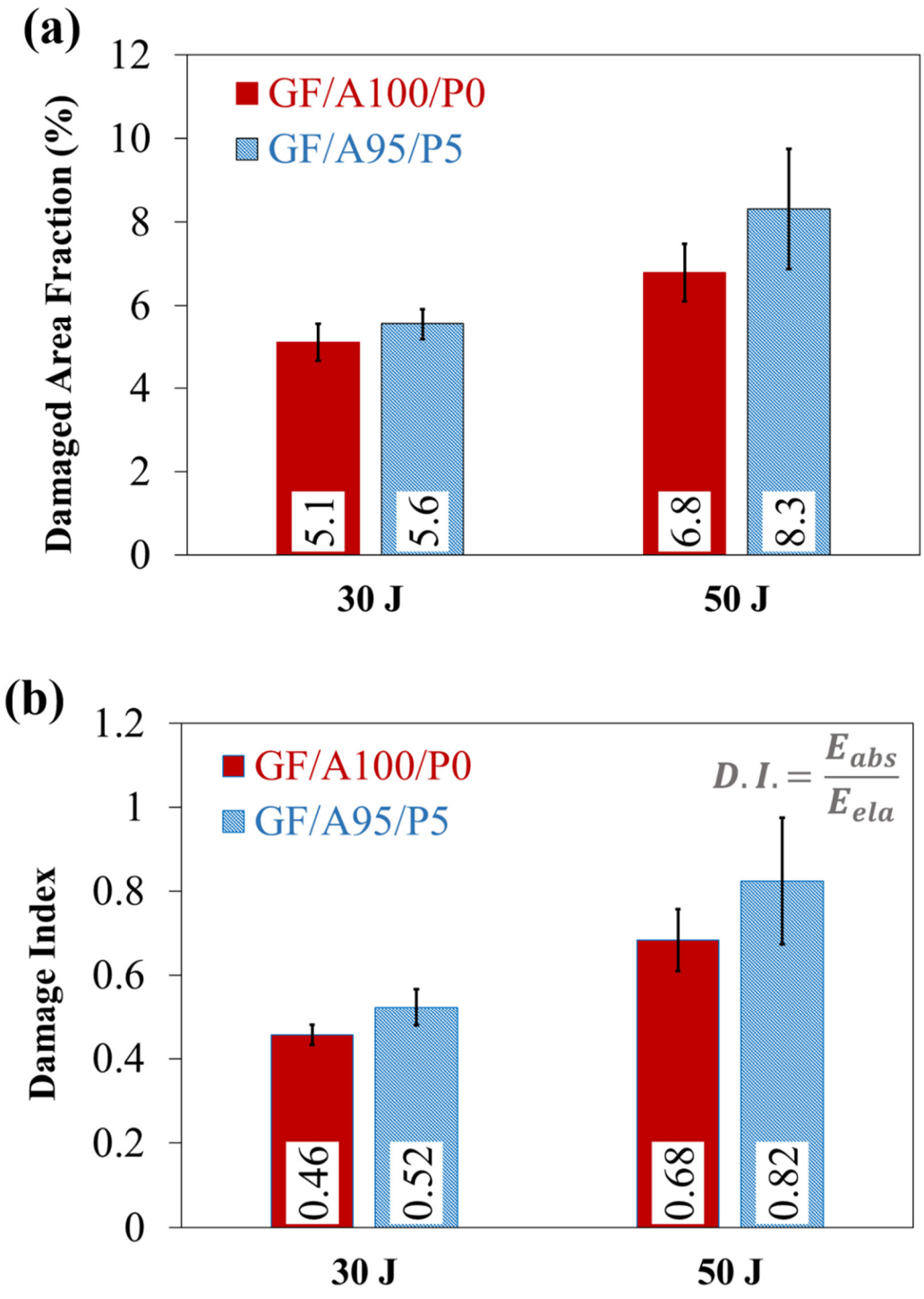


Figure 7-24. (a) Damaged area fraction and (b) damage index as functions of impact energy for GF/A100/P0 and GF/A95/P5. Lay-up: $[0/90/90/0]_S$.

It can be seen that for both 30 J and 50-J impacts, GF/A100/P0 coupons favour more of an elastic response, with 13 % and 21 % lower damage indices. Thus, the higher deflections exhibited by the GF/A95/P5 were most likely due to inelastic deformation and damage development processes; the latter may have inadvertently lowered the contact stiffness of the coupons.

In terms of their sensitivity to impact energy level, increasing the energy to 50 J resulted in 33 % and 48 % increases in GF/A100/P0 for damaged area fraction and damage index, and 48 % and 58 % increases for the same in GF/A95/P5, respectively. Thus, it can be seen that the hybrid matrix exhibits a greater sensitivity to the impact energy levels under the conditions of these investigations. This may be attributed to increased steric hindrances posed by the relative bulky phenyl moieties and restricted (or trapped) grafted chains. At higher energies, it is expected that the dissipative ability of the matrix is governed by relaxation times; i.e., the time taken to rearrange the polymer chains for elastic energy storage during striker contact. Also, increasing the impact energy implies that additional energy is available to initiate and propagate damage.

Given that the damage initiation threshold of the GF/A95/P5 material was exceeded even at 30 J, its relative superiority in initiation fracture toughness is inconsequential at even higher energy levels. Rather, its relative inferiority in propagation fracture toughness (with respect to the unmodified acrylic-matrix composite) is expected to amplify differences in sensitivity to increasing energy levels. Moreover, the complex interplay of chain slipping and bond breaking mechanisms associated with shear-induced deformation may also play contributory roles in the observed behaviour [51].

As previously discussed in Section 5.2.7.1, an important consideration in assessing the drop-weight impact behaviour of laminated composites is their penetration and perforation thresholds. As shown in Figure 7-25, both materials significantly lie below the equal energy line for 30 J and 50-J impacts. These results indicate that the energy levels used in this study are not theoretically expected to produce penetration or perforation damage states in both materials. It is worth noting that the unmodified acrylic-matrix composite falls marginally lower than its PPE-modified counterpart. This is particularly

evident at 50 J and suggests that the GF/A95/P5 material may tend towards penetration and perforation faster than GF/A100/P0 at higher energy levels.

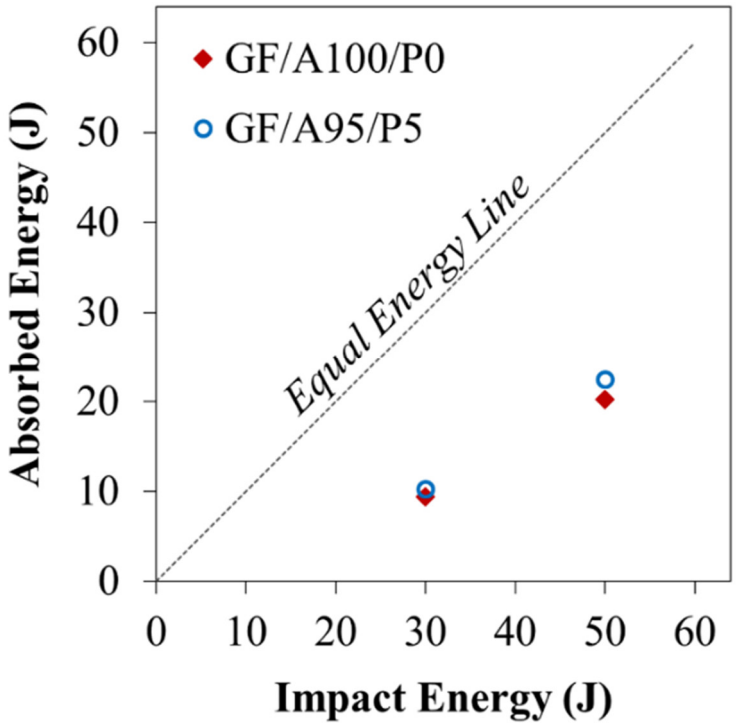


Figure 7-25. Energy profile diagram for GF/A100/P0 and GF/A95/P5 for drop-weight impacts performed at 30 J and 50 J. Lay-up: $[0/90/90/0]_S$.

Overall, these findings show that hybridisation did not enhance the impact damage resistance of the PPE-modified acrylic-matrix composite. An increase in sensitivity to increasing energy levels was also conferred as a result of hybridisation. These findings are not altogether unexpected in light of the findings concerning mode-I interlaminar fracture toughness for propagation (Section 7.2.8). However, the evidence of enhanced toughness observed from the areas bounded under curves shown in Sections 7.2.4 to 7.2.7 implies that the macroscopic fracture behaviour exhibited by the GF/A95/P5 composite is possibly linked to the transitional nature of the matrix. It has been shown to exhibit both highly ductile and brittle behaviour due to its plausibly heterogeneous morphology. Of course, the contributory factors proposed in Section 7.2.8 are expected to still hold for impact response, given that impact resistance is governed by the energy dissipative capacity of a material, both for the initiation of damage and propagation of same. Thus, the limited delamination propagation resistance [52] of GF/A95/P5 is likely to play a

crucial role in the observed behaviour. Further insights into the microstructure-property relations underpinning the observations in these sections are discussed in Section 7.3.

7.2.9.1 Impact tolerance

The post-impact residual properties of these materials are presented as was previously done in Section 5.2.7.2. From the flexural stress-strain curves shown in Figure 7-26, samples tested for both GF/A100/P0 and GF/A95/P5 exhibit similar evolution of stress with strain. Some scatter can be seen in the ultimate stress values of the GF/A95/P5 samples; however, key trends emerge that are worthy of discussion. Each curve shows a short linear-elastic region, followed by mild inelasticity up to ultimate failure. Interestingly, both materials did not show any discernible onset of damage until the ultimate flexural stress was reached. In all cases, mild plastic deformation can be seen leading up to the ultimate failure. Moreover, the GF/A95/P5 samples also appeared to possess marginally higher residual stiffness.

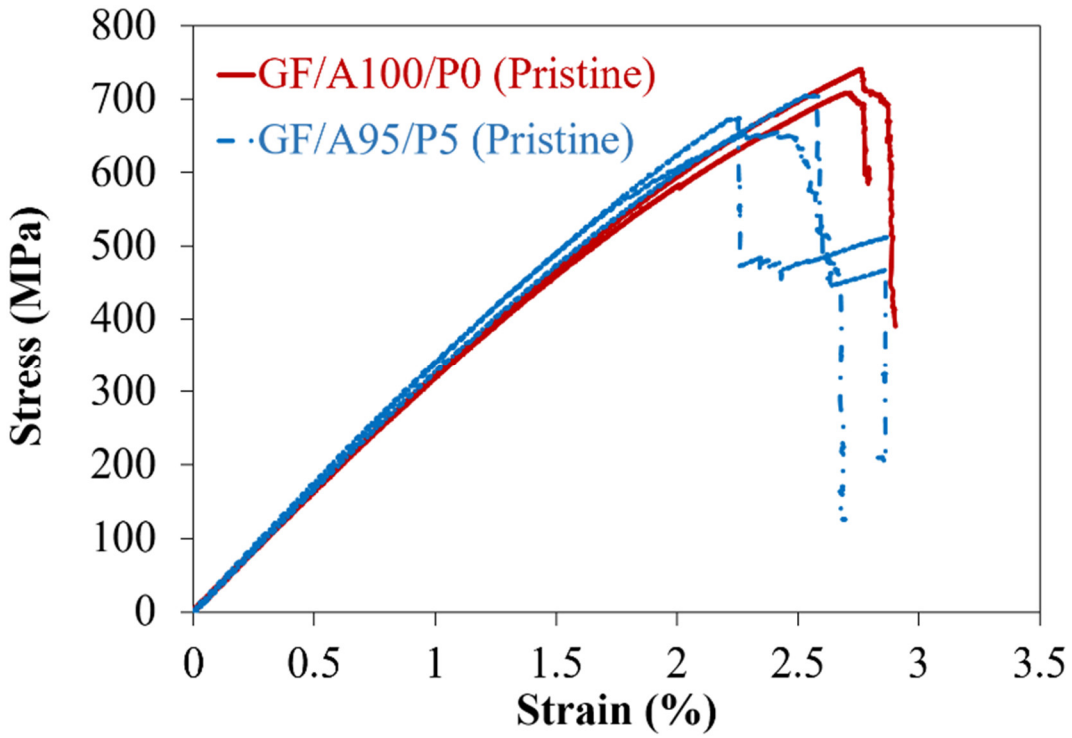


Figure 7-26. Flexural stress-strain curves for pristine (undamaged), bidirectional GF/A100/P0 and GF/A95/P5 samples. Lay-up: $[0/90/90/0]_S$.

The flexural stress-strain curves for GF/A100/P0 and GF/A95/P5 following impacts at 30 J are shown in Figure 7-27. As with the results in Figure 7-26, some scatter can be seen

in the ultimate stress values of these samples; however, discernible trends are discussed. While the GF/A95/P5 samples can be seen to exhibit marginally higher stiffness, they fail at lower stresses relative to GF/A100/P0 samples.

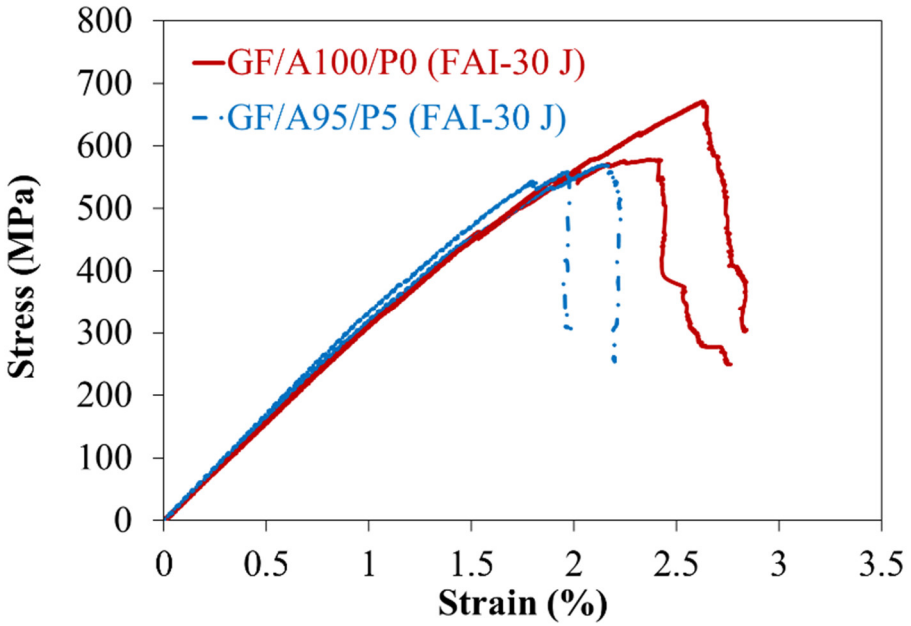


Figure 7-27. Flexural stress-strain curves for 30-J impact-damaged bidirectional GF/A100/P0 and GF/A95/P5 samples. Lay-up: $[0/90/90/0]_S$.

Although both materials show linear-elastic evolution of stress and inelasticity in the zone before ultimate failure stress, the GF/A100/P0 samples exhibited earlier damage onset after ~1.5 % strain. Moreover, while pristine GF/A95/P5 showed evidence of high residual stiffness in the post-peak zone, only GF/A100/P0 samples presented this characteristic for 30-J impact-damaged samples.

Similar observations were made for 50-J impact-damaged samples; however, GF/A100/P0 samples exhibited even earlier onsets of damage at ~0.8 % strain. Moreover, both materials' post-failure behaviour revealed more brittle behaviour in the PPE-modified acrylic-matrix composite samples. Load-drops in the GF/A100/P0 are indicative of post-peak damage extension. The more abrupt failure of GF/A95/P5 samples may confirm that after impact damage, cross-links play more of a dominant role

in deformation behaviour than the entangled linear species within the matrix. Of course, these results may also imply better retention of interfacial adhesion in the GF/A95/P5.

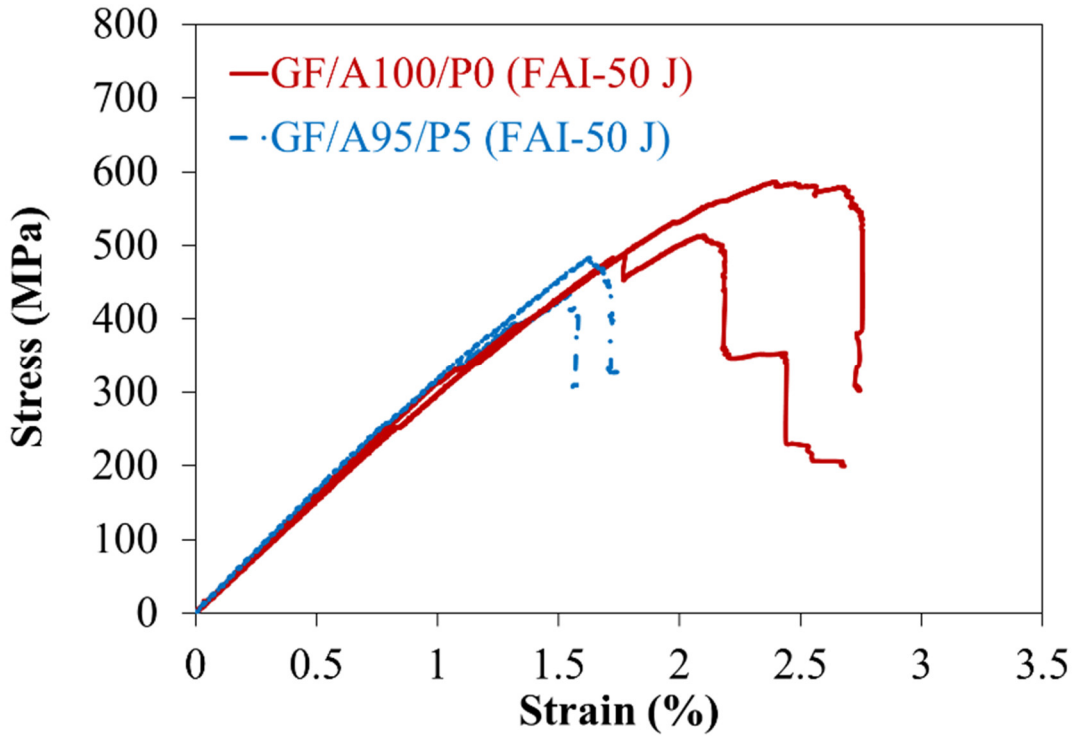


Figure 7-28. Flexural stress-strain curves for 50-J impact-damaged bidirectional GF/A100/P0 and GF/A95/P5 samples. Lay-up: $[0/90/90/0]_S$.

For all damage states, larger areas are bounded by the GF/A100/P0 curves, which indicate higher post-impact toughness with respect to the PPE-modified material. Interestingly, the reverse was the case for quasi-static loading conditions in preceding sections, where higher areas were typically bound under curves for the GF/A95/P5 material. However, this may reflect differences between quasi-unidirectional and bidirectional glass fibre-reinforced acrylic and PPE-modified acrylic composites. More importantly, geometry effects resulting from the use of a non-standard sample designation and test method may manifest in this way. As previously discussed, a more considerable extent of frictional energy dissipation is likely within the unmodified composite material. The use of bidirectional NCF as reinforcement in the materials within this section may provide frictional variations. Moreover, having lower propagation fracture toughness than the GF/A100/P0 material, the GF/A95/P5 hybrid-matrix composite is expected to

exhibit poorer resistance to damage extension. Thus, these results are possibly attributed to the differences in propagation fracture toughness.

For a more quantitative comparison of the results, post-impact flexural strengths and moduli are compared from Figure 7-29 and Figure 7-30, respectively. Beginning with residual strengths, as expected, increasing the impact energy reduces the residual strength of the materials. It is also important to note that the gap in residual strength for GF/A100/P0 and GF/A95/P5 widens progressively with increasing impact energy. As can be seen in Figure 7-29, the strengths of GF/A95/P5 samples are 6 %, 10 % and 17 % lower than those of pristine, 30-J impact-damaged and 50-J impact-damaged GF/A100/P0, respectively. Moreover, GF/A95/P5 samples appeared to have a greater extent of impact-damage related reduction in strength relative to the pristine strength. Its 30 J and 50-J impact-damaged coupons possessed 17 % and 32 % lower strengths than its pristine strength, respectively. Only 14 % and 24 % reductions occurred for GF/A100/P0.

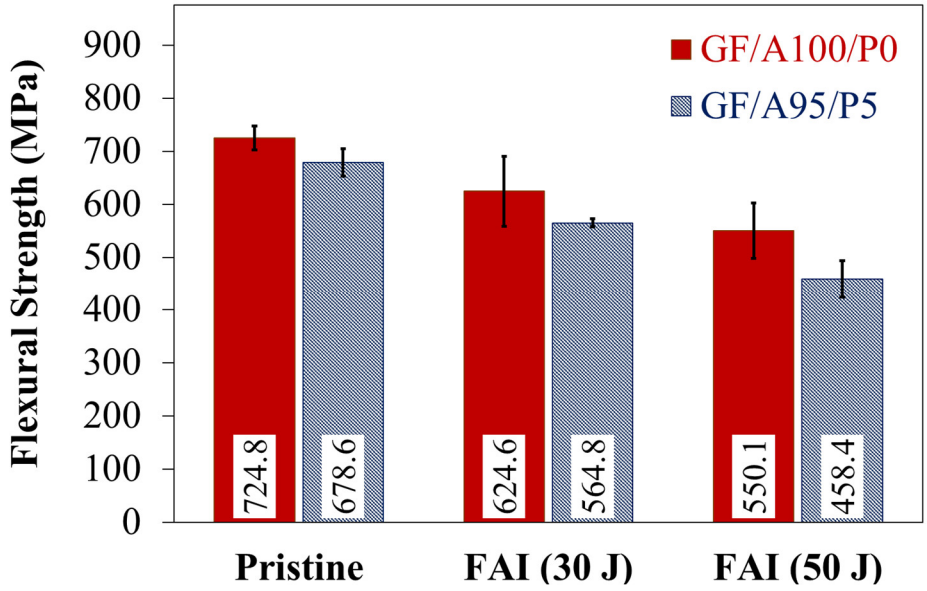


Figure 7-29. Post-impact flexural strength as a function of impact damage states for GF/A100/P0 and GF/A95/P5. Lay-up: $[0/90/90/0]_S$.

Conversely, flexural modulus appeared to be higher in GF/A95/P5 samples across all damage conditions, as shown in Figure 7-30. It exhibited 4 %, 7 % and 5 % higher modulus for pristine, 30 J and 50-J impact-damaged conditions relative to GF/A100/P0. Both materials did not exhibit discernible differences in terms of damage-induced

reductions in flexural modulus relative to the pristine condition. With the exception of the 30-J impact-damaged state of GF/A95/P5, for which only a 2 % reduction was recorded, all other cases showed a 5 % reduction. This may be evidence of the damage states within the impact-damaged coupons for both materials as damage mechanisms involving gross order delaminations, and fibre fractures are most likely to result in severe losses in modulus with respect to pristine modulus [53]. Thus, it is likely that much of the impact energies absorbed by both materials were used to create interfacial- and matrix-related damage. From the observations discussed on the post-peak failure behaviour of both materials, GF/A95/P5 samples appear to exhibit better retention of interfacial adhesion, with more abrupt failure behaviour. Moreover, residual flexural modulus may be less sensitive to damage size than residual strength [54].

However, it is worth considering that the GF/A95/P5 had a fibre volume fraction of 57 %, compared to that of the GF/A100/P0 (49.5 %). However, given the bidirectional orientation of the reinforcement system, it is not possible to conclusively remark on the sole contribution of fibres. Thus, it is highly likely that the damage states induced at 30 J and 50 J are significantly below the threshold of sensitivity for flexural modulus.

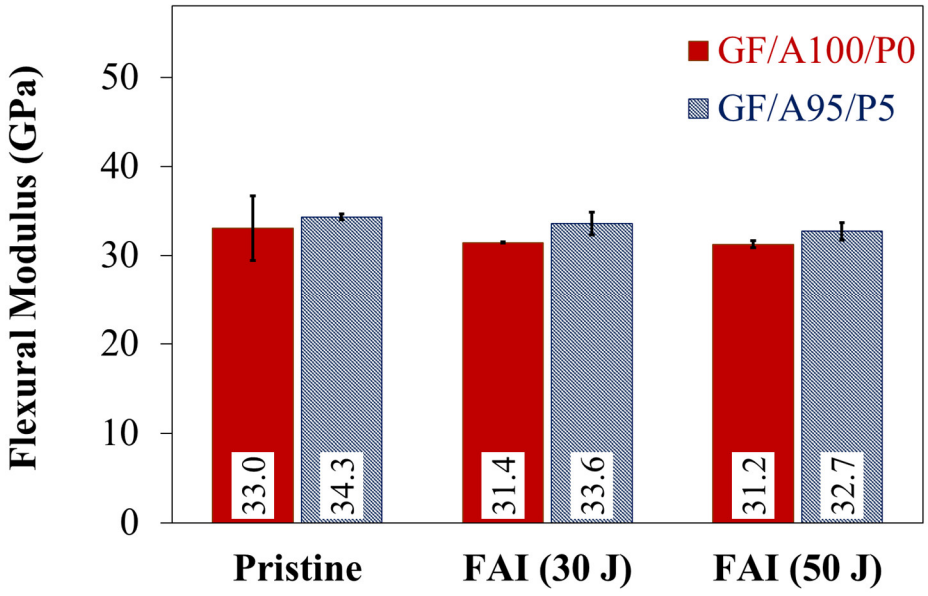
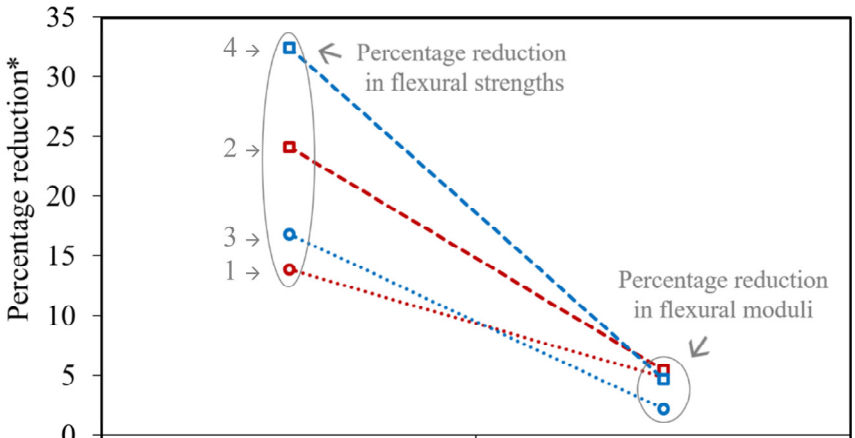


Figure 7-30. Post-impact flexural modulus as a function of impact damage states for GF/A100/P0 and GF/A95/P5. Lay-up: $[0/90/90/0]_S$.

Overall, the impact events likely produce considerably more transverse matrix cracks within the GF/A95/P5 samples, which under flexural loading may give way to

catastrophic failure by delamination initiation by coalescence of cracks and growth of existing delamination from the impact events. Finally, a summary of the residual properties is presented in Figure 7-31.



		% reduction in strength	% reduction in modulus
1 →	GF/acrylic (30 J)	14	5
2 →	GF/acrylic (50 J)	24	5
3 →	GF/A95/P5 (30 J)	17	2
4 →	GF/A95/P5 (50 J)	32	5

Figure 7-31. Residual post-impact properties as functions of matrix type and impact energy. *Percentage reductions are FAI strengths and moduli normalised with respect to corresponding nominal values. Lay-up: $[0/90/90/0]_S$.

Overall, both materials show expected reductions in post-impact strength and stiffness (marginal) with increasing impact damage area as the presence of larger damage would constitute greater stress concentrations at the interface between the damaged and undamaged regions of coupons and localised buckling of the damage-induced sublaminates.

From these results, it is clear that PPE-hybridisation does not result in enhanced impact damage tolerance under the conditions of this present study. Comparative propagation fracture toughness evaluations of the GF/A100/P0 and GF/A95/P5 materials revealed lower resistance to the extension of damage after initiation. Consequently, the PPE-modified acrylic composite likely underwent rapid damage development, culminating in abrupt failure. Interestingly, increments in damage area did not appear to influence the post-impact modulus. However, it is worth noting that flexural strength is more sensitive to more localised damage than flexural modulus [54].

7.3 Complementary summary of observations

In light of the intrinsic matrix toughening mechanisms identified for the unreinforced A95/P5 matrix, these observations highlight the contributions of microstructural fracture characteristics, which must not be ignored. Based on the assumption of the existence of entangled grafted acrylic/PPE and linear acrylic polymer chains within a lightly cross-linked network, the resultant macroscopic failure behaviour is likely a function of their relative contributions. Delamination initiation is thought to be associated with mode-I fracture behaviour, whereas delamination growth is believed to be influenced by the interlaminar longitudinal shear, transverse in-plane and interlaminar transverse shear stresses within the material system [55]. Thus, further exploration of the effects of fibres, fibre-matrix interface, and the intrinsic toughening mechanisms on macroscopic failure on the material response to these stress states may prove insightful.

When out-of-plane tensile stresses act on the hybrid-matrix composite, the resistance to failure initiation is likely governed by the complementary contributions of the cross-linked network and grafted chains within the proposed semi-IPN architecture. The ability of the matrix to dissipate energy and relieve stress without catastrophic fracture relies on the synergistic deformations of these integrated chains. The effects of linear homopolymeric acrylic are not explored in detail here as they are expected to be similar to those within the unmodified acrylic matrix. However, mutual sliding interactions with the grafted chains must be taken into account. The network and grafted acrylic/PPE reacted products are likely to resist the initiation of a crack under the applied out-of-plane tensile stress. The primary bonds in the networks must be able to withstand the applied stresses, and the network modulus must be stiff enough to confer localised rigidity and function in a load-bearing capacity.

Similarly, the grafted acrylic/PPE, which are assumed to be entangled and to interpenetrate the network must possess sufficiently high degrees of entanglement and free volume to facilitate the disentanglement phenomenon. Disentanglement, in this instance, can serve as a favourable dissipative mechanism [56]. Thus, the relative ratio of cross-linked-to-grafted interactions is essential to the resistance to fracture initiation. This

is strongly supported by hypotheses in published literature [56–58], where very similar architectures have been studied, albeit in unreinforced polymers.

7.4 Chapter conclusions

In this chapter, an array of characterisation techniques have been employed to assess the effects of incorporating PPE as a higher performance thermoplastic modifier within the lower-performance liquid thermoplastic acrylic resin. Glass fibre-reinforced laminates were produced by room temperature liquid resin infusion using an acrylic matrix and an acrylic-PPE matrix with 5 wt. % PPE loading. The following are observations from the chemical, thermomechanical and mechanical comparative characterisation of these materials:

- PPE hybridisation conferred enhanced solvent resistance in acetone. Following 60-minute and 72-hour exposures, the GF/A95/P5 samples lost 0 % and 2 % of their original masses, compared to 10 % and 28 % for GF/A100/P0, respectively. Note: the glass fibres accounted for a substantial portion of the residual masses.

- PPE-modification of the acrylic matrix in GF/A95/P5 resulted in a 50 % reduction of tan delta peak height. Mild peak splitting was also evident, with two discrete T_g values: ~106°C and 120°C. The second unique T_g suggest the presence of random/graft copolymers, cross-linked polymer, or a combination, likely coexisting within a semi-interpenetrating polymer network structure.

- TGA results also revealed a positive effect of PPE modification of the acrylic matrix. Enhanced thermal stability was observed in the GF/A95/P5 composite, evidenced by onset retardation and residual mass compared to the GF/A100/P0 material.

- The incorporation of PPE into the matrix system also enhanced ductility in the hybrid-matrix composite relative to the unmodified-matrix composite: failure strains increased under transverse tension (+58 %), transverse flexure (+24 %) and longitudinal flexure (+18 %).

- Longitudinal flexural strengths and moduli for GF/A100/P0 and GF/A95/P5 were normalised to 50 % V_f due to the different laminate volume fractions achieved. Normalisation revealed 20 % and 23 % reductions in strength and modulus, respectively due to PPE-modification of the acrylic-matrix composite. These results highlight the possible deleterious effects of higher V_f on performance, which warrant further exploration.

- It was observed that the GF/A95/P5 composite exhibited improved composite transverse flexural strength (+15 %) and modulus (+18 %) relative to GF/A100/P0, which suggest enhancements in matrix strength, modulus and interfacial adhesion.

- A 5 % increase was observed in the initiation fracture toughness of the GF/A95/P5 material with respect to the GF/A100/P0 reference material. This was possibly due to the effects of a multiple-crazing mechanism in the hybrid matrix system. However, its propagation fracture toughness was 29 % lower than that of the GF/A100/P0 material. This may be associated with diminished contributions from fibre bridging and possibly an inadequate thickness of the inter-ply matrix-rich region. The former is known to be an essential dissipative mechanism, and the latter is a prerequisite for plastic zone development, which controls the extent of plastic deformation at the crack tip.

Chapter references

[1] Fox TG. Influence of diluent and of copolymer composition on the glass temperature of a polymer system. Bull Am Phys Soc 1956;1:123-undefined.

[2] Karabanova L V, Boiteux G, Seytre G, Stevenson I, Lloyd AW, Mikhalovsky S V, et al. Phase separation in the polyurethane/ poly(2-hydroxyethyl methacrylate) semi-interpenetrating polymer networks synthesized by different ways. Polym Eng Sci 2008. https://doi.org/10.1002/pen.20965.

[3] Devotta I, Badiger M V, Rajamohanan PR, Ganapathy S, Mashelkar RA. Unusual retardation and enhancement in polymer dissolution: role of disengagement dynamics. Chem Eng Sci 1995;50:2557–69.

[4] Miller-Chou BA, Koenig JL. A review of polymer dissolution. Prog Polym Sci 2003;28:1223–70. https://doi.org/10.1016/S0079-6700(03)00045-5.

[5] Andrzejewska E. Free-radical photopolymerization of multifunctional monomers. Three-Dimensional Microfabr. Using Two-phot. Polym., 2019. https://doi.org/10.1016/B978-0-12-817827-0.00002-3.

[6] Vallittu PK. Oxygen inhibition of autopolymerization of polymethylmethacrylate-glass fibre composite. J Mater Sci Mater Med 1997. https://doi.org/10.1023/A:1018578210453.

[7] Alizadeh N, Barde M, Minkler M, Celestine AD, Agrawal V, Beckingham B, et al. High-fracture-toughness acrylic–polyurethane-based graft-interpenetrating polymer networks for transparent applications. Polym Int 2020. https://doi.org/10.1002/pi.6149.

[8] SABIC. NORYL™ SA9000 resin solubility guide 2019. https://www.sabic.com/en/products/documents/sabic-noryl-sa9000-solvent-guide/en.

[9] Fujiyabu T, Yoshikawa Y, Chung U, Sakai T. Structure-property relationship of a model network containing solvent. Sci Technol Adv Mater 2019.

https://doi.org/10.1080/14686996.2019.1618685.

[10] Hawke LGD, Ahmadi M, Goldansaz H, van Ruymbeke E. Viscoelastic properties of linear associating poly(n-butyl acrylate) chains. J Rheol (N Y N Y) 2016. https://doi.org/10.1122/1.4942231.

[11] Huang C, Huang G, Li S, Luo M, Liu H, Fu X, et al. Research on architecture and composition of natural network in natural rubber. Polymer (Guildf) 2018. https://doi.org/10.1016/j.polymer.2018.08.057.

[12] Bandzierz K, Reuvekamp L, Dryzek J, Dierkes W, Blume A, Bielinski D. Influence of network structure on glass transition temperature of elastomers. Materials (Basel) 2016;9. https://doi.org/10.3390/MA9070607.

[13] Romanzini D, Lavoratti A, Ornaghi HL, Amico SC, Zattera AJ. Influence of fiber content on the mechanical and dynamic mechanical properties of glass/ramie polymer composites. Mater Des 2013;47:9–15. https://doi.org/10.1016/j.matdes.2012.12.029.

[14] Idicula M, Malhotra SK, Joseph K, Thomas S. Dynamic mechanical analysis of randomly oriented intimately mixed short banana/sisal hybrid fibre reinforced polyester composites. Compos Sci Technol 2005;65:1077–87. https://doi.org/10.1016/j.compscitech.2004.10.023.

[15] Ibarra L, Paños D. Dynamic properties of thermoplastic butadiene-styrene (SBS) and oxidized short carbon fiber composite materials. J Appl Polym Sci 1998;67:1819–26. https://doi.org/10.1002/(SICI)1097-4628(19980307)67:10<1819::AID-APP15>3.0.CO;2-R.

[16] Poletto M. Mechanical, dynamic mechanical and morphological properties of composites based on recycled polystyrene filled with wood flour wastes. Cienc y Tecnol 2017;19:433–42. https://doi.org/10.4067/S0718-221X2017005000301.

[17] Lamri A, Shirinbayan M, Pereira M, Truffault L, Fitoussi J, Lamouri S, et al. Effects of strain rate and temperature on the mechanical behavior of high-density

polyethylene. J Appl Polym Sci 2020. https://doi.org/10.1002/app.48778.

[18] Nakajima T, Takedomi N, Kurokawa T, Furukawa H, Gong JP. A facile method for synthesizing free-shaped and tough double network hydrogels using physically crosslinked poly(vinyl alcohol) as an internal mold. Polym Chem 2010. https://doi.org/10.1039/c0py00031k.

[19] Bandyopadhyay A, Valavala PK, Clancy TC, Wise KE, Odegard GM. Molecular modeling of crosslinked epoxy polymers: The effect of crosslink density on thermomechanical properties. Polymer (Guildf) 2011. https://doi.org/10.1016/j.polymer.2011.03.052.

[20] Bandyopadhyay A, Odegard GM. Molecular modeling of crosslink distribution in epoxy polymers. Model Simul Mater Sci Eng 2012. https://doi.org/10.1088/0965-0393/20/4/045018.

[21] Yang S, Qu J. Computing thermomechanical properties of crosslinked epoxy by molecular dynamic simulations. Polymer (Guildf) 2012. https://doi.org/10.1016/j.polymer.2012.08.045.

[22] Shenogina NB, Tsige M, Patnaik SS, Mukhopadhyay SM. Molecular modeling approach to prediction of thermo-mechanical behavior of thermoset polymer networks. Macromolecules 2012. https://doi.org/10.1021/ma3007587.

[23] Clancy TC, Frankland SJ V, Hinkley JA, Gates TS. Molecular modeling for calculation of mechanical properties of epoxies with moisture ingress. Polymer (Guildf) 2009. https://doi.org/10.1016/j.polymer.2009.04.021.

[24] Brydson JA. Other Thermoplastics Containing p -Phenylene Groups. Plast. Mater., 1999. https://doi.org/10.1016/b978-075064132-6/50062-0.

[25] Gradin P, Howgate PG, Seldén R, Brown RA. Dynamic-mechanical Properties. Compr. Polym. Sci. Suppl., 1989. https://doi.org/10.1016/b978-0-08-096701-1.00053-7.

[26] Flore D, Wegener K. Influence of fibre volume fraction and temperature on fatigue life of glass fibre reinforced plastics. AIMS Mater Sci 2016. https://doi.org/10.3934/matersci.2016.3.770.

[27] Bowen CR, Dent AC, Nelson LJ, Stevens R, Cain MG, Stewart M. Failure and volume fraction dependent mechanical properties of composite sensors and actuators. Proc Inst Mech Eng Part C J Mech Eng Sci 2006. https://doi.org/10.1243/09544062JMES255.

[28] Adams D. Transverse flexure testing□ : CompositesWorld. Compos World 2010.

[29] Kazemi ME, Shanmugam L, Lu D, Wang X, Wang B, Yang J. Mechanical properties and failure modes of hybrid fiber reinforced polymer composites with a novel liquid thermoplastic resin, Elium®. Compos Part A Appl Sci Manuf 2019;125:105523. https://doi.org/10.1016/j.compositesa.2019.105523.

[30] Selezneva M, Swolfs Y, Katalagarianakis A, Ichikawa T, Hirano N, Taketa I, et al. The brittle-to-ductile transition in tensile and impact behavior of hybrid carbon fibre/self-reinforced polypropylene composites. Compos Part A Appl Sci Manuf 2018. https://doi.org/10.1016/j.compositesa.2018.02.034.

[31] Tan W, Naya F, Yang L, Chang T, Falzon BG, Zhan L, et al. The role of interfacial properties on the intralaminar and interlaminar damage behaviour of unidirectional composite laminates: Experimental characterization and multiscale modelling. Compos Part B Eng 2018. https://doi.org/10.1016/j.compositesb.2017.11.043.

[32] Zhou J, Li Y, Li N, Hao X, Liu C. Interfacial shear strength of microwave processed carbon fiber/epoxy composites characterized by an improved fiber-bundle pull-out test. Compos Sci Technol 2016. https://doi.org/10.1016/j.compscitech.2016.07.033.

[33] Qiao Y. A modeling framework of brittle and ductile fractures coexistence in composites. University of Central Florida [Doctoral Thesis], 2018.

[34] Pini T. Fracture behaviour of thermoplastic acrylic resins and their relevant unidirectional carbon fibre composites: rate and temperature effects. Politecnico Milano 1863 [Doctoral Thesis], 2017.

[35] Pini T, Caimmi F, Briatico-Vangosa F, Frassine R, Rink M. Fracture initiation and propagation in unidirectional CF composites based on thermoplastic acrylic resins. Eng Fract Mech 2017;184:51–8. https://doi.org/10.1016/j.engfracmech.2017.08.023.

[36] Seo Y, Hwang SS, Kim KU, Lee J, Hong S. Influence of the mechanical properties of the dispersed phase upon the behaviour of nylon/rubber blends: crosslinking effect. Polymer (Guildf) 1993. https://doi.org/10.1016/0032-3861(93)90326-6.

[37] Chen Q, Dai C, Fang C, Chen M, Zhang S, Liu R, et al. Mode I interlaminar fracture toughness behavior and mechanisms of bamboo. Mater Des 2019. https://doi.org/10.1016/j.matdes.2019.108132.

[38] Kim KY, Ye L, Yan C. Fracture behavior of polyetherimide (PEI) and interlaminar fracture of CF/PEI laminates at elevated temperatures. Polym Compos 2005;26:20–8. https://doi.org/10.1002/pc.20062.

[39] Pal S, Ray BC. Molecular Dynamics Simulation of Nanostructured Materials: An Understanding of Mechanical Behavior. CRC Press; 2020.

[40] Zhang Q, Liang S, Sui G, Yang X. Influence of matrix modulus on the mechanical and interfacial properties of carbon fiber filament wound composites. RSC Adv 2015;5:25208–14. https://doi.org/10.1039/c5ra00098j.

[41] Ming Chong H. Toughening mechanisms of block copolymer and graphene nanoplatelet modified epoxy polymers. Imperial College London [Doctoral Thesis], 2015.

[42] Masanai K. Toughening mechanisms of silica nanoparticle-modified epoxy polymers. Imperial College London [Doctoral Thesis], 2010.

[43] Arencón D, Velasco JI. Fracture toughness of polypropylene-based particulate composites. Materials (Basel) 2009;2:2046–94. https://doi.org/10.3390/ma2042046.

[44] Saghafi H, Fotouhi M, Minak G. Improvement of the impact properties of composite laminates by means of nano-modification of the matrix-A review. Appl Sci 2018. https://doi.org/10.3390/app8122406.

[45] Klingler A, Bajpai A, Wetzel B. The effect of block copolymer and core-shell rubber hybrid toughening on morphology and fracture of epoxy-based fibre reinforced composites. Eng Fract Mech 2018. https://doi.org/10.1016/j.engfracmech.2018.06.044.

[46] Salzano De Luna M, Filippone G. Effects of nanoparticles on the morphology of immiscible polymer blends - Challenges and opportunities. Eur Polym J 2016. https://doi.org/10.1016/j.eurpolymj.2016.02.023.

[47] Brown HR, Deline VR, Green PF. Evidence for cleavage of polymer chains by crack propagation. Nature 1989. https://doi.org/10.1038/341221a0.

[48] Bhudolia SK, Joshi SC. Low-velocity impact response of carbon fibre composites with novel liquid Methylmethacrylate thermoplastic matrix. Compos Struct 2018;203:696–708. https://doi.org/10.1016/j.compstruct.2018.07.066.

[49] Shah SZH, Megat-Yusoff PSM, Karuppanan S, Choudhry RS, Ahmad F, Sajid Z, et al. Performance comparison of resin-infused thermoplastic and thermoset 3D fabric composites under impact loading. Int J Mech Sci 2021. https://doi.org/10.1016/j.ijmecsci.2020.105984.

[50] Panettieri E, Fanteria D, Montemurro M, Froustey C, Panettieri E, Fanteria D, et al. Low-velocity impact tests on carbon/epoxy composite laminates: A benchmark study. Compos Part B Eng 2016;107:9–21. https://doi.org/10.1016/j.compositesb.2016.09.057ï.

[51] Zhao J, Lu L, Rabczuk T. The tensile and shear failure behavior dependence on

chain length and temperature in amorphous polymers. Comput Mater Sci 2015. https://doi.org/10.1016/j.commatsci.2014.03.071.

[52] Ku H, Cheng YM, Snook C, Baddeley D. Drop weight impact test fracture of vinyl ester composites: Micrographs of pilot study. J Compos Mater 2005. https://doi.org/10.1177/0021998305051111.

[53] Hart KR, Chia PXL, Sheridan LE, Wetzel ED, Sottos NR, White SR. Comparison of Compression-After-Impact and Flexure-After-Impact protocols for 2D and 3D woven fiber-reinforced composites. Compos Part A Appl Sci Manuf 2017;101:471–9. https://doi.org/10.1016/j.compositesa.2017.07.005.

[54] Cromer KR. Impact and post-impact response of a composite material to multiple non-coincident impacts. University of Delaware, 2010.

[55] Foreman C. Delamination investigation for novel damage states within coupon and structural elements. University of Surrey, 2016.

[56] Shams Es-Haghi S, Leonov AI, Weiss RA. Deconstructing the double-network hydrogels: The importance of grafted chains for achieving toughness. Macromolecules 2014. https://doi.org/10.1021/ma500815d.

[57] Djukic S, Bocahut A, Bikard J, Long DR. Study of Damage Mechanisms of Amorphous and Low Semicrystalline Polymers under Tensile Deformation by Ultrasmall-Angle X-ray Scattering. Macromolecules 2020. https://doi.org/10.1021/acs.macromol.0c00534.

[58] Meijer HEH, Govaert LE. Mechanical performance of polymer systems: The relation between structure and properties. Prog. Polym. Sci., 2005. https://doi.org/10.1016/j.progpolymsci.2005.06.009.

PART IV: INSIGHTS, THESIS CONTRIBUTIONS & CONCLUSIONS

Chapter 8 Thesis contributions to the current state of knowledge

The distinctive novelty of this body of work lies in the development and direct application of a room-temperature processible thermoplastic hybrid matrix to composite for performance tailoring. Moreover, this work has produced several contributions to the current state of knowledge within the composites community, which are presented herein.

8.1 Comparative study of thermoplastic (acrylic) and thermoset (epoxy) composites

A key objective of this body of work was to comparatively assess the nominal performance of the acrylic-matrix composite with respect to a traditional thermoset epoxy-based composite. This was done to attain baselines of chemical, mechanical and thermomechanical performance to which the properties of the hybrid-matrix composite were to be compared. Moreover, benchmarking results were essential to fill the gaps identified as part of the literature survey for this thesis. Thus, the findings reported in Chapters 4 and 5 fulfil a broader objective of contributing to and developing a more robust database of performance, a prerequisite for reaching the level of maturity that thermoset-based composites have attained.

8.2 Development of a novel hybridisation route for composite applications using in-situ polymerisable thermoplastic matrices

This thesis presents a novel implementation of the room-temperature in-situ polymerisation process for the cost-effective fabrication of acrylic-PPE hybrid composites. Before this study, non-reactive PPE had been historically used with thermoplastic polymers in melt blended hybrids, with the earliest use of reactive PPE being with polyamide precursors [1–3], which necessitated elevated temperature methodologies. However, this work's distinctive novelty lies in developing and applying a room-temperature-processible hybrid matrix directly to composites for performance tailoring.

To promote chemical reactivity between the acrylic monomer and the thermoplastic modifier was deemed an important criterion. A specialised grade of oligomeric PPE with multiple vinyl functional groups was selected as the second constituent of the hybrid due

to the potential for interactions with the reactive acrylic resin as the first constituent. This was successfully done without compromising glass transition temperature; in both unreinforced and reinforced hybrid materials, incorporating PPE into the acrylic resin improved the glass transition temperature.

This work opens up a world of possibilities for alternative routes by which cost-effective tailoring of composite matrices may be realised. This has economic and ecological implications for the wider composites community. Before now, the combination of a reactive thermoplastic resin with a suitably selected reactive engineering thermoplastic for the low-cost hybrid-matrix composites was limited by the cost-prohibitive mould-heating requirements. With the insights gained from this research, several open challenges emerge that are worthy of further research attention.

8.3 Insights into chemical interactions in acrylic-PPE hybrid matrices and composites

Applied chemical analyses played a pivotal part in the process of development of the PPE-modified acrylic blends. Chemical interactions between acrylic and PPE within the hybrid polymers and their composite were not only evidenced by changes to the thermal degradation behaviour, damping behaviour and confocal Raman microscopy, but was substantiated by the observation of the partial solubility of blends in three different solvents. Unlike the neat acrylic polymer and composite, which fully dissolved after exposure to acetone, chloroform and toluene, acrylic-PPE blends and their composites partially dissolved, leaving behind residual reacted products. Using the insights gained from these investigations, the tentative representation of the blend structure in Figure 6-26 and Figure 9-3, comprising a high-solubility, acrylic-rich phase and a lower solubility acrylic-PPE reacted species.

While this reacted product could not be analysed using the techniques employed within this work, a characteristic thermogravimetric valley associated with PPE coincided with similar behaviour observed in the thermal degradation curves for PPE-modified blends (Figure 6-13, Zone 3). No such degradation event was observed for the neat acrylic polymer. It is worth noting that a lack of chemical interactions would have produced mutual exclusive (or discrete) valleys in the blended polymers with characteristically separate acrylic and PPE parts. Most importantly, the presence of a lightly cross-linked

network in the blend structure was shown to not affect its reshapability after polymerisation, which is expected to extend to the thermoformability of the reinforced and unreinforced acrylic/PPE blend. Thus, such an approach can offer performance tailoring opportunities without deleterious effects on the desirable thermoplastic attributes of the base acrylic resin.

8.4 The development of potential repair and joining methodologies for thermoplastic acrylic-matrix composites

Waste management at the end of service and during the production cycle constitute critical issues faced by the composites community today, particularly in the bid to attain circularity and minimise environmental impact. Considering the paucity of published literature, which address these issues for acrylic-matrix composites, valuable insights gained as part of this research and other research involvements on repairability were broadly described and discussed in Section B.1.3. Furthermore, two types of waste management are addressed. The development of robust infusion repair methodologies is paramount to scrap minimisation, meaning the potentials of pre-service resources can be fully exploited. Moreover, such a method may be readily employed for joining multi-component assemblies and selectively tailoring parts using an adapted overmoulding technique. Finally, hot-press moulding of impact-damaged coupons was demonstrated as a viable approach towards post-impact healing of acrylic-matrix composites. Under the conditions investigated within this research project, the coupons appeared visibly healed. However, unknown factors were at play that limited the effective restoration of structural integrity towards the pre-impacted condition. Thus, this work's principal contribution is the establishment of a foundation of knowledge for further exploration of both intrinsic and extrinsic factors, some of which have also been defined. Perhaps, the most critical of these involves the effects of subjecting the impacted coupons to heat and pressure. Under the conditions employed for this research, deleterious effects were observed. Future research aimed at methodological refinements will benefit from the findings presented within this thesis and may facilitate heat processing of acrylic-matrix composites, which offers possibilities for re-use and recycling of used and discarded composite components.

8.5 Considerations for the use of acrylic resins

It is worth mentioning that for industrial applications, flammability constitutes a major limitation that must be taken into consideration. Random chain scission was identified as the primary mechanism by which an acrylic polymer undergoes major thermal degradation (Section 2.1.1). This highlights the importance of further exploration of the flammability of reactive acrylic polymers and their composites. Acrylics are known to depolymerise at elevated temperatures owing to the aforementioned scission mechanism, releasing flammable monomers, which pose in-service fire hazard implications. This is particularly important, given the contributions of poly (methyl methacrylate) sheet glazing (Oroglas) to the Summerland disaster in 1973 [4,5]. Already, it has been shown that, by using non-woven intumescent mats [6] and a phosphorus-carbon-based flame retardant [7], that the flame-retardant and smoke suppression properties of acrylic-matrix composites can be significantly enhanced.

8.6 Recommendations for further research

In light of the findings of this research and the insights gained via collaborative research involvements (Appendix B), emerging opportunities for further research have been highlighted. Herein are the identified gaps in existing contributions and challenges yet to be addressed with acrylic-matrix composites and hybrids based on reactive acrylic technology.

1. The desire to address current environmental challenges associated with end-of-life decommissioning and waste management will continue to be a key driver of research activities within the composites industry. The following areas are worthy of further exploration towards the goal of futureproofing these liquid acrylic resins as ideal candidate materials for the recyclable materials' market:

    a. **Reshapability:** Building on the author's work discussed in Section 5.1 and the success of the preliminary trial on the blends considered in this work (Section 6.5; Figure 6-25), can large-scale fibre-reinforced acrylics be readily thermoformed to meet the requirements for serial production?

    b. **Recyclability:** In the context of the works reviewed in Section 2.8.1, are there other more environmentally friendly routes to complete reclamation of

continuous fibres from acrylic-based composites? Are there viable routes to economically reusing the reclaimed materials from decommissioned acrylic-based components?

c. **Repairability:** The insights presented in Appendix D have attempted to answer the question: *"Can the reactivity of liquid acrylic resins be exploited for repair operations?"* using infusion repair, and hot-press impact damage repair approaches. These feasibility studies are not without limitation; due to material constraints, the number of tests required to draw statistically robust conclusions is yet to be conducted. Comprehensive investigations based on the foundational insights provided by these studies will be of interest to the broader composites community. Besides, other questions such as the following remain unanswered for reactive liquid acrylic resin-based composites.

(1) *What are the chemical characteristics of the 'weld lines' in infusion-repaired laminates with in-situ polymerisation of the reactive acrylic resin in the presence of a consolidated acrylic polymer-based substrate?*

(2) *Can large-scale structures be repaired on-site at room temperature without the need for costly decommission?*

2. The works discussed in Section 2.8.2 on thermal joining of acrylic-matrix composites have highlighted the need for scaling joining methodologies for larger structures. The development of thermally stable sizing for the conductive fibre-reinforced heating elements is an essential step towards this goal. The use of conductive heating elements also necessitates extensive lightning protection research, particularly for wind turbine blades. The durability of welded joints, particularly building on the reviewed works on joining, is worthy of research attention. Finally, the adaptability of these lab-based joining techniques to field joining operations must be adequately explored.

3. Despite the extensive efforts towards a comprehensive database on the performance of acrylic-matrix composites (Section 2.3), there still exists a paucity of published literature on their compressive performance, long-term durability and resilience, particularly due to the time scales required and the infancy of this resin technology. As such, the following topics must be further explored:

a. Compressive behaviour
b. Long-term creep performance
c. UV sensitivity
d. Long-term fatigue degradation of large scale components
e. End-notch-flexure behaviour

4. While efforts have been made towards enhancing the performance of acrylic-matrix composites, the standard practice involves the incorporation of a nanoscale rubber phase into the thermoplastic resin (Section 2.6). Thermoplastic-thermoplastic hybrid systems have not been extensively explored due to the processing challenges associated with traditional thermoplastic manufacturing processes. Consequently, other routes of modification must be considered that do not compromise matrix and composite performance. Being amorphous thermoplastics, composites based on these acrylic matrices exhibit poor solvent resistance. The present research has demonstrated a simple, yet viable route towards attaining performance tailoring, details of which have been presented and discussed in Chapters 6 & 7. Moreover, exciting opportunities for further exploration have been highlighted. It has been shown that the PPE oligomer and acrylic monomer interact during the free-radical polymerisation of the acrylic monomer. Some vital insights have been gained, which suggest the formation of multi-species mixtures within the hybrid-matrix composites manufactured in this research. However, the enhanced solvent resistance attained by PPE-hybridisation of the acrylic matrix system precluded the determination of the exact species formed using a solution-state NMR technique. Thus, alternative routes to analysing hybrid chemistry are pivotal to advancing the development of these hybrids. Other research questions raised by these findings include the following:

a. What are the effects of PPE-based hybridisation on the fibre-matrix interface?
b. Does the vinyl functionality of the PPE play a role in interfacial bonding?
c. Can specialised sizing technology enhance the effectiveness of the employed hybridisation approach?
d. Can an admixed acrylic-PPE resin be infused into a preform with interlaminar-dispersed PPE (or other suitably selected engineering thermoplastic) for targeted performance tailoring?
e. Are there any effects of temperature on acrylic monomer's reactivity with the vinyl functionality of the PPE oligomer employed in this work?

f. *Are there ways to control and measure the size and distribution of the PPE-rich domains, even at higher loadings?*
g. *Can the proposed semi-interpenetrating polymer network considered in this work be enhanced by targeted evaluation and control of the molecular parameters such as cross-link density, degree of entanglement, molecular weight distribution and inter-species interactions?*
h. *What mechanisms are responsible for the deleterious effects of hybridisation on impact damage resistance and tolerance?*
i. *Can such hybridisation positively affect the time-dependent deformation behaviours such as creep and stress relaxation of the purely amorphous acrylic matrix?*
j. *Are there effects of PPE incorporation on the flammability and smoke suppression characteristics of hybrid acrylic-matrix composites?*

5. The reactive nature of these liquid resins makes them ideally suited for use in multi-material systems such as fibre-metal laminates, the success of which has been highlighted in Sections 2.7 and D.1.1 of this thesis. Extensive exploration of the unique interfaces within such material systems should be undertaken to address research questions such as

a. *What are the effects of varying the organic adhesion promoter coatings on interfacial adhesion?*
b. *Can the same benefits gained with the use of fibre-based hybridisations in thermoset-matrix FMLs be exploited with TP-FMLs?*
c. *How much of a challenge is posed by the mismatch of thermal expansion coefficient, moisture sensitivity, and creep resistance of the dissimilar constituents within the TP-FMLs?*
d. *Does the use of room temperature processing offer any additional benefits by minimising thermal stresses at the interface, which are associated with high-temperature manufacturing?*
e. *Can blanks of TP-FMLs be produced and subsequently reprocessed by thermoforming?*

6. The works presented in Sections 2.1 and 2.2 provide essential foundations for understanding the polymerisation behaviour and current processing methods for these liquid acrylic resin systems. Innovative process-related research may pave the way for even greater adoption potential for these reactive thermoplastic acrylic resins. Given the challenges posed by foaming during polymerisation (of neat acrylic resin) within this work, alternative manufacturing methods for the production of unreinforced plaques for

characterisation must be considered. Moreover, routes that facilitate the integration of reactive acrylic technology into alternative processing methods; e.g., prepreg-inspired products with selective activation profiles must be explored.

Chapter references

[1] Stack S, O'Donoghue O, Birkinshaw C. The thermal stability and thermal degradation of blends of syndiotactic polystyrene and polyphenylene ether. Polym Degrad Stab 2003. https://doi.org/10.1016/S0141-3910(02)00235-5.

[2] Li Y, Xie T, Yang G. Effects of polyphenylene oxide content on morphology, thermal, and mechanical properties of polyphenylene oxide/polyamide 6 blends. J Appl Polym Sci 2006;99:2076–81. https://doi.org/10.1002/app.22687.

[3] Liu A, Xie T, Yang G. Effect of Na+-MMT Platelets on Monomer Casting Polyamide 6/Polyphenylene Oxide Blends. Macromol Chem Phys 2006;207:2180–7. https://doi.org/10.1002/macp.200600358.

[4] Qin Y, Summerscales J, Graham-Jones J, Meng M, Pemberton R. Monomer selection for in situ polymerization infusion manufacture of natural-fiber reinforced thermoplastic-matrix marine composites. Polymers (Basel) 2020;12:1–25. https://doi.org/10.3390/polym12122928.

[5] National Materials Advisory Board, of Sciences NA. Fire Safety Aspects of Polymeric Materials, Volume 1. National Academy of Sciences; 1977.

[6] Khalili P, Blinzler B, Kádár R, Blomqvist P, Sandinge A, Bisschop R, et al. Ramie fabric Elium®composites with flame retardant coating: Flammability, smoke, viscoelastic and mechanical properties. Compos Part A Appl Sci Manuf 2020;137:105986. https://doi.org/10.1016/j.compositesa.2020.105986.

[7] Khalili P, Blinzler B, Kádár R, Bisschop R, Försth M, Blomqvist P. Flammability, smoke, mechanical behaviours and morphology of flame retarded natural fibre/Elium®composite. Materials (Basel) 2019;12. https://doi.org/10.3390/ma12172648.

Chapter 9 Thesis conclusions

This thesis simultaneously addressed gaps in existing knowledge and demonstrate the viability of an innovative and methodical approach for performance tailoring of liquid acrylic resin systems for composite applications. A relatively inexpensive, and strategically selected engineering thermoplastic has been combined with a room-temperature-processible reactive thermoplastic resin. This process was employed to produce added-value composite materials, geared towards improving the cross-sectoral appeal of acrylic resins, which are considered commodity thermoplastic resins.

Unreinforced acrylic and PPE-modified acrylic polymers were prepared for complementary analyses using a combination of chemical, thermomechanical and mechanical techniques by a casting process. It was found that multi-component mixtures were formed upon in-situ polymerising, with species including soluble phases of neat acrylic and neat PPE, and an insoluble reacted acrylic-PPE product. PPE-hybridisation appeared to enhance the blends' solvent resistance, indicating chemical interactions between the acrylic and PPE constituents. While desirable from a material performance perspective, the enhanced solvent resistance prohibited the use of solution-state and solid-state nuclear magnetic resonance and gas permeation chromatography analyses to interrogate the precise chemical composition and structure of the insoluble phase.

Miscibility trials (Figure 9-1) and findings of complementary studies (Figure 9-2) of unreinforced polymer samples were employed to identify the optimum composition of acrylic and PPE. 5 wt. % was identified as the optimum loading of PPE by weight of acrylic resin to fabricate test laminates. Favourable energy dissipation mechanisms such as crack deflection, crazing and shear banding were observed during microscopic inspections of the acrylic/PPE blend fracture surfaces.

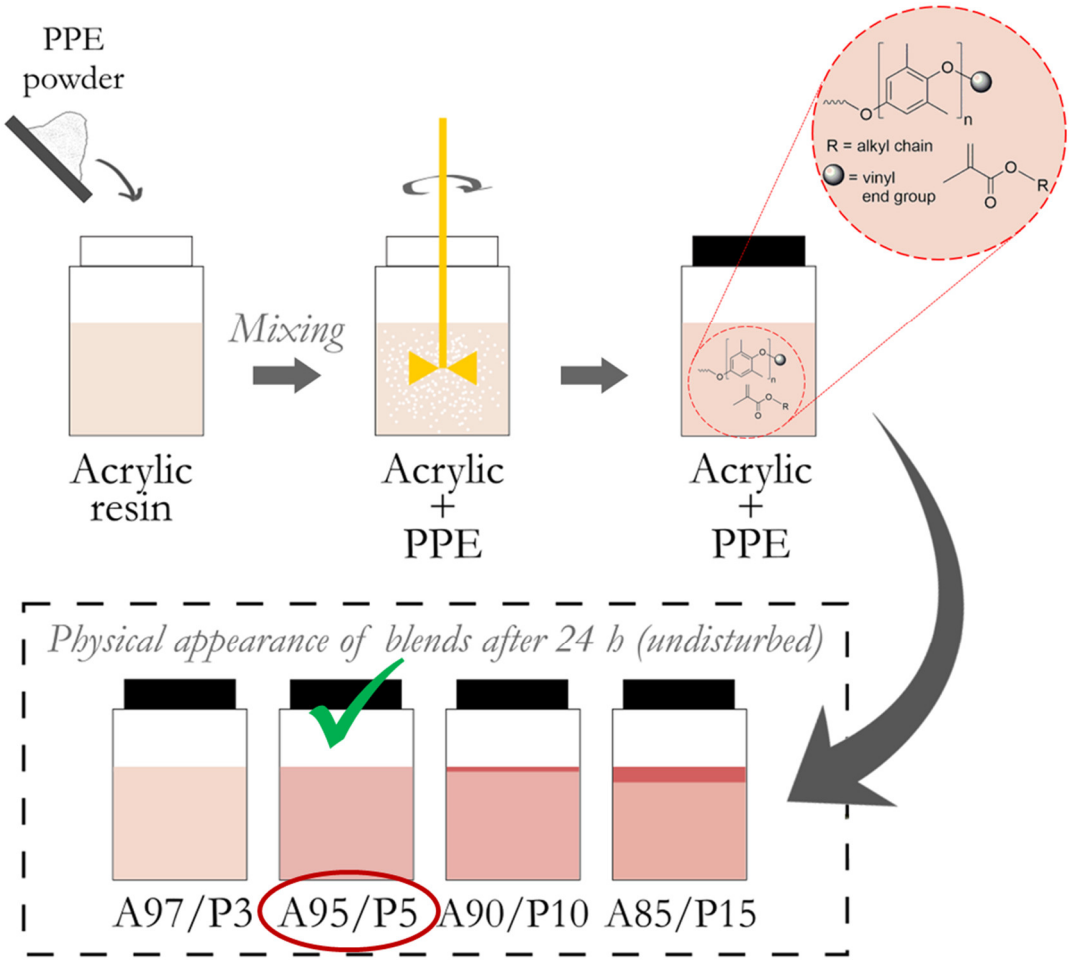


Figure 9-1. Illustrative summary of the preliminary miscibility trials conducted to assess the phase stability of the acrylic/PPE resin blends for room-temperature resin infusion processing. Further details are available in Chapter 6.

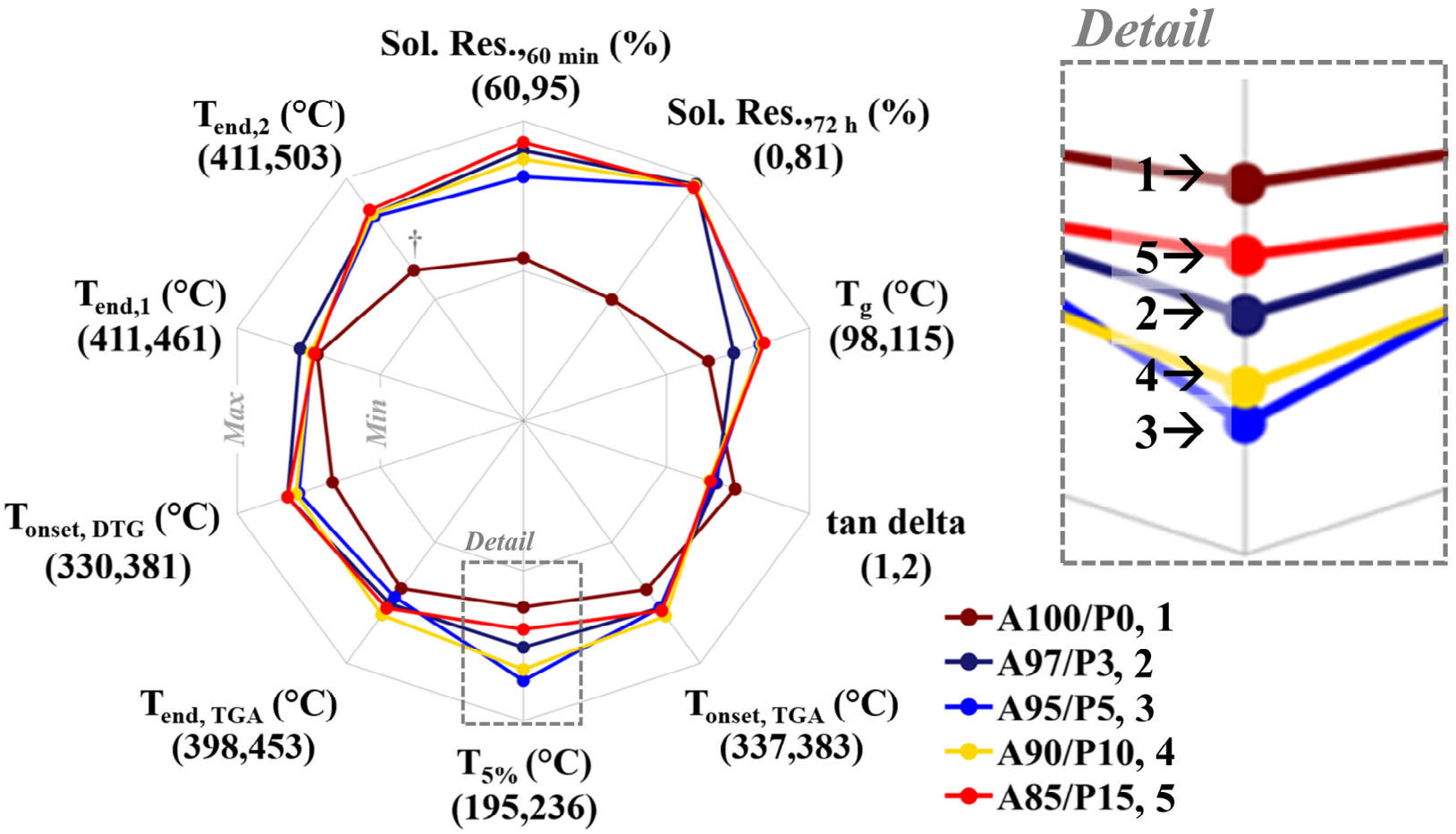


Figure 9-2. A summary of the key findings of this chapter. Axis Min and Max values are provided in parenthesis for scaling purposes. †: No T_{end}^2 value for A100/P0; the T_{end}^1 value was used for graphing purposes only. Note: Solvent resistance is the inverse of mass fraction lost during exposure to acetone; subscripts, 60 min and 72 h for solvent resistance imply the results for 60 min and 72 h exposure, respectively.

Furthermore, the obtained results were utilised with accepted polymer blend theory to propose the most likely blend architecture based on the reactants' chemical structures. The proposed structure is presented in Figure 9-3.

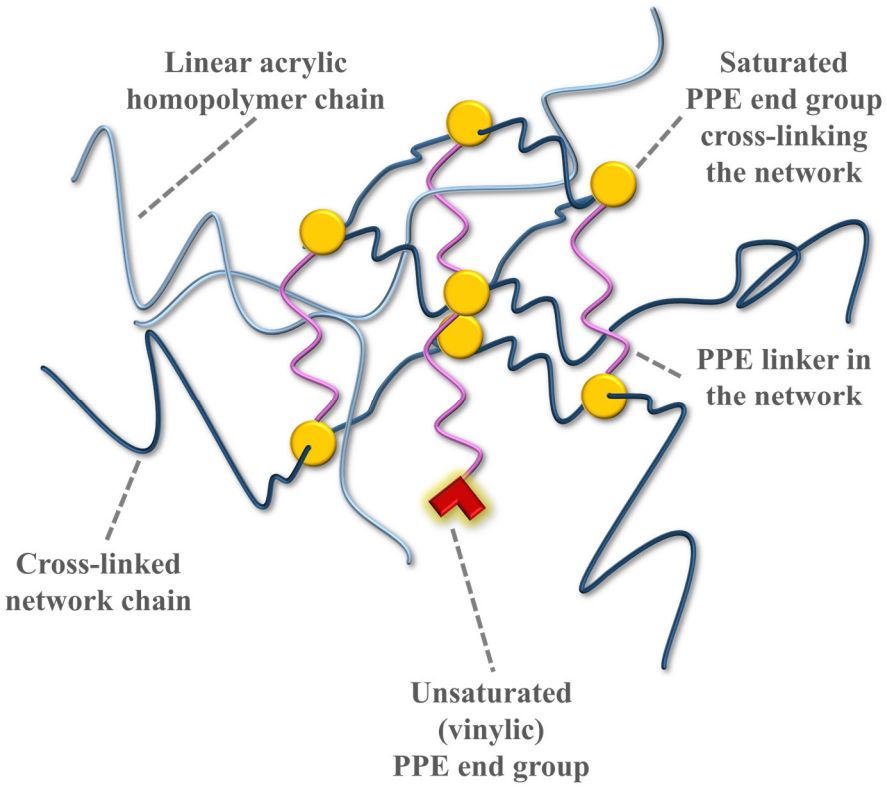


Figure 9-3. The proposed polymer architecture within the PPE-modified acrylic blends, showing a lightly cross-linked acrylic/PPE network, a branched or grafted acrylic/PPE species, and a highly entangled, linear acrylic polymer species. A detailed description of all considerations and theories that informed the identification of this structure can be found in Chapter 6 (Section 6.5).

Before the fabrication of fibre-reinforced PPE-modified acrylic composites, thermoformability was successfully demonstrated for all unreinforced blends to rule out the deleterious effects of the proposed cross-linked structures realised — evidenced by the deformability of the samples in Figure 9-4.

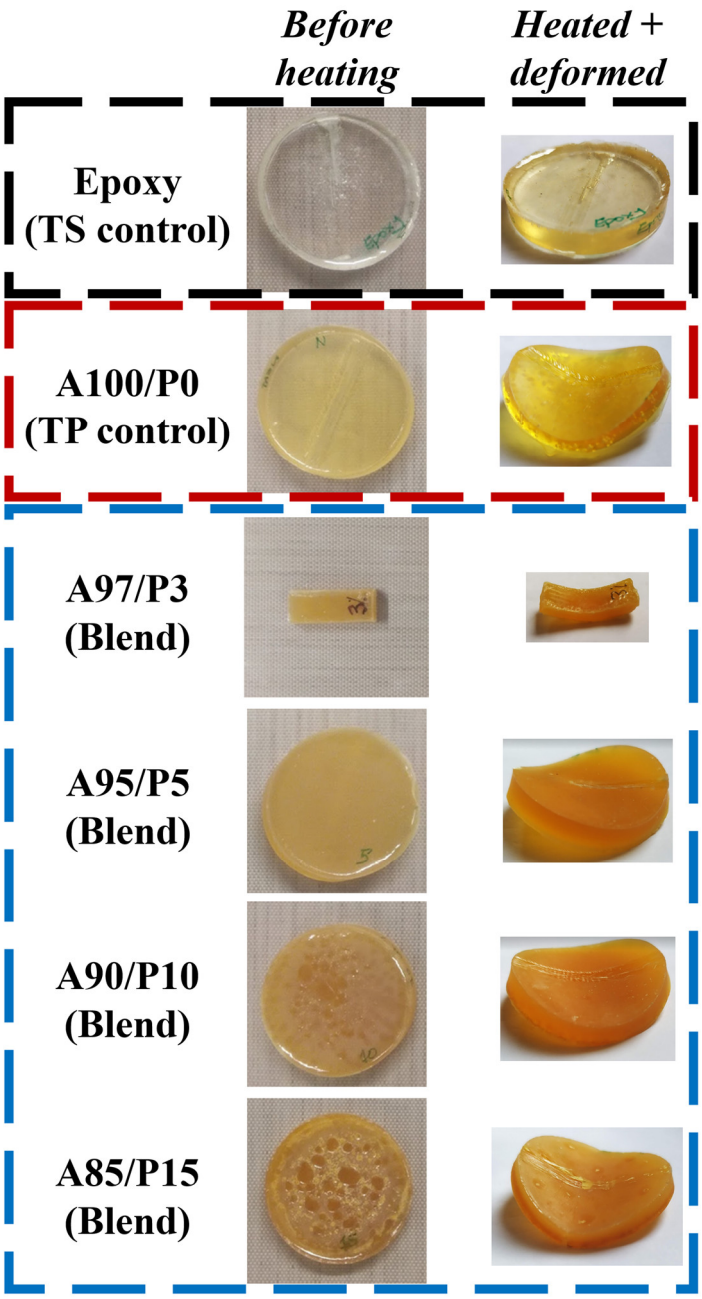


Figure 9-4. Results of thermoformability trials conducted on the acrylic/PPE blends, A100/P0 as the thermoplastic control, and epoxy as a thermoset control. All samples are 40-mm dia. discs except for A97/P3, which measures 25 mm × 8 mm × 4 mm due to material availability constraints. Previously presented in Section 6.5 and prepared as detailed in Appendix C.1.1.2 (Figure C-2).

Glass fibre-reinforced laminates of neat acrylic and 5 wt. % acrylic-PPE were comparatively assessed under various conditions to ascertain the effects of PPE-incorporation of the chemical, thermal, thermomechanical, mechanical and drop-weight impact performance. PPE-hybridisation conferred enhanced solvent resistance, thermal stability, increased glass transition temperatures and ductility on the acrylic-PPE-matrix composite with respect to unmodified acrylic-matrix composite. Transverse tensile properties were also improved, providing strong evidence for the successful tailoring of matrix-dominated properties. Initiation mode-I interlaminar fracture toughness was improved due to hybridisation, with a multiple-crazing mechanism being observed.

Based on the finding of this research, collaborative involvements and trends identified in existing scientific knowledge, recommendations for future research have also been proposed in Section 8.2. While current tailoring practices for liquid thermoplastic acrylic composites often incorporate elastomeric particulates into the matrix, such approaches may offer limited possibilities in terms of the retention of thermomechanical properties with the incorporation of elastomeric particulates. As the industry demands continue to drive research towards adopting practices for improved circularity, the demand for reactive resin systems will potentially see unrivalled growth. Liquid acrylics are ideal emergent solutions that meet market needs from an ecological and economic standpoint, being low-cost, commodity thermoplastic resins. The tailoring route demonstrated as part of this research offers a world of possibilities for realising innovative thermoplastic hybrid-matrix composites with added value for the composites community. Such methodologies will likely facilitate the cross-sectoral adoption of these liquid thermoplastic resins.

Presented below are charts summarising the key findings of this body of work.

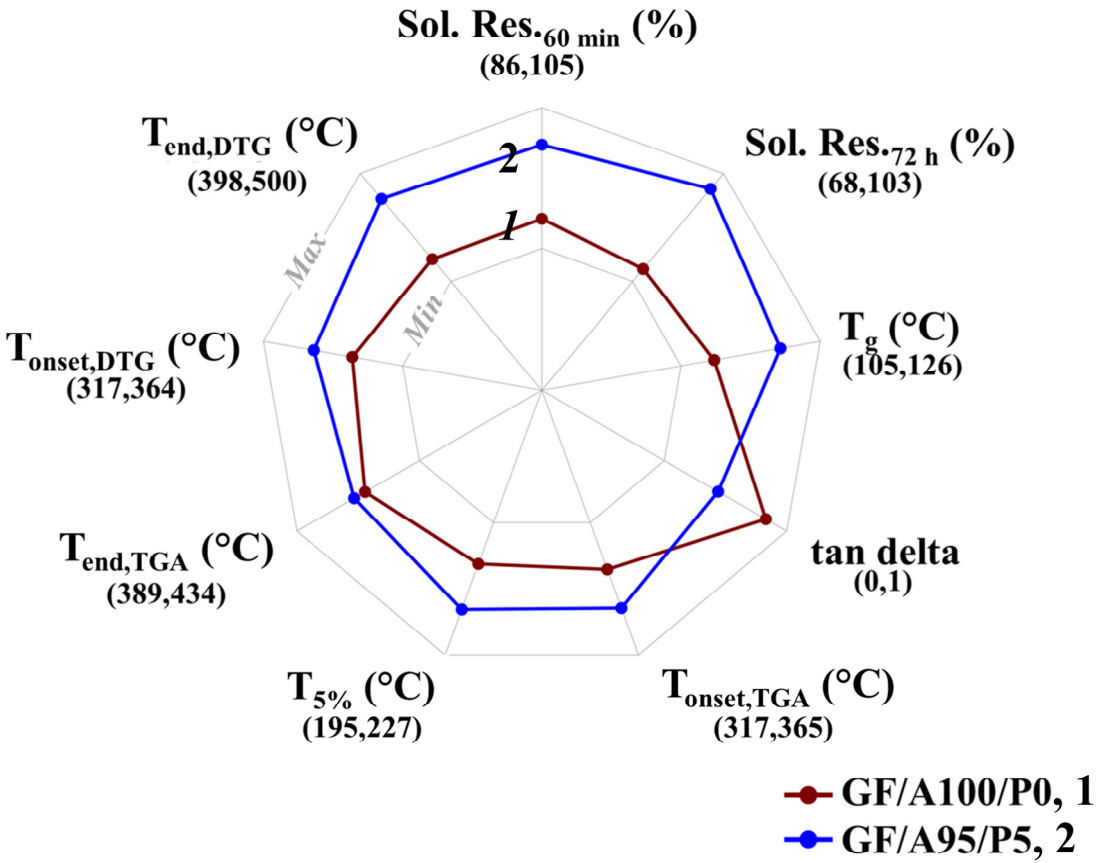


Figure 9-5. Summary of the chemical and thermal analyses results for glass fibre-reinforced acrylic (GF/A100/P0) and PPE-modified acrylic (GF/A95/P5) composites as presented in Chapter 7. All symbols are used as listed in the Nomenclature section (Appendix A).

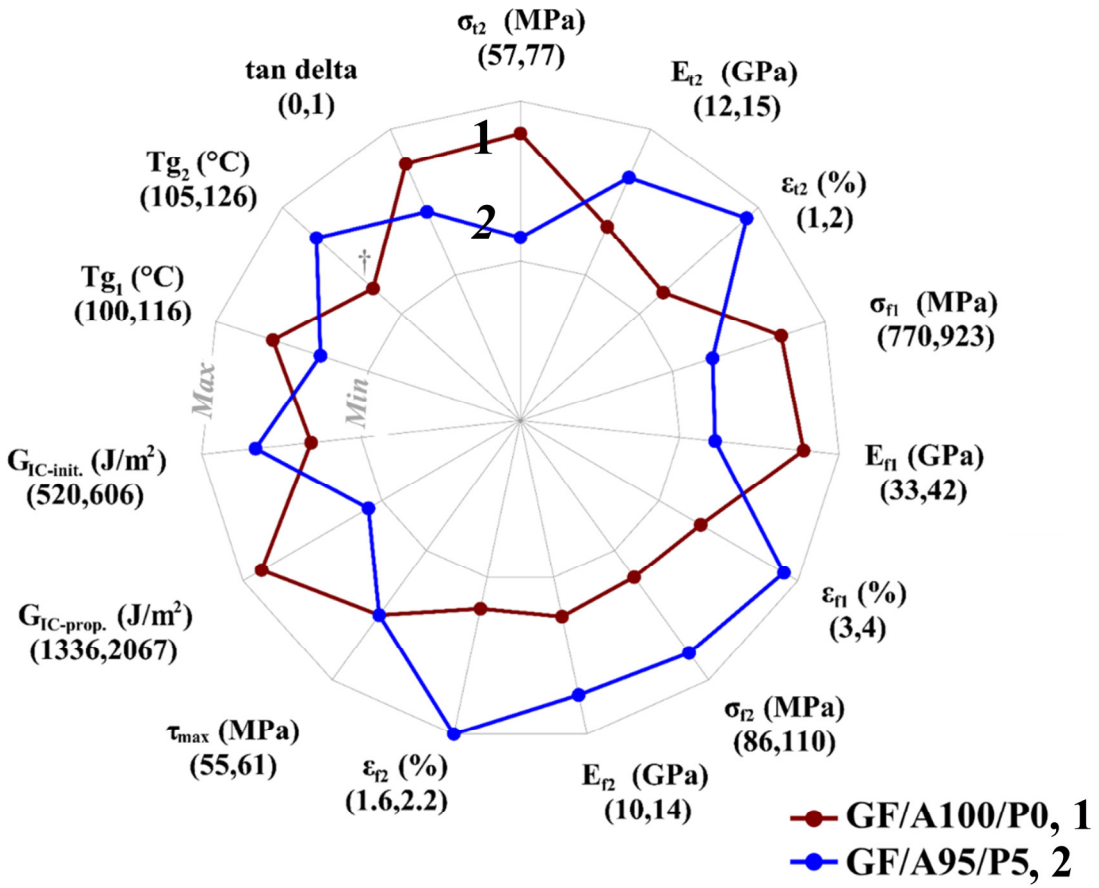


Figure 9-6. Summary of the mechanical and thermomechanical properties for glass fibre-reinforced acrylic (GF/A100/P0) and PPE-modified acrylic (GF/A95/P5) composites as presented in Chapter 7. All symbols are used as listed in the Nomenclature section (Appendix A).

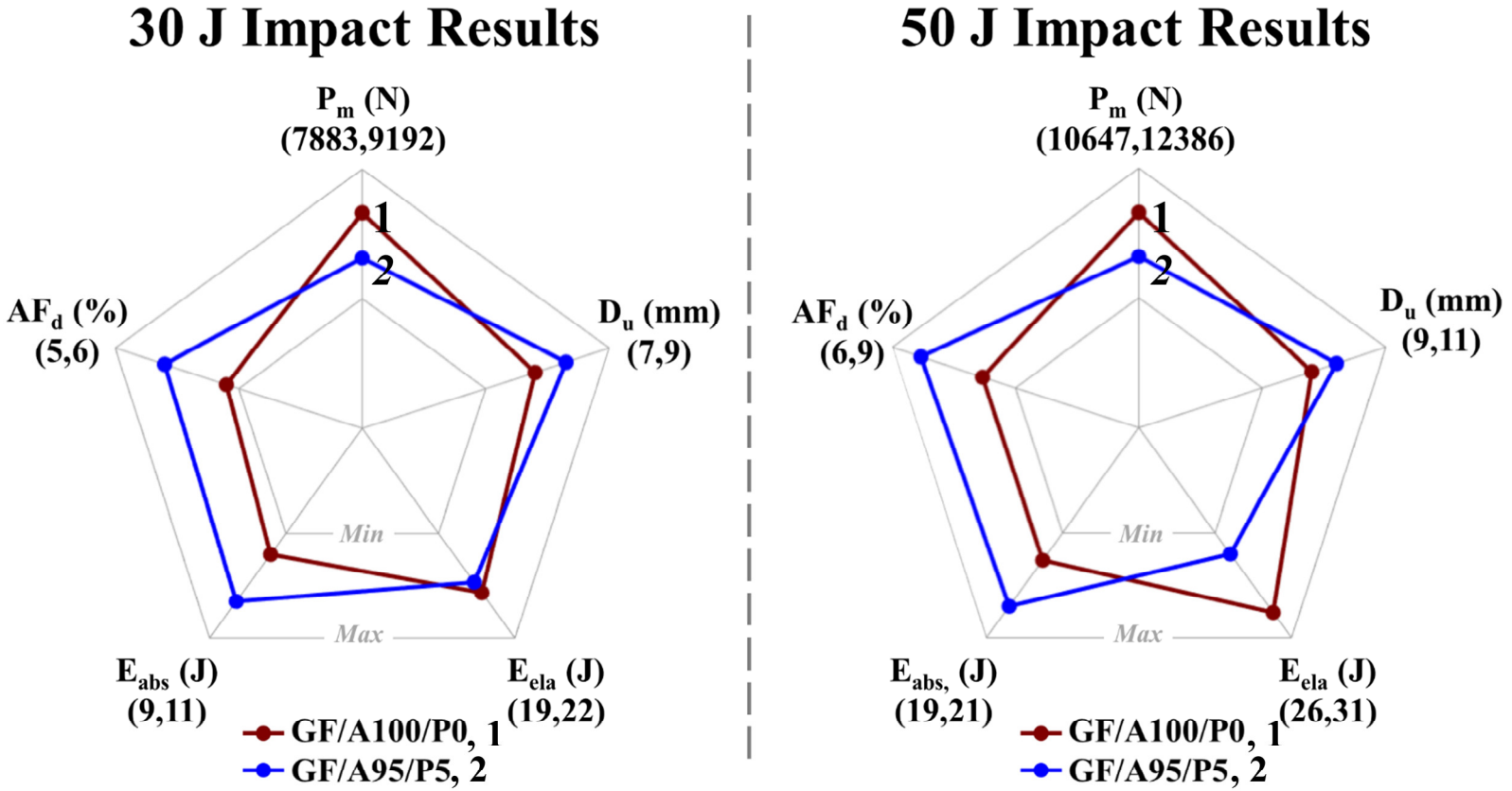


Figure 9-7. Summary of the drop-weight impact performance of glass fibre-reinforced acrylic (GF/A100/P0) and PPE-modified acrylic (GF/A95/P5) composites as presented in Chapter 7. All symbols are used as listed in the Nomenclature section (Appendix A).

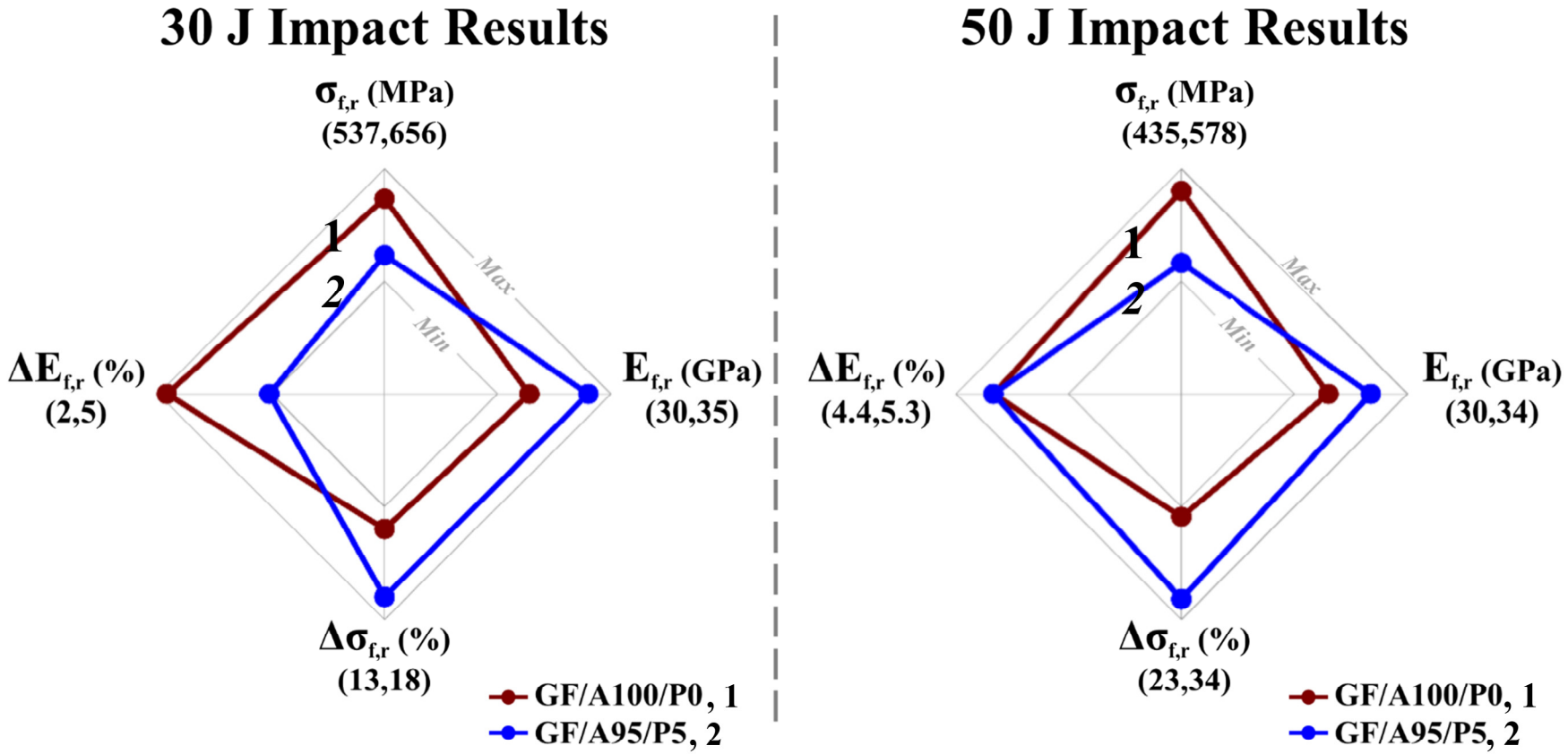


Figure 9-8. Summary of the impact tolerance (the post-impact flexural properties) of glass fibre-reinforced acrylic (GF/A100/P0) and PPE-modified acrylic (GF/A95/P5) composites as presented in Chapter 7. All symbols are used as listed in the Nomenclature section (Appendix A).

PART V: AUXILIARY CHAPTERS

Appendix A

Nomenclature and Acronyms

A.1 Acronyms and Material Designations

A0/P100	Oligomeric PPE
A100/P0	Unmodified acrylic (Elium® 188 O)
A85/P15	15 wt. % PPE-modified acrylic based on Elium® 188 O
A90/P10	10 wt. % PPE-modified acrylic based on Elium® 188 O
A95/P5	5 wt. % PPE-modified acrylic based on Elium® 188 O
A97/P3	3 wt. % PPE-modified acrylic based on Elium® 188 O
ABS	Acrylonitrile butadiene styrene
AC	Acrylic-compatible
ARALL®	Aramid-reinforced aluminium laminate
BATP	Brittle amorphous thermoplastic
BPO	Dibenzoyl peroxide
CARALL®	Carbon-reinforced aluminium laminate

CBT	Cyclic butylene terephthalate
CF	Carbon fibre
CNT	Carbon nanotubes
COSY	COrrelated SpectroscopY
DCB	Double cantilever beam
DEA	Dielectric analysis
DMA	Dynamical mechanical analysis
DOSY	Diffusion Ordered SpectroscopY
DSC	Differential scanning calorimetry
DTG	Derivative thermograms
FAI	Flexure-after-impact
FED	Flat energy director
FF	Flax fibre
FML	Fibre-metal laminates

FML	Fibre-metal laminates
FRP	Fibre-reinforced polymer
FRP	Fibre-reinforced polymer
GF	Glass fibre
GF/A100/P0	Glass-reinforced acrylic (based on Elium® 188 O)
GF/A95/P5	Glass fibre-reinforced A95/P5
GF/acrylic	Glass-reinforced acrylic (based on Elium® 188 O)
GF/E180	Glass fibre-reinforced Elium® 180 acrylic
GF/epoxy	Glass fibre-reinforced Sicomin SR epoxy
GF/IN-2	Glass fibre-reinforced IN-2 infusion epoxy
GLARE®	Glass Laminate Aluminium Reinforced Epoxy
GPC	Gel permeation chromatography
HSQC	Heteronuclear Single Quantum Coherence
IED	Integrated energy director

IFSS	Interfacial shear strength
IPNs	interpenetrating polymer networks
JF	Jute fibre
LCM	Liquid composite moulding
LRI	liquid resin infusion
M	Acrylic monomer (Elium® 188 O – as received)
MC	Multi-compatible
MF	Multi-frequency
MMA	Methyl methacrylate
MWCNT	Multi-walled carbon nanotubes
NCF	Non-crimp fabric
NCF	Non-crimp fabric
NMR	Nuclear magnetic resonance
NR	Non-reactive mixtures of acrylic monomer and PPE oligomer

NS	No sizing
O	Oligomeric PPE (as received)
O+BPO	Oligomeric PPE (mixed with dibenzoyl peroxide)
P	Polymeric form of acrylic and acrylic/PPE blends
PA6	Polyamide-6
PBT	Polybutylene terephthalate
PDA	Polydopamine
PEI	Poly(ether imide)
PEQ	UHMWPE Plain weave fiber from QuantaFlex
PES	UHMWPE Plain weave fiber from SOVETL
PETG	Glycol-modified polyethylene terephthalate
PFA	Perfluoroalkoxy alkane
PP	Polypropylene
PPE	poly(phenylene ether)

PPO	Poly(phenylene oxide)
PS	Polystyrene
RTM	Resin transfer moulding
S_B	Total blended system
SBS	Short beam shear
SEM	Scanning electron microscopy
SEM	Scanning electron microscopy
SF	Single-frequency
Sol. res.	Solvent resistance
sPS	Syndiotactic polystyrene
TGA	Thermogravimetric analysis
THF	Tetrahydrofuran
TP	Thermoplastic
TS	Thermosetting

TS	Thermosetting
UHMWPE	Ultra-high molecular weight polyethylene
VARTM	Vacuum-assisted resin transfer moulding
VARTM	Vacuum-assisted resin transfer moulding

A.2 Variables and Parameters

Latin Letters, Variables and Symbols

AF_d	Damaged area fraction	%
AW_f	Fibre areal weight	g/m^2
DA	Damage area	mm^2
DI	Damaged index	–
$d^i{}_{11}$	Mechanical damage index up to the ith cycle	–
E	Modulus	GPa
$E^o{}_{11}$	Initial Young's modulus	GPa
E_{ab} or E_{abs}	Absorbed energy	J
E_{aml}	Energy after max load	J

E_{bml}	Energy before max load	J
E_{diss}	Dissipated energy	J
E_{el} or E_{ela}	Elastic energy	J
$E_{f,r}$	Residual flexural modulus	GPa
E_{f1}	Longitudinal tensile modulus	(GPa)
E_{f2}	Transverse tensile modulus	(GPa)
E^{i}_{11}	Young's modulus after the ith cycle	GPa
E_p	Peak energy	J
E_{t2}	Transverse tensile modulus	(GPa)
G_{IC}	Mode-I interlaminar fracture toughness	kJ/m^2
$G_{IC\text{-}init.}$	Mode-I interlaminar fracture initiation toughness	kJ/m^2
$G_{IC\text{-}prop.}$	Mode-I interlaminar fracture propagation toughness	kJ/m^2
K_{max}	Sample stiffness	N/mm
L_m	Maximum load	kN

M_R	Residual mass at the end of the thermal cycle for TGA experiments	%
N	Number of piles	–
PD_m	Projectile displacement at maximum load	mm
PD_u or D_u	Ultimate projectile displacement	mm
PD_u-PD_m	Residual deflection	mm
P_m	Peak load	°C
t	Thickness	m
T	Temperature	°C
$T_{100\%}$	The temperature at 100% conversion during polymerisation	°C
tan delta	damping/dissipative capacity	–
$T_{end,\ DTG\text{-}N}$	Thermal decomposition end temperature from DTG thermograms; where N is used for multi-stage decompositions	°C
$T_{end,\ TGA}$	End temperatures for the main degradation event as determined from the TGA thermograms	°C
T_g	Glass transition temperatures	°C
T_{gel}	Gel temperature	°C

T_{gN}	Glass transition temperature for a blended system with multiple values	°C
$T_{gN,A}$	Glass transition temperature contribution by blend component A for a blended system with multiple values	°C
$T_{gN,B}$	Glass transition temperature contribution by blend component B for a blended system with multiple values	°C
$T_{max\text{-}DSC}$	Peak temperature from DSC thermograms	°C
$T_{max\text{-}DTG}$	The temperature corresponding to the maximum rate of degradation; i.e., the valleys or peaks of DTG thermograms	°C
$T_N\%$	Temperatures corresponding to N% of mass loss using TGA thermograms	°C
$T_{onset,\ DSC}$	Onset temperature for the polymerisation reaction using DSC thermograms	°C
$T_{onset,\ DTG}$ or $T_{onset,\ DTG\text{-}N}$	Thermal decomposition onset temperature from DTG thermograms; where N is used for multi-stage decompositions	°C
$T_{onset\text{-}TGA}$	Onset temperatures for the main degradation event as determined from TGA thermograms	°C
V_f	Fibre volume fraction	%
V_v	Void volume fraction	%

Greek Letters and Symbols

$\Delta E_{f,r}$	Post-impact reduction in flexural modulus as a percentage of nominal modulus	%
ΔH	Enthalpy change	J/g
$\Delta\sigma_{f,r}$	Post-impact reduction in flexural strength as a percentage of the nominal strength	%
δ	Penetration depth	mm
ε	Strain	
ε_{f1}	Longitudinal tensile failure strain	%
ε_{f2}	Transverse tensile failure strain	%
ε_{t2}	Transverse tensile failure strain	%
σ	strength	MPa
$\sigma_{f,r}$	Residual flexural strength	MPa
σ_{f1}	Longitudinal tensile strength	MPa
σ_{f2}	Transverse tensile strength	MPa
σ_{t2}	Transverse tensile strength	MPa
τ_{max}	Ultimate shear stress	MPa

φ_1	Mass fraction of constituent 1 in a blended polymer system for T_{g1}	–
$\varphi_{2,A}$	Mass fraction of constituent A in a blended polymer system for T_{g2}	–
$\varphi_{2,B}$	Mass fraction of constituent B in a blended polymer system for T_{g2}	–

Appendix B Insights from complementary research and collaborations

B.1 New possibilities with liquid acrylic resins and their hybrids

B.1.1 Thermoplastic fibre-metal laminates

Fibre-metal laminates (FML) are a family of hybrid composite materials that comprise fibre fabric plies and metal sheets stacked in alternating layers with a polymeric matrix phase as in aramid-reinforced aluminium laminate (ARALL®), carbon-reinforced aluminium laminate (CARALL®) and Glass Laminate Aluminium Reinforced Epoxy (GLARE®). FMLs have replaced their monolithic metal counterparts in applications where good fatigue performance, corrosion resistance, and excellent specific strength and stiffness properties are desirable. The presence of the metal sheets also provides enhanced impact performance compared to conventional all-fibre-reinforced polymer (FRP) laminates. Consequently, FMLs have become choice materials in the aerospace sector for primary and secondary structures. Out-of-autoclave manufacturing processes with shorter cycle times and lower associated costs are required to facilitate continued cross-sectoral growth for these hybrid materials. Vacuum-assisted resin transfer moulding (VARTM), a cost-effective process [1,2] with relatively short cycle times has proven to be a viable alternative production technique for FMLs. VARTM-fabricated FMLs can now be produced by replacing the non-permeable metallic sheets in traditional FMLs with strategically perforated sheets. The perforations serve as resin flow paths during processing and as such, facilitate through-thickness permeation of resin. As a result, this process is well established for FMLs with low-viscosity thermosetting (TS) matrices but has had limited applicability to thermoplastic (TP) FMLs due to their high melt viscosities. Consequently, there is a paucity of published literature on VARTM-fabricated TP-FMLs.

In recent years, infusible grades of reactive thermoplastic resins have made it possible to produce TP-matrix composites comprising long reinforcing fibres. The suitability of liquid TP acrylic resins for the production and characterisation of FMLs using vacuum infusion and in-situ polymerisation processes has been demonstrated by way of research involvement with an EPSRC-funded feasibility project. Working with Dr Dimitrios Mamalis as the Postdoctoral Researcher and Dr Dipa Roy as Principal Investigator,

thermoplastic fibre-metal laminates were successfully produced by a room-temperature vacuum infusion process as shown in Figure B-1 using the liquid acrylic resin.

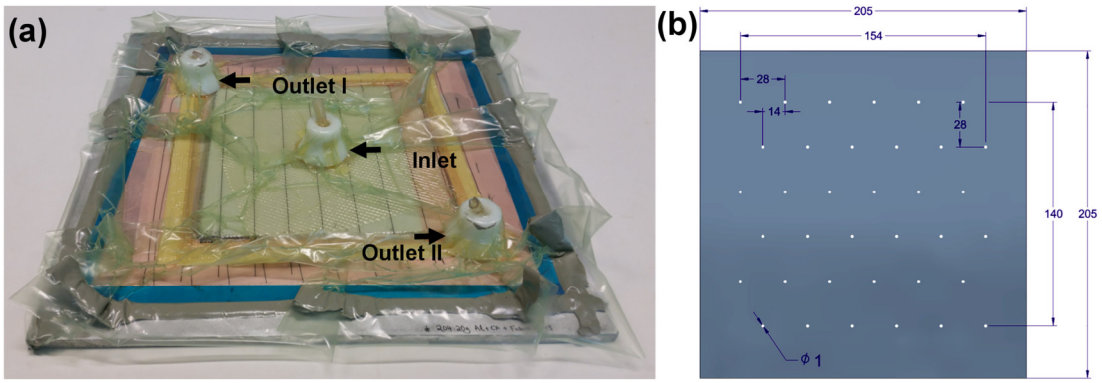


Figure B-1. (a) VARTM set-up and (b) perforation design of the Al alloy sheet utilised for TP-FML fabrication [3].

Taking advantage of the resin's reactivity, an adhesion-promoting epoxy acrylate coating was applied to enhance the interfacial bond between the interlaminar metal substrate and the adjacent laminate. Scanning electron microscopy (SEM) inspections of the interface, as shown in Figure B-2 confirmed that good interfacial bonding was achieved.

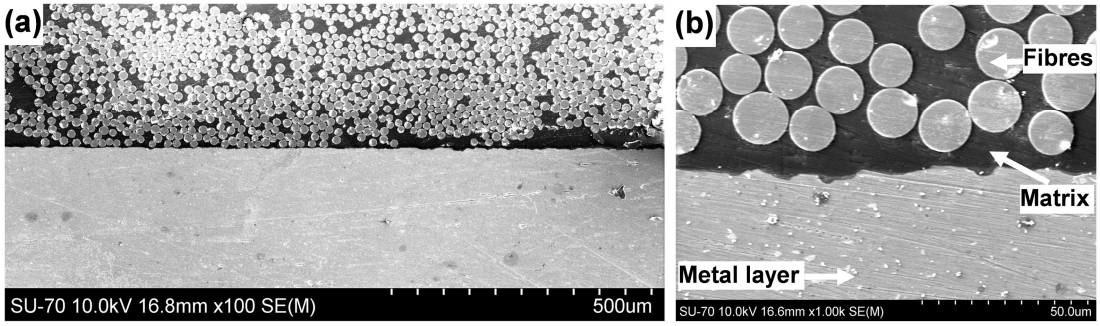


Figure B-2. (a) Low- and (b) high-magnification SEM micrographs showing the interface between the fibre-reinforced acrylic and the aluminium substrates of the TP-FML [3].

B.1.2 Waste management and infusion repair

At the heart of decision-making across many industries in today's cost- and green- driven market, there has been a shift of focus towards sustainable development which "seeks to meet the needs and aspirations of the present without compromising the ability to meet those of the future" [4]. Within the composites industry, the desire to attain circularity continues to be a significant research driver. Recent technological developments on enhancing the repair- and recycle- (reuse and repurpose) potential of FRPs to ensure that

minimal threat is posed to the environment and that near-absolute reclamation of resources from production operations to end-of-service decommissioning. The development of solutions to long-standing issues with production and end-of-life waste is an important area of current research activities.

Thermoplastic (TP) matrices have a demonstrated superiority over their thermoset (TS) counterparts in terms of recyclability, weldability, thermoformability and repairability. Having historically lagged behind TS matrices due to cost-prohibitive production methodologies, technological advancements in the form of novel reactive TP resins provide more cost-effective alternatives than their high melt-viscosity predecessors. These low-viscosity liquid thermoplastics are suited to liquid composite moulding (LCM) techniques, which were once exclusively used for TS-FRP production [3,5–11].

In terms of LCM production techniques, one of the most common sources of production-related waste is resin-starvation. This type of defect typically occurs due to one or more factors such as low preform permeability, high resin viscosity, and poor tooling design. Novel semipermeable membranes as auxiliary process materials and process simulation have gained significant research attention in recent years as viable solutions to this issue [12–15]; however, the cost and skill involved in the use of such systems may limit cross-sectoral adoption.

By way of a complementary Masters Research project [16], it has been demonstrated that liquid acrylic resins can serve as reactive diluents to aid in defect repair. A laminate was produced in a two-stage resin infusion process at room temperature. This was done to understand the effects of re-infiltration and polymerisation of liquid resin on resin-starved laminates in defect repair operations. The laminate's mechanical and thermomechanical characteristics were comparatively evaluated alongside a conventionally produced laminate. Laminates were fabricated using a liquid thermoplastic acrylic resin. As schematically represented in Figure B-3, the two-stage production process involved the primary infusion of a unidirectional 2 mm-thick preform, comprising four plies of dry glass non-crimp fabric (NCF) reinforcement. Following room temperature polymerisation of this primary laminate, a secondary preform was assembled for infusion. This preform comprised the primary laminate as one half and four new plies dry NCF as

the second half. A perfluoroalkoxy alkane (PFA) insert at the mid-plane created an artificial crack for subsequent bond strength tests.

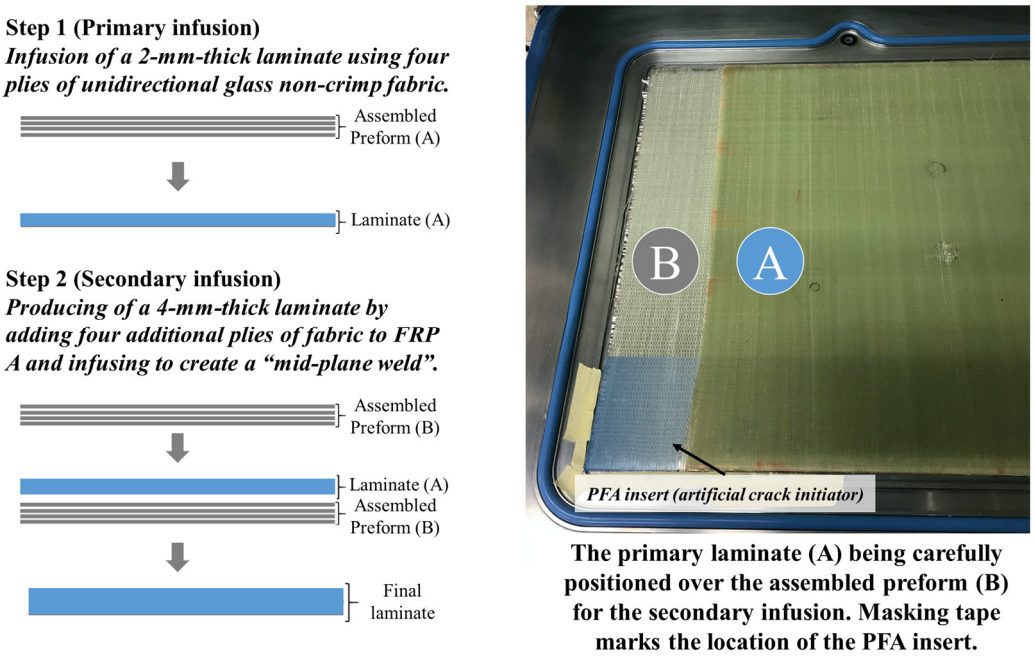


Figure B-3. Two-stage production sequence for the fabrication of the "repaired" laminate. Adapted from a Masters project report by O'Rourke [16].

As shown in the summary of properties obtained by O'Rourke [16], the repaired laminate exhibited superior performance in terms of its transverse tensile strength, mode-I interlaminar fracture toughness (initiation) and short beam shear strength. The reference laminate possessed superior transverse tensile modulus.

Table B-1. Summary of the results reported for infusion repair by O'Rourke [14].

Property	***Reference laminate***	***Repaired laminate***
Fibre volume fraction (%)	74	69
Transverse tensile strength (MPa)	49 ± 2.4	55 ± 4.9
Transverse tensile modulus (GPa)	7.3 ± 1.8	5.7 ± 0.5
Initiation fracture toughness (J/m²)	181 ± 42	448 ± 97
Short beam shear strength (MPa)	42 ± 1.4	52 ±0.9
Glass transition temperature (°C)	108	104

The reported improvements were attributed to the plausible formation of a semi-interpenetrating polymer network at the interface between the two halves of the repaired laminate; i.e., at the mid-plane. It was concluded that this zone favoured the formation of entangled and inter-diffused polymer chains. This possibly increased the resin-rich

region's thickness, which was deemed an important factor in the increased fracture toughness.

B.1.3 Impact damage repair

A feasibility study was also conducted to assess the repairability of impact-damaged acrylic-matrix composite materials. This was done by subjecting impact damaged coupons to heat and pressure on a LAB 450 PEI hot-press. Samples were resized (150 mm × 45 mm) as described in Section 5.1.4.8, and heated to 200°C between rigid steel platens and held isothermally for 3 minutes. Active cooling was performed at 10°C/min to bring the samples to 30°C while pressure was maintained at 29.5 bar throughout the heating and cooling segments. This repair operation was performed on two samples per energy level. Back-lit images of the impact-damaged coupons were taken as previously described in Section 4.2. to assess the extent of repair attained. Moreover, pristine samples were also subjected to the same repair procedure to assess the effects of the procedure on the properties under investigation. Representative before and after images are shown in Figure B-4.

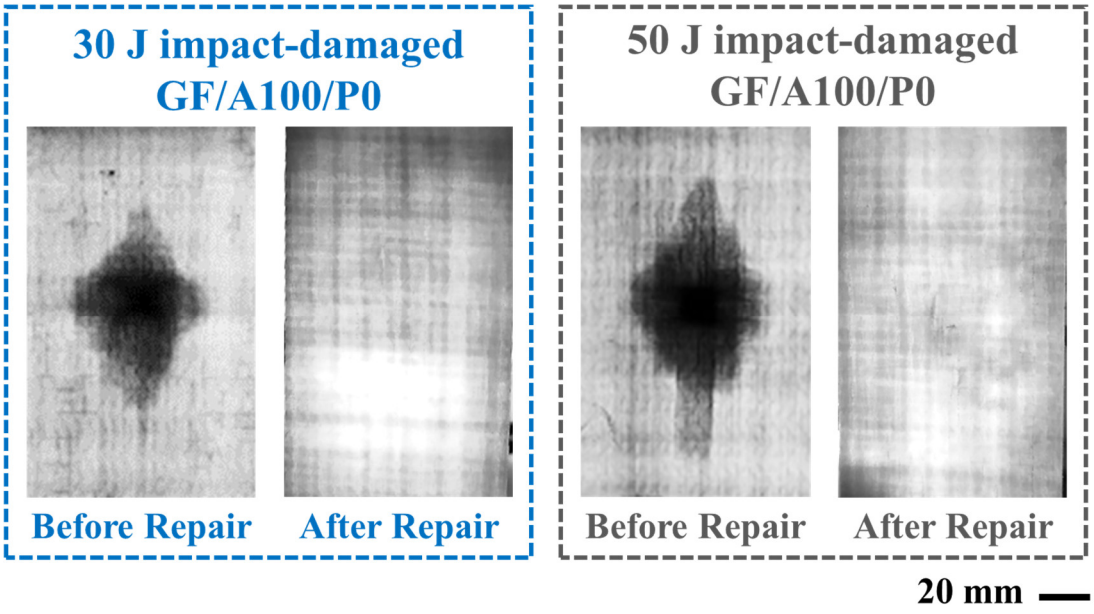


Figure B-4. High-contrast back-lit images of impact-damaged coupons before and after hot-press repair (Temperature: 200°C; Pressure: 29.5 bar; Duration: 3 minutes).

Samples were loaded in flexure to failure using the methodology reported in Section 5.1.4.8 to evaluate this method's repair efficiency. The comparative strengths, moduli and failure strains are presented in Figure B-5.

As shown in Figure 8-5a, despite effectively 'healing' of the damaged site, the repair operation did not appear to restore the samples' structural integrity. Understandably, thermal repair can only be deemed effective for matrix cracks, and would not restore interfacial debonding and fibre fractures. Thus, where matrix cracks are the dominant impact-damage mechanism, the proposed methodology would perhaps offer more considerable repair efficiency. However, it is worth noting that when the comparative performance of the pristine samples before and after the repair operation was assessed, reductions were observed in the corresponding strengths and moduli after the operation was performed. These reductions suggest that the temperature and pressure employed for repair were not favourable for the materials, as evidenced by the deleterious effects on the structural integrity of the damage-free samples.

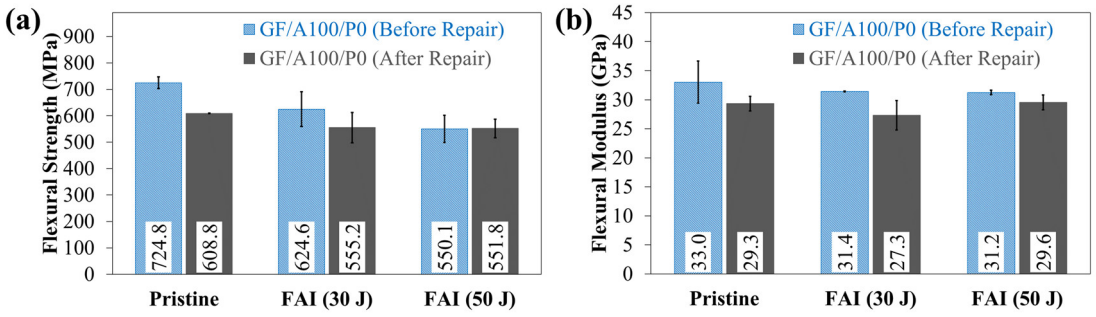


Figure B-5. Post-impact flexural (a) strength, (b) modulus as functions of damage and repair conditions.

While care was taken to perform the repair below the major thermal degradation temperature as determined by thermogravimetric methods in Section 7.2.3, performing the repair procedure in the presence of oxygen may likely have resulted in degradation below the major degradation temperature. An additional thermogravimetric analysis similar to the technique described in Chapters 6 and 7 would need to be carried out in the presence of air to gain insights into possible oxidative thermal degradation of this material. Although it is feasible to realise healing of damage using heat and pressure, other intrinsic factors such as the effects of existing interfacial failures must also be investigated. However, these findings provide vital insights that are intended to inform further investigations towards the development of an appropriate repair methodology that takes advantage of the post-processibility of the acrylic matrix. Moreover, it concomitantly demonstrates the viability of these resins for thermoforming and thermal joining applications.

B.1.4 Selective modification strategies

Besides the hybridisation route developed as part of this PhD research, other methodologies were explored by way of a Masters Research project [17]. This project aimed to develop alternative methodologies for incorporating PPE into the laminate to facilitate higher loadings without compromising the low viscosity of the acrylic resin. Thus, two techniques involving the dispersal of PPE directly within the preform were employed. The first approach applied the PPE powder between plies of the glass fibre reinforcement before resin infusion was performed at room temperature. The second employed an intermediate preforming step to consolidate the powder under a vacuum bag over a heated mould (180°C) for 20 minutes. This preform was subsequently cooled down passively overnight while maintained under vacuum. Furthermore, two PPE loadings (7.5 wt. % and 20 wt. %) were investigated to study the effect of PPE content on performance. Thus, the following three PPE-modified acrylic-matrix laminates summarised in Table B-2 were produced and compared to a reference acrylic laminate.

Table B-2. Summary of PPE-modified acrylic laminates investigated by Jones [17].

PPE content (wt. %)	PPE incorporation method	Fibre volume fraction (%)	Void volume fraction (%)
7.5	Loose powder dispersal	57	2.5
7.5	Preformed	56	7
20	Preformed	54	2.3

As shown in Figure B-6, traces of PPE are evident for the preformed sample, which was reported to be due to differences in PPE surface area within both systems. Moreover, preforming appeared to inhibit resin infiltration, evidenced by the characteristics of poor wetting, such as the presence of voids and poor interfacial adhesion. The zone of unreacted PPE is likely to have been due to the limited flow of resin occurring as a result of partial PPE consolidation after the preforming process.

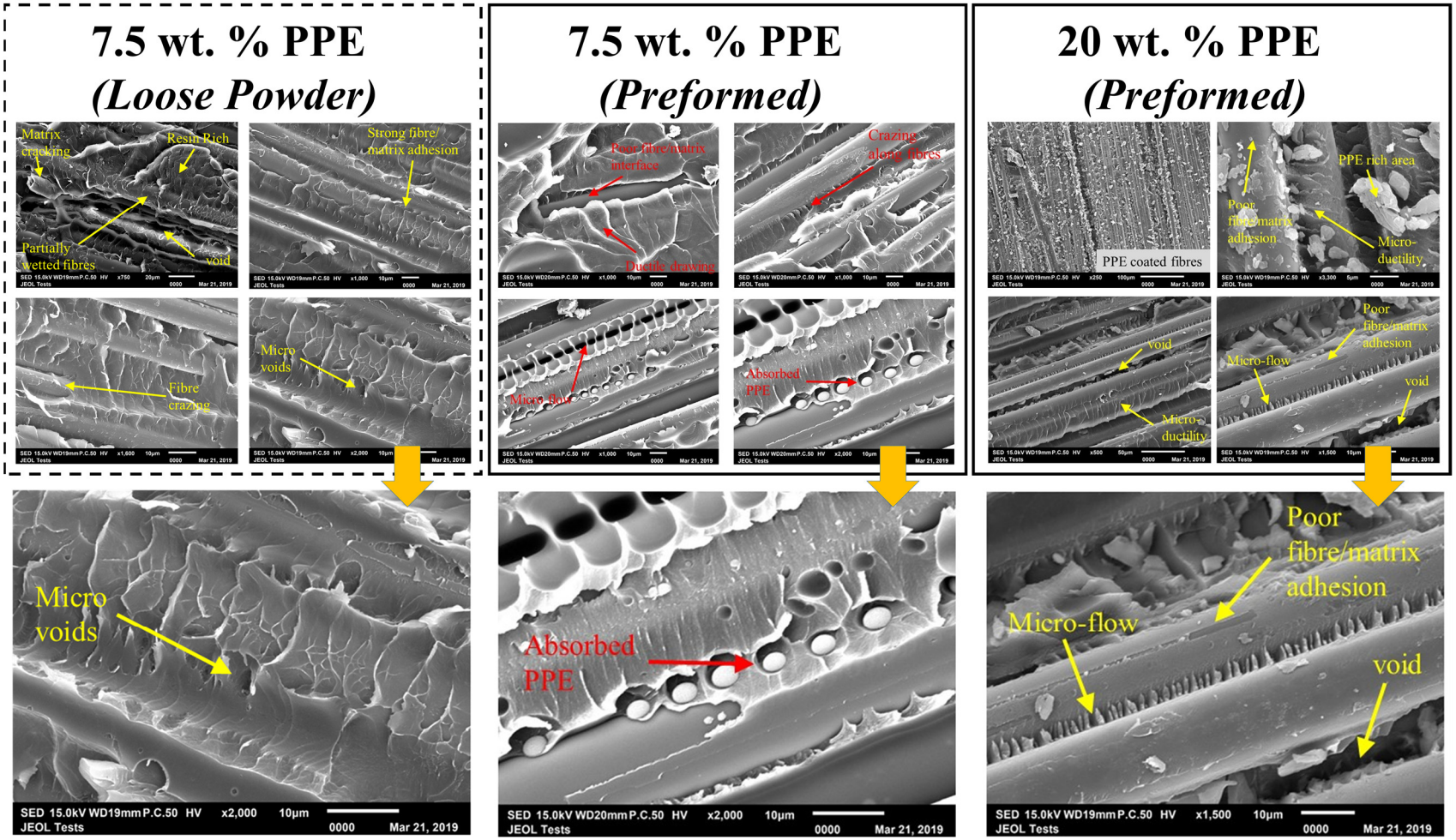


Figure B-6. Scanning electron micrographs of mode-I interlaminar fracture surfaces of acrylic-PPE hybrid matrix composites prepared using loose powder and preforming approaches. Note: these micrographs are a compilation of those reported by Jones [17].

Interestingly, increasing PPE content to 20 wt. % appeared to produce more brittle matrix fracture characteristics, whereas, some evidence of microstructural ductility can be observed in the micrographs of the 7.5 wt. % PPE-content samples. However, transverse tensile testing revealed higher strain-to-failure in the samples containing 20 wt. % of PPE than those containing 7.5 wt. % of PPE prepared using the same method. These findings constitute insightful findings and can serve as foundational knowledge for future research.

Most importantly, this study's findings highlight the possibility of interlaminar dispersal of modifiers into the acrylic-matrix composite system. It opens up opportunities for exploring other grades of materials to enhance the resulting hybrid composite material. Moreover, other similar grades of PPE and suitably selected catalysts may be considered for effective hybridisation of acrylic resins that require higher-temperature polymerisation cycles.

References

[1] Naik NK, Sirisha M, Inani A. Permeability characterization of polymer matrix composites by RTM/VARTM. Prog Aerosp Sci 2014;65:22–40. https://doi.org/10.1016/j.paerosci.2013.09.002.

[2] Jensen BJ, Cano RJ, Hales ' SJ, Alexa2 JA, Weiser ES, Loos AC, et al. Fibre metal laminates made by the VARTM process 2009. https://ntrs.nasa.gov/api/citations/20090028660/downloads/20090028660.pdf (accessed May 30, 2021).

[3] Mamalis D, Obande W, Koutsos V, Blackford JR, Ó Brádaigh CM, Ray D. Novel thermoplastic fibre-metal laminates manufactured by vacuum resin infusion: The effect of surface treatments on interfacial bonding. Mater Des 2019;162. https://doi.org/10.1016/j.matdes.2018.11.048.

[4] Rosen MA, Kishawy HA. Sustainable manufacturing and design: Concepts, practices and needs. Sustainability 2012;4:154–74. https://doi.org/10.3390/su4020154.

[5] Obande W, Ray D, Ó Brádaigh CM. Viscoelastic and drop-weight impact properties of an acrylic-matrix composite and a conventional thermoset

composite – A comparative study. Mater Lett 2019;238. https://doi.org/10.1016/j.matlet.2018.11.137.

[6] Obande W, Mamalis D, Ray D, Yang L, Ó Brádaigh CM. Mechanical and thermomechanical characterisation of vacuum-infused thermoplastic- and thermoset-based composites. Mater Des 2019;175. https://doi.org/10.1016/j.matdes.2019.107828.

[7] Cousins DS, Suzuki Y, Murray RE, Samaniuk JR, Stebner AP. Recycling glass fiber thermoplastic composites from wind turbine blades. J Clean Prod 2019;209:1252–63. https://doi.org/10.1016/j.jclepro.2018.10.286.

[8] Murray RE, Jenne S, Snowberg D, Berry D, Cousins D. Techno-economic analysis of a megawatt-scale thermoplastic resin wind turbine blade. Renew Energy 2019;131:111–9. https://doi.org/10.1016/j.renene.2018.07.032.

[9] Murray J, Mccarthy ED, Murray JJ, Gleich K, Mccarthy ED, Brádaigh CÓ. Properties of Polyamide-6 Composites Using a Low-Cost Thermoplastic Resin Transfer Moulding System. 22nd Int Conf Compos Mater 2019.

[10] Ó Máirtín P, McDonnell P, Connor M, Eder R, Ó Brádaigh CM. Process investigation of a liquid PA-12/carbon fibre moulding system. Compos Part A 2001;32:915–23.

[11] Coll SM, Murtagh AM, Ó Brádaigh CM. Resin film infusion of cyclic pBT composites: a fundamental study. Proc. SAMPE Eur. 25th Int. Jubil. Conf., Paris: 2004.

[12] Heider D, Gillespie JW. VARTM Variability and Substantiation. n.d.

[13] Heider D, Simacek P, Dominauskas A, Deffor H, Advani S, Gillespie JW. Infusion design methodology for thick-section, low-permeability preforms using inter-laminar flow media. Compos Part A Appl Sci Manuf 2007;38:525–34. https://doi.org/10.1016/j.compositesa.2006.02.016.

[14] Han K, Jiang S, Zhang C, Wang B. Flow modeling and simulation of SCRIMP for composites manufacturing. Compos Part A Appl Sci Manuf 2000;31:79–86. https://doi.org/10.1016/S1359-835X(99)00053-6.

[15] Garschke C, Weimer C, Parlevliet PP, Fox BL. Out-of-autoclave cure cycle study of a resin film infusion process using in situ process monitoring. Compos Part A Appl Sci Manuf 2012;43:935–44.

https://doi.org/10.1016/j.compositesa.2012.01.003.

[16] O'Rourke K. Investigating repairability of in-situ polymerisable thermoplastic composites. The University of Edinburgh [Masters Thesis], 2020.

[17] Jones MCS. Enhancing mechanical properties of acrylic matrix composites. The University of Edinburgh [Masters Thesis], 2019.

Appendix C Supplementary Information

C.1 Supplementary Information for Chapter 6

C.1.1.1 Activation energy for thermal decomposition

Using the data presented in Section 6.4.4, activation energies for thermal decomposition were assessed as described in work by Ray et al. [1]. Figure C-1 shows the influence of PPE content on the determined activation energies associated with total thermal decomposition for polymeric blend samples. Activation energy is a critical energy level that must be overcome by the reactants within a system for a reaction to occur. Thus, an increase in activation energy typically indicates an increase in thermal stability for decomposition [2]. From Figure C-1, activation energy did not appear to change drastically with increasing PPE content. However, up to 5 wt. % (A95/P5) a slight increase can be observed. While it is likely that increasing the PPE content beyond the scope of the range considered within this work would result in more significantly increased activation energies, the higher concentrations (10 wt. % and 15 wt. % appear to exhibit lower activation energies. Evidently, 5 wt. % is the upper limit within the range of concentrations explored. Unfortunately, it was not possible to consider higher contents due to the potential for instability in the miscibility for the processing conditions employed in this work.

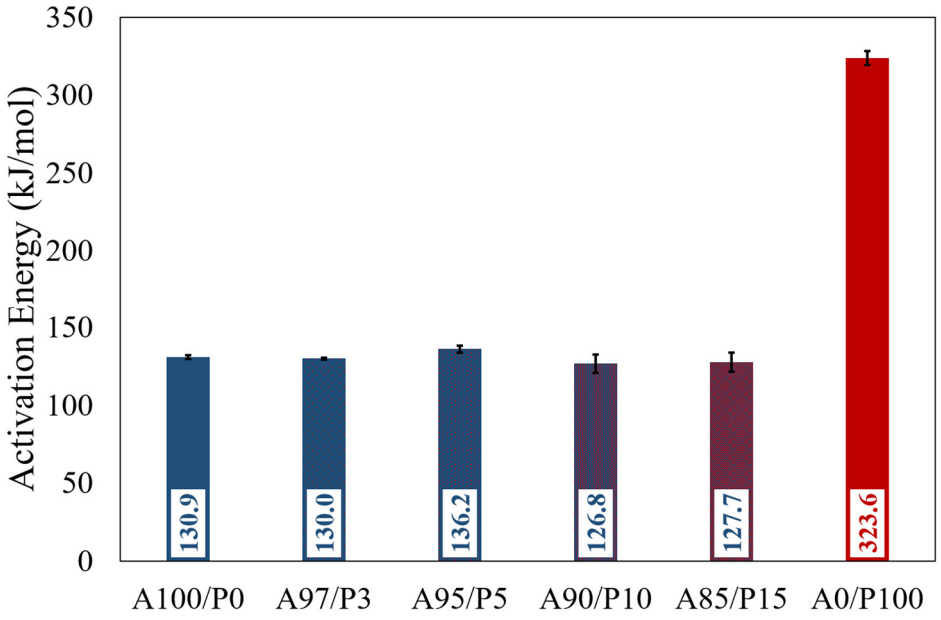


Figure C-1. Activation energies for degradation reactions for acrylic and PPE-modified acrylic polymers; results show the influence of PPE content on thermal stability. These energies were assessed using the data in Section 6.4.4.

C.1.1.2 Reshapability trials on unreinforced neat and PPE-modified acrylic samples

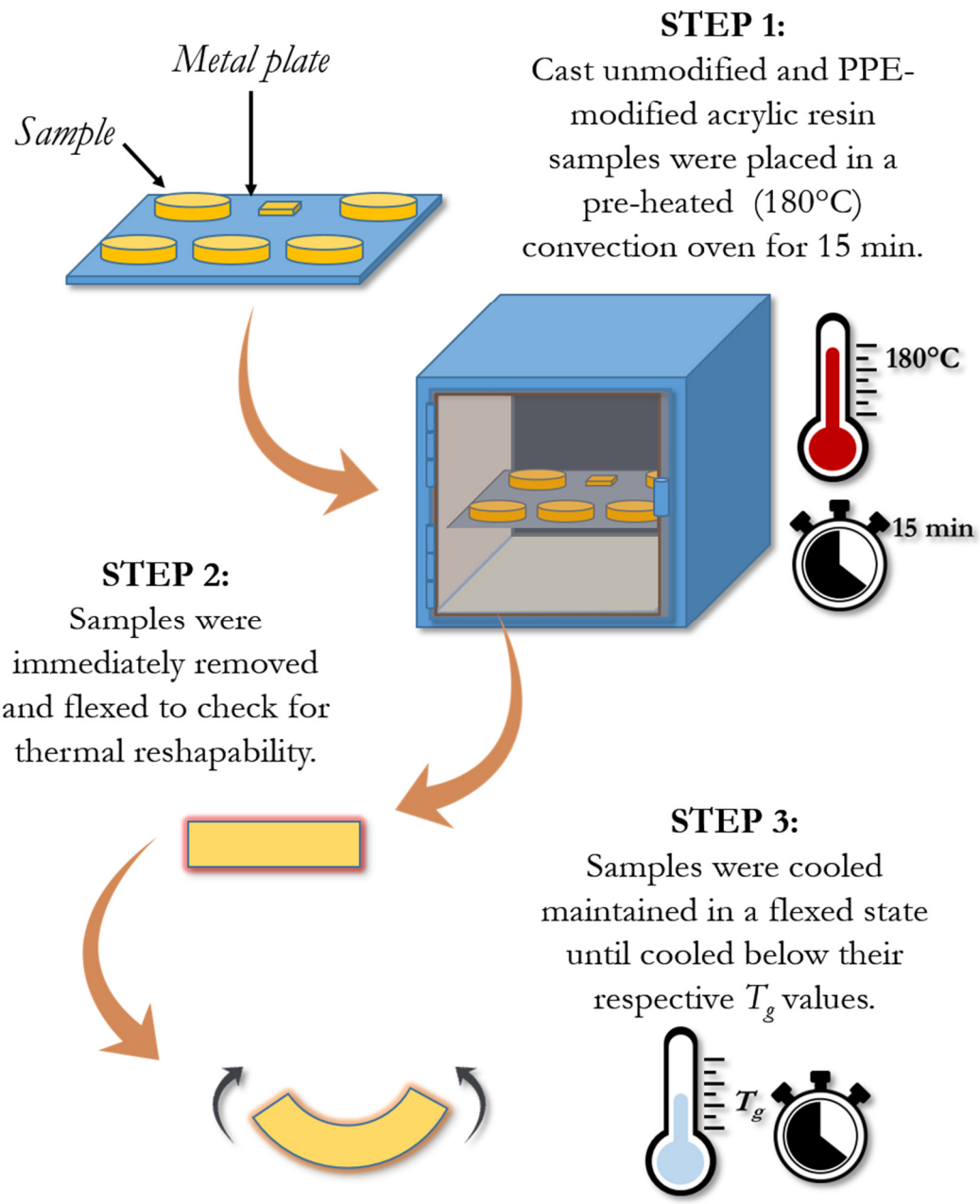


Figure C-2. Methodology for ascertaining the reshapability of unreinforced neat and PPE-modified acrylic samples. 40-mm dia. disc samples were used for an epoxy reference, A100/P0, A95/P5, A90/P10 and A85/P15 samples. Due to material availability, a different geometry was used for the A97/P3 sample, which measured (25 × 8 × 4) mm. The associated results are presented and discussed in Section 6.5 (Figure 6-25).

C.2 Supplementary Information for Chapter 7

C.2.1.1 Supplementary charts for mechanical testing reported in Chapter 7

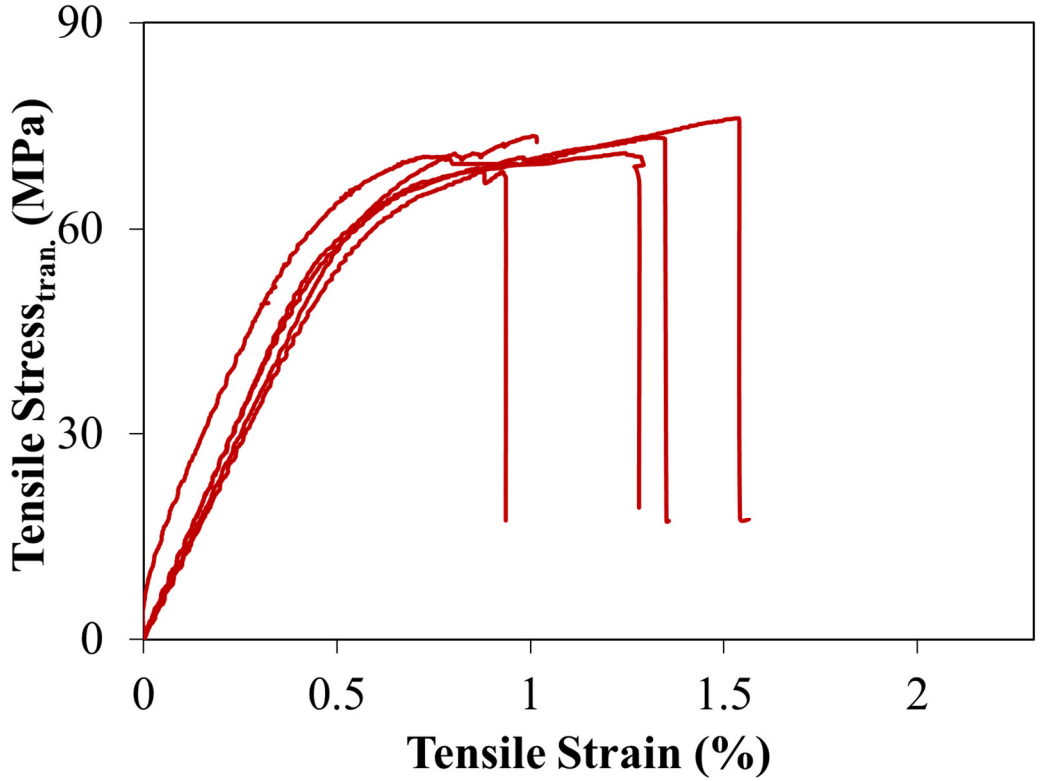


Figure C-3. Transverse tensile stress-strain responses for all GF/A100/P0 samples. A representative chart was presented for this material in Section 7.2.4 (Figure 7-7).

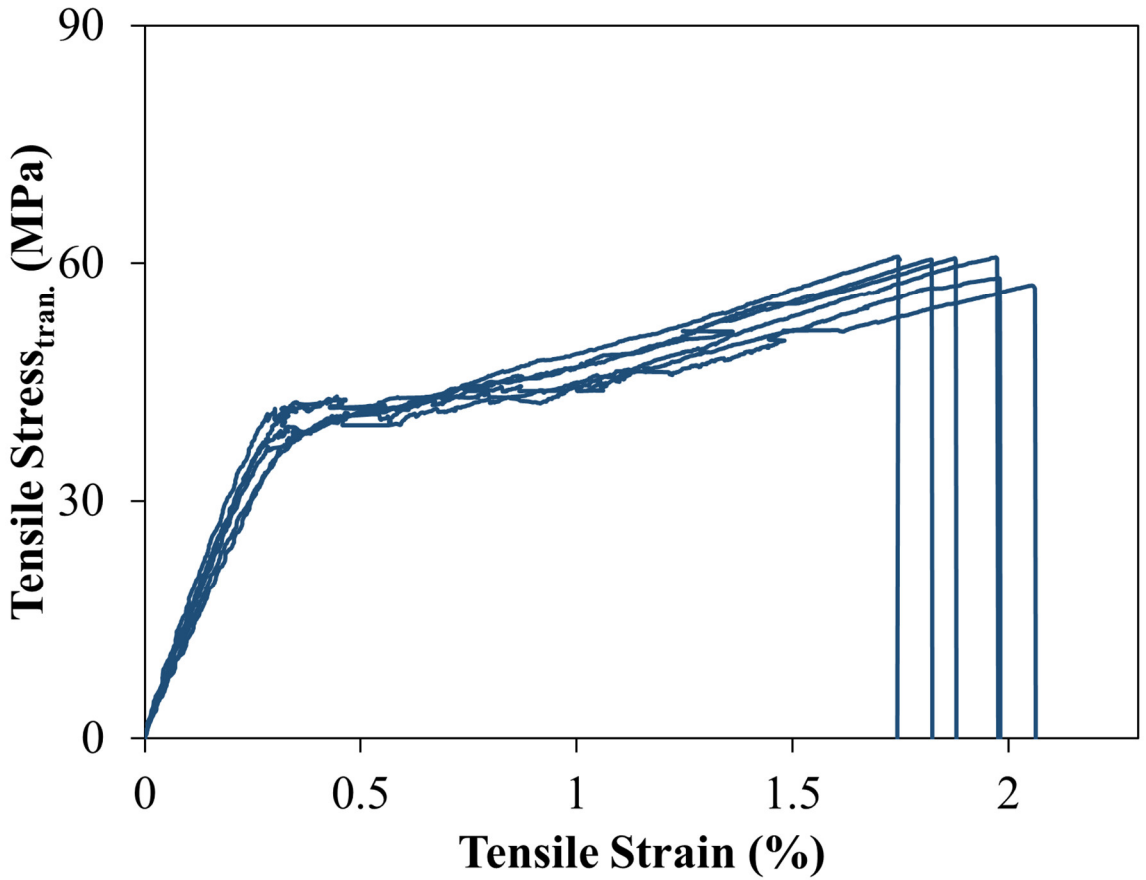


Figure C-4. Transverse tensile stress-strain responses for all GF/A95/P5 samples. A representative chart was presented for this material in Section 7.2.4 (Figure 7-7).

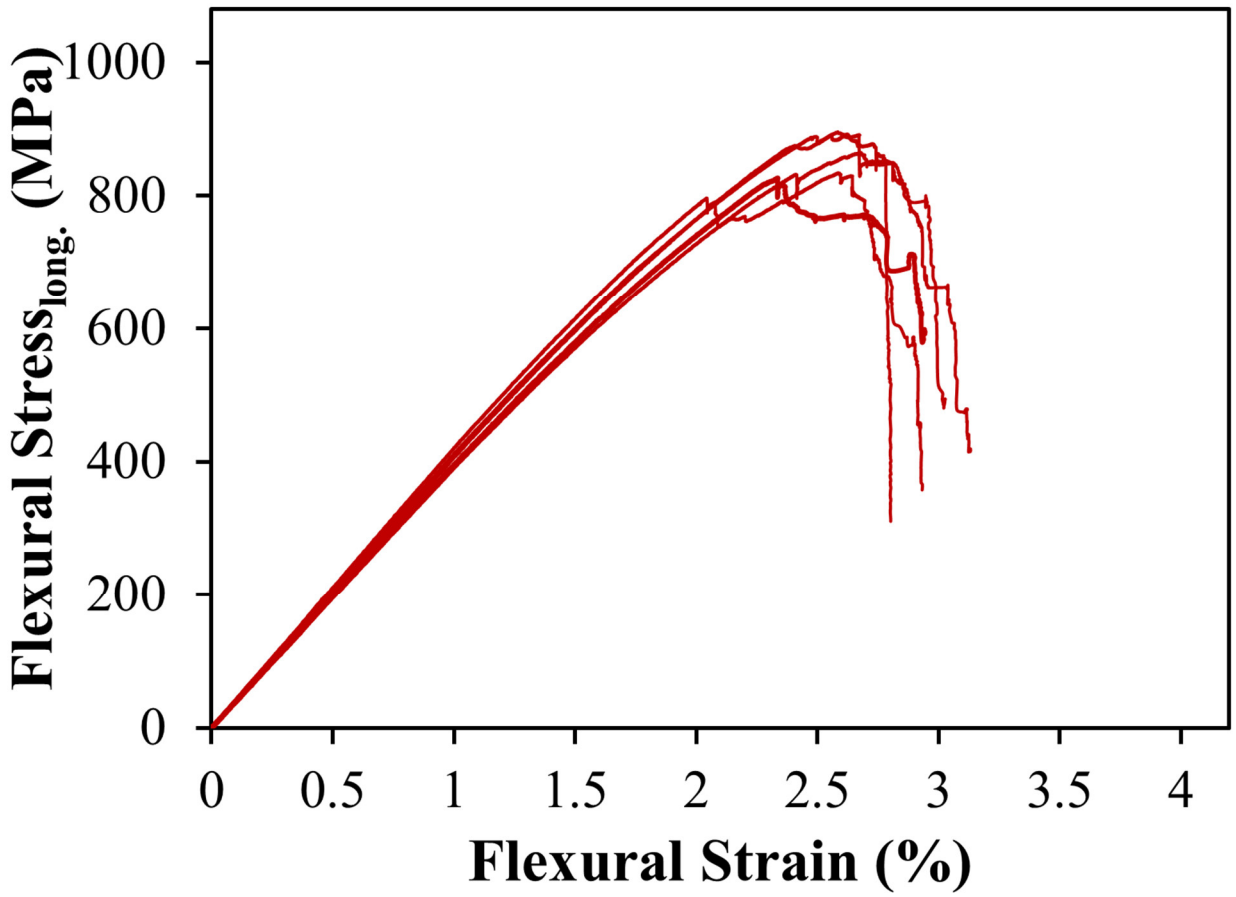


Figure C-5. Longitudinal flexural stress-strain responses for all GF/A100/P0 samples. A representative chart was presented for this material in Section 7.2.5 (Figure 7-9).

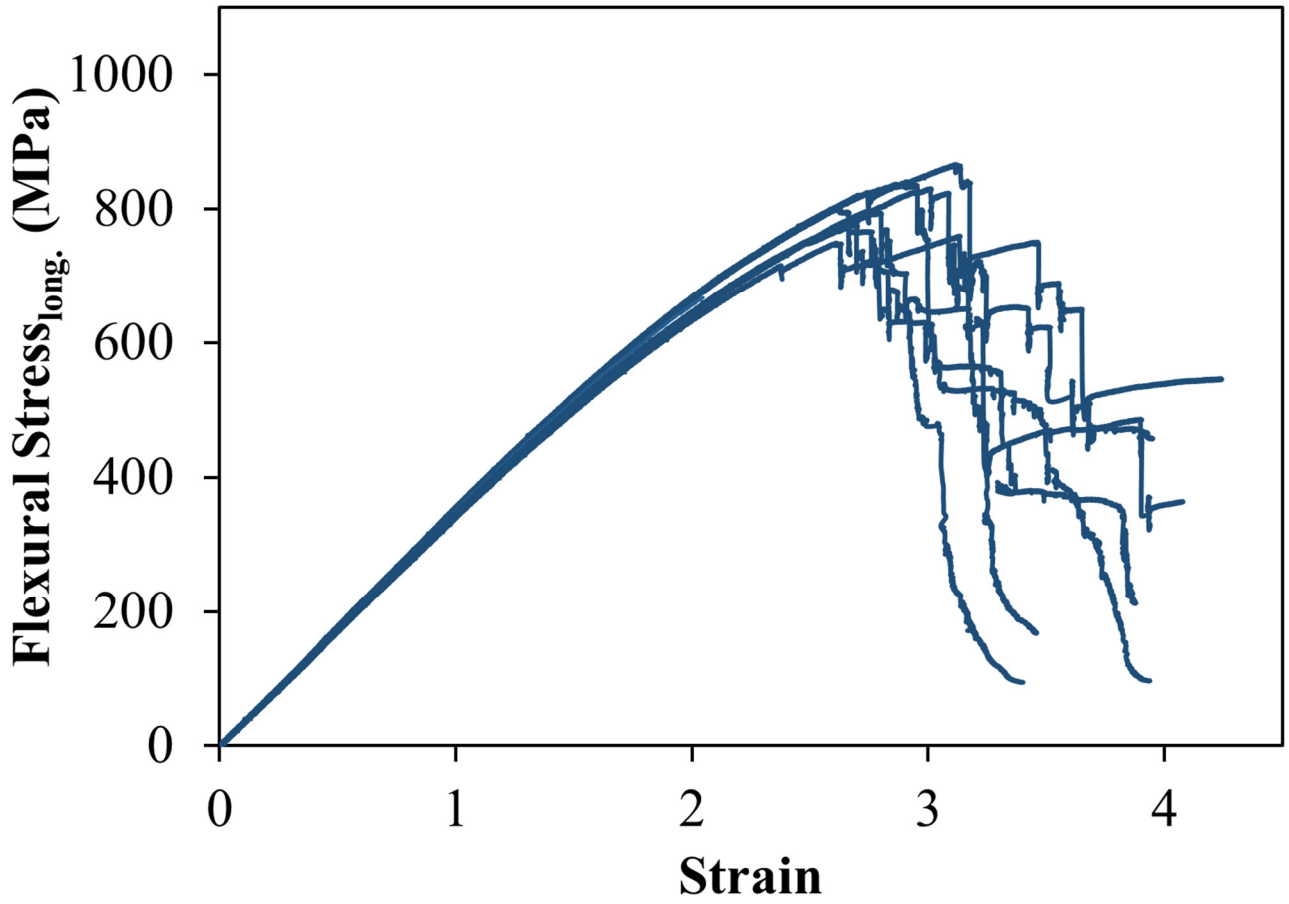


Figure C-6. Longitudinal flexural stress-strain curves for quasi-unidirectional, glass fibre-reinforced GF/A100/P0. A representative chart was presented for this material in Section 7.2.5 (Figure 7-9).

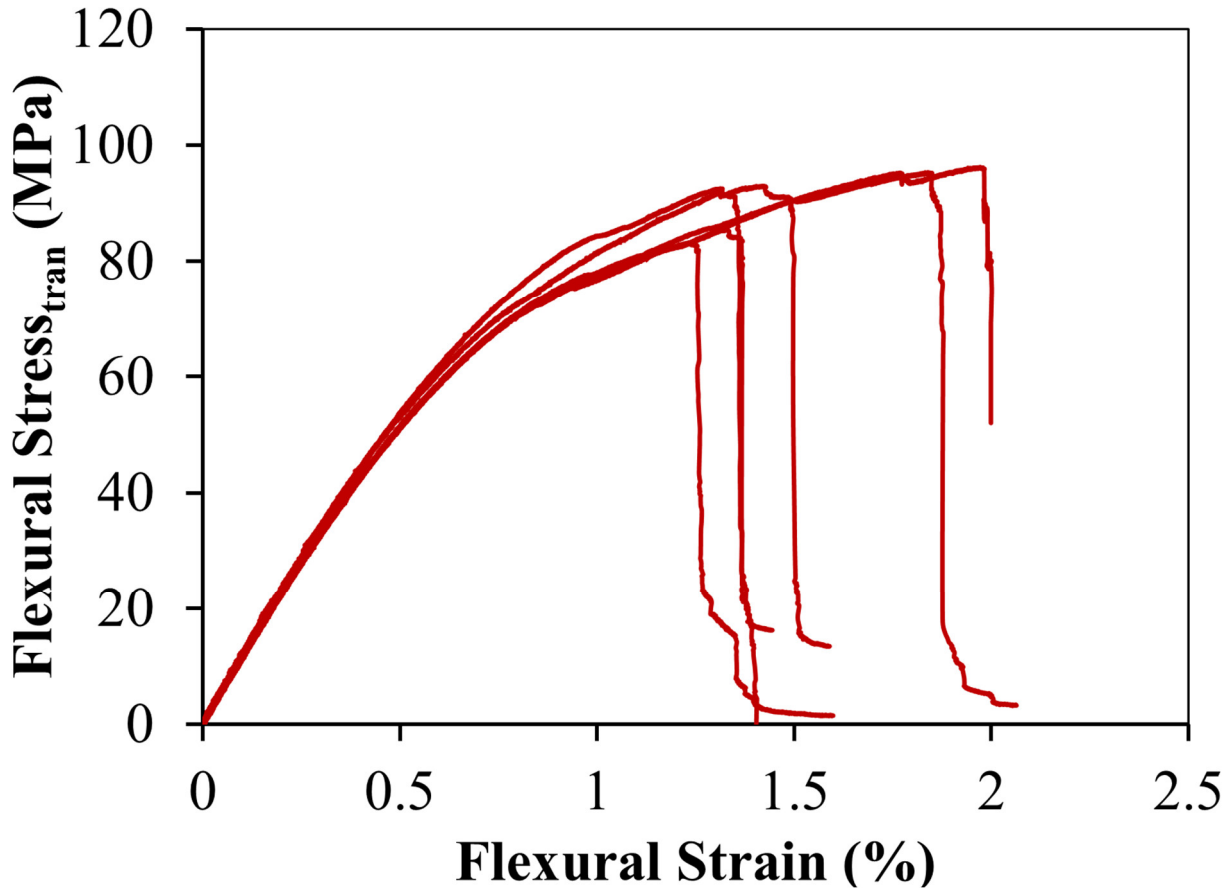


Figure C-7. Transverse flexural stress-strain curves for quasi-unidirectional, glass fibre-reinforced GF/A100/P0. A representative chart was presented for this material in Section 7.2.6 (Figure 7-11).

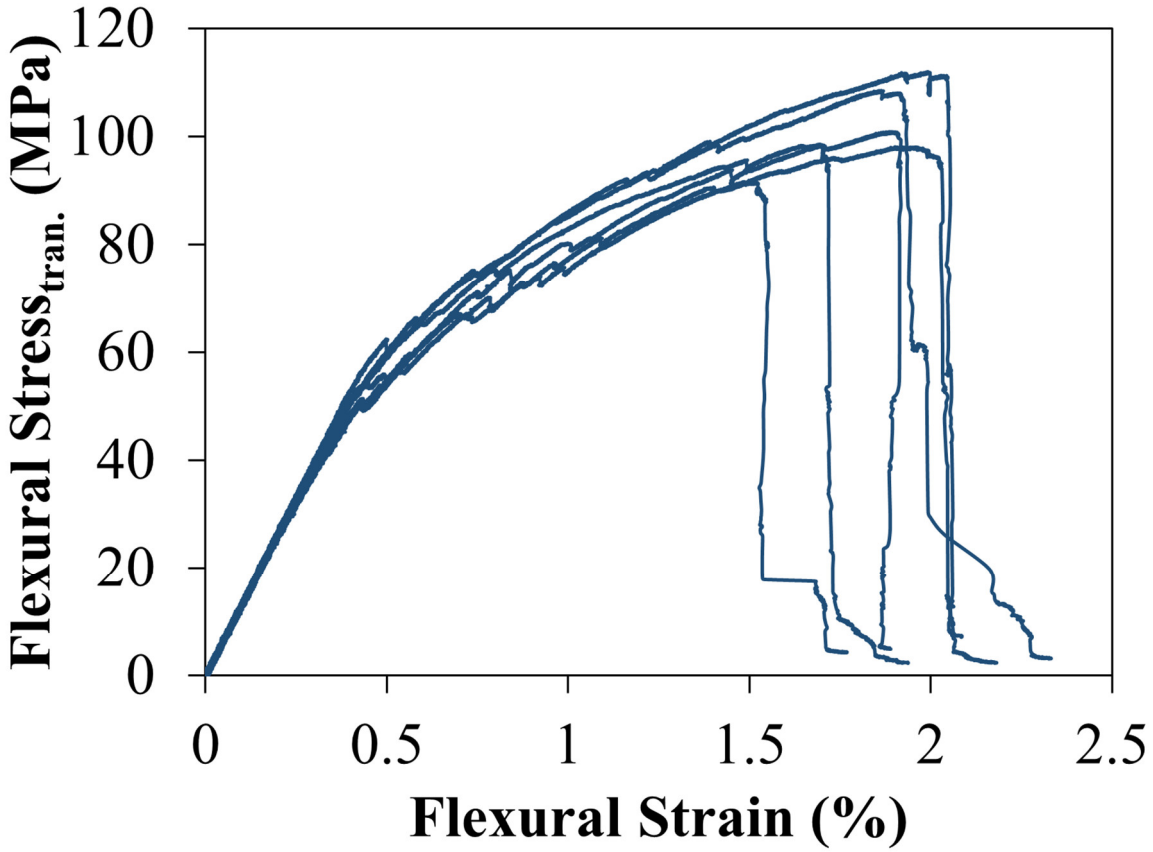


Figure C-8. Transverse flexural stress-strain curves for quasi-unidirectional, glass fibre-reinforced GF/A95/P5. A representative chart was presented for this material in Section 7.2.6 (Figure 7-11).

C.2.1.2 Details of unsuccessful fabrication and characterisation experiments

C.2.1.2.1 Hot-press moulding of neat, unreinforced PPE

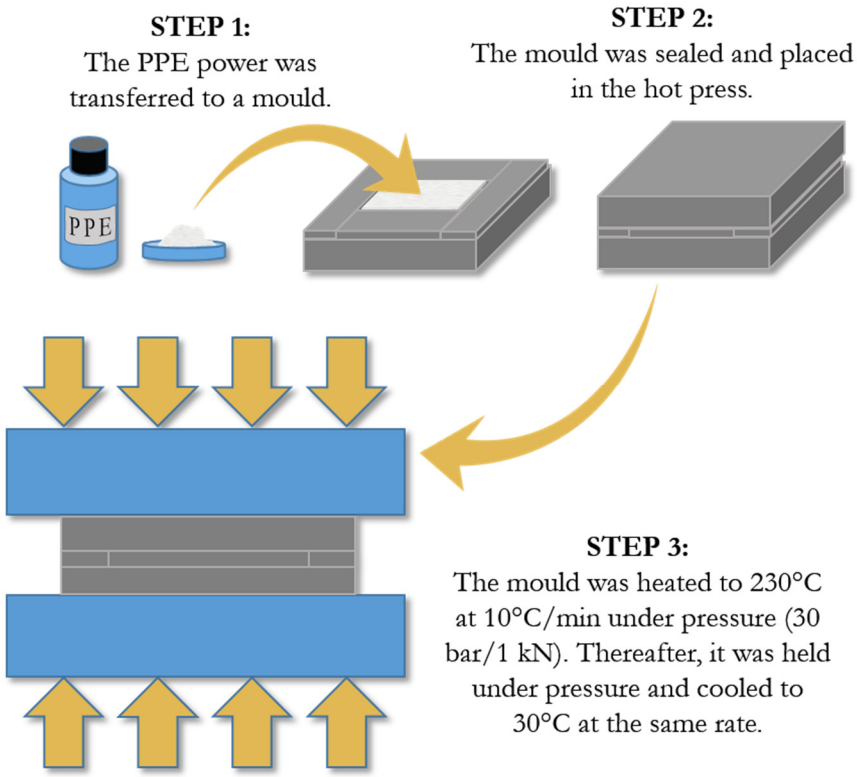


Figure C-9. Illustrative representation of the hot-press moulding attempted for the production of neat unreinforced PPE for characterisation. Results were unfavourable for testing as shown in Figure C-3.

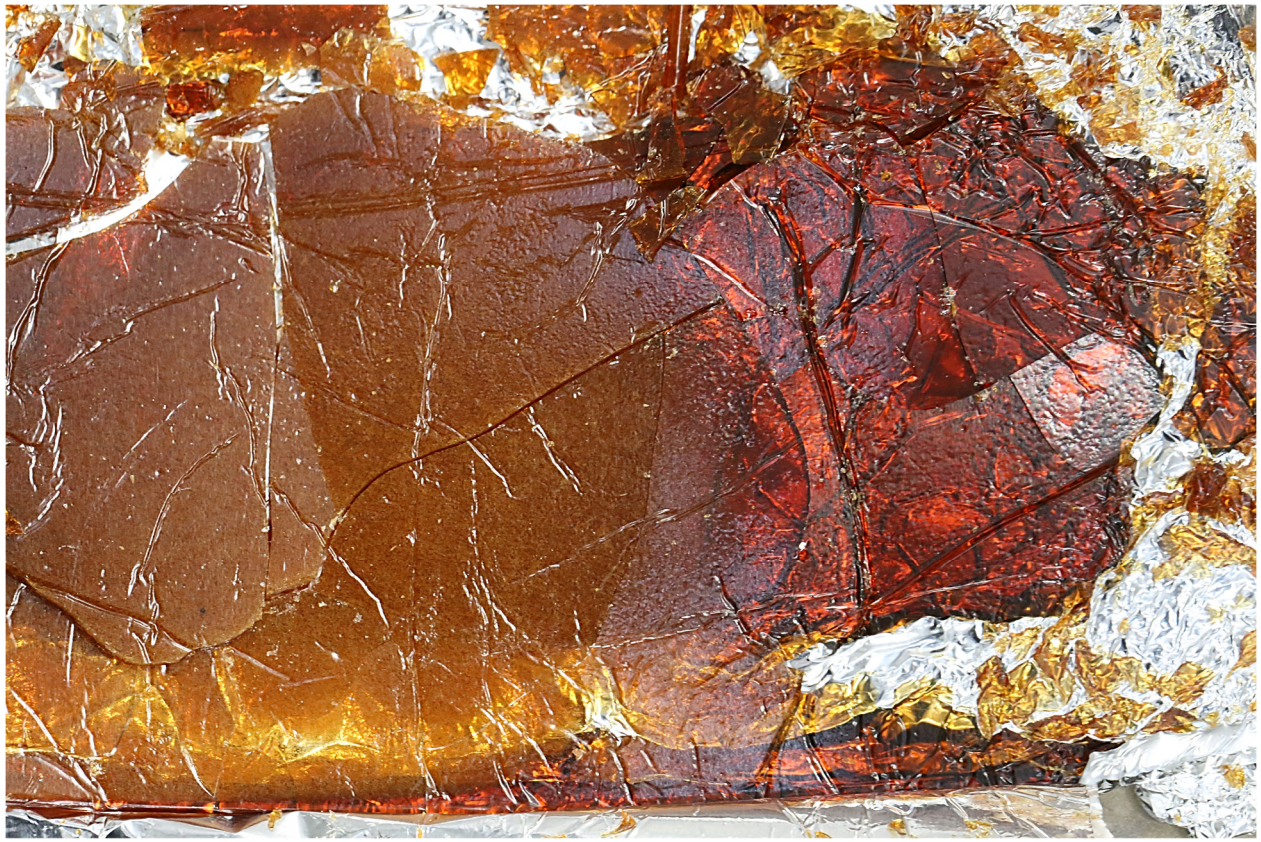


Figure C-10. Fragments of neat, unreinforced PPE obtained from the attempted hot-press moulding of plaques for testing as detailed in Figure C-2. The plaque exhibited poor handleability and was not suited for the extraction of samples for testing.

C.2.1.2.2 Characterisation of interfacial strength of unmodified and PPE-modified acrylic with glass fibre reinforcement by the micro-droplet technique

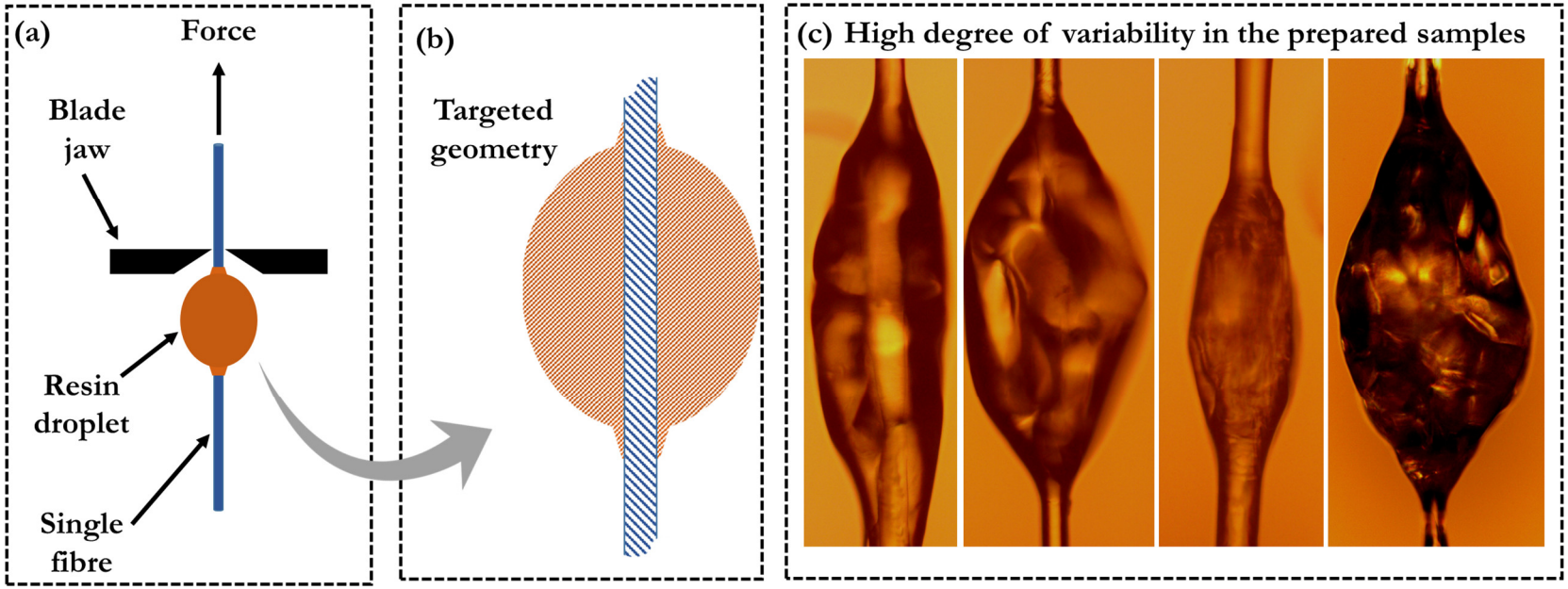


Figure C-11. (a)A graphical representation of the microdroplet test method attempted for characterising the fibre-matrix interface, (b) the targeted geometry, and (c) the obtained samples were not suitable for testing.

C.2.1.3 Fox equation computations

Using Equation 7-1 (Section 7.2.2), the mass fractions of acrylic ($\varphi_{2,A}$) and PPE ($\varphi_{2,B}$) required to attain a T_g value of 393 K were estimated as follows:

$$\frac{1}{T_{gN}} = \frac{\varphi_{2,A}}{T_{gN,A}} + \frac{\varphi_{2,B}}{T_{gN,B}} = \frac{\varphi_{2,A}}{T_{gN,A}} + \frac{1-\varphi_{2,A}}{T_{gN,B}}$$

$$\frac{1}{393} = \frac{\varphi_{2,A}}{377} + \frac{1-\varphi_{2,A}}{433}$$

$$\frac{1}{393} = \frac{56\varphi_{2,A} + 377}{(377)(433)}$$

$$56\varphi_{2,A} = 38.37$$

$$\varphi_{2,A} = 0.69$$

$$\varphi_{2,B} = 1 - 0.68 = 0.31$$

Where and $\varphi_{2,B}$ are mass fractions of acrylic and PPE, respectively, the sum of which equals unity; T_{gN} is the glass transition temperature corresponding to the peaks shown in Figure 7-4; $T_{gN,A}$ and $T_{gN,B}$ are the glass transition temperatures of the acrylic and PPE constituents, respectively. Note: all T_g values were used in Kelvin.

C.2.1.4 SEM micrographs of DCB fracture behaviour

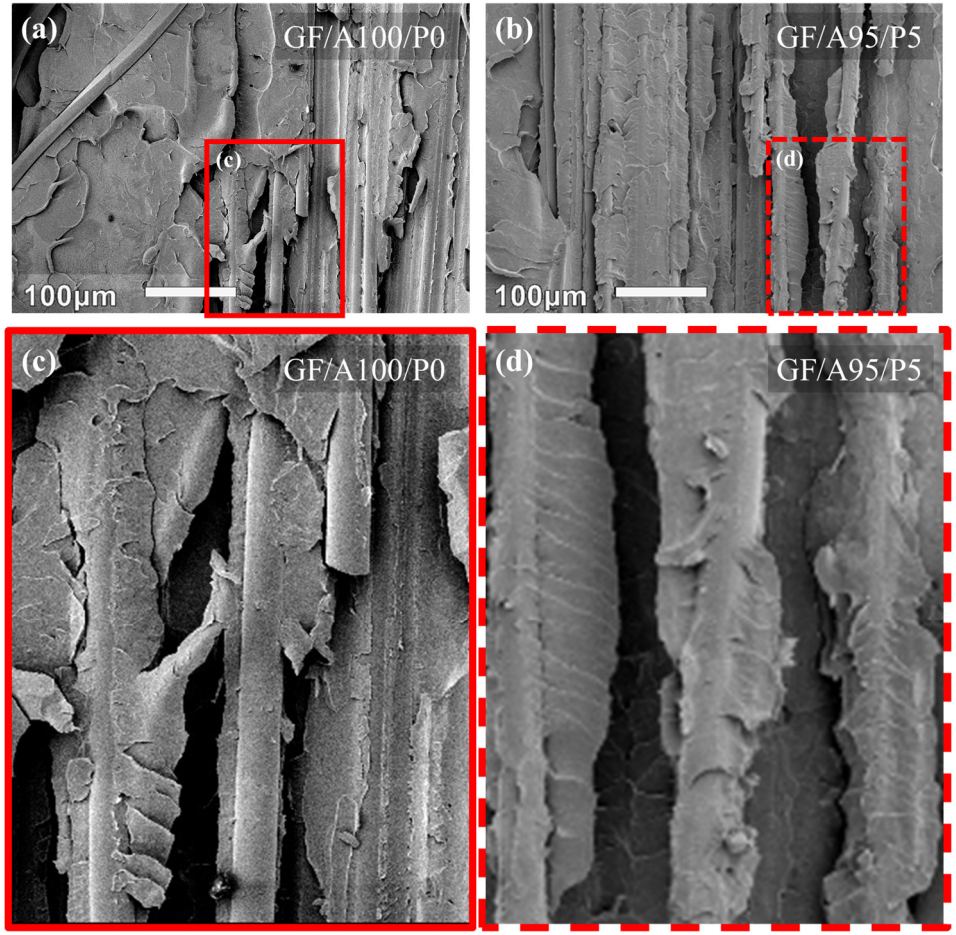


Figure C-12. SEM micrographs of GF/A100/P0 ((a) & (c), and GF/A95/P5 (b) & (d) fracture surfaces. Greater matrix coverage on fibres on GF/A95/P5 is indicative of enhanced interfacial adhesion.

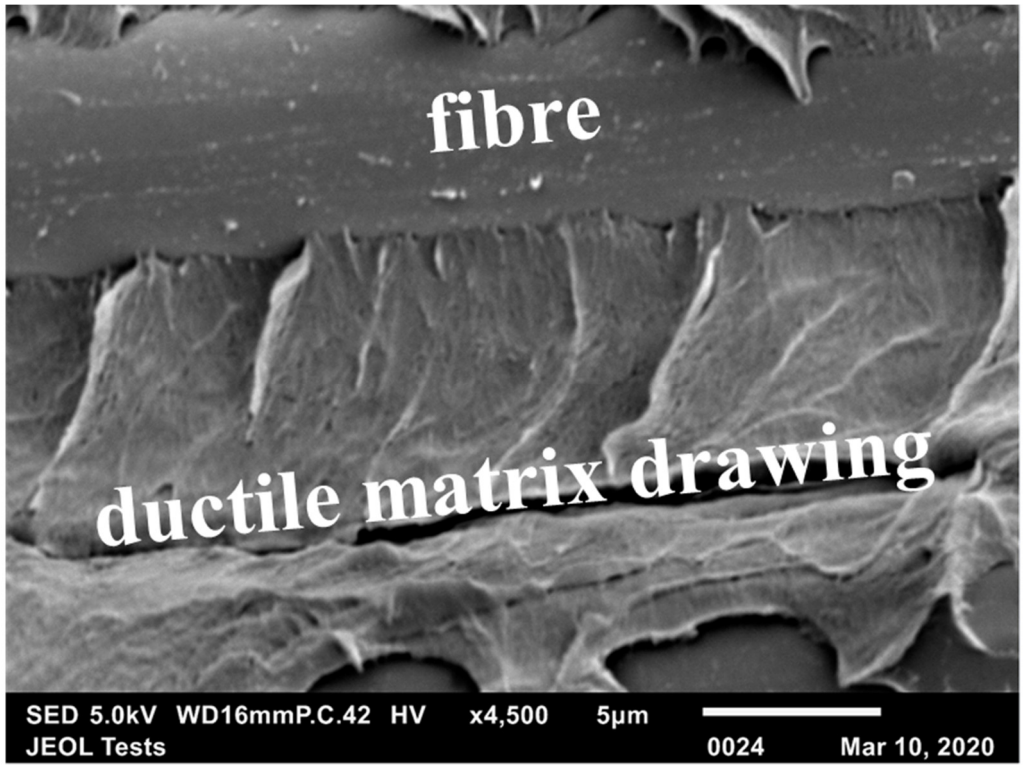


Figure C-13. Evidence of pronounced matrix ductility on the DCB fracture surface of a GF/A95/P5 sample.

References

[1] Ray D, Banerjee S, Mohanty AK, Misra M. Thermal and electrical behavior of vinylester resin matrix composites filled with fly ash particles. Polym Compos 2008;29:58–62. https://doi.org/10.1002/pc.20354.

[2] Mishra R, Tripathy SP, Fink D, Dwivedi KK. A study of the activation energy of thermal decomposition of irradiated polymers. Radiat Eff Defects Solids 2004;159:569–73. https://doi.org/10.1080/10420150412331326958.

Appendix D: Peer-Reviewed Publications of the Author

The respective studies presented in this PhD thesis (Chapters 2 – 7) are based on peer-reviewed publications. Details of published works are presented in Appendix D.1 and summarised in Chapter 1 (Table 1-1).

D.1 Published Journal Articles

Obande, W., Gruszka, W., Garden, J., Wurzer, C., Ó Brádaigh, C. M., Ray, D., 2021. Enhancing the solvent resistance and thermomechanical properties of thermoplastic acrylic polymers and composites via reactive hybridisation. *Materials & Design*, 109804, https://doi.org/10.1016/j.matdes.2021.109804.

Obande, W., Ó Brádaigh, C. M., Ray, D., 2021. Continuous fibre-reinforced thermoplastic acrylic-matrix composites prepared by liquid resin infusion–A review. *Composites Part B: Engineering*, 108771, https://doi.org/10.1016/j.compositesb.2021.108771.

Obande, W., Ó Brádaigh, C. M., Ray, D., 2020. Thermoplastic hybrid-matrix composites prepared by a room-temperature vacuum infusion and in-situ polymerisation process. *Composites Communications*, 22, https://doi.org/10.1016/j.coco.2020.100439.

Obande, W., Mamalis, D., Ray, D., Ó Brádaigh, C. M., 2019. Mechanical and thermomechanical characterisation of vacuum-infused thermoplastic- and thermoset-based composites. *Materials & Design*, 175, https://doi.org/10.1016/j.matdes.2019.107828.

Obande, W., Ray, D., Ó Brádaigh, C. M., 2019. Viscoelastic and drop-weight impact properties of an acrylic matrix composite and a conventional thermoset composite – a comparative study. *Materials Letters*, 238, https://doi.org/10.1016/j.matlet.2018.11.137.

D.2 Research collaborations and involvements

Some of the insights presented in Appendix B were gained through complementary collaborative research with other researchers within the School of Engineering at The University of Edinburgh. Key outputs from these research involvements are detailed below:

Robert, C., Mamalis, D., Obande, W., Koutsos, V., Ó Brádaigh, C. M, Ray, D., 2021. Interlayer bonding between thermoplastic composites and metals by in-situ polymerization technique. *Journal of Applied Polymer Science*, 51188, https://doi.org/10.1002/app.51188.

- Published as part of an EPSRC-funded project: "*Manufacturing Thermoplastic Fibre Metal Laminates by the In-Situ Polymerisation Route*". Principal Investigator: Dr Dipa Roy; Post-doctoral Researcher: Dr Dimitrios Mamalis.

Mamalis, D., Obande, W., Koutsos, V., Blackford, J., Ó Brádaigh, C. M, Ray, D., 2019. Novel thermoplastic fibre-metal laminates manufactured by vacuum resin infusion: The effect of surface treatments on interfacial bonding. *Materials and Design*, 162, https://doi.org/10.1016/j.matdes.2018.11.048.

- Published as part of an EPSRC-funded project: "*Manufacturing Thermoplastic Fibre Metal Laminates by the In-Situ Polymerisation Route*". Principal Investigator: Dr Dipa Roy; Post-doctoral Researcher: Dr Dimitrios Mamalis.

Materials & Design 206 (2021) 109804

Contents lists available at ScienceDirect

Materials & Design

journal homepage: www.elsevier.com/locate/matdes

Enhancing the solvent resistance and thermomechanical properties of thermoplastic acrylic polymers and composites via reactive hybridisation

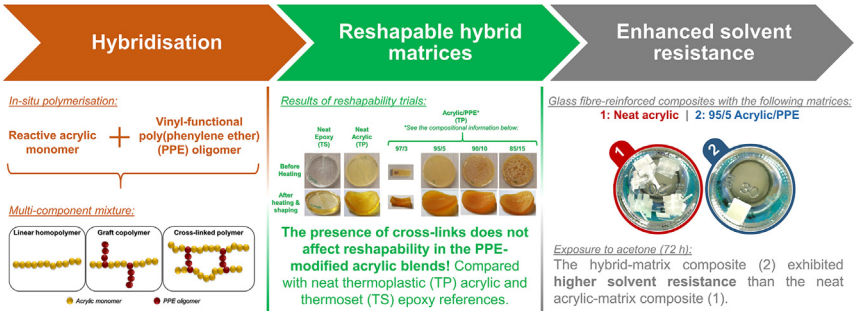
Winifred Obande [a], Weronika Gruszka [b], Jennifer A. Garden [b], Christian Wurzer [c], Conchúr M. Ó Brádaigh [a], Dipa Ray [a,*]

[a] School of Engineering, Institute for Materials and Processes, The University of Edinburgh, Sanderson Building, Robert Stevenson Road, Edinburgh EH9 3FB, Scotland, United Kingdom
[b] EaStCHEM School of Chemistry, The University of Edinburgh, Joseph Black Building, David Brewster Road, Edinburgh EH9 3FJ, Scotland, United Kingdom
[c] School of GeoSciences, UK Biochar Research Centre, The University of Edinburgh, Edinburgh EH9 3FF, Scotland, United Kingdom

HIGHLIGHTS

- Reactive acrylic/poly(phenylene ether) (PPE) blends were studied.
- Acrylic-PPE blends exhibited improved solvent resistance.
- Room-temperature vacuum processing of glass fibre-acrylic/PPE was demonstrated.
- Acrylic/PPE blends maintained full reshapability upon heating after polymerisation.

GRAPHICAL ABSTRACT



ARTICLE INFO

Article history:
Received 7 February 2021
Revised 1 May 2021
Accepted 3 May 2021
Available online 6 May 2021

Keywords:
Polymer-matrix composite
Thermoplastic composite
Thermoplastic resin
Chemical analysis
Thermal analysis
Hybrid-matrix composite

ABSTRACT

This work demonstrates the use of an engineering thermoplastic, poly(phenylene ether) (PPE) to enhance the solvent resistance and thermomechanical properties of liquid acrylic resin-based composites by a reactive hybridisation route. Oligomeric PPE with vinyl functionality was employed to attain chemical reactivity between the two constituents during the in-situ polymerisation process. Both unreinforced polymer blends and glass fibre-reinforced composites were studied; physical insights into the polymer structure and properties were obtained through complementary spectroscopic analysis, thermal analysis and microscopy. Spectroscopic analysis revealed the formation of multi-component mixtures in the blends, containing both $CDCl_3$-soluble and -insoluble constituents, with the latter likely corresponding to a reacted acrylic/PPE species. These findings show that incorporating reactive PPE into a reactive acrylic resin to produce a hybrid-matrix system is a simple, yet effective strategy towards enhancing solvent resistance (mass retention: 98% – PPE-modified; 72% – unmodified), while simultaneously enhancing the glass transition temperature (+9%) in acrylic-matrix composites.

© 2021 Published by Elsevier Ltd. This is an open access article under the CC BY-NC-ND license (http://creativecommons.org/licenses/by-nc-nd/4.0/).

1. Introduction

Processing methodologies for thermoplastic polymer matrix composites can be expensive for low part volumes, owing to high melt-viscosity, which must be overcome with high-cost tooling at elevated temperatures and pressures. More recently, a family

* Corresponding author.
E-mail address: dipa.roy@ed.ac.uk (D. Ray).

https://doi.org/10.1016/j.matdes.2021.109804
0264-1275/© 2021 Published by Elsevier Ltd.
This is an open access article under the CC BY-NC-ND license (http://creativecommons.org/licenses/by-nc-nd/4.0/).

of monomeric acrylic resins, which are suited to liquid resin infusion (LRI) processing of composites at room temperature, has become the subject of extensive research [1–9]. Such research efforts have focused on benchmarking their mechanical and thermomechanical performance against those of commodity-to-intermediate-performance epoxy systems. It has been established that the acrylic composites exhibit comparable performance with their epoxy counterparts [1,10–22].

Acrylics, as amorphous commodity thermoplastic polymers, are highly susceptible to solvent attack [23], which makes them unsuitable for application in particular environments. Improved solvent resistance can be highly beneficial for acrylic matrix composites, increasing their acceptance in a broader range of applications. This is particularly of importance in automotive applications, where solvent and chemical resistance are desirable in composite matrices to overcome the effects of prolonged in-service exposure to chemicals such as gasoline, motor oil, antifreeze, paint, cleaning solvents and road salts [24]. Moreover, in terms of their thermomechanical performance, lower glass transition temperatures have been reported (compared to epoxy-based composites) [19]. Thus, any efforts to enhance solvent resistance should ideally maintain or increase the glass transition temperature and overall thermal stability.

Low-viscosity, liquid thermoplastic acrylic resins are ideal candidate materials for the reactive modification methodologies employed for liquid thermosetting resin systems in composite applications [25–33]. Notably, liquid thermosetting resins can be used as reactive solvents within which higher molecular weight (higher performance) thermoplastics can be dissolved for subsequent processing by liquid composite moulding methods. This is an attractive way to produce composite structures from hybrid matrices with tailored performance [34,35].

The novelty of this current work compared with previous publications lies in the following aspects. *First*, the attainment of solvent-resistant blends using a telechelic PPE oligomer with chain-end vinyl functionality to promote reactivity with a liquid thermoplastic acrylic resin. *Second*, the ability to obtain said blends without compatibilisers or intermediates [36,37], and without sacrificing thermal stability and thermomechanical performance. *Third*, the direct application of oligomeric PPE as a co-reactant with a reactive, liquid acrylic monomer to produce room-temperature vacuum-infused composite laminates. Ultimately, the findings presented herein open up opportunities for new applications of acrylic/PPE-matrix composites, such as their potential use for components requiring in-service or periodic exposure to harsh chemical and thermal conditions. Examples include body and structural parts in automobiles, where the risk of contact with fuels, lubricants and cleaners/disinfectants may be significant enough to limit the drop-in replacement of thermosetting resin systems with thermoplastic acrylic resins.

To this end, the present work combines complementary analytical techniques to assess the effects of hybridisation on the chemical structure, phase morphology, solvent resistance and thermal characteristics of the PPE-modified acrylic materials, compared to an unmodified acrylic polymer counterpart. Solvent resistance and thermomechanical properties are evaluated in both unreinforced and reinforced forms.

2. Materials and methods

2.1. Materials

A liquid thermoplastic acrylic resin (Elium® 188O – Arkema GRL, France) was reactively modified with an oligomeric PPE to investigate an innovative route for modifying these liquid resins for composite applications. The PPE used was NORYL™ SA9000 resin (SABIC) – a low-molecular-weight grade (number average molecular weight (M_n): 2300 Da) with vinyl functional groups. Hereafter, the polymer samples (unmodified reference and blends) will be referred to as A100/P0, A97/P3, A95/P5, A90/P10, A85/P15 and A0/P100 as per the compositions and identification scheme: A#/P*, where # and * are weight fractions of acrylic and PPE in the blend, respectively.

The composite laminates described in Section 2.2.2 are reinforced by a glass, non-crimp fabric (TEST2594) supplied by Ahlstrom-Munksjö Glassfibre OY, Finland, where GF is appended to the designation defined for the unreinforced polymers and polymer blends to imply the use of glass fibre reinforcement. The glass fabric had a quasi-unidirectional construction, comprising 1200 TEX 0°-fibres (94%), 68 TEX 90°-fibres (6%) and polyester stitching. A $[0]_8$ preform was assembled using eight plies, laid up symmetrically about the mid-plane of the laminate. For both unreinforced polymers and reinforced composites, polymerisation was initiated with a dibenzoyl peroxide initiator (BP50FT) supplied by United Initiators GmbH, Germany.

2.2. Sample preparation

2.2.1. Unreinforced polymer and polymer blends

PPE was dissolved into liquid acrylic resin in the compositional range of 3% to 15% by weight of the acrylic resin. The liquid acrylic resin acted as a reactive solvent for the PPE oligomer. BP50FT, a dibenzoyl peroxide (BPO) initiator was added to the resin blends 24 h after preparation at a mix ratio of 100:3 (by weight). The same initiator content was used for the neat acrylic resin. Samples measuring 50 mm × 8 mm × 4 mm (nominally) were polymerised at room temperature for 24 h in silicone moulds. Polytetrafluoroethylene (PTFE)-covered steel plates were used to cover the moulds throughout the polymerisation to prevent the evaporation and foaming of the liquid resin. The sample specifications used for characterisation are provided in the relevant methodology sections of this paper.

2.2.2. Glass fibre-reinforced composites

To assess the potential enhancements conferred by using the PPE-modified acrylic matrix for composite applications, glass fibre-reinforced acrylic and PPE-modified acrylic laminates were also produced by vacuum infusion processing as detailed in the supporting information (Section S1). The PPE-modified acrylic laminate composition was selected based on the miscibility and phase stability trial results in the supplementary material (Section S1, Figure S1), which revealed 5 wt% (A95/P5) as the most stable blend for the resin infusion conditions employed in this work. Hereafter, the laminates will be referred to as GF/A100/P0 and GF/A95/P5. The burn-off technique was employed to determine their fibre volume fractions as 49.5% and 57%, and fibre weight fractions of 68% and 75%, respectively. The corresponding void contents for these materials were 0.4% and 0.8%, respectively. Their solvent resistance and thermomechanical behaviour have been comparatively assessed and will be discussed in Sections 3.1.2 and 3.2.2, respectively. Average thicknesses for the GF/A100/P0 and GF/A95/P5 were 3.8 mm and 3.3 mm, respectively. For solvent resistance studies, samples measuring 8 mm × 8 mm were used, whereas, for thermomechanical analysis, nominal sample dimensions were 40 mm × 8 mm.

2.3. Solvent resistance characterisation by prolonged acetone immersion

Non-standard solvent resistance experiments were performed in acetone to study the influence of PPE-modifier content on the

unreinforced acrylic matrix system. Two independent sets of experiments were conducted (one sample per material type, per set); polymerised samples of unmodified acrylic and acrylic/PPE blends (PPE content: 3–15 wt%) were sectioned, weighed (216–275 mg) and placed in acetone at room temperature for 60 min and 72 h. Samples with a 60-min exposure time were immersed in acetone for the test duration and carefully removed, dried and weighed after completing the experiment. Data collection for the 72-h study involved routine inspections at set intervals up to 300 min, during which visible geometrical changes were recorded until the end of the experiment. After 300 min had elapsed, samples were inspected at the 24-h mark and 72-h mark. All coupons were removed from the solvent, dried and weighed at the end of the respective test durations. The same procedure was followed for glass fibre-reinforced composite samples (GF/A100/P0 and GF/A95/P5) with starting weights of 410 – 490 mg to assess their comparative resistance to acetone.

2.4. Characterisation of thermomechanical properties by dynamic mechanical analysis

The dynamic mechanical analysis (DMA) was performed on polymer samples to study the influence of PPE-modifier content on T_g and damping behaviour using a DMA 8000 analyser (Perkin Elmer, USA). Two samples (per set), measuring 40 mm × 8 mm × 4 mm (nominal dimensions) were dynamically loaded at a fixed frequency of 1 Hz using a dual cantilever bending configuration. Each sample was heated from ambient temperature to 180°C at 3°C/min.

2.5. Thermogravimetric analysis of unreinforced polymer and polymer blend samples

Thermogravimetric analysis (TGA) was performed using a TGA/DSC 1 analyser (Mettler Toledo, USA) to analyse the thermal stability of polymeric samples. Samples weighing 10 mg were heated from 25°C to 600°C at 10°C/min under a nitrogen flow rate of 50 ml/min. The evolution of mass loss and derivative thermograms (DTG) were compared. Results are averages of duplicates (two samples per material).

2.6. Confocal Raman microscopy of fractured polymer blend surfaces

Fractured samples were non-destructively imaged using a Confocal Raman microscopy technique to spatially assess the chemical composition of each blend. This method was complementary to the rest of the characterisation methods, as it provided insights into the phase morphology and interactions between the blend components. Single polymeric samples were fractured using the non-standard flexural testing method described by Obande et al. [38]. To enhance the visualisation precision across the fracture surface (irrespective of topographical variations), the sample was maintained at constant focus using a *TrueSurface*® tool. An Alpha 300 AR instrument (WiTec GmbH, Germany) was used for this study.

2.7. Solution-state nuclear magnetic resonance (NMR) spectroscopy of polymer and polymer blend samples

The chemical structures of unmodified acrylic and PPE in the presence and absence of BPO (i.e., polymers and unpolymerised liquid resins, respectively), as well as acrylic/PPE blends (PPE content: 5–10 wt%), were analysed using ^{1}H and 2D NMR experiments (^{1}H–^{1}H COrrelated SpectroscopY (COSY), ^{1}H–^{13}C Heteronuclear Single Quantum Coherence (HSQC) spectroscopy and Diffusion-Ordered SpectroscopY (DOSY)). NMR spectra were recorded on a Bruker AVA500 (USA) spectrometer at 298 K (500 MHz) in $CDCl_3$ and were referenced to the residual $CDCl_3$ peaks (^{1}H: δ 7.26 ppm, ^{13}C: 77.2 ppm). Only the soluble portions of the reactive A95/P5 and A90/P10 blends were analysed by NMR spectroscopy in $CDCl_3$. The solubility of the reactive blends in $CDCl_3$ was improved by heating (50°C) and sonicating the blends in $CDCl_3$ for approximately 2 h or leaving the samples in excess $CDCl_3$ overnight. Both blends also exhibited low solubility in other common NMR spectroscopy solvents (tetrahydrofuran (THF)-d_8, pyridine d_5 and toluene d_8).

3. Results and discussions

3.1. Solvent resistance

3.1.1. Unreinforced polymer and polymer blend samples

Fig. 1 shows the results of solvent resistance experiments on unreinforced polymers. Following exposure to acetone for 60 min at room temperature, all acrylic/PPE blend polymer samples exhibited lower mass losses after 60 min in acetone than the unmodified acrylic (A100/P0) sample. A 37% mass loss was observed with the A100/P0 sample, whereas the blends sustained mass losses in the range of 10–18 %. Except for the A97/P3 sample, which lost only 12% of its original mass, an increase in PPE content from 5 wt% (A95/P5) to 15 wt% (A85/P15) results in a consistent increase in solvent resistance, evidenced by corresponding terminal mass losses of 18% and 10%, respectively.

Following the 72-h exposure experiments, the A100/P0 was found to completely dissolve after 300 min, following a visible, progressive loss of volume. In contrast, all blends sustained only 23–25% of mass loss, showing significant improvements in their solvent resistance. Increasing PPE concentration within the blends did not, however, appear to result in significant changes in the terminal mass in acetone after 72 h. These observations provide strong evidence that PPE content plays a vital role in the dissolution rate and consequently, initial mass loss of acrylic/PPE blends.

The dissolution rate of polymers is influenced by polymer characteristics such as molecular weight, the chemical structure and composition of the polymer backbone, segmental stiffness, and dispersity. Given that the addition of PPE into the hybrid matrices adds aromatic groups within their structure, where the unmodified acrylic only contains aliphatic polymer chains, obvious differences in backbone structure, composition, molecular weight and segmental stiffness are likely to arise between the polymer matrices. The variations in initial dissolution behaviour observed in the 60-min experiments with increasing PPE content are possibly linked with differences in polymer chain mobility [39,40]. At a molecular level, the variation of respective chain mobilities may be substantial enough to give rise to varying reptation times and thus, disengagement rates. This may provide evidence of interchain interactions between the phenyl groups within the PPE modifier.

Moreover, the A100/P0 sample can be seen to undergo progressive mass loss until complete dissolution at 300 min. In contrast, the PPE-modified hybrid matrices appear to exhibit whitening, with considerable swelling being observed across all samples until the full study duration elapsed. These results suggest a significant effect of PPE incorporation on the molecular weight [40] and the possibility of cross-linked [41] acrylic/PPE species arising from the reactions of monomeric acrylic with multi-vinyl oligomeric PPE. Moreover, dispersity also plays a role in the rate of dissolution and may explain the enhanced solvent resistance observed with the hybrid matrices [40].

It is worth noting that white sediments were observed in the solvent from 60 min for all hybrid matrices. These sediments remained in solution until the experiment was completed. The size of dispersed sediment appeared to increase with increasing PPE

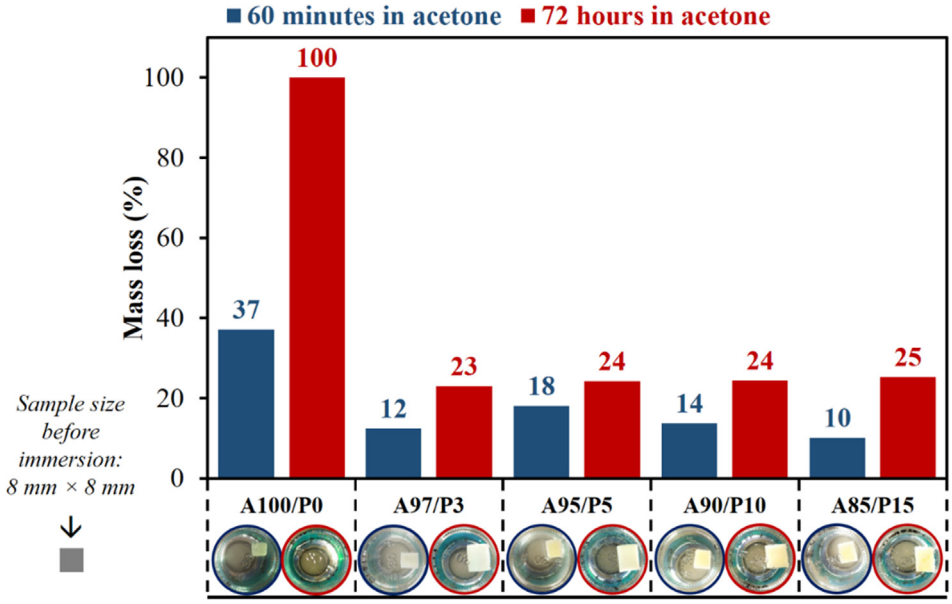


Fig. 1. Results of solvent resistance experiments after exposure of unreinforced polymer samples to acetone for 60 min (blue) and 72 h (red). Mass losses are presented for unmodified acrylic (A100/P0) and PPE-modified acrylic (A97/P3-A85/P15) where a lower mass loss corresponds to superior solvent resistance. Note: results are based on one sample per material, per set. (For interpretation of the references to colour in this figure legend, the reader is referred to the web version of this article.)

content. These observations may indicate the presence of unreacted oligomeric PPE within the polymerised samples, which is in agreement with observations from NMR analysis of these materials, as discussed in Section 3.5.

3.1.2. Glass-fibre reinforced composite samples

Fig. 2 shows the results of solvent resistance experiments on glass fibre-reinforced acrylic (GF/A100/P0) and acrylic/PPE (GF/A95/P5) composite samples. 60-min solvent resistance experiments on the fibre-reinforced acrylic (GF/A100/P0) and acrylic/PPE (GF/A95/P5) revealed that the incorporation of PPE into the acrylic resin system contributes positively to the resistance to initial solvent ingress and subsequent dissolution. No evidence of mass loss was measured after 60 min. In the unmodified acrylic composite sample (GF/A100/P0), a 10% loss in mass was recorded.

Given that the rate of dissolution is influenced by chain mobility at a molecular scale, these results suggest significant differences in the reptation times and disengagement rates [39,40] between both matrices. The differences in respective chain mobilities may be substantial enough to give rise to varying reptation times and disengagement rates at a molecular level. These variations can result from the presence of the cross-linked species or the presence of phenyl moieties within the backbone.

Following the longer time-scale exposure (72 h), it becomes clear that the use of the PPE-modified matrix results in even more significant improvement of the solvent resistance of the GF/A95/P5

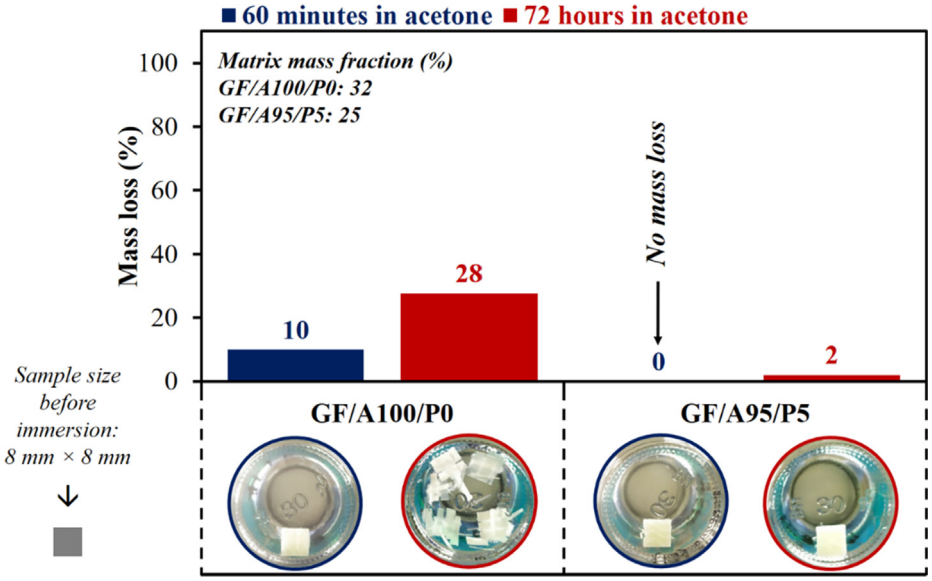


Fig. 2. Mass losses after the exposure of glass fibre-reinforced acrylic (GF/A100/P0) and PPE-modified acrylic (GF/A95/P5) composite samples to acetone for 60 min (blue) and 72 h (red) showing the influence of PPE modifier content on solvent resistance. Note: A lower mass loss corresponds to superior solvent resistance. (For interpretation of the references to colour in this figure legend, the reader is referred to the web version of this article.)

(only 2% of mass loss) over its unmodified acrylic counterpart (GF/A100/P0), which lost 28% of its original mass. With a matrix mass fraction of 32 ± 0.3% in the composite, this recorded mass loss for the GF/A100/P0 sample is similar in magnitude to its matrix mass fraction. As such, it indicates that complete dissolution of the acrylic matrix occurred, which is in agreement with visual observations during data collection (Fig. 2).

3.2. Characterisation of thermomechanical properties by dynamic mechanical analysis

3.2.1. Unreinforced polymer and polymer blend samples

From single-frequency DMA scans at 1 Hz, the effects of PPE-modification on the glass transition temperatures and tan delta peak heights were studied alongside the unmodified acrylic polymer matrix material. T_g values were determined as the temperatures corresponding to the maximum tan delta values. The representative thermograms obtained from each material presented in Fig. 3a reveal single tan delta peaks for all blends. A lowering effect was also observed for the tan delta peak heights, with values decreasing by up to ~ 0.2 (-12%). These trends are more pronounced up to 5 wt% addition of PPE, as in the A95/P5 material; however, as PPE content is increased up to 15 wt% (A85/P15), the contributions are less prominent. Moreover, a mild T_g shift is evident with increasing PPE content. Given that the PPE used had a higher T_g (160°C) than the acrylic constituent, such a shift is expected with the in-situ polymerisation of acrylic in the presence of PPE.

Increasing the PPE content within the blends causes an overall increase in T_g by up to ~ 6°C (Fig. 3c). This suggests decreased chain mobility owing to increased rigidity and π- π interactions due to the phenyl rings [42] of the PPE phase. Given that tan delta is a ratio of loss modulus to storage modulus, and describes the degree of viscoelastic damping within a material and the extent of polymer segmental mobility, the overall reductions in tan delta peak height with increasing PPE content suggests a reduction in the viscoelastic response of the blends compared to the unmodified acrylic polymer matrix.

The reductions in tan delta peak height may be due to increased rigidity caused by the phenyl moieties in PPE or may indicate the existence of a cross-linked species, which would likely decrease the chain mobility [43]. Despite the absence of a cross-linking agent, the presence of vinyl-functionalised PPE oligomer may have triggered spontaneous localised cross-linking alongside the formation of a non-cross-linked acrylic-rich constituent. Using a high-molecular-weight vinyl-pendant PPO, Huang et al. [44] proposed that a higher vinyl-pendant ratio was more likely to undergo a cross-linking reaction during polymerisation than a lower ratio. Interestingly, increasing glass transition temperatures were also thought to be attributed to the presence of cross-links within the vinyl-pendant PPO structure.

While this present research employed a low-molecular-weight, vinyl-end-functionalised PPE, it is plausible that increased glass transition temperatures in the blends with respect to A100/P0 was a contribution of cross-linked structures.

The effects of PPE modification on half peak width and peak factor were also assessed. Half peak width is typically used to evaluate the relative reduction of relaxation-induced molecular mobility [45]. Peak factor is a representation of the intrinsic heterogeneity within the polymer system [46]. It is calculated as the ratio of the corresponding half peak width (Fig. 3b) and peak height (Fig. 3b) for each material. Within blended polymeric systems with

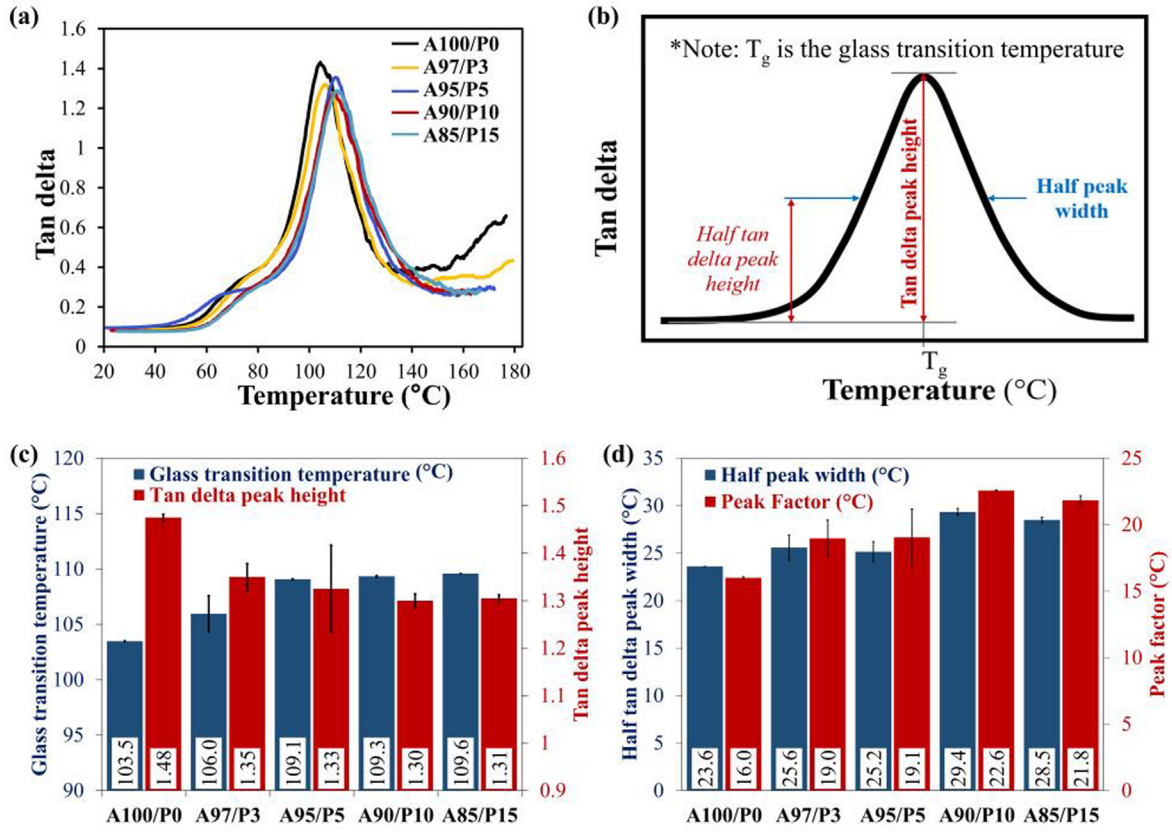


Fig. 3. (a) Representative DMA results, showing the effects of PPE content on damping behaviour (tan delta) and T_g, (b) graphical representation of the reported parameters, (c) T_g values and tan delta peak heights, and (d) half tan delta peak widths and peak factors from DMA experiments on polymer matrix samples. Results are averages of duplicates.

dissimilar T_g values, broad tan delta peaks indicate the formation of diffuse domains [47,48]. Both peak width [49] and peak factor are attributed to the heterogeneity or broad dispersity within the polymer [46,50]; however, peak width also correlates to the distribution of relaxation times within the polymer [51]. The parameters in Fig. 3d, obtained as depicted in Fig. 3b, highlight a correlation between the PPE content and both peak width and peak factor. This suggests the co-existence of composition-dependent acrylic-rich and PPE-rich phases within the blends.

3.2.2. Glass-fibre reinforced composite samples

Fig. 4 shows representative thermograms obtained from DMA experiments on glass fibre-reinforced PPE-modified acrylic (GF/A95/P5) matrix composite and an unmodified acrylic composite (GF/A100/P0). Prominent differences in damping behaviour are observed. The GF/A100/P0 material exhibits a distinct, single tan delta peak. In contrast, despite the observation of single peaks for the unreinforced A95/P5 in Section 3.2.1, the peak for GF/A95/P5 appears to broaden with mild evidence of peak splitting, indicating the presence of multi-species phases within the blend-matrix composite. The distance between tan delta peaks in blends correlates to the extent of phase separation between their constituents [52].

The dissimilarities in the unreinforced and reinforced A95/P5 matrix provide further evidence of the differences between the polymerisation conditions between both materials. Moreover, the effects of fibres on the growth kinetics of the polymer chains is also another possible source of variation between the two methodologies.

Although the Fox empirical model has limited applicability for blends with intermolecular interactions, it has been applied to gain preliminary insights into the plausible proportions of the hybrid matrix constituents. A similar approach has been previously reported in work by Karabanova et al. [53] who studied semi-interpenetrating polymer networks (semi-IPNs) based on polyurethane and poly(2-hydroxyethyl methacrylate), which provides insights into the structure of the polymer blends under consideration. Additionally, mass data from the solvent resistance characterisation described in Section 3.1 have been used in conjunction with the Fox equation to obtain better approximations of the compositions of the soluble and insoluble constituents of the blend. The corresponding T_g values for GF/A95/P5 are 105°C and 120°C (393 K), as shown in Fig. 4. The T_g values for neat acrylic and PPE are 104°C (rounded value from results in Fig. 3, 377 K) and 160°C (433 K) [7], respectively. Thus, T_{g1} is most likely attributed to the presence of an acrylic homopolymer species, as evidenced by NMR spectroscopy in Fig. 7.

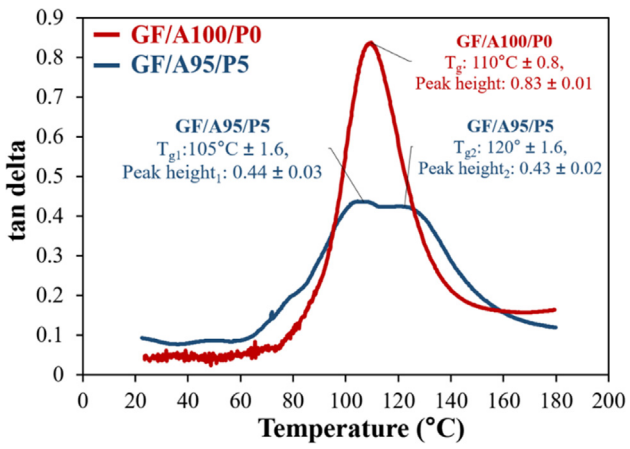


Fig. 4. Representative DMA results for glass fibre-reinforced acrylic (GF/A100/P0 – in red); and (b) PPE-modified acrylic (GF/A95/P5 – in blue) composites. Results are based on averaged duplicates (Figure S8). Lay-up: $[0]_8$. (For interpretation of the references to colour in this figure legend, the reader is referred to the web version of this article.)

On the other hand, T_{g2} is a unique intermediate temperature between the two blend components, and possibly provides evidence of a reacted product of the acrylic and PPE constituents coexisting with the acrylic homopolymer. Based on the observed T_g values, the hybrid matrix system was assumed to be bi-phasic in nature, comprising an acrylic (or acrylic-rich phase) and a PPE-rich acrylic/PPE. The Fox equation was applied using Equation (1) and as detailed in Section S3.1 to estimate acrylic/PPE reacted product's composition that would give rise to a secondary glass transition temperature, T_{g2}.

$$\frac{1}{T_{gN}} = \frac{\varphi_{2,A}}{T_{gN,A}} + \frac{\varphi_{2,B}}{T_{gN,B}} \tag{1}$$

Where $\varphi_{2,A}$ and $\varphi_{2,B}$ are mass fractions of acrylic and PPE, respectively, the sum of which equals unity; T_{gN} is the glass transition temperature corresponding to the peaks shown in Figure S8 and illustrated in Figure S9; $T_{gN,A}$ and $T_{gN,B}$ are the glass transition temperatures of the acrylic and PPE constituents, respectively. Note: all T_g values were used in Kelvin. For the determined T_{g2}, $T_{g2,A}$ and $T_{g2,B}$ values of 393 K, 377 K, and 433 K, respectively, $\varphi_{2,A}$ and $\varphi_{2,B}$ within the reacted product were estimated to be 0.69 and 0.31, respectively. The interested reader is referred to Section S3.1 for the employed procedure.

Moreover, based on the observation of two T_g values, the full blended system (S_B) can be represented by a summation of the mass fractions corresponding to T_{g1} (φ_1) and T_{g2} ($\varphi_{2,A} + \varphi_{2,B}$). T_{g1} relies solely on contributions from the acrylic phase, and T_{g2} involves contributions from both acrylic and PPE phases. Thus, assuming that all the PPE (5 wt%) within the full blended system (S_B) is directly proportional to $\varphi_{2,B}$ (0.31) according to the Fox Equation (Equation (1)), $\varphi_{2,A}$ yields a corresponding mass fraction estimate in S_B of $\left(\frac{0.69\times0.05}{0.31}\right) = 0.11$. The total mass fraction of acrylic/PPE reacted product is 16 wt%, based on combined acrylic and PPE mass fractions in S_B, i.e. 11 wt% and 5 wt%. Accordingly, 84% of the total 95 wt% of acrylic supplied for the polymerisation reaction was consumed in the formation of the acrylic homopolymer, whereas 16% formed a reacted product with PPE.

These results provide further evidence of the formation of a complex co-reacted acrylic/PPE species. Although no traditional cross-linker was employed as part of this study, the hybridisation of the acrylic matrix using a PPE oligomer with multiple vinyl functional groups facilitated the formation of a lightly cross-linked structure.

In light of the relative mass loss of the GF/A95/P5 sample following prolonged exposure to acetone in Section 3.1.2, these estimated mass fractions may hold the key to understanding the hybrid-matrix structure. Solvent resistance studies revealed that a mass retention of approximately 98% (of the original mass) was possible due to PPE incorporation. However, in this section, it was estimated that the acrylic homopolymer constituted 84 wt% of the full hybrid matrix system. Neat acrylic has been shown in Section 3.1.1 to be fully vulnerable to acetone attack under the same conditions. Given that solvent resistance is influenced by disengagement and reptation times of polymer chains, the blend architecture must, therefore, provide favourable shielding and trapping of entanglements, which act as anchors for a large extent of the vulnerable acrylic homopolymer [54–56].

Furthermore, changes in T_g are typically indicative of changes in chain length and mobility. The increase in T_g with the addition of PPE indicates relative reductions in chain flexibility, available free volume and chain mobility, possibly due to the contributions of

phenyl moieties in the PPE and cross-links to the overall rigidity [42]. It is also apparent that the PPE-modified-matrix composite exhibited a broader peak, providing further evidence of structural and molecular heterogeneity within the matrix.

Interestingly, the severity of peak height reduction in the GF/A95/P5 samples supports the hypothesis that the presence of cross-links and phenyl moieties within the PPE-modified acrylic composite enhances the rigidity of the matrix. Cross-links are known to give rise to reduced intensities in damping peaks [57]. Moreover, the low tan delta peak values may also provide crucial information on the fibre–matrix interfacial behaviour. It is well known that composites with poor interfacial strength exhibit superior damping ability, evidenced by increased peak heights [58,59]. Thus, a diminished peak height provides strong evidence that incorporating PPE into the acrylic matrix does not appear to deteriorate interfacial adhesion between the blend matrix and the reinforcing fibres.

3.3. Thermogravimetric analysis of unreinforced polymer and polymer blend samples

The thermal stability of the acrylic and PPE-modified acrylic blends were analysed by thermogravimetric analysis (TGA). Table 1 summarises the key results from TGA thermograms obtained for each sample. The interested reader is referred to Figure S10 for the thermograms.

Oligomeric PPE (A0/P100) appears to undergo a single-stage degradation process under the experimental conditions employed (Figure S10). Negligible mass loss was observed below 438 ± 0.1° C, its onset temperature for major degradation ($T_{onset\text{-}TGA}$). This degradation behaviour is consistent with published literature, which cite a major step between 430 and 500°C occurring due to thermal Fries-type chain rearrangements [60,61]. The incorporation of PPE delays the onset of major degradation, $T_{onset\text{-}TGA}$ by 7–10°C under the degradation conditions used. In addition to comparing the effect of PPE content on $T_{onset\text{-}TGA}$, it may be useful to compare $T_{5\%}$ and $T_{10\%}$, which are temperatures corresponding to 5% and 10% mass losses, respectively. The PPE-modified acrylic blends possessed up to 10% and 12% higher $T_{5\%}$ and $T_{10\%}$ values, respectively relative to the unmodified acrylic polymer. Thus, incorporating PPE oligomer into the acrylic polymer system results in improved thermal stability in terms of delaying thermal degradation events. However, at the PPE concentrations employed in this present work, no distinct trends or correlations were discernible between PPE loading and the extent of improvements attained. The representative DTG plots shown in Fig. 5 reveal that A100/P0 undergoes a major degradation event with a valley occurring at ca. 300–445°C. Evidence of a unique, minor degradation event in the A100/P0 material can be seen between 225°C and 300°C

Polymethylmethacrylate-based polymers are reported to undergo three-stage thermal degradation processes; with head-to-head linkage-induced scission (150°C–264°C), unsaturated chain-end-induced scission (264°C–335°C) and random main chain scission (335°C–425°C) [62–64]. However, two-stage degradations have also been previously reported [65], namely a minor event (108°C–115°C) and a major event (298°C–326°C).

In this present work, the occurrence of the unique, minor degradation event in A100/P0 between 225°C and 300°C is attributed to the degradation of unsaturated chain ends [65]. Interestingly, no preceding major degradation events were observed. The main stage of degradation occurring between 300°C and 445°C is linked to random scission of main polymer chains [62,63]. Moreover, while TGA thermograms showed minor mass losses between 90°C and 110°C for all acrylic-based polymers and blends, the early-onset degradation step reported by de Andrade Raponi et al. [65] as occurring between 150°C and 230°C was characteristically absent from the DTG thermograms of the materials in this present work. This step is induced by the breakdown of weak head-to-head linkages formed during the termination reaction (by combination) of the polymerisation process. Thus, this absence may indicate that alternative termination reactions were prevalent within the polymers under investigation [64]. The absence of this step may also suggest that shorter chain lengths dominate within each polymer material. Longer chain lengths are more susceptible to defects such as head-to-head linkages and are thus, more thermally labile [66].

Furthermore, all PPE-modified acrylic blends exhibit elevated temperature degradation events, occurring between ~ 430°C and ~ 480°C, where a slower degradation rate is evident. This late-stage event is likely due to contributions from PPE-rich phases within the blended polymer systems and may be linked with the aforementioned Fries-type rearrangements associated with PPE chains. This distinct behaviour with the blends provides strong evidence of chemical interactions between the acrylic and PPE components of the blends, mainly because thermal degradation here is driven by main chain scission. Thus, this confirms that the PPE chemically interacts with the acrylic and alters the chemical structure of the blends compared to the acrylic reference. This is further supported by the fact that the blends' end-stage degradation events coincide with the A0/P100 valley's peak temperature, as shown in Zone 1 of (Fig. 5).

3.4. Confocal Raman microscopy of fractured polymer blend surfaces

As is evident from the Confocal Raman micrographs in Fig. 6, all blends exhibit binary phase separation. PPE-rich domains appear to be dispersed within an acrylic-rich host matrix. The dispersed domains appear to vary in size, distribution and intensity within each blend. These phases appear to interact and are not mutually exclusive. Some domains exhibit a more distinct boundary,

Table 1
Summary of thermogravimetric results for acrylic polymer and PPE-modified acrylic blends showing the effects of PPE-modification on thermal stability. Values are averaged from duplicates. Parameters were obtained from data presented in Figure S10, as graphically illustrated in Figure S11.

	$T_{onset,\ TGA}$ [a] (°C)	$T_{5\%}$ [b] (°C)	$T_{10\%}$ [c] (°C)	$T_{end,\ TGA}$ [d] (°C)	M_R [e] %
A100/P0	355 ± 3.2	205 ± 6	255 ± 4.6	419 ± 1.9	1 ± 0.6
A97/P3	362 ± 1.3	216 ± 6	274 ± 4.2	426 ± 0.1	4 ± 0.0
A95/P5	362 ± 2.2	225 ± 4	282 ± 2.8	423 ± 0.9	3 ± 0.4
A90/P10	365 ± 2.8	222 ± 13	286 ± 11.2	431 ± 0.2	4 ± 0.5
A85/P15	363 ± 0.1	211 ± 2	274 ± 3.9	428 ± 1.9	4 ± 0.3
A0/P100	438 ± 0.1	426 ± 1	438 ± 0.4	471 ± 0.7	23 ± 0.1

[a,d] $T_{onset,\ TGA}$ & $T_{end,\ TGA}$: Onset & end temperatures for major degradation as determined from TGA curves, respectively (see Figure S11).
[b,c] $T_{N\%}$: Temperatures corresponding to N% mass loss using the TGA thermograms.
[e] M_R: Residual mass at the end of the thermal cycle.

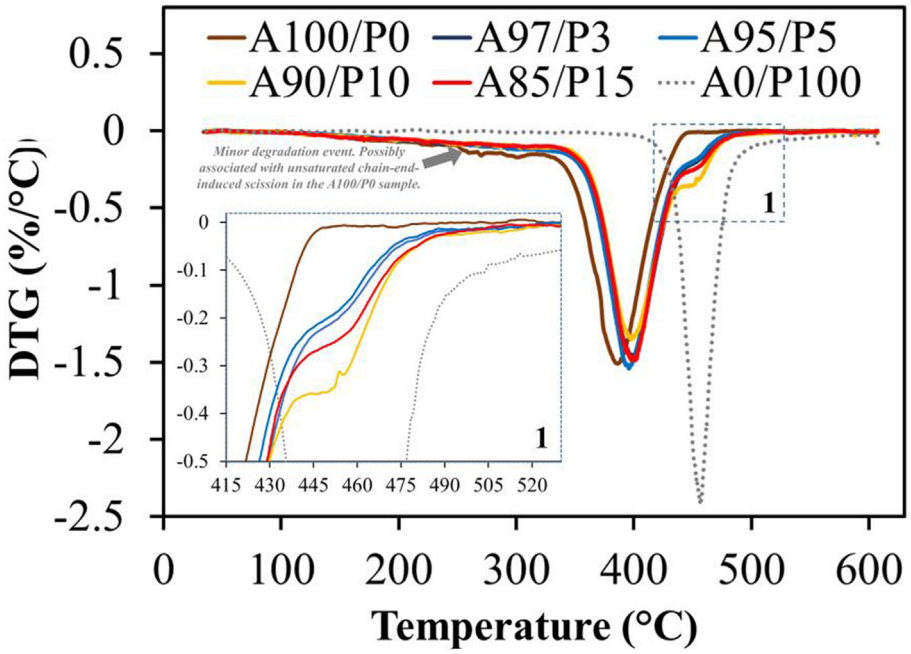


Fig. 5. Representative DTG thermograms for unmodified acrylic polymer (A100/P0), PPE oligomer (A0/P100) and their blends: A97/P3, A95/P5, A90/P10 and A85/P15. Zone 1 is an inset graph for improved visibility of unique degradation behaviour exhibited by all blends.

whereas other boundaries are more diffuse in appearance. It is worth noting that the exact proportion of each component (acrylic and PPE) within the domain and host matrix is not exactly discernible using this technique.

3.5. Solution-state nuclear magnetic resonance (NMR) spectroscopy of polymer and polymer blend samples

The chemical composition of acrylic/PPE blends A95/P5 and A90/P10 was probed by NMR spectroscopy in $CDCl_3$ and compared to monomeric and polymeric acrylic (A100/P0) and oligomeric PPE (A0/P100) in the absence and presence of BPO initiator (Fig. 7). While monomeric acrylic, polymeric acrylic and oligomeric PPE were all soluble in $CDCl_3$ at room temperature, partial dissolution of the A95/P5 and A90/P10 blends required heat (50°C), sonication (approx. 2 h) or excess $CDCl_3$. These differences in solubility suggest that A95/P5 and A90/P10 form reactive blends. Providing further evidence to support this, 95:5 and 90:10 blends (w/w) of the polymeric acrylic and oligomeric PPE were prepared by mixing the two individual components in the absence of BPO; these non-reactive blends displayed complete solubility in $CDCl_3$. These solubility differences suggest that the less soluble components of A95/P5 and A90/P10 are likely to be a high-molecular-weight copolymer or cross-linked polymeric acrylic/PPE species formed upon mixing monomeric acrylic and PPE in the presence of BPO. Both A95/P5 and A90/P10 reactive blends also exhibited noticeable swelling upon solvation in $CDCl_3$, whereas no swelling was observed with the non-reactive 95:5 and 90:10 polymeric acrylic/PPE blends (prepared in the absence of BPO). Swelling has previously been associated with the formation of cross-linked structures [41], with higher swelling ratios observed at lower cross-linker concentrations (<20%) of divinylbenzene in methyl methacrylate (MMA)-divinylbenzene cross-linked copolymers.

NMR analysis of polymeric and monomeric acrylic confirmed that polymerisation of the acrylic occurs under the reaction conditions employed to generate the reactive acrylic/PPE blends (Fig. 7). This was evidenced by the appearance of a new ^1H signal corresponding to –OR (R = alkyl) protons in the polymeric acrylic backbone. ^1H NMR analysis indicated incomplete conversion of the monomeric acrylic, which could be due to polymerisation becoming diffusion-limited upon the formation of a high-molecular-weight polymeric acrylic, the rate of radical initiator formation or the experimental conditions employed, or both (refer to supporting information for further details).

Conversely, the reaction of oligomeric PPE with BPO produced no change in the ^1H NMR spectrum (Fig. 7), which suggests that PPE does not homopolymerise under the reaction conditions employed. Notably, ^1H NMR spectra of PPE with and without BPO displayed low-intensity ^1H signals in the downfield region ($^1H^{3\text{-}5}$), which were tentatively attributed to vinylic end groups in oligomeric PPE (Fig. 7 and Figure S2).

The relative integrals of these signals suggested a 1:1 ratio of $^1H^3$: [$^1H^4$ + $^1H^5$], with coupling between $^1H^4$ and $^1H^5$ detected by COSY analysis (Figure S2). HSQC analysis indicated that the $^1H^3$ signal correlates with a different, more downfield ^{13}C resonance compared to the $^1H^4$ and $^1H^5$ signals; $^1H^4$ and $^1H^5$ correlated with a single ^{13}C resonance within the expected ^{13}C NMR shift range for a disubstituted vinyl moiety. Therefore, the NMR analysis suggests that $^1H^3$ protons are most likely aromatic, whereas $^1H^4$ and $^1H^5$ correspond to vinyl protons on disubstituted vinyl moieties in PPE oligomer end groups [67]. Using the M_n of the commercially available PPE oligomer (2300 Da), along with the relative integrals of the $^1H^{3\text{-}5}$ and aromatic PPE oligomer backbone signals, suggests that the PPE oligomer contains multiple reactive aromatic vinyl end groups per chain and may, therefore, form cross-links between polymeric acrylic chains. Although these vinyl functional groups appear to be unreactive towards homopolymerisation under the conditions tested, these groups are likely involved in copolymerisation/cross-linking reactions in the presence of the acrylic monomer.

The reactivity differences between the acrylic and PPE, combined with NMR studies, suggest that the formation of block copolymers does not occur under the conditions employed in this work. The generation of random/gradient copolymers or cross-linked polymers (or both) is more likely (Fig. 8, refer to the supporting information for further details).

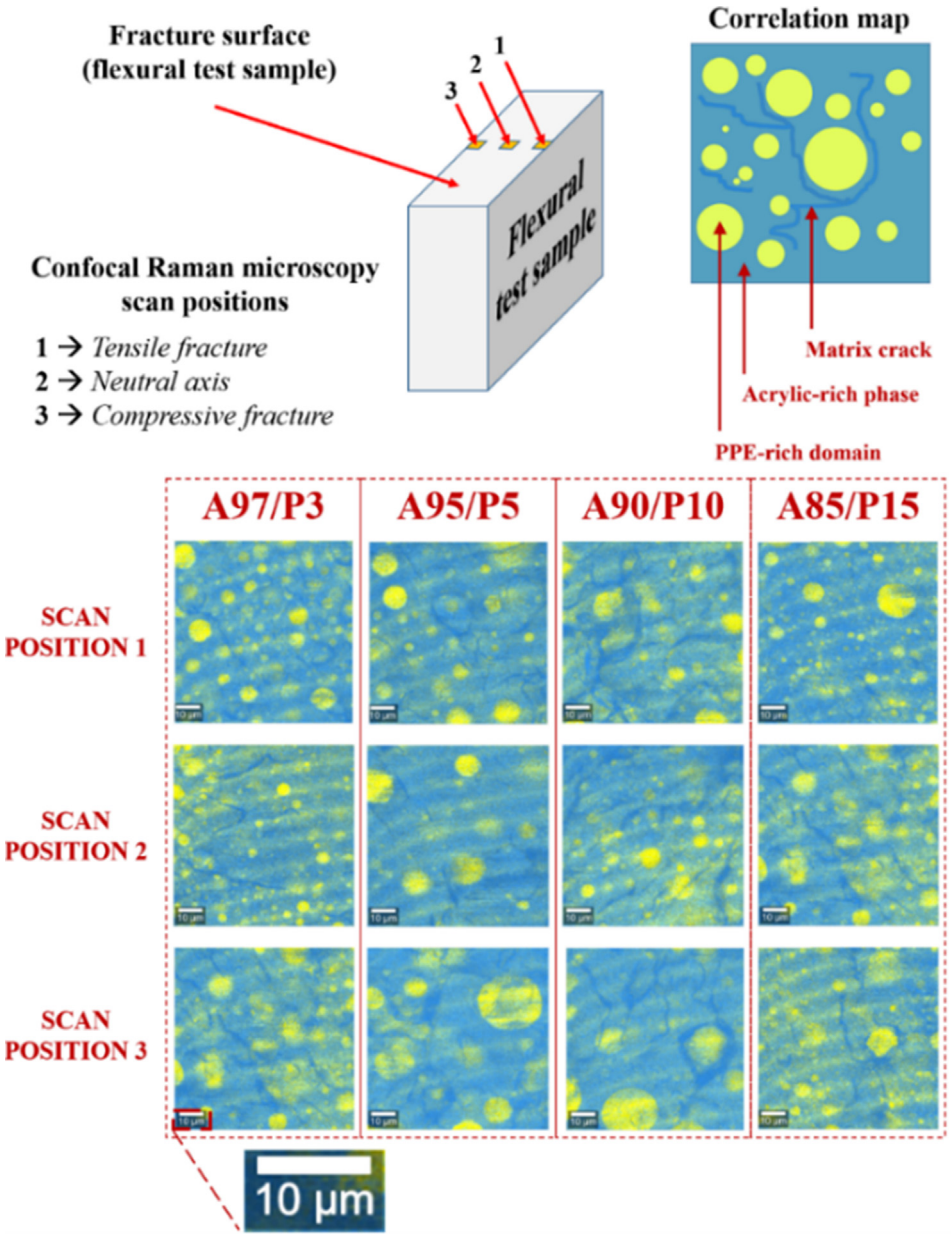


Fig. 6. Confocal Raman micrographs showing compositional maps for A97/P3, A95/P5, A90/P10 and A85/P15. Cyan and yellow regions depict an acrylic-rich phase and PPE-rich domain, respectively. (For interpretation of the references to colour in this figure legend, the reader is referred to the web version of this article.)

Although in-depth characterisation of the blends was limited by their enhanced solvent resistance in common NMR solvents, ^{1}H NMR analysis of the soluble portions of A95/P5 and A90/P10 blends indicated multi-component mixtures, which comprised polymeric acrylic, unreacted oligomeric PPE and monomeric acrylic, as well as BPO (Fig. 7, refer to supporting information for more details on the presence of BPO signals).

The same multi-component mixture was also present in the non-reactive polymer blends (95:5 and 90:10 polymeric acrylic: PPE, Figures S6 & S7, respectively). While the insoluble portions of the reactive blends (A95/P5 and A90/P10) could not be analysed, ^{1}H NMR analysis showed that the polymeric acrylic is the major component of the soluble portions (based on the relative intensities of the polymeric acrylic -OR ^{1}H NMR signal *vs*. the monomeric acrylic and oligomeric PPE). Although close inspection of baseline signals in the ^{1}H NMR spectra revealed the presence of several unknown species, these could be attributed to trace components present in the starting materials and impurities from sample preparation (Fig. 7); none were associated with polymeric acrylic/PPE linkages. These observations were supported by DOSY NMR analysis, which revealed the presence of separate oligomeric PPE and polymeric acrylic molecules in the soluble portions of the reactive A95/P5 and A90/P10 blends, as well as the non-reactive blends, as these species give different diffusion coefficients (Figures S3 to S5).

Due to the insolubility of the reactive A95/P5 and A90/P10 blends, solid-state NMR was investigated as a method of providing further insight into the polymer structure. However, it was not possible to obtain suitably pulverised samples from the A95/P5 and A90/P10 blends using standard and cryogrinding techniques.

Taken together with the ^{1}H NMR data of the soluble components, the insolubility, resistance to mechanical grinding, and swelling of the A95/P5 and A90/P10 blends suggest that these are reactive blends, rather than (non-reactive) blended aggregates of polymeric acrylic and oligomeric PPE. Indeed, the enhanced solvent resistance and swelling suggest the formation of high-

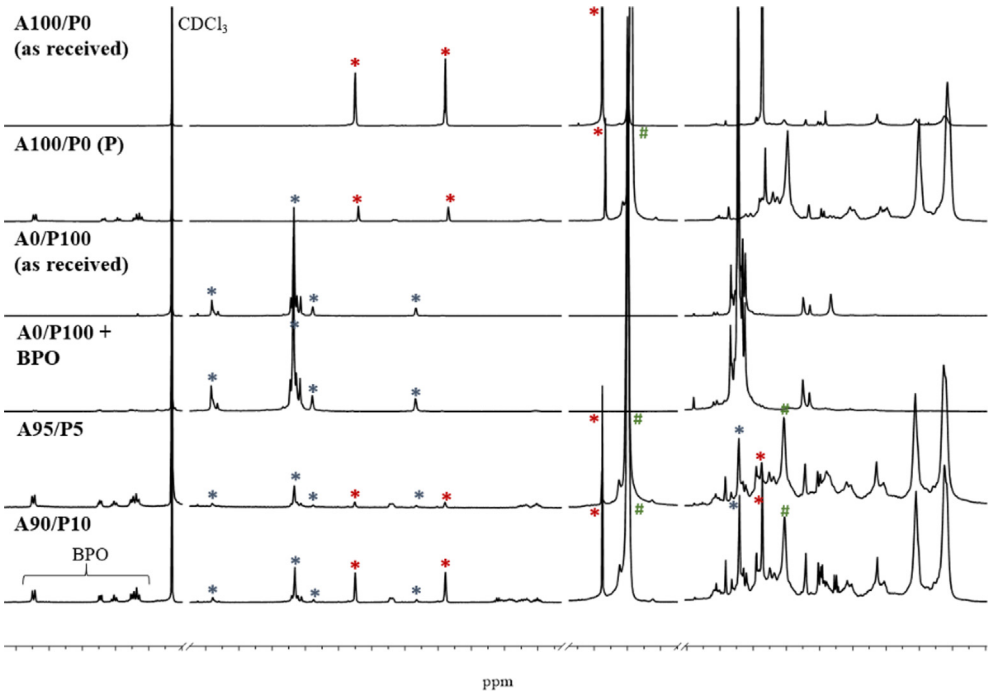


Fig. 7. Overlaid ^{1}H NMR spectra of the acrylic/PPE blends A95/P5 and A90/P10 and the starting materials in the presence and absence of BPO in $CDCl_3$. The key ^{1}H NMR signals from the monomeric acrylic (*, red), oligomeric PPE (*, blue) and polymeric acrylic (#, green) are highlighted. (For interpretation of the references to colour in this figure legend, the reader is referred to the web version of this article.)

molecular-weight copolymeric or cross-linked acrylic/PPE species. While the resistance to mechanical grinding and lack of solubility limited determination of the precise chemical structure of the A95/P5 and A90/10 blends by both solid- and solution-state NMR spectroscopy, this low solubility implies potential benefits in terms of solvent resistance. Moreover, the observed resistance to pulverisation in the blends suggests enhanced mechanical properties.

3.6. Proposed polymer blend architecture

Based on a vinyl functionality of 1.9 for the PPE formulation (specified by the manufacturer [68]), the formation of cross-linked acrylic/PPE species is highly likely within the blends based on the number of reactive sites as shown in Fig. 9.

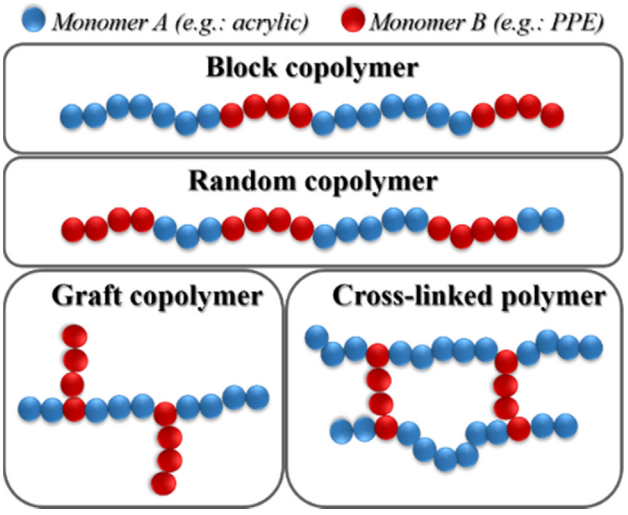


Fig. 8. General structures of block, random and graft copolymers and cross-linked polymers.

Moreover, as discussed in Section 3.5, the PPE grade used cannot homopolymerise; meaning no PPE-PPE interactions are expected during the polymerisation process. Instead, the telechelicity of PPE facilitates its participation in the propagation reaction with growing acrylic chains.

The study illustrated in Fig. 10a was conducted to explore the effects of the presence of crosslinks on the reshapability of the blends. As shown in Fig. 10b, these trials revealed that the presence of cross-links did not have deleterious effects on the post-

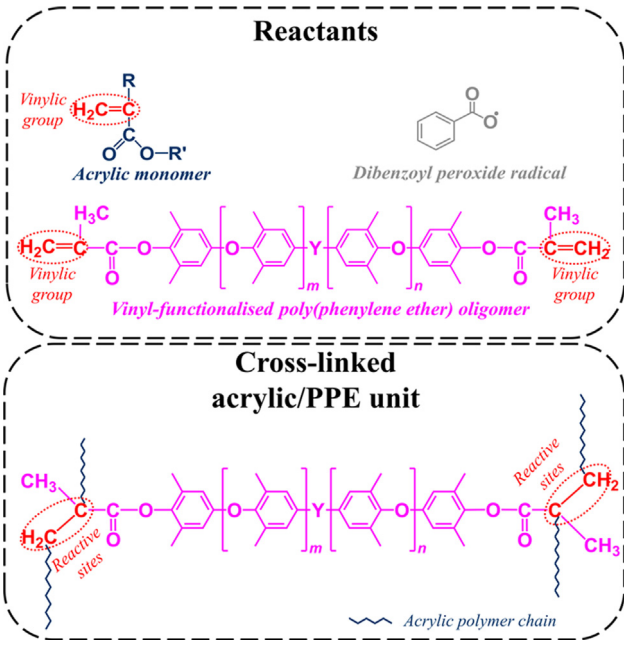


Fig. 9. Chemical structures of the reactants (acrylic monomer, PPE oligomer and dibenzoyl peroxide radical) and the proposed cross-linked acrylic/PPE structure formed.

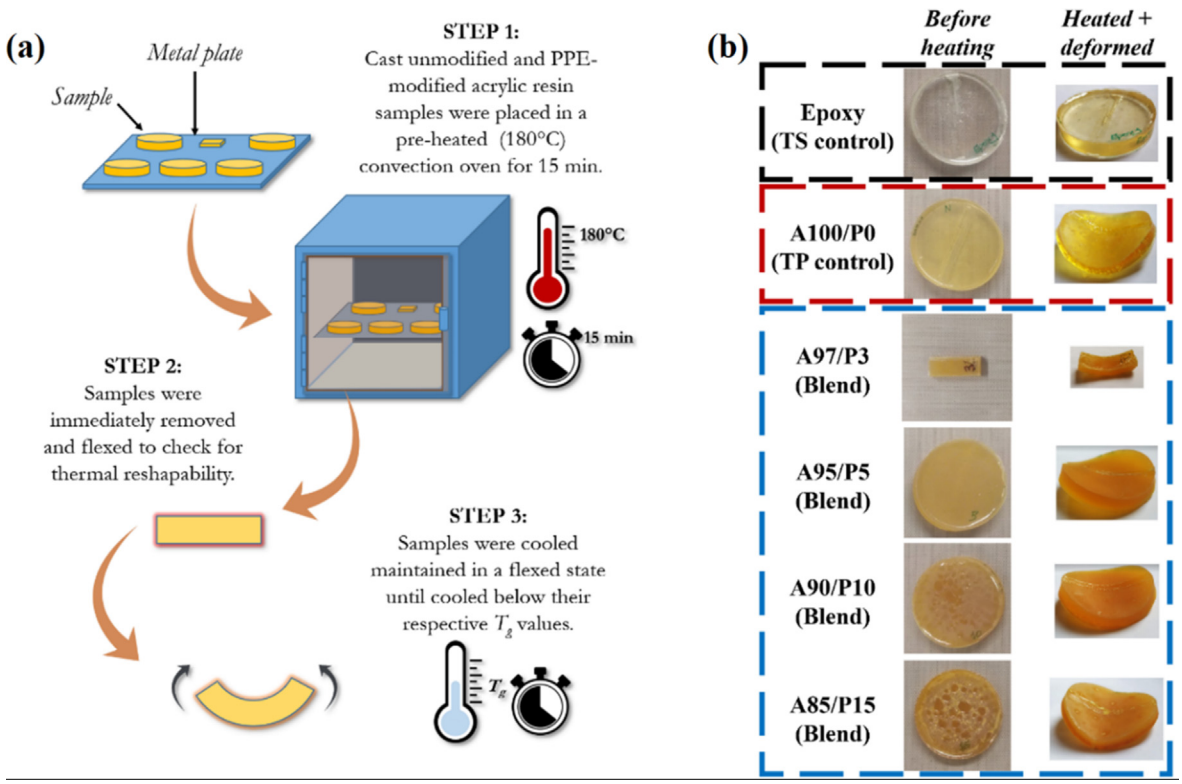


Fig. 10. (a) Methodology and (b) results of reshapability trials performed on unreinforced neat and PPE-modified acrylic samples. 40-mm dia. disc samples were used for an epoxy reference, A100/P0, A95/P5, A90/P10 and A85/P15 samples. The sample for A97/P3 measures 25 mm × 8 mm × 4 mm due to material availability constraints.

processibility of the unreinforced PPE-modified acrylic blends. The unreinforced acrylic/PPE blends and the unreinforced neat acrylic samples can be seen to be deformable upon heating and retain the deformed shape upon cooling. Thus, it was demonstrated that the thermoplastic blends produced in this work exhibit the desirable characteristics of thermosets (possessing excellent solvent resistance, thermal stability, and easy infusibility at room temperature), while also retaining the post-processibility of thermoplastics.

Such duality of characteristics has been previously reported for materials such as vitrimers and covalent adaptable networks (CANs), which are known to offer excellent reprocessibility despite containing cross-linked networks [69–71]. In addition to retaining the post-processibility of thermoplastics, which facilitates reshaping even after polymerisation and solidification, these attributes are highly advantageous and offer numerous potentials for composite applications.

Combined with the micrographic evidence from confocal Raman imaging and SEM imaging, thermogravimetric analysis and solvent resistance trials, the thermoformability of these blends confirms that both acrylic-rich and cross-linked acrylic/PPE remain reshapable following in-situ polymerisation and consolidation. Moreover, the results of thermoforming trials suggest a good extent of chain mobility must be possible despite the presence of cross-links. Thus, these results confirm that the blends may only be slightly cross-linked or that the cross-links form clusters.

The degree and density of cross-linking are expected to be highly influenced by the relative reactivities of PPE and acrylic. Variations in the extent of steric hindrance resulting from the presence of bulky phenyl groups [72,73] will likely result in volumetric congestion around each successive acrylic/PPE interaction at the reactive site. In addition, an increase in the solution viscosity is expected to result in the trapping or burying of some substituents. Consequently, some of the PPE macromolecules may only be partially saturated upon the termination of the polymerisation reaction, with perhaps trace amounts of unreacted PPE remaining entrapped by cross-linked and grafted chains. The latter may account for the aforementioned observation of unreacted PPE during NMR analysis. Branched or grafted chains can effectively become anchored and trapped within the network within such structures, restricting disengagement. As such, their presence is not expected to compromise the solvent resistance of the blends [74].

Moreover, no specialised approach was adopted for tuning or controlling the cross-linking or grafting processes; thus, spatial variations are expected within each blend system. Finally, based on these observations and discussions, the chain architecture is proposed in Fig. 11.

This is supported by the analysis of results presented in Section 3.1.2, where the two distinct glass transition temperatures observable at the tan delta peaks provided evidence of the formation of a complex reacted acrylic/PPE species. Although these temperatures revealed that the acrylic homopolymer contributed approximately 84 wt% of the total blended system within the GF/A95/P5 material, with the reacted product constituting approximately 16 wt%, the relatively high residual mass following exposure to acetone provides even more insights into the blend architecture. The linear, acrylic homopolymer is likely shielded within a protective reacted network and is expected to interpenetrate the cross-linked acrylic/PPE network alongside a graft copolymer. In such a structure, the network can effectively serve as a scaffold and may promote a great extent of entanglement between linear acrylic and PPE-grafted acrylic chains.

Remarkably, such architecture has been previously reported by Röttger [75], who showed that dioxaborolane-based vitrimers exhibit excellent solvent resistance in THF, retaining up to 95% of their original mass. The same materials were reported to remain thermoformable even with cross-linked constituents. This is simi-

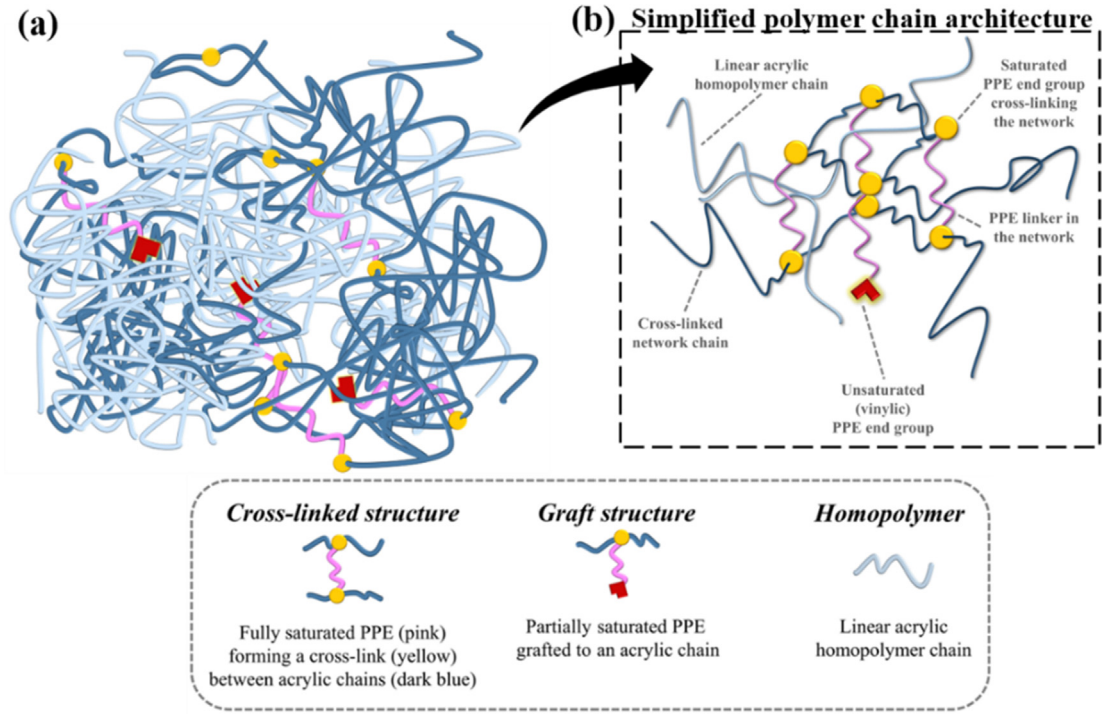


Fig. 11. (a) The proposed polymer architecture within the PPE-modified acrylic blends, showing a lightly cross-linked acrylic/PPE network, a branched or grafted acrylic/PPE species, and a highly entangled, linear acrylic polymer species; (b) a simplified form of same.

lar to the findings presented herein and may provide interesting insights into the behaviour of the blends considered in this present work. The formation of a vitrimer is highly unexpected, however, as vitrimers characteristically require ester-alcohol transesterification reactions. Thus, it is not believed that the blends in this work are vitrimeric in nature.

Moreover, the process employed in this paper produces a similar material to interpenetrating polymer networks (IPNs) in that at least one of the polymers is synthesised in the presence of the other [53,76–80]. A distinguishing characteristic of IPNs is that one (semi-IPN) or both (full IPN) are cross-linked to form a network. Although the novel polymer blends presented in this chapter were not prepared with a traditional cross-linker, it has been shown that the telechelic PPE employed can promote cross-linking. Thus, the resulting blend architecture is likely similar to a semi-IPN with both linear acrylic and branched/grafted acrylic/PPE species interpenetrating within a lightly cross-linked acrylic/PPE network.

4. Conclusions

This paper demonstrates a simple, yet practical reactive hybridisation approach for tailoring the performance of liquid acrylic resins for composite applications. Unique insights into the structure–property relationships, which underpin the observed effects of hybridisation, were provided via a combination of spectroscopic, thermal and microscopic analytical techniques. Incorporating reactive oligomeric PPE with functional vinylic groups into reactive monomeric acrylic resin results in enhanced solvent resistance (in $CDCl_3$ and acetone) and higher glass transition temperature of unreinforced (up to 6% increase) and glass fibre-reinforced (+9%) acrylic/PPE hybrid material systems, with respect to their neat acrylic counterparts. While unreinforced blend samples retained up to 77% of their original masses after 72 h of acetone exposure, the unreinforced, unmodified acrylic sample fully dissolved after 300 min. Reinforced samples exhibited similar trends: 98% and 72% mass-retentions in the PPE-modified and unmodified samples, respectively. In addition to the enhanced solvent resistance, the hybrids exhibited exceptional resistance to mechanical grinding; thus, suitable samples for solid-state NMR spectroscopic analysis were not readily obtained. However, solution-state NMR spectroscopic analysis of the soluble portions (in $CDCl_3$) indicated the formation of multi-component mixtures comprising individual molecules of monomeric and polymeric acrylic, oligomeric PPE and BPO. This suggests that the insoluble portions are more complex and likely to be copolymeric or cross-linked acrylic/PPE species while retaining reshapability with applied heat and pressure after in-situ polymerisation. These findings open up new opportunities for scalable and low-temperature fabrication of thermoplastic amorphous hybrid-matrix composites with tailored properties for a wide range of practical applications. Finally, while this work demonstrated positive hybridisation effects using only glass fibres, we believe that the insights presented herein should be applicable to other appropriately sized fibre systems (for the base reactive acrylic resin).

Funding sources

Ms W. Gruszka and Dr J. A. Garden would like to thank the CRITICAT Centre for Doctoral Training and Engineering and Physical Sciences Research Council (PhD studentship to W. G.; Grant EP/L016419/1), Royal Society (J. A. G., Grant RSG/R1/180101), British Ramsay Memorial Trust (J. A. G.) and L'Oréal-UNESCO For Women in Science (J. A. G.) for funding. C. Wurzer received funding from the European Union's Horizon 2020 research and innovation programme under the Marie Skłodowska-Curie grant agreement No 721991.

Declaration of Competing Interest

The authors declare that they have no known competing financial interests or personal relationships that could have appeared to influence the work reported in this paper.

Acknowledgements

The authors gratefully acknowledge Arkema GRL, France and SABIC for the provision of materials and technical support towards this research. SABIC and brands marked with ™ are trademarks of SABIC or its subsidiaries or affiliates, unless otherwise noted. Moreover, the authors also wish to acknowledge the support of the Henry Royce Institute for Ms O. W. Obande through the Royce PhD Equipment Access Scheme enabling access to Confocal Raman facilities at Royce@CCFE; EPSRC Grant Number EP/R00661X/1.

Data availability

The raw data required to reproduce these findings cannot be shared at this time due to technical or time limitations.

Appendix A. Supplementary material

Supplementary data to this article can be found online at https://doi.org/10.1016/j.matdes.2021.109804.

References

[1] W. Obande, C.M. Ó Brádaigh, D. Ray. Continuous fibre-reinforced thermoplastic acrylic-matrix composites prepared by liquid resin infusion – A review. Compos Part B Eng 2021:108771. https://doi.org/10.1016/j.compositesb.2021.108771

[2] N. Han, I. Baran, J.S.M. Zanjani, O. Yuksel, L.L. An, R. Akkerman, Experimental and computational analysis of the polymerization overheating in thick glass/Elium® acrylic thermoplastic resin composites, Compos Part B Eng (2020), https://doi.org/10.1016/j.compositesb.2020.108430.

[3] S.K. Bhudolia, G. Gohel, L.K. Fai, R.J. Barsotti, Investigation on ultrasonic welding attributes of novel carbon/Elium® composites, Materials (Basel) 13 (2020) 10–15, https://doi.org/10.3390/ma13051117.

[4] S.K. Bhudolia, G. Gohel, L. Kah Fai, R.J. Barsotti, Fatigue response of ultrasonically welded carbon/Elium® thermoplastic composites, Mater Lett 264 (2020), https://doi.org/10.1016/j.matlet.2020.127362 127362.

[5] M.E. Kazemi, L. Shanmugam, S. Chen, L. Yang, J. Yang, Novel thermoplastic fiber metal laminates manufactured with an innovative acrylic resin at room temperature, Compos Part A Appl Sci Manuf 138 (2020) 106043, https://doi.org/10.1016/j.compositesa.2020.106043.

[6] M.E. Kazemi, L. Shanmugam, Z. Li, R. Ma, L. Yang, J. Yang, Low-velocity impact behaviors of a fully thermoplastic composite laminate fabricated with an innovative acrylic resin, Compos Struct 250 (2020) 112604, https://doi.org/10.1016/j.compstruct.2020.112604.

[7] H. Bel Haj Frej, R. Léger, D. Perrin, P. Ienny, Effect of aging temperature on a thermoset-like novel acrylic thermoplastic composite for marine vessels, J Compos Mater (2021), https://doi.org/10.1177/0021998321996780. 002199832199678.

[8] L. Shanmugam, M.E. Kazemi, C. Qiu, M. Rui, L. Yang, J. Yang, Influence of UHMWPE fiber and Ti6Al4V metal surface treatments on the low-velocity impact behavior of thermoplastic fiber metal laminates, Adv Compos Hybrid Mater 3 (2020) 508–521, https://doi.org/10.1007/s42114-020-00189-7.

[9] S.K. Bhudolia, G. Gohel, S.C. Joshi, K.F. Leong, Quasi-static indentation response of core-shell particle reinforced novel NCCF/Elium® composites at different feed rates, Compos Commun 21 (2020) 100383, https://doi.org/10.1016/j.coco.2020.100383.

[10] A. Chilali, W. Zouari, M. Assarar, H. Kebir, R. Ayad, Analysis of the mechanical behaviour of flax and glass fabrics-reinforced thermoplastic and thermoset resins, J Reinf Plast Compos 35 (2016) 1217–1232, https://doi.org/10.1177/0731684416645203.

[11] G. Kinvi-Dossou, R. Matadi Boumbimba, N. Bonfoh, S. Garzon-Hernandez, D. Garcia-Gonzalez, P. Gerard, et al., Innovative acrylic thermoplastic composites versus conventional composites: Improving the impact performances, Compos Struct 217 (2019) 1–13, https://doi.org/10.1016/j.compstruct.2019.02.090.

[12] A. Aronica, D. Fossati, Mechanical Properties of Carbon Fiber Composite Materials, Politecnico di Milano [Master's Thesis] (2014).

[13] A. Aronica, D. Fossati, Effects of resin and processing on mechanical properties of carbon fibre composites, Politecnico di Milano [Master's Thesis] (2015).

[14] C. Baley, M. Lan, A. Bourmaud, A. Le Duigou, Compressive and tensile behaviour of unidirectional composites reinforced by natural fibres: Influence of fibres (flax and jute), matrix and fibre volume fraction, Mater Today Commun 16 (2018) 300–306, https://doi.org/10.1016/j.mtcomm.2018.07.003.

[15] W. Obande, D. Ray, C.M. Ó Brádaigh. Viscoelastic and drop-weight impact properties of an acrylic-matrix composite and a conventional thermoset composite – A comparative study. Mater Lett 2019;238:38–41. https://doi.org/10.1016/j.matlet.2018.11.137

[16] A. Chilali, M. Assarar, W. Zouari, H. Kebir, R. Ayad, Effect of geometric dimensions and fibre orientation on 3D moisture diffusion in flax fibre reinforced thermoplastic and thermosetting composites, Compos Part A Appl Sci Manuf 95 (2017) 75–86, https://doi.org/10.1016/j.compositesa.2016.12.020.

[17] S.K.K. Bhudolia, P. Perrotey, S.C.C. Joshi, Optimizing polymer infusion process for thin ply textile composites with novel matrix system, Materials (Basel) 10 (2017), https://doi.org/10.3390/ma10030293.

[18] T. Lorriot, J. El Yagoubi, J. Fourel, F. Tison. Non-conventional glass fiber NCF composites with thermoset and thermoplastic matrices. 20th Int. Conf. Compos. Mater., Copenhagen: 2015

[19] W. Obande, D. Mamalis, D. Ray, L. Yang, C.M. Ó Brádaigh. Mechanical and thermomechanical characterisation of vacuum-infused thermoplastic- and thermoset-based composites. Mater Des 2019;175:107828. https://doi.org/10.1016/j.matdes.2019.107828

[20] R.E. Murray, D. Penumadu, D. Cousins, R. Beach, D. Snowberg, D. Berry, et al., Manufacturing and Flexural Characterization of Infusion-Reacted Thermoplastic Wind Turbine Blade Subcomponents, Appl Compos Mater 27 (2019) 1–17, https://doi.org/10.1007/s10443-019-9760-2.

[21] P. Davies, M. Arhant, Fatigue behaviour of acrylic matrix composites: influence of seawater, Appl Compos Mater 26 (2019) 507–518, https://doi.org/10.1007/s10443-018-9713-1.

[22] S.K. Bhudolia, P. Perrotey, S.C. Joshi, Mode I fracture toughness and fractographic investigation of carbon fibre composites with liquid Methylmethacrylate thermoplastic matrix, Compos Part B Eng 134 (2018) 246–253, https://doi.org/10.1016/j.compositesb.2017.09.057.

[23] Chemical Resistance of Thermoplastics, Plastics Design Library, Volume 1, 2012, p. 1–106. https://doi.org/10.1016/b978-1-4557-7896-6.00001-7.

[24] P.K. Mallick, Thermoplastics and thermoplastic-matrix composites for lightweight automotive structures, Mater. Des. Manuf. Light. Veh., Elsevier Ltd. (2010) 174–207, https://doi.org/10.1533/9781845697822.1.174.

[25] S.E. Lee, E. Jeong, M.Y. Lee, M.K. Lee, Y.S. Lee, Improvement of the mechanical and thermal properties of polyethersulfone-modified epoxy composites, J Ind Eng Chem 33 (2016) 73–79, https://doi.org/10.1016/j.jiec.2015.09.022.

[26] K. Mimura, H. Ito, H. Fujioka, Improvement of thermal and mechanical properties by control of morphologies in PES-modified epoxy resins, Polymer (Guildf) 41 (2000) 4451–4459, https://doi.org/10.1016/S0032-3861(99)00700-4.

[27] P. Zhao, X. Liang, J. Chen, Q. Ran, Y. Gu, Poly(ether imide)-modified benzoxazine blends: Influences of phase separation and hydrogen bonding interactions on the curing reaction, J Appl Polym Sci 128 (2013) 2865–2874, https://doi.org/10.1002/app.38459.

[28] N. Biolley, T. Pascal, B. Sillion, Polyimide-modified epoxy system: time-temperature-transformation diagrams, mechanical and thermal properties, Polymer (Guildf) 35 (1994) 558–564, https://doi.org/10.1016/0032-3861(94)90511-8.

[29] I. Hamerton, L.T. McNamara, B.J. Howlin, P.A. Smith, P. Cross, S. Ward, Toughening mechanisms in aromatic polybenzoxazines using thermoplastic oligomers and telechelics, Macromolecules 47 (2014) 1946–1958, https://doi.org/10.1021/ma5002436.

[30] T. Orhan, S. Ates, J. Hacaloglu, Y. Yagci, Thermal degradation characteristics of polysulfones with benzoxazine end groups, J Anal Appl Pyrolysis 94 (2012) 146–152, https://doi.org/10.1016/j.jaap.2011.12.001.

[31] B. Del Saz-Orozco, D. Ray, A. Kervennic, P.T. McGrail, W.F. Stanley, Toughening of carbon fibre/polybenzoxazine composites by incorporating polyethersulfone into the interlaminar region, Mater Des 93 (2016) 297–303, https://doi.org/10.1016/j.matdes.2015.12.138.

[32] G. Di Pasquale, O. Motta, A. Recca, J.T. Carter, P.T. McGrail, D. Acierno, New high-performance thermoplastic toughened epoxy thermosets, Polymer (Guildf) 38 (1997) 4345–4348, https://doi.org/10.1016/S0032-3861(96)01031-2.

[33] I. Hamerton, L.T. McNamara, B.J. Howlin, P.A. Smith, P. Cross, S. Ward, Developing toughened aromatic polybenzoxazines using thermoplastic oligomers and telechelics, part 1: Preparation and characterization of the functionalized oligomers, J Appl Polym Sci (2014;131.), https://doi.org/10.1002/app.40875.

[34] B. Ronak. Fracture mechanics of nanostructured polymer blends with janus particles. University of Bayreuth [Doctoral Thesis], 2018.

[35] Nelissen LNIH. A novel route to blends of polystyrene and poly(2,6-dimethyl-1,4-phenylene ether) : synthesis, properties and applications 1991. https://doi.org/10.6100/IR352941.

[36] J.G. Bennett, R.M. Summers, Composition of a polyphenylene ether and an acrylic resin modified polyisoprene (1974), https://doi.org/10.1145/178951.178972.

[37] F.J. Viersen, P. Colantuoni, I. Mamalis, Compatibilization of poly(2,6-dimethyl-1,4-phenylene ether)/poly(vinylidene difluoride) blends, Die Angew Makromol Chemie (1993), https://doi.org/10.1002/apmc.1993.052060111.

[38] W. Obande, C.M. Ó Brádaigh , D. Ray. Thermoplastic hybrid-matrix composite prepared by a room-temperature vacuum infusion and in-situ polymerisation process. Compos Commun 2020. https://doi.org/10.1016/j.coco.2020.100439

[39] I. Devotta, M.V. Badiger, P.R. Rajamohanan, S. Ganapathy, R.A. Mashelkar, Unusual retardation and enhancement in polymer dissolution: role of disengagement dynamics, Chem Eng Sci 50 (1995) 2557–2569.

[40] B.A. Miller-Chou, J.L. Koenig, A review of polymer dissolution, Prog Polym Sci 28 (2003) 1223–1270, https://doi.org/10.1016/S0079-6700(03)00045-5.

[41] F.M. Uhl, G.F. Levchik, S.V. Levchik, C. Dick, J.J. Liggat, C.E. Snape, et al., Thermal stability of cross-linked polymers: Methyl methacrylate with divinylbenzene and styrene with dimethacrylates, Polym Degrad Stab 71 (2001) 317–325, https://doi.org/10.1016/S0141-3910(00)00181-6.
[42] T. Nakano, π-stacked polymers and molecules: Theory, synthesis, and properties. (2014), https://doi.org/10.1007/978-4-431-54129-5.
[43] M. Zhang, O. Bareille, M. Salvia, Cure and damage monitoring of flax fiber-reinforced epoxy composite repairs for civil engineering structures using embedded piezo micro-patches, Constr Build Mater (2019), https://doi.org/10.1016/j.conbuildmat.2019.07.179.
[44] C.C. Huang, M.S. Yang, M. Liang, Synthesis of new thermosetting poly(2,6-dimethyl-1, 4-phenylene oxide)s containing epoxide pendant groups, J Polym Sci Part A Polym Chem (2006), https://doi.org/10.1002/pola.21679.
[45] J.P. Correa-Aguirre, F. Luna-Vera, C. Caicedo, B. Vera-Mondragón, M.A. Hidalgo-Salazar, The Effects of Reprocessing and Fiber Treatments on the Properties of Polypropylene-Sugarcane Bagasse Biocomposites, Polymers (Basel) 12 (2020) 1440, https://doi.org/10.3390/polym12071440.
[46] A. Romo-Uribe, Dynamic Mechanical Thermal Analysis of Epoxy/Thermoplastic Blends 23, Handb. Epoxy Blends (2017) 675–706, https://doi.org/10.1007/978-3-319-40043-3_23.
[47] K.S. Arora, F. Baah, G.M. Canard, D.E. Setze, DMA of new acrylic- polyurethane hybrids, Eur Coatings J (2001). 2001.
[48] N.J.W. Gamage, D.J.T. Hill, C.A. Lukey, P.J. Pomery, Thermal characterization of polyester-melamine coating matrices prepared under nonisothermal conditions, J Polym Sci Part A Polym Chem 41 (2003) 1603–1621, https://doi.org/10.1002/pola.10698.
[49] A. Bacchi, J.A. Yih, J. Platta, J. Knight, C.S. Pfeifer, Shrinkage/stress reduction and mechanical properties improvement in restorative composites formulated with thio-urethane oligomers, J Mech Behav Biomed Mater 78 (2018) 235–240, https://doi.org/10.1016/j.jmbbm.2017.11.011.
[50] H. Miyagawa, M.J. Rich, L.T. Drzal, Amine-cured epoxy/clay nanocomposites. I. Processing and chemical characterization, J Polym Sci Part B Polym Phys (2004), https://doi.org/10.1002/polb.20288.
[51] A.R. Kannurpatti, J.W. Anseth, C.N. Bowman, A study of the evolution of mechanical properties and structural heterogeneity of polymer networks formed by photopolymerizations of multifunctional (meth)acrylates, Polymer (Guildf) 39 (1998) 2507–2513, https://doi.org/10.1016/S0032-3861(97)00585-5.
[52] N. Alizadeh, M. Barde, M. Minkler, A.D. Celestine, V. Agrawal, B. Beckingham, et al., High-fracture-toughness acrylic–polyurethane-based graft-interpenetrating polymer networks for transparent applications, Polym Int (2020), https://doi.org/10.1002/pi.6149.
[53] L.V. Karabanova, G. Boiteux, G. Seytre, S. Isabelle, A.W. Lloyd, S.V. Mikhalovsky, et al., Phase separation in the polyurethane/poly(2-hydroxyethyl methacrylate) semi-interpenetrating polymer networks synthesized by different ways, Polym Eng Sci 48 (2008) 588–597, https://doi.org/10.1002/pen.
[54] T. Fujiyabu, Y. Yoshikawa, Chung U il, T. Sakai. Structure-property relationship of a model network containing solvent. Sci Technol Adv Mater 2019. https://doi.org/10.1080/14686996.2019.1618685.
[55] L.G.D. Hawke, M. Ahmadi, H. Goldansaz, E. van Ruymbeke, Viscoelastic properties of linear associating poly(n-butyl acrylate) chains, J Rheol (N Y N Y) (2016), https://doi.org/10.1122/1.4942231.
[56] C. Huang, G. Huang, S. Li, M. Luo, H. Liu, X. Fu, et al., Research on architecture and composition of natural network in natural rubber, Polymer (Guildf) (2018), https://doi.org/10.1016/j.polymer.2018.08.057.
[57] K. Bandzierz, L. Reuvekamp, J. Dryzek, W. Dierkes, A. Blume, D. Bielinski, Influence of network structure on glass transition temperature of elastomers, Materials (Basel) (2016;9.), https://doi.org/10.3390/MA9070607.
[58] D. Romanzini, A. Lavoratti, H.L. Ornaghi, S.C. Amico, A.J. Zattera, Influence of fiber content on the mechanical and dynamic mechanical properties of glass/ramie polymer composites, Mater Des 47 (2013) 9–15, https://doi.org/10.1016/j.matdes.2012.12.029.
[59] M. Idicula, S.K. Malhotra, K. Joseph, S. Thomas, Dynamic mechanical analysis of randomly oriented intimately mixed short banana/sisal hybrid fibre reinforced polyester composites, Compos Sci Technol 65 (2005) 1077–1087, https://doi.org/10.1016/j.compscitech.2004.10.023.
[60] E.N. Peters, Poly(phenylene ether) based amphiphilic block copolymers, Polymers (Basel) 9 (2017), https://doi.org/10.3390/polym9090433.
[61] G. Wypych, Data on Specific Polymers, Handb Mater Weather (2013) 351–546, https://doi.org/10.1016/b978-1-895198-62-1.50017-2.
[62] S.G. Castellanos, V.V.A. Fernández, J. Aguilar, F.J. Moscoso-Sánchez, I. Ceja, G. Canché-Escamilla, et al., Synthesis and characterization of poly(methyl methacrylate)-boehmite nanocomposites by direct microemulsion polymerization combined with the in-situ sol-gel method, Polymer (Guildf) 163 (2019) 134–143, https://doi.org/10.1016/j.polymer.2018.12.053.
[63] E.T. Röchow, L. Häußler, A. Korwitz, D. Pospiech, Thermal decomposition of phosphonate-containing methacrylate-based copolymers, Polym Degrad Stab 152 (2018) 235–243, https://doi.org/10.1016/j.polymdegradstab.2018.04.036.
[64] W. Viratyaporn, R.L. Lehman, Effect of nanoparticles on the thermal stability of PMMA nanocomposites prepared by in situ bulk polymerization, J Therm Anal Calorim 103 (2011) 267–273, https://doi.org/10.1007/s10973-010-1051-y.
[65] Raponi O de Andrade, L.C.M. Barbosa, B.R. de Souza, A.C. Ancelotti Junior, Study of the influence of initiator content in the polymerization reaction of a thermoplastic liquid resin for advanced composite manufacturing, Adv Polym Technol 37 (2018) 3579–3587, https://doi.org/10.1002/adv.22142.
[66] V. Percec, C. Pugh, O. Nuyken, Pask SD. Macromonomers, Oligomers and Telechelic Polymers, Compr. Polym. Sci. Suppl., Elsevier (1989) 281–357, https://doi.org/10.1016/b978-0-08-096701-1.00189-0.
[67] H.J. Reich, Chem 605 - Structure Determination Using Spectroscopic, Methods (2020).
[68] SABIC. NORYLTM SA9000 resin solubility guide 2019.
[69] H. Han, X. Xu, Poly(methyl methacrylate)–epoxy vitrimer composites, J Appl Polym Sci (2018), https://doi.org/10.1002/app.46307.
[70] Q. Li, S. Ma, N. Lu, J. Qiu, J. Ye, Y. Liu, et al., Concurrent thiol–ene competitive reactions provide reprocessable, degradable and creep-resistant dynamic–permanent hybrid covalent networks, Green Chem (2020), https://doi.org/10.1039/d0gc02823a.
[71] N.J. Van Zee, R. Nicolaÿ, Vitrimers: Permanently crosslinked polymers with dynamic network topology, Prog Polym Sci (2020), https://doi.org/10.1016/j.progpolymsci.2020.101233.
[72] Flory PJ. Principles of polymer chemistry. 1953.
[73] B. Yamada, P.B. Zetterlund, E. Sato, Utility of propenyl groups in free radical polymerization: Effects of steric hindrance on formation and reaction behavior as versatile intermediates, Prog Polym Sci 31 (2006) 835–877, https://doi.org/10.1016/j.progpolymsci.2006.08.005.
[74] R.A. Plenderleith, C.J. Pateman, C. Rodenburg, J.W. Haycock, F. Claeyssens, C. Sammon, et al., Arginine-glycine-aspartic acid functional branched semi-interpenetrating hydrogels, Soft Matter (2015), https://doi.org/10.1039/c5sm00695c.
[75] M. Röttger, T. Domenech, R. Van Der Weegen, A. Breuillac, R. Nicolaÿ, L. Leibler, High-performance vitrimers from commodity thermoplastics through dioxaborolane metathesis, Science 356 (2017) 62–65, https://doi.org/10.1126/science.aah5281.
[76] V.D. Athawale, S.L. Kolekar, S.S. Raut, Recent developments in polyurethanes and poly(acrylates) interpenetrating polymer networks, J Macromol Sci - Polym Rev (2003), https://doi.org/10.1081/MC-120018018.
[77] L.V. Karabanova, S.V. Mikhalovsky, A.W. Lloyd, G. Boiteux, L.M. Sergeeva, T.I. Novikova, et al., Gradient semi-interpenetrating polymer networks based on polyurethane and poly(vinyl pyrrolidone), J Mater Chem (2005), https://doi.org/10.1039/b410178b.
[78] L.H. Sperling, V. Mishra, The current status of interpenetrating polymer networks, Polym Adv Technol (1996), https://doi.org/10.1002/(SICI)1099-1581(199604)7:4<197::AID-PAT514>3.0.CO;2-4.
[79] L.H. Sperling, R. Hu, Interpenetrating polymer networks. Polym. Blends Handb. (2014), https://doi.org/10.1007/978-94-007-6064-6_8.
[80] Y.S. Lipatov, T.S. Chramova, L.M. Sergeeva, L.V. Karabanova, Some properties of intermediate regions in interpenetrating polymeric networks, J. Polym. Sci. Polym. Chem. Ed (1977), https://doi.org/10.1002/pol.1977.170150216.

Composites Part B 215 (2021) 108771

Contents lists available at ScienceDirect

Composites Part B

journal homepage: www.elsevier.com/locate/compositesb

Continuous fibre-reinforced thermoplastic acrylic-matrix composites prepared by liquid resin infusion – A review

Winifred Obande, Conchúr M. Ó Brádaigh, Dipa Ray *

School of Engineering, Institute for Materials and Processes, The University of Edinburgh, Sanderson Building, Robert Stevenson Road, Edinburgh, EH93FB, Scotland, United Kingdom

ARTICLE INFO

Keywords:
A. polymer-matrix composites (PMCs)
A. Thermoplastic resin
B. Mechanical properties
E. Liquid composite moulding

ABSTRACT

Increasing demand for lightweight materials is a major driving force for the steady growth of the continuous fibre-reinforced polymer composite industry. In recent years, strict global targets demanding greater environmental responsibility have led to a shift in research focus to address the end-of-life challenges posed by the use of thermoset matrices. Thermosets offer lower-cost processibility than thermoplastics, which historically required cost- and energy-intensive production methodologies. Consequently, despite their well-demonstrated recyclability, thermoformability and weldability, thermoplastics are yet to attain the same technological maturity as thermosets. *In situ* polymerisable thermoplastic resins have been identified as attractive emerging solutions for improving the processibility of thermoplastics. Thus, are essential materials in meeting the demand for fibre-reinforced thermoplastic composites. This review presents a comprehensive summary of recent works on room-temperature-processible liquid thermoplastic acrylic resins and their composites. Moreover, open problems and research opportunities are identified and discussed.

1. Introduction

In parallel to the increasing demand for fibre-reinforced polymer (FRP) composites, there is renewed interest in thermoplastic (TP) matrices across many sectors where their thermoset (TS) counterparts are dominant. While it has long been established that TP matrices offer more favourable benefits than TS matrices in terms of recyclability, welding and thermoformability [1–3], their high-melt viscosities necessitate high processing temperatures and pressures, and thus, renders them cost-prohibitive and impractical for most sectors [4,5]. Research efforts to address this have paved the way for the application of innovative *in situ* polymerisation methodologies for the production of continuous fibre-reinforced TP composites. Early-generation reactive TP precursors such as cyclic butylene terephthalate (CBT) [6–10], caprolactam [11,12] and laurolactam [13,14] now facilitate the production of fibre-reinforced polybutylene terephthalate (PBT), polyamide-6 (PA-6) and polyamide-12 (PA-12) by liquid composite moulding, respectively. These materials do, however, require mould heating to achieve temperatures above 150°C (PA-6 and PA-12) and 180°C (PBT), which makes the fabrication of large-scale structures relatively challenging. This additional requirement for mould heating may be impracticable for the wind energy sector, for instance, where blade lengths continue to increase to meet growing global demand [15–17].

The study of bulk polymerisation of acrylic resins started in the 1940s, and only few studies were reported on the reactive processing of acrylic composites [18]. The growing interest in the field of TP-FRPs has led to the development of Elium®, a family of liquid TP acrylic resins, which are suitable for manufacturing large composite structures with continuous fibre reinforcement at room temperature via *in situ* polymerisation. With viscosities as low as 100 mPa s, these acrylic resins are considered more cost-effective than the aforementioned first-generation reactive resins. Moreover, their suitability for the production of large-scale components by resin infusion [19–21]; and their thermoformability and recyclability [22] have recently been demonstrated.

The present article reviews the advancements to-date in the use of reactive acrylic resins as attractive solutions to the challenges associated with traditional thermosetting and thermoplastic matrices for composite applications. Published works on the mechanical and thermomechanical performance of *in situ* polymerisable acrylic matrices and their composites are reviewed and discussed in this article. A comprehensive summary of comparative analyses performed to-date alongside comparable thermosetting composites is also presented. This article is intended

* Corresponding author.
E-mail address: dipa.roy@ed.ac.uk (D. Ray).

https://doi.org/10.1016/j.compositesb.2021.108771
Received 28 December 2020; Received in revised form 26 February 2021; Accepted 6 March 2021
Available online 11 March 2021
1359-8368/© 2021 Elsevier Ltd. All rights reserved.

Table 1
Summary of the resins in the works under review and new name assignations, with unreinforced matrix properties.

Commercial name	Elium® 150	Elium® RT150	Elium® 180	Elium® 188, Elium® 188 O	Elium® 280	Elium® C595 E
New name assignation	E−150	E−RT150	E−180	E−188O	E−280	E−C595E
Recommended process	Infusion	Injection	Infusion; injection	Infusion; injection	–	Pultrusion; wet compression; winding
Viscosity at 25°C (m.Pas)	100	100	100	100	–	500
Process temp. (°C)	15–25	15–25	20–60	20–60	–	20–115
Process time @ 25°C (min)	55–60	55–60	45–60	45–60	–	Adjustable
Initiator/Catalyst	Dibenzoyl peroxide	Dibenzoyl peroxide	Dibenzoyl peroxide	Dibenzoyl peroxide	–	Peroxide blend
Tensile strength (MPa)	76	76	66	66	76	66
Tensile modulus (GPa)	3.3	3.3	3.17	3.17	3.3	3.17
Elongation (%)	6	6	2.8	2.8	6	–
Compressive strength (MPa)	130	130	116	116	–	–
Compressive modulus (GPa)	–	–	3.83	3.83	–	–
Flexural strength (MPa)	130	130	111	111	–	–
Flexural modulus (GPa)	3.25	3.25	2.91	2.91	–	–

for the composites community, so a detailed description of the polymerisation chemistry of the acrylic resins has not been included within the scope of this article.

In the sections that follow, new name assignations have been applied as detailed in Table 1; e.g.: the use of E−150 now implies Elium® 150.

2. Polymerisation reaction of liquid reactive acrylic resins

2.1. Studies on polymerisation behaviour

Acrylics polymerise by free radical polymerisation and undergo the three characteristic reactions: (i) Initiation is typically brought about by radical peroxides (initiators or catalysts), which comprise unpaired electrons that open double bonds (unsaturation) in the monomers, resulting in the creation of reactive radical sites on the monomers; (ii) The chain propagation reaction ensues, with unreacted monomer molecules successively being 'captured' and newly unpaired electrons becoming available at growing chain ends; (iii) Termination can subsequently occur by recombination, usually in the presence of another radical, or a termination agent to bring growth to an end. Process parameters such as initiator concentration, temperature and pressure, have been reported to significantly influence the rates of radical polymerisation reactions and consequently, the resultant molecular weight and molecular weight distribution [23,24]. Understanding their effects on the resulting acrylic polymer system is an essential step in fostering an established knowledge base on optimum processing conditions. Presented herein, is a brief overview of published works on polymerisation behaviour of acrylics as a function of processing conditions.

2.1.1. Influence of initiator content

Using the E−150 grade of liquid acrylic resin and a commercial organic peroxide, it was reported that initiator content influences the reaction stages of free radical polymerisation [25]. Both high (1.6%) and low (0.8%) initiator contents promote slower initiation and termination reaction rates than an intermediate concentration (1.2%). Combined with higher onset temperatures (75°C) for the high and low concentrations, and lower temperature (58°C) for the intermediate concentration, the authors concluded that these observations were associated with the availability of the radical species provided by the initiator. It was suggested that at the lower radical concentration (0.8%), fewer acrylic monomer molecules were initiated and thus, the growth of a few long chains culminated in the observed behaviour. In contrast, higher concentration (1.6%) promoted concurrent growth of several short chains. It can thus be deduced that in all cases, these effects are combinatory effects of the competitive chain growth and ultimate termination reactions. Interestingly, the lowest initiator content was found to cause an

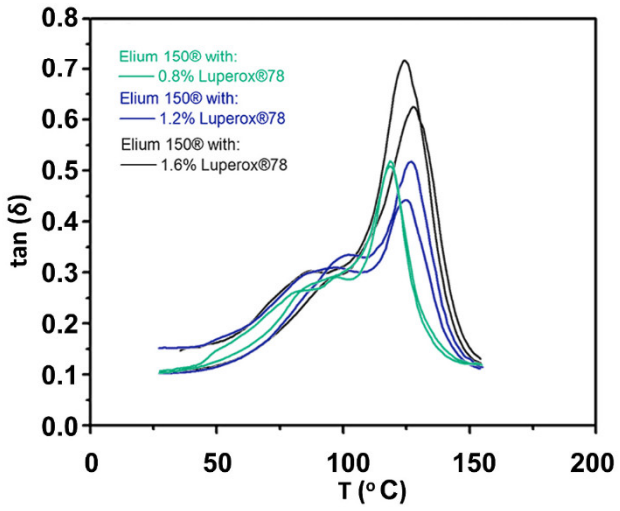


Fig. 1. Dynamic-mechanical analysis results showing effect of initiator contents of (a) 0.8%, (b) 1.2%, and (c) 1.6% on tangent delta (tan (δ)) as a function of temperature (T) (Copyright permission from Wiley. Adapted from Fig. 7 in Ref. [25]).

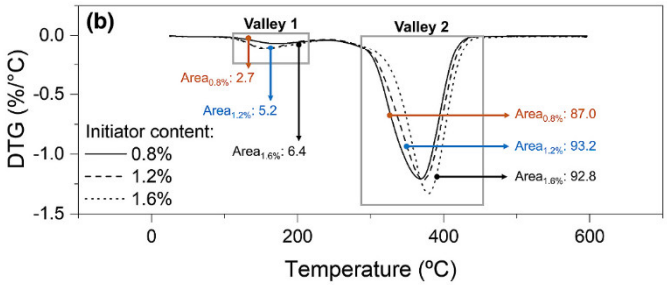


Fig. 2. Results of the thermogravimetric analyses on samples polymerised with initiator contents of 0.8 wt %, 1.2 wt % and 1.6 wt %. Valleys corresponding to the first and second mass loss events are marked as 1 and 2, respectively (Copyright permission from Wiley. Adapted from Fig. 8 in Ref. [25]).

instantaneous, exponential increase in viscosity up to the terminal cycle temperature (rheological study). Increasing the initiator content was reported to reduce the viscosity at all polymerisation reaction stages.

A positive correlation exists between the initiator content and glass transition temperature (Fig. 1), with equivalent values reported for 1.2%

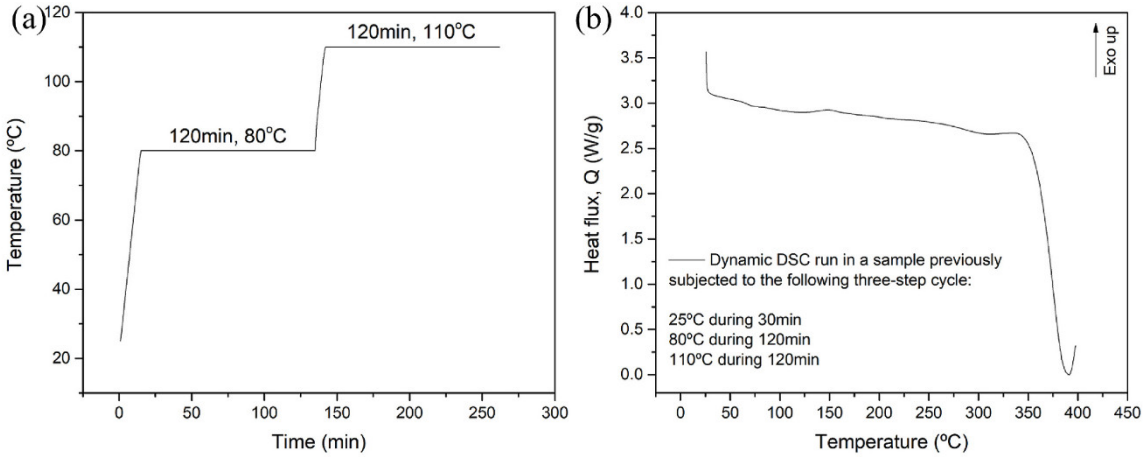


Fig. 3. Degree of conversion as a function of temperature for E−150 samples polymerised with 0.8 wt %, 1.2 wt % and 1.6 wt % of initiator (Copyright permission from Wiley [25]).

Table 2
Summary of critical findings on the influence of initiator content on polymerisation behaviour of liquid acrylic resins. Data sourced from Ref. [25].

Initiator content (wt. %)	Polymerisation				Rheology	Glass transition	Decomposition	
	$T_{100\%}$ (°C)	T_{onset} (°C)	T_{max} (°C)	-ΔH (J/g)	T_{gel} (°C)	T_g (°C)	T_{onset} Peak 1 (°C)	T_{onset} Peak 2 (°C)
0.8	199.3	75.9	82.6	129.4	87.0	116.2	113	298
1.2	122.4	57.9	70.4	150.7	84.4	123.4	115	302
1.6	163.9	74.0	81.8	210.7	87.5	123.3	108	326

and 1.6% concentrations [25]. While no effects were observed on tan delta peak amplitudes between the samples containing 0.8% and 1.2% of initiator content, a pronounced increase was observed for the sample polymerised with 1.6 wt % of the initiator. These differences were reported to be related to differences in polymer chain lengths between the samples.

The same authors reported no major effects of initiator content on the thermal degradation behaviour on polymerised samples. All samples were reported to undergo two mass loss stages, evidenced by the two valleys in the derivative thermogravimetric (DTG) curves (Fig. 2). For samples polymerised using initiator contents of 0.8%, 1.2% and 1.6%, respectively, the valleys are as follows. (i) *Valley 1*: occurred at 113°C, 115°C and 108°C, and was said to be related to the depolymerisation of head-to-head linkages (from recombination termination reactions) and residual monomers. (ii) *Valley 2*: occurred at 298°C, 302°C and 326°C. This valley was said to be associated with random scission. Evidently, an increase in initiator content promoted the formation of more head-to-head linkages. Finally, a third characteristic decomposition valley, which is observed for acrylic-based polymers due to the decomposition of unsaturated chain ends at temperatures of around 230°C was said to be absent due to copolymerisation with oxygen during the polymerisation process.

On the influence of initiator content on the degree of conversion, the samples containing 0.8 wt % and 1.6 wt % of initiator appear to exhibit slower initiation and propagation rates as shown in Fig. 3 [25]. The work by de Andrade Raponi et al. [25] provides an understanding of the influence of initiator content for E−150 resin; key findings are summarised in Table 2. While this is an essential study in advancing knowledge on the behaviour of E−150, it is worth noting that compositional differences exist between the grades of this novel family of acrylic resins. As such, research attention towards understanding the effects of initiator content for other grades of Elium® is essential.

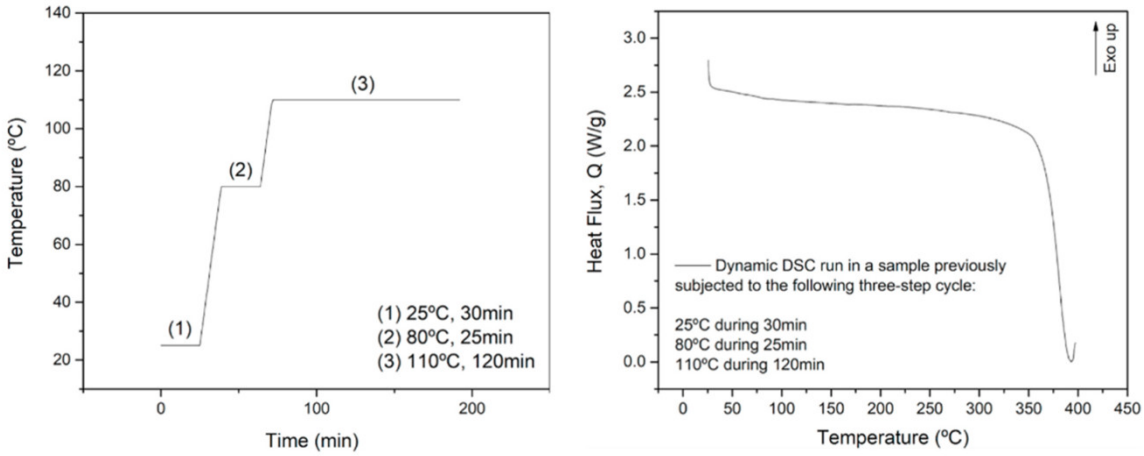


Fig. 4. An (a) optimised three-step thermal cycle for E−150 resin and (b) DSC validation results for the cycle as developed by de Andrade Raponi et al. [26] (Copyright permission from Elsevier. From Figs. 9 and 10 in Ref. [26]).

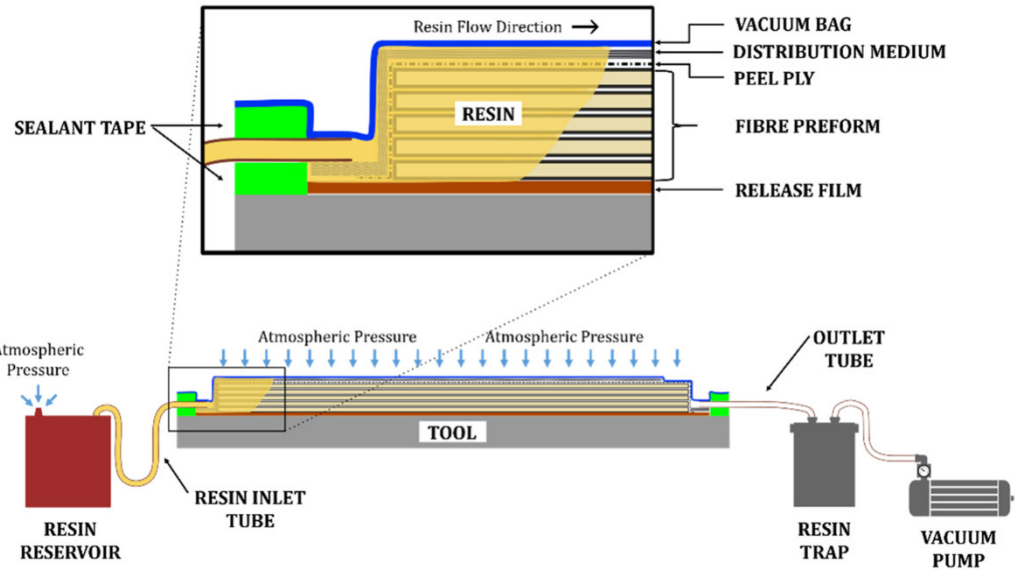


Fig. 5. Conventional liquid resin infusion process under a flexible membrane set-up.

2.1.2. Influence of temperature

The polymerisation of first-generation acrylate monomers has been shown to be influenced by temperature due to effects on the polymerisation time, the formation of voids, and the risk of exothermic runaways [18]. de Andrade Raponi et al. [26] showed that temperature significantly influences the termination step of polymerisation reactions for unreinforced E−150 containing 1.2% of a commercial organic peroxide, and invariably, its degree of conversion. A key contribution of this work was the proposal of a three-stage thermal processing cycle (Fig. 4a) comprising sequential isothermal segments at 25°C (25 min), 80°C (30 min) and 110°C (120 min), with heating rates of 4°C/min. The first segment was employed to promote a slow reaction rate to limit the formation of thermally-induced voids. DSC analysis on the polymerised sample (Fig. 4b) revealed no exothermic peak; no further polymerisation was detected. As with the work reviewed in 2.1.1, an obvious limitation is that this study focused solely on process optimisation for this specific grade of acrylic resin, and the proposed process parameters may not be directly applicable to other grades given the compositional variations that may exist in this family of acrylic resins. Thus, further studies of this nature covering several grades may prove beneficial. Interestingly, the manufacturer remarks on the suitability of this resin grade for room-temperature polymerisation, however, suggests a post-polymerisation heating step at 80°C for 4 h to realise enhanced mechanical performance [27].

2.1.3. Polymerisation exotherm

Murray et al. [28] reported the need for a proprietary exothermic control agent for the production of thick sections of glass fibre-reinforced acrylic laminates. Murray et al. [19] highlighted the need for such measures in the production of thick components (>12 mm). These findings are supported by Charlier et al. [29] who reported constant heat flow and reaction rate up to 40% conversion, followed by an instantaneous increase in reaction rate up to 100% conversion. This rate change was believed to be attributed to an auto-acceleration phenomenon (the gel effect), reported to induce a high degree of exotherm in bulk free radical polymerisation. Peak exotherm temperatures of 45°C [30] and 77–90°C [22] have been reported for thin and thick sections, respectively. An increase in laminate thickness from 3.8 mm to 11.3 mm has been shown to result in a corresponding increase in peak exotherm temperature of 21.5°C [31].

3. Fabrication of continuous fibre-reinforced acrylic-matrix composites

Most published works on the properties of *in situ* polymerised acrylic-matrix composites have employed a liquid resin infusion technique

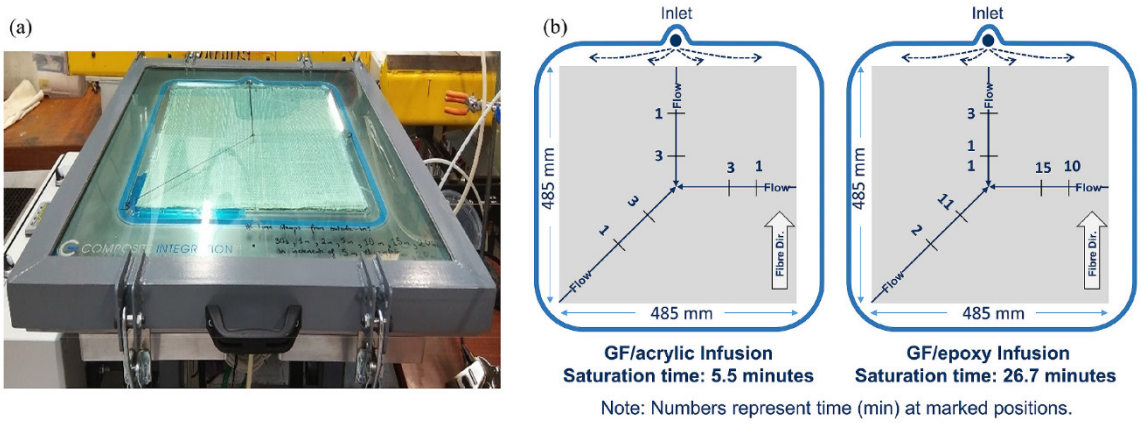


Fig. 6. (a) Composite Integration liquid resin infusion equipment and (b) graphical representation of flow fronts during the fabrication of glass fibre-reinforced acrylic and epoxy laminates (Copyright permission from Elsevier. From Fig. 1 in Ref. [37]).

Table 3
Summary of reported processing techniques of acrylic matrix composites and resulting fibre (V_f) and void (V_v) volume fractions, by resin grade and fibre type.

Reinforcement	Resin	Process	V_f (%)	V_v (%)	Reference
Carbon	E-280	i. Liquid resin infusion	i. 48 – 60	i. 0.1 – 1	i. [33,35,57,63]
		ii. RTM	ii. 57	ii. N/S	ii. [34]
Carbon	E-150	i. Hand layup & vacuum moulding[a]	i. N/S	i. N/S	i. [106]
		ii. Liquid resin infusion	ii. N/S	ii. N/S	ii. [58]
Carbon	N/S	Liquid resin infusion	60	N/S	[65]
Glass	E-180, E-188 O	i. Liquid resin infusion	47-49.5	0.4	[37,51]
		ii. VRTM			
Glass	E-150	Liquid resin infusion	N/S	N/S	[54]
Glass	N/S	Liquid resin infusion	i. 54.2	i. N/S	i. [28]
			ii. 46.5	ii. 7	ii. [36]
			iii. 52.4	iii. 1.3	iii. [45]
Flax	E-RT150	i. Hand layup & press moulding	i. 48	i. N/S	i. [41]
		ii. Liquid resin infusion	ii. 35 – 40	ii. 2.5 – 7.5	ii. [107]
Flax	N/S	Liquid resin infusion	37.1	5	[45]

[a] Thermally post-processed, **N/S:** Not specified.

[32–37]; however, resin transfer moulding (RTM) [34,38–40], wet lay-up and press moulding [41] have also been used.

Depending on the variant of liquid resin infusion method used (such as those in Hindersmann's overview [42]), an array of auxiliary materials are used to aid liquid resin infusion and the subsequent release or demoulding process. In most cases, the set-up shown in Fig. 5 is employed, where a flexible membrane or bag is used in conjunction with a rigid tool base. Traditional liquid resin infusions are typically preceded by a resin degassing process for the removal of dissolved gases and micro-bubbles within liquid resins such as epoxy [43]. However, the short pot life and infusion window (~40 min) of these acrylic resin systems makes degassing impractical. Where it has been attempted on E−280, no significant benefits were reported [33]. With the exception of the work done by Cousins et al. [22], no authors reported a resin degassing step for acrylic-based laminates. Across most of the reviewed works, a conventional liquid resin infusion configuration with a flexible membrane was employed. Additionally, vacuum RTM (VRTM) or RTM Light was also reported using an innovative adjustable-thickness tool (Fig. 6) with two rigid mould halves [37,44], where vacuum is used for both clamping and resin flow [42].

A two-stage technique for the fabrication of flax fibre-reinforced acrylic was reported by Baley et al. [41]. (i) The initial manual impregnation stage produced fully wetted-out preforms, which were subsequently (ii) hot-press moulded for enhanced void-elimination and consolidation. While this resin grade (E−150) does not require heating during the polymerisation process [27], the use of heat during and after the polymerisation step is reported by the authors as manufacturer's recommendations. Heating was also empoyed by Boufaida et al. [40] for RTM fabrication of acrylic-based laminates; however, this was reported by the authors as a requirement to thermally activate the polymerisation process due to the incompatibility of the fibre sizing on the reinforcements employed with the intrinsic activation agent in the initiator. It was suggested that the activator within the initiator reacted with the epoxide groups within the multi-compatible sizing formulation. Thus, thermal activation was required in-lieu of chemical activation. While the precise grade of acrylic resin used was not specified in the work by Boufaida et al. [40], the suitability of the RTM process for producing acrylic-matrix laminates has also been demonstrated by Bhudolia et al. [34] using E−280 with carbon fibre reinforcements (with a thermoplastic-compatible sizing agent). Table 3 presents an overview of the most adopted fabrication processes of acrylic matrix composites and the laminate quality achieved by resin grade and fibre type.

4. Properties of acrylic-matrix composites

4.1. Glass fibre-reinforced acrylic-matrix composites

4.1.1. Tensile properties

Lorriot et al. [36] reported comparable longitudinal tensile strengths (~860 MPa) and moduli (40 GPa) in glass fibre-reinforced acrylic and epoxy laminates, reporting marginally higher (5%) failure strain in the acrylic-based composite. Similar comparability was reported by Chilali et al. [45]. However, despite a relatively high fibre volume fraction (~52% for the acrylic-based material), the reported tensile strength (380 MPa) and modulus (23 GPa) are considerably lower than indicated by other authors. Cousins [46] identified a marked superiority in the tensile strength of an acrylic composite over its epoxy counterpart, reporting strengths of 916 MPa and 723 MPa, respectively for both materials. Even higher longitudinal tensile strength (1241 MPa) and modulus (52.7 GPa) were reported by Zoller et al. [47], possibly owing to higher fibre weight fractions (81%), the use of a different grade of acrylic resin (E-C595E) or the effects of the pultrusion process on fibre

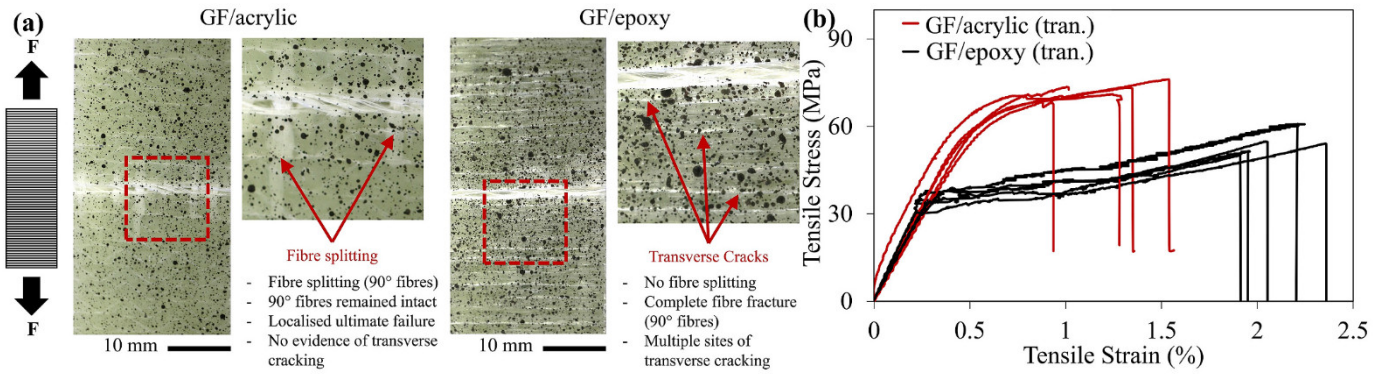


Fig. 7. (a) Macroscopic failure behaviour and (b) stress-strain responses of glass fibre-reinforced acrylic and epoxy composites subjected to transverse tensile loading (Copyright permission from Elsevier. Reproduced from Figs. 2 and 3 [37]).

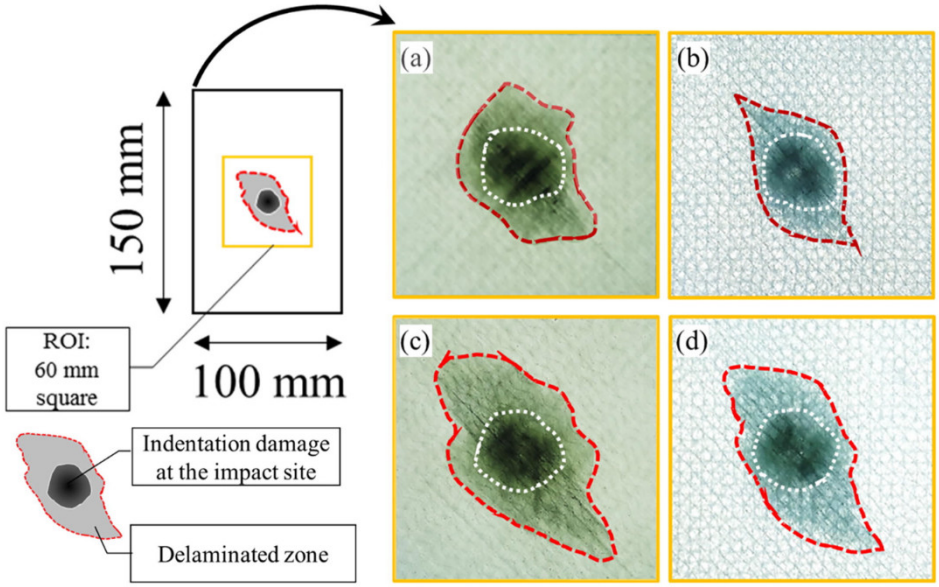


Fig. 8. Representative damage states for glass fibre-reinforced (a) acrylic at 15 J, (b) epoxy at 15 J, (c) acrylic at 30 J, and (d) epoxy at 30 J. ROI: region of interest (Copyright permission from Elsevier. Adapted from Fig. 2 in Ref. [51]).

alignment. Obande et al. [37] characterised the tensile properties of acrylic- and epoxy-based glass FRPs and reported marked superiority in transverse strength for the acrylic system; strengths of 73 MPa and 54 MPa were reported, respectively. Equivalent transverse tensile moduli were reported for both materials at 13 GPa. As shown in Fig. 7, the authors reported distinct failure characteristics in both materials. The stress-strain behaviour (Fig. 7b) for the epoxy-matrix composite showed an earlier onset of non-catastrophic damage; the authors suggested a link between this behaviour and the multiple transverse cracks observed on test samples (Fig. 7a). These were shown to accumulate along the sample gauge length during loading up to failure. This phenomenon was not reported for acrylic-based samples; rather, fibre splitting along the loading direction was evident. These were identified as originating from 90° reinforcing yarns in the fabric.

4.1.2. *Compressive properties*

The compressive performance of glass fibre-reinforced acrylics has not been extensively studied. Cousins [46] comparatively assessed glass fibre-reinforced acrylic and epoxy composites and reported equivalent strengths (~600 MPa) and moduli (~34 GPa) for both materials. Substantially higher average compressive strength (1044 MPa) and modulus (~52 GPa) values were reported for pultruded glass fibre-reinforced acrylic based on E-C595E E by Zoller et al. [47]. While no details of fibre volume or mass fractions were provided for the materials reported by Cousins [46], the high fibre mass fraction of 81% reported by Zoller et al. [47] possibly explains the high compressive strength and modulus. Besides, the use of the pultrusion process may confer a high degree of fibre alignment, which are known to influence the longitudinal compressive performance of composites [48]. To the best of our knowledge, no other works focus on assessing the compressive performance of glass fibre-reinforced acrylic composites. The lack of published literature on this area highlights the need for more benchmarking studies on the compressive properties of glass-reinforced acrylic composites alongside more traditional thermoset matrix-based composites.

4.1.3. *Flexural properties*

Cousins [46] measured higher flexural strengths in the acrylic-based composite (1006 MPa) than the epoxy-based reference material (809 MPa); the authors reported moduli of values of ~37.5 GPa and ~35 GPa, respectively. No fibre volume fractions were reported for these materials. As with the tensile and compressive properties in Sections 4.1.1 and 4.1.2., Zoller et al. [47] showed that it was possible to achieve high-flexural-performance glass fibre-reinforced acrylics based on E-C595E E by pultrusion. The average longitudinal flexural strength and modulus for this material were 1291 MPa and 44.7 GPa, respectively. Davies and Arhant [49] reported flexural strengths of 703 MPa and 606 MPa, and moduli of 40.1 GPa and 38.2 GPa for glass fibre-reinforced acrylic and epoxy composites with fibre volume fractions of 52 and 53%, respectively. These trends were also observed by Obande et al. [37], who reported strengths of 879 MPa and 869 MPa, and moduli of 40 GPa and 38 GPa for glass fibre-reinforced acrylic and epoxy composites, with fibre volume fractions of 49.5%, respectively. In the same study, the authors reported the opposite trend for transverse flexural performance, reporting strengths of 91 MPa and 94 MPa and moduli of 11 GPa and 12 GPa for the acrylic- and epoxy-based materials. Interestingly, despite possessing consistently higher longitudinal characteristics than composites produced from other grades of the acrylic resin and produced using other techniques, the material studied by Zoller et al. [47], exhibited inferior transverse flexural strength (68.9 MPa) and marginally higher modulus (11.5 GPa) than that reported by Obande et al. [37].

4.1.4. *Shear properties*

In-plane shear properties of a glass fibre-reinforced acrylic matrix and an epoxy-based counterpart were studied by Lorriot et al. [36]. The authors reported higher shear modulus (~31%) in the epoxy-matrix composite and comparable shear strengths in both materials. Chilali et al. [45] reported comparable performance during in-plane shear strengths, with both acrylic- and epoxy-matrix composites yielding strengths of ~68 MPa and moduli or ~6 GPa. Cousins [46] found that an acrylic-based FRP possessed 8% lower short-beam shear strength than its epoxy-based counterpart, reporting strengths of ~50 MPa and 54 MPa, respectively. Obande et al. [37] also studied the short-beam shear behaviour of glass fibre-reinforced acrylic and epoxy composites and reported comparable shear strengths in both materials, with the acrylic-based composite being marginally higher at 58 MPa (+2%) than its epoxy counterpart. Dissimilar damage evolution was described by the authors, who found that epoxy-matrix samples exhibited a more pronounced onset of failure beyond load peaks, dropping by up to 30% from the peak load. In contrast, a smoother and more gradual drop in load was observed with acrylic samples. For unidirectional glass-fibre reinforced acrylics, Davies and Arhant [49] reported 21% higher short-beam shear

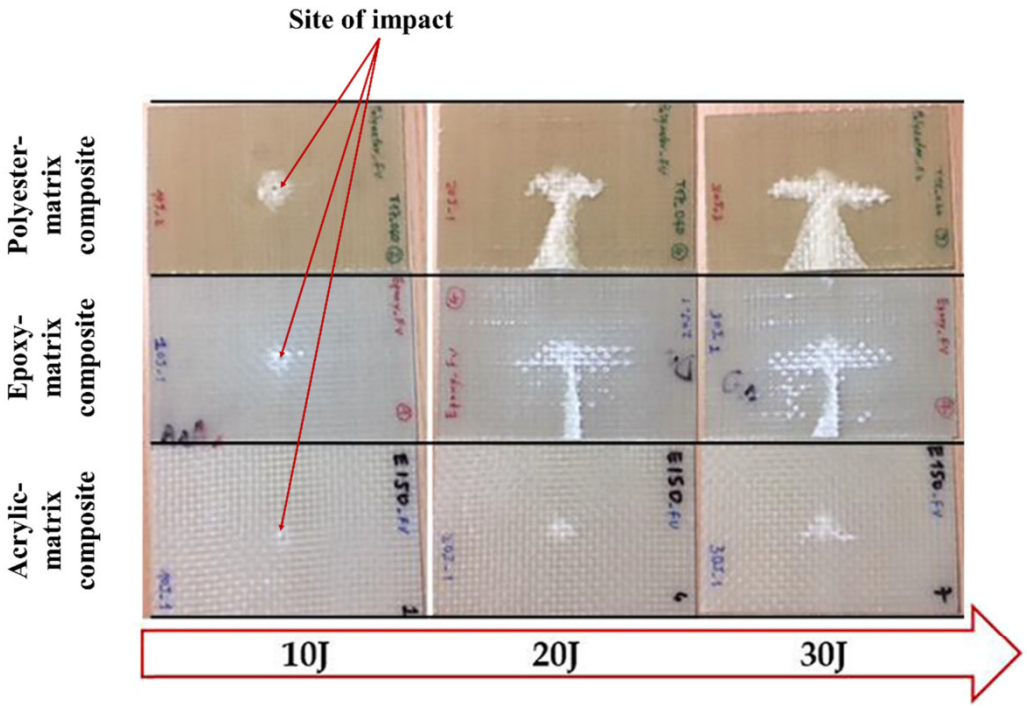


Fig. 9. Impact-face damage states on glass fibre-reinforced polyester, epoxy and acrylic composites subjected to impact events of 10 J, 20 J and 30 J (Copyright permission from Elsevier. Adapted from Fig. 8 in Ref. [52]).

strengths than a comparable epoxy-based composite. Despite the authors exploiting specialised acrylic-compatible sizing on their reinforcements, an average short-beam shear strength of 46 GPa was reported for the acrylic-based samples. The grade of acrylic resin used in this work (E−180) and that was used by Obande et al. [37], E−188 belong to the same family of resins [50] and as such, should exhibit similar performance for the same type of reinforcement. Moreover, short-beam shear behaviour should ideally be enhanced in work by Davies and Arhant [49], particularly given the benefits that specialised sizing formulation potentially confer and marginally higher fibre volume fraction (52%) than that reported by Obande et al. [37] (49.5%). While these authors employed different stacking sequences, these observations highlight the need for comparative benchmarking studies on sizing technology for these acrylic matrices.

4.1.5. Impact properties

Obande et al. [51] comparatively assessed the drop-weight impact behaviour of glass fibre reinforced acrylic composites with an epoxy-based reference. Following impact events at 15 and 30 J, the authors measured the resultant damage area as shown in Fig. 8 to assess impact damage resistance. Expressing average damage area as percentages of the total sample face area in acrylic- and epoxy-based materials, 15 J impact events produced damage areas of 4.4 ± 0.9% and 3.9 ± 0.3%, respectively, whereas, 30 J impacts resulted in 7.4 ± 0.5% and 6.6 ± 0.5%, respectively.

From these findings, it was concluded that the reference epoxy-based material sustained a lesser extent of measurable damage, and thus, was deemed more damage resistant than the acrylic-based composite at the energy levels used in the study. Kinvi-Dossou et al. [52] conducted a similar study and although the authors did not quantify the extent of impact-induced damage, their study ranked acrylic-matrix composites more damage resistant than its polyester- and epoxy-based counterparts. As shown in Fig. 9, the damaged envelope grows considerably for the polyester- and epoxy-matrix composites, with evidence of gross delamination being observable. Only minimal damage states are presented for the acrylic composite samples at these energy levels. The authors believe that the superior impact strength is attributed to improved interfacial adhesion between the glass fibres and the acrylic matrix, but provide no strong evidence to support this claim. In addition, the impact performance of the acrylic laminate was also reported to be enhanced by shear banding within the matrix, which contributes to the dissipation of bulk strain energy and gives way to shear localisation. A further remark by the authors suggests that this acrylic is considerably more ductile than the epoxy and polyester matrix, which are described as brittle. However,

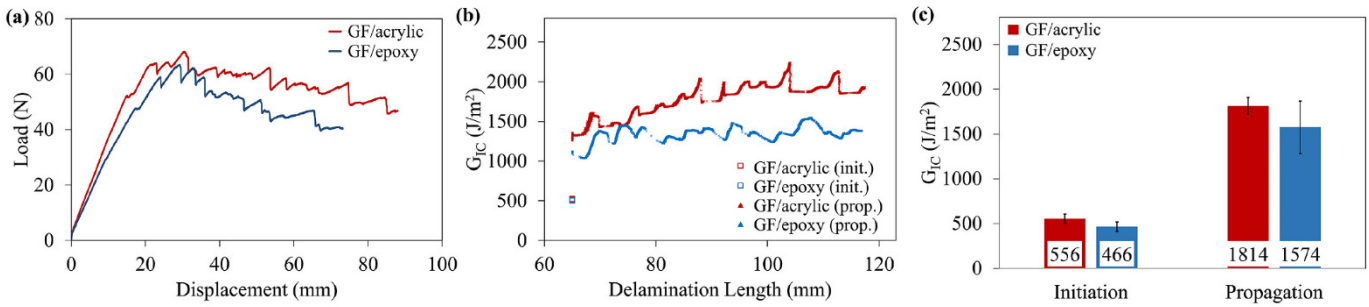


Fig. 10. (a) Load-displacement curves and (b) resistance curves (R-curves) for glass fibre-reinforced acrylic and epoxy composites, and (c) initiation and propagation fracture toughness values of same (Copyright permission from Elsevier. From Fig. 12 in Ref. [37]).

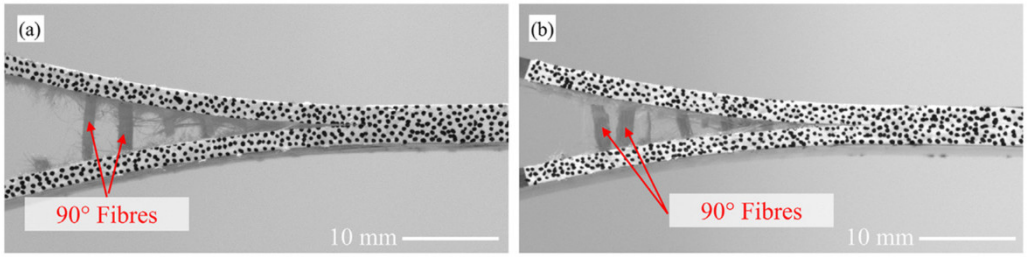


Fig. 11. Delamination behaviour of glass fibre-reinforced acrylic and epoxy samples undergoing double cantilever beam testing at equivalent test times (Copyright permission from Elsevier. From Fig. 13 in Ref. [37]).

acrylics have been shown to possess low failure strain and strain-dependent embrittlement [37,51,53] as brittle amorphous thermoplastic materials. However, it is worth noting that woven reinforcement was used in the study by Kinvi-Dossou et al. [52], whereas Obande et al. [51] presented results for a quasi-isotropic laminate. Cadieu et al. [54] assessed the effects of rate on the out-of-plane loading response of glass fibre-reinforced E−150 using quasi-static indentation and drop-weight impact; it was concluded that higher loading rates result in lower penetration depth and higher stiffness, which results in higher elastic energy and conversely, lower dissipated energy. At low impact energies and low indentation, no rate effects were reported for the area of the damaged zone. At higher energy levels, however, a more substantial reduction is observed in the damaged area at the shorter timescale. Damage mechanisms were not found to be affected by the loading rate; the authors observed delamination, matrix cracking and fibre-related failure at all loading rates.

4.1.6. *Interlaminar fracture toughness*

4.1.6.1. Mode-I interlaminar fracture toughness. Obande et al. [37] showed that glass fibre-reinforced acrylic laminates exhibited superior (+15%) Mode-I interlaminar fracture toughness than their epoxy-based counterparts. As shown in Fig. 10, the acrylic composite also possessed higher (+19%) initiation fracture toughness. Progressive unstable delamination growth was reported by the authors, with evidence of stick-slip propagation mechanisms observed. From the higher slope of the R-curve for the acrylic-based sample in Fig. 10b, the authors reported the superiority of the thermoplastic acrylic composite in damage resistance over its epoxy counterpart. Both materials exhibited some extent of fibre bridging at the crack tip, as shown in Fig. 11; however, this was more prominent in the acrylic-matrix composite. In terms of fractographic behaviour, the presence of distinctly ductile characteristics was reported in the case of the acrylic-matrix composite, with more brittle features being observed on the epoxy composite. They also remark on the likelihood of tow-rupture and debonding occurring along the interface of these 90° tows, which would inadvertently be pathways for damage-related energy absorption. As such, the results presented were not deemed representative of unidirectional fracture behaviour. With the exception of this work, no other authors have reported findings on the Mode-I interlaminar fracture behaviour of glass fibre-reinforced acrylic composites, highlighting the need for further exploration of this topic for these materials.

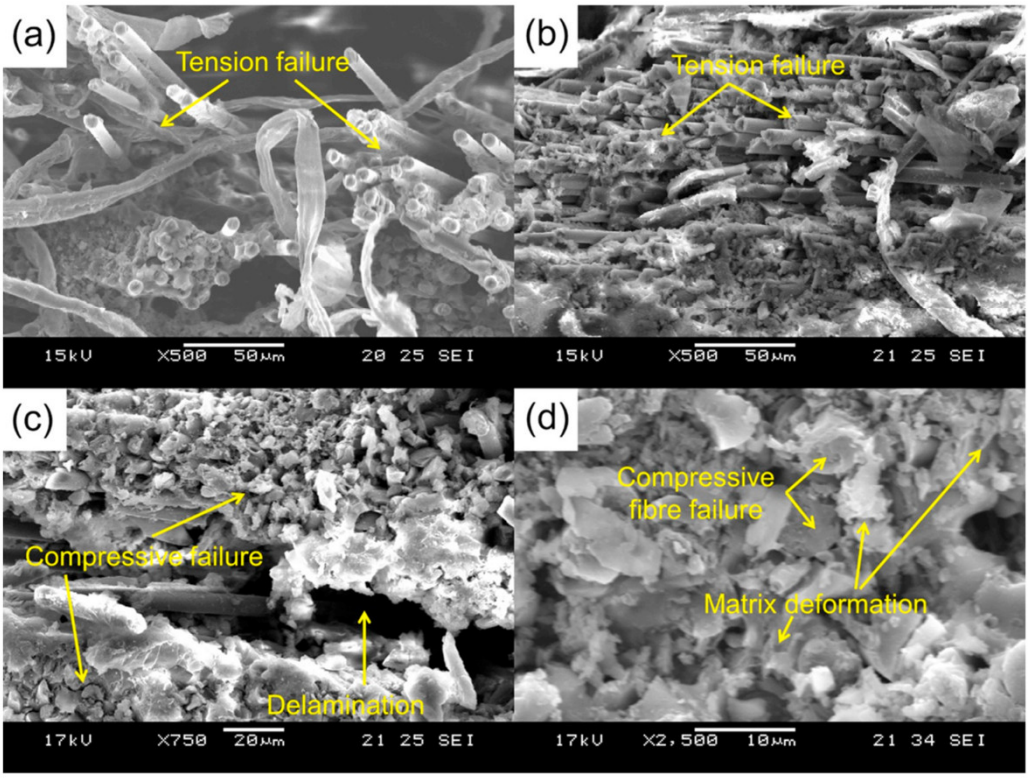


Fig. 12. Scanning electron micrographs showing flexural failure modes of thin-ply carbon fibre-reinforced (a) & (c) epoxy and (b) & (d) acrylic composites (Copyright permission from Elsevier. From Fig. 2 in Ref. [55]).

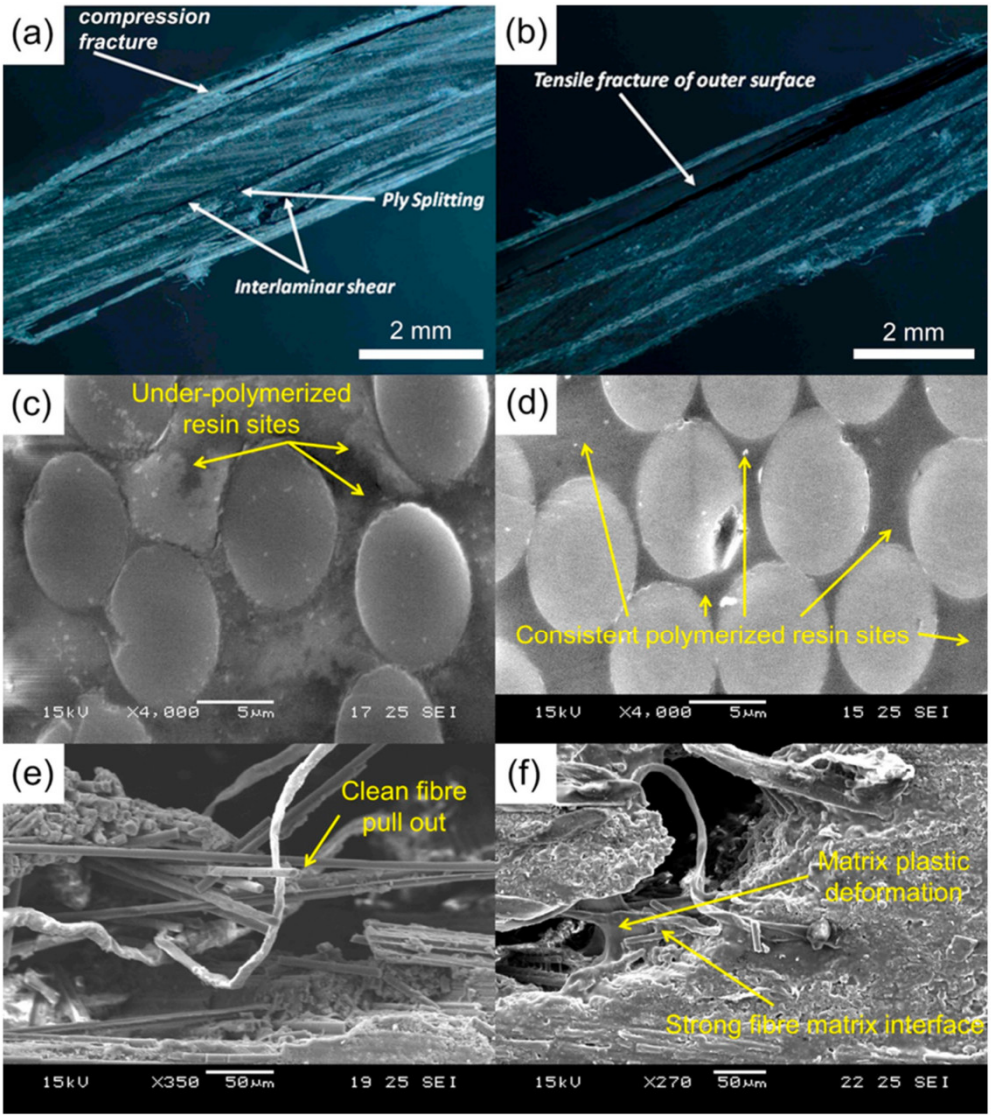


Fig. 13. Flexural failure modes of thin-ply carbon fibre-reinforced acrylic composites: (a), (c) & (e) without annealing; and (b), (d) & (f) with annealing (Copyright permission from Elsevier, From Fig. 3 in Ref. [55]).

4.2. Carbon fibre-reinforced acrylic-matrix composites

4.2.1. Tensile properties

The tensile properties of cross-ply carbon acrylic and epoxy FRPs were studied by Bhudolia et al. [35]. While localised brittle fractures were observed in the epoxy-based material, fibre splitting and fracture, and delamination were reported as the predominant modes in the acrylic-based FRP. Ultimately, the epoxy material had superior strength (1217 MPa) and modulus (66.7 GPa) than its thermoplastic counterpart, which had corresponding values of 1004 MPa and 53.1 GPa. A major limitation of this study is that dissimilar carbon reinforcement systems were used, making it challenging to draw definitive conclusions. Interestingly, Davies and Arhant [49] reported lower tensile strength (831 MPa) and higher modulus (71.9 GPa) for thick-ply carbon fibre-reinforced acrylic composite.

4.2.2. Flexural properties

The flexural properties of an acrylic-based material were comparatively evaluated alongside a baseline epoxy system. In this work, Bhudolia et al. [35] reported 33.3% and 9.5% higher strength and modulus values, respectively for the epoxy FRP, which failed on both the tensile and compressive sides. However, only compressive failure was observed in the acrylic composite, which had average strength and modulus values of 671.1 MPa and 52.1 GPa, respectively. These findings were, however, affected by the ply configuration in each laminate – conventional thick-ply non-crimp fabric (NCF) was used in the fabrication of the acrylic laminate, whereas its epoxy-based counterpart contained thin-ply NCF reinforcement.

In another work by Bhudolia et al. [55], the authors presented findings on flexural behaviour of thin-ply carbon fibre-reinforced acrylic and epoxy composites. Using quasi-isotropic laminates with fibre volume fractions of 58.3% and 60%, respectively, the authors reported flexural strengths of 813 MPa and 835 MPa for the acrylic- and epoxy-based materials, respectively. Their moduli were found to be comparable at ~51 GPa. Differences in failure behaviour were highlighted. For thick-ply laminates with similar stacking sequence, Davies and Arhant [49] reported lower mean flexural strength (590 MPa) and higher modulus (103 GPa). Fig. 12 shows the failure characteristics reported by Bhudolia et al. [55]. A greater extent of visible matrix deformation on the side in compression was reported for the acrylic-based composite; delamination was observed in its epoxy counterpart. This work also represents the first implementation of annealing for this family of acrylic resins. Although similar to the post-processing cycles recommended by the manufacturers for some grades of Elium®

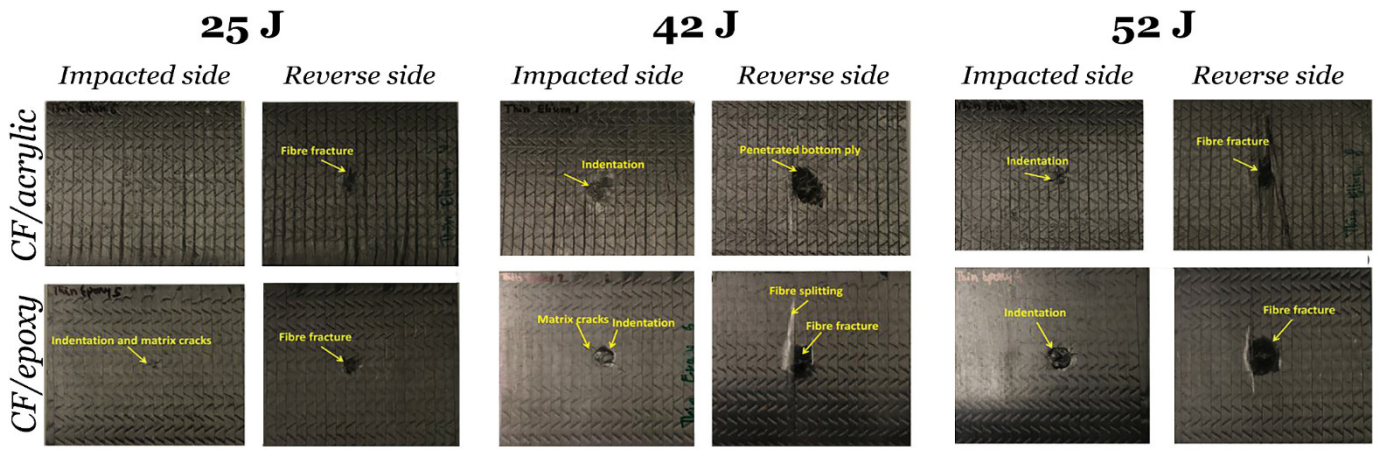


Fig. 14. Impact side and reverse side damage following impact events at 25, 42 and 52 J (Copyright permission from Elsevier. Reproduced from Figs. 12, 14 and 16 in Ref. [34]).

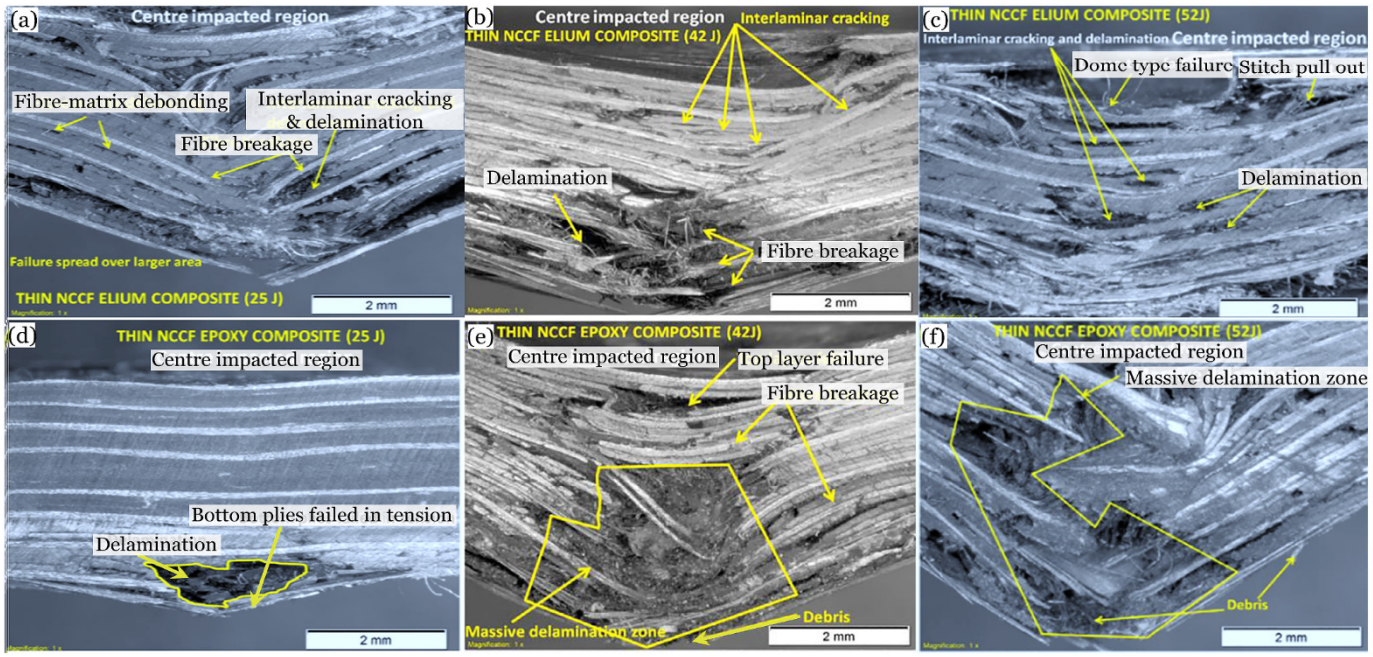


Fig. 15. Micrographs showing damage sustained by carbon fibre-reinforced (a), (b) & (c) acrylic and (d), (e) & (f) epoxy composites following drop-weight impacts at 25, 42 and 52 J, respectively (Copyright permission from Elsevier. Reproduced from Figs. 13–15 [34]).

resin, it was performed in a hot press (80°C for 2 h) as opposed to a free-standing heating cycle. This annealing process was said to facilitate targeted microstructural reorganisation, a more complete polymerisation reaction, enhanced matrix ductility and interfacial adhesion as shown in Fig. 13. The grade of Elium® under consideration in this work was not disclosed, which indirectly limits the transferability of the findings presented therein to other grades. It is unclear if the insufficient polymerisation was associated with sizing effects as previously suggested by Boufaida et al. [40].

4.2.3. *Impact properties*

Carbon fibre-reinforced acrylic composites have been shown to possess superior structural integrity during impact compared to an equivalent epoxy-based composites. The acrylic-matrix composite was reported to be capable of undergoing more elastic deflection before the maximum impact load was reached [34]. The authors also reported strain sensitivity in this material, with increasing energy levels giving rise to greater elastic-plastic deformations relative to the epoxy-matrix composite. This had direct consequences on the resulting damage states of both materials (Fig. 14 and Fig. 15); a larger extent of delamination and catastrophic failure characteristics were observed in the carbon fibre-reinforced epoxy samples for 42-J and 52-J impacts. Interestingly, impacts at a lower energy level (25 J) appeared to produce more severe and extensive damage states in the acrylic-based material such as fibre fractures and interlaminar cracking (Fig. 15a); delamination and tensile failure of back-face plies can be seen for the epoxy-matrix composite (Fig. 15d). The authors also suggested that plastic zone development at the tips of interlaminar cracks contributed positively to enhancing the ductility of the acrylic-matrix composite. It was also proposed that shear crack propagation was favoured by superior interfacial strength in the carbon fibre-reinforced acrylic material. In a similar study, the use of thin-ply carbon fibre reinforcement has also been shown by Bhudolia et al. [56] to produce more impact damage-resistant acrylic-matrix composites than is possible with standard thick-ply reinforcement. Thin-ply carbon fibre-reinforced acrylic composites were found to exhibit more favourable elastic-plastic

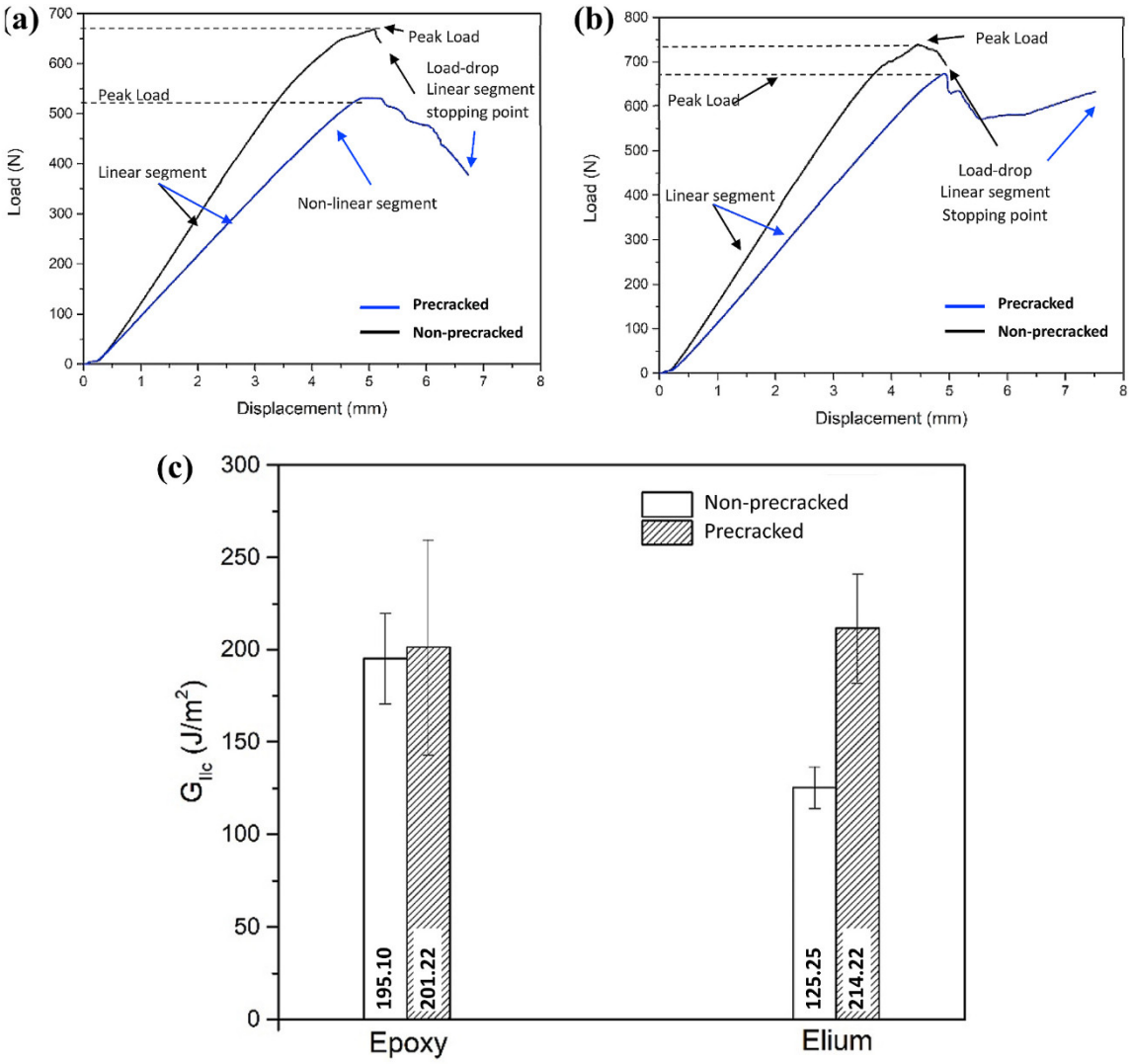


Fig. 16. Load-displacement curves for carbon fibre-reinforced (a) E−150, (b) epoxy; and (c) Mode-II interlaminar fracture toughness determined from same (Copyright permission from Elsevier. Reproduced from Figs. 6–8 in Ref. [58]).

deformation, leading to smaller delamination zones than in the thick-ply variant.

4.2.4. *Interlaminar fracture toughness*

4.2.4.1. Mode-I interlaminar fracture toughness. Quasi-isotropic thin-ply carbon fibre-reinforced acrylic composites have been reported to exhibit superior Mode-I fracture toughness than equivalent epoxy-based composites due to the prevalence of crack arresting mechanisms such as crack deflection behind the crack tip, crack branching and multi-plane propagation of cracks [57]. The authors reported fibre bridging, strong interfacial strength, ductile drawing and crazing, fibre splitting and pull-out for the acrylic-matrix composite material, whereas the epoxy-based composite was reported to exhibit clean fibre failure and pull out, brittle propagation of matrix cracks and scarp formation. Higher peak loads were reported for the acrylic-based samples than their epoxy counterpart, indicating superior resistance to crack initiation. The authors reported a superiority in bond strength and adhesion in both thick- and thin-ply carbon fibre-reinforced acrylic composites relative to the thin-ply epoxy-matrix composite. This work also highlighted the effects of ply thickness on the Mode-I interlaminar fracture toughness, which are believed to have their origins in the size of the interlaminar resin-rich layer thickness. This is supported by the findings reported by Bhudolia et al. [35]. More importantly, these works highlight that even thick-ply acrylic-matrix composite outperforms its thin-ply epoxy counterpart in both initiation and propagation fracture toughness.

4.2.4.2. Mode-II interlaminar fracture toughness. Barbosa et al. [58] found that woven carbon fibre-reinforced acrylic exhibited superior Mode-II propagation toughness (+40%) than its epoxy-matrix counterpart. The load-displacement responses for both materials are presented in Fig. 16 (a) and Fig. 16 (b). The authors state that the higher peak load in the epoxy-matrix composite is indicative of superiority in *suppressing* the occurrence of delamination; i.e., a higher energy requirement for initiation. It was also suggested that the superior propagation fracture toughness exhibited by this thermoplastic-matrix composite stems from two mechanisms – plastic matrix deformation and interfacial debonding; which the authors remarked are beneficial in composites subjected to Mode-II loading. In addition to crack propagation, some of the energy absorbed was said to be linked with plastic deformation within matrix-rich zones. This plastic deformation is thought to alter the fracture surface considerably and may mask important fractographic characteristics. SEM fractographic inspection (Fig. 17) revealed characteristic Mode-II fracture behaviour on the surfaces of both materials, namely, shear cusps. Cusps are shear-induced fracture features that develop at the interface due to interlaminar shear stresses, which

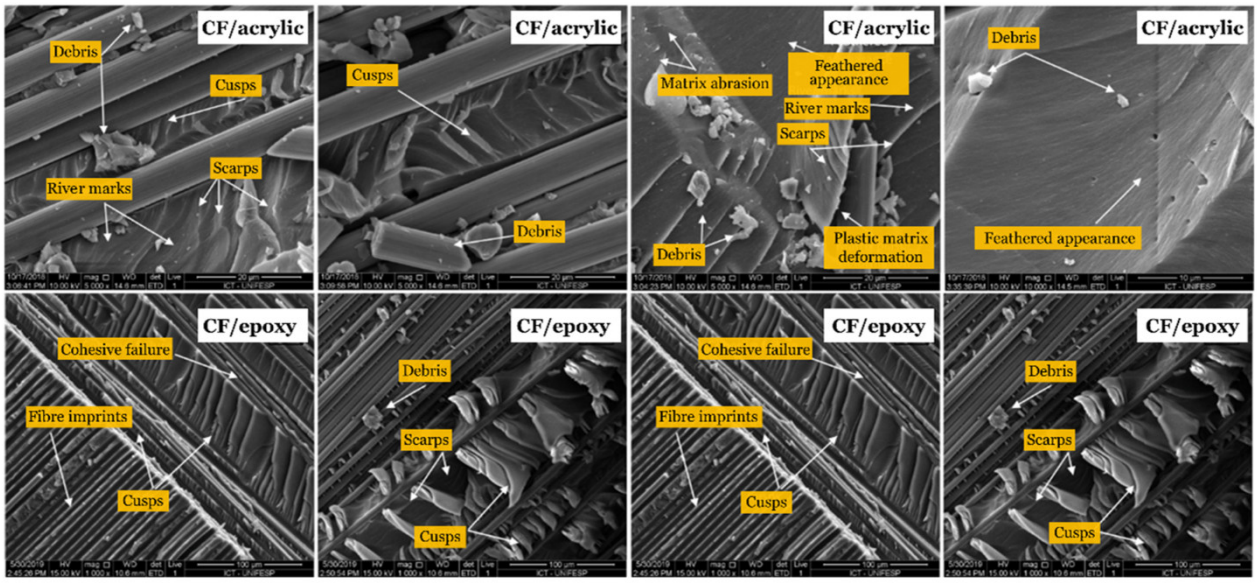


Fig. 17. SEM micrographs of Mode-II fracture surfaces of CF/acrylic and CF/epoxy (Copyright permission from Elsevier. Reproduced from Figs. 11 and 12 in Ref. [58]).

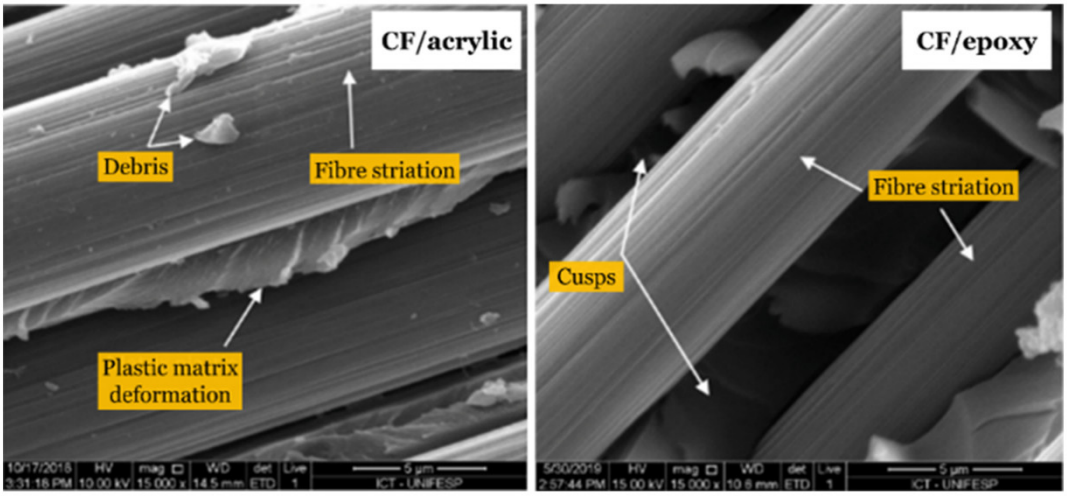


Fig. 18. SEM micrographs of exposed fibre surfaces following Mode-II fracture toughness testing on CF/acrylic and CF/epoxy composites (Copyright permission from Elsevier. Reproduced from Figs. 11 and 12 in Ref. [58]).

may cause matrix cleavage. They develop in the matrix-rich regions between fibres, following the direction of failure propagation. Micrographs of the fibre surfaces shown in Fig. 18 reveal comparable fibre coverage following fracture, indicating that the use of multi-compatible sizing technology may not adversely affect the performance of the acrylic-based system. Thus, the variations in G_{IIC} between precracked and non-precracked test configurations may not be linked with variations in interfacial adhesion. The authors did, however, remark that even further enhancements may be realised in the crack resistance of the acrylic-based composites by using specially sized fabrics compatible with acrylic resin systems.

4.3. Flax fibre-reinforced acrylic-matrix composites

4.3.1. Tensile properties

Baley et al. [41] conducted a parametric study to assess the longitudinal tensile behaviour of flax fibre-reinforced acrylic composites alongside polyamide-, polypropylene-, and epoxy-based counterparts. For the purpose of this review, the measurements reported by the authors have been normalised to equivalent fibre volume fractions of 50%. Although matrix type yielded marginal effects on the tensile moduli across all samples, the most significant influence was observed in strengths. The acrylic-matrix composite was found to be superior in tensile strength to the flax fibre-reinforced polypropylene (+23%) and maleic anhydride-grafted polypropylene (+7%). However, its tensile strength was 58% lower than the epoxy-based laminate and comparable to the polyamide-based material. Chilali et al. [45] also studied the static tensile behaviour of woven flax fibre-reinforced epoxy and acrylic laminates alongside their unreinforced forms. The authors observed ductile and quasi-linear behaviour in the unreinforced acrylic and epoxy matrices, with failure strains of 2.3% and 1.1%, respectively. For reinforced composites, three distinct stress-strain characteristic regions were identified. Both the acrylic- and epoxy-based materials were reported to exhibit an initial linear elastic region. This region was preceded by a region of slight non-linearity, with a loss of stiffness being reported. Lastly, stress increases linearly up to ultimate failure, with both materials failing abruptly thereafter. This variation has also been reported in other works by Haggui et al. [59,60], who describe the same trend in

Table 4
Summary of tensile properties reported for flax fibre-reinforced acrylic composites.

	V_f	V_f*	σ (MPa)	σ** (MPa)	E (GPa)	E** (GPa)
Baley et al. [41]	48	50	243.8	**254.0**	27.6	**28.8**
Chilali et al. [45]	37.1	50	130	**175.2**	13.53	**18.2**
Haggui et al. [59,60]	38	50	210	**276.3**	23	**30.3**
Monti et al. [107]	~37.5	50	225	**300**	23.3	**31.1**

All data has been normalised to a target V_f (marked *) of 50% for the purpose of this review.
Reported data and normalised data (marked **) have been presented.

stress-strain response for unidirectional flax fibre-reinforced acrylics. All authors attribute the second stage (non-linear) with the creation and evolution of damage. However, the authors present different explanations for the third and final stage. Haggui et al. [59,60] suggest that this quasi-linear behaviour is associated with multiplication or intensification of damage, leading up to ultimate failure, whereas, Chilali et al. [45] proposed contributions from microfibrillar reorientation associated with flax fibres. As shown in Table 4, the tensile properties reported by Chilali et al. [45] appear to be significantly lower than those reported by other authors. However, this may be due to the differences in reinforcement architecture used and the high variability of flax fibres being natural fibres [61].

4.3.2. Compressive properties

Baley et al. [41] presented findings of a study on the comparative compressive performance of unidirectional flax fibre-reinforced acrylic and epoxy composites. The authors reported 7%, 27% and 5% lower compressive strength in the acrylic-based material than its epoxy (115 MPa), polyamide (134 MPa), and polypropylene/maleic anhydride-grafted polypropylene (110 MPa) counterparts, respectively. However, it had 28% higher compressive strength than flax fibre-reinforced polypropylene (75 MPa). In terms of tensile strength, it was superior to the flax fibre-reinforced polypropylene (193 MPa; +23%) and maleic anhydride-grafted polypropylene (234 MPa; +7%). However, its tensile strength was 58% lower than the epoxy-based laminate (408 MPa) and comparable to the polyamide-based material (258 MPa). These results clearly show a more considerable influence of the matrix used on compressive strength than on tensile strength, a property known to be fibre-dominated. The authors attribute the poor compressive performance of the acrylic to weak interfacial strength between the flax fibres and acrylic matrix. These results clearly show a considerable influence of the matrix used on compressive strength, which itself is known to be matrix-dominated.

4.3.3. Flexural properties

Haggui et al. [59] evaluated the flexural behaviour of bidirectional flax fibre-reinforced acrylic laminates using three-point bend tests. A three-stage stress-strain behaviour was described, with an initial linear region preceding a nonlinear and terminal quasi-linear one. The authors also reported transverse microcracking as the incipient damage mechanism, occurring during the nonlinear phase of testing. Haggui et al. [59] studied the cyclic flexural performance of flax fibre-reinforced acrylics and identified a two-stage degradation of stiffness. The authors concluded that a critical number of cycles (c. 10^4) exists, below which the rate of degradation is relatively slow. This was believed to be related to damage initiation and microcracking phenomena, which precede the rapid accumulation of transverse cracking and subsequent delamination growth up to 9×10^5 cycles.

4.3.4. Shear properties

Chilali et al. [45] assessed the shear performance of flax fibre-reinforced acrylic and epoxy laminates by in-plane shear testing and reported a superiority (~10%) in shear modulus for the epoxy-based material. Both flax fibre-reinforced acrylic and epoxy materials were reported to exhibit equivalent ultimate shear strengths at approximately 23 GPa; however, normalising the reported data revealed an even greater difference in the measured values. The epoxy-based laminate possessed higher (+16%) shear strength than the acrylic material.

4.4. Dynamic mechanical (thermomechanical) properties

Several works have studied the thermomechanical behaviour of thermoplastic acrylic matrices and their glass fibre-reinforced composites. Acrylic-based composites have been reported to exhibit comparable (and in some case, superior) performance to their thermosetting counterparts, such as epoxy-matrix composites with T_g values in the range of 67°C–127°C being reported [25,37,47,51,62–65]. Table 5 presents a

Table 5
Summary of some thermomechanical properties reported in published works for acrylic-based matrices and composites.

Materials	Results	References
Matrix: E−180, E−188 Reinforcement: UD Glass NCF Sizing: Multi-compatible	i. T_g: 115°C Tan delta peak: 0.53 ii. T_g: 106°C Tan delta peak: 0.76	[51] [37]
Matrix: (E-X) Grade not specified Reinforcement: Not specified Sizing: Not specified	i. T_g: 125°C Tan delta peak: ii. T_g: 127°C Tan delta peak:	[65] [64]
Matrix: E−150† Reinforcement: Not specified Sizing: Not specified †Various initiator contents: 0.8–1.6 wt %	T_g: 116°C, 123°C, 123°C Tan delta peak: ~0.5, ~0.45, ~0.65 0.8 wt %, 1.2 wt % and 1.6 wt %, respectively	[25]
Matrix: E-C595E Reinforcement: Not specified Sizing: Not specified Matrix: E-C595E Reinforcement: UD Glass Sizing: contains a vinyl group	T_g: 109°C As produced T_g: 119°C Processed at 190°C; 10 min T_g: 122°C	[47]
Matrix: E−150 Reinforcement: Sizing: Not specified Reinforcement: Carbon fabric* (thin- and thick-ply) Sizing: Not specified *quasi-isotropic lay-up	T_g: 110–120°C Tan delta peak: 1.3 (matrix only) Tan delta peak: 0.59 (thin-ply) Tan delta peak: 0.51 (thick-ply	[63]

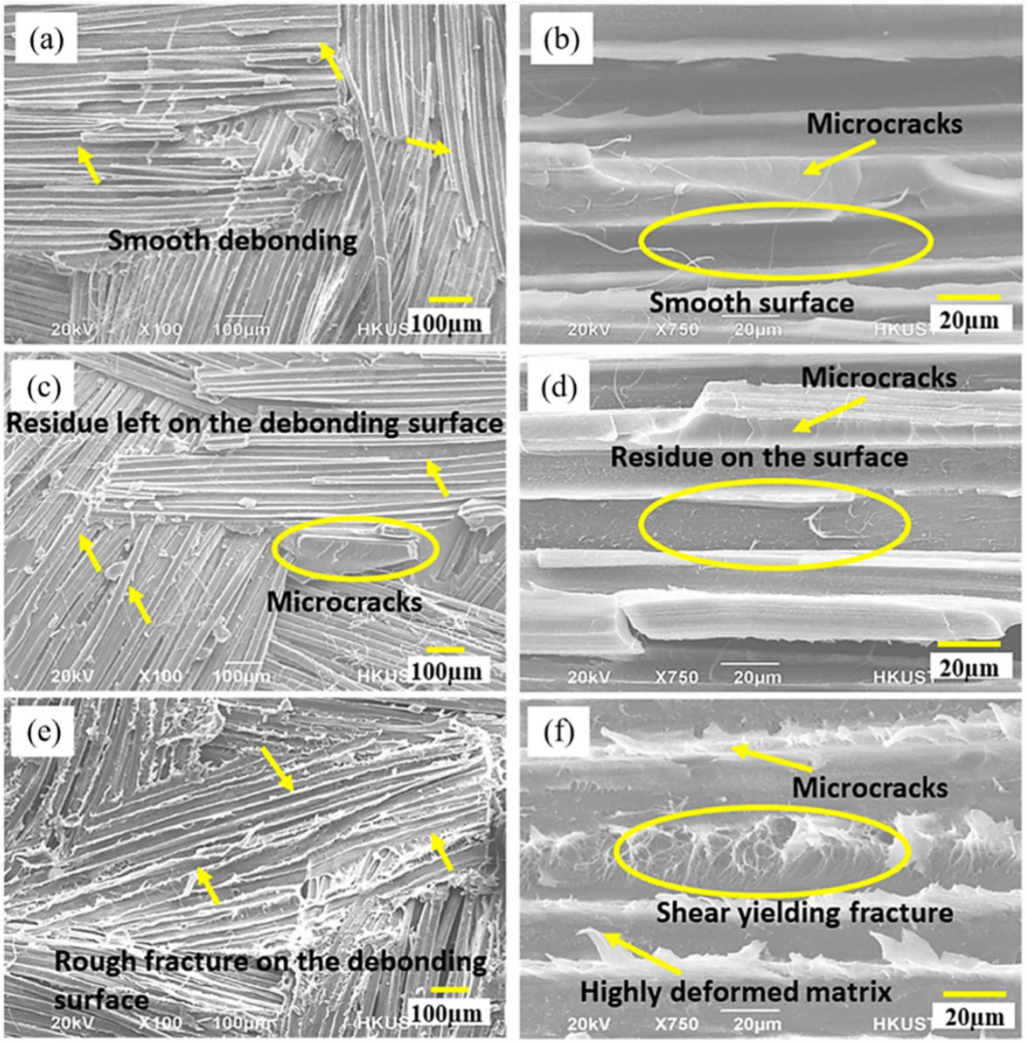


Fig. 19. Low- and high-magnification SEM micrographs of double cantilever fracture surfaces of UHMWPE-acrylic samples containing (a & b) untreated fibres, (c & d) PDA-treated fibres, and (e & f) PDA + MWCNT-treated fibres (Copyright permission from Elsevier. Adapted from Fig. 7 in Ref. [68]).

summary of some of the key reported thermomechanical properties of acrylic matrix composites in published literature.

4.5. The effects of fibre sizing on the properties of acrylic-matrix composites

Given the infancy of this class of resins, its chemistry is not as well-known as that of traditional thermosets, which are associated with well-established supply chains and dedicated sizing technology. Until recently, much of the published literature on acrylic-matrix composites comprised fibre reinforcements with multi-compatible sizing. With advancing research, there are now specially sized reinforcement systems available for acrylic matrix composites. However, being based on novel technology, these systems require comprehensive characterisation. Several authors have investigated the effects of such acrylic-sized reinforcements against their multi-compatible counterparts. The following section summarises the findings to date.

Boufaida et al. [40] studied the influence of sizing on the properties of glass fibre-reinforced acrylic composites using fibres sized with multi-compatible (MC) and acrylic-compatible (AC) formulations. Fibre-matrix strength was assessed in the materials using monotonic and fatigue in-plane shear testing. Although no notable influences were reported on modulus and strength, the authors reported a lower threshold for the development of progressive damage in MC-sized samples in response to monotonic loading, with an enhancement of only 4% in strength reported for the use of AC sizing. On the influence of sizing on fatigue damage development, damage-induced heat build-up was reported for both materials alongside a reference with no sizing (NS). It



poly[(methyl)methacrylate]-b- poly(butyl acrylate)-b-poly[(methyl)methacrylate]

Fig. 20. Structure of self-assembling acrylic block copolymer (Copyright permission from Elsevier. Reproduced from Fig. 1a in Ref. [32]).

Table 6
Overview of works on the effects of toughening on the impact performance of acrylic-matrix composites.

Materials	Summary of results	Comments	Ref.

E−150
Nanostrength® (5–15 wt %)
Glass fibre (woven)
Drop-weight impact
	• Enhanced impact damage resistance (20°C and 80°C impacts only). Increase in matrix ductility and reduced damage extension with Nanostrength® toughening.
	• 10 wt % loading conferred superior performance in most cases as shown by changes in absorbed energy relative to the unmodified material:
	  • -80°C impacts → −4% (30 J); −35% (40 J); −13% (50 J)
	  • 20°C impacts → −31% (30 J); −5% (40 J); +7% (50 J)
	  • 80°C impacts → −6% (30 J); −17% (40 J); −10% (50 J)
	• Proposed toughening mechanisms: crack-bridging, micelle cavitation, shear banding and crack tip shielding.
		Explored a breadth of variables, which are insightful for the composites community in terms of the impact behaviour of toughened acrylic-matrix composites.
		However, the effects of individual variables was not readily understood. Moreover, no quantitative damage zone assessments were performed.
			[32]

E−150
ABS (10 wt %)
Nanostrength® (10 wt %)
Glass fibre
Drop-weight impact & Charpy impact
	• Nanostrength® and ABS toughening of acrylic polymer and composite only moderately enhanced the absorbed energy in toughened laminates for drop-weight impact:
	  • ABS-toughened acrylic →-19% (40 J); −0% (50 J); −7% (60 J)
	  • Nanostrength®-toughened acrylic →-16% (40 J); +8% (50 J); −2% (60 J)
	• Significant improvements in Charpy impact resistance unreinforced samples:
	  • ABS-toughened acrylic →+238% (unreinforced polymer)
	  • Nanostrength®-toughened acrylic →+43% (unreinforced polymerProposed toughening mechanisms for Nanostrength® and ABS: crack-bridging, void coalescence, micelle cavitation, shear banding and crack tip shielding.
		Findings are logically presented and discussed with the effects of toughening, reinforcements and energy levels considered.
		However, no quantitative damage zone assessments were performed.
			[52]

Table 7
A summary of the effects of Nanostrength®-toughening on glass transition temperatures of unreinforced acrylic polymers.

Matrix	Glass transition temperature (°C)	Reference
Elium®	125	Pini et al. [65]
	127	Pini et al. [64]
Elium Impact®	−25, 125	Pini et al. [65]
	−25, 130	Pini et al. [64]

was found that the use of MC-sized fabrics results in enhanced fatigue performance (+7% compared to the NS reference). However, a more significant difference was reported for the AC-sized material, corresponding to a 22% improvement with respect to the NS reference. Although this study evaluated macromechanical performance, their findings were in agreement with those of Beguinel et al. [66], who studied the effects of fibre sizing on the interfacial shear strength (IFSS) of glass fibres with acrylic-compatible and polypropylene-compatible sizings, and carbon fibres with acrylic-compatible- and epoxy-sizings. Microbond test samples were prepared using a reactive acrylic matrix on single tensioned fibres. Improved IFSS values were reported for glass- and carbon-reinforced acrylic samples comprising fibres with acrylic-compatible sizing (compared to those employing multi-compatible sizing formulations). Interestingly, Davies et al. [67] suggest that the use of appropriate sizings may affect the durability of glass fibre-reinforced acrylic composites.

Shanmugam et al. [68] demonstrated fibre surface functionalisation of ultra-high molecular weight polyethylene (UHMWPE) as a viable means of improving Mode-I interlaminar fracture toughness. The authors studied the effect of treating fibres with two polydopamine (PDA)-based coatings for composite applications. As evident in Fig. 19, the effects of these treatments on fracture behaviour were significant. Comparing the fracture behaviour of the FRP (Fig. 19a and b) with untreated fibre to that containing PDA-treated fibres (Fig. 19c and d), the authors reported smooth fibre surfaces with the use of untreated fibres and the presence of residue on treated fibre. Thus, it was evident that fibre functionalisation with PDA alone resulted in enhanced interfacial adhesion with the E−188 matrix used, corresponding to 19.6% improvement in average fracture toughness. Furthermore, the enhancements achieved with the sample shown in Fig. 19e and f were realised with the incorporation of 0.03 wt % of multi-walled carbon nanotubes (MWCNT) into the PDA coating. For this sample, an improvement of 42.5% in fracture toughness was reported against its untreated counterpart.

These works highlight the requirement of specialised sizing technologies for these acrylic resins; however, several authors [28,37,38,51,69] have shown that the use of MC-sized reinforcement does not result in any adverse effects on the quality and performance of the composites. Interestingly, these authors report the use of E−180 or 188 resins with MC-sized glass fibre reinforcement. These studies may highlight the suitability of the Elium® 18* family of resins for use with existing glass fibre sizing technologies. Besides, in a study by Charlier et al. [69], the

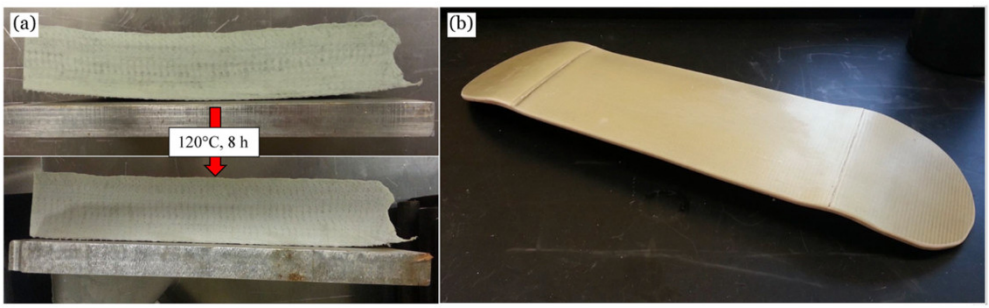


Fig. 21. Demonstration of thermoformability: (a) flattening a curved section and (b) producing a curved prototype from glass-reinforced acrylic laminates (Copyright permission from Elsevier. Reproduced from Figs. 9 and 10 in Ref. [22]).

Configuration		Resin Volume (mm^3)
ELC_IED		150.7
ELC_FED (0.5mm ELF)		312.5

Fig. 22. Welding configuration used by Bhudolia et al. [39] (Copyright permission from Elsevier. Fig. 1 in Ref. [39]).

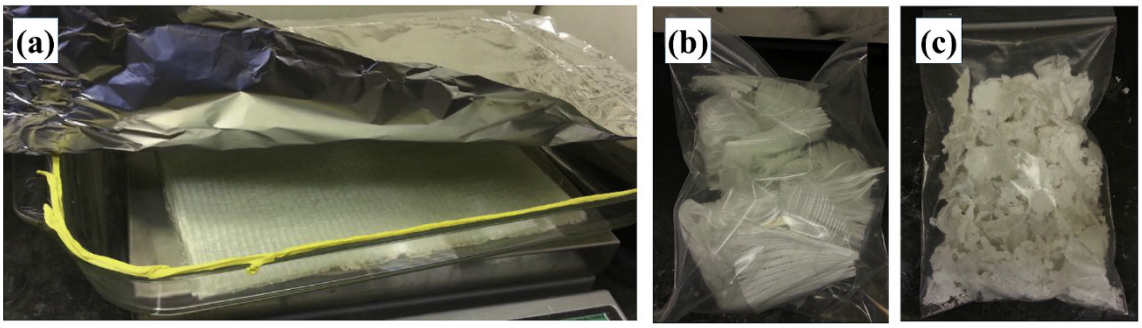


Fig. 23. Recovery of fibres and polymer matrix from *in situ* polymerised glass/acrylic laminate by dissolution as demonstrated by Cousins et al. [22] (Copyright permission from Elsevier. Reproduced from Fig. 5 in Ref. [22]).

IFSS of an unspecified Elium® resin with MC-sized and AC-sized glass fibres were micromechanically assessed by fragmentation and microdroplet testing. No significant improvements in IFSS were reported with the use of specialised sizings for acrylic matrices on glass fibres. These findings constitute important knowledge, given that the use of appropriate glass fibre sizing technology is a prerequisite for effective interfacial stress transfer, desirable fibre strength and the ultimate resistance to aggressive physical, chemical and environmental degradation agents [70].

4.6. Toughening of acrylic-matrix composites

Matrix toughness is known to contribute significantly to the behaviour of a laminate, particularly its interlaminar fracture behaviour [64], which affects damage tolerance [65]. Thermoplastic matrices are naturally superior in toughness to their thermosetting counterparts and as such, typically exhibit higher Mode-I interlaminar fracture toughness and other matrix-dominated characteristics. However, in these works [34,35,57], acrylic-based composites were only marginally higher in Mode-I interlaminar fracture toughness than their epoxy-based counterparts – highlighting a requirement for the development of appropriate toughening strategies. To date, the intrinsic toughness of traditional high-performance thermoplastic matrices obviates the requirement for toughening; as such, the effects of a strategically developed approach for acrylic-based composites need to be understood.

The influence of toughening on unreinforced and reinforced acrylic matrices have been investigated in several works [32,52,64,65,71,72]. All studies focused on benchmarking a toughened acrylic matrix – Elium Impact® alongside an untoughened grade. This modified grade reportedly contains 10 wt % of a self-assembling acrylic block copolymer additive, Nanostrength®. However, the base grade of Elium® within the so-called Elium Impact® is not specified in any of the cited works. Nanostrength® is based on Arkema's proprietary alcoxyamine technology, comprising polymethylmethacrylate-b-polybutylacrylate-b-polymethylmethacrylate (shown in Fig. 20).

In addition to Nanostrength®, acrylonitrile butadiene styrene (ABS) has also been applied as a toughening agent [52]. Like Nanostrength®, ABS is a block copolymer but contains a uniformly dispersed phase of rubber within a styrene-acrylonitrile matrix. The effects of the incorporation of these toughening agents on the performance of acrylic-matrix composites will be discussed herein. Table 6 presents an overview of published works in this area.

The use of Nanostrength® within a glass fibre-reinforced acrylic hybrid laminate has been shown to reduce the energy absorbed for damage development when compared to the equivalent untoughened laminate [32]. Similarly, Kinvi-Dossou et al. [52] reported enhanced impact strength in Nanostrength®-toughened acrylic, both in unreinforced and glass fibre-reinforced forms, as detailed in Table 6. However, ABS-toughening proved more effective at enhancing polymer and composite impact strengths than the use of Nanostrength®. In the same work, the authors also studied drop-weight impact performance of the same materials; however, impacts under 40 J did not appear to be influenced by toughening. Both tougheners contain rubber nanophases, which become grafted to the matrix during the *in situ* polymerisation process, rendering it more ductile. This enhanced ductility facilitates plastic deformation within the matrix in response to low-velocity impacts. In the case of Nanostrength®, it is believed to play a vital role in crack bridging and suppressing coalescence of voids and microcracks. The authors also suggest that the self-assembling ability of Nanostrength® is essential to the micelle cavitation mechanism, which not only toughens the matrix but induces shear banding and resists the initiation of delamination. These conclusions are in agreement with those drawn by Boumbimba et al. [32]. They are further supported by the works of Pini et al. [65,72,73], who extensively studied the fracture behaviour of untoughened and toughened acrylic matrix systems and identified the dominant roles played by crazing, cavitation and shearing in Nanostrength®-toughened acrylic matrices. Pini et al. [65] suggested a transition from crazing to cavitation and shearing depending on temperature and strain-rate conditions and reported differences in the respective dependences of Mode-I fracture toughness on crack propagation rates for the toughened and untoughened acrylic-matrix composites. The fracture toughness of the toughened-matrix composite exhibited inverse proportionality to strain-rate; as the crack propagation rate increased, the authors reported a decreasing trend in fracture toughness. Interestingly, no rate effects were reported for the unmodified-matrix composite. These observations are further explained in work by Pini [53], which showed that higher displacement rates (and lower temperatures) promote multiple crazing in the Nanostrength®-toughened acrylic matrix. Conversely, cavitation and shear yielding are the dominant mechanisms at lower displacement rates (and

Table 8
Aluminium alloy surface treatment study parameters as reported for acrylic-based fibre-metal laminates by Mamalis et al. [88] (Copyright permission from Elsevier. From Table 2 in Ref. [88]).

Time (min)	Treatment					
	NaOH 10 wt %	Acid solution (ANPE 80/5/5/10)	NaOH 10 wt% + acid solution	Acid solution + NaOH 10 wt%	Sulphuric acid anodising	Atmospheric plasma treatment
2	–	✓	–	–	Def Stan 2003–25/4	1 scan at 1 mm/s
5	✓	✓	✓	✓		1 scan at 2 mm/s
10	✓	✓	✓	✓		3 scan at 1 mm/s
20	✓	✓	✓	✓		3 scan at 2 mm/s

Table 9
Summary of the metal and fibre surface treatments used in acrylic-based fibre-metal laminates by Shanmugam et al. [89].

Laminate	Titanium treatment condition	Fibre surface coating
1. Ti-Pris + UHWPE-Pris	Untreated	No coating
2. Ti-Ann + UHWPE-Pris	Treated	No coating
3. Ti-Ann + UHWPE-PDA	Treated	PDA
4. Ti-Ann + UHWPE-PDA + CNT	Treated	PDA + CNT

higher temperatures). The rubber particles within the toughened acrylic matrix are said to both initiate and control the crazing behaviour. While a few larger crazes were reported for unmodified acrylic matrix, toughening was said to give rise to the formation of a large number of smaller crazes; the relative increase in the volume saturated by these smaller crazes is believed to contribute to favourable energy absorption within the toughened matrix. Cavitation in the vicinity of rubber particles was said to promote matrix plasticity as opposed to being a primary energy absorption mechanism. Another role of cavitation in the toughened matrix is to shear yielding, which like crazing, constitutes a major energy absorption mechanism.

Pini [53] also reported positive effects of toughening on the interfacial adhesion; unmodified acrylic-matrix composites exhibited inferior interfacial strength to the toughened composites, which showed evidence of cohesive fracture of the fibre-matrix interface. However, fibre bridging was more prevalent in the unmodified composite during testing. Finally, the author reported more effective toughness transfer from unreinforced matrix to reinforced composite in the case of the unmodified matrix for which full transfer was reported due to the absence of interactions between the fibres and the process zone in the matrix-rich layer. This was not the case for the toughened materials, where only a partial transfer was reported. The author attributes this to contributions from fibre-process zone interactions. A smaller process zone (as in the untoughened matrix) was thought to be constrained by adjacent fibres. As the size of the process zone increases (with the incorporation of a toughening phase), its development is thought to be more affected by the presence of the fibres. Furthermore, the crack tip opening distance and thickness of the interlaminar resin-rich layer were shown to be influenced by the presence of a toughening phase within the matrix. Pini cites rheological differences in the toughened and untoughened material as the source of these observed differences.

In general, rubber toughening of polymeric materials is known to compromise their mechanical [74,75] and thermomechanical performance by decreasing T_g [76]. Owing to their non-reactive backbone, block copolymers like Nanostrength® are said to be unique, in that their use reportedly yields no reduction in T_g [77]. To date, mechanical and thermomechanical characterisation of Nanostrength®-toughened acrylic matrices and their composites remain mostly unexplored. However, the work of Pini [53] provides valuable insights into the fracture behaviour. The author reported a deleterious effect of Nanostrength®-toughening on matrix stiffness due to the presence of the rubber phase. The authors reported enhancements in tensile failure strains at a constant displacement rate of 1 mm/min over a range of test temperatures (0–60°C). Unmodified acrylic matrix (grade unspecified) exhibited brittle failure characteristics with strains of ~0.025–0.2, whereas the incorporation of 10 wt % of Nanostrength into the same matrix system produced more ductile failure with strains of ~0.2–0.9. Table 7 presents a summary of key published works on the thermomechanical performance of Nanostrength®-toughened acrylic (Elium Impact®). Due to the paucity of works on the thermomechanical properties of toughened acrylic-matrix composites, only findings on toughened unreinforced acrylic polymer have been presented in Table 7.

Table 10
Overview of some published works on acrylic-matrix hybrid composites.

Materials	Fabrication Methodology	Summary of results	Ref.

• E–188
• BPO
• UHMWPE (woven; 12 plies)
• Ti6Al4V titanium (1.5-mm thick)
• PDA
• CNT (multi-walled)
	A multi-stage process was employed as illustrated in Fig. 27b and detailed in Table 9:
	• Alloy surface activation → anodisation, alkali etching and annealing of the alloy sheet.
	• Fibre surface functionalisation → PDA or PDA & CNT fibre coating.
	  • Laminate 1 → Untreated
	  • Laminate 2 → Only alloy surface activation
	  • Laminate 3 → Alloy surface activation + PDA fibre treatment;
	  • Laminate 4 → Alloy surface activation + PDA & CNT fibre treatment.
		• Mode-I fracture toughness improvements relative to the untreated reference laminate (Laminate 1) as shown in Fig. 28b:
		  • Laminate 2 → +528%;
		  • Laminate 3 → +636%;
		  • Laminate 4 → +916%.
		• The most significant improvements in crack growth resistance were exhibited by Laminate 4 as evidenced in Fig. 28a, c and d. Failure mechanisms are shown in Fig. 28d.
			[89]

• E–180
• BPO
• Glass fabric (UD; 6 plies)
• 6082-T6 aluminium (0.71-mm thick)
• CN104 epoxy acrylate coating
	Multi-stage process the process parameters are summarised in Table 8:
	• Alloy surface activation → chemical etching (alkali, acid, acid-alkali and alkali-acid) or anodisation or atmospheric plasma. The resulting surface morphologies are shown in Fig. 24.
	• Alkali-etched aluminium was used in FMLs to promote mechanical interlocking in addition to enhanced chemical adhesion using the CN104 coating.
	  • Laminate 1 → Acrylic-matrix FRP
	  • Laminate 2 → TP-FML
		• Performance of Laminate 2 (relative to the conventional reference laminate (Laminate 1) as shown in Fig. 26:
		  • Flexural strength → +10%;
		  • Flexural modulus → +23%;
		  • Interlaminar shear strength → +41%;
		  • Mode-I fracture toughness → −78%.
			[88]

FML: fibre-metal laminate; **BPO:** dibenzoyl peroxide initiator; **UHMWPE:** ultra-high molecular weight polyethylene; **PDA:** polydopamine; **CNT:** carbon nanotubes; **UD:** unidirectional; **FRP:** fibre-reinforced polymer; **TP-:** thermoplastic.

5. Advantages of thermoplastic acrylic-matrix composites

5.1. Reshaping by thermoforming

Cousins et al. [22,46] successfully demonstrated the thermoformability of continuous fibre-reinforced acrylic composites. An acrylic-matrix prototype spar cap section was flattened (120°C, 5.4 kPa, 8 h; radio-frequency press) as shown in Fig. 21a, and a prototype single-curvature component (Fig. 21 b) was also produced as part of this study. Such works are essential to the cross-sectoral appeal; particularly for the automotive industry, where *in situ* polymerised blanks could be readily thermoformed, facilitating mass-production. However, further investigation would be essential to understanding the effects of thermal reprocessing on matrix, fibre and interfacial properties.

5.2. Joining of acrylic-matrix composites

Welding is an attractive alternative to mechanical fasteners and adhesive joining. The former adds undesired weight and may cause drilling-induced delamination and bearing failure. The bondline achieved with the latter is sensitive to harsh chemical environments, which can compromise static and dynamic structural performance [38]. Some recent works have demonstrated the weldability of glass fibre-reinforced acrylic composites [38,39,78]. Fusion welding of glass fibre-reinforced acrylic substrates to form lap-shear coupons was readily realised above 110°C (T_g of E−188) using several element types (fine stainless steel mesh, woven carbon and unidirectional carbon fabrics) [38]. Bhudolia et al. [39] comparatively assessed ultrasonically welded and adhesively bonded carbon fibre-reinforced acrylic joints based on E−150. The authors reported the use of an integrated semi-hemispherical energy director design for some of the welded joints and Arkema's methacrylate-based adhesive system (Bostik SAF 30-5) for the adhesively bonded reference coupons. The joint configurations used for welded samples are schematically represented in Fig. 22 with the volume of neat resin used in forming the energy director within the joints. Energy directors have also been shown by Bhudolia et al. [39,78] to cut down on joining time compared to adhesive bonding by 99.8%. Additionally, Bhudolia et al. [39] reported 23% higher static lap shear strengths and 12% higher fatigue strengths in welded joints compared to their adhesively bonded counterparts. The authors observed fibre impingement and shear cusps as the primary failure mechanisms, concluding that these promoted strong interfacial adhesion. Murray et al. [38] reported up to 100% higher static lap shear strengths in resistance and induction welded coupons relative to the adhesively bonded variants. It was also suggested even greater potential enhancements of joint performance may be realised using fibre-reinforced heating elements with improved sizing technology and infusion quality.

5.3. Recycling and recovery of constituents

Cousins et al. [22] demonstrated the viability of acrylic-matrix composites for recycling by conventional recovery methodologies employed today such as pyrolysis, mechanical grinding and dissolution. The authors compared the recoverable constituents as well as the energy and cost requirements for all techniques, concluding that dissolution was the most favourable approach based on full-scale fibre and polymer recovery as shown in Fig. 23. Compared to virgin fibres, recovered fibres were reported to exhibit no loss in tensile strength, with a 12% reduction in stiffness. This loss in stiffness was attributed to operator-induced fibre misalignments during the dissolution recovery process. Additionally, pyrolysis was reported to result in the loss of fibre length scale and sizing; dissolution facilitated not only their retention but also the recovery of the acrylic polymer. Pyrolysis was deemed less viable for the acrylic-matrix composite, as this required 78% more decomposition energy than the requirement for the epoxy-based reference. Grinding and dissolution consumed the lowest and highest energy, respectively, per unit of mass. The works of these authors essentially answer the questions raised by Baley et al. [41] on the recyclability of these novel acrylic-matrix composites. Although the findings reported by Cousins et al. [22] suggest no loss of sizing using the dissolution approach, surface analyses could substantiate this conclusion and contribute to increased confidence in these materials as potential future-proof solutions in terms of overall end-of-life value. Dissolution in acetone has also been demonstrated as a potential route to material recovery [79].

One of the challenges associated with composites recycling is that recovery methodologies only facilitate down-cycling, with low-level application of the recyclates due to process-related loss of structural integrity. The attainment of higher levels in the recycling hierarchy is therefore, more crucial than ever to realise true circularity in this market [80]. Ultimately, processes like pyrolysis and dissolution offer better prospects in terms of fibre length-maintenance; however, dissolution affords even greater benefits in terms of polymer matrix recovery [22]. In particular, the potential for selective dissolution combined with the reshapability of continuous fibre-reinforced acrylic composites as discussed in Section 5.1 could be attractive. The property-retention facilitated by dissolution recycling processes may enable the exploration of high-value recycling and reuse of end-of-life acrylic-matrix composites.

These works go a long way to answering important research questions, which have profound ecological implications. Full or partial recovery of resources from end-of-life components manufactured from acrylic-matrix composites can mean better end-of-life waste management. In terms of tonnage, retired thermoset-matrix composite blades account for a large percentage of landfill-bound waste. It is said that current practices in the marine sector mean that all end-of-life composite waste is typically disposed of in landfill due to contamination with oils, paints and core materials [81]. Given the energy-intensive production methods involved in the fabrication of such components, the use of thermoplastic-based composites has not only been identified as a viable solution to minimising environmental impact, but also potentially has far-reaching economic implications [22].

6. Hybrid thermoplastic composites using *in situ* polymerised acrylics

Matrix- and fibre-based hybridisation have been shown as viable means of providing essential performance enhancements, while concurrently targeting the reduction of mass and overall costs [82,83]. Recent advancements in liquid acrylic-matrix hybrid composites are discussed herein.

Kazemi et al. [84] reported improvements of up to 150% in the compressive strength of woven carbon fibre/ultra-high molecular weight polyethylene (UHMWPE) fibre-reinforced acrylic hybrid composite systems, with respect to UHMWPE-only fibre-reinforced acrylic reference laminates. Unsurprisingly, this corresponded to 27% lower strengths in the hybrids, relative to the carbon fibre-reinforced acrylic reference laminate, due to the superiority of carbon fibres in performance. While studies of this type play vital roles in improving our understanding of carbon and UHMWPE as reinforcements in acrylic-matrix hybrid composites, the authors fail to provide comprehensive conclusions of their findings. No remark was made on the implication of such hybrids. Nonetheless, this study does demonstrate the potential for realising more economical (compared to carbon-only FRPs), stronger and stiffer (compared to UHMWPE-only FRPs) thermoplastic hybrid systems by a conventional room-temperature vacuum infusion process. In another study by Kazemi et al. [85], similar hybrids were shown to enhance impact performance, evidenced by a lesser (−47%) reduction in structural integrity and 18% reduction in absorbed energy.

Fibre-metal laminates (FMLs) are a class of hybrids comprising thin metal sheets interleaving FRP layers. They were developed to exploit the weight-saving benefits of composites in a relatively cost-effective manner with possible enhancements in fire resistance, damage tolerance, fatigue and impact properties [86,87]. Some of the earliest works

in this area focused on the use of thermosetting matrices with glass-reinforced epoxies. This was due to the historic challenges associated with melt processing methodologies for thermoplastic alternatives. The rise in the popularity of liquid reactive thermoplastic resins has opened doors of opportunity for this class of hybrids, as they facilitate resin infusion processing of thermoplastic FMLs. An overview of works in this area, demonstrating the suitability of liquid thermoplastic acrylic resins is presented in Table 10. While Mamalis et al. [88] relied on drilled holes for through-thickness resin flow during vacuum infusion processing (Fig. 25), Shanmugam et al. [89] did not report similar measures to enhance flow. Additionally, it is worth pointing out that although the Mode-I interlaminar fracture toughness reported by Mamalis et al. [88] was lower than the reference acrylic-based laminate, the authors remarked that the value reported for the FML was ~237% higher than values reported in literature for a thermoset FML.

7. Important consideration for the use of acrylic resins in composite applications

7.1. History of flammability

Random chain scission was identified as the primary mechanism by which an acrylic polymer undergoes major thermal degradation (Section 2.1.1). This highlights the importance of further exploration of the flammability of reactive acrylic polymers and their composites. Acrylics are known to depolymerise at elevated temperatures owing to the aforementioned scission mechanism, releasing flammable monomers, which pose in-service fire hazard implications. This is particularly important, given the contributions of poly (methyl methacrylate) sheet glazing (Oroglas) to the Summerland disaster in 1973 [90,91]. Already, it has been shown that, by using non-woven intumescent mats [92] and a phosphorus-carbon-based flame retardant [93], that the flame-retardant and smoke suppression properties of acrylic-matrix composites can be significantly enhanced.

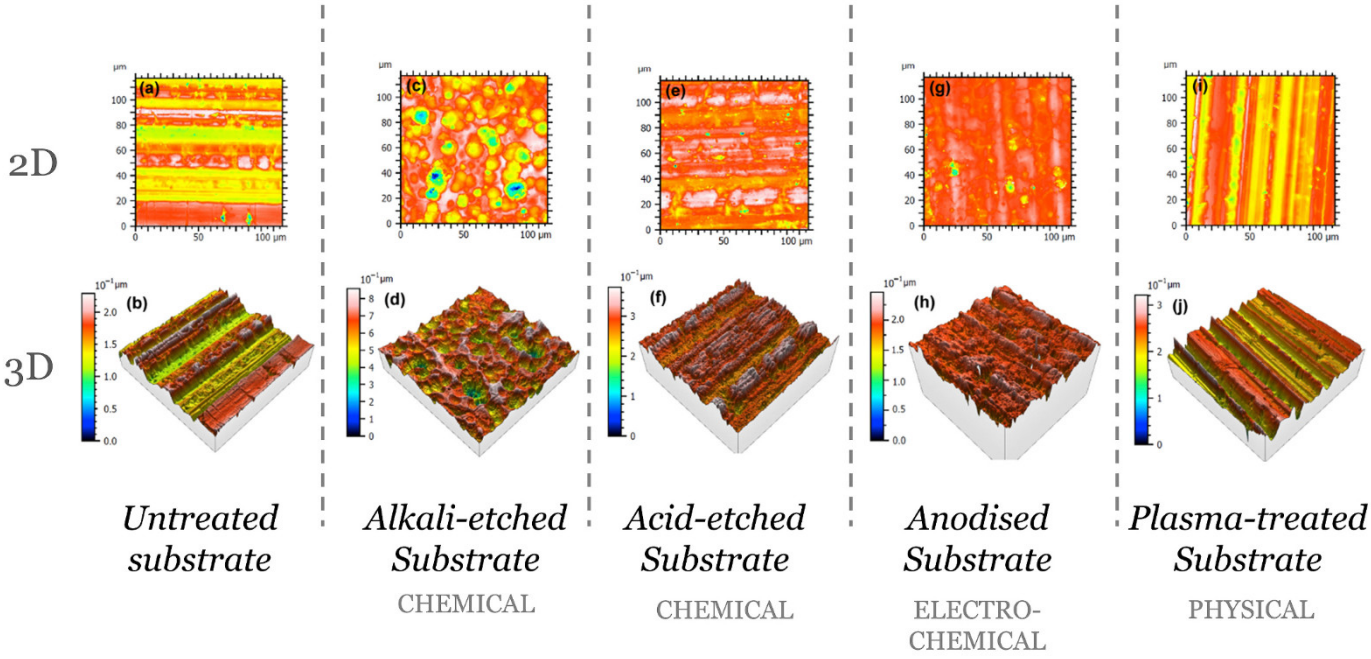


Fig. 24. 2D and 3D height profiles for an untreated substrate (a) & (b); and alkali-etched (c) & (d), acid-etched (e) & (f), anodised (g) & (h), and plasma-treated (i) & (j) substrates (Copyright permission from Elsevier. Reproduced from Fig. 2 in Ref. [88]).

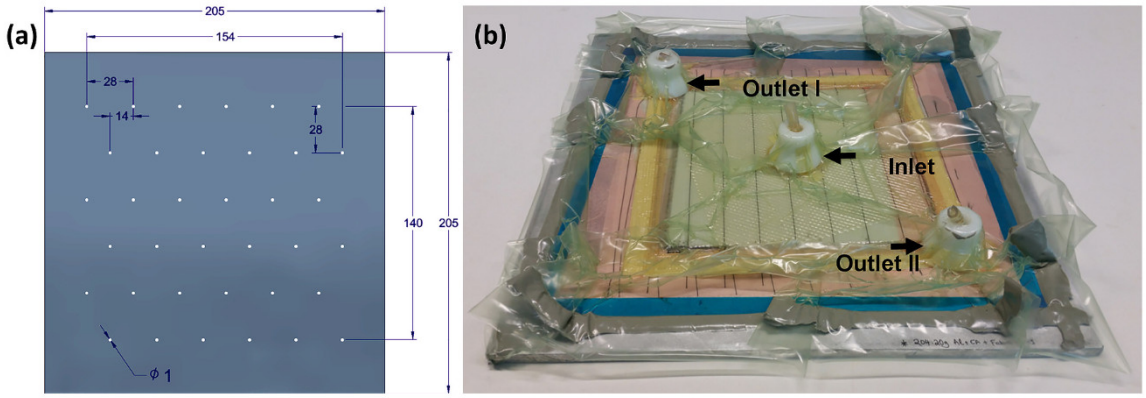


Fig. 25. (a) Perforated aluminium sheet (b) Experimental set-up for radial vacuum infusion process as used Mamalis et al. [88] (Copyright permission from Elsevier. Adapted from Fig. 1 in Ref. [88]).

Table 11
Summary of some comparative attributes of liquid resin infusible acrylic, polyamide-6 and epoxy and melt-processible isotactic polypropylene.

Polymer	Temperature (°C)			Shrinkage (%)	Tensile strength (MPa)	Elongation (%)	[b]Avg. material cost (£/kg)	Water uptake 24 h, 23°C (%)	Resistance		
	Processing	Glass transition	Max service						Solvent	UV	Fuel
Acrylic [LRI]	25 [27]	120 [33]	90 [108]	0.8 [109]	66 [37]	3 [37]	4.90 [110]	0.2–0.4 [111]	★ [112]	★★★ [112]	★★ [112]
iPP [MP]	225 [113]	145 [113]	130 [108]	3 [109]	34 [113]	350 [113]	1.30 [114]	0.01–0.1 [111]	★ [112]	★★ [112]	★★ [112]
PA-6 [LRI]	110 [115]	65 [116]	120 [108]	1.6 [109]	83 [117]	30 [117]	1.20 [118]	1.6–1.9 [111]	★★★★ [112]	★★ [112]	★★★ [112]
Epoxy [LRI][a]	25 [37]	127 [37]	90 [119]	6.9 [120]	78 [37]	4 [37]	2.40 [110]	0.1–0.15 [119]	★★★★ [121]	★ [122]	★★★★ [123]

The numbers in square brackets represent references corresponding to the sourced values; **iPP**: isotactic polypropylene; **PA-6**: polyamide-6; **LRI:** suited to liquid resin infusing; **MP:** suited to melt processing.

[a] Reported values are from literature/sources on commodity, non-aerospace grade epoxies.

[b] £/GBP equivalents as of the 26th of February, 2021 for the €/EUR and $/USD values reported in the referenced sources. The ratings for resistance to exposure under various conditions are: 'Poor (★)', 'Fair (★★)', 'Good (★★★)' and 'Excellent (★★★★)'.

7.2. Vulnerability to solvent attack

Furthermore, while the dissolution of acrylic-matrix composites in acetone offers favourable end-of-life resource recovery prospects as discussed in Section 5.3, it highlights the vulnerability of these materials to solvent attack. Low solvent resistance therefore constitutes a challenge to the extended applicability of acrylic-matrix composites.

7.3. Sustainable production and application of bio-based acrylic resins

Finally, considering the ongoing market shift from petroleum-based polymers to bio-based polymers for composite applications, the development and application of reactive bio-based monomers is highly attractive for establishing improved supply chain sustainability [94,95]. In fact, the availability of bio-based variants has been considered a key criterion in the material selection process for composites in marine applications [90]. For the purpose of this review, the term *'bio-based'* is used to imply monomers and polymers produced from bio-sourced feedstock (naturally and bio-engineered). Already, technological advances on the synthesis of bio-acrylate monomers bearing great structural similarity to petroleum-derived acrylates has been demonstrated by Voronov and Tarnavchyk [96,97]. Moreover the use of more sustainable feedstocks in the production of methyl methacrylates adhesives and monomers by Lucite, Evonik and Arkema holds promise for the exploration of bio-based acrylics [98].

Technological development continues in this area, but thus far, the most viable bio-sources are epoxidised and hydroxylated soybean oil, pine tree resin and various lignin derivatives [95,96,98–101]. While these approaches offer promise for revolutionising the supply chain and environmental impact of thermoplastic acrylic monomers and their end-products, further exploration is critical to continued advancements. Today, bio-based polymers are said to account for less than 1% of the global production of polymers. Their use is often associated with inferior performance compared to their traditional counterparts [102]. Thus, performance-tailoring research activities aimed at enhancing rigidity, thermal stability and overall compatibility with existing both fibre and sizing technologies, are pivotal to extending their long-term adoption potential. Mono-acrylate isosorbide (derived from cellulose) has been shown to potentially confer favourable thermal and mechanical characteristics on the derived acrylic [103]. The broad availability of bio-feedstocks such as carbohydrates, triglycerides and proteins as viable alternatives to petroleum-based building blocks, therefore offers ecological and technological advantages [104]. Some challenges that need to be overcome in this area for the successful adoption of more sustainable practices includes the lack of cost-competitiveness of bio-renewable feedstocks compared to existing petroleum-based alternatives; an overall lack of maturity; and possibly the true sustainability of feedstocks and synthesis methodologies. The interested reader is referred to an exhaustive overview by Fouilloux and Thomas on current production and polymerisation pathways of bio-based acrylates [102].

7.4. Critical overview of comparative performance

Some characteristics of LRI-processible acrylic polymer (unreinforced) alongside other LRI-processible polymers (isotactic polypropylene and non-aerospace-grade epoxy), and melt-processible isotactic polypropylene can be summarised (as shown in Table 11) to facilitate comparisons between processing routes and attainable properties for different potential applications. In particular, the maximum continuous service temperatures reported in the literature and their resistance to exposure to various conditions and environments are presented to provide an overview of properties, which are expected to directly influence the applicability of these resin systems. Similarly, some representative longitudinal tensile strengths and moduli discussed in this review have been summarised in Fig. 29. To provide further insights on the quality of the interfacial adhesion across these composite

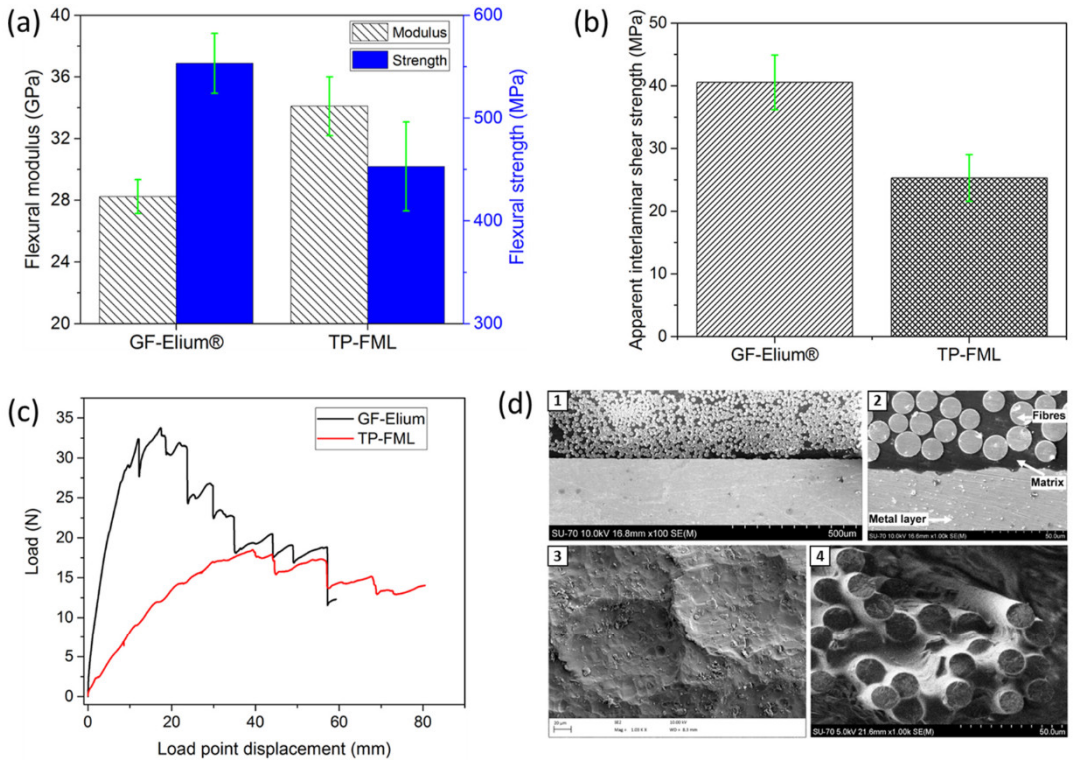


Fig. 26. Summary of comparative (a) flexural, (b) interlaminar shear, and (c) Mode-I interlaminar fracture toughness performance of thermoplastic FML and an equivalent FRP reference. (d) Microscopic characteristic of thermoplastic FML studied by Mamalis et al. [88] (Copyright permission from Elsevier. Reproduced from Figs. 5–8 in Ref. [88]).

systems and variability, theoretical predictions for strengths (Fig. 29a) and moduli (Fig. 29b) were obtained. This was done for multiaxial carbon, UD glass and woven glass fibre-reinforced acrylics. In the interest of simplicity, multiaxial and woven reinforcements were assumed to offer comparable contributions. Given the similarities between the various grades of the acrylic resin, the predicted properties were relatively consistent across all grades. The interested reader is referred to the supporting document for further methodological information.

As can be seen in Fig. 29a, all experimental values were inferior to the theoretical values, with the exception of the multiaxial carbon-reinforced E−280 material, which appeared to be marginally superior. Interestingly, the highly aligned, pultruded UD glass fibre-reinforced E-C595E material exhibits comparable V_f-normalised strength to the multiaxial carbon and UD glass E−150 material. All glass fibre reinforced samples exhibited only marginally lower experiment strength with respect to theoretically-derived strengths. While these results may highlight contributions of the interface and fibre alignment, the theoretical and experimental values appear to be comparable in terms of orders of magnitude. Fig. 29b reveals good agreement between experimental and theoretical data.

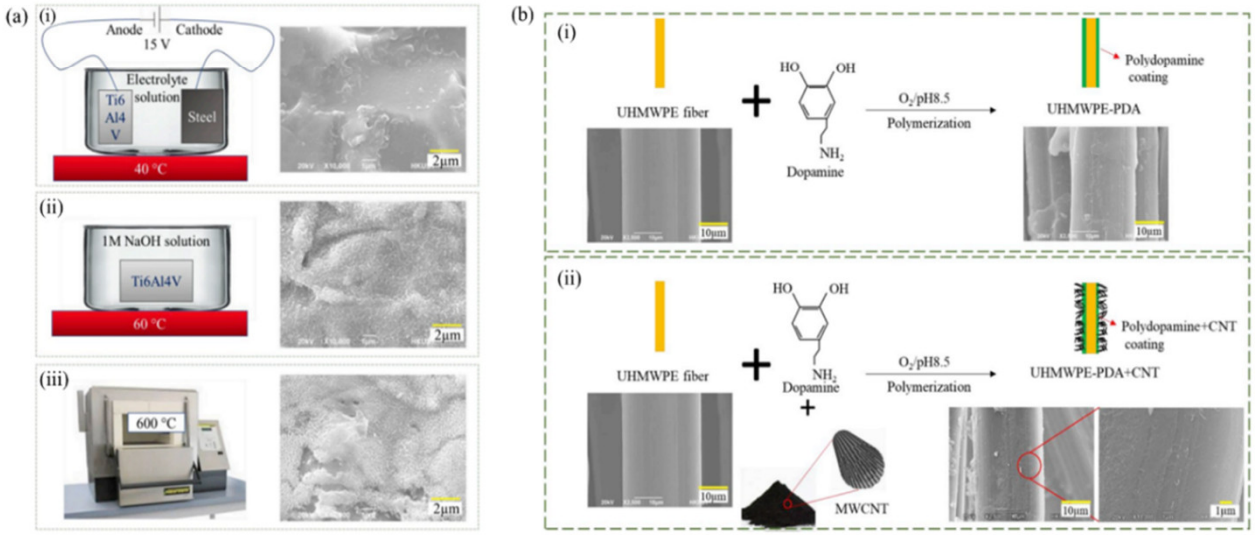


Fig. 27. (a) Schematic of the titanium alloy surface treatment sequence; (b) UHMWPE fibre surface treatments using (i) a polydopamine coating only and (ii) a polydopamine coating-impregnated carbon nanotube coating (Copyright permission from Elsevier. Reproduced from Figs. 1 and 2 in Ref. [89]).

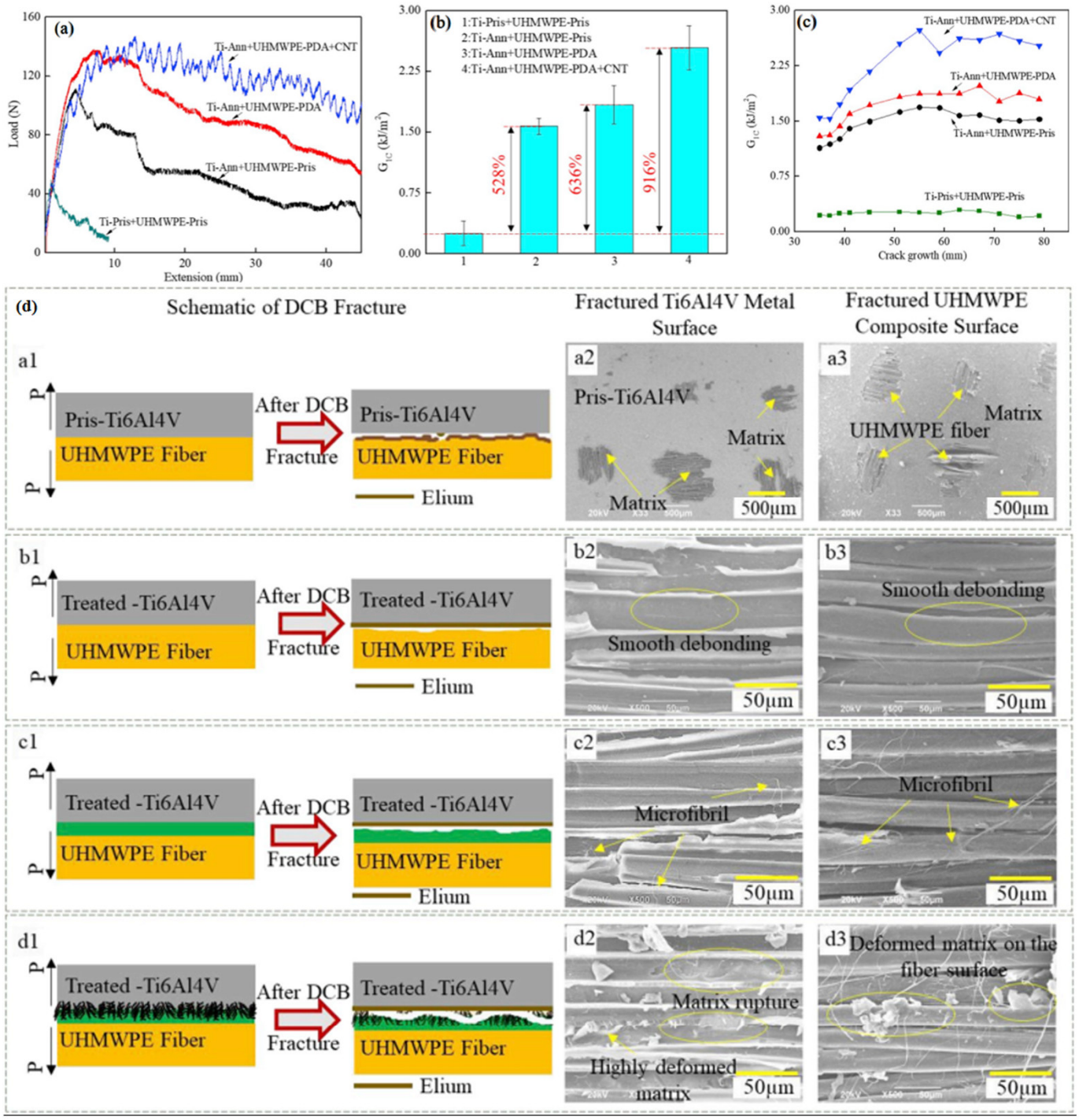


Fig. 28. (a) Load-displacement behaviour, (b) Mode-I interlaminar fracture toughness, (c) resistance curves for four FMLs, showing the effects of fibre-surface and metal-surface treatments (Copyright permission from Elsevier. Reproduced from Figs. 5 and 7 in Ref. [89]).

8. Future research directions

Pivotal to this process is the identification of existing challenges and associated opportunities to steer and guide future research. Already, we have discussed some important consideration and challenges for the adoption of liquid, *in situ* polymerisable acrylic monomer resins into newer application as substitutes for existing polymer and resin technologies. Herein, we present thoughts on gaps in existing contributions and propose further related challenges yet to be addressed.

1. Addressing the current environmental challenges associated with end-of-life decommissioning and waste management will continue to be a key driver of research activities within the composites industry. To futureproof these liquid acrylic resins as ideal candidate materials for a greener market, the following areas are worthy of further exploration:
   a. **Reshapability**: Building on the work of the authors discussed in Section 5.1, can large-scale fibre-reinforced acrylics be readily thermoformed to meet the requirements for serial production? Are there viable routes to reuse of reclaimed materials from decommissioned acrylic-based components?

b. **Recyclability**: In the context of the works reviewed in Section 5.3, are there other more environmentally friendly routes to complete reclamation of continuous fibres from acrylic-based composites?
c. **Repairability**: Can the reactivity of liquid acrylic resins be exploited for repair operations? Can large-scale structures be repaired on-site at room temperature without the need for costly decommissioning?
d. **Sustainability**: Can bio-sourced feedstock be reliably and sustainably employed to develop more value-added products based on acrylic monomer technology? Can performance-tailoring be performed to enhance the appeal of bio-derived acrylic building blocks with sustainable natural fibres and other bio-derived monomers, macromonomers and polymers to concomitantly confer desirable functionality?

2. The works discussed in Section 5.2 on thermal joining of acrylic-matrix composites have highlighted the need for scaling joining methodologies for larger structures. The use of conductive heating elements necessitates extensive lightning protection research, particularly for wind turbine blades. The durability of welded joints needs to be investigated, particularly building on the reviewed works on fatigue resistance; investigation of their water absorption behaviour would also be beneficial. Finally, the adaptability of these lab-based joining techniques to field joining operations must be adequately explored.
3. Despite the extensive efforts towards a comprehensive database on the performance of acrylic-matrix composites (Section 4), there still exists a paucity of published literature on their compressive performance, long-term durability and resilience, particularly due to the timescales required and the infancy of this resin technology. As such, the exploration of the comparative compressive behaviour, long-term performance (creep and fatigue) and UV sensitivity are essential.
4. While efforts have been made towards enhancing the mechanical and thermomechanical performance of acrylic-matrix composites, the standard practice involves the incorporation of a nanoscale rubber phase into the thermoplastic resin (Section 4.6). The use of thermoplastic modifiers remains unexplored for these resins. Furthermore, being amorphous thermoplastics, composites based on these acrylic matrices may exhibit poor solvent resistance as discussed in Section 7. These must also be considered in studies on tailoring of bulk matrix performance. Finally, a complementary approach to assessing the resulting interfaces must be explored.
5. The reactive nature of these liquid resins makes them ideally suited for use in multi-material systems such as fibre-metal laminates, the success of which has been highlighted in *Section* 6 of this review. Extensive exploration of the unique interfaces within such material systems should be undertaken. Moreover, the combination of dissimilar constituents presents unique challenges in terms of thermal expansion coefficient mismatch, moisture sensitivity and non-destructive damage evaluation. These areas may necessitate dedicated research efforts.
6. Innovative process-related research may pave the way for even greater adoption-potential for these reactive thermoplastic acrylic

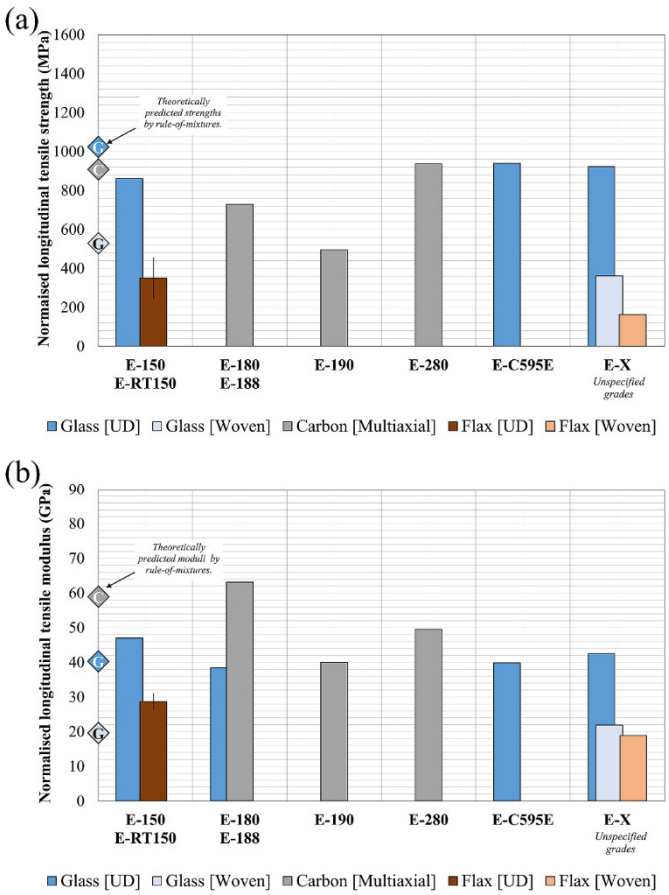


Fig. 29. Summary of (a) Vf-normalised longitudinal tensile strengths and (b) corresponding Vf-normalised longitudinal tensile moduli. All reported data were normalised to a Vf of 50% to facilitate comparisons. Respective rule-of-mixtures-derived predictions, labelled C and G (on the y-axis) were assessed for multiaxial carbon, and UD and woven glass materials. The diamond-shaped markers maintain the same colours designation shown in the legend. (For interpretation of the references to colour in this figure legend, the reader is referred to the Web version of this article.)

resins. Routes that facilitate the integration of reactive acrylic technology into alternative processing methods; e.g.: prepreg-inspired products with selective activation profiles must be explored. An indicator of innovation in this area is the recent patented approach for preparing acrylic-matrix thermoplastic prepreg composites by Zhang et al. [105]. Extending the technological advancement demonstrated therein requires the exploration of routes to address the challenges posed by the inherent low boiling point of acrylic monomers. The works presented in Sections 2 & 3 provide an essential foundation on the polymerisation behaviour and current processing methods for these liquid acrylic resin systems. To make these resins successful candidates for industrial applications, the suitable selection of initiators with delayed (or temperature-controlled) activity can be effective for the fabrication of large-scale components in the industrial environment.

9. Concluding remarks

In this paper, the research contributions on *in situ* polymerisable acrylic resins and their composites have been reviewed. From research contributions to-date, their role in the cost-effective production of continuous fibre-reinforced thermoplastics at favourably low temperature and pressures; current challenges, and future research opportunities have also been identified. These matrices have been shown to exhibit competitive thermomechanical and mechanical performance to more established epoxy resin systems. The room temperature infusibility, thermoformability, weldability and recyclability of *in situ* polymerised acrylic-matrix composites have been demonstrated. Based on the trends highlighted in this review of research contributions to-date on *in situ* polymerised acrylic composites, as the demands on industry continue to drive research towards adopting practices for improved circularity, the demand for reactive resin systems will potentially see high growth. It is our belief that these liquid resins will gain increasing cross-sectoral acceptance, if the challenges in understanding their durability and enhancing their mechanical and thermomechanical performance are addressed.

CRediT author statement

Winifred Obande: Conceptualisation, investigation, project administration, writing – original draft preparation.

Conchúr M. Ó Brádaigh: Supervision, resources, writing – reviewing and editing.

Dipa Ray: Conceptualisation, supervision, resources, project administration, writing – reviewing and editing.

Declaration of competing interest

The authors declare that they have no known competing financial interests or personal relationships that could have appeared to influence the work reported in this paper.

Appendix A. Supplementary data

Supplementary data to this article can be found online at https://doi.org/10.1016/j.compositesb.2021.108771.

References

[1] Hinkley J, Johnston N, O'Brien T. Interlaminar fracture toughness of thermoplastic composites. Adv Thermoplast Matrix Compos Mater 1989:251–63. https://doi.org/10.1520/stp24606s.

[2] Nash NH, Young TM, McGrail PT, Stanley WF. Inclusion of a thermoplastic phase to improve impact and post-impact performances of carbon fibre reinforced thermosetting composites - a review. Mater Des 2015;85:582–97. https://doi.org/10.1016/j.matdes.2015.07.001.

[3] Kim K-Y, Ye L, Phoa K-M. Interlaminar fracture toughness of CF/PEI and GF/PEI composites at elevated temperatures. Appl Compos Mater 2004;11:173–90.

[4] Howes JC, Loos AC, Hinkley JA. The effect of processing on autohesive strength development in thermoplastic resins and composites. In: Newaz GM, editor. Adv. Thermoplast. Matrix compos. Mater. ASTM STP 1044. Florida: American Society for Testing and Materials; 2008. p. 33–49. https://doi.org/10.1520/stp24593s.

[5] Akca E, Gursel A. A review on the matrix toughness of thermoplastic materials. Period Eng Nat Sci 2015;3:1–8. https://doi.org/10.21533/pen.v3i2.52.

[6] Coll SM, Murtagh AM, Ó Brádaigh CM. Resin film infusion of cyclic pBT composites: a fundamental study. In: Proc. SAMPE Eur. 25th Int. Jubil. Conf., Paris; 2004.

[7] Parton H, Verpoest I. In situ polymerization of thermoplastic composites based on cyclic oligomers. Polym Compos 2005;26:60–5.

[8] Yan C, Liu L, Zhu Y, Xu H, Liu D. Properties of polymerized cyclic butylene terephthalate and its composites via ring-opening polymerization. J Thermoplast Compos Mater 2018;31:181–201. https://doi.org/10.1177/0892705717697774.

[9] Abt T, Sánchez-Soto M. A review of the recent advances in cyclic butylene terephthalate technology and its composites. Crit Rev Solid State Mater Sci 2017;42:173–217. https://doi.org/10.1080/10408436.2016.1160820.

[10] Balogh G. Development of cyclic butylene terephthalate matrix composites [Doctoral Thesis]. Budapest University of Technology and Economics; 2012.

[11] Van Rijswijk K, Teuwen JJE, Bersee HEN, Beukers A. Textile fiber-reinforced anionic polyamide-6 composites. Part I: the vacuum infusion process. Compos Part A Appl Sci Manuf 2008;40:1–10. https://doi.org/10.1016/j.compositesa.2008.03.018.

[12] Pillay S, Vaidya UK, Janowski GM. Effects of moisture and UV exposure on liquid molded carbon fabric reinforced nylon 6 composite laminates. Compos Sci Technol 2009;69:839–46. https://doi.org/10.1016/j.compscitech.2008.03.021.

[13] Ó Máirtín P, McDonnell P, Connor M, Eder R, Ó Brádaigh CM. Process investigation of a liquid PA-12/carbon fibre moulding system. Compos Part A 2001;32:915–23.

[14] Zingraff L, Michaud V, Bourban PE, Månson JAE. Resin transfer moulding of anionically polymerised polyamide 12. Compos Part A Appl Sci Manuf 2005;36:1675–86. https://doi.org/10.1016/j.compositesa.2005.03.023.

[15] Ó Brádaigh CM, Doyle A, Doyle D, Feerick P. Electrically-heated ceramic composite tooling for out-of-autoclave manufacturing of large composite structures. SAMPE J 2011;47:6–14.

[16] Doyle A, Feerick P, Mallon P, Ó Brádaigh C, Doyle D. A heated mould for moulding polymeric composites, a method for making such mould and its use. European Patent EP 2344312B1, 2012.

[17] Gardiner G. Thermoplastic wind blades: to be or Not? CompositesWorld 2012. 30–5, http://www.compositesworld.com/articles/thermoplastic-wind-blades-to-be-or-not.

[18] van Rijswijk K, Bersee HEN. Reactive processing of textile fiber-reinforced thermoplastic composites - an overview. Compos Part A Appl Sci Manuf 2007;38:666–81. https://doi.org/10.1016/j.compositesa.2006.05.007.

[19] Murray RE, Snowberg D, Berry D, Beach R, Rooney S, Swan D. Manufacturing a 9-meter thermoplastic composite wind turbine blade. In: Am. Soc. Compos. 32nd Tech. Conf., west Lafayette, Indiana; 2017.

[20] Arkema. Elium resin: a disruptive innovation in the world of composites. Innov Webzine 2019. https://www.arkema.com/global/en/webzine/post/elium-resin-a-disruptive-innovation-in-the-world-of-composites/.

[21] Murray RE, Beach R, Barnes D, Snowberg D, Berry D, Rooney S, et al. Structural validation of a thermoplastic composite wind turbine blade with comparison to a thermoset composite blade. Renew Energy 2021;164:1100–7. https://doi.org/10.1016/j.renene.2020.10.040.

[22] Cousins DS, Suzuki Y, Murray RE, Samaniuk JR, Stebner AP. Recycling glass fiber thermoplastic composites from wind turbine blades. J Clean Prod 2019;209:1252–63. https://doi.org/10.1016/j.jclepro.2018.10.286.

[23] Ehrenstein GW. Polymeric materials. Munich: Carl Hanser Verlag; 2001.

[24] McCrum NG, Buckley CP, Bucknall CB. Principles of polymer engineering. second ed. Oxford University Press; 1997.

[25] de Andrade Raponi O, Barbosa LCM, de Souza BR, Ancelotti Junior AC. Study of the influence of initiator content in the polymerization reaction of a thermoplastic liquid resin for advanced composite manufacturing. Adv Polym Technol 2018;37:3579–87. https://doi.org/10.1002/adv.22142.

[26] de Andrade Raponi O, de Souza BR, Barbosa LCM, Ancelotti Junior AC. Thermal, rheological, and dielectric analyses of the polymerization reaction of a liquid thermoplastic resin for infusion manufacturing of composite materials. Polym Test 2018;71:32–7. https://doi.org/10.1016/j.polymertesting.2018.08.024.

[27] Arkema. ELIUM® 150 technical datasheet – liquid thermoplastic resin for glass-reinforced composite 2017. https://cstjmateriauxcomposites.files.wordpress.com/2017/11/elium_150_tech_data_sheet_grp_160908.pdf. [Accessed 21 December 2020].

[28] Murray RE, Penumadu D, Cousins D, Beach R, Snowberg D, Berry D, et al. Manufacturing and flexural characterization of infusion-reacted thermoplastic wind turbine blade subcomponents. Appl Compos Mater 2019;27:1–17. https://doi.org/10.1007/s10443-019-9760-2.

[29] Charlier Q, Fontanier J-C, Lortie F, Pascault J-P, Gerard J-F. Rheokinetic study of acrylic reactive mixtures dedicated to fast processing of fiber-reinforced thermoplastic composites. J Appl Polym Sci 2019;136:47391. https://doi.org/10.1002/app.47391.

[30] Pantelelis N, Bistekos E, Emmerich R, Gerard P, Zoller A, Gallardo RR. Compression RTM of reactive thermoplastic composites using microwaves and cure monitoring. Procedia CIRP 2019;85:249–54. https://doi.org/10.1016/j.procir.2019.10.005.

[31] Han N, Baran I, Zanjani JSM, Yuksel O, An LL, Akkerman R. Experimental and computational analysis of the polymerization overheating in thick glass/Elium®

acrylic thermoplastic resin composites. Compos B Eng 2020. https://doi.org/10.1016/j.compositesb.2020.108430.
[32] Matadi Boumbimba R, Coulibaly M, Khabouchi A, Kinvi-Dossou G, Bonfoh N, Gerard P. Glass fibres reinforced acrylic thermoplastic resin-based tri-block copolymers composites: low velocity impact response at various temperatures. Compos Struct 2017;160:939–51. https://doi.org/10.1016/j.compstruct.2016.10.127.
[33] Bhudolia SKK, Perrotey P, Joshi SCC. Optimizing polymer infusion process for thin ply textile composites with novel matrix system. Materials (Basel) 2017;10. https://doi.org/10.3390/ma10030293.
[34] Bhudolia SK, Joshi SC. Low-velocity impact response of carbon fibre composites with novel liquid Methylmethacrylate thermoplastic matrix. Compos Struct 2018;203:696–708. https://doi.org/10.1016/j.compstruct.2018.07.066.
[35] Bhudolia SK, Perrotey P, Joshi SC. Experimental investigation on suitability of carbon fibre thin plies for racquets. Proc Inst Mech Eng P J Sports Eng Technol 2016;230:64–72. https://doi.org/10.1177/1754337115598489.
[36] Lorriot T, El Yagoubi J, Fourel J, Tison F. Non-conventional glass fiber NCF composites with thermoset and thermoplastic matrices. In: 20th Int. Conf. Compos. Mater., copenhagen; 2015.
[37] Obande W, Mamalis D, Ray D, Yang L, Ó Brádaigh CM. Mechanical and thermomechanical characterisation of vacuum-infused thermoplastic- and thermoset-based composites. Mater Des 2019;175:107828. https://doi.org/10.1016/j.matdes.2019.107828.
[38] Murray RE, Roadman J, Beach R. Fusion joining of thermoplastic composite wind turbine blades: lap-shear bond characterization. Renew Energy 2019;140:501–12. https://doi.org/10.1016/j.renene.2019.03.085.
[39] Bhudolia SK, Gohel G, Kah Fai L, Barsotti RJ. Fatigue response of ultrasonically welded carbon/Elium® thermoplastic composites. Mater Lett 2020;264:127362. https://doi.org/10.1016/j.matlet.2020.127362.
[40] Boufaida Z, Farge L, André S, Meshaka Y. Influence of the fiber/matrix strength on the mechanical properties of a glass fiber/thermoplastic-matrix plain weave fabric composite. Compos Part A Appl Sci Manuf 2015;75:28–38. https://doi.org/10.1016/j.compositesa.2015.04.012.
[41] Baley C, Lan M, Bourmaud A, Le Duigou A. Compressive and tensile behaviour of unidirectional composites reinforced by natural fibres: influence of fibres (flax and jute), matrix and fibre volume fraction. Mater Today Commun 2018;16:300–6. https://doi.org/10.1016/j.mtcomm.2018.07.003.
[42] Hindersmann A. Confusion about infusion: an overview of infusion processes. Compos Part A Appl Sci Manuf 2019. https://doi.org/10.1016/j.compositesa.2019.105583.
[43] Afendi M, Banks WM, Kirkwood D. Bubble free resin for infusion process. Compos Part A Appl Sci Manuf 2005;36:739–46. https://doi.org/10.1016/j.compositesa.2004.10.030.
[44] Obande W, Ó Brádaigh CM, Ray D. Thermoplastic hybrid-matrix composite prepared by a room-temperature vacuum infusion and in-situ polymerisation process. Compos Commun 2020. https://doi.org/10.1016/j.coco.2020.100439.
[45] Chilali A, Zouari W, Assarar M, Kebir H, Ayad R. Analysis of the mechanical behaviour of flax and glass fabrics-reinforced thermoplastic and thermoset resins. J Reinforc Plast Compos 2016;35:1217–32. https://doi.org/10.1177/0731684416645203.
[46] Cousins DS. Advanced thermoplastic composites for wind turbine blade manufacturing [Doctoral Thesis]. Colorado School of Mines; 2018.
[47] Zoller A, Escalé P, Gérard P. Pultrusion of bendable continuous fibers reinforced composites with reactive acrylic thermoplastic Elium® resin. Front Mater 2019;6:1–9. https://doi.org/10.3389/fmats.2019.00290.
[48] Lee J, Soutis C. A study on the compressive strength of thick carbon fibre-epoxy laminates. Compos Sci Technol 2007;67:2015–26. https://doi.org/10.1016/j.compscitech.2006.12.001.
[49] Davies P, Arhant M. Fatigue behaviour of acrylic matrix composites: influence of seawater. Appl Compos Mater 2019;26:507–18. https://doi.org/10.1007/s10443-018-9713-1.
[50] Arkema. Liquid thermoplastic resin for tougher composites. n.d.;1, https://www.arkema-americas.com/export/shared/.content/media/downloads/products-documentations/incubator/brochure-elium-2017.pdf.
[51] Obande W, Ray D, Ó Brádaigh CM. Viscoelastic and drop-weight impact properties of an acrylic-matrix composite and a conventional thermoset composite – a comparative study. Mater Lett 2019;238:38–41. https://doi.org/10.1016/j.matlet.2018.11.137.
[52] Kinvi-Dossou G, Matadi Boumbimba R, Bonfoh N, Garzon-Hernandez S, Garcia-Gonzalez D, Gerard P, et al. Innovative acrylic thermoplastic composites versus conventional composites: improving the impact performances. Compos Struct 2019;217:1–13. https://doi.org/10.1016/j.compstruct.2019.02.090.
[53] Pini T. Fracture behaviour of thermoplastic acrylic resins and their relevant unidirectional carbon fibre composites: rate and temperature effects [Doctoral Thesis]. Politecnico Milano; 2017. 1863.
[54] Cadieu L, Kopp JB, Jumel J, Bega J, Froustey C. Strain rate effect on the mechanical properties of a glass fibre reinforced acrylic matrix laminate. An experimental approach. Compos Struct 2019;223:110952. https://doi.org/10.1016/j.compstruct.2019.110952.
[55] Bhudolia SK, Joshi SC, Bert A, Di YB, Makam R, Gohel G. Flexural characteristics of novel carbon methylmethacrylate composites. Compos Commun 2019;13:129–33. https://doi.org/10.1016/j.coco.2019.04.007.
[56] Bhudolia SK, Joshi SC, Bert A, Gohel GR, Raama M. Energy characteristics and failure mechanisms for textile spread tow thin ply thermoplastic composites under low-velocity impact. Fibers Polym 2019;20:1716–25. https://doi.org/10.1007/s12221-019-9295-z.
[57] Bhudolia SK, Perrotey P, Joshi SC. Mode I fracture toughness and fractographic investigation of carbon fibre composites with liquid Methylmethacrylate thermoplastic matrix. Compos B Eng 2018;134:246–53. https://doi.org/10.1016/j.compositesb.2017.09.057.
[58] Barbosa LCM, Bortoluzzi DB, Ancelotti AC. Analysis of fracture toughness in mode II and fractographic study of composites based on Elium® 150 thermoplastic matrix. Compos B Eng 2019;175:107082. https://doi.org/10.1016/j.compositesb.2019.107082.
[59] Haggui M, El Mahi A, Jendli Z, Akrout A, Haddar M. Damage analysis of flax fibre/elium composite under static and fatigue testing. In: Haddar M, Chaari F, Benamara A, Chouchane M, Karra C, Aifaoui N, editors. Des. Model. Mech. Syst. Cham: Springer International Publishing; 2018. p. 681–91.
[60] Haggui M, El Mahi A, Jendli Z, Akrout A, Haddar M. Static and fatigue characterization of flax fiber reinforced thermoplastic composites by acoustic emission. Appl Acoust 2019;147:100–10. https://doi.org/10.1016/j.apacoust.2018.03.011.
[61] Virk AS, Hall W, Summerscales J. Failure strain as the key design criterion for fracture of natural fibre composites. Compos Sci Technol 2010;70:995–9. https://doi.org/10.1016/j.compscitech.2010.02.018.
[62] Barbosa LCM, Gomes G, Junior ACA. Prediction of temperature-frequency-dependent mechanical properties of composites based on thermoplastic liquid resin reinforced with carbon fibers using artificial neural networks. Int J Adv Manuf Technol 2019. https://doi.org/10.1007/s00170-019-04486-4.
[63] Bhudolia SK, Perrotey P, Joshi SC. Enhanced vibration damping and dynamic mechanical characteristics of composites with novel pseudo-thermoset matrix system. Compos Struct 2017;179:502–13. https://doi.org/10.1016/j.compstruct.2017.07.093.
[64] Pini T, Caimmi F, Briatico-Vangosa F, Frassine R, Rink M. Fracture initiation and propagation in unidirectional CF composites based on thermoplastic acrylic resins. Eng Fract Mech 2017;184:51–8. https://doi.org/10.1016/j.engfracmech.2017.08.023.
[65] Pini T, Briatico-Vangosa F, Frassine R, Rink M. Time dependent fracture behaviour of a carbon fibre composite based on a (rubber toughened) acrylic polymer. Procedia Struct Integr 2016;2:253–60. https://doi.org/10.1016/j.prostr.2016.06.033.
[66] Johanna B, Jean-François G, Frédéric L, Pierre G, Jérôme M. New continuous fiber reinforced thermoplastic composites: an analysis of interfacial adhesion from the micro scale to the macro scale. In: ICCM Int conf compos mater 2015; 2015-July. 19–24.
[67] Davies P, Le Gac PYY, Le Gall M. Influence of sea water aging on the mechanical behaviour of acrylic matrix composites. Appl Compos Mater 2017;24:97–111. https://doi.org/10.1007/s10443-016-9516-1.
[68] Shanmugam L, Kazemi ME, Rao Z, Lu D, Wang X, Wang B, et al. Enhanced Mode I fracture toughness of UHMWPE fabric/thermoplastic laminates with combined surface treatments of polydopamine and functionalized carbon nanotubes. Compos B Eng 2019;178:107450. https://doi.org/10.1016/j.compositesb.2019.107450.
[69] Charlier Q, Lortie F, Gerard P, Gerard JF. Interfacial adhesion between glass fibers and acrylic-based matrices as studied by micromechanical testing. In: ICCM Int conf compos mater 2015; 2015-July. p. 19–24.
[70] Thomason JL. Glass fibre sizing: a review. Compos Part A Appl Sci Manuf 2019;127. https://doi.org/10.1016/j.compositesa.2019.105619.
[71] Pini T, Briatico-Vangosa F, Frassine R, Rink M. Matrix toughness transfer and fibre bridging laws in acrylic resin based CF composites. Eng Fract Mech 2018;203:115–25. https://doi.org/10.1016/j.engfracmech.2018.03.026.
[72] Pini T, Castellani L, Briatico-Vangosa F, Frassine R, Rink M. Damage mechanisms in a toughened acrylic resin: effect of temperature and thermal history. Polym Eng Sci 2019;59:566–72. https://doi.org/10.1002/pen.24971.
[73] Pini T, Briatico-Vangosa F, Frassine R, Rink M. Fracture toughness of acrylic resins: viscoelastic effects and deformation mechanisms. Polym Eng Sci 2018;58:369–76. https://doi.org/10.1002/pen.24583.
[74] Keskin R, Adanur S. Improving toughness of polypropylene with thermoplastic elastomers in injection molding. Polym Plast Technol Eng 2011;50:20–8. https://doi.org/10.1080/03602559.2010.512344.
[75] Tamas-Benyei P, Bitay E, Kishi H, Matsuda S, Czigany T. Toughening of epoxy resin: the effect of water jet milling on worn tire rubber particles. Polymers (Basel) 2019;11. https://doi.org/10.3390/polym11030529.
[76] Utaloff K, Kothmann MH, Ciesielski M, Döring M, Neumeyer T, Altstädt V, et al. Improvement of fracture toughness and glass transition temperature of DGEBA-based epoxy systems using toughening and crosslinking modifiers. Polym Eng Sci 2019;59:86–95. https://doi.org/10.1002/pen.24870.
[77] Barsotti R, Fine T, Inoubli R, Gerard P, Schmidt S, Macy N, et al. Nanostrength ® block copolymers for epoxy toughening. https://www.trfa.org/erc/docretrieval/uploadedfiles/Technical Papers/2008 Meeting/Barsotti-Arkema_paper-Block_copolymers.pdf; 2008.
[78] Bhudolia SK, Gohel G, Fai LK, Barsotti RJ. Investigation on ultrasonic welding attributes of novel carbon/Elium® composites. Materials (Basel) 2020;13:10–5. https://doi.org/10.3390/ma13051117.
[79] Gebhardt M, Chakraborty S, Manolakis I, Meiners D. Closed-loop room temperature recycling of Elium CFRPs and its influence on the 2nd generation composite properties. J Sci Alliance Plast Technol 2020;16:179–210.
[80] Lee P, Sims E, Bertham O, Symington H, Bell N, Pfaltzgraff L, et al. Towards a circular economy – waste management in the EU. https://www.europarl.europa.eu/RegData/etudes/STUD/2017/581913/EPRS_STU%282017%29581913_EN.pdf. [Accessed 24 February 2021].

[81] Summerscales J, Singh MM, Wittamore K. Disposal of composite boats and other marine composites. Mar. Appl. Adv. Fibre-Reinforced Compos., Elsevier Inc. 2016:185–213. https://doi.org/10.1016/B978-1-78242-250-1.00008-9.

[82] Safri SNA, Sultan MTH, Jawaid M, Jayakrishna K. Impact behaviour of hybrid composites for structural applications: a review. Compos B Eng 2018;133:112–21. https://doi.org/10.1016/j.compositesb.2017.09.008.

[83] Bunea M, Cîrciumaru A, Buciumeanu M, Bîrsan IG, Silva FS. Low velocity impact response of fabric reinforced hybrid composites with stratified filled epoxy matrix. https://doi.org/10.1016/j.compscitech.2018.11.024; 2018.

[84] Kazemi MEE, Shanmugam L, Lu D, Wang X, Wang B, Yang J. Mechanical properties and failure modes of hybrid fiber reinforced polymer composites with a novel liquid thermoplastic resin. Elium®. Compos Part A Appl Sci Manuf 2019; 125:105523. https://doi.org/10.1016/j.compositesa.2019.105523.

[85] Kazemi ME, Shanmugam L, Dadashi A, Shakouri M, Lu D, Du Z, et al. Investigating the roles of fiber, resin, and stacking sequence on the low-velocity impact response of novel hybrid thermoplastic composites. Compos B Eng 2021; 207:108554. https://doi.org/10.1016/j.compositesb.2020.108554.

[86] Vlot A, Gunnik JW. Fibre metal laminates: an introduction. 2011. https://doi.org/10.1007/978-94-010-0995-9.

[87] Vogelesang LB, Vlot A. Development of fibre metal laminates for advanced aerospace structures. J Mater Process Technol 2000;103:1–5. https://doi.org/10.1016/S0924-0136(00)00411-8.

[88] Mamalis D, Obande W, Koutsos V, Blackford JR, Ó Brádaigh CM, Ray D. Novel thermoplastic fibre-metal laminates manufactured by vacuum resin infusion: the effect of surface treatments on interfacial bonding. Mater Des 2019;162:331–44. https://doi.org/10.1016/j.matdes.2018.11.048.

[89] Shanmugam L, Kazemi ME, Rao Z, Yang L, Yang J. On the metal thermoplastic composite interface of Ti alloy/UHMWPE-Elium® laminates. Compos B Eng 2020;181:107578. https://doi.org/10.1016/j.compositesb.2019.107578.

[90] Qin Y, Summerscales J, Graham-Jones J, Meng M, Pemberton R. Monomer selection for in situ polymerization infusion manufacture of natural-fiber reinforced thermoplastic-matrix marine composites. Polymers (Basel) 2020;12: 1–25. https://doi.org/10.3390/polym12122928.

[91] National Materials Advisory Board. Sciences NA of. Fire safety aspects of polymeric materials, vol. 1. National Academy of Sciences; 1977.

[92] Khalili P, Blinzler B, Kádár R, Blomqvist P, Sandinge A, Bisschop R, et al. Ramie fabric Elium® composites with flame retardant coating: flammability, smoke, viscoelastic and mechanical properties. Compos Part A Appl Sci Manuf 2020;137: 105986. https://doi.org/10.1016/j.compositesa.2020.105986.

[93] Khalili P, Blinzler B, Kádár R, Bisschop R, Försth M, Blomqvist P. Flammability, smoke, mechanical behaviours and morphology of flame retarded natural fibre/Elium® composite. Materials (Basel) 2019;12. https://doi.org/10.3390/ma12172648.

[94] Sun XS. Overview of plant polymers: resources, demands, and sustainability. Bio-Based Polym. Compos. 2005:1–14. https://doi.org/10.1016/B978-0-12-763952-9.X5000-X.

[95] Wu N, Demchuk Z, Voronov A, Pourhashem G. Sustainable manufacturing of polymeric materials: a techno-economic analysis of soybean oil-based acrylic monomers production. J Clean Prod 2021:286. https://doi.org/10.1016/j.jclepro.2020.124939.

[96] Voronov A, Tarnavchyk I. Bio-based acrylic monomers. United States Patent US10315985B2, 2019.

[97] Voronov A, Tarnavchyk I. Bio-based acrylic monomers and polymers thereof. United States Patent US10584094B2, 2020.

[98] Sweeney N. Biobased acrylic adhesives. third ed. Handb. Adhes. Technol.; 2017. https://doi.org/10.1201/9781315120942.

[99] Tajbakhsh S, Hajiali F, Maric M. Nitroxide-mediated miniemulsion polymerization of bio-based methacrylates. Ind Eng Chem Res 2020. https://doi.org/10.1021/acs.iecr.0c00840.

[100] Lebeau J, Efromson JP, Lynch MD. A review of the biotechnological production of methacrylic acid. Front Bioeng Biotechnol 2020. https://doi.org/10.3389/fbioe.2020.00207.

[101] Veith C, Diot-Néant F, Miller SA, Allais F. Synthesis and polymerization of bio-based acrylates: a review. Polym Chem 2020;11:7452–70. https://doi.org/10.1039/d0py01222j.

[102] Fouilloux H, Thomas CM. Production and polymerization of biobased acrylates and analogs. Macromol Rapid Commun 2021;42. https://doi.org/10.1002/marc.202000530.

[103] Veregin RPN, Sacripante GG. Bio-based acrylate and (meth)acrylate resins. United States Patent US9581924B2, 2014.

[104] Yu D, Zhao J, Wang W, Qi J, Hu Y. Mono-acrylated isosorbide as a bio-based monomer for the improvement of thermal and mechanical properties of poly (methyl methacrylate). RSC Adv 2019;9:35532–8. https://doi.org/10.1039/c9ra07548h.

[105] Zhang M, Gleich KF, Yohannes A, Block MJ, Asrar J, Bristol DC, et al. System for producing a fully impregnated thermoplastic prepreg. United States Patent US20200368979A1, 2020.

[106] Fredi G, Dorigato A, Pegoretti A. Novel reactive thermoplastic resin as a matrix for laminates containing phase change microcapsules. Polym Compos 2019. https://doi.org/10.1002/pc.25233.

[107] Monti A, El Mahi A, Jendli Z, Guillaumat L. Mechanical behaviour and damage mechanisms analysis of a flax-fibre reinforced composite by acoustic emission. Compos Part A Appl Sci Manuf 2016;90:100–10. https://doi.org/10.1016/j.compositesa.2016.07.002.

[108] SpecialChem SA. Maximum continuous service temperature. Max Contin Serv Temp; 2021. https://omnexus.specialchem.com/polymer-properties/properties/max-continuous-service-temperature. [Accessed 23 February 2021].

[109] SpecialChem SA. Shrinkage value of plastics material. Shrinkage value plast mater. https://omnexus.specialchem.com/polymer-properties/properties/shrinkage. [Accessed 23 February 2021].

[110] Murray RE, Jenne S, Snowberg D, Berry D, Cousins D. Techno-economic analysis of a megawatt-scale thermoplastic resin wind turbine blade. Renew Energy 2019; 131:111–9. https://doi.org/10.1016/j.renene.2018.07.032.

[111] SpecialChem SA. Water absorption 24 hour - (ASTM D570) test of plastics. n.d. https://omnexus.specialchem.com/polymer-properties/properties/water-absorption-24-hours. [Accessed 23 February 2021].

[112] Co RTP. Chemical & environmental resistance of thermoplastics. Chem Environ Resist Thermoplast 2021. https://www.rtpcompany.com/technical-info/chemical-resistance/. [Accessed 23 February 2021].

[113] Maddah HA. Polypropylene as a promising plastic: a review. Am J Polym Sci 2016;6:1–11. https://doi.org/10.5923/j.ajps.20160601.01.

[114] Plastic Portal. Average resin prices I PlasticPortal.eu n.d. https://www.plasticportal.eu/en/polymer-prices/lm/14/. [Accessed 23 February 2021].

[115] van Rijswijk K, van Geenen AA, Bersee HEN. Textile fiber-reinforced anionic polyamide-6 composites. Part II: investigation on interfacial bond formation by short beam shear test. Compos Part A Appl Sci Manuf 2009. https://doi.org/10.1016/j.compositesa.2009.02.018.

[116] van Rijswijk K, Lindstedt S, Vlasveld DPN, Bersee HEN, Beukers A. Reactive processing of anionic polyamide-6 for application in fiber composites: a comparitive study with melt processed polyamides and nanocomposites. Polym Test 2006. https://doi.org/10.1016/j.polymertesting.2006.05.006.

[117] Murray JJ, Robert C, Gleich K, McCarthy ED, Ó Brádaigh CM. Manufacturing of unidirectional stitched glass fabric reinforced polyamide 6 by thermoplastic resin transfer moulding. Mater Des 2020;189. https://doi.org/10.1016/j.matdes.2020.108512.

[118] SunSirs. SunSirs: caprolactam price was from rising to falling in June, how is the market going in the future? SunSirs caprolactam price was from rising to falling June, how is mark going futur. http://www.sunsirs.com/uk/detail_news-2845.html. [Accessed 23 February 2021].

[119] East Coast Fibreglass Supplies. EC157 epoxy infusion resin technical data sheet. Tech data sheet. n.d. http://www.ecfibreglasssupplies.co.uk/images/TechnicalDataSheet/3207.pdf. [Accessed 23 February 2021].

[120] Li C, Potter K, Wisnom MR, Stringer G. In-situ measurement of chemical shrinkage of MY750 epoxy resin by a novel gravimetric method. Compos Sci Technol 2004;64:55–64. https://doi.org/10.1016/S0266-3538(03)00199-4.

[121] Zheng S, Lucas PA. Understanding chemical resistance in epoxy system. Underst Chem Resist Epoxy Syst; 2020. https://www.coatingsworld.com/issues/2020-06-01/view_technical-papers/understanding-chemical-resistance-in-epoxy-system/. [Accessed 23 February 2021].

[122] Nikafshar S, Zabihi O, Ahmadi M, Mirmohseni A, Taseidifar M, Naebe M. The effects of UV light on the chemical and mechanical properties of a transparent epoxy-diamine system in the presence of an organic UV absorber. Materials (Basel) 2017. https://doi.org/10.3390/ma10020180.

[123] Engineering ToolBox. Epoxy - chemical resistance. Epoxy - Chem Resist; 2004. https://www.engineeringtoolbox.com/chemical-resistance-epoxy-d_786.html. [Accessed 23 February 2021].

Composites Communications 22 (2020) 100439

Contents lists available at ScienceDirect

Composites Communications

journal homepage: www.elsevier.com/locate/coco

Short Communication

Thermoplastic hybrid-matrix composite prepared by a room-temperature vacuum infusion and in-situ polymerisation process

Winifred Obande, Conchúr M. Ó Brádaigh, Dipa Ray *

School of Engineering, Institute for Materials and Processes, The University of Edinburgh, Sanderson Building, Robert Stevenson Road, Edinburgh, EH9 3FB, Scotland, United Kingdom

ARTICLE INFO

Keywords:
Polymer-matrix composite
Hybrid matrix
Liquid thermoplastic resin
Mechanical properties
Resin infusion
Fibre-reinforced composite

ABSTRACT

This work explores a novel route for the fabrication of hybrid-matrix composites based on a recently developed liquid thermoplastic acrylic resin. This resin was modified using a poly(phenylene ether) (PPE) oligomer with vinyl functionality. Glass fibre-reinforced laminates based on acrylic and PPE-modified acrylic matrices were produced by a room-temperature vacuum infusion and in-situ polymerisation process. Comparative assessments of their mechanical performance and mode-I interlaminar fracture behaviour revealed enhanced matrix ductility, transverse flexural properties and initiation fracture toughness. Crazing was identified as the dominant mechanism for improved resistance to crack initiation.

1. Introduction

Innovative low-viscosity liquid thermoplastic resins can readily infiltrate into fibrous reinforcement under conditions of relatively low temperature and pressure in the same way that thermoset (TS) resins can [1–4]. Room-temperature infusible acrylic resins with viscosities as low as 100 mPa.s have received considerable research attention in recent years [5–13]. In our previous work, we presented comparisons between the mechanical performance of acrylic composites with equivalent epoxy composites and reported inferior transverse flexural performance [7] and impact damage resistance [8] in the acrylic-matrix composites.

Structural composites typically comprise a thermoset matrix or a semi-crystalline thermoplastic matrix. Cross-linked networks and crystalline domains contribute to enhanced matrix rigidity, making them ideal candidates for high-performance applications. In contrast, purely amorphous matrices such as acrylics do not contain cross-links or crystalline regions within their molecular structure. Thus, this might influence composite properties, particularly when matrix strength plays a key role.

Therefore, there is a significant scope to tailor the structure of acrylic-matrix composites for enhanced performance under different loading conditions. Recent works on this topic have used Nanostrength™ triblock copolymers comprising polymethylmethacrylate-*b*-polybutylacrylate-*b*-polymethylmethacrylate [9–11] and hybrid-fibre reinforcements [12] to realise improved composite properties. However, TP-TP hybridisation of an acrylic matrix, via in-situ polymerisation, is novel and has never been investigated before.

Poly(phenylene ether) (PPE) – an amorphous engineering thermoplastic, is arguably one of the most successfully applied modifiers in TS-matrix composites [14–16]. Unlike the acrylic matrix, which is a purely aliphatic amorphous TP, PPE contains aromatic rings, which may confer some rigidity in a hybrid system and is thus, worthy of exploration.

This present study investigates an innovative route to obtaining vacuum-infusible hybrid-matrix composites based on acrylic and PPE. To promote reactive blending during in-situ polymerisation of the hybrid matrix, PPE with vinyl functionality was selected for this study. The effects of hybridisation on mechanical and morphological properties are presented herein.

2. Experimental

2.1. Materials and fabrication

Two 4-mm thick (nominally) test laminates were prepared by a room-temperature vacuum infusion and in-situ polymerisation process. Table 1 provides an overview of the materials used. Full details of the materials and fabrication processes used are supplied in Appendix A.

* Corresponding author.
E-mail address: dipa.roy@ed.ac.uk (D. Ray).

https://doi.org/10.1016/j.coco.2020.100439
Received 19 June 2020; Received in revised form 24 July 2020; Accepted 7 August 2020
Available online 24 August 2020
2452-2139/© 2020 Elsevier Ltd. All rights reserved.

Table 1
Summary of materials used for composite fabrication with constituent ratios by weight (Elium and NORYL resins only) and fibre volume fractions for composites (Q-UD reinforcement only).

	Elium® 188 O[a]	*NORYL™ SA9000*[b]	*Q-UD Glass*[c]
Unreinforced polymer samples [d]			
A100/P0	100	0	0
A95/P5	95	5	0
Composite samples [d]			
GF/A100/P0	100	0	50
GF/A95/P5	95	5	57

[a] Liquid acrylic resin [A] supplied by Arkema GRL, France.
[b] An oligomeric PPE resin [P] with vinyl functionality, supplied by SABIC.
[c] TEST2594 – a quasi-unidirectional (UD) glass non-crimp fabric (NCF) supplied by Ahlstrom-Munksjö. GF: glass fibre. Fibre volume fraction.
[d] Polymerised using a dibenzoyl peroxide initiator – BP50FT supplied by United Initiators.

2.2. Mechanical and thermomechanical characterisation

2.2.1. Tensile testing
Tensile properties were evaluated in accordance with ASTM D3039 in transverse tension.

2.2.2. Short beam shear testing
Short beam shear properties were evaluated by short beam shear testing using a span-to-thickness ratio of 4:1 in accordance with ASTM D2344.

2.2.3. Flexural testing
Non-standard flexural testing was performed on unreinforced matrix samples as detailed in Appendix B. To gain further insights on differences in fracture behaviour of the matrices, SEM inspections were also performed.

Flexural properties of glass fibre-reinforced composite samples were determined by three-point bending (ASTM D7264 – Procedure A) using a span-to-thickness ratio of 32:1 under longitudinal and transverse loading.

2.2.4. Mode-I interlaminar fracture toughness (ILFT) testing
Mode-I ILFT was evaluated using double cantilever beam tests per ASTM D5528. SEM inspections were conducted on DCB fracture surfaces to assess fracture behaviour.

The interested reader is referred to Appendix B for supplementary specimen and test specifications.

3. Results and discussions

3.1. Flexural test results of unreinforced matrices

PPE modification appears to improve flexural strength and stiffness of the GF/A95/P5 sample as evidenced by the stress-displacement curves in Fig. 1(a). Although mid-span deflections were not measured during testing, the observed increase in stiffness may tentatively indicate an increase in modulus. These results are based on single-sample tests and are thus, not conclusive; however, they provide interesting insights that are worthy of further investigation.

The micrographs from the respective regions of interest, diagrammatically shown in Fig. 1(b), reveal relatively flat fracture topography for A100/P0 (Fig. 1(c)). Multi-planar fractures were observed for the A95/P5 matrix (Fig. 1(d)), which suggest an interplay of crack deflection and crack penetration mechanisms as detailed in Appendix C [17]. At higher magnifications, the A100/P0 matrix appears homogenous (Fig. 1(e)); a biphasic morphology comprising discrete domains was observed for the A95/P5 matrix (Fig. 1(f)). These domains are likely PPE-rich phase, surrounded by an acrylic-rich phase.

3.2. Results of composites testing

3.2.1. Transverse tensile test results
Representative stress-strain responses and average transverse tensile strengths, moduli and failure strains of the GF/A100/P0 and GF/A95/P5 materials are presented in Fig. 2(a). Both materials exhibit similar linear behaviour initially; however, an earlier onset of damage initiation (matrix cracking) was observed with the GF/A95/P5 samples. From Points 1 to 3 Fig. 2(a), matrix crack accumulation occurs before ultimate

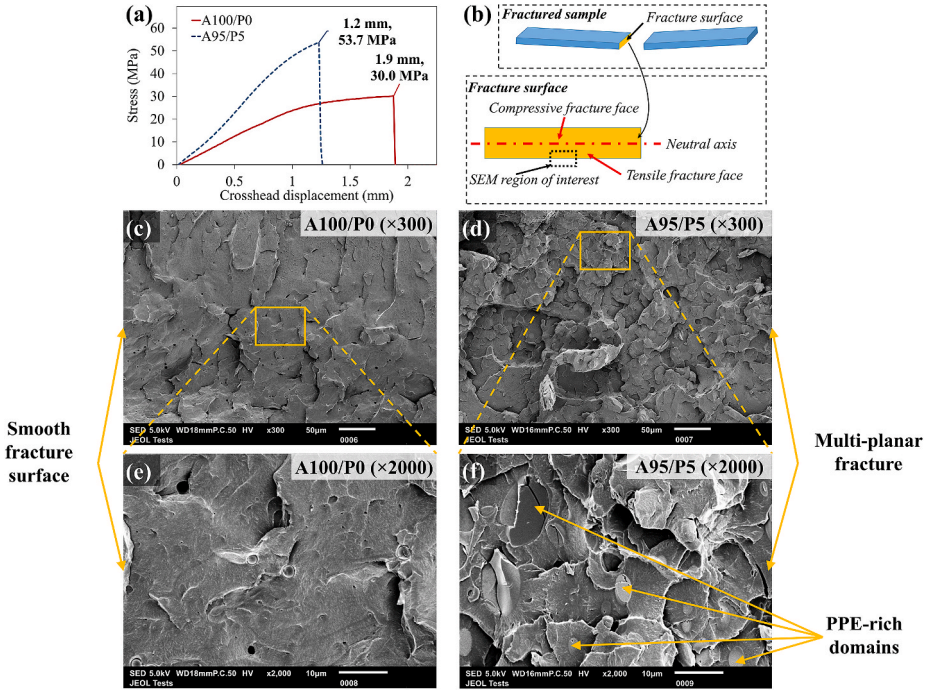


Fig. 1. Flexural stress-displacement curves (a) and diagrammatic representation of the SEM region of interest (b). SEM micrographs of fracture surfaces of unreinforced (c) & (e) A100/P0 and (d) & (f) A95/P5 samples at different magnifications (× 300 & × 2000).

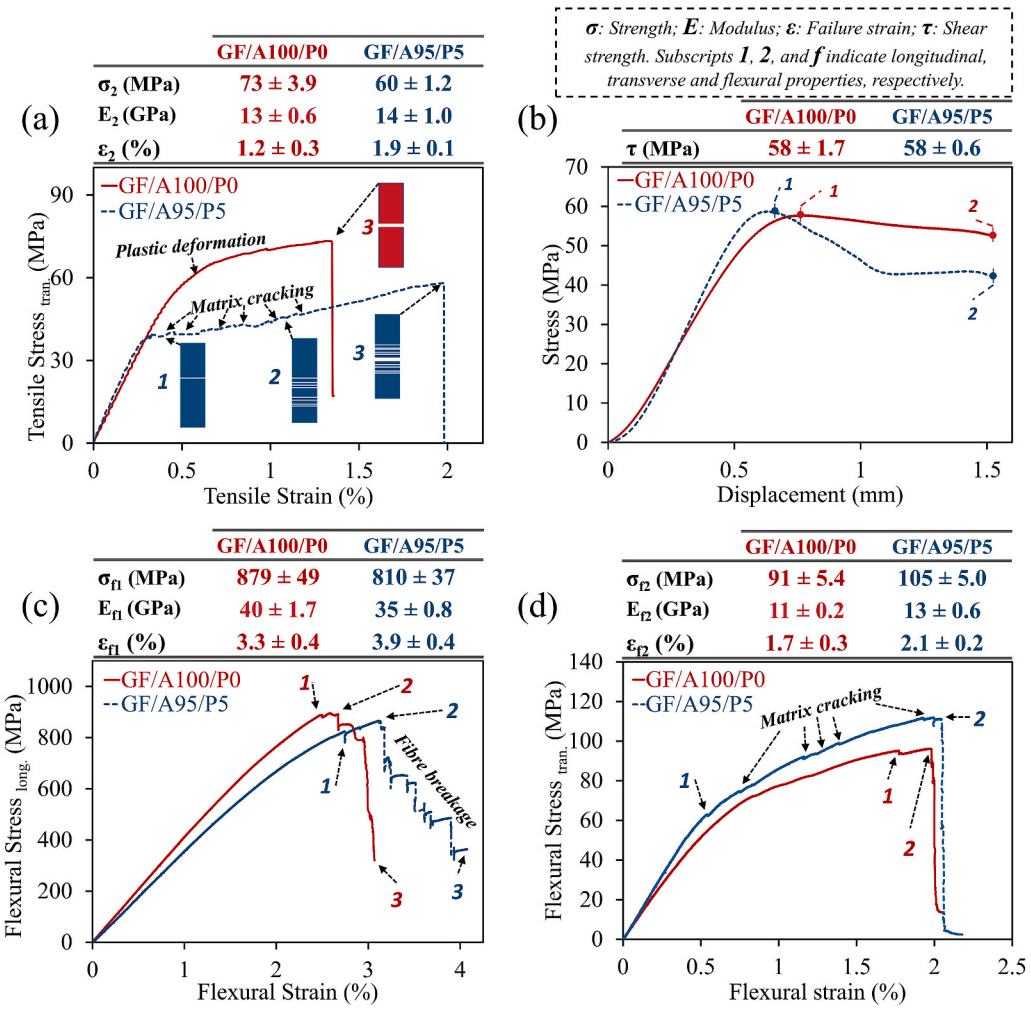


Fig. 2. Representative curves and results for GF/A100/P0 (red) and GF/A95/P5 (blue) following loading in (a) transverse tension; (b) short beam shear; (c) longitudinal flexure and (d) transverse flexure. (For interpretation of the references to colour in this figure legend, the reader is referred to the Web version of this article.)

failure. In contrast, the GF/A100/P0 material undergoes plastic deformation up to failure. Matrix hybridisation resulted in reduced (−18%) transverse tensile strength with a slight increase in modulus (+8%) and a significant increase in failure strain (+58%). Thus, hybridisation appears to increase both transverse composite modulus and ductility. Moreover, higher areas bounded under GF/A95/P5 curves may suggest enhanced toughness.

3.3. Short beam shear test results

Fig. 2(b) shows the results of short beam shear tests performed on the GF/A100/P0 and GF/A95/P5 materials. For both materials, all samples exhibited plastic deformation up to their respective ultimate shear stress values (Point 1). However, beyond this point, the curves of GF/A95/P5 samples exhibited a more abrupt loss in stiffness with increasing displacement between Points 1 and 2.

3.3.1. Flexural test results

Results from longitudinal flexural tests are presented in Fig. 2(c). All samples of both materials exhibited a three-stage stress-strain evolution: (i) an initial linear-elastic region, (ii) a region of slight nonlinearity, and (iii) the onset of damage (Point 1). Post-peak strain evolution between Points 2 and 3 was relatively more confined in GF/A100/P0 samples than in GF/A95/P5. Progressive fibre fractures over a broader range of strains may provide evidence of superior damage resistance and possibly toughness in the GF/A95/P5 material. Moreover, it exhibited markedly higher (18%) average failure strain than the GF/A100/P0 reference material.

Hybridisation did, however, produce a laminate with lower longitudinal flexural strength (−8%) and modulus (−18%).

In Fig. 2(d), the results of transverse flexural tests are presented. All samples across both materials exhibited an initial region of linearity, beyond which, plastic deformation ensued with a distinct onset of failure (Point 1) and abrupt ultimate failure at Point 2. All GF/A95/P5 samples underwent cumulative matrix cracking in plies under tension, such as those shown between Points 1 and 2. The hybrid-matrix composite exhibited improved transverse flexural strength (+15%), modulus (+18%) and failure strain (+24%) relative to the unmodified reference.

Differences in the trends between the comparative transverse tensile and flexural performance were likely attributed to the sensitivity of the former to defect distribution across the gauge length. Thus, it can be concluded that hybridisation improved the composite transverse strength, modulus, ductility and overall interfacial strength.

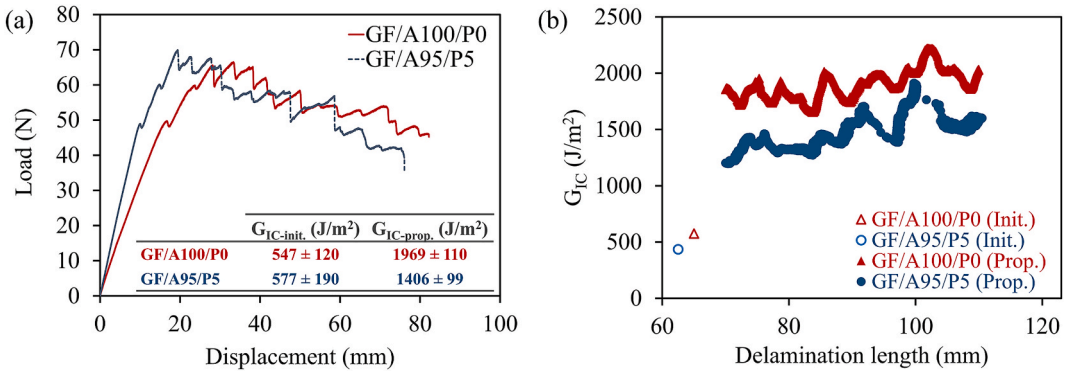


Fig. 3. (a) Representative load-displacement curves and (b) R-curves for GF/A100/P0 (red) and GF/A95/P5 (blue) following double cantilever beam testing. (For interpretation of the references to colour in this figure legend, the reader is referred to the Web version of this article.)

3.3.2. *Mode-I interlaminar fracture toughness test results*

Representative DCB load-displacement curves and the obtained results are shown in Fig. 3(a). Despite exhibiting superior longitudinal flexural stiffness, GF/A100/P0 samples had unexpectedly lower crack opening stiffness up to initiation, which may be explained by a higher fibre volume fraction in the GF/A95/P5 laminate. Both materials underwent unstable crack growth due to the presence of 90° fibres within the fabric.

Hybridisation conferred a 5% increase in the initiation fracture toughness ($G_{IC\text{-}init.}$); however, propagation fracture toughness ($G_{IC\text{-}prop.}$) decreased by 29%. Similar results were reported by Lee et al. [18] who found that hybridisation only enhanced $G_{IC\text{-}init.}$, but $G_{IC\text{-}prop.}$ was

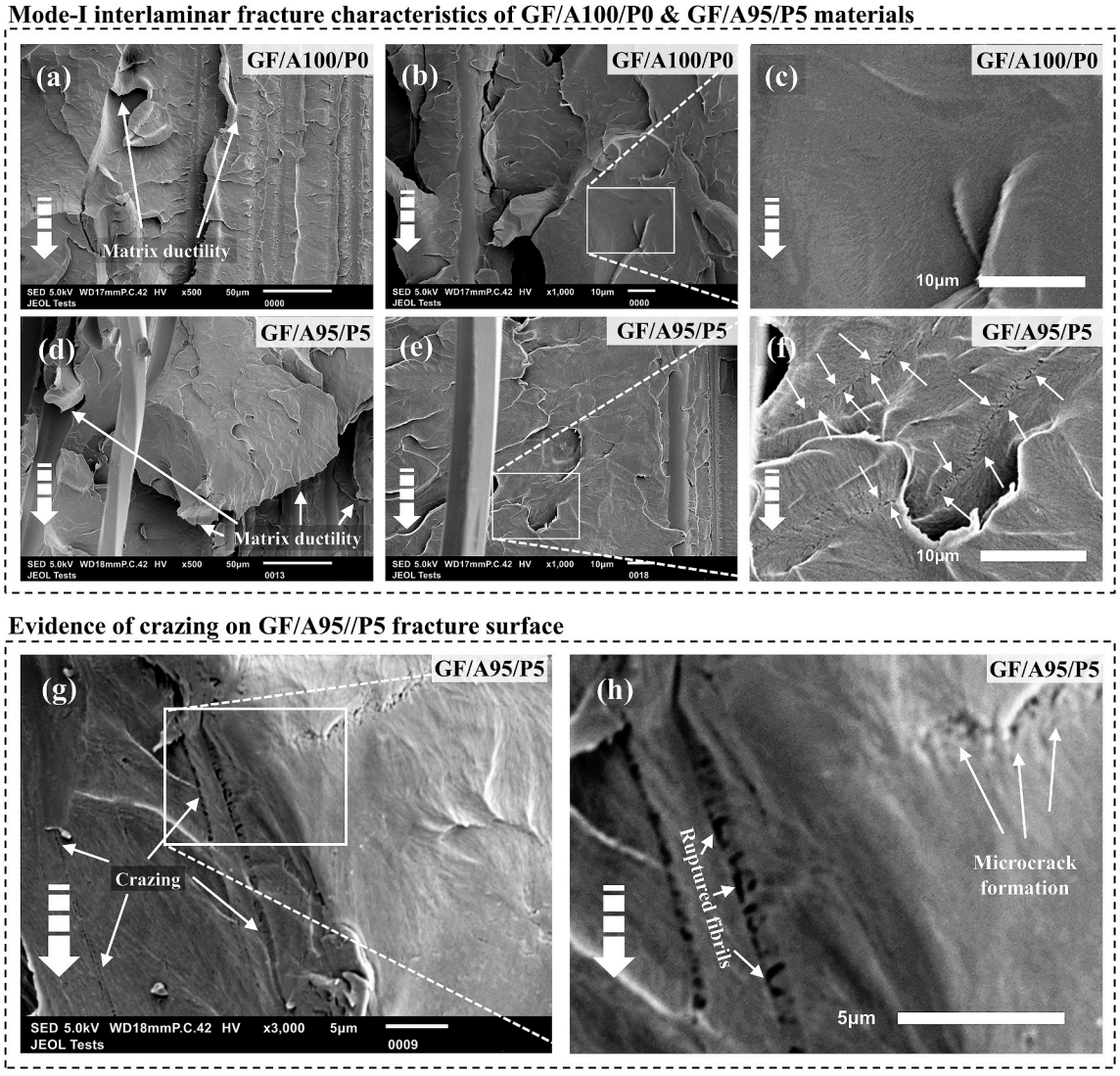


Fig. 4. SEM micrographs showing mode-I fracture surfaces of (a), (b) & (c) GF/A100/P0 and (d)–(h) GF/A95/P5. The larger broken arrows show the direction of crack propagation. In (f), arrows highlight paths of microcrack formation.

reduced due to limited fibre bridging in the hybrid composite. This is supported by literature on factors affecting propagation behaviour [11,19,20]. Moreover, other factors limiting fibre bridging in the GF/A95/P5 material may be its plausibly higher matrix modulus [17] (evidenced by the higher stiffness reported in 3.1) and enhanced interfacial strength as discussed in 3.2.3 [21,22]. Interestingly, R-curves (Fig. 3(b)) did not reveal discernibly distinct propagation behaviour between both materials.

Fig. 4 (a)-(f) present DCB fracture surfaces of GF/A100/P0 and GF/A95/P5 samples obtained using SEM. Both surfaces appear texturally coarse and dull, indicating comparable ductility on a microscopic scale.

The GF/A95/P5 sample showed evidence of microcrack formation (Fig. 4(f)) and multiple sites of crazing (Fig. 4(g)), features which were not observed for GF/A100/P0. The microcracks appeared as long craze-like interpenetrating paths across the fracture surface; however, no coalescence was observed at their points of intersection. Crazing is a dominant plastic deformation mechanism in amorphous TP matrices [23,24], which may explain the increased $G_{IC\text{-}init.}$.

The absence of discernible PPE-rich domains in the micrographs of the GF/A95/P5 sample compared with those of the A95/P5 sample may highlight the effects of fibres on the resulting phase morphology. However, further investigation would be required to substantiate this hypothesis.

4. Conclusions

This study represents the first implementation of a novel approach for room-temperature vacuum infusion of continuous fibre, thermoplastic hybrid-matrix composites. The approach exploits the low viscosity of liquid TP acrylic resins and the vinyl functionality of a higher performance poly(phenylene ether) to realise enhanced reactivity during the in-situ polymerisation processing. The following are the key observations and conclusions from the benchmarking of mechanical performance with respect to an unmodified acrylic reference laminate:

- **Enhanced ductility in the hybrid-matrix composite:** failure strains increased under transverse tension (+58%), transverse flexure (+24%) and longitudinal flexure (+18%).
- **Improved composite transverse flexural strength (+15%) and modulus (+18%):** this may suggest enhancements in matrix strength, modulus and interfacial adhesion.
- **A 5% increase in initiation fracture toughness**, possibly due to the effects of a multiple-crazing mechanism in the hybrid matrix system.
- **Decreased propagation fracture toughness by 29%**, possibly due to diminished contributions from fibre bridging.

The investigation of the reaction kinetics and mechanism between acrylic resin and PPE, and how this relates to phase separation and morphology is recommended as future work.

CRediT authorship contribution statement

Winifred Obande: Conceptualization, Methodology, Validation, Formal analysis, Investigation, Data curation, Visualization, Project administration, Writing - original draft, Project administration. **Conchúr M. Ó Brádaigh:** Supervision, Resources, Writing - review & editing, Funding acquisition. **Dipa Ray:** Conceptualization, Supervision, Resources, Project administration, Writing - review & editing, Funding acquisition.

Declaration of competing interest

The authors declare that they have no known competing financial interests or personal relationships that could have appeared to influence the work reported in this paper.

Acknowledgements

The authors gratefully acknowledge Arkema GRL, France and SABIC for the provision of materials and technical support towards this research. SABIC and brands marked with ™ are trademarks of SABIC or its subsidiaries or affiliates, unless otherwise noted.

Appendix A. Supplementary data

Supplementary data to this article can be found online at https://doi.org/10.1016/j.coco.2020.100439.

References

[1] H. Parton, I. Verpoest, In situ polymerization of thermoplastic composites based on cyclic oligomers, Polym. Compos. 26 (2005) 60–65.
[2] K. Van Rijswijk, J.J.E. Teuwen, H.E.N. Bersee, A. Beukers, Textile fiber-reinforced anionic polyamide-6 composites. Part I: the vacuum infusion process, Compos. Part A Appl. Sci. Manuf. 40 (2008) 1–10, https://doi.org/10.1016/j.compositesa.2008.03.018.
[3] J.J. Murray, C. Robert, K. Gleich, E.D. McCarthy, C.M. Ó Brádaigh, Manufacturing of unidirectional stitched glass fabric reinforced polyamide 6 by thermoplastic resin transfer moulding, Mater. Des. 189 (2020) 108512, https://doi.org/10.1016/j.matdes.2020.108512.
[4] Y. Zhao, X. Ma, T. Xu, D.R. Salem, H. Fong, Hybrid multi-scale thermoplastic composites reinforced with interleaved nanofiber mats using in-situ polymerization of cyclic butylene terephthalate, Compos. Commun. 12 (2019) 91–97, https://doi.org/10.1016/j.coco.2019.01.005.
[5] R.E. Murray, D. Snowberg, D. Berry, R. Beach, S. Rooney, D. Swan, Manufacturing a 9-meter thermoplastic composite wind turbine blade, in: Am. Soc. Compos. 32nd Tech. Conf., West Lafayette, Indiana, 2017. www.nrel.gov/publications. (Accessed 1 January 2019).
[6] D.S. Cousins, Advanced Thermoplastic Composites for Wind Turbine Blade Manufacturing [Doctoral Thesis], Colorado School of Mines, 2018.
[7] W. Obande, D. Mamalis, D. Ray, L. Yang, C.M. Ó Brádaigh, Mechanical and thermomechanical characterisation of vacuum-infused thermoplastic- and thermoset-based composites, Mater. Des. 175 (2019) 107828, https://doi.org/10.1016/j.matdes.2019.107828.
[8] W. Obande, D. Ray, C.M. Ó Brádaigh, Viscoelastic and drop-weight impact properties of an acrylic-matrix composite and a conventional thermoset composite – a comparative study, Mater. Lett. 238 (2019) 38–41, https://doi.org/10.1016/j.matlet.2018.11.137.
[9] M.R. Boumbimba, M. Coulibaly, A. Khabouchi, G. Kinvi-Dossou, N. Bonfoh, P. Gerard, Glass fibres reinforced acrylic thermoplastic resin-based tri-block copolymers composites: low velocity impact response at various temperatures, Compos. Struct. 160 (2017) 939–951, https://doi.org/10.1016/j.compstruct.2016.10.127.
[10] G. Kinvi-Dossou, R. Matadi Boumbimba, N. Bonfoh, S. Garzon-Hernandez, D. Garcia-Gonzalez, P. Gerard, A. Arias, Innovative acrylic thermoplastic composites versus conventional composites: improving the impact performances, Compos. Struct. 217 (2019) 1–13, https://doi.org/10.1016/j.compstruct.2019.02.090.
[11] T. Pini, Fracture Behaviour of Thermoplastic Acrylic Resins and Their Relevant Unidirectional Carbon Fibre Composites : Rate and Temperature Effects [Doctoral Thesis], Politecnico di Milano, 2017.
[12] M.E. Kazemi, L. Shanmugam, D. Lu, X. Wang, B. Wang, J. Yang, Mechanical properties and failure modes of hybrid fiber reinforced polymer composites with a novel liquid thermoplastic resin, Elium®, Compos. Part A Appl. Sci. Manuf. 125 (2019) https://doi.org/10.1016/j.compositesa.2019.105523.
[13] S.K. Bhudolia, S.C. Joshi, Low-velocity impact response of carbon fibre composites with novel liquid methylmethacrylate thermoplastic matrix, Compos. Struct. 203 (2018) 696–708, https://doi.org/10.1016/j.compstruct.2018.07.066.
[14] R.W. Venderbosch, H.E.H. Meijer, P.J. Lemstra, Processing of Intractable Polymers Using Reactive Solvents: 1. Poly(2,6-dimethyl-1,4-phenylene ether)/epoxy resin, 1993.
[15] R.W. Venderbosch, H.E.H. Meijer, P.J. Lemstra, Processing of intractable polymers using reactive solvents. 2. poly(2,6-dimethyl-1,4-phenylene ether) as a matrix material for high-performance composites, Polymer (Guildf) 36 (1995) 1167–1178, https://doi.org/10.1016/0032-3861(95)93918-C.
[16] H. Cong, B. Yu, H. Yuan, C. Tian, S. Yang, Preparation and characterization of nanocomposites with polyphenylene oxide, in: V. Mittal (Ed.), Manuf. Nanocomposites with Eng. Plast, Woodhead Publishing, 2015.
[17] Q. Zhang, S. Liang, G. Sui, X. Yang, Influence of matrix modulus on the mechanical and interfacial properties of carbon fiber filament wound composites, RSC Adv. 5 (2015) 25208–25214, https://doi.org/10.1039/c5ra00098j.
[18] J.J. Lee, S.L. Ogin, P.A. Smith, Interlaminar Fracture Toughness of Glass Fiber Laminates Additionally Reinforced with Carbon Bead, in: ASTM Spec, Tech. Publ., 1995, https://doi.org/10.1520/stp14007s.
[19] T. Pini, F. Briatico-Vangosa, R. Frassine, M. Rink, Matrix toughness transfer and fibre bridging laws in acrylic resin based CF composites, Eng. Fract. Mech. 203 (2018) 115–125, https://doi.org/10.1016/j.engfracmech.2018.03.026.

[20] P. Compston, P.B. Jar, The transfer of matrix toughness to composite mode I interlaminar fracture toughness in glass-fibre/vinyl ester composites, Appl. Compos. Mater. 9 (2002) 291–314.
[21] H. Ming Chong, Toughening Mechanisms of Block Copolymer and Graphene Nanoplatelet Modified Epoxy Polymers, 2015.
[22] K. Masanai, Toughening Mechanisms of Silica Nanoparticle-Modified Epoxy Polymers, Imperial College London, 2010.
[23] K.Y. Kim, L. Ye, C. Yan, Fracture behavior of polyetherimide (PEI) and interlaminar fracture of CF/PEI laminates at elevated temperatures, Polym. Compos. 26 (2005) 20–28, https://doi.org/10.1002/pc.20062.
[24] S. Pal, B.C. Ray, Molecular Dynamics Simulation of Nanostructured Materials: an Understanding of Mechanical Behavior, 2020.

Materials and Design 175 (2019) 107828

Contents lists available at ScienceDirect

Materials and Design

journal homepage: www.elsevier.com/locate/matdes

Mechanical and thermomechanical characterisation of vacuum-infused thermoplastic- and thermoset-based composites

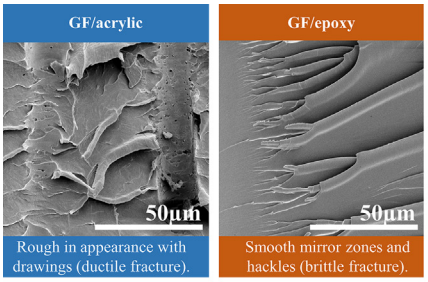
Winifred Obande [a], Dimitrios Mamalis [a], Dipa Ray [a,*], Liu Yang [b], Conchúr M. Ó Brádaigh [a]

[a] School of Engineering, Institute for Materials and Processes, The University of Edinburgh, Sanderson Building, Robert Stevenson Road, Edinburgh EH9 3FB, Scotland, United Kingdom
[b] University of Strathclyde, Department of Mechanical and Aerospace Engineering, 75 Montrose Street, Glasgow G1 1XJ, United Kingdom

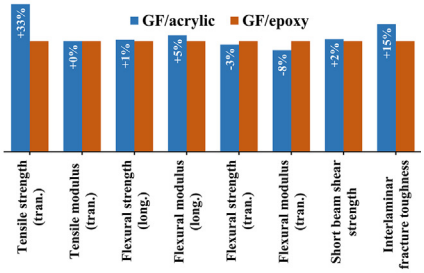
HIGHLIGHTS

- An in-situ polymerised thermoplastic acrylic composite was manufactured by liquid resin infusion.
- The mechanical and thermomechanical characteristics of the acrylic material have been benchmarked against an epoxy reference.
- The acrylic composite exhibited superior tensile (90°), flexural (0°), interlaminar shear and fracture toughness properties.
- "Thermomechanical characterisation revealed marked superiority in the damping behaviour of the acrylic composite.

GRAPHICAL ABSTRACT



SEM micrographs of fractured samples from mode-I interlaminar fracture toughness testing.



GF/acrylic exhibited comparable and marginally superior mechanical performance to GF/epoxy.

ARTICLE INFO

Article history:
Received 14 January 2019
Received in revised form 30 April 2019
Accepted 2 May 2019
Available online 3 May 2019

Keywords:
Thermoplastic polymer
Vacuum infusion
In-situ polymerisation
Polymer-matrix composites (PMCs)
Mechanical properties
Thermomechanical properties

ABSTRACT

In this work, a comparative performance study was conducted on glass fibre-reinforced thermoplastic acrylic and thermosetting epoxy laminates produced by vacuum-assisted resin transfer moulding. Mechanical characterisation revealed that the acrylic-based composite had superior transverse tensile strength and mode-I fracture toughness to the epoxy composite, while longitudinal flexural properties and short beam shear strength were found to be comparable. Dissimilar damage evolution behaviour was observed in both materials during tensile testing. The thermomechanical behaviour of the materials has been assessed as a function of temperature. Finally, fractographic investigations of shear and mode-I fracture behaviour revealed distinct fracture mechanisms that complement the findings from mechanical and thermomechanical analyses.

© 2019 The Authors. Published by Elsevier Ltd. This is an open access article under the CC BY-NC-ND license (http://creativecommons.org/licenses/by-nc-nd/4.0/).

1. Introduction

Fibre-reinforced polymer composites (FRPs) are particularly attractive for their exceptional specific strength and stiffness properties; and are known to be highly durable. Thus, they are ideal candidate materials across many sectors, particularly for weight-critical applications. They typically comprise fibrous reinforcement encapsulated within a polymer matrix, which may be thermosetting (TS) or thermoplastic (TP). TS polymers form dense three-dimensional, crosslinked networks upon polymerisation and are not thermo-softening materials; as a result, they cannot be reshaped, joined and readily recycled like their TP counterparts. Consequently, from an ecological viewpoint, TP matrices are more desirable for FRP applications; however, high melt-viscosity has been a major limitation to their cross-sectoral adoption. They typically require high-cost processing techniques where elevated

* Corresponding author.
E-mail address: dipa.roy@ed.ac.uk (D. Ray).

https://doi.org/10.1016/j.matdes.2019.107828
0264-1275/© 2019 The Authors. Published by Elsevier Ltd. This is an open access article under the CC BY-NC-ND license (http://creativecommons.org/licenses/by-nc-nd/4.0/).

temperatures and pressures are used to realise infiltration viscosities and optimal consolidation. TS matrices possess inherently low viscosities, making them ideal for low-cost processing. In recent years, lightweighting has been identified by several sectors as an effective strategy towards meeting the strict global government targets on addressing current environmental challenges [1,2]. In the context of minimising ecological impact, TP resins possess a unique combination of characteristics that make them ideal candidate matrices for FRPs. Furthermore, TP resins have a well-documented superiority in toughness – a property that controls numerous matrix and laminate properties [3,4]. As such, the development of lower cost alternatives for TP-FRP fabrication has been the subject of extensive research.

Previous research has focussed on infusion and in-situ polymerisation of engineering polymers such as polyamide-12 (PA-12 using the laurolactam monomer system) [5], polyamide-6 (PA-6 using the caprolactam system [6,7]) and polybutylene terephthalate (PBT using cyclic oligomer precursors, known as CBT) [8–10]. In each of these cases, however, elevated mould temperatures are required in order to polymerise the matrix system after infusion into the fibre bed. Temperatures above 150 °C in the case of the PA-6 and PA-12 systems, and as high as 180 °C for the CBT are required. This can add significant expense in terms of high temperature mould tooling, especially for large structures such as wind turbine blades [11–13].

A notable advancement in this area has been the recent development of novel reactive TP resins such as Arkema's acrylic-based Elium®. These resins are low-viscosity liquids (100–200 mPa.s) at room temperature and are suited to processing by liquid composite moulding techniques using room-temperature tooling, which were once exclusively used for TS-FRP production. This technology has already been demonstrated through the production of a 9 m long glass-fibre reinforced prototype wind turbine blade using resin infusion [14]. Furthermore, the recyclability and thermoformability of these materials have also been demonstrated [15].

The properties of this infusible acrylic and its composites have been studied by many authors. These works have effectively established the knowledge base on the material's mechanical characteristics, with extensive efforts in characterising tensile, compressive, shear, impact, and fracture toughness [16–30]. Much applied research has been conducted on understanding the material's fatigue [23,31,32]; moisture diffusivity and marine ageing [33–37]; interfacial adhesion [38,39]; damage evolution and fracture behaviour [24,36,40–43]; and even the effects of processing on properties [25,44]. Moreover, the thermomechanical properties of this acrylic family and their composites have also been studied by a number of researchers [29,40,45,46].

Several authors have published works on the comparative performance of acrylic composites with respect to comparable thermoset composites. An overview of existing literature by characterisation and reinforcement type is presented in Table 1.

Chilali et al. [24] reported comparable tensile and shear performance in both acrylic-based and epoxy-based composites. They also observed superior damage resistance in flax-acrylic composites with respect to a comparable flax-epoxy material, no differences in extent of damage and residual performance were reported between their glass-reinforced counterparts. Their findings on the tensile performance of the glass-reinforced composites are in agreement with published work by Lorriot et al. [47]; however, Baley et al. [16] reported significantly lower (−40%) tensile strength in glass-reinforced acrylic than glass-reinforced epoxy. Kinvi-Dossou et al. [28] reported superior impact performance in glass-acrylic composites than their thermoset counterparts; however, Obande et al. [29] found that despite exhibiting more energy dissipative behaviour, glass-acrylic composites were less impact damage resistant than their epoxy counterparts.

With the exception of work published by Cousins [48], the general mechanical properties (tensile, compressive, flexural and shear) of acrylic and comparable epoxy composites have not been evaluated comprehensively. As shown in Table 1, no one study comparatively evaluates general mechanical properties, fracture toughness, damage behaviour and thermomechanical characteristics in a complementary fashion. This clearly highlights the need for rigorous benchmarking to develop the robustness of the material performance database on acrylic matrices in composites, which despite attracting considerable research interest is not as well understood as traditional matrix systems such as epoxies. Such benchmarking analyses will serve to improve the understanding of areas in which acrylic composites may be most effectively applied.

In this present study, an acrylic-based glass fibre composite was benchmarked against a traditional thermosetting epoxy-based counterpart. Mechanical (tensile, flexural, short beam shear, mode-I fracture toughness) and thermomechanical characterisation techniques were used to evaluate both materials. Fractographic inspections were conducted, using scanning electron microscopy to assess shear crack modes and mode-I fracture surfaces.

Table 1
Summary of published literature on comparative performance of acrylic composites against comparable epoxy composites.

Characterisation										
Tensile	Compressive	Flexural	Shear	Fracture toughness	Impact	Fatigue	Moisture diffusivity & ageing	Damage and fracture behaviour	Damage & viscoelasticity	
F, G			F, G					F, G		Chilali et al. [24]
					G				G	Obande et al. [29]
G, C		G, C				G, C	G, C			Davies and Arhant [23]
				C						Bhudolia et al. [30]
					G					Kinvi-Dossou et al. [28]
					C					Bhudolia and Joshi [27]
			C							Bhudolia et al. [25]
			C		C					Aronica and Fossati [17]
F, J	F, J									Baley et al. [16]
							F, G			Freund et al. [35]
							G, C			Davies et al. [34]
							C			Davies [33]
							F			Chilali et al. [37]
							F	F		Chilali et al. [36]
								C	C	Bhudolia et al. [45]
G			G							Lorriot et al. [47]
G	G	G	G							Cousins [48]
G, C		G, C	G, C				G, C			Davies et al. [49]
		G								Murray et al. [50]

F, G, C and J indicate the usage of flax, glass, carbon and jute reinforcements in the cited work(s).

Table 2
Summary mechanical and thermomechanical properties reported as specified in matrix technical datasheets.

Property	Elium® 188 O	SR 1710/SD 7820
Tensile strength (MPa)	66	78
Tensile modulus (GPa)	3.2	2.8
Elongation at break (%)	2.8	6.2
Flexural strength (MPa)	111	117
Flexural modulus (GPa)	2.9	2.8
Glass transition temperature (°C)	120[a]	127

[a] Value for Elium® 280 sourced from literature [25].

2. Materials and fabrication

2.1. Materials

The materials under investigation in this study were glass fibre-reinforced acrylic (GF/acrylic) and epoxy (GF/epoxy) laminates, comprising eight plies of non-crimp E-glass fabric (TEST2594-125-50; Ahlstrom-Munksjö). Fibres in 0°- and 90°-directions and PES stitching account for 600, 36 and 10 g/m^2, respectively of the total areal weight of 646 g/m^2. For the GF/acrylic laminate, Elium® 188 O resin (Arkema) was used with BP-50-FT organic peroxide initiator (United Initiators). A two-part epoxy resin system SR 1710/SD 7820 (Sicomin Epoxy Systems), was used for the GF/epoxy laminate. The comparability of glass transition temperature (T_g) of unreinforced matrices was the main selection criterion for the reference epoxy system. It is worth noting that the mixed resin viscosities (as specified by the manufactures) were dissimilar for both resins. Elium® 188 O had a viscosity of 100 mPa.s at 25 °C, whereas the value specified for the epoxy was 450 mPa.s at 30 °C. Table 2 shows properties of both resin systems. With the exception of T_g for Elium® 188 O, all values have been sourced from relevant datasheets. Reinforcement with multi-compatible sizing was sourced for this investigation due to the limited availability of specially sized fabrics for acrylics at the time.

2.2. Manufacturing method

Laminates were manufactured using an adjustable-cavity vacuum infusion mould supplied by Composite Integration. For each processing cycle, square fabric plies measuring 485 mm in length were cut and dried in a convection oven (60 °C overnight). Eight unidirectional plies were carefully assembled into the cavity with a pre-set height of 4 mm; the entire mould surface had been pre-treated with Zyvax® Watershield, a chemical release agent. Following the vacuum-assisted clamping and evacuation of the mould cavity, a 2-minute leak test was performed for a target maximum leak rate of 5 mbar/min. All infusions were performed at room temperature, followed by 24 h at room temperature. The GF/epoxy laminate was subjected to a two-part, free-standing post-cure (8 h at 60 °C and 4 h at 100 °C). The GF/acrylic laminate did not require post-processing; however, the recommended time of 8 h was extended to 24 h to ensure full polymerisation. As can be seen in Fig. 1, the use of the low-viscosity acrylic resin resulted in significantly shorter infusion times (up to five times shorter) than the use of its epoxy counterpart.

2.3. Preparation of test specimen

A water-lubricated diamond-coated saw blade was used to cut specimens from the fabricated laminates in accordance with relevant test standards. Drying was performed in a convection oven at 50 °C for 72 h to ensure samples were free of moisture from the cutting process prior to testing. With the exception of transverse tensile and flexural test specimens, longitudinal specimens were utilised for all other test methods.

Fibre volume and void fractions were determined by the matrix burn-off technique (ASTM D3171) to assess the quality of the laminates produced. Fibre volume fractions were the same (49.5%) in both cases; however, the void contents were 0.4% and 1.3% in GF/acrylic and GF/epoxy, respectively. The lower void content in the case of GF/acrylic can be attributed to the low infusion viscosity of the acrylic resin and is in agreement with observations by Chilali et al. [24].

3. Experimental methods

3.1. Tensile testing

Transverse tensile testing was conducted in accordance with ASTM D3039. Six samples measuring 250 mm × 25 mm were loaded at 2 mm/min until failure on an MTS Criterion (Model 45) 300-kN capacity test frame. To prevent slippage between the grip face and specimen ends during testing, 240 grit emery cloths were used at sample ends; hydraulic gripping jaws were used (grip pressure: 60 bar). Using video extensometry (Imetrum UVX & Manta G-146B/G-146C), strains were computed from recorded real-time deformations; all samples were speckled with matt black paint prior to testing.

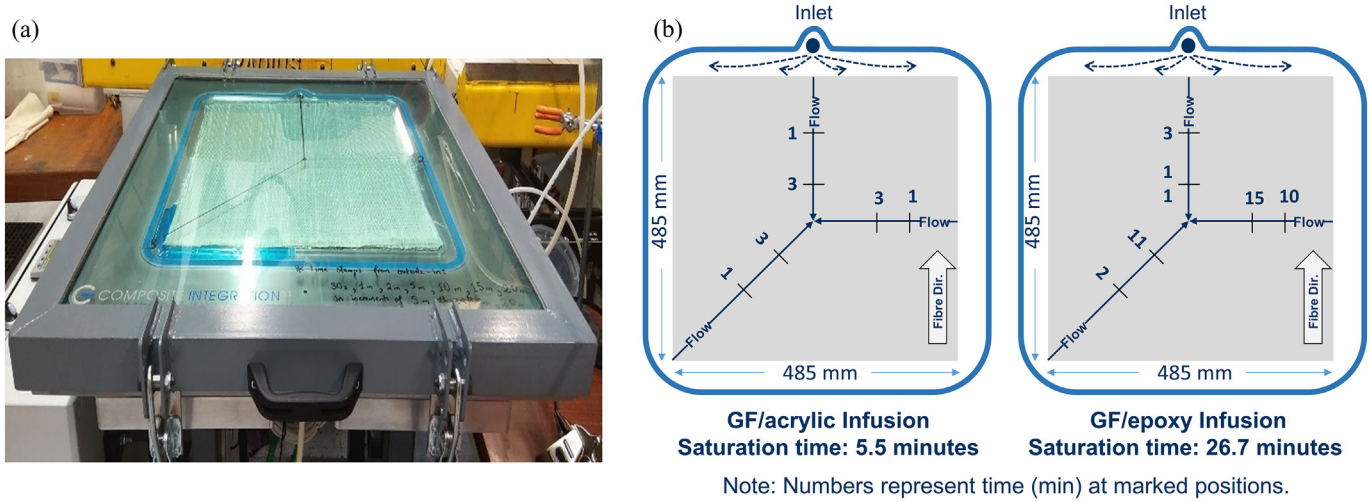


Fig. 1. (a) Experimental set-up for the production of test laminates; (b) graphical representation of observed flow fronts for GF/acrylic and GF/epoxy.

Table 3
Details of test parameters and specimen dimensions.

Analyser	Q800-V21.1 TA instruments
Mode	Three-point bending (longitudinal)
Nominal specimen dimensions	60 mm × 10 mm × 4 mm (50-mm span)
Temperature profile	Ambient – 180 °C (3 °C/min)
Displacement amplitude	50 μm
Frequency	1 Hz

3.2. Flexural testing

The longitudinal and transverse flexural properties (strengths and moduli) of GF/acrylic and GF/epoxy were determined by three-point loading in accordance with ASTM D7264 using a sample span-to-thickness ratio of 32:1, corresponding to sample lengths of 154 mm and crosshead speed of 1 mm/min. Loading nose and supports were hardened steel pins of 6 mm diameter. Six samples were tested for each material under transverse loading conditions, whereas five samples were loaded longitudinally from each laminate. Testing was performed on an Instron (3369) test frame fitted with a 10 kN load cell (Instron 2530-10 kN). Mid-span deflections were tracked and recorded by means of the video extensometer described in Section 3.1. Sample edges were speckled with a fine-tip permanent marker to facilitate video extensometry.

3.3. Short beam shear testing

To evaluate the short beam shear performance of GF/acrylic and GF/epoxy, six coupons measuring 8 mm × 24 mm were loaded to failure by short beam shear testing (in accordance with ASTM D2344). The test frame detailed in Section 3.2 was used. Testing was performed at a crosshead speed of 1 mm/min. A span-to-thickness ratio of 4:1 was used to ensure samples were subjected to a shear stress state. Cylindrical loading nose and supports were used with diameters of 6 mm and 3 mm, respectively.

3.4. Mode-I fracture toughness testing

Double cantilever beam (DCB) testing was performed in accordance with ASTM D5528 for the determination of mode-I interlaminar fracture toughness. Testing was performed on the Instron test frame detailed in Section 3.2. Self-releasing films (13-μm thick perfluoroalkoxy alkane) were implanted at the mid-plane of each laminate during fabrication to create a 63-mm long initiation site for delamination. Samples were carefully cut from the test laminate to maintain the length of the original initiation site and dimensions (175 mm × 25 mm). Steel loading blocks (25 mm × 25 mm × 16 mm) were bonded to the *pre-cracked* sample ends for load introduction and high-contrast speckles were applied as described in Section 3.2 to sample edges to facilitate automatic tracking of delamination length using a video extensometer (refer to Section 3.1 for specifications). For each test, loading was performed at a rate of 1 mm/min for a minimum delamination length of 50 mm. Load, opening (crosshead) displacement and delamination length were recorded.

3.5. Dynamic mechanical analysis

Dynamical mechanical analysis (DMA) was performed in accordance with BS ISO 6721-11 to assess the thermomechanical properties of both materials. The test and specimen specifications are detailed in Table 3. Storage and loss moduli, and tan delta were recorded as functions of temperature throughout testing.

3.6. Scanning electron microscopy

Scanning electron microscopy was used as a means of qualitatively assessing failure behaviour following short beam shear (SBS) and DCB testing. Samples were prepared with a 40-nm sputter coating of gold to enhance surface conductivity and imaged at 5 kV on a JEOL JSM series instrument. SBS sample edges were coated; whereas on DCB samples, coating was applied to exposed interlaminar fracture surfaces (created during testing).

4. Results and discussion of manufactured laminates

4.1. Results of mechanical characterisation

A summary of the tensile, flexural and short beam shear properties reported and discussed in Sections 4.1.1 to 4.1.4 is presented in Table 4.

4.1.1. Transverse tensile test results

Representative stress-strain responses for GF/acrylic and GF/epoxy are presented in Fig. 2 and are given in Table 4. GF/acrylic exhibited significantly higher average transverse tensile strengths at 73 MPa, compared to 54 MPa for the GF/epoxy specimens. For both materials, strain is observed to increase linearly with increasing applied stress. GF/acrylic samples showed evidence of plastic deformation at strains in excess of 0.4% and continue to yield gradually until the point of ultimate specimen fracture. In contrast, lower transverse tensile strengths were observed for the GF/epoxy samples, with higher strains observed at failure. GF/epoxy had higher failure strains (2.1 ± 0.2%) than GF/acrylic (1.2 ± 0.3%).

As shown in Fig. 3, a series of horizontal cracks were observed in all GF/epoxy specimens. In the case of GF/acrylic, only a few cracks were seen to appear prior to the main failure event. Evidence of fibre-splitting along the loading direction, originating from the sparsely distributed 90°-fibres were only observed in GF/acrylic samples.

Table 4
Tensile, flexural and shear properties.

		GF/acrylic	GF/epoxy
Tensile properties (transverse)	Strength (MPa)	73 ± 3.9	54 ± 4.1
	Modulus (GPa)	13 ± 0.6	13 ± 0.5
	Failure strain (%)	1.2 ± 0.3	2.1 ± 0.2
Flexural properties (longitudinal)	Strength (MPa)	879 ± 49	869 ± 42
	Modulus (GPa)	40 ± 1.7	38 ± 2.3
	Failure strain (%)	3.3 ± 0.4	3.4 ± 0.6
Flexural properties (transverse)	Strength (MPa)	91 ± 5.4	94 ± 7.2
	Modulus (GPa)	11 ± 0.2	12 ± 0.4
	Failure strain (%)	1.7 ± 0.3	2.0 ± 0.2
Short beam shear properties	Strength (MPa)	58 ± 1.7	57 ± 1.0

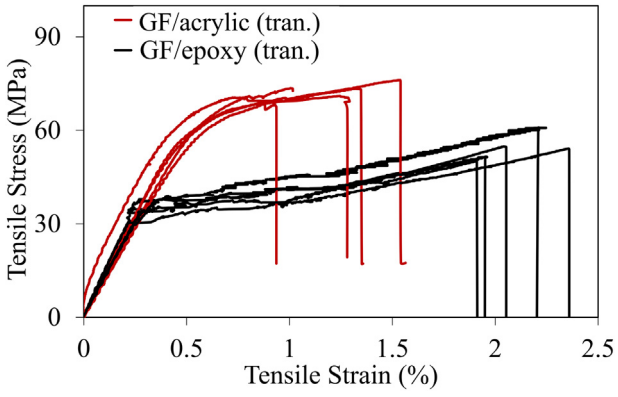


Fig. 2. Transverse stress-strain behaviour of all GF/acrylic and GF/epoxy samples. Reinforcements are a non-crimp stitched unidirectional E-glass fabric with fibre volume fraction of 49.5% in each case.

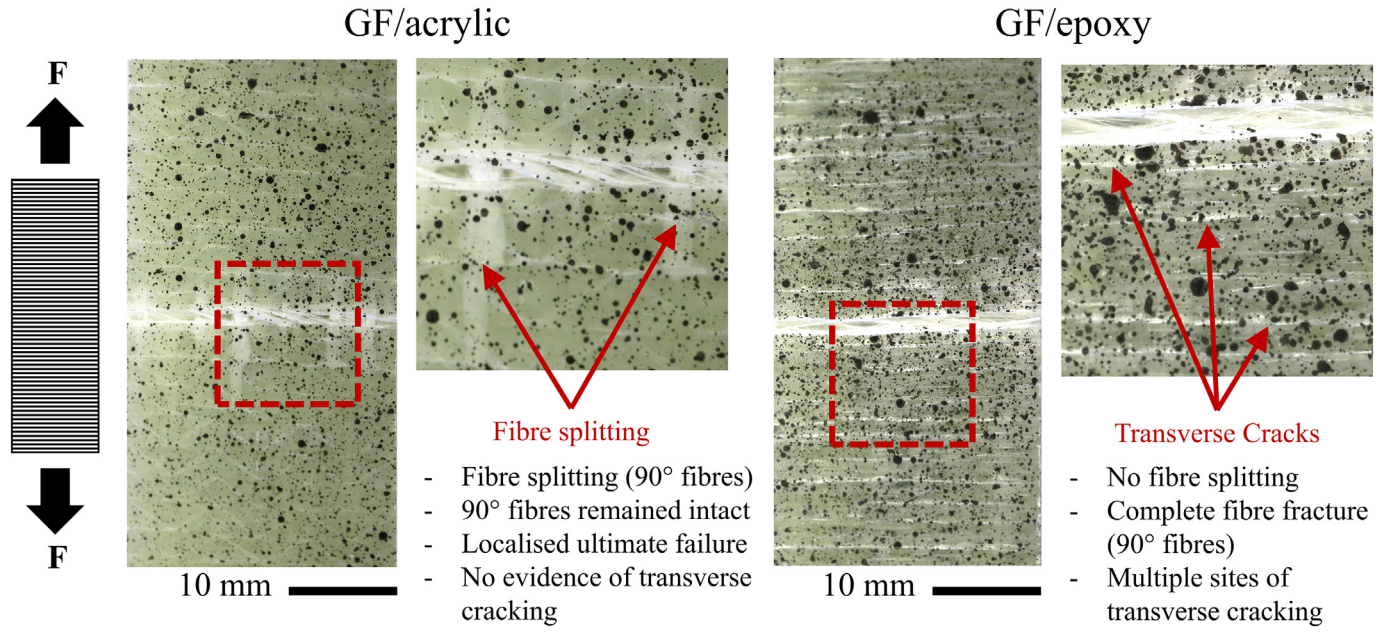


Fig. 3. Representative failure modes in both materials following transverse tensile testing with loading direction schematically represented.

Strain maps (obtained from video extensometer) have been presented in time-lapse sequences (Fig. 4) to highlight the difference in strain development (and thus, damage evolution) between both material systems. GF/acrylic strain maps are more uniform throughout the testing. The effects of accumulating transverse cracks in GF/epoxy, however, are highly evident; high-strain domains dominate the strain maps between 40 min and t*. The time stamp, t* represents the strain distribution at the time of ultimate failure in both materials.

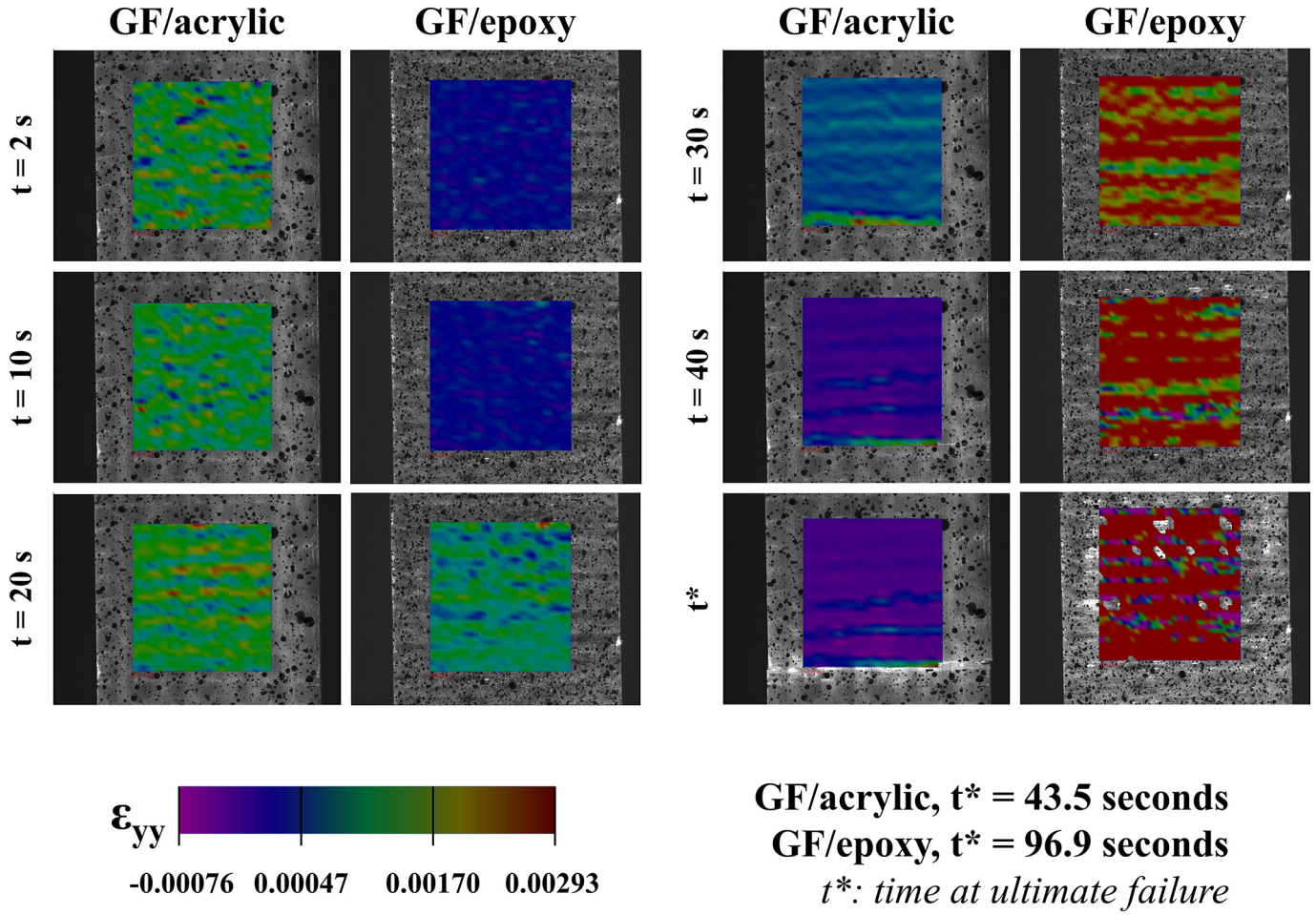


Fig. 4. Time-lapse compilation of representative strain maps obtained during transverse tensile loading of GF/acrylic and GF/epoxy samples.

4.1.2. Longitudinal flexural test result

Fig. 5 shows representative stress-strain behaviour of the materials under investigation following longitudinal flexural loading to failure. As previously presented in Table 4, GF/acrylic exhibited marginally higher strength (average of 880 MPa) and modulus (average of 40 GPa) compared to averages of 870 MPa and 38 GPa for GF/epoxy, respectively. In addition, up to failure, its stress-strain response was similar to that of GF/epoxy.

A monotonic linear increase in stress exists in both materials up to the limit of proportionality; thereafter, evidence of plastic deformation is seen until the onset of severe compressive failure (Point 1). However, they exhibit dissimilar damage evolution beyond this point. In both materials, ultimate tensile fibre fracture (Point 2) is observed as a discrete and sudden loss in stiffness; however, in GF/acrylic samples, this was preceded by an extended period where marginal stress reductions were observed with increasing strain. This behaviour is thought to be indicative of progressive matrix cracking [51]. In the case of the GF/epoxy samples, more sudden load drops and stepped reduction in stress are observed until ultimate failure. The strain window between onset and ultimate failure events, i.e., between Points 1 and 2 was broader (~26%) in GF/acrylic samples.

Damage initiation in both materials occurred on the side in compression, with evidence of compressive fibre fractures being observed before tensile fibre fracture. In the case of GF/epoxy samples, tensile matrix failure events coincided with compressive fibre fracture. It is worth noting however, that as these observations were reliant on edge detection of failure, other undetected failure events may have occurred prior to those reported.

Post-mortem inspections of ultimate compressive, tensile and through-thickness (edge) failure modes were conducted on all samples. Representative images obtained during these inspections are presented in Fig. 6. Focusing on the damage on the compressive sides (Fig. 6a & d) of test samples from both materials, distinct failure types are observed; GF/acrylic samples showed evidence of micro-buckling under the loading nose and severe delamination in tows on outer edges. On the other hand, matrix crushing was more prominent in GF/epoxy, without edge effect as observed with GF/acrylic. A lesser extent of surface buckling was evident. Distinct, ultimate tensile failure modes were also observed in both materials. While all samples showed characteristics of tow separation and delamination, GF/acrylic tows remained mostly intact (Fig. 6b), whereas GF/epoxy tows suffered more intra-tow matrix cracks and debonding, leading to a shinier appearance (Fig. 6e). Damage in GF/acrylic was spread over a longer length, while more localised damage occurred in GF/epoxy. Comparing the distribution of damage mechanisms through the thickness as shown in Fig. 6c and f, a similar extent of fibre-related damage processes (such as kinking and fracture) were observed in both materials. Although distinct regions of compressive and tensile failure were observed in all samples, GF/acrylic samples showed more *hourglass-shaped* distribution of these regions, with upper and lower regions joining. In contrast, GF/epoxy samples had two discrete upper and lower bounds in the distribution of failure.

4.1.3. Transverse flexural test results

Representative stress-strain responses to transverse flexural loading are shown in Fig. 7. and strengths and moduli were presented in Table 4.

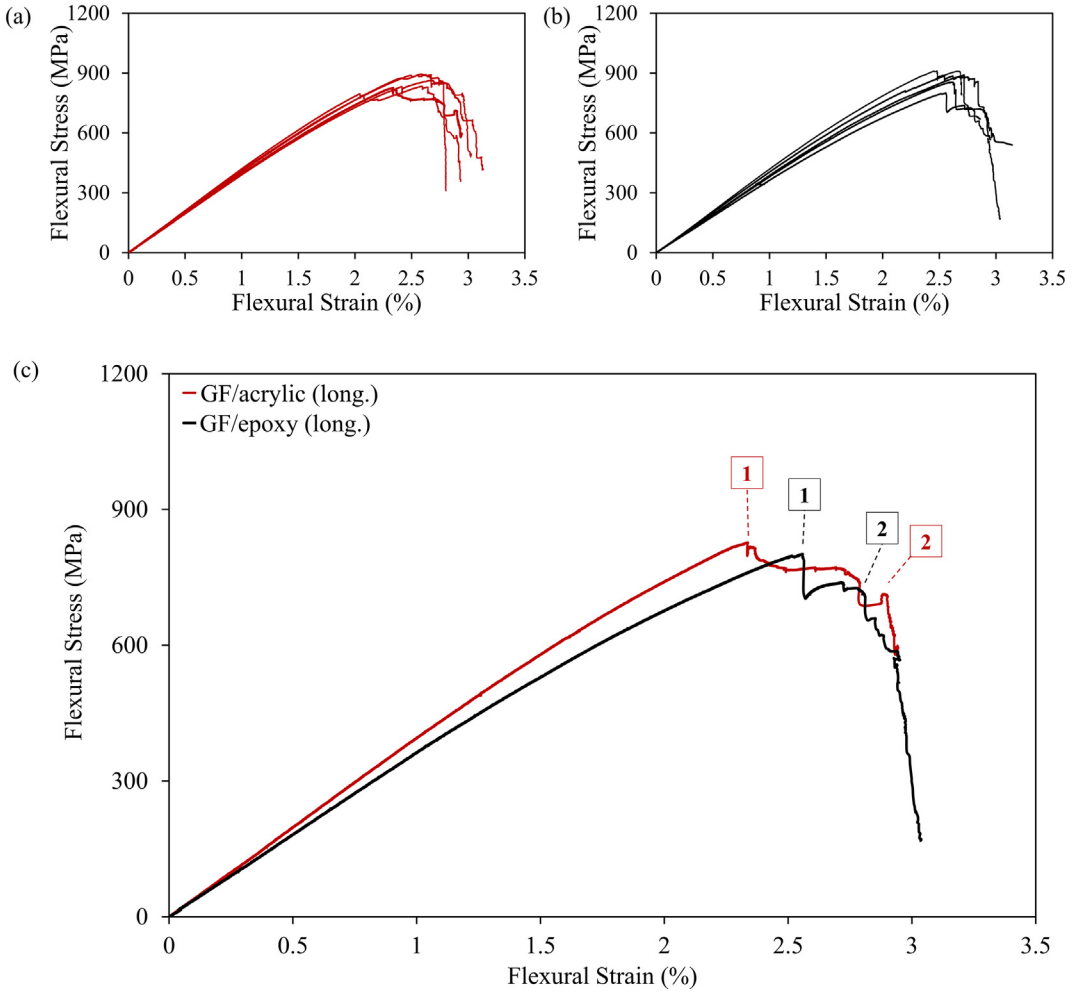


Fig. 5. Stress-strain curves of (a) GF/acrylic, (b) GF/epoxy and (c) representative curves showing characteristic behaviour of both materials in response to longitudinal flexural loading.

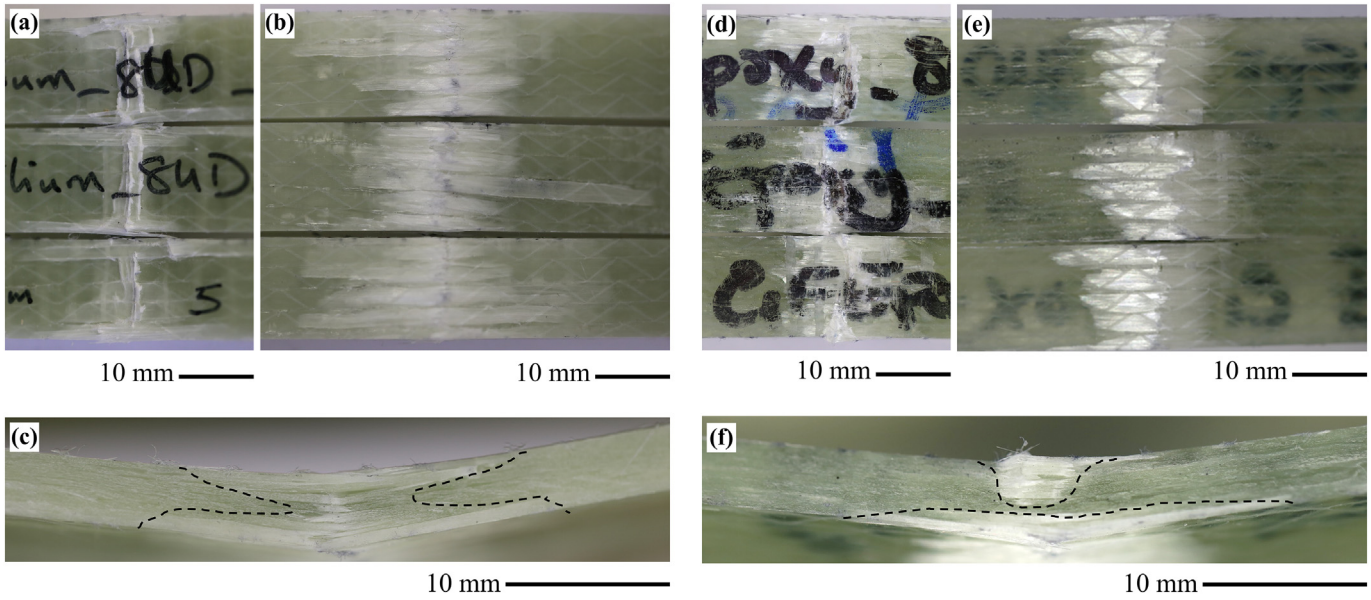


Fig. 6. Images showing representative modes of (a) compressive failure, (b) tensile failure, on upper and lower surfaces, respectively; and (c) regions of compressive and tensile failure on GF/acrylic sample edges of longitudinal flexure specimens. Note: (d), (e) and (f) are same features on GF/epoxy samples, respectively.

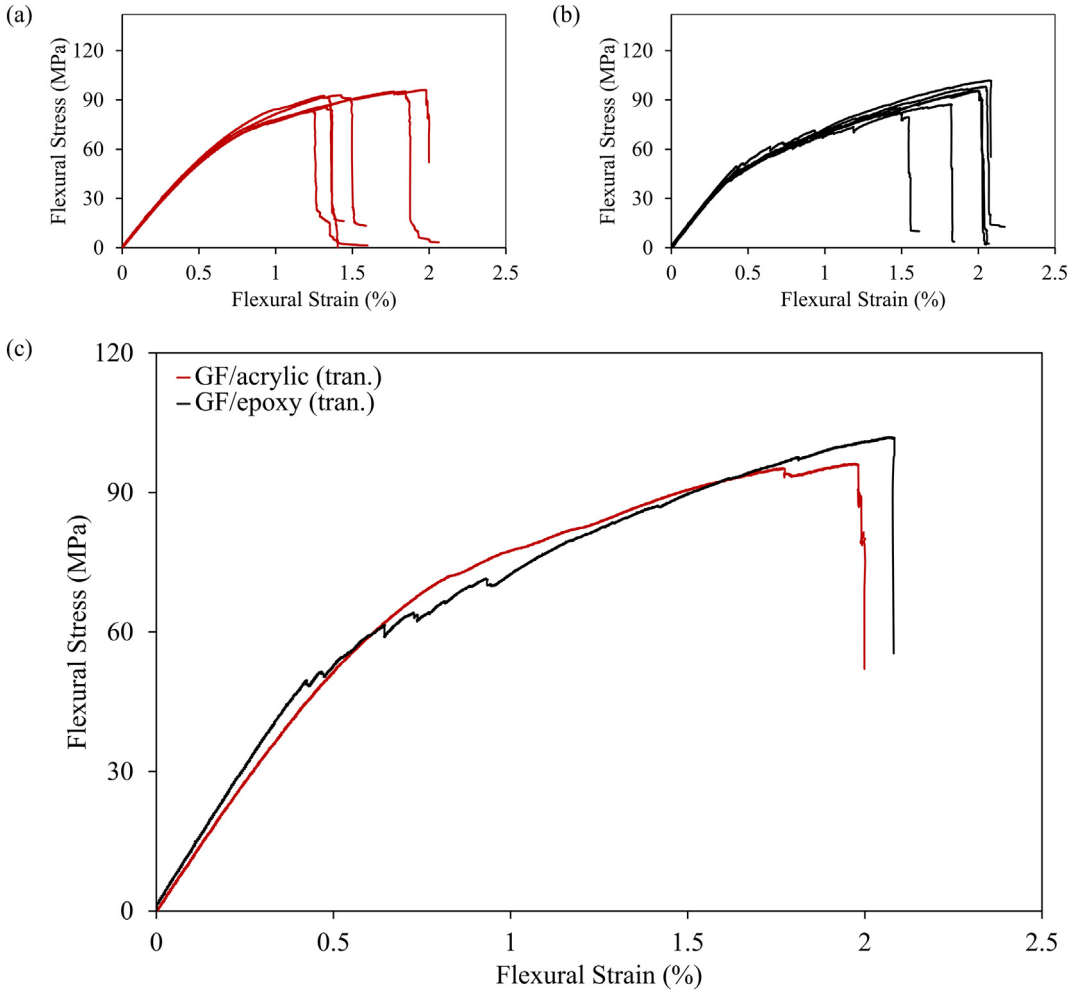


Fig. 7. Stress-strain curves of (a) GF/acrylic and (b) GF/epoxy and (c) representative curves showing characteristic behaviour of both materials in response to transverse flexural loading.

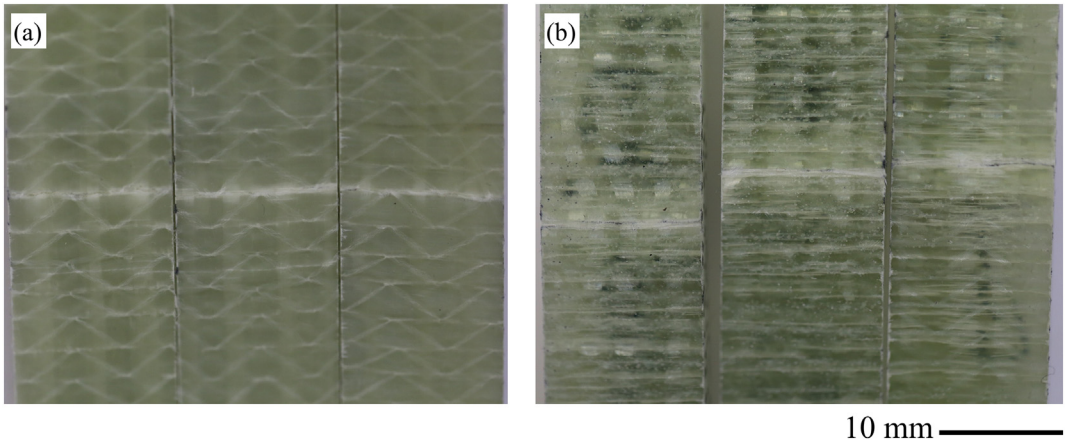


Fig. 8. Images of representative failures (tensile side) on three samples of (a) GF/acrylic and (b) GF/epoxy following transverse flexural testing.

Despite its superior transverse tensile performance, with strength of 91 MPa and modulus of 11 GPa, GF/acrylic had marginally lower transverse flexural properties than GF/epoxy, which had average strength of 94 MPa and modulus of 12 GPa.

As seen in Fig. 7, both materials exhibit a short linear elastic region, however, in the case of GF/acrylic; this region is followed by some non-linearity until failure, indicating a higher degree of plastic deformation before failure. Conversely, GF/epoxy samples showed evidence of earlier onset of damage after the initial linear region. In all epoxy-based samples, this region was followed by oscillations in stress-strain response (indicating progressive accumulation of minor damage events) until the occurrence of ultimate failure. Unlike the longitudinal stress-strain responses where a broader region of linearity was observed (indicating fibre-dominated flexural behaviour), a high extent of non-linearity

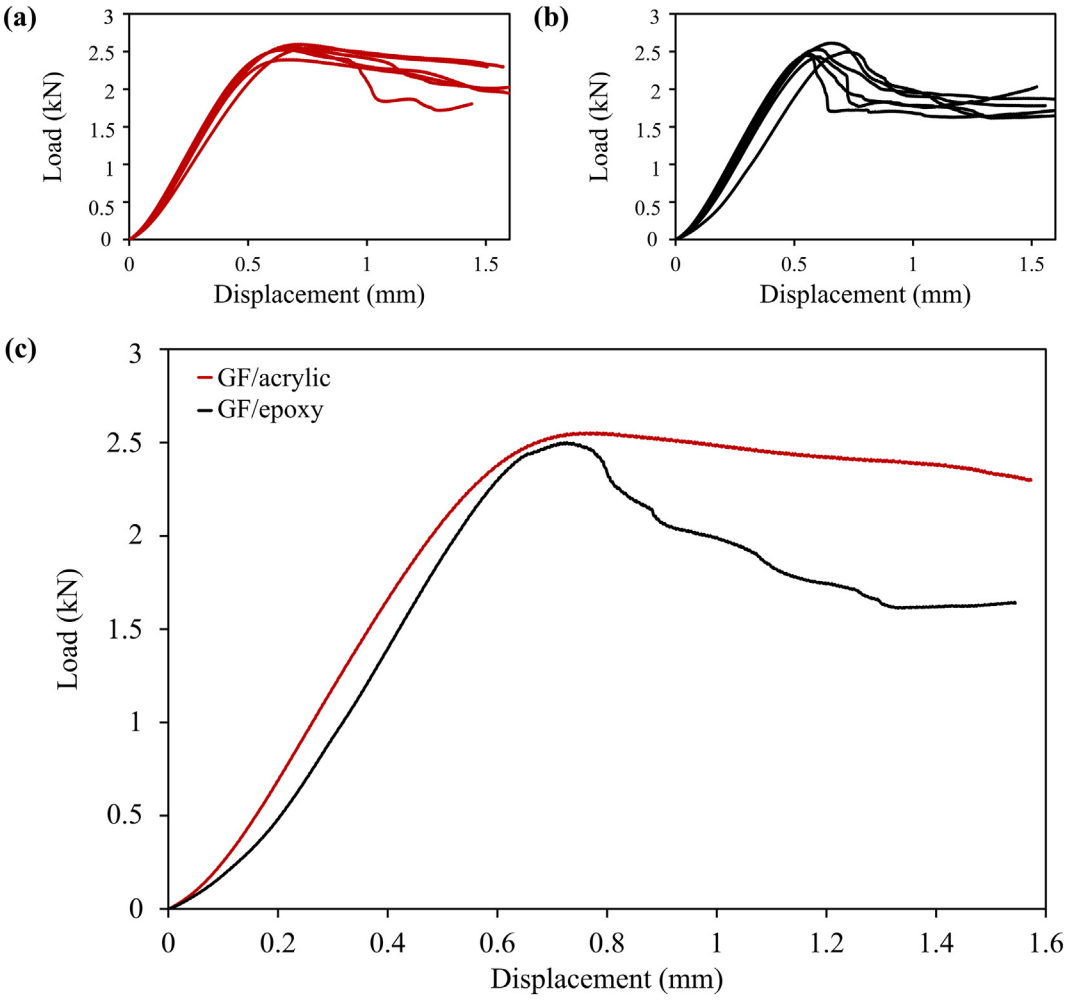


Fig. 9. Load-displacement curves obtained from short beam shear tests for all (a) GF/acrylic and (b) GF/epoxy samples and (c) a comparison of two representative curves from both materials.

exists in the transverse stress-strain curves due to the matrix-dominated nature of failure.

As shown in Fig. 8, multiple transverse cracks were observed on GF/Epoxy samples, explaining the oscillations observed in stress-strain behaviour (Fig. 7) leading to ultimate failure. In GF/acrylic, fewer cracks were evident; however, these were concentrated around the main site of matrix fracture.

4.1.4. Short beam shear test results

In this section, the results of short beam shear testing for the determination of short shear strengths are presented in Table 4 and discussed. GF/acrylic had marginally higher average shear strength (58 MPa) than GF/epoxy (57 MPa). Fig. 9 shows all load-displacement curves for both materials.

Load-displacement curves reveal similar pre-peak behaviour in both materials. A linear region is observed for all samples and is followed by some nonlinear deformation prior to peak load. Beyond this point, GF/acrylic samples did not exhibit abrupt load drops; their curves revealed evidence of severe inelastic deformation with localised stable crack propagation. In contrast, a more noticeable onset of failure is observed in GF/epoxy samples as load drops of about 20–30% from respective load peaks. Larger areas are bounded by the GF/acrylic curves than those observed under GF/epoxy curves, indicating higher energy absorption. It can thus be assumed that more fracture energy was available within GF/acrylic samples.

Post-mortem SEM inspections on edges of failed specimens were conducted to substantiate observed load-displacement behaviour. As shown in Fig. 10, evidence of interlaminar shear and plastic deformation are visible in GF/acrylic, with ductile fracture characteristics observed. The damage characteristics of GF/epoxy shown in Fig. 11 are consistent with interlaminar shear failure; brittle shear cusps [52] were present, with no plasticity being observed. Both materials had multiple cracks uniformly dispersed throughout the thickness.

All cracks observed in the GF/epoxy sample were near 90° fibres, which were dispersed throughout each ply. In contrast, cracks in GF/acrylic did not occur around these fibres. The observation of more delamination in GF/acrylic than GF/epoxy are in agreement with the assumptions made from the load-displacement curves in terms of fracture energy absorption.

4.1.5. Interlaminar fracture toughness

It has been shown in preceding sections that GF/acrylic significantly outperforms GF/epoxy in terms of transverse tensile strength, while exhibiting similar interlaminar short beam shear and flexural properties (in both longitudinal and transverse directions). This section discusses the observations from double cantilever beam fracture testing. The mode-I fracture toughness values reported here are average strain energies released during initiation ($G_{IC\text{-}Init.}$) and propagation ($G_{IC\text{-}Prop.}$), calculated using the modified beam theory method as per the test standard, with the onset of nonlinearity being used to evaluate the former.

GF/acrylic exhibited superior mode-I fracture toughness, with a mean $G_{IC\text{-}Prop.}$ of 1814 J/m^2 compared to the value of 1574 J/m^2 for GF/epoxy, with 19% higher initiation fracture toughness than GF/epoxy. Representative load-displacement curves, R-curves and comparison of mean initiation and propagation toughness values are presented in Fig. 12.

All samples exhibited an initial non-linearity during the *take-up* portion of load introduction and simultaneous opening of the specimen prior to crack initiation. Following this, a monotonic increase in load

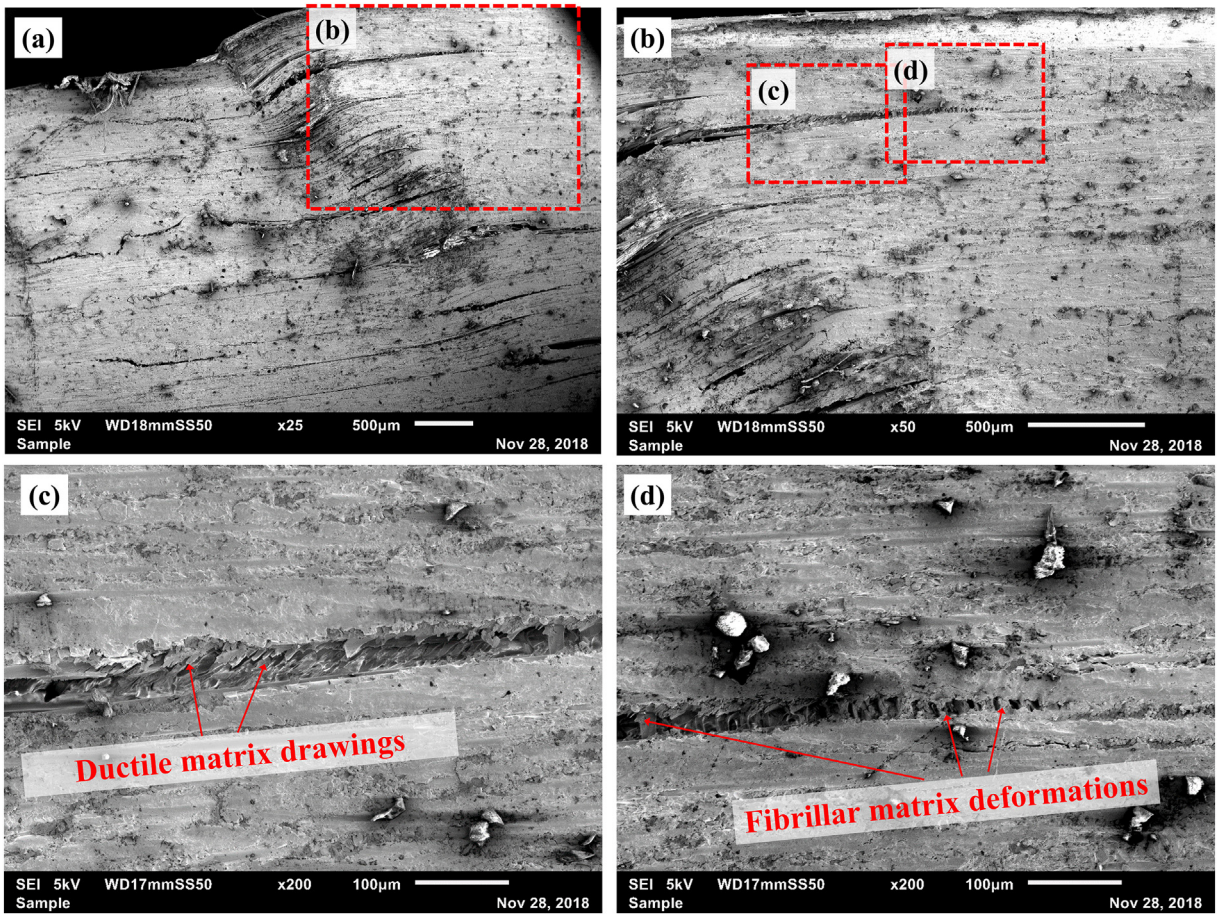


Fig. 10. SEM micrographs showing representative GF/acrylic short beam shear failure modes at magnifications of 25× in (a), 50× in (b), and 200× in (c) and (d).

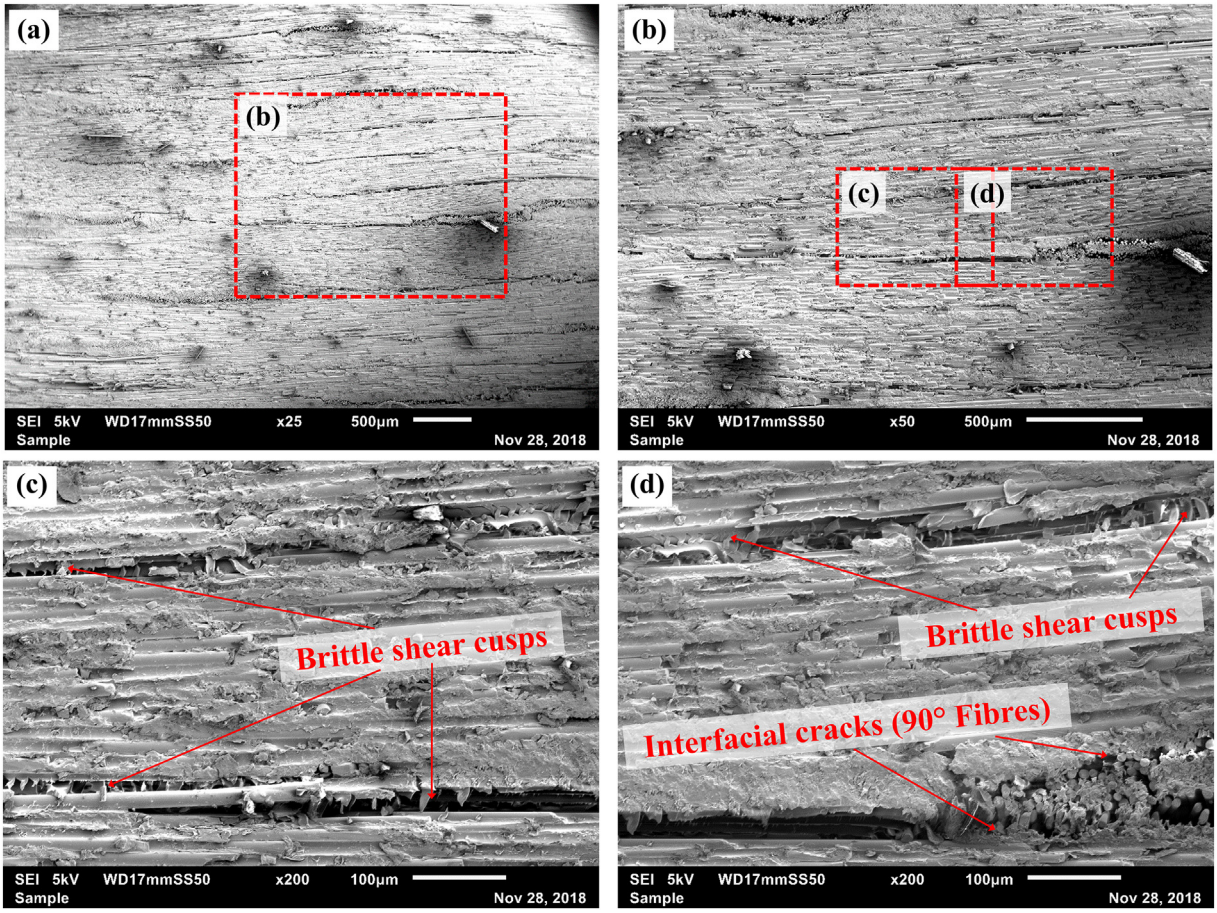


Fig. 11. SEM micrographs showing representative GF/epoxy short beam shear failure modes at magnifications of 25× in (a), 50× in (b), and 200× in (c) and (d).

was observed prior to delamination initiation. A minor pre-peak load-drop is evident in both materials. Upon initiation, the load-displacement curves of both materials showed minor oscillations and load-drops, which are consistent with stick-slip delamination behaviour (indicative of unstable propagation) [53,54].

From Fig. 13, a higher extent of fibre bridging (at the crack tip) is observed in GF/acrylic than in GF/epoxy. Moreover, crack bridging occurred throughout testing due to the presence of 90° tows in the fabric used. This was evident in both materials and occurred throughout testing; as such, the load-displacement curves (Fig. 12a) and the R-curves (Fig. 12b) are not representative of purely unidirectional specimens. It is highly likely that some of the load drops and evolution of mode-I fracture resistance with increasing crack length correspond to secondary energy-dissipation processes such as tow rupture and/or debonding events [54]. However, as the same reinforcement was used in both materials, the associated effects on the comparability of these materials are considered negligible. As is evident in Fig. 12b, the delamination resistance of GF/acrylic increases with increasing crack growth, whereas that of GF/epoxy remains relatively constant.

Focusing on electron micrographic inspections of fracture surfaces (Fig. 14) however, distinct failure modes are visible in both materials. The presence of ductile matrix deformation and risers on the GF/acrylic

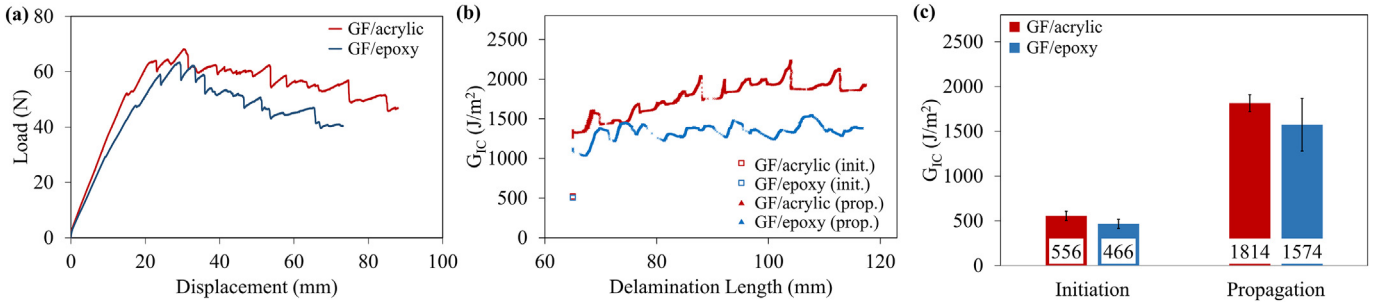


Fig. 12. Representative (a) load-displacement curves and (b) resistance curves (R-curves) obtained from DCB testing of GF/acrylic and GF/epoxy; and (c) is a chart comparing their average $G_{IC\text{-}Init.}$ and $G_{IC\text{-}Prop.}$ values.

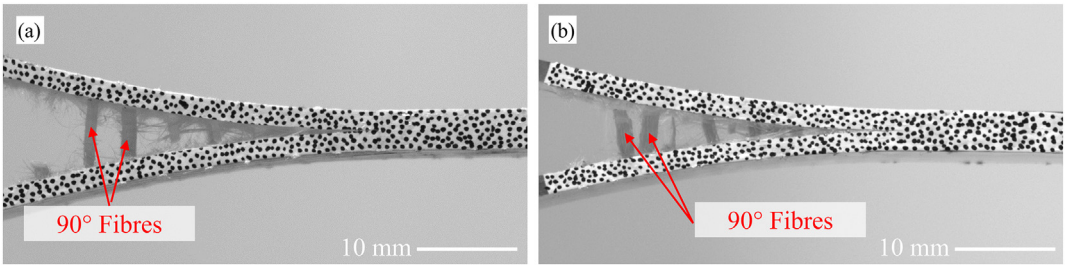


Fig. 13. Images of representative delamination behaviour observed during DCB testing of (a) GF/acrylic and (b) GF/epoxy at equivalent test times.

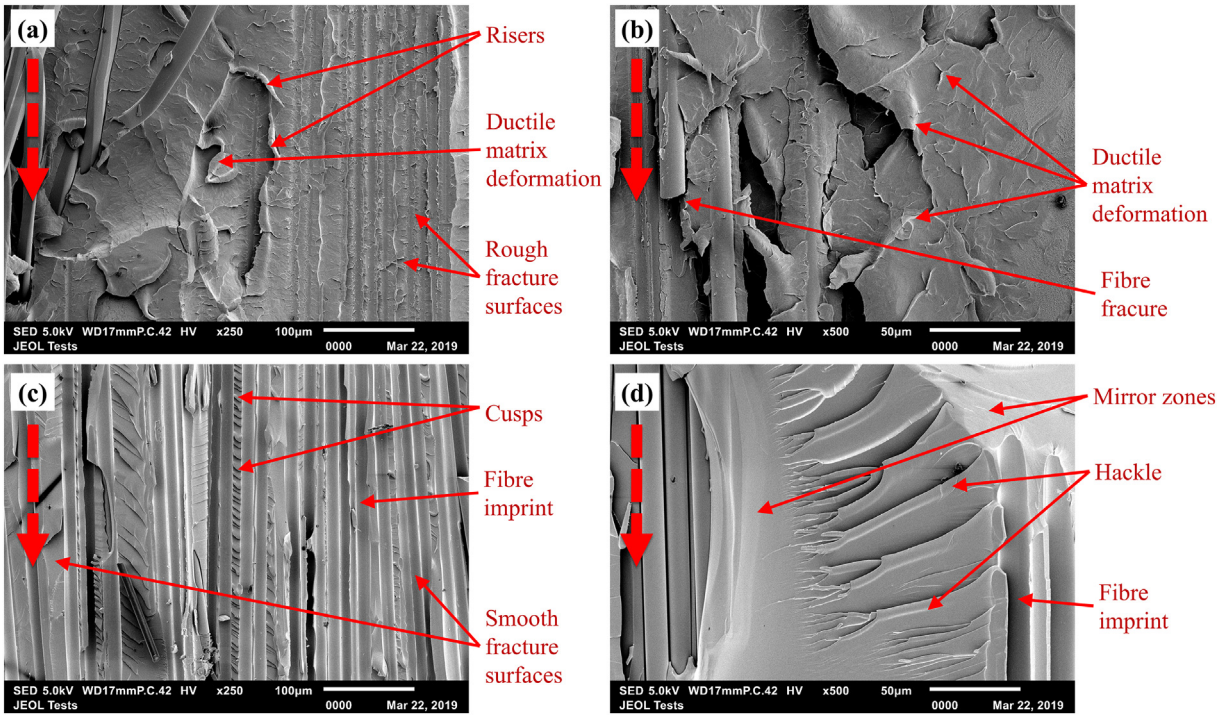


Fig. 14. SEM micrographs of mode-I fracture surfaces of GF/acrylic (a–b) and GF/epoxy (c–d).

fracture surface indicated ductile matrix fracture, whereas the cusps, mirror zones and hackle zones observed in GF/epoxy are characteristics of brittle matrix fracture. In the context of ductile and brittle matrix fracture characteristics, these micrographic observations are consistent with those from short beam test specimens. Moreover, an exceptional level of fibre-matrix adhesion was observed in GF/acrylic compared with its epoxy counterpart. This explains the superiority in transverse tensile strength in the GF/acrylic material and confirms that the use of fabric with multi-compatible sizing resulted in a desirable strong interfacial adhesion. In addition to the presence of risers, matrix fractures observed in GF/acrylic were distinctly duller in appearance and seemed to have a rougher texture, further confirming microscopic ductile fracture. All epoxy matrix fractures had brittle characteristics (sheen and smoothness).

4.2. Dynamic mechanical analysis

The viscoelastic response of both materials with temperature are shown in Fig. 15. The section that follows discusses differences in tan delta and storage modulus for both materials in the context of damping behaviour associated with each matrix type.

The thermomechanical properties of GF/acrylic and GF/epoxy obtained from the DMA experiments are presented in Table 5.

GF/acrylic was found to exhibit superior damping behaviour, as evidenced by the higher tan delta peak and the larger area under this peak, compared to GF/epoxy. The term "damping" here is used to indicate the energy dissipative efficiency of the materials [55,56]. The area bounded

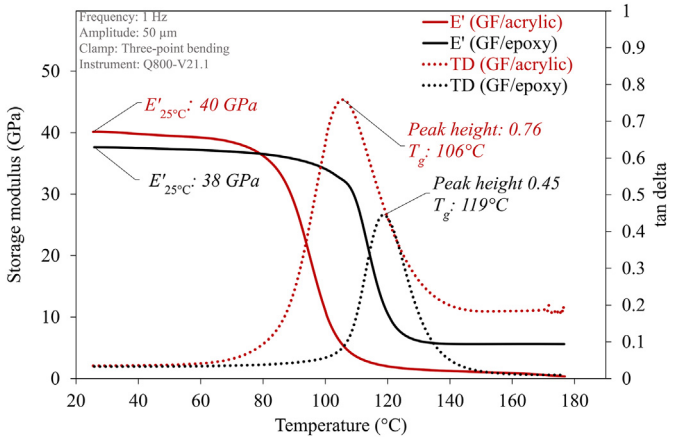


Fig. 15. Thermomechanical results showing the effect of temperature on storage modulus and tan delta in DMA testing. Testing carried out in the longitudinal direction.

Table 5
Summary of thermomechanical results.

	T_g, tan delta (°C)	Height of tan delta peak	Storage modulus at onset (GPa)
GF/acrylic	106	0.76	40
GF/epoxy	119	0.45	38

under the tan delta curve is proportional to the degree of molecular mobility, which in turn correlates to damping properties [57,58]. Thus, having higher peak intensity and larger area under its tan delta curve, GF/acrylic exhibits better damping behaviour. Being a thermoplastic amorphous polymer, i.e., possessing no crosslinks, the polymer chains in GF/acrylic can undergo instantaneous short-range deformation to dissipate the applied stresses. Conversely, the crosslinked 3D-network structure of the matrix in GF/epoxy inhibits deformations of the same magnitude as observed in GF/acrylic. The effects of crosslinks on the height of tan delta peaks have been previously studied by Bandzierz et al. [59]. These results indicate that GF/acrylic would tend towards highly inelastic response, whereas elastic response dominates in GF/epoxy.

5. Conclusions

The present research comparatively assessed the mechanical and thermomechanical performance of a vacuum-infused thermoplastic acrylic composite against a traditional epoxy based system. The processing of the thermoplastic system was associated with shorter cycle times (due to low viscosity infiltration and no requirement for post-processing). Moreover, the use of multi-sized reinforcement fabric resulted in good interfacial adhesion in GF/acrylic.

The following are the relevant findings and observations in relation to the benchmarking of GF/acrylic against GF/epoxy:

- GF/acrylic had 33% higher transverse tensile strength and equivalent modulus.
- It had comparable longitudinal flexural strength (+1%) and modulus (+5%).
- Its short beam shear strength was comparable (+2%).
- It had slightly lower transverse flexural strength (−3%) and modulus (−8%).
- It exhibited superior fracture toughness and delamination resistance with its $G_{IC\text{-}Init.}$ and $G_{IC\text{-}Prop.}$ being 19% and 15% higher, respectively.
- Micrographs revealed microstructural ductility in GF/acrylic and brittle fracture mechanisms in GF/epoxy.
- GF/acrylic had a higher tan delta peak (+69%) than GF/epoxy.

The findings and observations presented in this paper will serve to foster an understanding of acrylic matrices in continuous fibre-reinforced composite applications. Such knowledge is essential for highlighting applications where acrylic-based composite may most effectively be employed, and may provide guidance on necessary performance enhancing modifications.

CRediT authorship contribution statement

Winifred Obande: Conceptualization, Data curation, Formal analysis, Investigation, Methodology, Project administration, Resources, Visualization, Writing - original draft, Writing - review & editing. **Dimitrios Mamalis:** Data curation, Formal analysis, Investigation, Writing - review & editing. **Dipa Ray:** Conceptualization, Funding acquisition, Methodology, Project administration, Resources, Supervision, Validation, Visualization, Writing - review & editing. **Liu Yang:** Formal analysis, Resources, Validation. **Conchúr M. Ó Brádaigh:** Funding acquisition, Resources, Supervision, Validation, Writing - review & editing.

Acknowledgments

The authors would like to thank Arkema GRL, France for providing material samples towards this research.

Declaration of conflicting interests

The authors declared no potential conflicts of interest with respect to the research, authorship, and/or publication of this article.

The raw/processed data required to reproduce these findings cannot be shared at this time due to technical or time limitations.

References

[1] H.J. Kim, G.A. Keoleian, S.J. Skerlos, Economic assessment of greenhouse gas emissions reduction by vehicle lightweighting using aluminum and high-strength steel, J. Ind. Ecol. 15 (2011) 64–80, https://doi.org/10.1111/j.1530-9290.2010.00288.x.
[2] H. Helms, U. Lambrecht, The potential contribution of light-weighting to reduce transport energy consumption, Int. J. Life Cycle Assess. 12 (2006) 58–64, https://doi.org/10.1065/lca2006.07.258.
[3] N.H. Nash, T.M. Young, P.T. McGrail, W.F. Stanley, Inclusion of a thermoplastic phase to improve impact and post-impact performances of carbon fibre reinforced thermosetting composites - a review, Mater. Des. 85 (2015) 582–597, https://doi.org/10.1016/j.matdes.2015.07.001.
[4] K.-Y. Kim, L. Ye, K.-M. Phoa, Interlaminar fracture toughness of CF/PEI and GF/PEI composites at elevated temperatures, Appl. Compos. Mater. 11 (2004) 173–190 https://link.springer.com/content/pdf/10.1023%2FB%3AACMA.0000026586.12629.7e.pdf (accessed December 7, 2018).
[5] P. Ó Máirtín, P. McDonnell, M. Connor, R. Eder, C.M. Ó Brádaigh, Process investigation of a liquid PA-12/carbon fibre moulding system, Compos. Part A 32 (2001) 915–923www.elsevier.com/locate/compositesa, Accessed date: 29 December 2018.
[6] K. Van Rijswijk, J.J.E. Teuwen, H.E.N. Bersee, A. Beukers, Textile fiber-reinforced anionic polyamide-6 composites. Part I: the vacuum infusion process, Compos. Part A Appl. Sci. Manuf. 40 (2008) 1–10, https://doi.org/10.1016/j.compositesa.2008.03.018.
[7] S. Pillay, U.K. Vaidya, G.M. Janowski, Effects of moisture and UV exposure on liquid molded carbon fabric reinforced nylon 6 composite laminates, Compos. Sci. Technol. 69 (2009) 839–846, https://doi.org/10.1016/j.compscitech.2008.03.021.
[8] S.M. Coll, A.M. Murtagh, C.M. Ó Brádaigh, Resin film infusion of cyclic pBT composites: a fundamental study, in: Proc. SAMPE Eur. 25th Int. Jubil. Conf., Paris, 2004.
[9] H. Parton, I. Verpoest, In situ polymerization of thermoplastic composites based on cyclic oligomers, Polym. Compos. 26 (2005) 60–65.
[10] C. Yan, L. Liu, Y. Zhu, H. Xu, D. Liu, Properties of polymerized cyclic butylene terephthalate and its composites via ring-opening polymerization, J. Thermoplast. Compos. Mater. 31 (2018) 181–201, https://doi.org/10.1177/0892705717697774.
[11] C.M. Ó Brádaigh, A. Doyle, D. Doyle, P. Feerick, Electrically-heated ceramic composite tooling for out-of-autoclave manufacturing of large composite structures, SAMPE J. 47 (2011) 6–14http://hdl.handle.net/10379/3542, Accessed date: 1 January 2019.
[12] A. Doyle, P. Feerick, P. Mallon, C. Ó Brádaigh, D. Doyle, A heated mould for moulding polymeric composites, a method for making such mould and its use, European Patent EP (2012) 2344312B1http://www.freepatentsonline.com/WO2010040576.html, Accessed date: 1 January 2019.
[13] G. Gardiner, Thermoplastic Wind Blades: To be or not? 2012 https://www.compositesworld.com/articles/thermoplastic-wind-blades-to-be-or-not (accessed January 1, 2019).
[14] R.E. Murray, D. Snowberg, D. Berry, R. Beach, S. Rooney, D. Swan, Manufacturing a 9-meter thermoplastic composite wind turbine blade, Am. Soc. Compos. 32nd Tech. Conf., West Lafayette, Indiana, 2017www.nrel.gov/publications, Accessed date: 1 January 2019.
[15] D.S. Cousins, Y. Suzuki, R.E. Murray, J.R. Samaniuk, A.P. Stebner, Recycling glass fiber thermoplastic composites from wind turbine blades, J. Clean. Prod. 209 (2019) 1252–1263, https://doi.org/10.1016/j.jclepro.2018.10.286.
[16] C. Baley, M. Lan, A. Bourmaud, A. Le Duigou, Compressive and tensile behaviour of unidirectional composites reinforced by natural fibres: influence of fibres (flax and jute), matrix and fibre volume fraction, Mater. Today Commun. 16 (2018) 300–306, https://doi.org/10.1016/j.mtcomm.2018.07.003.
[17] A. Aronica, D. Fossati, Effects of Resin and Processing on Mechanical Properties of Carbon Fibre Composites, Politecnico di Milano, 2015 Master's Thesis.
[18] T. Pini, F. Caimmi, F. Briatico-Vangosa, R. Frassine, M. Rink, Fracture initiation and propagation in unidirectional CF composites based on thermoplastic acrylic resins, Eng. Fract. Mech. 184 (2017) 51–58, https://doi.org/10.1016/j.engfracmech.2017.08.023.
[19] T. Pini, F. Briatico-Vangosa, R. Frassine, M. Rink, Matrix toughness transfer and fibre bridging laws in acrylic resin based CF composites, Eng. Fract. Mech. 203 (2018) 115–125, https://doi.org/10.1016/j.engfracmech.2018.03.026.
[20] T. Pini, F. Briatico-Vangosa, R. Frassine, M. Rink, Time dependent fracture behaviour of a carbon fibre composite based on a (rubber toughened) acrylic polymer, Procedia Struct. Integr. 2 (2016) 253–260, https://doi.org/10.1016/j.prostr.2016.06.033.
[21] A. Aronica, D. Fossati, Mechanical Properties of Carbon Fiber Composite Materials, Politecnico di Milano, 2014 [Master's Thesis].

[22] A. Monti, A. El Mahi, Z. Jendli, L. Guillaumat, Mechanical behaviour and damage mechanisms analysis of a flax-fibre reinforced composite by acoustic emission, Compos. Part A Appl. Sci. Manuf. 90 (2016) 100–110, https://doi.org/10.1016/j.compositesa.2016.07.002.

[23] P. Davies, M. Arhant, Fatigue behaviour of acrylic matrix composites: influence of seawater, Appl. Compos. Mater. (2018) 1–12, https://doi.org/10.1007/s10443-018-9713-1.

[24] A. Chilali, W. Zouari, M. Assarar, H. Kebir, R. Ayad, Analysis of the mechanical behaviour of flax and glass fabrics-reinforced thermoplastic and thermoset resins, J. Reinf. Plast. Compos. 35 (2016) 1217–1232, https://doi.org/10.1177/0731684416645203.

[25] S.K. Bhudolia, P. Perrotey, S.C. Joshi, Optimizing polymer infusion process for thin ply textile composites with novel matrix system, Materials (Basel) 10 (2017)https://doi.org/10.3390/ma10030293.

[26] M.R. Boumbimba, M. Coulibaly, A. Khabouchi, G. Kinvi-Dossou, N. Bonfoh, P. Gerard, Glass fibres reinforced acrylic thermoplastic resin-based tri-block copolymers composites: low velocity impact response at various temperatures, Compos. Struct. 160 (2017) 939–951, https://doi.org/10.1016/j.compstruct.2016.10.127.

[27] S.K. Bhudolia, S.C. Joshi, Low-velocity impact response of carbon fibre composites with novel liquid methylmethacrylate thermoplastic matrix, Compos. Struct. 203 (2018) 696–708, https://doi.org/10.1016/j.compstruct.2018.07.066.

[28] G. Kinvi-Dossou, R. Matadi Boumbimba, N. Bonfoh, S. Garzon-Hernandez, D. Garcia-Gonzalez, P. Gerard, A. Arias, Innovative acrylic thermoplastic composites versus conventional composites: improving the impact performances, Compos. Struct. 217 (2019) 1–13, https://doi.org/10.1016/j.compstruct.2019.02.090.

[29] W. Obande, D. Ray, C.M. Ó Brádaigh, Viscoelastic and drop-weight impact properties of an acrylic-matrix composite and a conventional thermoset composite – a comparative study, Mater. Lett. 238 (2019) 38–41, https://doi.org/10.1016/j.matlet.2018.11.137.

[30] S.K. Bhudolia, P. Perrotey, S.C. Joshi, Mode I fracture toughness and fractographic investigation of carbon fibre composites with liquid methylmethacrylate thermoplastic matrix, Compos. Part B Eng. 134 (2018) 246–253, https://doi.org/10.1016/j.compositesb.2017.09.057.

[31] M. Haggui, A. El Mahi, Z. Jendli, A. Akrout, M. Haddar, Damage analysis of flax fibre/elium composite under static and fatigue testing, in: M. Haddar, F. Chaari, A. Benamara, M. Chouchane, C. Karra, N. Aifaoui (Eds.), Des. Model. Mech. Syst, Springer International Publishing, Cham 2018, pp. 681–691.

[32] M. Haggui, A. El Mahi, Z. Jendli, A. Akrout, M. Haddar, Static and fatigue characterization of flax fiber reinforced thermoplastic composites by acoustic emission, Appl. Acoust. 147 (2019) 100–110, https://doi.org/10.1016/j.apacoust.2018.03.011.

[33] P. Davies, Environmental degradation of composites for marine structures: new materials and new applications, Philos. Trans. R. Soc. A Math. Phys. Eng. Sci. 374 (2016) 1–14 (doi:ARTN 20150272\r10.1098/rsta.2015.0272).

[34] P. Davies, P.-Y. Le Gac, M. Le Gall, M. Arhant, Marine ageing behaviour of new environmentally friendly composites, in: P. Davies, Y.D.S. Rajapakse (Eds.), Durab. Compos. a Mar. Environ, vol. 2, Springer International Publishing, Cham 2018, pp. 225–237, https://doi.org/10.1007/978-3-319-65145-3_12.

[35] L. Freund, V. Bouchart, H. Perrin, P. Chevrier, Hydrothermal aging of natural fibers composite: determination of diffusivity parameters, ECCM17 - 17th Eur. Conf. Compos. Mater, 2016.

[36] A. Chilali, W. Zouari, M. Assarar, H. Kebir, R. Ayad, Effect of water ageing on the load-unload cyclic behaviour of flax fibre-reinforced thermoplastic and thermosetting composites, Compos. Struct. 183 (2017) 309–319, https://doi.org/10.1016/j.compstruct.2017.03.077.

[37] A. Chilali, M. Assarar, W. Zouari, H. Kebir, R. Ayad, Effect of geometric dimensions and fibre orientation on 3D moisture diffusion in flax fibre reinforced thermoplastic and thermosetting composites, Compos. Part A Appl. Sci. Manuf. 95 (2017) 75–86, https://doi.org/10.1016/j.compositesa.2016.12.020.

[38] J. Beguinel, J.-F. Gérard, F. Lortie, P. Gérard, J. Maupetit, New continuous fiber reinforced thermoplastic composites: an analysis of interfacial adhesion from the micro scale to the macro scale, 20th Int. Conf. Compos. Mater, 2015.

[39] Z. Boufaida, L. Farge, S. André, Y. Meshaka, Influence of the fiber/matrix strength on the mechanical properties of a glass fiber/thermoplastic-matrix plain weave fabric composite, Compos. Part A Appl. Sci. Manuf. 75 (2015) 28–38, https://doi.org/10.1016/j.compositesa.2015.04.012.

[40] T. Pini, F. Briatico-Vangosa, R. Frassine, M. Rink, Fracture toughness of acrylic resins: viscoelastic effects and deformation mechanisms, Polym. Eng. Sci. 58 (2018) 369–376, https://doi.org/10.1002/pen.24583.

[41] T. Pini, Fracture Behaviour of Thermoplastic Acrylic Resins and Their Relevant Unidirectional Carbon Fibre Composites: Rate and Temperature Effects, Politecnico di Milano, 2017 [Doctoral Thesis].

[42] M. Haggui, Z. Jendli, A. Akrout, A. El Mahi, Damage identification in flax fibre composite with thermoplastic matrix under quasi-static loading, Int. Conf. Adv. Mater. Mech. Manuf 2016, pp. 1–4.

[43] M. Haggui, A. El Mahi, Z. Jendli, A. Akrout, Damage characterization of flax fibre composite using linear and nonlinear vibration resonant techniques, 26th Annu. Int. Conf. Compos. Eng, 2018.

[44] Q. Lin, M. Ferriol, M. Cochez, H. Vahabi, C. Vagner, Continuous fiber-reinforced thermoplastic composites: influence of processing on fire retardant properties, Fire Mater 41 (2017) 646–653, https://doi.org/10.1002/fam.2406.

[45] S.K. Bhudolia, P. Perrotey, S.C. Joshi, Enhanced vibration damping and dynamic mechanical characteristics of composites with novel pseudo-thermoset matrix system, Compos. Struct. 179 (2017) 502–513, https://doi.org/10.1016/j.compstruct.2017.07.093.

[46] G. Fredi, A. Dorigato, A. Pegoretti, Novel reactive thermoplastic resin as a matrix for laminates containing phase change microcapsules, Polym. Compos. (2019)https://doi.org/10.1002/pc.25233.

[47] T. Lorriot, J. El Yagoubi, J. Fourel, F. Tison, Non-conventional glass fiber NCF composites with thermoset and thermoplastic matrices, 20th Int. Conf. Compos. Mater., Copenhagen, 2015https://www.researchgate.net/publication/301684388, Accessed date: 17 January 2019.

[48] D.S. Cousins, Advanced Thermoplastic Composites for Wind Turbine Blade Manufacturing, Colorado School of Mines, 2018 [Doctoral Thesis].

[49] P. Davies, P.Y. Le Gac, M. Le Gall, Influence of sea water aging on the mechanical behaviour of acrylic matrix composites, Appl. Compos. Mater. 24 (2017) 97–111, https://doi.org/10.1007/s10443-016-9516-1.

[50] R.E. Murray, D. Penumadu, D. Cousins, R. Beach, D. Snowberg, D. Berry, Y. Suzuki, A. Stebner, Manufacturing and flexural characterization of infusion-reacted thermoplastic wind turbine blade subcomponents, Appl. Compos. Mater. 27 (2019) 1–17, https://doi.org/10.1007/s10443-019-9760-2.

[51] D. Zhang, A.M. Waas, C.-F. Yen, Progressive damage and failure response of hybrid 3D textile composites subjected to flexural loading, part I: experimental studies, Int. J. Solids Struct. 75–79 (2015) 309–320, https://doi.org/10.1016/j.ijsolstr.2015.06.034.

[52] M.J. Hiley, Fractographic study of static and fatigue failures in polymer composites Fractographic study of static and fatigue failures in polymer composites, Plast. Tubber Compos. 28 (1999) 210–227, https://doi.org/10.1179/146580199101540358.

[53] F.A. Almansour, H.N. Dhakal, Z.Y. Zhang, Effect of water absorption on mode I interlaminar fracture toughness of flax/basalt reinforced vinyl ester hybrid composites, Compos. Struct. 168 (2017) 813–825, https://doi.org/10.1016/j.compstruct.2017.02.081.

[54] F. Bensadoun, I. Verpoest, A.W. Van Vuure, Interlaminar fracture toughness of flax-epoxy composites, J. Reinf. Plast. Compos. 36 (2017) 121–136, https://doi.org/10.1177/0731684416672925.

[55] T. Eliades, S. Zinelis, D. Kim, W. Brantley, Structure/property relationships in orthodontic polymers, Orthod. Appl. Biomater 2017, pp. 39–59, https://doi.org/10.1016/B978-0-08-100383-1.00002-3.

[56] M. Sudheer, Thermomechanical properties of epoxy/PTW composites, J. Mech. Eng. Autom. 6 (2016) 18–21, https://doi.org/10.5923/c.jmea.201601.04.

[57] V. Chaudhari, H. Chandekar, J. Saboo, A. Mascarenhas, Studies on thermo-mechanical properties of chemically treated jute-polyester composite, IOP Conf. Ser. Mater. Sci. Eng, vol. 330, 2018, pp. 1–9, https://doi.org/10.1088/1757-899X/330/1/012032.

[58] A. Mousa, G. Heinrich, U. Wagenknecht, Wood-like material from thermoplastic polymer and landfill bio-materials: DMA, TGA and solvent resistance properties, Polym. from Renew. Resour. 6 (2015) 25–42 http://www.polymerjournals.com/pdfdownload/1189819.pdf (accessed April 29, 2019).

[59] K. Bandzierz, L. Reuvekamp, J. Dryzek, W. Dierkes, A. Blume, D. Bielinski, , Influence of network structure on glass transition temperature of elastomers Materials (Basel) 9 (2016) 1–17, https://doi.org/10.3390/MA9070607.

Materials Letters 238 (2019) 38–41

Contents lists available at ScienceDirect

Materials Letters

journal homepage: www.elsevier.com/locate/mlblue

Viscoelastic and drop-weight impact properties of an acrylic-matrix composite and a conventional thermoset composite – A comparative study

Winifred Obande, Dipa Ray *, Conchúr M. Ó Brádaigh

School of Engineering, Institute for Materials and Processes, The University of Edinburgh, Scotland, United Kingdom

ARTICLE INFO

Article history:
Received 30 June 2018
Received in revised form 23 October 2018
Accepted 24 November 2018
Available online 30 November 2018

Keywords:
Polymeric composites
Amorphous materials
Viscoelasticity
Thermoplastic matrices

ABSTRACT

Novel reactive thermoplastic resin systems such as Elium® have attracted significant research attention for composite applications because they combine the low-cost processibility of thermosets and the recyclability of TPs. In this work, the viscoelastic and impact behaviours of glass fibre-reinforced composites, containing Elium® and a commercial epoxy matrix were evaluated. To complement observations from both characterisation techniques, the fracture characteristics of both materials were also investigated by scanning electron microscopy.

© 2018 Elsevier B.V. All rights reserved.

1. Introduction

In light of recent global directives such as 2009/33/EC and 2008/98/EC, which stipulate strict targets for weight-reduction in the transport sector and cross-sectoral reduction of landfill-bound waste streams, respectively, thermoplastic (TP)-based fibre-reinforced polymer (FRP) composites are uniquely placed to future-proof FRPs as replacements for traditional materials. TP matrices are high-viscosity melts, requiring high-cost FRP fabrication processes [1,2]. Consequently, their low-viscosity thermoset (TS) counterparts dominate the FRP industry due to ease of processing. Recently, novel low-viscosity (~100 mPa.s; 25 °C) liquid TP resin systems such as the acrylic-based Elium® by Arkema have opened up new opportunities for the fabrication of TP-FRPs using low-cost TS-FRP production methodologies.

The mechanical and thermomechanical properties of Elium®-matrix FRPs have been studied by several authors [3–6], however, there is a paucity of published comparative data (with conventional TS-FRPs). In this work, the viscoelastic and impact behaviours of glass fibre-reinforced Elium® (GF/Elium®) and glass fibre-reinforced epoxy (GF/Epoxy) FRPs have been studied comparatively. The damping characteristics of these materials provide valuable insights into internal molecular mobility and dissipation of energy [7,8]. Fracture behaviours were also investigated to assess their associated failure processes.

2. Experimental

2.1. Materials and fabrication

Elium® 180 (Arkema GRL, France) and IN2 Infusion Epoxy (Easy Composites Ltd., UK) laminates were fabricated by a room temperature (RT) vacuum infusion method. Eight plies $[45/0/-45/90]_S$ of a non-crimp E-glass fabric (Saertex GmbH & Co. KG, Germany) were used to produce 4 mm-thick laminates (0.47 fibre volume fraction). The processing schedules are as follows:

- GF/Elium®: 24 h at RT. No post-cure.
- GF/Epoxy: 24 h at RT. Post-cure: 40 °C to 70 °C; 10 °C increments with a 2-hour isothermal segment at each temperature.

2.2. Mechanical and thermomechanical characterisation

Single-frequency (SF) and multi-frequency (MF) dynamical mechanical analyses (DMA) were performed to study the viscoelastic behaviours of both materials. Their damage resistance following drop-weight impact events at 15 J and 30 J were also assessed by measuring respective damage areas; six specimens were tested at each energy level per material. This was done by

* Corresponding author.
E-mail address: Dipa.Roy@ed.ac.uk (D. Ray).

https://doi.org/10.1016/j.matlet.2018.11.137
0167-577X/© 2018 Elsevier B.V. All rights reserved.

high-contrast imaging of the translucent coupons using backlight illumination. Damage areas were measured using a digital image processing software (Image J, National Insitutes of Health). Relevant information on specimens and test parameters are presented in Table 1.

Fractographic analyses were performed by scanning electron microscopy (SEM – Jeol JSM series microscope) to qualitatively assess the fibre-matrix interface and matrix ductility in both materials. Given that flexural stresses play a significant role in the impact damage processes, flexural testing was performed to obtain fracture surfaces. Single coupons measuring 65 mm in length were flexurally loaded at 10 mm/min over a span of 30 mm. Fracture on the lower surfaces (i.e., resulting from tensile stress) were inspected for both materials. It is worth noting that being obtained from a quasi-static test regime, the fracture behaviours will not be directly comparable to those observed in impact loading, where failure occurs in shorter time scales.

3. Results and discussion

Glass transition (T_g) temperatures were determined as temperatures corresponding to the damping peak as shown in Fig. 1a. These were 67 °C and 115 °C for GF/Epoxy and GF/Elium®, respectively. GF/Elium® was also found to have a higher damping peak compared to that of GF/Epoxy.

Given their dissimilar T_g values, multi-frequency scan results were analysed at a reference temperature of 25 °C to facilitate direct comparisons between the materials' viscoelastic behaviours. As is evident in Fig. 1b., GF/Elium® not only exhibited higher (8.7%) damping behaviour, but had a higher damping retention than GF/Epoxy at higher frequencies (66%, from 0.01 Hz to 100 Hz, compared to 26%).

As an amorphous TP, the chains within the Elium® matrix are able to dissipate the applied energy and subsequently expend it by means of short-range motion. The rigid nature of the crosslinked chains within the GF/Epoxy reduces the extent to which it can dissipate energy at 25 °C. For both materials, there is a time-dependent response because at higher frequencies, the molecules undergo limited dissipation. Both SF and MF scans showed higher energy dissipation in the case of GF/Elium®.

The observations from the viscoelastic study were not reflected in the impact testing. The damage areas for GF/Elium® and GF/Epoxy were measured as 4.4 ± 0.9% and 3.9 ± 0.3% for coupons subjected to 15 J impacts, and 7.4 ± 0.5% and 6.6 ± 0.5% for 30 J impacts, respectively. Thus, GF/Epoxy was marginally more damage resistant. Representative images for these estimations are presented in Fig. 2a.–d.

The impact performance of FRPs involves a combination of several complex and interrelated processes, which include energy dissipation (elastic deflection and rebound) and absorption (creation of fracture surfaces); the extent of the latter controls the resultant damage processes. From a stress perspective, the inherent anisotropy of laminated FRPs gives rise to two states of stress – namely bending and interlaminar shear [10]. Their interplay results in matrix cracking and interfacial debonding, which ultimately lead to delamination and fibre fracture. As such, matrix toughness, ductility and interfacial strength play significant roles in impact performance.

To understand the lack of correlation between the viscoelastic and impact responses of GF/Elium® and GF/Epoxy, some possible influencing factors are proposed. Complementary fractographic observations on GF/Elium® (Fig. 3a.) and GF/Epoxy (Fig. 3b.) will be discussed in light of the theoretical fracture behaviours of amorphous thermoplastic and crosslinked thermoset matrices; and their respective composites.

Although the fracture surfaces of both GF/Elium® (Fig. 3a.) and GF/Epoxy (Fig. 3b.) show brittle matrix failure, certain differences are observed. Brittle amorphous thermoplastics (BATPs) such as acrylics exhibit microscopic ductility and undergo ductile-to-brittle transition at high strain rates due to strain localisation [11,12]. Microductility predominates on the GF/Elium® fracture surfaces, whereas mirror (smooth) zones are evident in GF/Epoxy. Mirror zones indicate brittle failure with unstable crack growth.

Table 1
DMA and Impact test information.

Test Method	Test Parameters	
DMA	Standard	BS ISO 6721 – 11
	Specimen dimensions (mm)	35 × 5
	Instrument	Triton 2000 series
	Mode	3-point bending
	Heating rate (°C/min)	3
	Amplitude (μm)	10
	Temperature range (°C)	SF: Ambient – 170 MF: Ambient – 45
	Frequency (Hz)	SF: 1 MF: 0.01 – 100
	Span (mm)	30
Impact	Standard	ASTM D7136
	Specimen dimensions (mm)	150 × 100
	Impactor mass (kg)	4.2
	Drop height (m)	15 J: 0.55 30 J: 1.05

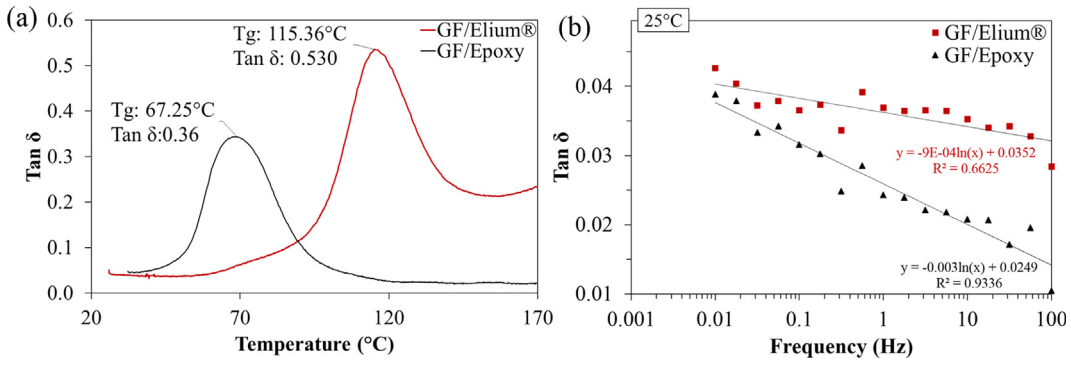


Fig. 1. Results from (a) single frequency DMA scans showing damping as a function of temperature and (b) multi-frequency DMA scans showing the evolution of damping with frequency at 25 °C.

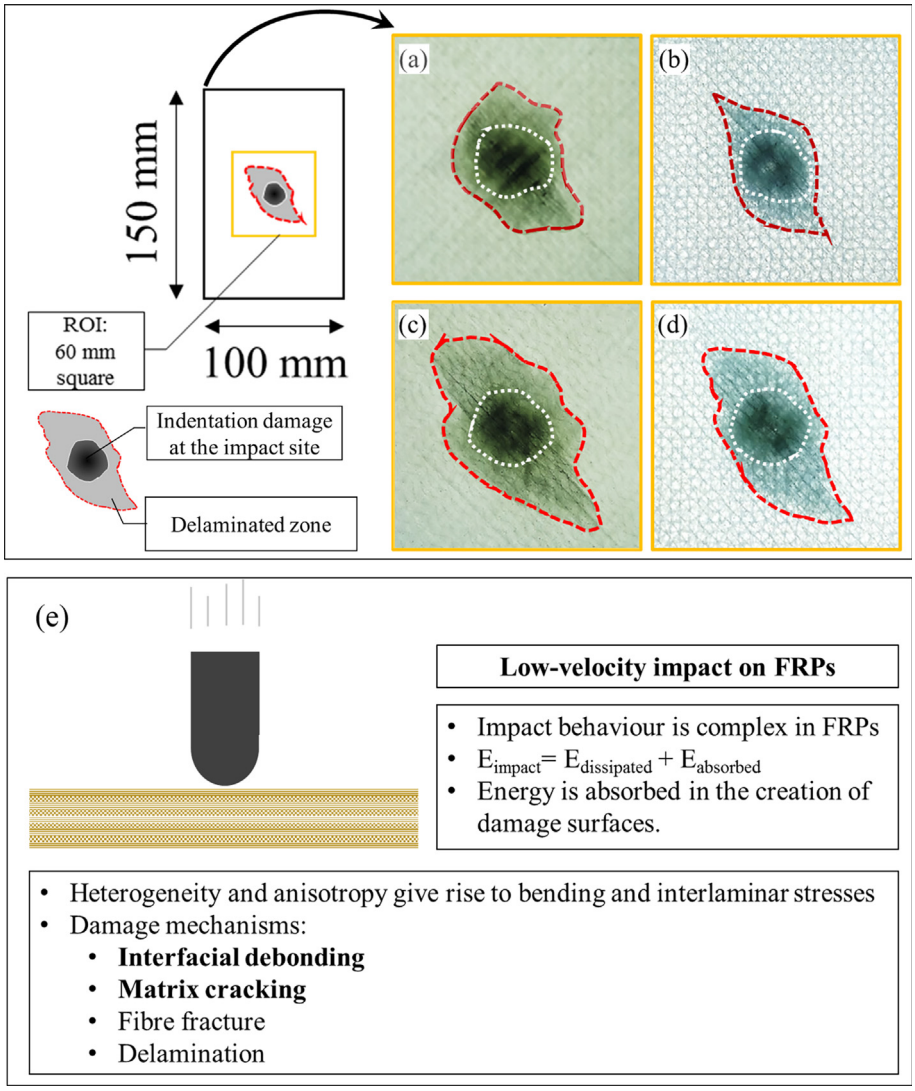


Fig. 2. Representative damage states for (a) GF/Elium® at 15 J, (b) GF/Epoxy at 15 J, (c) GF/Elium® at 30 J, and (d) GF/Epoxy at 30 J. ROI: region of interest.

The aforementioned microscopic ductility in matrices like Elium® typically does not translate into macroscopic failure behaviour because of their post-yield behaviour. This is because crazes form normal to the applied stress direction as a result of macroscopic strain softening and limited strain hardening, the latter of which gives rise to low failure strain [11,12]. Additionally, the presence of fibres in BATPs inhibits plastic zone development [13], which induces a triaxial stress state in the matrix and limits the dissipation of energy [14]. Despite being brittle and amorphous, epoxies do not commonly exhibit this post-yield deformation behaviour because their crosslinks increase their strain hardening moduli [13].

Despite having superior dissipative characteristics, GF/Elium® contains an acrylic matrix, which is prone to strain-dependent embrittlement [11] and has low failure strain [12]. Furthermore, a high damping peak does not necessarily predict high impact strength, because the nature of chain deformation occurring within the polymer – i.e., main or side chain – determines how much of a correlation exists between both behaviours [15].

4. Conclusions

A comparative study was conducted to evaluate the viscoelastic and impact behaviours of GF/Elium® and GF/Epoxy. GF/Elium® was found to have higher (~9%) damping parameter and superior (66%) retention of this property at the highest test frequency of 100 Hz. Improved damping characteristics typically predict impact damage resistance; however, when subjected to 15 and 30 J impact events, GF/Elium® was less damage resistant. Our observations are in agreement with those of Heijboer [15] on viscoelastic and impact responses of unreinforced acrylic polymer. These findings are important for benchmarking Elium® as a new resin system for composite applications. SEM micrographs revealed brittle matrix failure in both materials with evidence of unstable crack propagation (smoother fracture surfaces) in GF/Epoxy and microductility in the case of GF/Elium®. Further investigations are required to substantiate the tentative explanations discussed on fractographic behaviour.

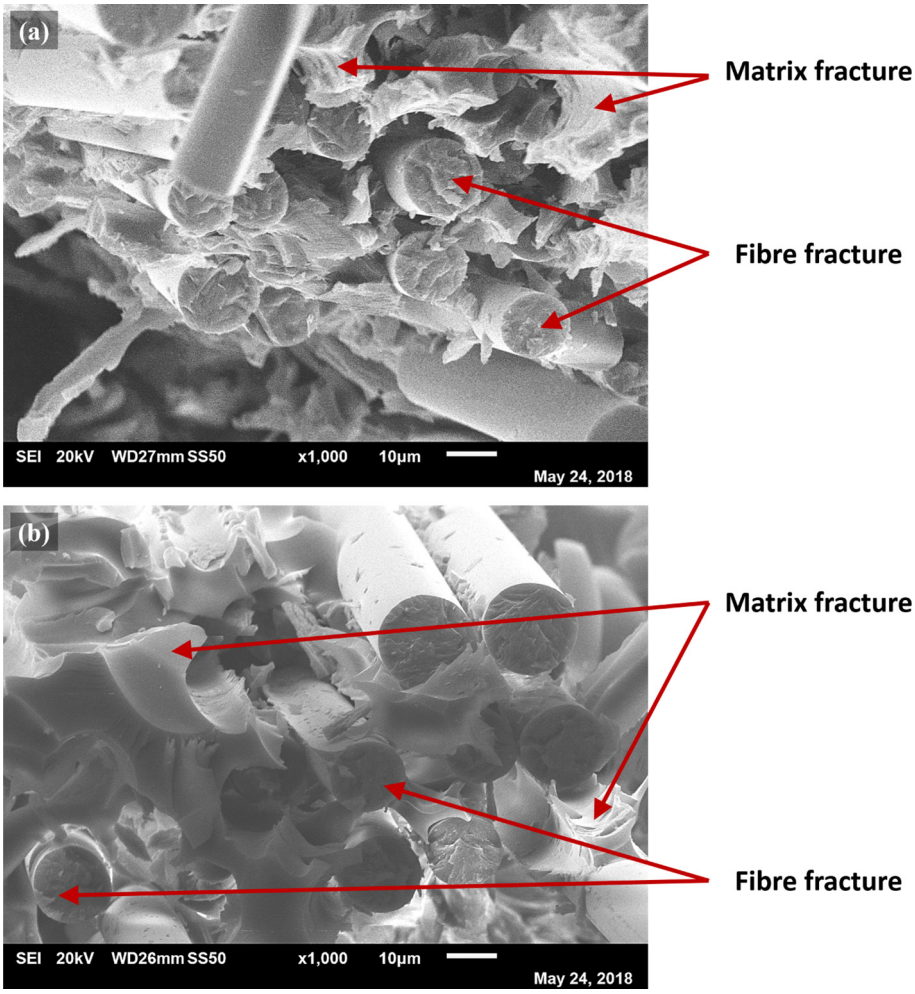


Fig. 3. SEM micrographs of tensile fracture surfaces from flexural specimens showing brittle matrix failure for (a) GF/Elium® and (b) GF/Epoxy.

Acknowledgements

We would like to thank Arkema GRL, France for providing material samples towards this research; and the School of Engineering, University of Limerick, Ireland, for access to their testing facilities. The authors gratefully acknowledge the financial support of the University of Edinburgh via a PhD scholarship awarded to Ms. O. W. Obande.

Appendix A. Supplementary data

Supplementary data to this article can be found online at https://doi.org/10.1016/j.matlet.2018.11.137.

References

[1] D.M. Bigg, D.F. Hiscock, J.R. Preston, E.J. Bradbury, High performance thermoplastic matrix composites, J. Thermoplast. Compos. Mater. (1988) 146–160.
[2] S. Béland, High Performance Thermoplastic Resins and Their Composites, 1st ed., Noyes Data Corporation, New Jersey, 1990.
[3] A. Chilali, W. Zouari, M. Assara, H. Kebir, R. Ayad, Analysis of the mechanical behaviour of flax and glass fabrics-reinforced thermoplastic and thermoset resins, J. Reinf. Plast. Compos. 35 (16) (2016) 1217–1232.
[4] S.K. Bhudolia, P. Perrotey, S.C. Joshi, Enhanced vibration damping and dynamic mechanical characteristics of composites with novel pseudo-thermoset matrix system, Compos. Struct. 179 (2017) 502–513.
[5] S.K. Bhudolia, P. Perrotey, S.C. Joshi, Mode-I fracture toughness and fractographic investigation of carbon fibre composites with liquid methylmethacrylate thermoplastic matrix, Compos. B Eng. 134 (2018) 246–253.
[6] A. Chilali, W. Zouari, M. Assarar, H. Kebir, R. Ayad, Effect of water ageing on the load-unload cyclic behaviour of flax fibre-reinforced thermoplastic and thermosetting composites, Compos. Struct. 183 (2018) 309–319.
[7] J.F. McCabe, H. Arikawa, Rheological properties of elastomeric impression materials before and during setting, J. Dent. Res. 77 (11) (1998) 1874–1880.
[8] Saba, M. Jawaid, O.Y. Alothman, M.T. Paridah, A review on dynamic mechanical properties of natural fibre reinforced polymer composites, Constr. Build. Mater. 106 (2016) 106.
[10] S. Abrate, Impact Engineering of Composite Structures, SpringerWienNewYork, Udine, 2011.
[11] H. Wu, G. Ma, Y. Xia, Experimental study of tensile properties of PMMA at intermediate strain rate, Mater. Lett. 58 (2004) 3681–3685.
[12] I.A. van Casteren, Control of Microstructures to Induce Ductility in Brittle Amorphous Polymers, Technische Universiteit Eindhoven, Einhoven, 2003.
[13] W.L. Bradley, Relationship of matrix toughness to interlaminar fracture toughness, in: Application of Fracture Mechanics to Composite Materials, Elsevier Science Publishers, Amsterdam, 1989, pp. 159–186.
[14] J.M.M. de Kok, Deformation, Yield and Fracture of Unidirectional Composites in Transverse Loading, Technische Universiteit Eindhoven, Eindhoven, 1995.
[15] J. Heijboer, Dynamic mechanical properties and impact strength, J. Polym. Sci.: Part C 16 (1968) 3755–3763.